Porphyrins as Complexing Ligands for Modular Syntheses of Rigid Homo and Heteromultimetallic Complexes

Zur Erlangung des akademischen Grades eines

DOKTORS DER NATURWISSENSCHAFTEN

(Dr. rer. nat.)

von der KIT-Fakultät für Chemie und Biowissenschaften

des Karlsruher Instituts für Technologie (KIT)

genehmigte

DISSERTATION

von

M. Sc. Christoph Schissler

aus Heilbronn-Neckargartach

Dekan: Prof. Dr. Hans-Achim Wagenknecht

Referent: Prof. Dr. Stefan Bräse

Korreferent: PD. Dr. Patrick Weis

Tag der mündlichen Prüfung: 14. Dezember 2021

“The mind is not a vessel to be filled but a fire to be kindled.”

-Plutarch

German Title of the Thesis

Porphyrine als Komplexliganden für Modulare Synthesen Rigider Homo- und Heteromultimetallischer Komplexe

Chronology of the Ph.D. research

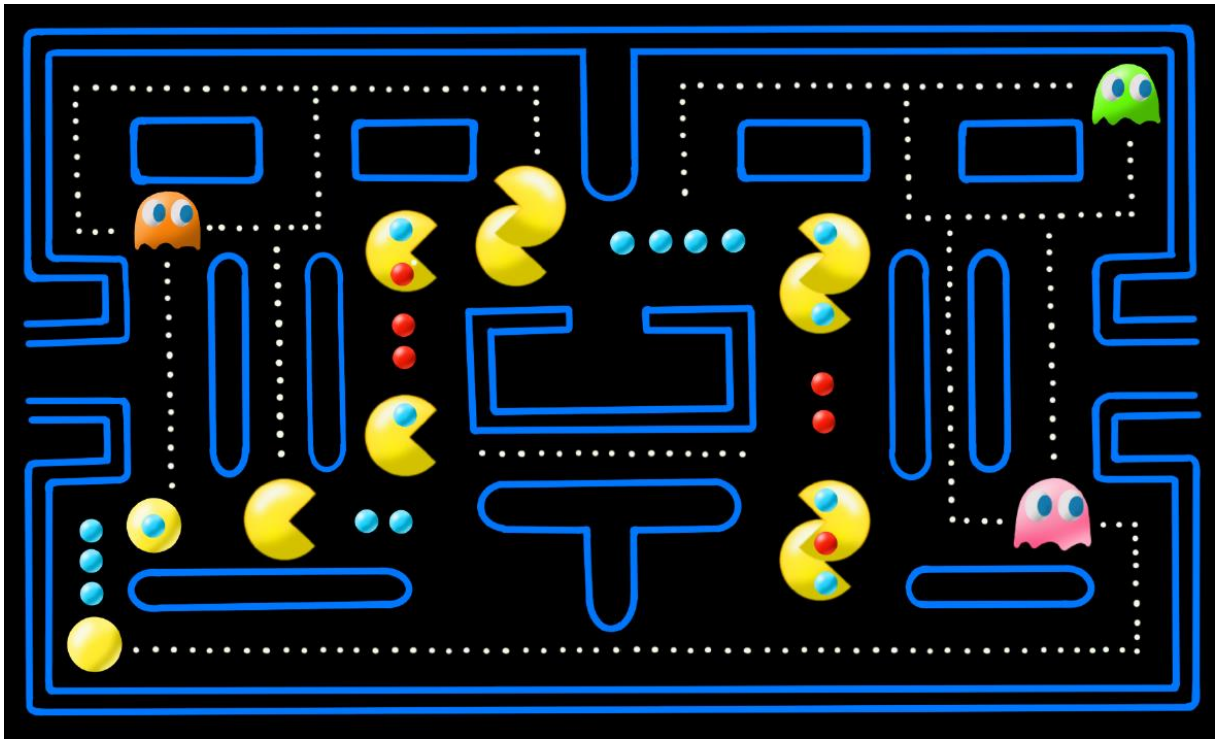

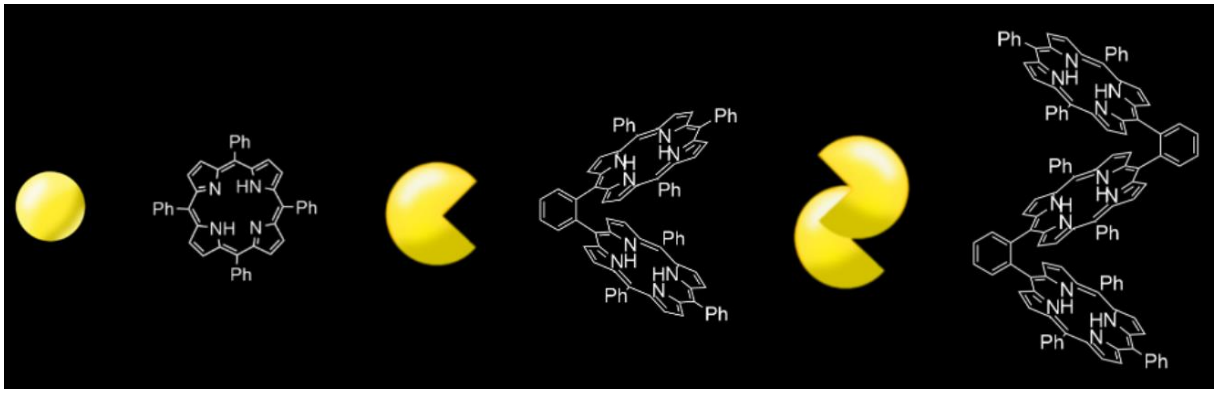

Table of Contents

Abstract

The molecular class of porphyrins combines a universal ligand system with versatile functionality, thus providing all the requirements for synthesizing tailor-made multimetallic centers. Complex biological systems such as the Fe(II)-Ni(II) center of the carbon monoxide dehydrogenase, enabling CO_2 reduction under physiological conditions, can consequently be recreated and investigated in a simplified form. This makes a valuable contribution towards a better understanding of biological models to apply cooperative metal-metal interaction in catalysis in the future.

The present work provides a synthetic contribution towards porphyrin-based cofacial metal complexes and their characterization. To this end, linker systems were tested to arrange the porphyrin ligands at defined distances spatially. Thereby, three analogs of the cofacial *o*-phenylene-bisporphyrin ligand were obtained and successfully coordinated twice with Mn(III), Fe(III), Ni(II), Cu(II), Zn(II), Pd(II), Pb(II) and Bi(III). The first crystal structure of this class of compounds was obtained from an unsymmetrical 2Ni(II) complex. For the Fe(III) derivative, an antiparallel coupling between the two centers *via* an μ-oxo bridge to an overall diamagnetic complex could be attested using *Mössbauer* spectroscopy.
Furthermore, a combination of ion mobility measurements and DFT calculations revealed a ligand-dependent distance trend, which was correlated to a shoulder arising in the *Soret*-band region of the UV-Vis absorption spectrum. Due to the modular incorporation of metal centers, by the developed synthesis strategy, the heterobimetallic complexes Fe(III)-Ni(II)/Cu(II)/Pd(II)/Pt(II) and Mn(III)-Cu(II) were synthesized and characterized. Advancements of the protocol pave the way towards cofacial porphyrin trimers for both homo- and heterotrimetallic complexes. The *cis*-isomer was characterized as the first conformationally restricted planar-chiral porphyrin trimer. The corresponding mono-, di- and trimeric porphyrin-based Pd(II) complexes show a disproportional increase in the intensity of the $^1O_2$ emission in the luminescence spectrum and thus an increase in efficiency triggered by cooperative effects on potential active drugs in photodynamic therapy. Furthermore, a modified protocol was developed to cofacially connect an N-fused-porphyrin with a regular porphyrin *via* an *o*-phenylene-residue, which can stabilize different oxidation states of the same metal, as demonstrated for the Mn(I)-Mn(III)-case. *Via* the successful 6-fold sulfonation reaction of the dimeric ligand, water-soluble compounds were obtained, facilitating further insights into the electronic structure of the systems by photodissociation and photoelectron spectroscopy.

Kurzzusammenfassung

Die Molekülklasse der Porphyrine vereint ein universelles Ligandensystem mit vielseitiger Funktionalisierbarkeit und liefert damit alle Voraussetzungen zum Aufbau modularer multimetallischer Zentren. Komplexe biologische Systeme wie das Fe(II)-Ni(II) Zentrum der Kohlenstoffmonoxid Dehydrogenase, das unter physiologischen Bedingungen die CO_2 Reduktion katalysiert, können somit in vereinfachter Form nachgebaut und untersucht werden. Damit kann ein wertvoller Beitrag für ein besseres Verständnis biologischer Vorbilder geleistet werden, um in Zukunft kooperative Metall-Metall Interaktionen in Katalysen anzuwenden.

Die vorliegende Arbeit liefert einen synthetischen Beitrag zum Aufbau porphyrin-basierter cofacialer Metallkomplexe und deren Charakterisierung. Dazu sollten zunächst Linkersysteme getestet werden, die Porphyrinliganden in unterschiedlichen Abständen räumlich fixieren. Hierbei konnten drei Analoga des cofacialen *o*-Phenyl-bisporphyrin Liganden dargestellt werden, die erfolgreich Mn(III), Fe(III), Ni(II), Cu(II), Zn(II), Pd(II), Pb(II) und Bi(III) zweifach komplexieren können. Von einem unsymmetrischer 2Ni(II) Komplex konnte hierbei die erste Kristallstrukur dieser Verbindungsklasse erhalten werden. Den Fe(III) Komplexen konnte über mößbauerspektroskopische Untersuchungen eine antiparallele Kopplung über eine μ-oxo Brücke zu einem diamagnetischen Komplex attestiert werden. Des Weiteren wurde über eine Kombination aus Ionenmobiliätsmessungen und DFT Rechnungen ein ligandenabhängiger Abstandstrend verdeutlicht, der zudem mit einer Schulter in der *Soret*-Bande des UV-Vis Absorptionsspektrums korreliert. Durch die entwickelte modulare Synthese konnten außerdem die heterobimetallischen Komplexe Fe(III)-Ni(II)/Cu(II)/Pd(II)/Pt(II) und Mn(III)-Cu(II) synthetisiert und charakterisiert werden. Die Weiterentwicklung des Protokolls, ermöglichte die Synthese cofacialer Porphyrintrimere als homo- und heterotrimetallische Komplexe. Dabei wurde das entsprechende *cis*-Isomer als erstes konformationelleingeschränktes planar-chirales Porphyrintrimer charakterisiert. Die entsprechenden mono-, di- und trimeren Pd(II) Komplexe zeigen im Lumineszenz Spektrum einen überproportionalen Intensitätsanstieg der Singulett-O_2 Emission und damit eine Effizienzsteigerung, ausgelöst von kooperativen Effekten, auf potentielle Wirkstoffe der photodynamischen Therapie. Des Weiteren wurde ein N-fused Porphyrin mit einem regulären Porphyrin cofacial über einen *o*-phenyl Linker verknüpft, das in der Lage ist, unterschiedliche Oxidationsstufen gleicher Metalle, wie für Mn(I)-Mn(III) gezeigt, zu stabilisieren. Über eine 6-fach Sulfonierung des dimeren Liganden konnten wasserlösliche Strukturen erhalten werden, die per Photodissoziations- und Photoelektronenspektroskopie weitere Einblicke in die elektronische Struktur der Systeme ermöglichen.

1 Introduction

In nature, the catalytically active sites of metalloenzymes are often highly conserved structural motives in adaptive protein matrices that have evolved over millions of years. Already *Leonardo Da Vinci* noticed that the systematic recognition of solutions in living nature should be the main source of inspiration for research and expressed that as follows:

"*The human creative spirit can make various inventions (...), but it will never succeed in one that is more beautiful, more economical and more straightforward than that of nature, because nothing is missing in its inventions and nothing is too much*."[1]

Even though this citation from the early 16th century rather comprises the thought of transferring biological knowledge toward technical applications in a macroscopic way, without a doubt, this can also be transferred to chemical research.

Never before has humankind faced a comparable threat to climate change alongside the world's energy problem. To master this challenge, the duty of science is nothing less than groundbreaking discoveries in the field of, e.g., novel sustainable energy sources.

A promising approach is the reduction of CO_2 as an essential reaction to generate new types of renewable raw materials and curb the greenhouse effect.[2] However, the conversion of CO_2 into a usable, reduced form is one of the greatest challenges in synthetic chemistry since it is thermodynamically extremely stable.[3]

Inspired by the binuclear Ni(II)-Fe(II) center of carbon monoxide dehydrogenase (CODH), which can efficiently catalyze the reduction of CO_2 to CO under physiological conditions,[4] increased efforts have been made to understand the working principle and structure-activity relation of the enzyme by, e.g., single-crystal diffraction measurements.[5, 6]

To understand how spatially close metal ions interact, a rigid molecular system that allows tuning the distance between the metal centers is best suited to conduct a systematic investigation. Cooperative effects between metals are examined in great detail in the research project "Cooperative Effects in Homo- and Heterometallic Complexes (3MET)". Everything is geared towards a fundamental understanding of the environment to recognize natural solutions to preserve nature from humankind.[7, 8]

1.1 Structure and nomenclature

Porphyrins rank among the most widespread macrocycles in nature and to the best-explored compounds in chemistry.[9] To represent the structure efficiently and in a defined manner, the nomenclature, represented in Figure 1, is introduced for the exemplary compounds **1** and **2**. The parent compound of porphyrins is called porphin (**3**) with the molecular formula $C_{20}H_{14}N_4$, consisting of four pyrrole subunits connected *via* methine bridges in a cyclic manner.

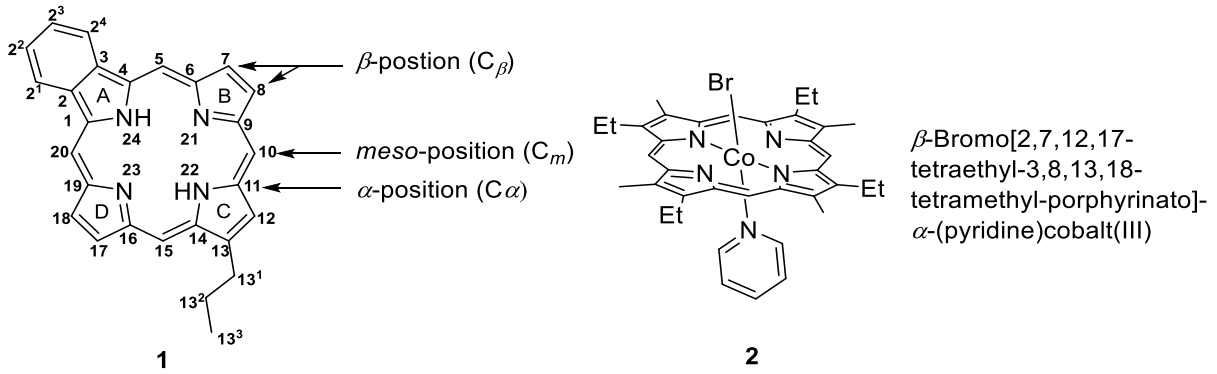

Figure 1: Nomenclature of the modified parent compound porphin explained *via* examples **1** and **2**. The general designations *α*– *β*– and *meso*-position are not according to the IUPAC but are commonly used terms to address positions in general (left). The *α* and *β*–denotation, according to IUPAC, defines the position of differing ligands orthogonal to the plane.[10]

The shown nomenclature is recommended by the International Union of Pure and Applied Chemistry (IUPAC) and the International Union of Biochemistry and Molecular Biology (IUBMB). All 24 positions of the porphin (**3**) were consecutively numbered – for carbons that expand the scaffold, superscripted numbers were introduced. The terms *α*-, *β*- and *meso*-position are not recommended by the IUPAC nomenclature but commonly address available positions. The base structure containing two acidic protons attached to the four nitrogen atoms of the pyrrole rings was denoted as free-base porphyrin.[11] Within the nomenclature of porphyrin-based metal complexes, the exact assignment regarding the coordination was not applied but generally treated as a double negatively charged ligand.[10] For that reason, to the macrocyclic ligand, the *suffix –ato* has to be added, followed by the name of the coordinated metal and its oxidation number in roman numerals in brackets. The denotation of the coordination of additional ligands above and below the porphyrin plane is listed alphabetically. In case of differing ligands orthogonal to the plane, the additional ligand below the in clockwise direction numbered porphyrin is denoted as *α*, in contrast to the additional ligand above, which is labeled *β*.[10]

As a general classification of *meso*-substituted porphyrins, the so-called ABCD-system can be applied. Different symmetries can easily be described using the *prefix trans*- for 5,15-substitution or *cis*- for 5,10-substitution *via* this notation (Figure 2).[11]

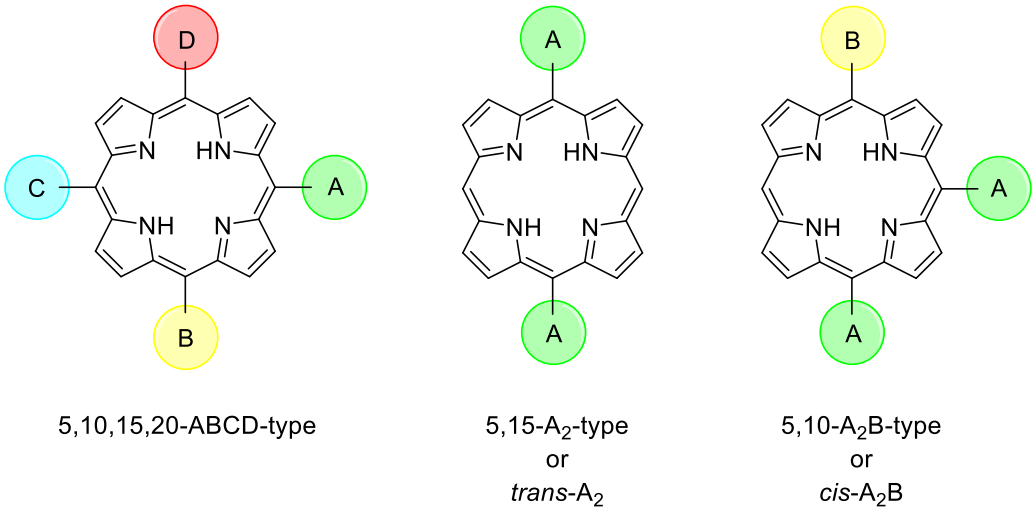

Figure 2: ABCD-nomenclature for *meso*-substituted porphyrins.

Over the years, many porphyrinoid structures have been discovered beside the classical porphyrin scaffold, including the isomers of porphin with a rearranged $C_{20}N_4$ core, defined reductions of double bonds and analogs with expanded or contracted skeleton ranging from subporphyrin **19** to dodecaphyrin **24** (Figure 3).[12-14]

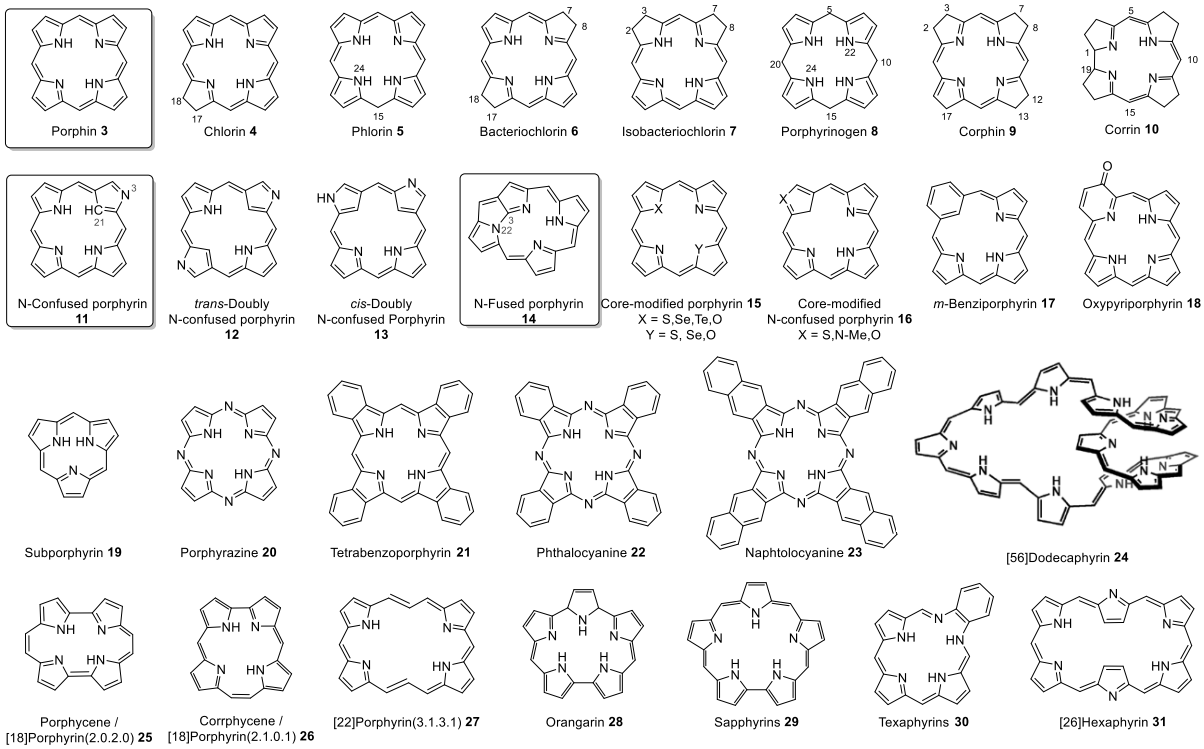

Figure 3: A selection of porphyrinoid structures. Squared derivatives represent the most relevant scaffolds in this work.

The rearrangement of the $C_{20}N_4$ skeleton to yield the 2-aza-21-carbaporphyrin is known as the N-confused porphyrin **11**. In 1994, *Naruta et al.* first noticed this structural motive as a new isomer of tetraphenylporphyrin, occurring as a side-product of the common acid-catalyzed condensation reaction of pyrrole and benzaldehyde.[15] As indicated in Figure 3, one of the pyrrole rings underwent a 2,4-instead of a 2,5-substitution. As a result, one pyrrole subunit is

inverted to replace a tertiary amine with a CH on the internal part of the porphin core. Consequently, the nitrogen atom substitutes one carbon atom at the *β*-position on the periphery of the ring.[15, 16] The IUPAC nomenclature follows the rules of a regular porphyrin without accounting for the change of the atoms (Figure 4).[17]

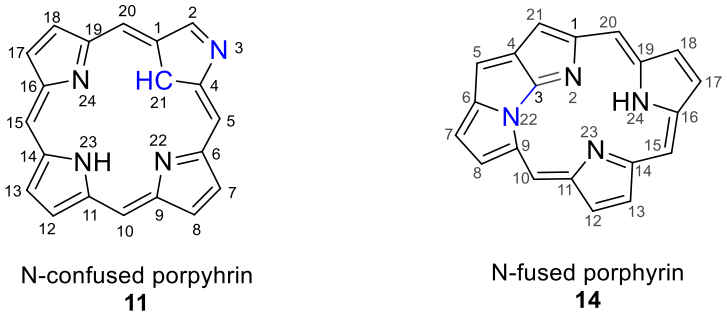

Figure 4: Nomenclature of the N-confused porphyrin (**11**) – a rearranged isomer of the porphin scaffold and the N-fused porphyrin (**14**) containing a [5.5.5]fused tri-pentacyclic ring.

The skeleton contains a [5,5,5]fused tri-pentacyclic ring, including two tertiary nitrogens, as depicted in Figure 4. N-confused porphyrins (**11**) can be converted into the N-fused porphyrin (**14**) *via* a rotation of the confused pyrrole and a subsequent nucleophilic attack of the adjacent pyrrole to form the C(3)-N(22) bond.[18, 19] The numbering stays following the IUPAC recommendation, starting with the carbon atom connected to a methin bridge of the previously inverted pyrrole. The interior N-atoms are therefore assigned to the numbers 2 and 22 – 24.

.

1.2 Properties of porphyrins

Porphyrins consist of a planar, conjugated π-electron system with 26 π-electrons, of which 18 are cyclically delocalized according to the (4n+2)-*Hückel*-rule of aromaticity.[20] The possibility of different resonance structures of the macrocycle and their contribution to the aromaticity has been under discussion for a long time. For porphin (**3**), a contributing structure with 26 π-electrons, three symmetrically distinguishable 22 π-electron and two 18 π-electron resonance forms can be constructed. Studies indicate that the aromatic resonance hybrid of porphin (**3**) has to be considered a superposition of all (4n+2)π mesomerisms, of which the dominating contributions stem from the 26 π- and the two 22 π-electron structures.[21, 22] The work of *Schleyer et al*. corroborates that appended 6 π aromatic sextets confer aromaticity more effectively than macrocyclic (4n+2)π electron conjugation.[23]

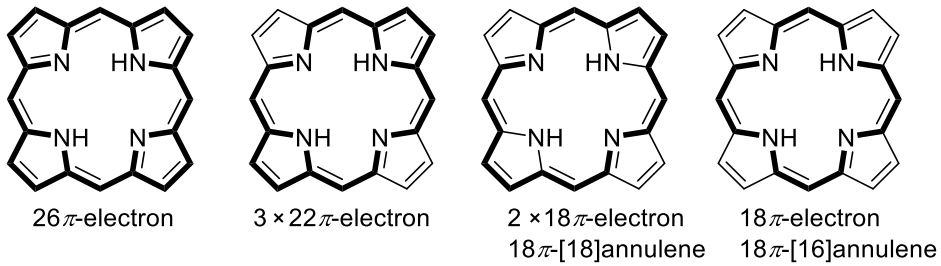

Figure 5: Four different π-electron pathways according to the (4n+2)-*Hückel*-rule of aromaticity.[21]

As is typical for aromatic compounds, the chemical shift of the involved protons arises in characteristic ranges in ^{1}H NMR spectra. The reason for that is a π-electron ring current generated by the spectrometer's external magnetic field. The resulting local magnetic field overlaps with the external field, which leads to deshielding effects on the outer protons and the occurrence of resonances at a chemical shift of up to 11 ppm. In contrast, the internal protons attached to the nitrogen atoms undergo shielding effects and occur in the region down to –4 ppm.[21]

1.2.1 Photophysical properties of free-base porphyrins

The cyclically delocalized π-electrons are the basis of many photophysical effects as the light absorption in the range of UV- to visible-light manifests in an intense red-purple color (Figure 6).

Figure 6: Tetraphenylporphyrin (TPP, **32**) as a solid (left), as 1.63×10^{-3} M solution in CH_2Cl_2 in day light (top-right) and under UV-radiation (λ = 395 nm) (bottom-right).

Porphyrins belong to the chromophores with the highest extinction coefficient ($\varepsilon = 3.72 \times 10^5$ $cm^{-1}M^{-1}$ in diethyl ether). Therefore, 10 mg TPP (**32**) dissolved in 10 mL CH_2Cl_2 (1.63×10^{-5} M) is enough to dye the solution dark red.[24] The macroscopic properties can be explained by looking into the UV-Vis absorption spectrum (Figure 7). The absorption spectrum of tetraphenylporphyrin TPP consists of two characteristic absorption bands resulting of π-π^*-transition within the π-electronic system.[25] The most intensive absorption band reaches from 380 – 430 nm and is named B-band or *Soret*-band after its discoverer. In the 500 – 650 nm region, four less intensive absorption bands are located, called Q-bands.[25] The transitions that lead to the Q-bands can be assigned to the electronic excitations from the ground state S_0 to the first excited state S_1. The excitation from the ground state S_0 to the second excited state S_2 can be assigned to the *Soret*-band. The free-base porphyrin has D_{2h} symmetry due to non-equivalent molecular symmetry in x- and y-direction. This results in a Q-band splitting in Q_x and Q_y, which leads to four Q-bands with different vibrational states $Q_{x(O,O)}$, $Q_{x(O,1)}$ and $Q_{y(O,O)}$, $Q_{y(O,1)}$ as shown in Figure 7. Substituting the *meso*-position with electron-donating groups leads to bathochromic effects manifesting in a red-shift of the absorption spectra. The substituent contributes to the π-electronic system and enhances the delocalization, whereby the excitation energy is lowered.[26]

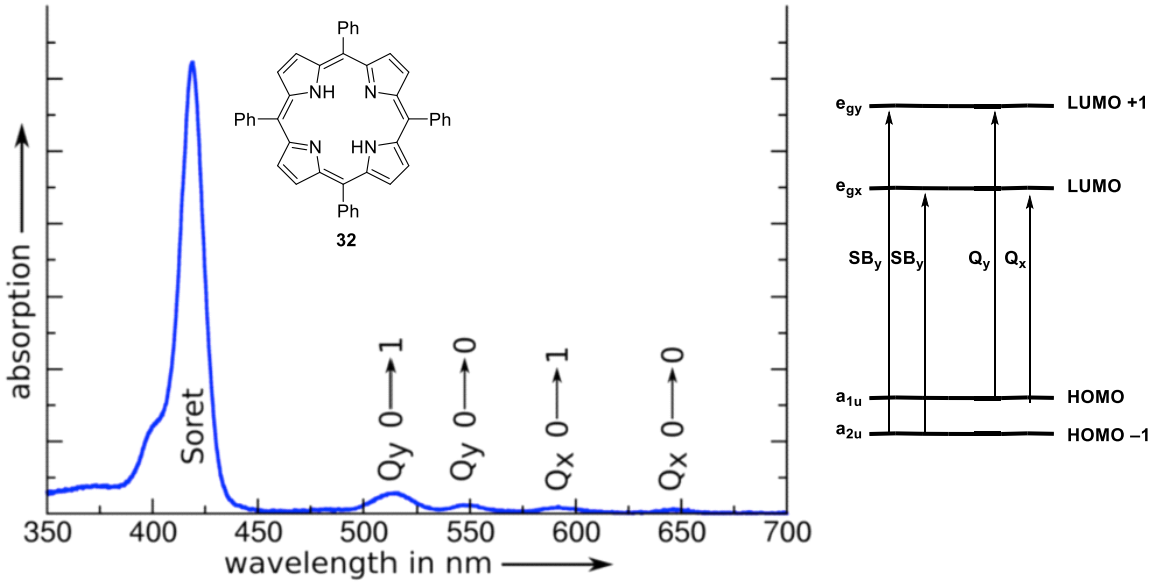

Figure 7: Condensed phase UV-Vis spectrum of TPP **32** and the assignment of the respective electron transitions to the corresponding bands (left). Representation of the relevant frontier orbitals for the porphyrin absorption (right). The depicted Figure is based on *Heine et al.*[27]

1.2.2 Properties of metalloporphyrins: square-planar coordination

In contrast to the D_{2h} symmetry of free-base porphyrins, the molecular symmetry of porphyrin-based metal complexes is identical in x- and y-direction and has thus D_{4h} symmetry. Due to the E_u symmetry of the transitions, the four Q-bands collapse into two or three Q-bands and can be assigned to the different vibrational states $Q_{(O,O)}$, $Q_{(O,1)}$ and $Q_{(O,2)}$. Based on the research of *Gouterman et al.*, the existence and appearance of the *Soret*- and Q-bands can be explained by molecular orbital theory (Figure 8).

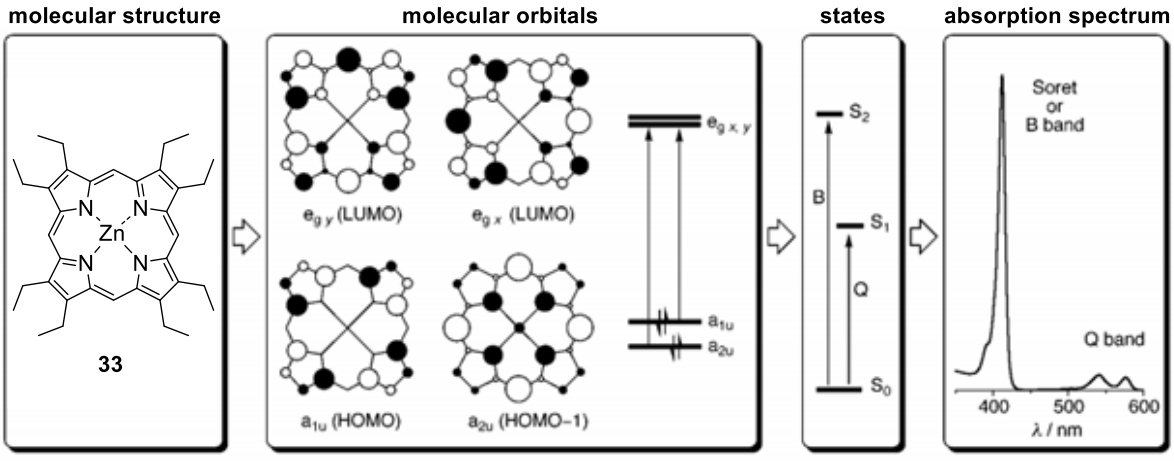

Figure 8: The *Gouterman* four orbital theory explained at a symmetric porphyrin-based metal complex Zn(II)-octaethylporphyrin (**33**). Figure based on *Anderson et al.*[28]

The developed model was based *inter alia* on the previous work of the groups of *Simpson*,[29] *Longuet-Higgins*[30] and *Platt*.[31] In the course of the *Gouterman* model, only the four frontier orbitals are taken into account. The highest occupied molecular orbitals (HOMOs) are π-orbitals with almost the same energy and a_{2u}- or a_{1u}-symmetry. The lowest unoccupied molecular orbitals (LUMOs) have degenerated π^*-orbitals with e_g-symmetry. This is represented in more detail in Figure 8 with Zn(II)-octaethylporphyrin (**33**) as an example. The linear combination of both transitions $a_{1u} \rightarrow e_g$ and $a_{2u} \rightarrow e_g$ results in interfering processes. Constructive interference of the transition dipoles results in the intensive short-wavelength *Soret*-bands, destructive interference results in long-wavelength Q-bands. The weakness of the Q-bands can, in addition to that, be assigned to the *pseudo*-parity-forbidden status that originated from the pairing properties of alternant hydrocarbons (Figure 8).[32]

Additionally, the pyrrole-type rings joined by four methine bridges give a planar N_4 macrocycle and provide a vacant site at its center, ideally prepared for metal incorporation as dianion. The *circa* 3.7 $Å^2$ cavity of the tetra dentate ligand is a flexible coordination sphere for *inter alia*, a square-planar, square-pyramidal and octahedral coordination.[33, 34] The essence of bonding between the central metal ion and the porphyrin-type ligand can be divided into σ-orbital interactions of the nitrogen lone pairs directed towards the center of the ring and π-orbital interactions of p_π- and/or d_π- metal orbitals with nitrogen p_π-orbitals. The symmetry aspects of these interactions fit according to trivial square-planar coordination spheres – the appropriate symmetry adapted linear combinations (SALCs) are shown schematically in Figure 9.

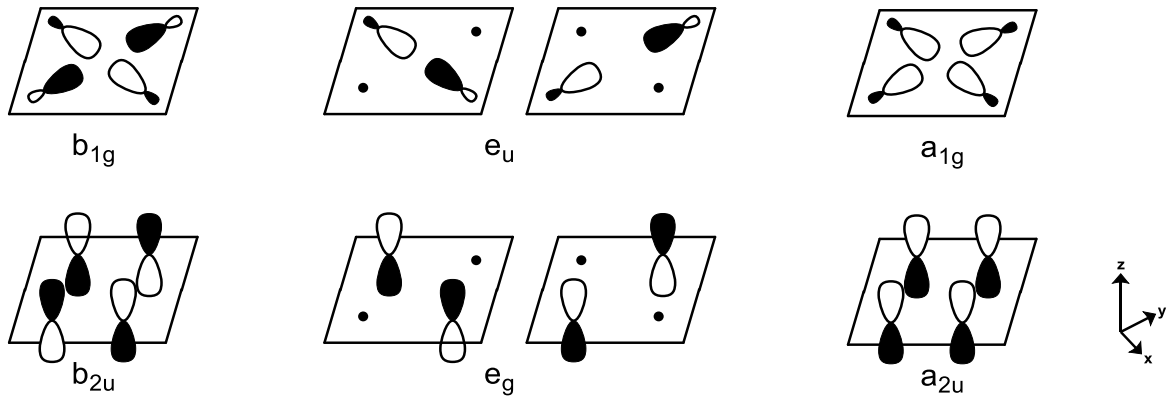

Figure 9: Schematic representation of the appropriate symmetry adapted linear combination of ligand orbitals in a square-planar coordination sphere.[35]

The coordination of the central metal ion surrounded by the tetra dentate ligand is realized through the interactions of $d_{x2-y2} - b_{1g}$, d_{xz} and $d_{yz} - e_g$, d_{z2} and $s - a_{1g}$, p_x and $p_y - e_u$ and $p_z - a_{2u}$ pairs.[35] Figure 10 represents the molecular orbital diagram for square-planar ML_4-σ-complexes with D_{4h} point symmetry. In the square-planar coordination sphere of porphyrin-

based metal complexes, π-interactions play a role *via* the interaction of the d_{xz} and d_{yz} – e_g pair. For clarity reasons, only a simplified MO diagram neglecting the π-interactions was chosen as representation in Figure 10.

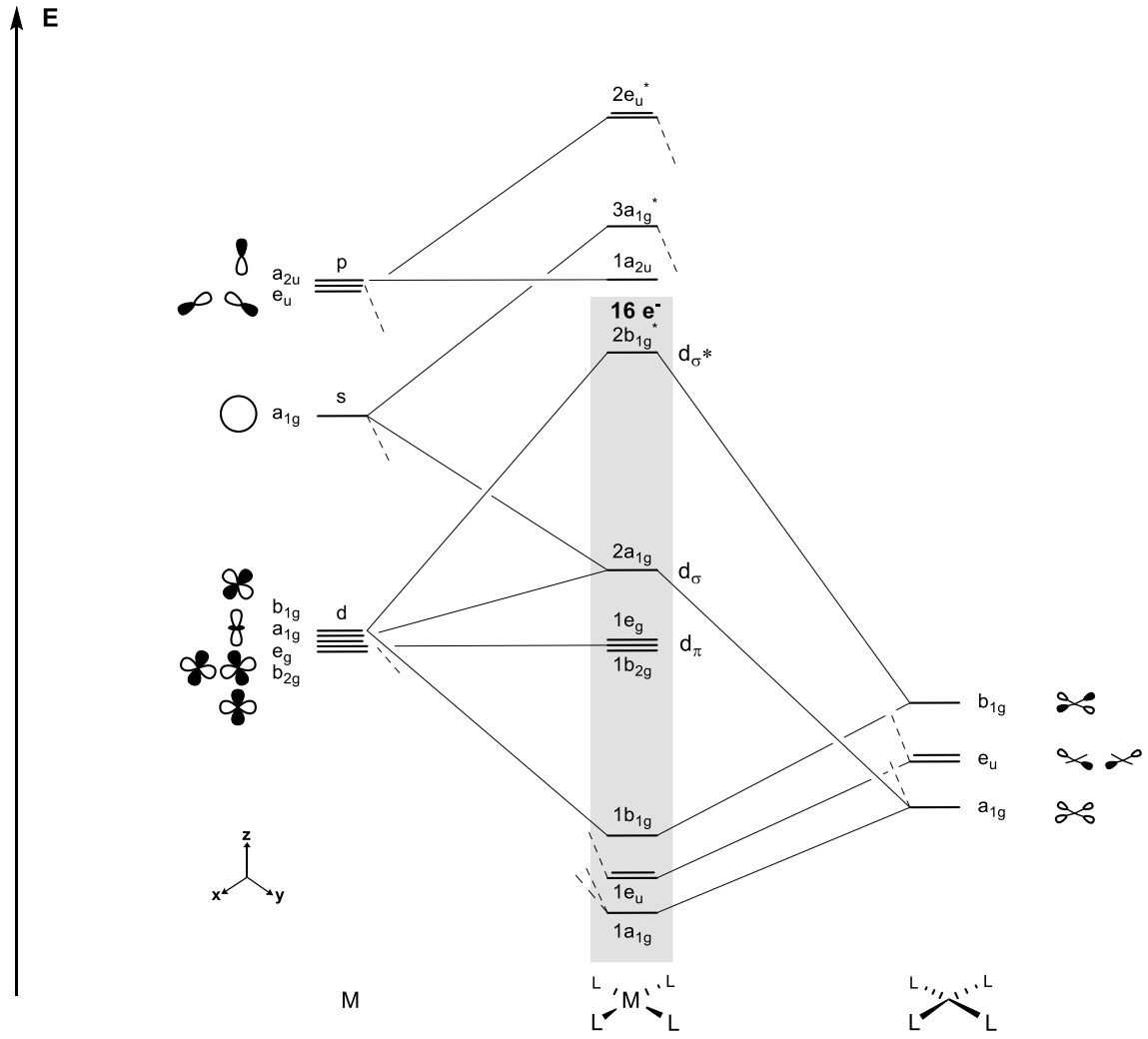

Figure 10: Molecular orbital diagram for square-planar ML_4-σ-complexes without π-interactions – D_{4h} point symmetry.[36]

Each interaction distributes over several orbitals in the porphyrin ligand – Figure 10 merely illustrates the symmetry types. The tetrapyrrolic ligand acts as a σ-donor with optimal stability if filled with 16 π-electrons. As mentioned above, the ligand additionally has the necessary orbitals to act as a π-donor and acceptor.[37] Calculations indicate that the donor side is more prominent – for instance, the N $2p_z$ orbital is occupied by net 1.61 electrons for the dianionic porphin model system of *Hoffmann et al.*[35] Considering this and combining it with the previously described *Gouterman* model, especially the possibility of the porphyrin ligand to operate as a π-acceptor can explain absorption behaviors. Metalloporphyrins can be divided into porphyrin metal complexes with fully occupied or empty orbitals (Zn(II)-d^{10} and Mg(II)-d^0) in contrast to coordinated but not fully occupied transitions metals (Cu(II)-d^9 or Pd(II)-d^8). In the first case, the metallic d_{xy}- and d_{yz}-orbitals are energetically very low-lying orbitals,

which do not significantly affect the $\pi \rightarrow \pi^*$ transition.[38] Generally, *Gouterman et al.* could show that the energy difference between the two excited singlets, i.e., $^1E(a_{2u},e_g) - {}^1E(a_{1u},e_g)$, decreases along with the series Pd(II)>Cu(II)>Zn(II)>2H, depending on the corresponding π-type orbital interactions. In addition to that, the $S_0 \rightarrow S_2$ transition energy decreases, which results in a hypsochromic shift along with the series 2H-porphyrin to Pd(II)-porphyrin (Figure 11).[39]

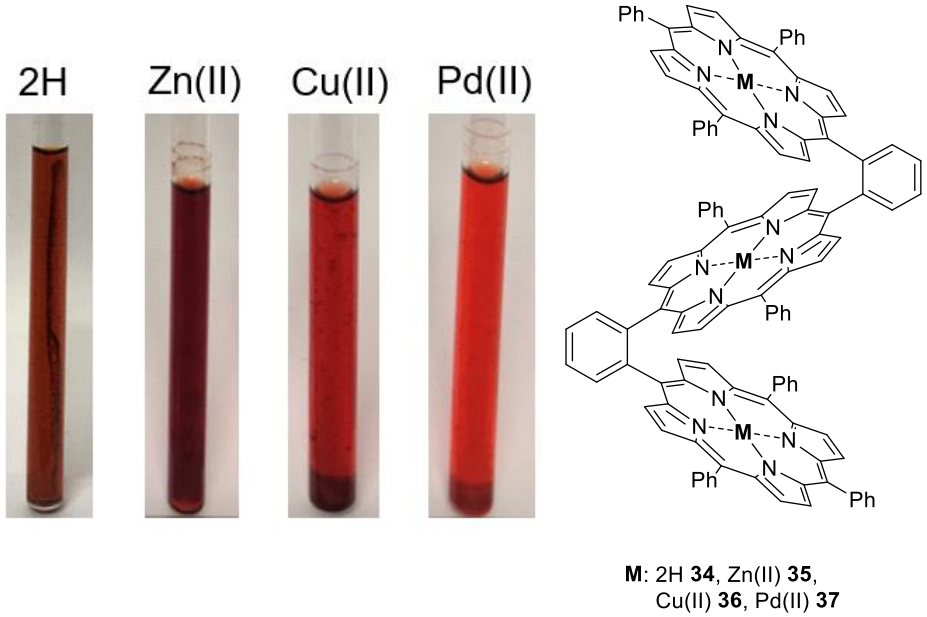

Figure 11: Saturated CD_2Cl_2 solutions of free-base-, 3Zn(II)-, 3Cu(II)-, 3Pd(II)-*o*-phenylene-trisporphyrin (**34** – **37**). Ordered by the energy gap between the two excited singlet states (low→high).

Due to the relatively flexible backbone of the porphyrin ligand, numerous cations can coordinate. The bonding tendency depends more on the cation than on the structure of the porphyrin ligand, whereby the ion radius plays a crucial role. Meanwhile, porphyrin complexes with every non-radioactive metal could be obtained – in the range of Si(IV) (0.42 Å) to Pb(II) (1.20 Å) in a square-planar fashion.[40] The square-planar ligand field ("in-plane") represents the most common coordination geometry where the cations are two times positively charged. Besides that, five-times coordinated metalloporphyrins arranged in a square-pyramidal fashion ("sitting atop") as shown in Figure 12.

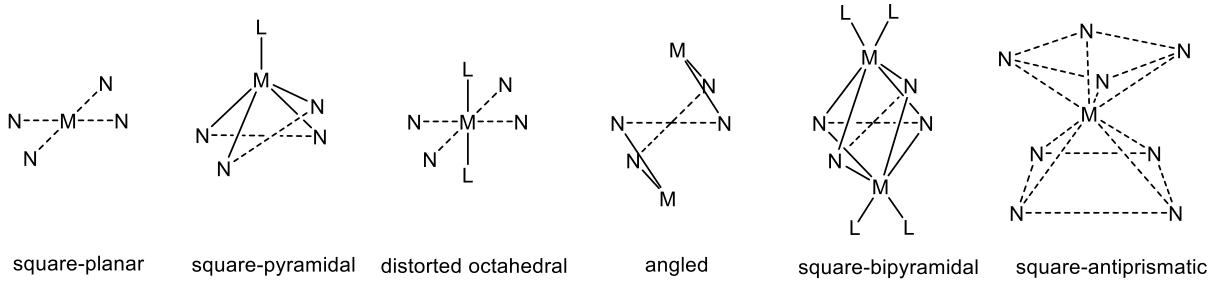

Figure 12: Schematic representation of different coordination geometries of porphyrin-based metal complexes.

This includes high-spin Fe(III) complexes with an Fe(III) cation sitting 0.5 Å above the plane with an orthogonal and negatively charged ancillary ligand such as Cl^-.[41] Al(III),[42] Ga(III)[43] and Ir(III),[37] for instance, show similar coordination geometries. Six-fold coordinating metalloporphyrins arranged in a distorted octahedral coordination geometry, for instance, in heme-protein or cytochromes in nature. Due to the fixed structure of the macrocycle, the distance of two axial ligands differs.[41] The Rh(III)-carbonyl-TPP-Cl^- is a prototype that follows the well-investigated octahedral porphyrin complexes found in nature.[44] The rather unusual angled or square-bipyramidal geometry occurs in bimetallic complexes containing univalent metals as Li(I), Na(I), K(I) and Ag(I).[45] In the case of larger metal cations, eight-fold coordinated porphyrin-based metal complexes occur in a square-antiprismatic ligand field in a sandwich-like arrangement. For larger metal cations as Y(III),[46] Zr(IV),[47] Hf(IV),[48] Ce(IV),[49] and most lanthanide and actinide metal ions such as La(III),[50] Th(IV)[51] and U(IV),[52] this is the preferred coordination sphere.

1.2.3 Properties of metalloporphyrins: square-antiprismatic coordination

Cofacially arranged porphyrin complexes are of fundamental interest as structural models of the photosynthetic reaction center. *Rhodopseudomonas viridis* has two bacteriochlorophyll units arranged face-to-face with an average plane distance of approximately 3 – 4 Å. The metal ions keep the macrocycles closer than their *van-der-Waals* distances, resulting in strong π-interactions, which mimic the electronic interactions occurring in the ´special pair`, the crucial part of the molecular system enabling photosynthesis. Consequently, the ease of the π-system oxidation and energetically low lying first singlet (π–π^*) exited states (→bathochromic shift of the Q-bands) compared to the corresponding monomers arise.[53]
Square-antiprismatic coordination spheres present for the bisporphyrin-Ce(IV)-complexes have monomer-like ground-state absorption features as the *Soret*- and Q-bands, while the former is slightly blue-shifted compared to the monomeric chromophore (Figure 13).

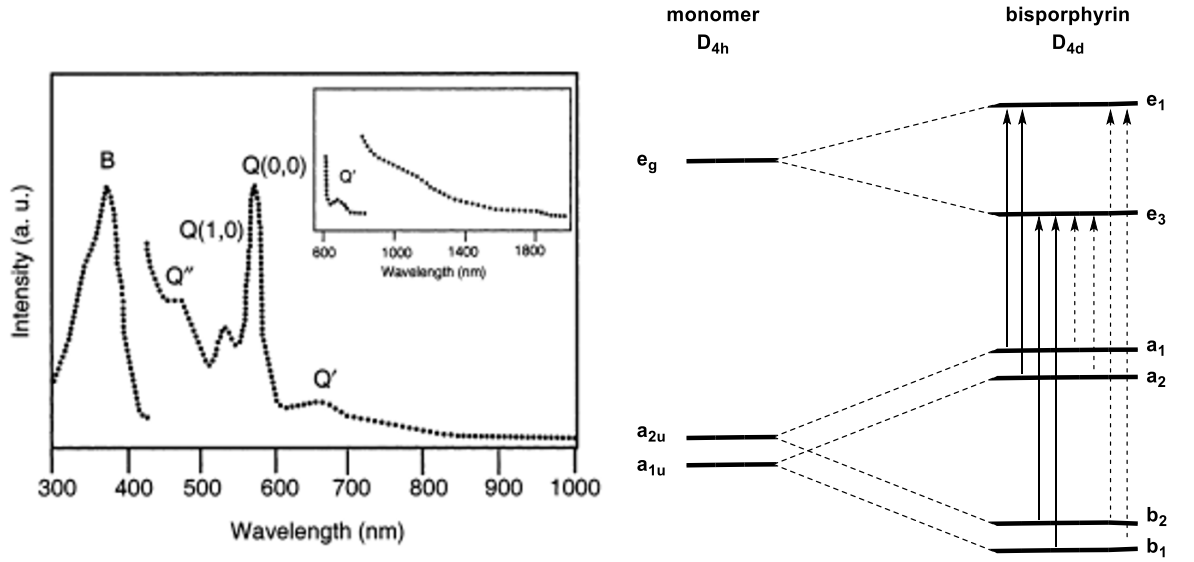

Figure 13: Absorption spectrum of $Ce(OEP)_2$ in CH_2Cl_2 (left). They simplified the diagram of the supermolecule molecular orbitals formed from the linear combination of the four-orbital MOs of the constituent monoporphyrin complex (right). The solid arrows denote dipole-allowed (E_1) one-electron transitions and the dashed arrows are used for the dipole-forbidden (E_3) one-electron transition. The Figure is based on *van Gisbergen et al.* and *Rosa et al.*[53, 54]

In contrast to monomeric porphyrins, Q-bands are further split into blue-shifted Q''- and red-shifted Q'-bands with a broad tailing directed to lower energy. A phosphorescence band in the NIR region also occurs due to cofacial arrangement. The positions of the additional Q-bands are strongly dependent on the distance between the cofacial chromophores. The general absorption band pattern can again be described by a symmetry-adapted version of the *Gouterman* four-orbital model. In the limit of the degeneracy of D_{4d} symmetric molecules, the dipole-allowed configurations consist of ($a_1 - e_1$), ($a_2 - e_1$), ($b_1 - e_3$) and ($b_2 - e_3$) transitions, which can be assigned to the four Q-bands in Figure 13. The NIR absorption band is associated with the low-energy Q'-band resulting from dipole-forbidden ($a_1 - e_3$) and ($a_2 - e_3$) transitions.[53]

1.2.4 Properties of metalloporphyrins: heteroatom-bridged coordination

According to the above-mentioned square-antiprismatic coordination sphere, heteroatom bridged face-to-face bimetallic complexes exist. Famous examples are in that case of the 2Mn(III) -, 2Fe(III) [55]- and 2Ru(IV) [56]-μ-oxo species (**38** – **40**) shown in Figure 14.

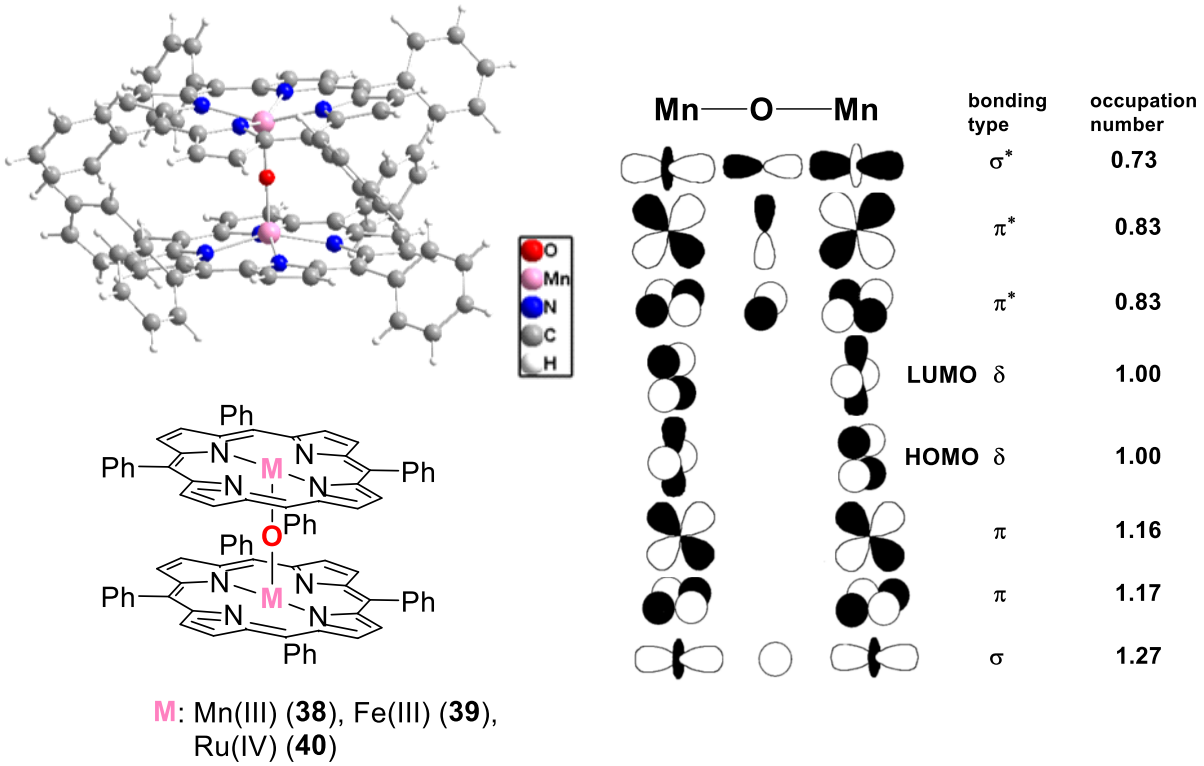

Figure 14: Left: X-ray structure of μ-oxo-bridged bimetallic Mn(III) tetraphenyl-porphyrin complexes **38**. A more detailed description of the X-ray structure analysis can be found in section 6.9. Right: relevant molecular orbitals of the metal-O-metal bridge based on *Koizumi et al.*[57]

The obtained crystal structure of compound **38** shows an Mn(III)-Mn(III) distance of 3.524 Å with an angle Mn(III)–O–Mn(III) angle of 177.96° while the averaged measured torsion angle between stacked planes is 28.37° and can be seen as a distorted square-antiprismatic arrangement. The O^{2-} anion is thereby attached to the two Mn(III) cations *via* σ- π- $\pi_{\perp}$- bondings, as shown in Figure 14. The oxygen bridge enables strong spin-spin coupling between the metal centers that leads to very rapid relaxation. *Mössbauer* spectroscopy indicates the coupling to be antiferromagnetic for the $^{5}/_{2}$ Fe(III) ions.[58]

Other porphyrinoid skeletons, as present in the N-confused and the N-fused porphyrins, can further adjust different properties and options for metal coordination.

1.2.5 Properties of N-confused porphyrins

A remarkable property of N-confused porphyrin (NC-porphyrin) is its isomerization between the inner 3H (**41**) and the inner 2H (**42**) tautomer as represented in Scheme 1.[59]

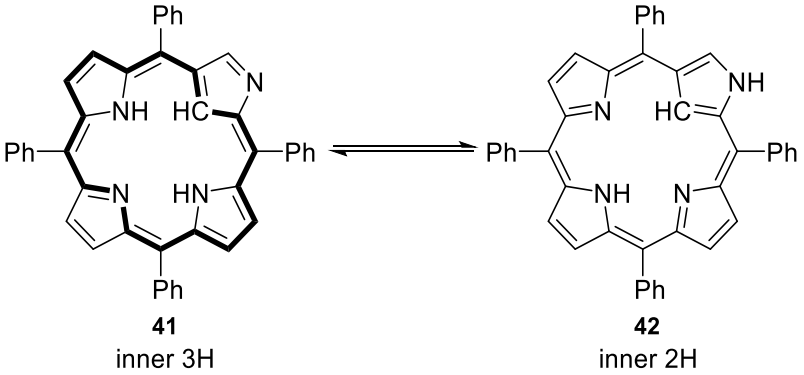

Scheme 1: Tautomeric forms of the N-confused TPP. **41**: inner 3H, **42**: inner 2H.

The isomeric ratio in solution is highly dependent on the polarity of the solvent. While polar or H-bond accepting solvents as DMAC favor the inner 2H species **42**, in non-polar solvents such as $CHCl_3$, the inner 3H analog **41** is most prominent.[60] Compound **41** exhibits a contiguous18 π-electron system and is therefore aromatic; for compound **42**, the annulene circuit is interrupted at the twisted pyrrole subunit. Besides the increased energy, the UV-Vis spectra differ significantly with regards to the Q-bands.

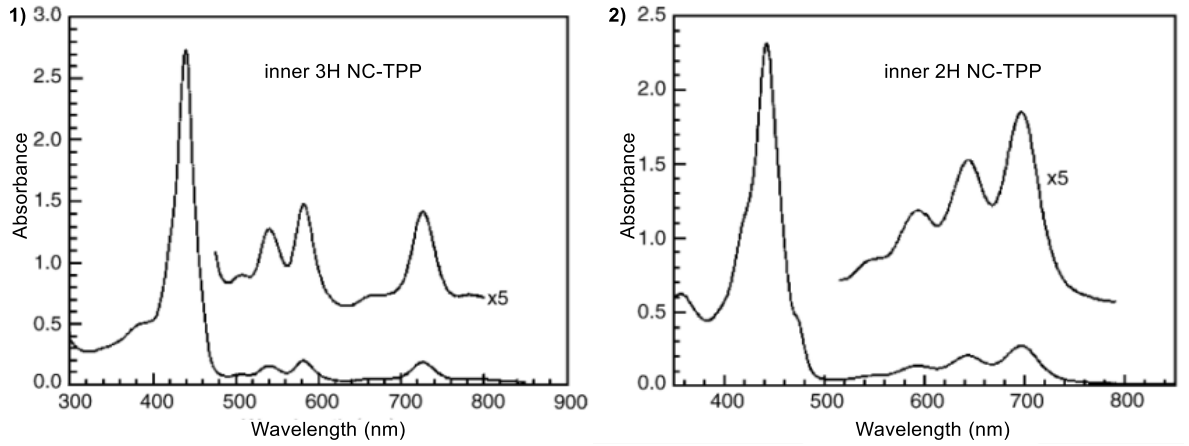

Figure 15: UV-Vis absorption spectra of both the inner 3H (**41**) (in $CHCl_3$, left) and the inner 2H (**42**) (in DMAC, left) N-confused porphyrin. The figure is based on *Ziegler et al.* and *Modarelli et al.*[16, 61]

Complete deprotonation of the inner 3H tautomer **41**, leads to a three-times negatively charged coordination site, stabilizing metal ions in higher oxidation states than regular porphyrins. For instance, Ag(III) can be bound in an N-confused porphyrin ligand.[62] The inner 2H tautomer **42** instead favors metal ions with oxidation state +2 as Ni(II) with a double negatively charged binding site.[63]

Different metal complexes with N-confused porphyrin ligands are known as e.g. Cu(II),[64] Fe(II),[65] Fe(III),[66] Ag(III),[62] Zn(II),[67] Rh(I), Rh(III), Rh(IV)[68] and Pd(II).[69]

1.2.6 Properties of N-fused porphyrins

Similar to the N-confused TPP analog, N-fused porphyrins (NFPs) exist in two relevant NH-tautomeric forms, whereby a proton can be exchanged between N(2) and N(24) (Scheme 2).

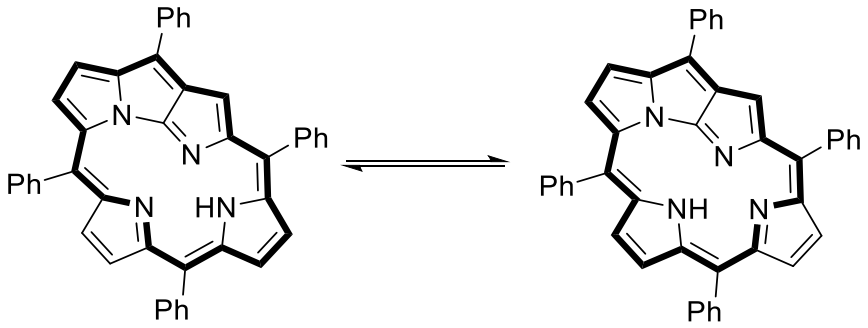

Scheme 2: Tautomeric forms of the N-fused TPP indicate the 18 π-electron circuits.

Tautomer A of the N-fused TPP **43** is, in most cases, the more stable isomer by 2 – 3 $^{kcal}/_{mol}$. By introducing a Br-substituent at C(21), tautomer B (**44**) becomes thermodynamically more stable by 1 $^{kcal}/_{mol}$. Both tautomers exhibit a continuous 18 π-aromatic circuit and are therefore almost equally stable. Since the N(2)–N(24) distances ranges between 2.469 – 2.558 Å for all NFPs in the solid-state, the tautomerism does not have a similarly large impact as it is present in NC-TPP and therefore does not influence the UV-Vis absorption bands (Figure 16) or the metal coordination.[18]

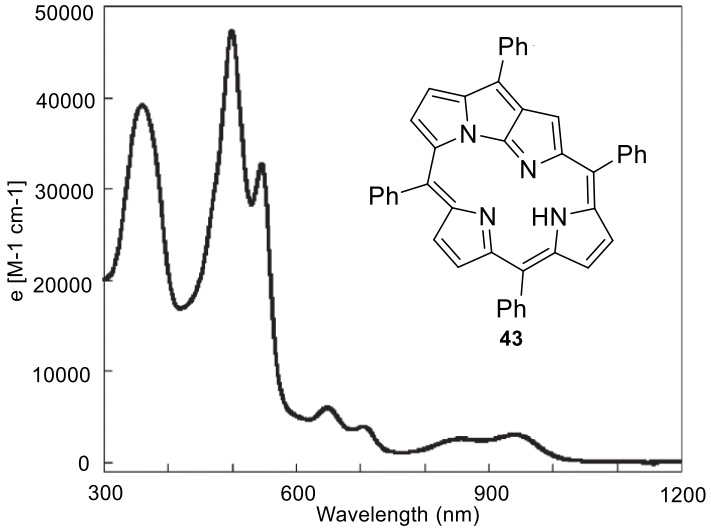

Figure 16: UV-Vis absorption spectrum of N-fused TPP **43** measured in CH_2Cl_2. Based on *Furuta et al.*[70]

The fusion of the two adjacent pyrrole rings in the porphyrinoid skeleton results in a decrease of the HOMO – LUMO band gap without increasing the number of π-electrons and impacting the optical properties. Strong absorption bands are observed at 360, 499 and 545 nm, while

weak absorption peaks are found at 647, 704, 852 and 941 nm. Despite the present 18 π-aromatic system, its absorption edge exceeds 1000 nm.[70]

Metal complexes of NFPs can be grouped into in-plane coordination and sitting atop coordination. Due to the tri-pentacyclic rings, only metal ions with small ion radii can be incorporated *via* an in-plane fashion, whereas P(V),[71] Mn(I),[72] W(VI)[73] and Re(I)[74, 75] coordinate above the NFPs' plane.

As the previously discussed possible coordination spheres of porphyrins comprised only the suitable arrangements of this thesis, the diversity can be imagined. Generally, due to the anionic nature of the porphyrin ligand, most metal ions with oxidation states +1, +2 and +3 are coordinated by the pyrrole nitrogen atoms.[76] The synthesis of cyclic tetrapyrroles was the focus of chemists very early on, particularly due to its enormous chemical flexibility and unique photophysical properties.

1.3 Syntheses of porphyrins

1.3.1 Porphyrins with A_4-symmetry

Willstätter, *Stoll* and *Küster* conducted the first investigations on porphyrins at the beginning of the 20th century – their postulated molecular structure was proven by *Hans Fischer* shortly after.[77, 78] *Rothemund* was the first to synthesize symmetric porphyrins in 1935 by stirring equimolar amounts of pyrrole and different aldehydes in MeOH or pyridine in a pressure vessel.[79, 80] After stirring the reaction mixture for several days between 90 °C for porphin (**3**) and tetramethylporphyrin **49** and 220 °C for TPP **32**, the symmetric porphyrins were formed in up to 10% yield (Scheme 3).[79, 81] In 1967, *Adler* and *Longo* increased the yield to 20% while conducting the condensation in propionic acid under reflux. The applied harsh conditions were tolerated only by a few functional groups.[82]

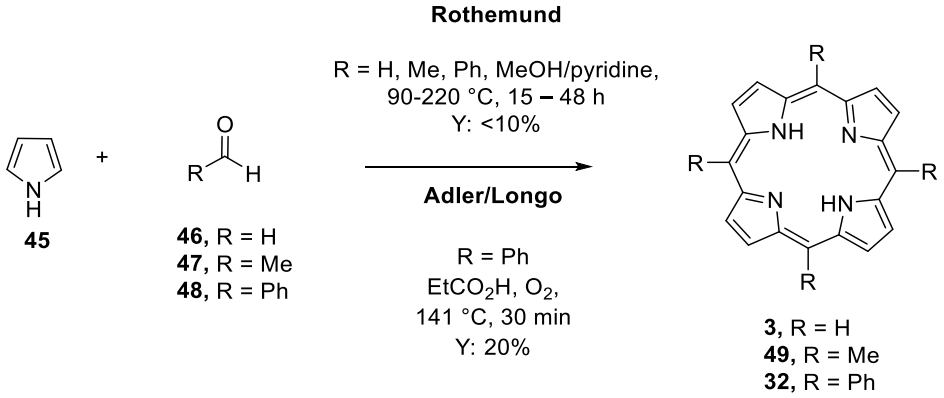

Scheme 3: First syntheses of *meso*-substituted A_4 porphyrins by *Rothemund* and the developed procedure by *Adler* and *Longo*.

In 1986, *Lindsey et al.* investigated milder reaction conditions and developed a new methodology by conducting the reaction in high dilution (10^{-2} M). Pyrrole and the aldehyde were dissolved in dry, chlorinated solvents, trifluoroacetic acid (TFA), *Lewis* acid boron trifluoride diethyl etherate ($BF_3 \bullet OEt_2$) were added in catalytic amounts and the reaction mixture was stirred at room temperature under an inert atmosphere. The intermediary porphyrinogen can then be oxidized by adding a *p*-chinone as *p*-chloranil or 2,3-dichloro-5,6-dicycano-1,4-benzoquinone (DDQ) in the second step of the porphyrin synthesis.[83] The mild reaction conditions enabled several aromatic and aliphatic aldehydes to tolerate thermally unstable functionalities such as azides. A better mechanistic understanding led to up to 50% yields under optimized reaction conditions depending on the used aldehyde.[84] For instance, *Lindsey et al.* observed the maximum yield (45%) for TPP **32** while performing the reaction at a 10^{-2} M concentration, while for tetrapentylporphyrin, the maximum yield (26%) was achieved by running the reaction at a 10^{-3} M concentration. Generally, they noticed differences depending

on the concentration, catalyst, solvent and reaction time for deployed aldehydes. Limiting factors such as the oligomerization as a competing reaction to the cyclization, remain (Scheme 4).[83]

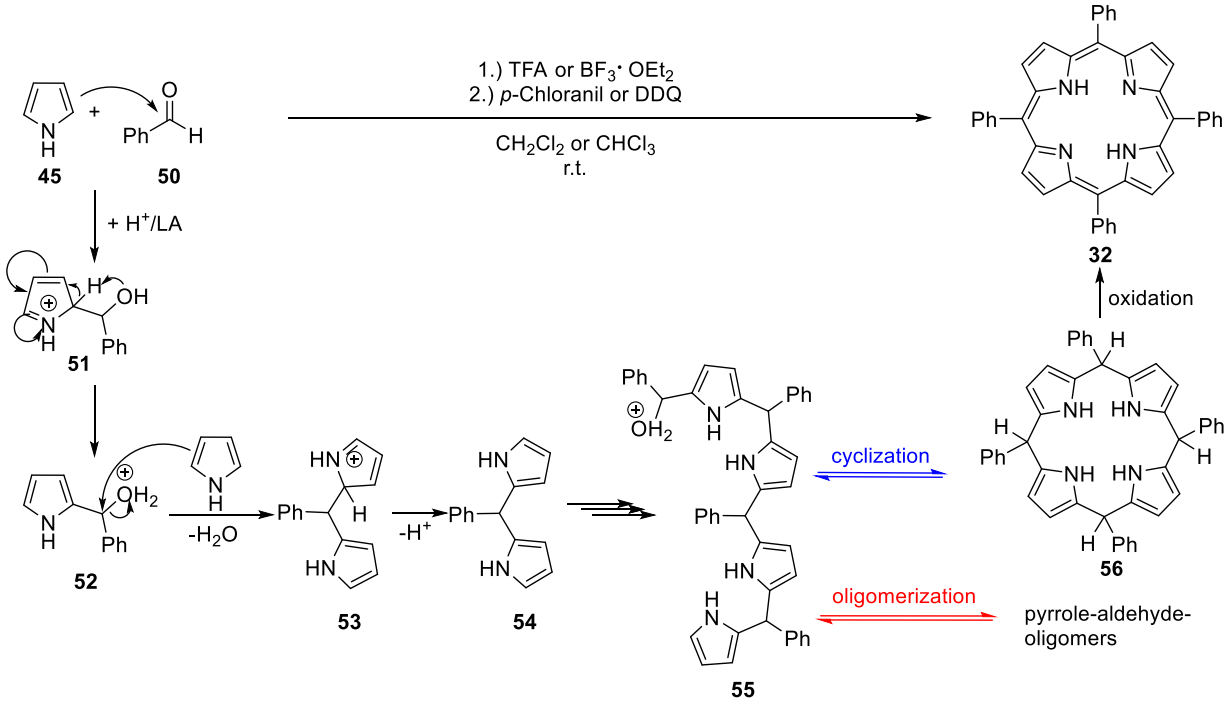

Scheme 4: General mechanism of the porphyrin synthesis towards TPP **32** under reaction conditions developed by *Lindsey et al*. – oligomerization *vs*. cyclization.[83]

The reaction starts with an acid-catalyzed, electrophilic addition of benzaldehyde (**50**) to the pyrrole-*α*-position to form the protonated phenyl(2H-pyrrol-2-yl)methanol (**51**). Under hydrolysis, the second pyrrole attacks the electrophilic carbon attached to the first pyrrole ring, which leads to the dipyrromethane derivative **54** after re-aromatization. Analogously the hydrated form of the bilane carbenium ion **55** is formed. For entropic reasons, the tetrapyrrole arranges in a helical structure, which can react following the shown steps to form long-chain pyrrole-aldehyde-oligomers or cyclizes to the porphyrinogen **56**. This intermediate can be oxidized in a one-pot fashion by adding *p*-chinone derivatives to form the porphyrin **32**.[83]

With this method, asymmetrical porphyrins are only accessible in the form of so-called mixed condensation reactions, in which the statistical distribution of the possible products can be controlled *via* the stoichiometry of the aldehydes used.[9] In addition to a significant loss in yield, the product separation can be challenging since the compound polarities are often similar. A step-by-step approach using dipyrromethane **57** as an intermediate is often superior to efficiently synthesizing a porphyrin with a defined substitution pattern.[85]

1.3.2 Syntheses of non-symmetric porphyrins

As shown in Scheme 5, the cyclization can be carried out with an equimolar ratio of 2,2'-dipyrromethane (**57**) and several types of aldehydes under (*Lewis*) acid catalysis according to the mechanism presented in Scheme 4.

Because of their contiguous π-electron system following the *Hückel* rule, porphyrins belong to the group of heteroaromatics. Electrophilic substitution reactions can therefore achieve modifications of the backbone at the *meso* and at the β-position, whereby the *meso*-position can have a comparatively more pronounced electrophilic character.[86] Additionally, the electrophilicity can be increased by coordinating *Lewis* acids such as Zn(II) to the pyrrole nitrogens, minimizing the deactivating effect that occurs by protonation.[11] Moreover, *Senge et al.* showed that porphyrins could react with organolithium compounds *via* an addition-oxidation mechanism in a nucleophilic aromatic substation reaction. The *meso*-position again turned out to be more reactive.[87]

Non-symmetrical porphyrins with a defined substitution pattern can generally be obtained *via* nucleophilic and electrophilic aromatic substitution reaction introducing, e.g., bromine, followed by C–C-cross-coupling reactions (Scheme 5).[87, 88]

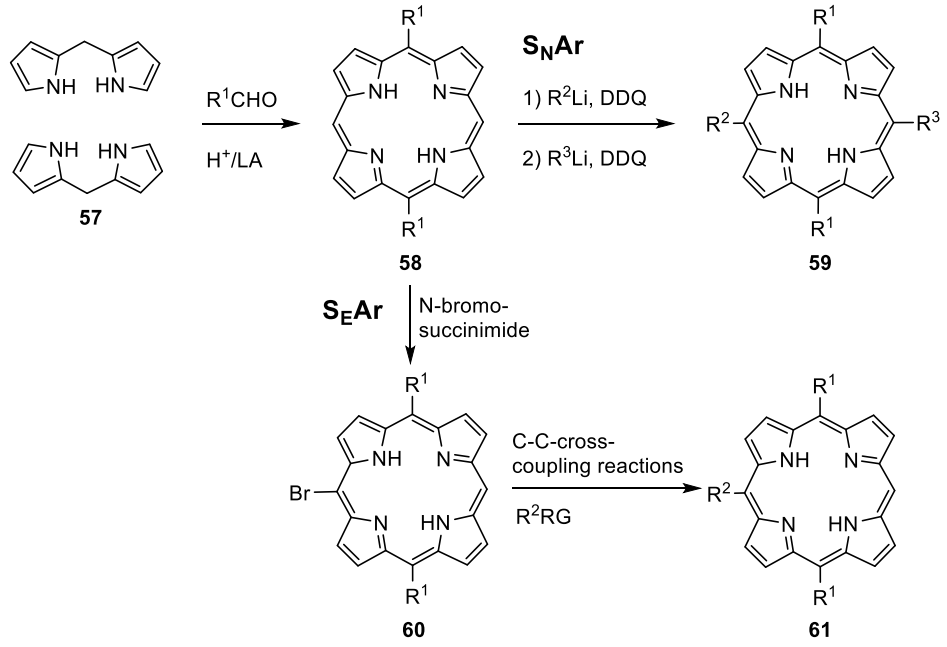

Scheme 5: Efficient methodology for the synthesis of unsymmetrical porphyrins with a defined substitution pattern. RG: C–C-cross-coupling reaction counter parts as $B(OH)_2$, terminal alkyne, etc.[87, 88]

The major disadvantage of the two-stage reaction protocol to build up the porphyrin skeleton *via* dipyrromethane **57** is an acid-catalyzed rearrangement, known as scrambling. The lability of dipyrromethane **57** towards acids leads to its acid-catalyzed fragmentation into pyrrole (**45**) and azafulvene **63** (Scheme 6). This allows the formation of substituent arrangements in the

porphyrinogen, which cannot be obtained *via* direct condensation of the aldehyde and dipyrromethane **57**.[89]

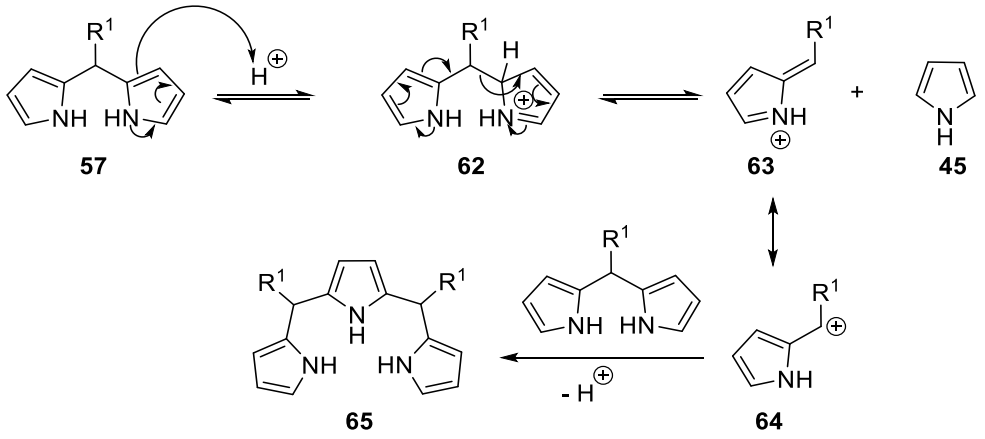

Scheme 6: Reaction mechanism and consequences of the acid-catalyzed rearrangement (scrambling) of the dipyrromethane scaffold **57**.[90]

In the extreme case, all six possible products can arise in the synthesis of A_2B_2 porphyrins, which corresponds to the product range of a mixed condensation reaction. There are also dipyrromethane derivatives for which no scrambling is observed. The influence of the *meso*-substituent seems to play a decisive role. *Litter et al.* were able to show that sterically demanding aryl substituents, such as aryls substituted in the *o*-position, almost completely suppress scrambling.[89] Electron-withdrawing groups can also prevent scrambling, as the positively charged azafulvene derivative **63** is destabilized.[91] In addition, a correlation was established between the porphyrin yield and the extent of scrambling. The higher the yield, the more pronounced the acid-catalyzed rearrangement. For this reason, attempts to reduce scrambling automatically led to a loss in the yield of the porphyrin.[92] The synthesis method with dipyrromethane **57** as a precursor can be carried out easily but is not suitable for all combinations of aldehydes and dipyrromethanes **57**. Especially in nature, the porphyrin scaffolds are frequently substituted in a sophisticated manner to fit the biochemical purpose perfectly. The *de novo* synthesis of these compounds usually demands a step-by-step total synthesis.

1.4 Porphyrins in nature

1.4.1 Monomeric representatives

Tetrapyrrolic systems take on an indispensable role in nature due to their function as ligands in catalysis or electron transportation (Figure 17), which in the form of protoporphyrin IX enables a reversible oxygen binding in hemoglobin in the erythrocytes and oxygen storage in the myoglobin of muscle tissue and is therefore essential to the energy supply of many breathing organisms.[93]

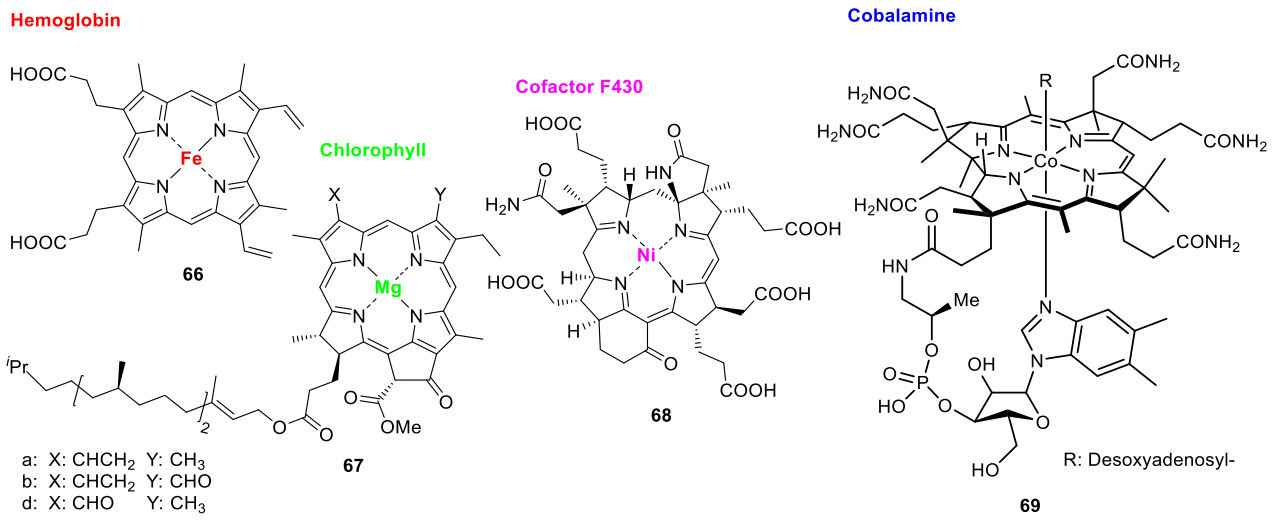

Figure 17: A selection of known porphyrin derivatives in nature: Heme b **66**, Chlorophyll (a,b,d) **67**, Cofactor F430 **68**, Cobalamine (= vitamin B12) **69**.[93, 94]

Cytochrome c, a derivative of the shown cofactor **66**, can function as an electron carrier *via* redox processes. Thus it plays a decisive role in oxidative phosphorylation in the mitochondria, enabling electron transport between complex (III) and complex (IV) in the respiratory chain.[95] The heme b **66** in its enzymatic surrounding can oxidize its substrates using molecular oxygen, for example, in the cytochrome P450 enzymes. The most important type of reaction is the hydroxylation of non-activated C–H bonds, which contribute to the metabolism of water-insoluble substances.[96] Furthermore, heme b **66** is essential for the activity of many peroxidases and catalases.[97-99] Iron-containing catalases consist of four prosthetic groups per enzyme (human catalase: 62 kDa per subunit) and enable the *in vivo* disproportionation reaction of H_2O_2 to H_2O and O_2.[100] In contrast to catalases, peroxidases dissociate H_2O_2 without releasing O_2 by directly oxidizing an organic substrate.[101] In both cases, the active iron center of the porphyrin is reduced while the substrate is oxidized and subsequently has to be regenerated in a cyclic fashion.[102]

By varying the coordinated metal ion and modifying the porphyrin framework, the functional variability can be increased. The cofactor in chlorophyll consists of Mg(II) chlorine complexes **67**. As represented in Figure 17, the C17 and the C18 in the periphery of the porphyrin skeleton are reduced, a typical characteristic of chlorine. Moreover, an additional saturated five-membered ring is fused onto the methine-, α- and β-carbon of the pyrrole subunit adjacent to the reduced pyrrole. The magnesium-based cofactor plays a crucial role in the oxidative photosynthesis of plants by serving as a ´photon catcher`, mediating electron transfer and therefore plays an important role in the oxidation of water to oxygen.[94] In aerobic bacteria, similar tasks are performed by bacteriochlorophyll, which also contains Mg(II). A nickel-based derivative was detected in methanogenic bacteria taking over the last stage of biomass's anaerobic microbial degradation. The so-called cofactor F430 **68**, for example, plays a key role in the conversion of CO_2 and H_2 to CH_4 and H_2O.[103]

Another example is vitamin B12 **69**, which consists of a corrin-Co(II) complex and is essential for the synthesis of DNA. The ligand framework consists of four doubly reduced pyrrole units that lack a methine bridge (Figure 17).[104]

1.4.2 Multimetallic representatives

In nature, the catalytically active sites of metalloenzymes often consist of multimeric agglomerations of prosthetic groups in adaptive protein matrices defining a spatial arrangement of the metal-containing ligands relative to each other. Correspondingly, strongly interacting metal sites are the basis for the unique catalytic activity of many multinuclear metalloproteins such as hemocyanin,[35, 105] hemerythrin,[106] superoxide dismutase,[107] carbon monoxide dehydrogenase[5] or cytochrome c oxidase.[108] The latter enzyme belongs to the superfamily of heme copper oxidases, the terminal electron acceptor of the respiratory chain in all aerobically breathing organisms. It receives an electron from four cytochrome c molecules and transfers them to one dioxygen molecule, converting the molecular oxygen to two water molecules. The oxidases are present in the inner mitochondrial membrane in eukaryotes and the inner cell membrane in prokaryotes.[109] Most of them use heme variants as cofactors for electron donation and consist of an additional heme group together with a copper ion in spatial proximity in the active center. As presented in Scheme 7, the reduced cytochrome Fe_c **70** transfers electrons onto cytochrome Fe_a **71** step-by-step and therewith influences the Fe_a–Cu_a (**71** + **72**) *vs.* Fe_{a3}–Cu_{a3} **73**. After the reduction of both redox centers, the Fe–S bond swings out and O_2 is bound by Fe_{a3} and Cu_{a3} instead, whereby a peroxide intermediate is formed, locating the two metal centers

in a 3.7 Å distance. After that, two electrons are transferred almost simultaneously from the Fe–Cu center. It is not finally determined when and where the four protons for the H_2O formation originate from but during that process another four protons are translocated from the inner to the outer side of the membrane. The resulting electrochemical potential can be used by the ATP synthase to synthesize ATP.[110]

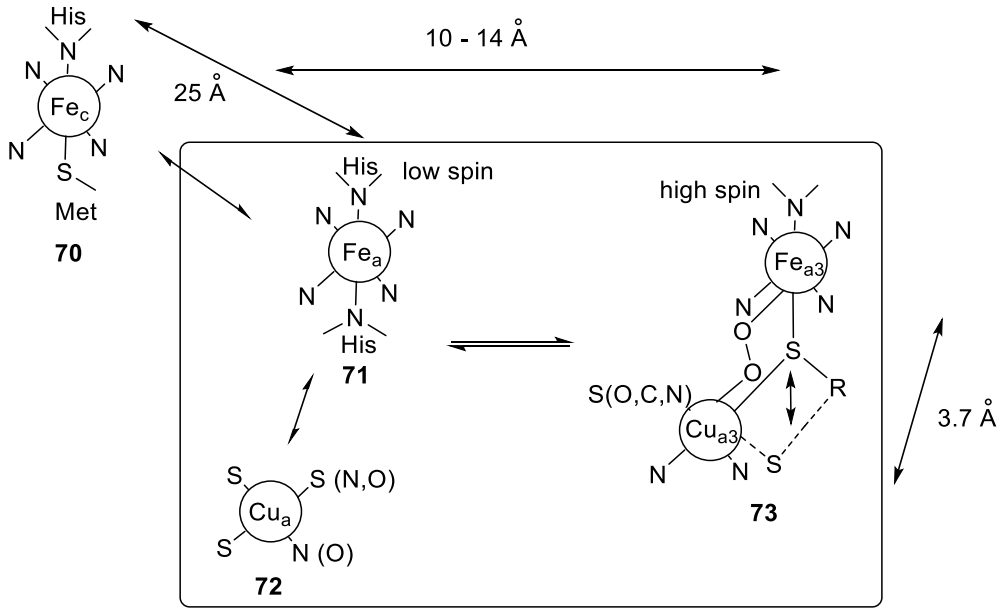

Scheme 7: The active center of cytochrome c oxidase (schematic). The four nitrogens around the Fe redox centers of the enzyme represent the porphyrin ring system. The lines towards the amino acids His/Met symbolize the 5th and 6th ligand on the iron. The nature of the four ligands on the copper ions is not exactly known (options in brackets). The reduced cytochrome (Fe_c) **70** transfers electrons onto cytochrome (Fe_a) **71** step-by-step and, in addition to that, influences the ratio of the arrangement Fe_a–Cu_a (**71** + **72**) *vs*. Fe_{a3}–Cu_{a3} **73**. The 6th coordination position of cytochrome Fe_{a3} differs with its oxidized state: ox: connected *via* a sulfur bridge; red: connected *via* O_2.[111]

This strongly evolved structural motif is responsible for almost all oxygen consumption by breathing organisms, by transferring four electrons from, e.g., cytochrome c to O_2 to generate H_2O without toxic intermediates such as H_2O_2 and O_2^{-}.[111]

Furthermore, porphyrin-based spatial arrangements catalyze reactions directly, but their enforced aggregations of various metal ions or prosthetic groups are often crucial *in vivo* electron transfer processes.[112] X-ray analysis of the bacterial photosynthetic reaction center has shown just how sophisticatedly nature has evolved the spatial arrangement of the six interacting tetrapyrroles involved in photosynthesis (Figure 18).[113] Among these six chromophores, the primary electron donor in the bacterial and green plant photosynthetic reaction center consists of a dimeric porphyrinoid pigment, the so-called ´special pair` with a minimal distance between the pyrrole rings of 3.2 Å as depicted on the right of Figure 18.[114]

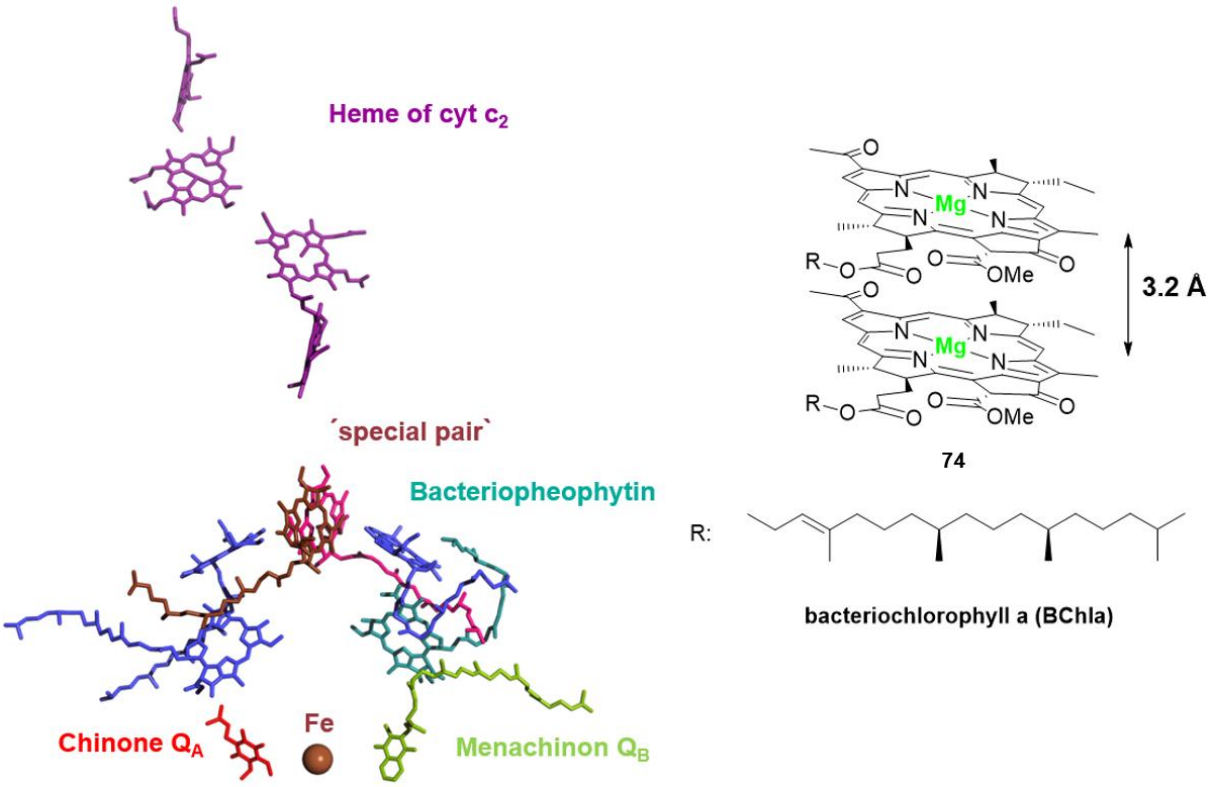

Figure 18: Bacterial photosynthetic reaction centers *in Rhodopseudomonas viridis* (left). Schematic representation of the ´special pair` **74** depicting the closes clearance of 3.2 Å (right). Taken and translated from *Yikrazuul*, who provided it as an open-source image.[115]

The charge separation by absorbing a photon and the subsequent electron transfer has been studied extensively but is still not fully determined.[116] Complete elucidation of the electron-transport processes after light-triggered charge separation remains one of the fundamental open tasks in photosynthesis.[117] Inspired by the three-dimensional orientation of bacterial photosynthetic reaction centers in *Rhodopseudomonas viridis*, several porphyrin-based synthetic models have been developed to investigate catalysts for photosynthetic charge separation and transfer.[118, 119]

1.5 Applications of optical properties of porphyrins

1.5.1 Technical application

Besides their biochemical importance, this class of natural substances also offers numerous possible applications in technology. Close to the natural purpose in photosynthesis, porphyrins serve as light-harvesting complexes in dye-sensitized solar cells (DSSC) for solar energy conversion. The principle of photoredox catalysis is exploited since the porphyrin–metal complex has lower ionization energy in the electronically excited state and can donate electrons into a conduction band more easily.[120] The regeneration can take place *via* organic redox couples including halogens,[121-124] pseudohalogens[125] and hydroquinons[126] or transition-metal complexes such as ferrocene/ferrocenium,[127] copper (I/II),[128] cobalt (II/III)[129] and nickel (III/IV)[130] on, e.g., a TiO_2 surface.[131] In photophysical terms, porphyrins are characterized by a high extinction coefficient greater than 10^5 (see Figure 6) and by non-linear optical behavior of the second and third-order.

Non-linear optics (NLO) is a collective term for effects that occur at high light intensities, resulting from the interaction of light with a non-linear medium. In the case of asymmetrical porphyrins with a high dipole moment, the 2nd order non-linearity is dominant, which is reflected in frequency doubling, frequency mixing and the linear change in the refractive index (*Pockel* effect).[132, 133] For 3rd order non-linear optics, an extended delocalized π-system is necessary.[124] The resulting non-linear optical phenomena of 3rd order are the *Kerr* effect, four-wave mixing and *Raman*, *Brillouin* and *Rayleigh* scattering.[134] Non-linear optics is used for telecommunication, data storage, computers, display technology and information processing, such as, e.g., optical switches to reduce light transmission depending on the exposure intensity.[124, 135]

1.5.2 Medicinal application

Besides the technical applications of porphyrins, this molecular class found its way into medicine, mostly in photodynamic therapy (PDT) or is used in luminescence diagnosis against malignant tumors.[136] Raising interest was attributed since porphyrins can accumulate in several types of cancer cells and tumorous micro vessels, which is the condition for local cancer treatment.[137] The working principle of PDT is based on a photochemical reaction between light and the tumor tissue with exogenous photosensitized agents. Mostly, porphyrin derivatives were utilized to catalyze the electronic transition of molecular triplet oxygen $^3O_2$ to singlet

oxygen $^1O_2$ when exposed to radiation with a defined wavelength. $^1O_2$ damages the surrounding cells due to its cytotoxicity and leads to apoptosis or necrosis. Apoptosis goes along with a contract of the cell, cell surface blebbing, chromatin condensation and chromosomal DNA fragmentation – necrosis manifests in the swelling of the cell and subsequent lyses.[138] The photosensitizer absorbs a photon leading to the promotion of the molecule into the short-lived excited singlet state (S_2) (Scheme 8). Either the molecule relaxes to the ground state (S_0) either by emitting light *via* fluorescence (F), internal conversion (IC) followed by vibrational relaxation (VR, heat dissipation) or is converted *via* the spin-forbidden intersystem crossing (ISC) to the long-lived triplet state (T_1). A good photosensitizer is characterized by a high quantum yield for the ISC process. The transition from T_1 to S_0 and *vice versa* is spin-forbidden according to the selection rules, which state that the value of the overall spin has to be conserved. Thus, transitions between states with differing spin multiplicity are not allowed[139] and transitions between orbitals with equal parity are forbidden (*Laport* rule).[140] Consequently, the radiative relaxation from T_1 to S_0 (phosphorescence) leads to a long-lived excited state. The longer the PS stays in its excited state and the more efficient subsequent reactions can be initiated. Depending on the type of the photosensitizer, the concentration of substrate and oxygen, two reaction pathways can be chosen.

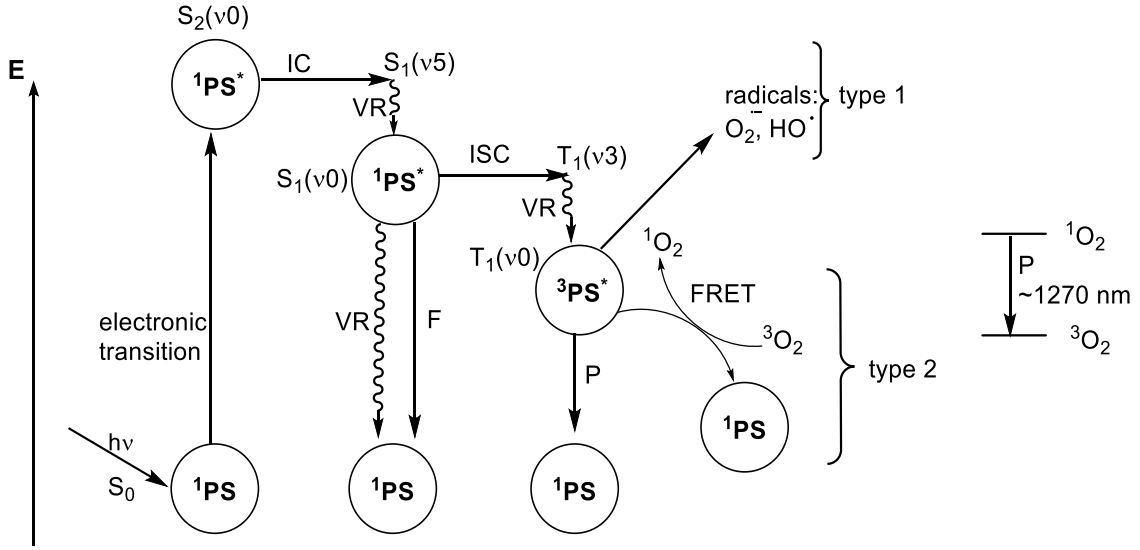

Scheme 8: Schematic representation of the working principle of photodynamic therapy (PDT). PS: photosensitizer; IC: internal conversion; VR: vibrational relaxation; ISC: inter system crossing; F: fluorescence; P: phosphorescence; FRET: *Förster* resonance energy transfer.[141]

In the traditional PDT treatment against tumors, the photosensitizer is injected into the patient. The active compound accumulates in the tumor tissue and can induce cell death *via* apoptosis or necrosis by local irradiation with visible light.[138]

The Type I process can occur independently from O_2 in the first step, whereby the PS directly reacts with organic molecules in the cellular microenvironment, acquiring an H atom or an electron to form radicals. In the following, the reduced PS can transfer an electron to O_2 to form the superoxide anionic radical $O_2^{\bullet-}$. Dismutation or single-electron reduction yield H_2O_2, which in turn can undergo a second single-electron reduction to the highly reactive hydroxyl radical $HO^{\bullet}$.[142, 143] Reactive oxygen species (ROS) generated *via* a type II reaction are usually the dominating pathway, only for bacteriochlorins as PS, which contributes significantly.[138]

In contrast to the Type I reaction pathway, the Type II mechanism suggests a direct reaction between $^3O_2$ and the excited PS to pass on energy *via Förster* resonance energy transfer. [141, 144-146] Thereby, the reactive $^1O_2$ is generated while the PS relaxes non-radiatively back to the ground state.[147] The singlet oxygen and the ROS can directly react with many molecules occurring in cells.[145, 148] For instance, the photooxidation of unsaturated oils[149] and peroxide formation on Trp, His, Tyr, Met and Cys, are reported.[150]

To circumvent that most photosensitizers are activated by visible or even UV-light with poor tissue-penetration capacity, current research focuses on (photon-)upconverting nanoparticles (UCNP) based on lanthanide- or other rare-earth-doped inorganic nanocrystals.

The upconverting process enables the absorption of two or more near-infrared photons and emits visible or near-UV photons.[151, 152] Minor energy radiation improves the signal-to-noise ratio significantly and improves the detection selectivity due to the minimized autofluorescence. That simplifies the *in vivo* imaging and treatment of large or internal tumors since deep tissue penetration is possible without photo damages as a side effect to the living organism.[151, 152]

1.5.3 Catalytical application

Since nature can efficiently use the thermodynamically stable O_2 as described in section 1.4.1 on cytochrome P450 and cytochrome c oxidase, the interest in transferring this onto industrial applications, oxidation of unreactive C–H bonds with O_2 as an inexpensive oxidant has enormous application potential. Co(II)-TPP **77** in concentrations of 1 – 5 ppm in the presence of cyclohexane (*c*Hex, **75**) and O_2 increases the yield for the cyclohexanone **76** syntheses from 4.8% – 7.1% to 77% – 87% and is applied on a ton-scale each year (Scheme 9).[68]

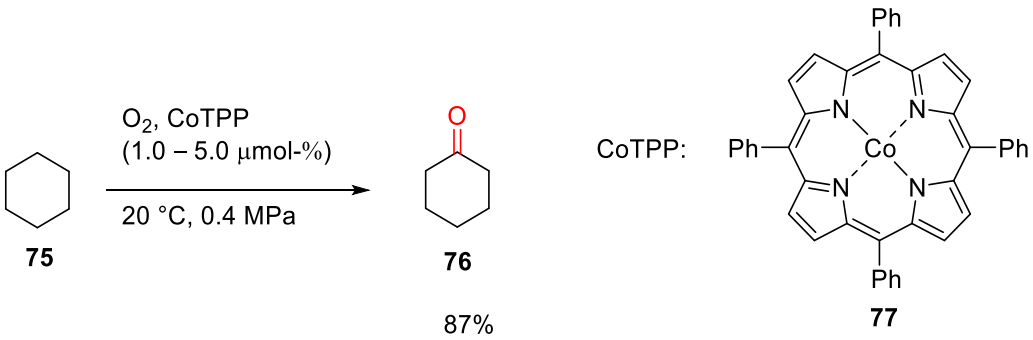

Scheme 9: First bioinspired, porphyrin-based oxidation reaction of cyclohexane **75** on a ton scale.[153]

Furthermore, various porphyrin-metal complexes found their way to industry and can catalyze epoxidations *via* Mn(III)-porphyrin complexes,[154, 155] sulfoxidations *via* Fe(III)-porphyrin complexes[156] and hydroxylations *via* Ru(II)-porphyrin complexes.[157] Moreover, the respective *meso*-positions enable attachment points to introduce chirality to the planar reaction center.

The ability of metalloporphyrins to catalyze chemical reactions of small molecules can also be exploited for reductions. In particular, the electrochemical reduction of CO_2 to valuable carbon sources catalyzed by porphyrin-metal complexes has experienced ever-increasing attention since the end of the last century. CO_2 is a thermodynamically stable molecule whose reduction to a radical anion (CO_2 / $CO_2^{\bullet-}$) with a potential of –2.2 V *vs.* the SCE (saturated calomel electrode) can only be achieved in an endergonic way.[158] Many homogenous and heterogenous catalysts mostly in non-aqueous solutions have been developed and evaluated to overcome efficiently this highly uphill conversion, including precious metals like Re,[159] Ru,[160] Ir,[161] Au[162] and non-precious metals like Fe,[163] Ni,[164] Co[165] and Mn[166]. Besides the chosen catalyst, the electrochemical reduction is dependent on the electrode material and the reaction medium.[167]

As represented in Scheme 10, three reaction pathways are possible for the radical anion $CO_2^{\bullet-}$ generated from the electrochemical reduction of CO_2. The observed reaction products are formiate (a), oxalate (b) and carbon monoxide CO (c).[168, 169] In the presence of water, the formiate generation is the dominant channel, as proven by *Liebens et al.* in 1904.[170]

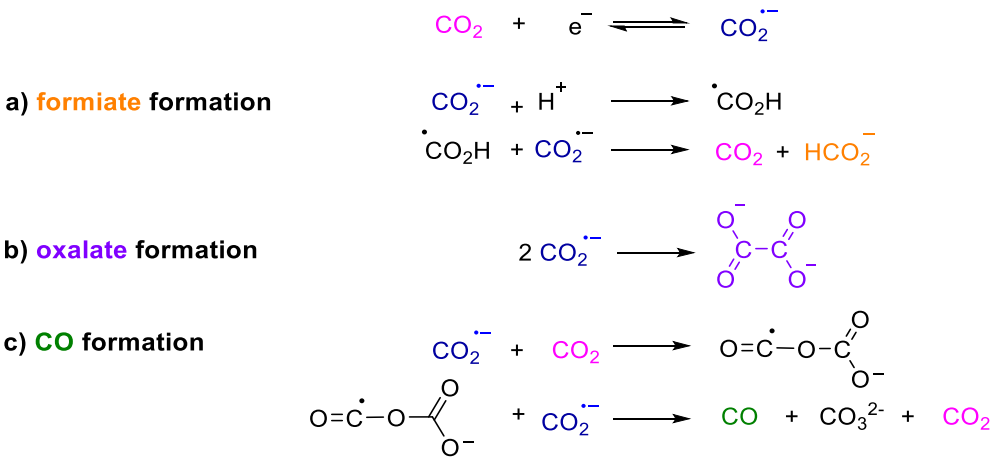

Scheme 10: Possible reaction pathways for the electrochemical CO_2 reduction.[167]

Since the reaction medium influences the product formation, catalysts were designed to reduce the over potential η of an electrochemical reaction, as shown in equation (I).[171]

$$\eta = E - E^{O}_{\frac{CO_2}{CO}} \qquad E^{O}_{\frac{CO_2}{CO}} = -0.69\ V\ in\ DMF \qquad \text{(I)}$$

In addition to the so-called redox catalysts, attempts were also made to selectively promote the product formation of one of the compounds shown in Scheme 10 with the aid of chemical catalysts. As the *Marcus* theory describes, the interaction between substrate and chemical catalyst is stronger than in a simple outer-sphere electron transfer catalysis.[171, 172] A transition metal can also act as a catalyst *via* forming a temporary metal-substrate adduct.[173]

In 1989, *Savéant et al.* observed an σ-alkyl-Fe-porphyrin adduct, giving hints that Fe porphyrin cannot only function as an outer-sphere-electron donor in the presence of CO_2 but could also be used as a chemical catalyst for the CO_2 reduction. In an ensuing work by *Savéant et al.*, carbene-like CO_2-Fe-porphyrin complexes were perceived, transferring electrons from the electron-rich porphyrin to the substrate.[167, 174] If a second CO_2 molecule enters the catalytic center, an acid-base reaction breaks the C–O bond yielding an Fe(II)–CO complex and CO_3^{-}-anion. The binding energy of Fe(II)–CO is weak so that CO leaves the complex at room temperature and the catalyst is regenerated. The catalytic cycle can be optimized by adding Mg(II) as *Lewis* acid, enabling a bimetallic catalytic cycle.[167]

Naruta et al. succeeded in synthesizing the cofacially stacked Fe(II) porphyrin dimer **78** in 2017, increasing the *Faraday* efficiency of the $CO_2 \rightarrow CO$ conversion from 70% to >90% in both aqueous and organic media.[7] Thereby a significant impact of the peripheral substitutions at the *meso*-position on the over-potential η could be attested. Furthermore, the bimetallic catalyst was attached *via* phosphoric acid anchors to a fluorine-doped tin oxide (FTO) surface enabling heterogeneous catalysis on a large scale (Scheme 11).

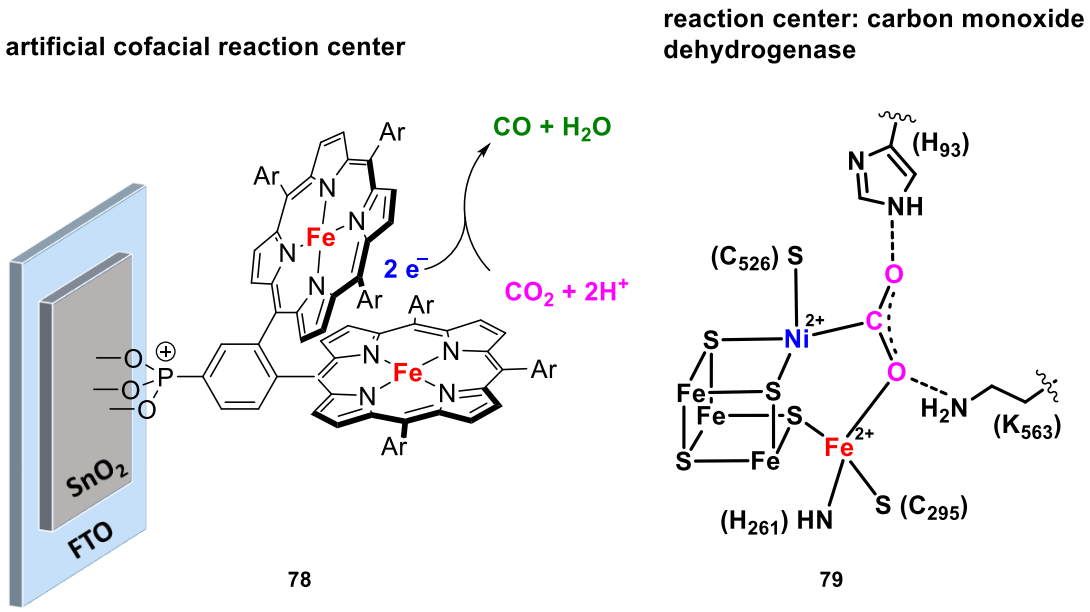

Scheme 11: Electrochemical reduction of $CO_2 \rightarrow CO$ at a fluorine-doped tin oxide (FTO) surface *via* the cofacial Fe(II) complex **78** (left). Analogs reaction center of the carbon monoxide dehydrogenase **79** (right).[7]

Naruta et al. impressively show that taking nature as inspiration for sophisticated catalyst design can significantly increase the efficiency of reactions. To push the abilities of artificial synthesis closer to performances reached by enzymes, a fundamental understanding of the spatial and electronic interaction of metal ions is essential. There has always been a driving force why *in vivo* molecular systems have evolved over millions of years to end up exactly at the given structure one finds today. Revealing the evolutionary decision-making in nature might pave the way for humankind out of the energy problem.

2 Aim of the work

In nature, the catalytical active sites of metalloenzymes are often rigidly fixed structures in an adaptive protein matrix, which defines a spatial arrangement of the metal-containing ligands relative to each other. In such systems, the proximity of several metal cations is typically required to achieve catalytic functions. To gain a deeper understanding of the unique coordination chemistry of such complexes, a rigid molecular system is ideal since it allows tuning the distances between the different metal centers without significantly changing the ligand field. It then becomes possible to vary the interactions between metal centers by slight variations of the rigid framework.

Porphyrins can be synthesized in a tailor-made way and can coordinate numerous metal ions without adapting the ligand.

Cooperative effects between metals will be examined in more detail in the research project "Cooperative Effects in Homo- and Heterometallic Complexes (3MET)". In this course, a linker system is to be established to connect porphyrin subunits *via* rigid backbones forcing metals into spatial proximity. Therefore, the required monomeric porphyrin precursors should first be synthesized to stack them later in a fixed arrangement using, e.g., *o*-phenylene, *m*-phenylene, [2.2]paracyclophane or 4,5-substituted triazoles as linker systems as shown in Figure 19 below.

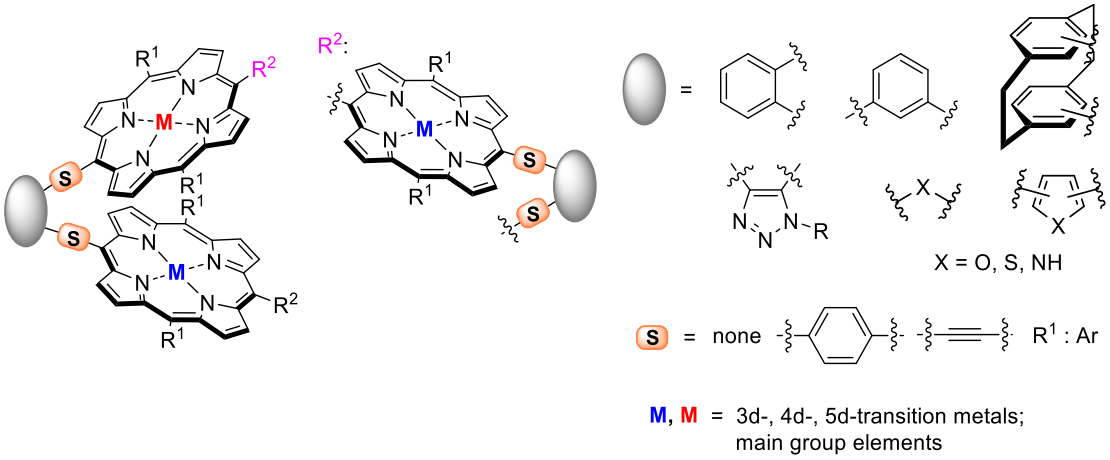

Figure 19: Schematic representation of porphyrin-based multimetallic centers with variable backbones (grey), spacers S and metals M.

The metal-metal separations are dependent on the tetrahedral angle defined by the chosen backbone and can be adjusted *via* the connective spacer group. 3d, 4d, or 5d transition metal complexes and main group compounds are to be examined. By building up the ligand system stepwise, heteromultimetallic complexes are aimed *via* the protocol to be developed. The chosen backbones should enforce strong π-stacking of the porphyrin subunits to bring metal

ions into distances where spatial interaction occurs. Preliminary studies by *Osuka et al.* proved that intramolecular stacking effects in cofacial structures could overcome the 60° bite angle for the *o*-phenylene backbone case.[175] As a result, the cofacial ligand system should be a model to understand elementary enzymatic reactivity and study cooperative magnetic, catalytic and optical properties.

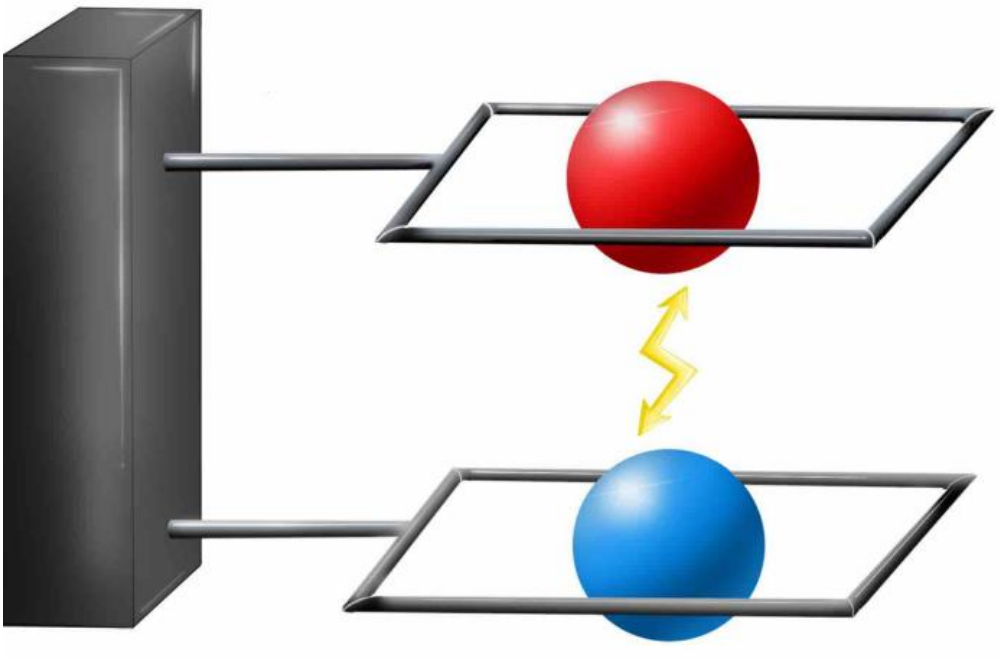

Figure 20: Cooperative effects between spatial close metal ions.

3 Main part

3.1 Syntheses of the monomeric porphyrin precursors

The porphyrin scaffold can be functionalized in three ways without affecting the metal-binding site and the circular π-electron system (Scheme 12). While for *meso*- and residue-functionalization, an asymmetric A_3 porphyrin is needed, the β-substitution only demands an A_4 porphyrin system. The remaining *meso*-residues can be chosen independently, but aryl residues combine rather high yields and rigidity.

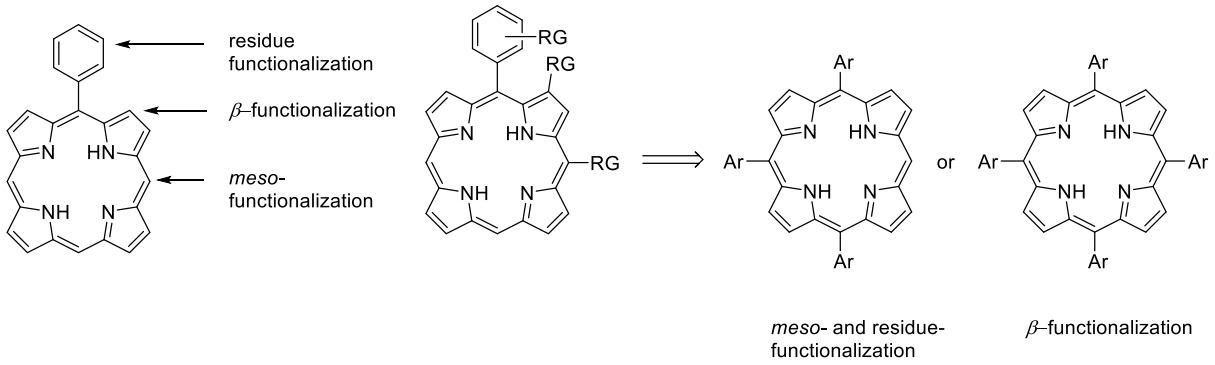

Scheme 12: Functionalization patterns at the porphyrin scaffold: *meso*-, β- and residue-functionalization.

Direct functionalization of the porphyrin core without adding ancillary spacer moieties is in favor due to smaller metal-metal distances and a stronger π-electron overlap of the future multimetallic complexes.

3.1.1 Syntheses of monomeric *meso*-substituted porphyrin precursors

As precursors for angled multimeric porphyrin complexes, asymmetric *meso*- and residue substituted porphyrin precursors were considered monomeric building blocks (Scheme 13). Therefore, the porphyrin scaffold ought to be built up *via* an A_3 porphyrin to choose the position of the reactive group.

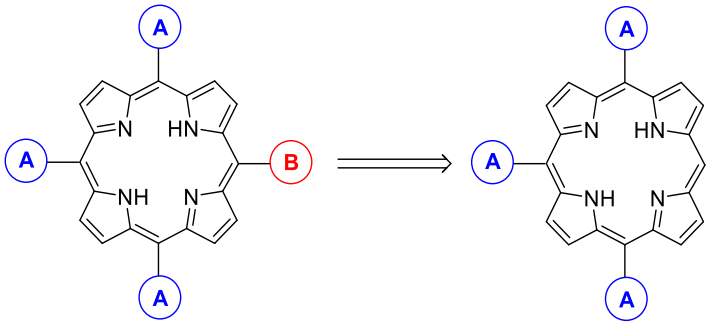

Scheme 13: Schematic representation of the synthesis towards A_3B-porphyrins.

A valid alternative is the mixed condensation approach as described in 1.3.1. However, this approach was not considered due to an anticipated significant drop in the yield.

To enable a high yielding synthesis route of A_3B-porphyrins, the described protocol in Scheme 14 *via* 2,2'-dipyrromethane (**57**) was used. Following the protocol developed by *Bein et al*., freshly distilled pyrrole (**45**) and paraformaldehyde were converted in the presence of $InCl_3$ as a *Lewis* acid at 55 °C for 3 h.[176] The air-sensitive 2,2'-dipyrromethane (**57**) can subsequently be applied in a TFA-catalyzed condensation reaction developed by *Lindsey et al.* to afford the 5,15-substituted porphyrinogen. This porphyrin species can be oxidized in the second step with DDQ to yield the *trans*-A_2 porphyrins **80** and **81**.[83] 5,15-Diphenylporphyrin (**80**) can be obtained in 41% yield starting from pyrrole (**45**) and benzaldehyde. In analog, the ethoxycarbonylphenyl-porphyrin **81** can be synthesized in an overall yield of 34% by applying the ethoxycarbonylphenyl-aldehyde instead of benzaldehyde. This result shows how sensitive the condensation reaction towards the choice of aldehyde is, significantly affecting the yield.

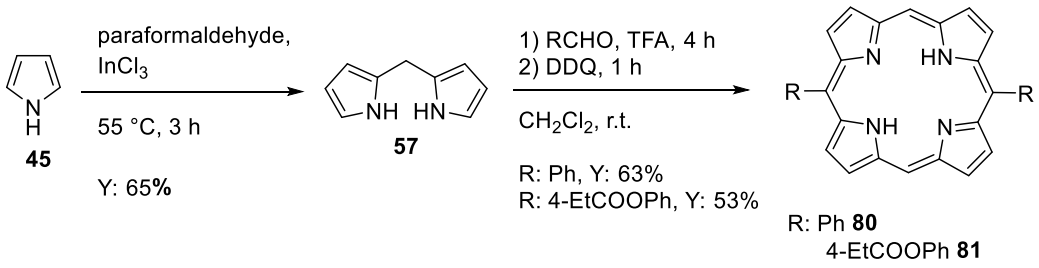

Scheme 14: Porphyrin synthesis using 2,2'-dipyrromethane (**57**) as a precursor.

According to the established protocol by *Senge et al.* for the efficient *meso*-functionalization *via* nucleophilic aromatic substitution, PhLi and subsequent oxidation afforded the 5,10,15-triphenylporphyrin (**82**) in 95% yield.[87] The subsequent bromination to obtain the 5-bromo-10,15,20-triphenylporphyrin (Scheme 15) by applying a small excess of N-bromosuccinimide (NBS) together with 1 mol% pyridine as a catalyst in $CHCl_3$ at room temperature for 2 h could be carried out in 97% yield. In a similar approach, the 5,15-(4-ethoxycarbonylphenyl)-porphyrin (**81**) was treated with NBS in the presence of 1 mol% pyridine in CH_2Cl_2 at 0 °C for 20 min to avoid dibromination to the thermodynamically more stable dibrominated product and afforded 5-bromo-10,20-(4-ethoxycarbonylphenyl)-porphyrin (**84**) in 60% yield.

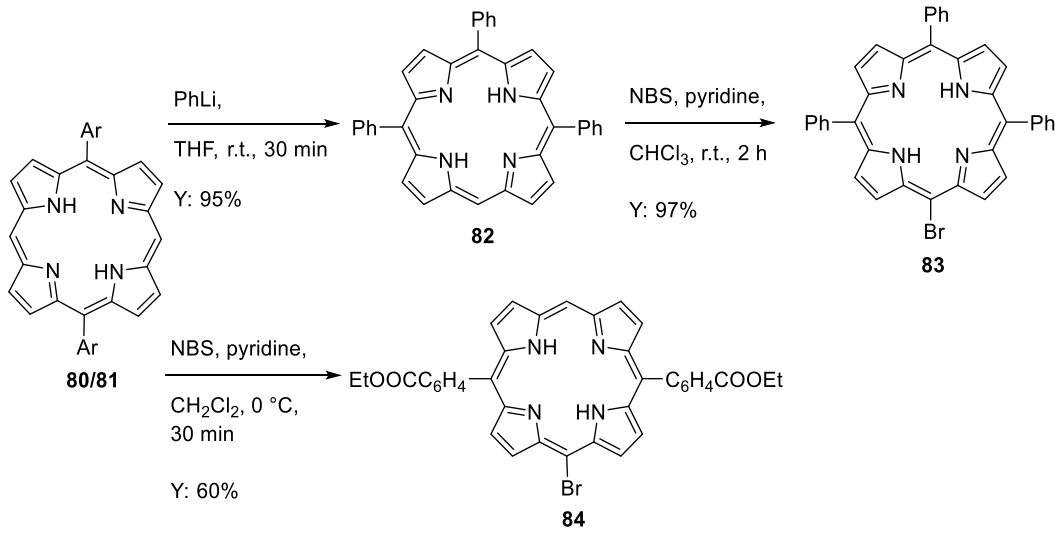

Scheme 15: Electrophilic bromination reaction of porphyrins in *meso*-position. Ar: Ph for the A_3B porphyrin synthesis, Ar: 4-EtCOOPh for the A_2B porphyrin synthesis.

3.1.2 Syntheses of the monomeric *β*-substituted porphyrin precursors

The *β*-substituted porphyrin precursors only demand A_4 porphyrin scaffolds, which can be synthesized as described in 1.3.1 or purchased commercially. Tetraphenylporphyrin (TPP) **32** can be mono brominated under rather harsh conditions, using an excess of NBS, in a refluxing solution of CH_2Cl_2 and 3 mol% pyridine for 8 h (Scheme 16). Two consecutive flash column chromatographies on silica gel were needed to separate the starting material and multiple brominated TPP molecules with similar R_f values to obtain 2-bromo-5,10,15,20-tetraphenylporphyrin (**85**) in 54% yield.

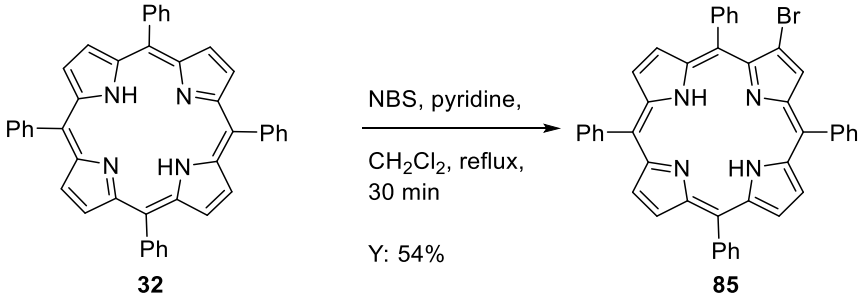

Scheme 16: Pyridine catalyzed *β*-bromination of the porphyrin scaffold with NBS.

The readily synthesized porphyrin precursors described in the last two sections have been used for the syntheses routes towards the respective metal complexes.

3.1.3 Syntheses of the metal-containing monomeric porphyrin precursors

As described in section 1.2, porphyrin molecules can bind various metal ions in different coordination spheres. For prebuilt metalated porphyrin precursors, diamagnetic metal ions in oxidation state +2 were used to avoid paramagnetic NMR spectra and charged complexes.
First, Zn(II) and Ni(II) precursors were applied in coordination reactions to obtain the respective Zn(II) complexes **87** and **88** and the Ni(II) complex **86**. While $Zn(OAc)_2$ can be used to bind Zn(II) under mild conditions into the porphyrin core, for the Ni(II) insertion, $Ni(acac)_2$ together with the porphyrin had to be heated up to 96 °C (Scheme 17).[177, 178]

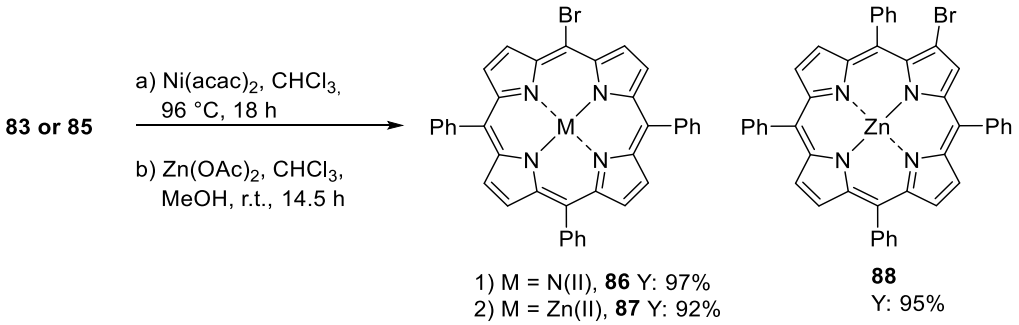

Scheme 17: Metalation reaction of the monomeric bromo-porphyrin precursors.

Generally, metal ions with unoccupied d-orbitals can be coordinated faster and stronger the more electron-rich the porphyrin core, since a stronger π-back bonding to the metal ion (e.g., Ni(II), d^8) occurs.[39] For this reason, Zn(II) porphyrin is superior to closed-shell metal ions. The metal ion can be removed easily and thus allows metal changes later under mild reaction conditions. While the Zn(II)-ion can be decoordinated by stirring the porphyrin metal complex in a 6 M HCl solution, Ni(II) porphyrins must be treated with *Grignard* reagents. This circumvents harsh conditions containing H_2SO_4 in TFA and the subsequent hydrolysis with 1 M HCl solution to release the Ni(II) ion and retain the free-base porphyrin.[179]
In the preceded master thesis,[180] a high dependency between electronic environment and reactivity at *meso*-position conditional to the inserted metal ion could be proven. While an azido functionality could be introduced in up to 65% yield for the Ni(II) case, the Zn(II) derivative showed no conversion to the azido-porphyrin. These findings agree with *Yamashita et al.*, who obtained no product for the free-base case.[181] That can be explained again with the metal-ligand π-back bonding, which reduces the ring system's electron density and nucleophilicity.
As described in section 1.3.2 and investigated in the master thesis, bromo-porphyrins can be applied in C–C cross-coupling reactions to install a spacer moiety. Therefore, the protocol of *Xu et al.* was used for a *Sonogashira* cross-coupling reaction with TMS-acetylene, followed by deprotection of the silyl protecting group (Scheme 18).[182]

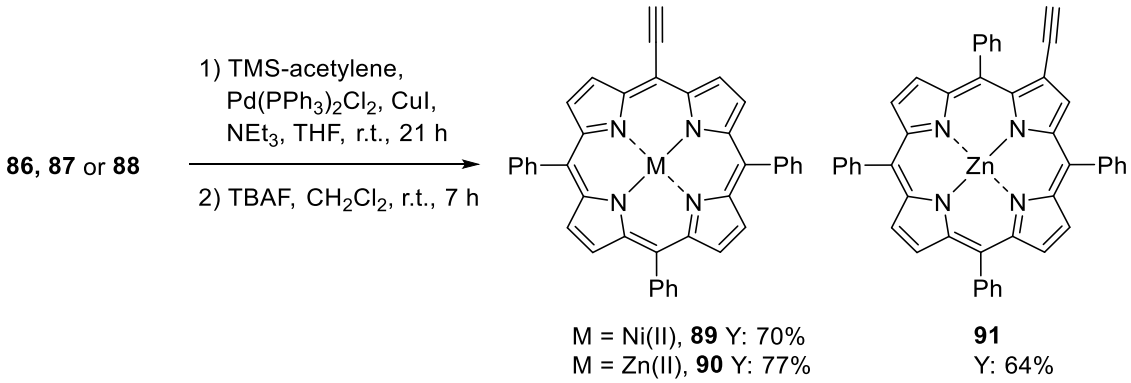

Scheme 18: *Sonogashira* cross-coupling reaction with TMS-acetylene and subsequent deprotection.

The synthesized monomeric porphyrin precursors were now deployed for the synthesis of *meso*- and *β*-connected porphyrin dimers.

3.2 Varying the backbone of angled dimeric porphyrin metal complexes

The metal-metal separations can be adjusted using the tetrahedral angle specified by the relative substitution position of the linker to the backbone as well as *via* the connectivity to the linker moiety. The chosen backbone has in these regards the most dominant effect on the plane distances. Depending on the linkage between the linker moiety and the porphyrin subunit, the coherent π-electrons system can be expanded.

3.2.1 Syntheses and functionalization of alkyne-linked porphyrin dimers

As already examined in the preceding master thesis, the Zn(II)-bromo-porphyrin **87** and the Zn(II)-ethinyl-porphyrin **90** can be coupled *via* a copper-free *Sonogashira* cross-coupling reaction[183, 184] or a Cu(II)-catalyzed *Glaser* coupling[185] (Scheme 19).

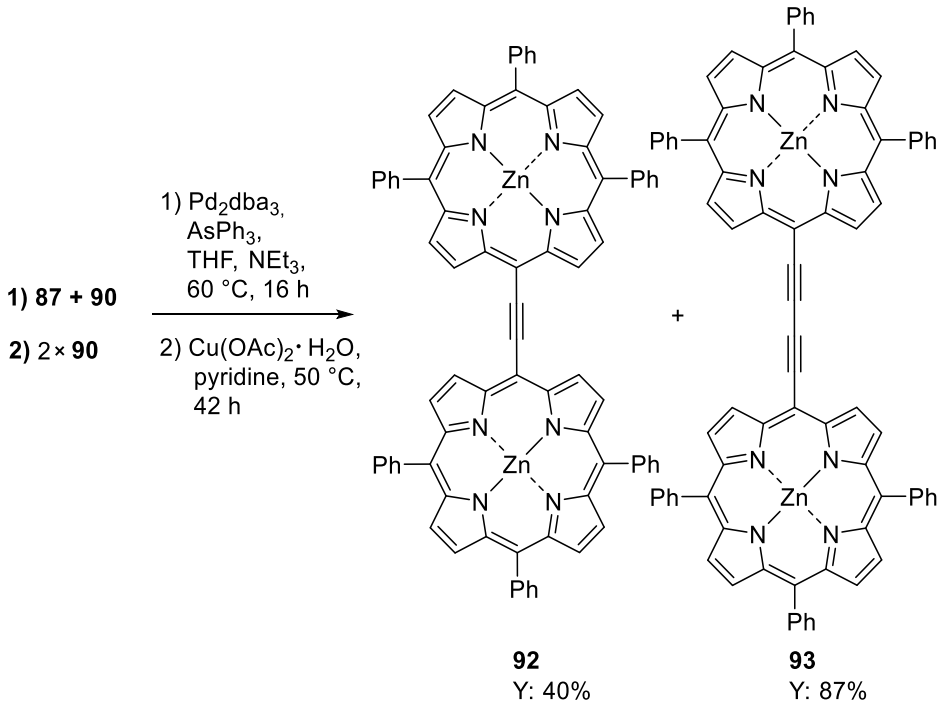

Scheme 19: Copper-free *Sonogashira* cross-coupling reaction and *Glaser* coupling reaction towards alkyne-connected porphyrin dimers **92** and **93**.

The *Glaser*-product **93** could successfully be used in a cyclization reaction in the presence of $Na_2S \bullet 9\ H_2O$ with 2-methoxyethanol in *p*-xylene at 130 °C in 90 h to form 2,5-substituted thiophene (Scheme 20).[186] These results of the preceding master thesis[180] prove that linearly connected porphyrins are reactive enough to be converted at a later stage.[186]

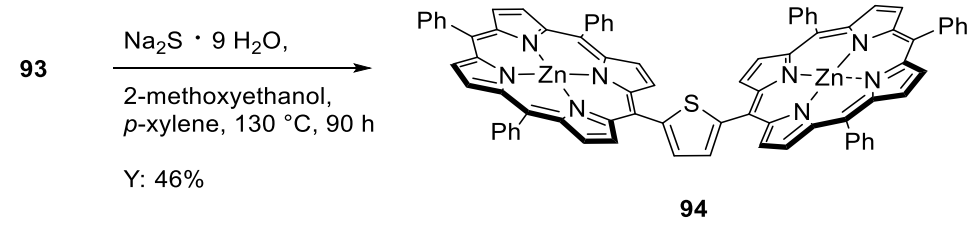

Scheme 20: Sulfide-based cyclization reaction to obtain a 2,5-substituted thiophene backbone between two Zn(II)porphyrin subunits.

Unfortunately, the exocyclic bond angle for the 2,5-thienyl backbone is 148° and in addition to that, too large to enforce spatial π-stacking between the porphyrin subunits.[187] In contrast, all functionalization attempts for the single alkyne-linked porphyrin dimer failed even though literature is known for tolane (Scheme 21).[188-190] The click reaction towards **95** and **96** yielded partly monomeric porphyrins and the cyclization approaches towards **97** and **99** as well as the *Diels-Alder* reaction towards **98** showed no conversion of the starting material. This suggests either a too electron-rich triple bond or the porphyrin residue is sterically too demanding.

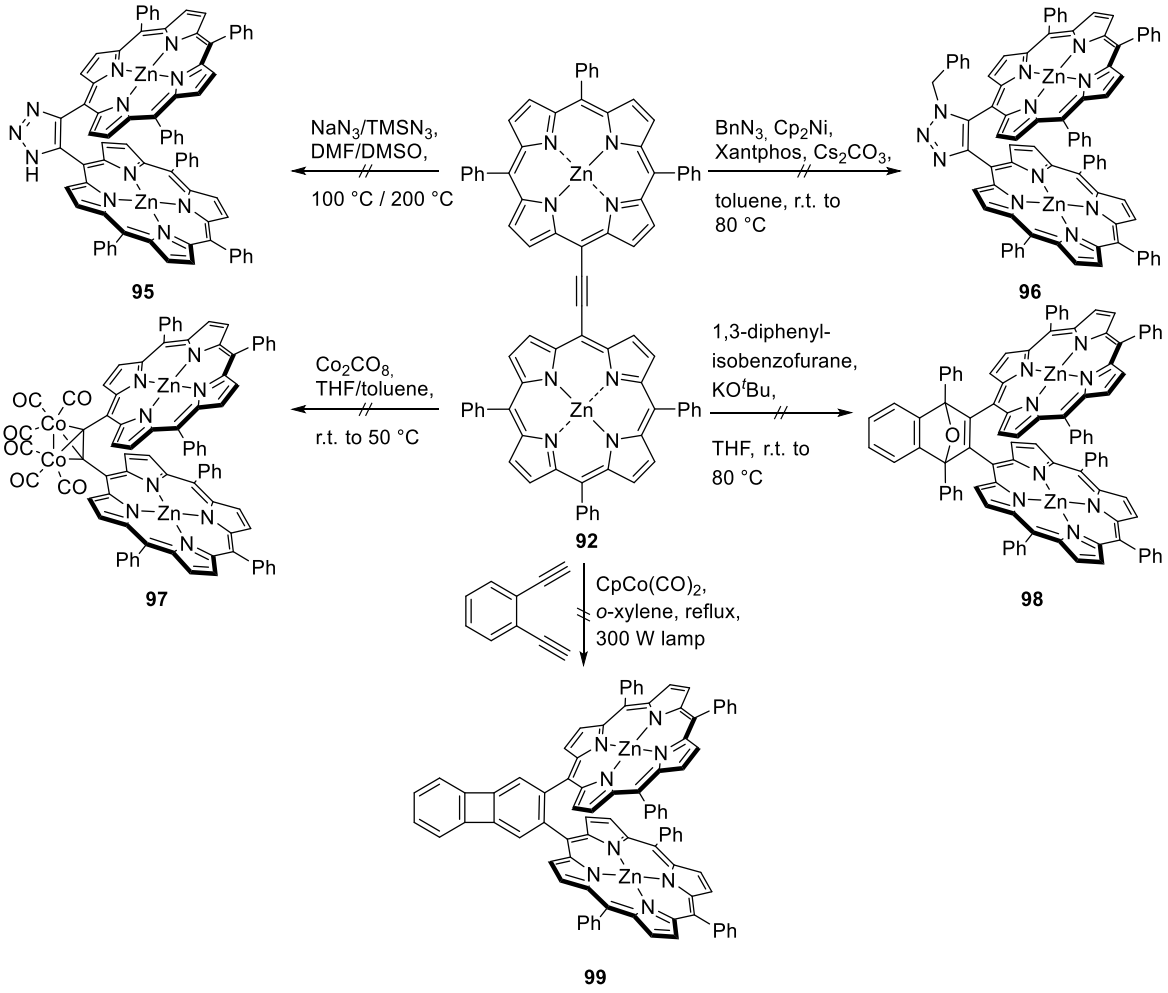

Scheme 21: Synthetic attempts to functionalize the internal alkyne *via* cycloaddition reactions and metal coordination.

Reevaluating the findings of section 3.1.3 that show a high dependency between the electronic environment and the reactivity of the *meso*-position encouraged further functionalization

attempts of the rather unreactive internal alkyne by altering the applied alkyne-linked porphyrin dimers.

Therefore, the Ni(II)2NH-alkyne-linked-porphyrin dimer and the 2Zn(II)-*β*-linked-alkyne-porphyrin dimer were synthesized, differing in coordination and linkage (Scheme 22).

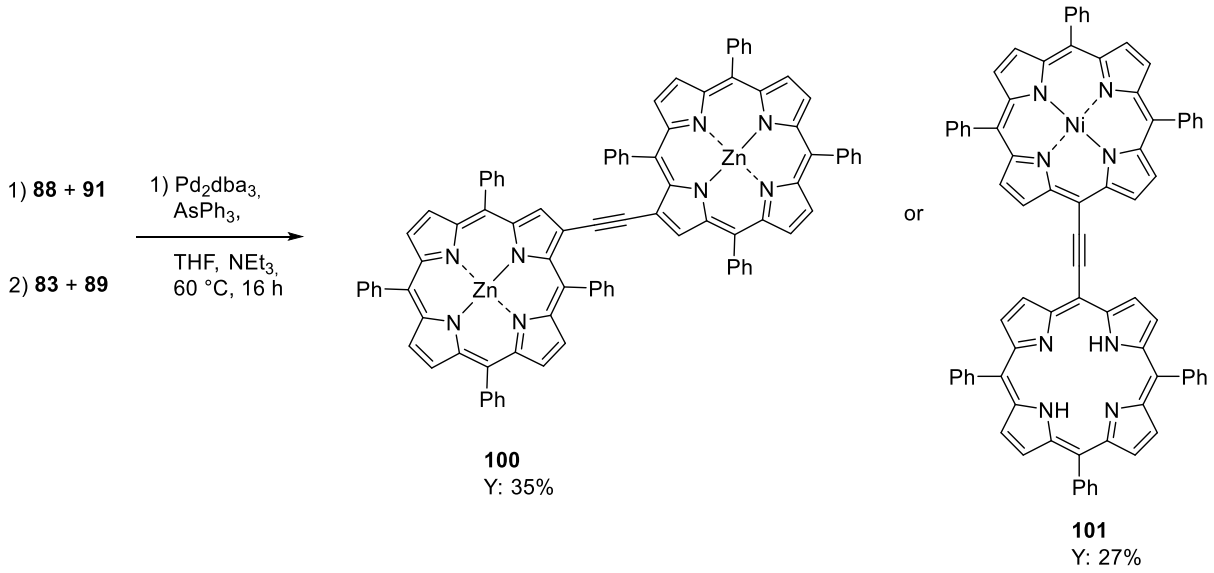

Scheme 22: Synthesis of other derivatives of the alkyne-bridged porphyrin dimers **100** and **101** varied by their connectivity or their metal insertion.

Both internal alkynes still failed to be converted into the respective 4,5-substituted 1,2,3-triazoles by performing the Click reaction at 70 °C in $TMSN_3$. While the reaction in boiling $TMSN_3$ showed no conversion, stirring under microwave irradiation led to degradation.

The *β*-linked-alkyne-porphyrin dimer was further investigated in a metal-templated [2+2+2] cycloaddition with 1,6-heptadiyne and $Co_2(CO)_8$ that should yield, as reported by *Therien et al.*, the face-to-face bis[(porphinato)zinc(II)] compound **102** in 45% yield. Even though *Fletcher* and *Therien* reported that the Co-mediated cycloaddition works smoothly even with trimeric Zn(II) porphyrin complexes,[191] no cofacial porphyrin dimer formation could be attested (Scheme 23).

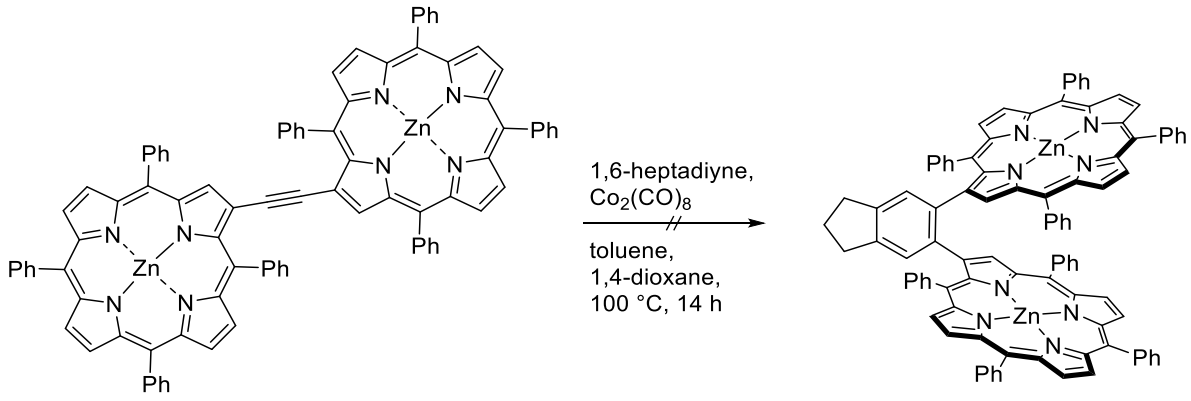

100 **102**

Scheme 23: Cycloaddition attempt with 1,6-heptadiyne and $Co_2(CO)_8$ at a less crowded internal alkyne functionality.

The presented substrate scope is limited, containing only electron-rich Zn(II) complexes substituted by less bulky alkyl residues for all *meso*-connected compounds. Porphyrins with aryl-residues could be converted by *Therien et al. via* the [2+2+2] cycloaddition, only if the sterically demand of the porphyrin rings against each other is decreased by the *β*-linkage. Since the presented work aims to develop a rather universally applicable cofacial ligand system, the conversion of pre-linked linear porphyrin multimers was discarded later.

3.2.2 N-joined porphyrin dimers

Due to the low reactivity of the internal alkynes, even under harsh reaction conditions as described in section 3.1.4, it was postulated that nitrogen, as a heteroatom, could be used to join two porphyrin subunits.

Even though the secondary amine with a bond angle of roughly 108°[192] cannot force the two porphyrins in a cofacial structure, it might show interesting properties due to the extended *π*-electron system. In addition, the step-by-step approach enables the defined synthesis of heterometallic porphyrin complexes by reacting two monomeric porphyrin subunits containing different metal ions with each other.

Osuka et al. reported a nucleophilic aromatic substitution of derivatives of Ni(II)amino-porphyrin **103** with Ni(II)chloro-porphyrin **105**. The necessary porphyrin monomers and the respective Zn(II)chloro-porphyrin **106** were synthesized (Scheme 24).

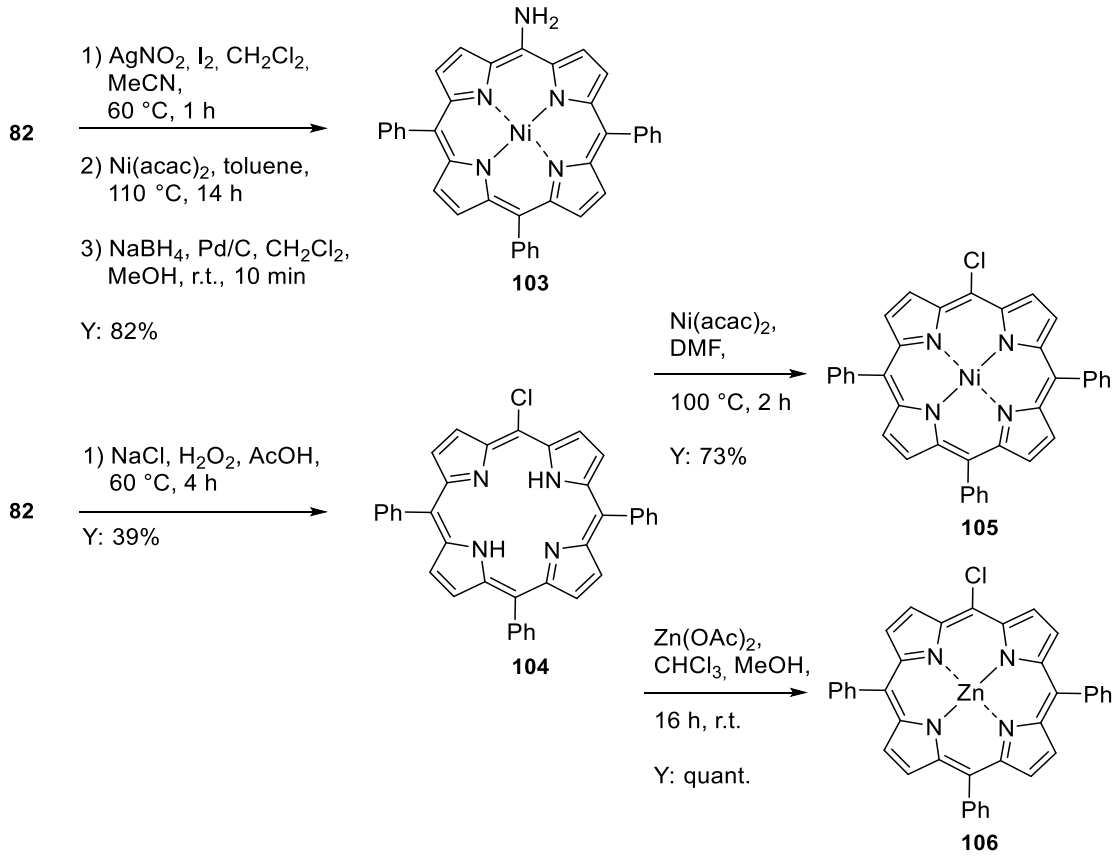

Scheme 24: Functionalization reactions at the porphyrin *meso*-position introducing NH_2- and Cl-functionalities.

In a one-pot procedure to synthesize Ni(II)-amino-porphyrin **103**, triphenylporphyrin **82** was first nitrated with $AgNO_2$ induced by elemental iodine. Subsequently, Ni(II) was introduced *via* $Ni(acac)_2$ followed by the reduction of the NO_2-group with $NaBH_4$ on Pd/C to give the desired compound **103** in a yield of 82%.[193] By substituting the Ni(II) insertion with a classical Zn(II) insertion using $Zn(OAc)_2$ in the second step, the respective Zn(II) complex could only be obtained in traces. Thereby it was noticed that the Zn(II) insertion decelerated and twice the amount of the Zn(II) salt was needed to guarantee full conversion into the Zn(II)-nitro-porphyrin. The subsequent reduction of the NO_2-group led to many by-products in a wide color range from orange to blue and green, indicating that reducing the porphyrin core to the respective chlorines might be preferred.[194]

The chloro-porphyrin **104** instead can be synthesized in a yield of 39% as free-base porphyrin, using NaCl and 30% H_2O_2 in AcOH.[195] The following Ni(II) and Zn(II) coordination reactions worked smoothly as described earlier for the Br-derivatives.

With the Ni(II)-amino-porphyrin **103** and the Ni(II)-chloro-porphyrin **105** in hand, the protocol developed by *Osuka et al.* was employed by stirring both porphyrin derivatives in DMF with NaH as a base. The nucleophilic aromatic substitution reaction in *meso*-position yielded [bis-(10,15,20-triphenylporphyrin-5-yl)amine]-dinickel(II) (**107**) with 48% (Scheme 25).[193]

The same procedure was now applied to the Zn(II)-chloro-porphyrin but only defunctionalized material and starting material could be isolated after reacting at 60 °C for 7 h. The electron-rich Zn(II)-chloro-porphyrin with its coordination of a d^{10} metal, instead of the d^8 electron configuration in the case of the Ni(II) species, inhibits the reaction. The back bonding of the π-electron system is not as strong as the system with vacant orbitals, increasing the overall electron density of the system and thus disfavoring the nucleophilic attack of the primary amine to substitute the chloride-ion at the second porphyrin subunit.

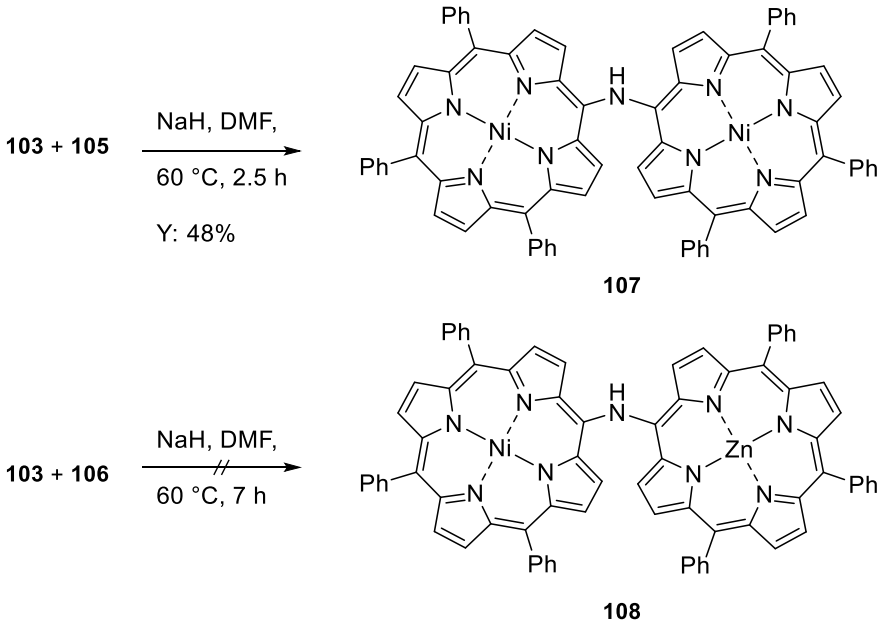

Scheme 25: Synthesis attempts to afford the homobimetallic 2Ni(II)- and the heterobimetallic Ni(II)Zn(II)-N-bridged-porphyrin dimers.

To circumvent the electronic obstacles to porphyrin-NH-porphyrin binding, a *Buchwald-Hartwig*-type cross-coupling reaction catalyzed by $Pd(OAc)_2$, DPEPhos as a ligand and Cs_2CO_3 as a base was tested (Scheme 26).[196] After 14 h stirring at 68 °C in dry THF, the product could be isolated *via* flash column chromatography on silica gel to afford the heterobimetallic Ni(II)-Zn(II)-porphyrin complex **108** in 55% yield.

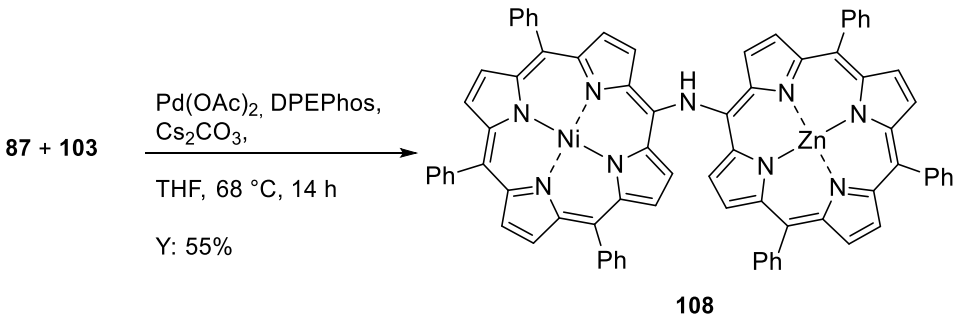

Scheme 26: Synthesis of the Ni(II)Zn(II)-N-bridged-porphyrin dimer *via* a *Buchwald-Hartwig* cross-coupling reaction.

The homobimetallic and the heterobimetallic complexes were investigated by UV-Vis spectroscopy. While the monomeric Ni(II)chlorido-porphyrin **105** and the Ni(II) amino-

porphyrin **103** exhibit rather narrow *Soret*-bands, the ones of the dimeric 2Ni(II) and Ni(II)Zn(II) N-joined-porphyrins **107** and **108** are broadened significantly, which is a result of the extended π-system (Figure 21).

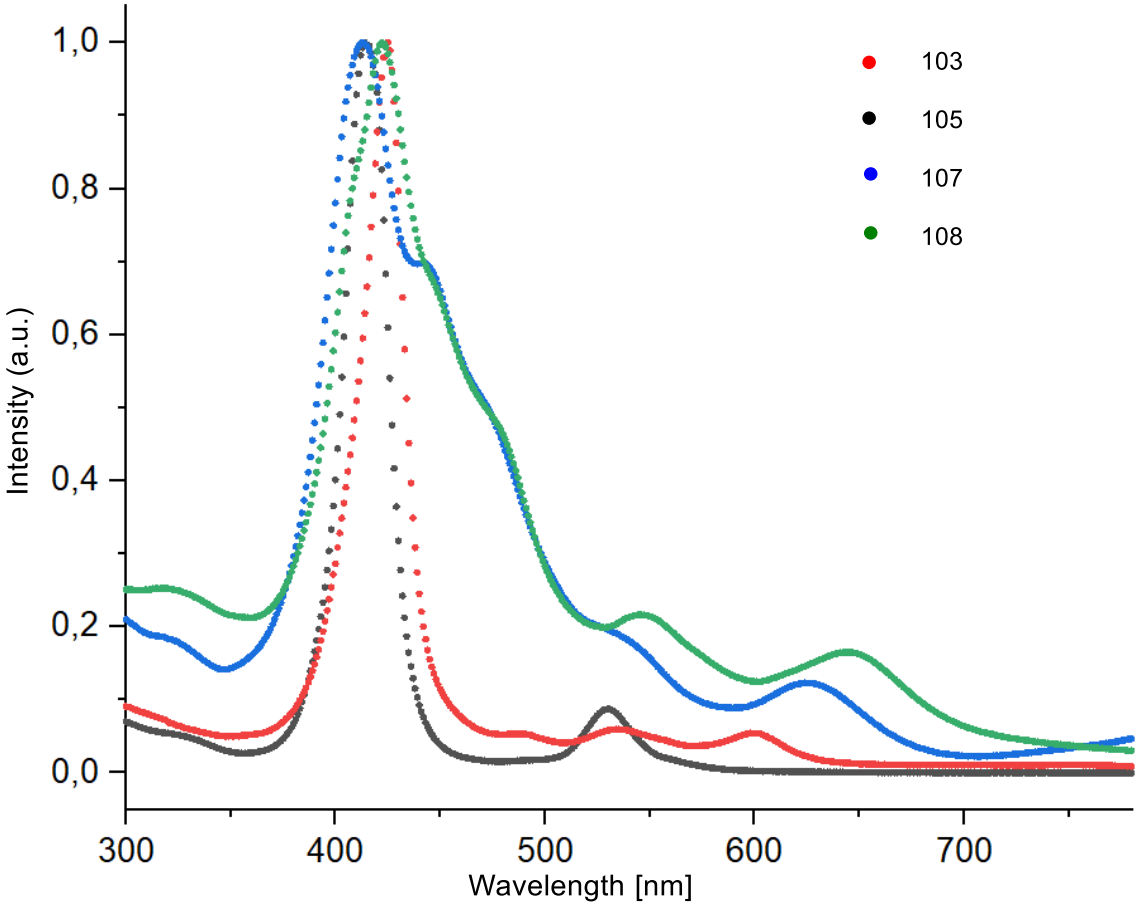

Figure 21: Normalized UV-Vis absorption spectra of the Ni(II)chloridoporphyrin **105**, Ni(II)aminoporphyrin **103**, 2Ni(II)-N-bridged-porphyrin dimers **107** and Ni(II)Zn(II)-N-bridged-porphyrin dimers **108**. Zn(II)bromidoporphyrin **87** is not shown due to the impact of the larger halogen onto the porphyrin core. The chart is normalized to an intensity of 1.0.

The complexed metal ions only affect the wavelength of peak maximum. For the 2Ni(II) porphyrin **107**, the absorption maximum is at 413 nm; for the Ni(II)Zn(II) case **108**, the maximum shifts bathochromically to 422 nm.

Since the modular synthesis to structure a heterobimetallic center was achieved as described above, [2.2]paracyclophane was investigated as a linking moiety to bring two different metal ions in spatial proximity.

3.2.3 [2.2]Paracyclophane porphyrin conjugates

[2.2]Paracyclophane represents a rather new platform for metal-binding sites that enables adjustable distances between metal centers. Generally, [2.2]paracyclophane can hold up to 16 substituents in a precise spatial orientation. The below-depicted substitution patterns represent double substitutions that are otherwise difficult to achieve (Figure 22). The prefix ´pseudo` is

used to indicate the substitution at the two different benzene rings. *Pseudo-para* substitutions bear the largest metal-metal distance, *pseudo-geminal* the lowest.

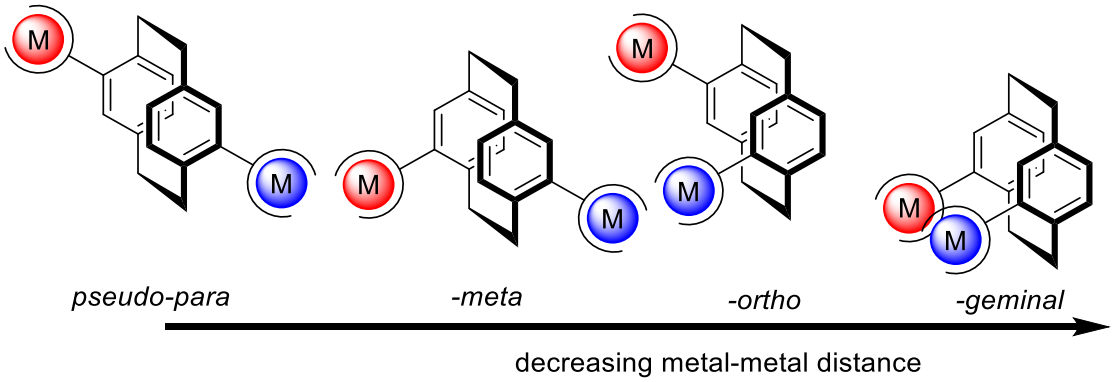

Figure 22: Variable substitution pattern of the *pseudo*-functionalized [2.2]paracyclophane scaffold.

[2.2]Paracyclophane has a ´bent and battered` 3D conformation built from two benzene rings bent out of the plane (Figure 23).[197]

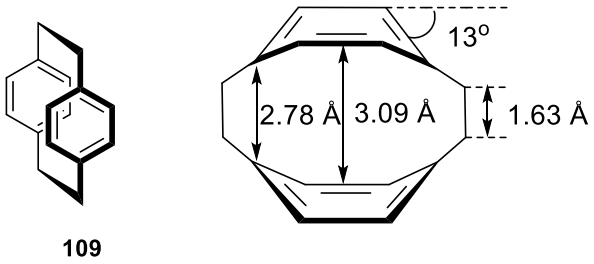

Figure 23: The ´bent and battered` 3D structure of [2.2]paracyclophane (**109**).

The two ethyl bridges force the bridgeheads of the benzene rings to a distance of 2.78 Å and the centers of the benzene moieties to a distance of 3.09 Å, thereby inducing a strain. The separation of the benzene rings is 0.31 Å below the *van-der-Waals* distance of the layers in graphene (3.40 Å),[198] inducing transannular through-space electronic communication *via* the π-system.[199]

The ´bent and battered` structure decreases the aromaticity of the *p*-xylene subunits, which is indicated by a significant upfield shift of the aromatic protons by up to 1.5 ppm. Besides spectroscopic effects, the reactivity can differ significantly from that of *p*-xylene.

As a result of the overlap of the π-systems on the benzene rings, a substitution at one ring affects the functionalization of the other ring. *Bräse et al.* could show that lithiation of one benzene moiety increases the electron density of both and therefore the second lithiation is hindered.[200] Spatial electronic communication is already deployed in molecular junctions[201] and molecular wires.[202]

Both above-outlined phenomena lead to chemical behavior distinctly from the isolated *p*-xylene or benzene; therefore, reactions cannot be directly transferred to [2.2]paracyclophane.

In this work, the ability of porphyrins as easily modifiable ligands forming stable transition metal complexes was combined with the [2.2]paracyclophane scaffold to bind an additional metal-binding site in spatial proximity rigidly.

3.2.3.1 Au(I)Zn(II)-[2.2]paracyclophane-porphyrin conjugates

The following part was examined in collaboration with Dr. Daniel Maximilian Knoll, who took over mainly the synthetic work of the [2.2]paracyclophane scaffold.[203]
With our first try, we envisioned selectively converting one of the two bromides of 4,16-bromo[2.2]paracyclophane (**110**) into a phosphine binding site to coordinate Au(I) and install a porphyrin subunit at the position of the second bromine (Scheme 27).

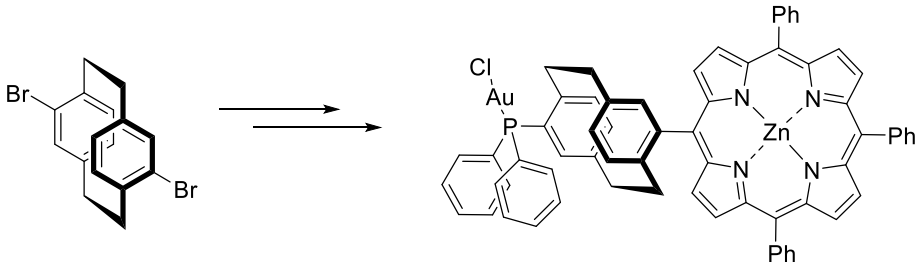

110 **111**

Scheme 27: Original idea of the first directly *meso*-connected [2.2]paracyclophane-porphyrin conjugate as a heterobimetallic Zn(II)Au(I) complex **111**.

Therefore, **110** was synthesized by reacting [2.2]paracyclophane (**109**) with elemental bromine. Subsequently, the dibromide **110** was unsymmetrically functionalized *via* selective lithium-halogen exchange reaction followed by reaction with DMF to afford 4-bromo-16-formyl[2.2]paracyclophane **112**.[203] The condensation reaction with pyrrole and benzaldehyde yielded the free-base bromo substituted [2.2]paracyclophane-porphyrin conjugate as the product of a mixed condensation. After the metal coordination, the Zn(II)-porphyrin-[2.2]paracyclophane conjugate **113** was obtained in an overall yield of 4.9% (Scheme 28).

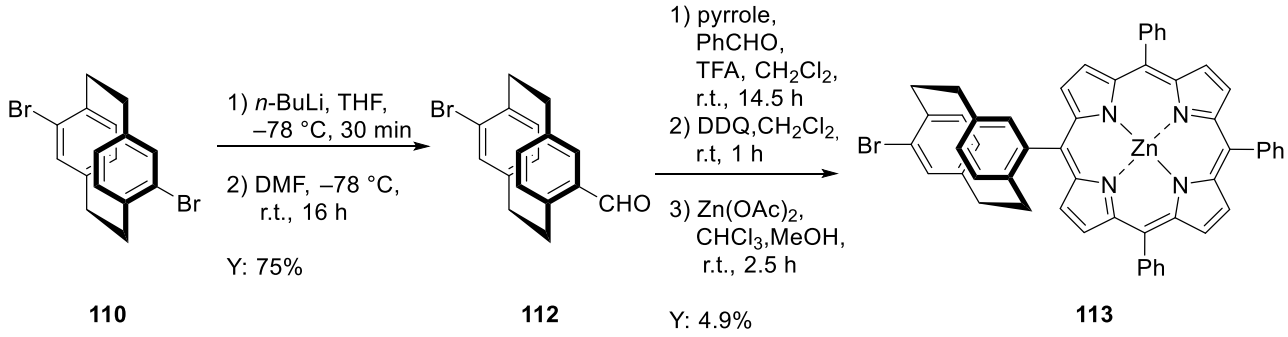

110 **112** **113**

Scheme 28: Synthesis of the *pseudo-para* substituted bromo[2.2]paracyclophane-Zn(II)porphyrin-conjugate **113**. Compound **112** was provided by Daniel Knoll.[203]

In the following, again, a lithium-halogen exchange was conducted, but this time with a subsequent phosphination with the air-sensitive PPh_2Cl to introduce the phosphine-binding site in *pseudo-para* position. However, even with a large excess of *n*-BuLi or *t*-BuLi, only starting material was recovered (Scheme 29). That underlines the transannular through-space electronic communication between the benzene rings *via* the π-system, inducing electron density of the electron-rich porphyrin ring into the second benzene moiety, which leads to resilience against lithiation agents.

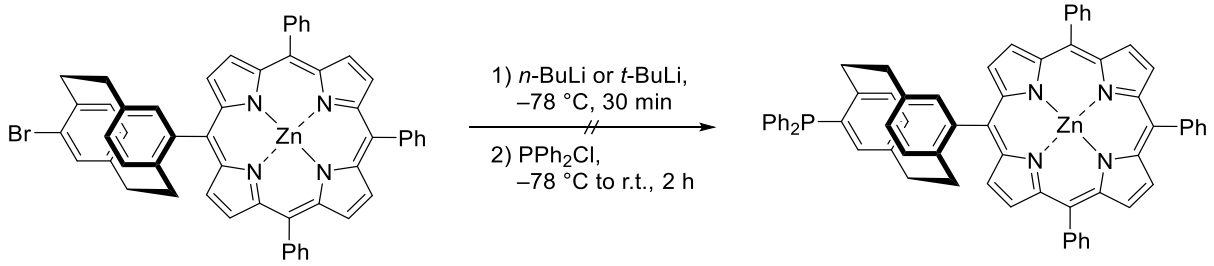

113 **114**

Scheme 29: Phosphination attempt of the bromo functionality of the [2.2]paracyclophane scaffold.

The synthetic approach was modified for the more ambitious *pseudo-ortho* substitution pattern, whereby the bromide was substituted before introducing the porphyrin moiety (Scheme 30). Therefore, the bromide-functionality of **115** underwent a Pd-catalyzed *Sonogashira* cross-coupling reaction with TMS-acetylene to afford 4-formyl-16-TMS-alkyne[2.2]paracyclophane (**116**) in 52% yield (Dissertation Daniel Knoll).[203] The subsequent TFA-catalyzed mixed condensation with pyrrole and benzaldehyde used the formyl-residue to build up the porphyrin core, coordinated with Zn(II) to give **117** in an overall yield of 2.6%.

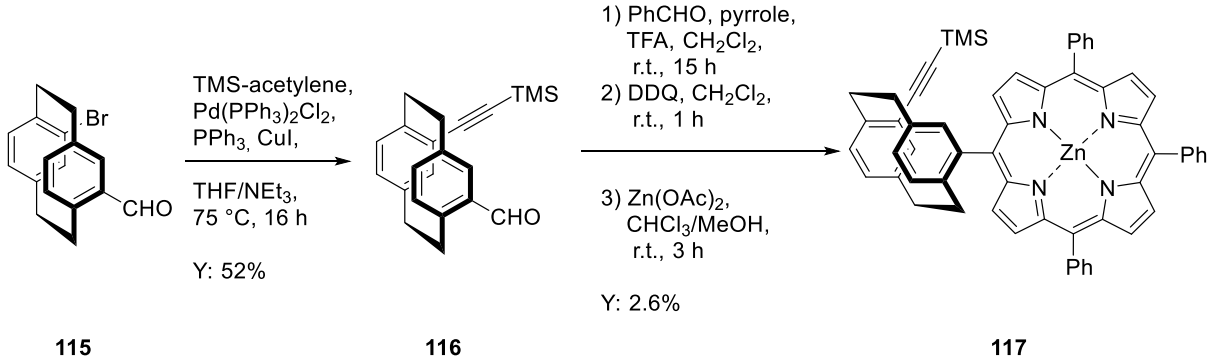

115 **116** **117**

Scheme 30: Synthesis of the Zn(II) complex of the *pseudo-ortho*-TMS-alkyne-[2.2]paracyclophane-porphyrin conjugate **117**. **116** was provided by Daniel Knoll.[203]

Since linear alkyne-Au(I)-PPh_3 complexes are literature known, the respective Ph_3AuCl complex **119** was synthesized starting from chloro(tetrahydrothiophene)gold(I) (**118**) as the Au(I) source in a yield of 78%.[204] After the silyl-protecting group was removed with TBAF, the alkyne **120** was deprotonated with KOH and the Au(I) salt was added to the solution (Scheme 31).

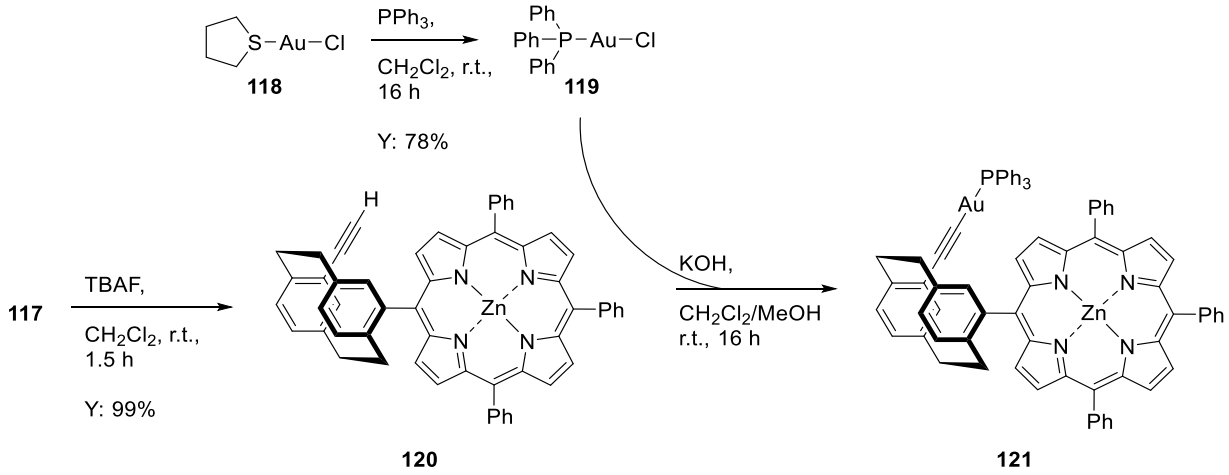

120 **121**

Scheme 31: Synthesis of the first heterobimetallic *pseudo-ortho*-[2.2]paracyclophane-porphyrin complex containing Zn(II) and Au(I) **121**.

Nevertheless, purification of the Au(I)-Zn(II) heterobimetallic complex using crystallization or flash column chromatography on silica gel did not yield the product, but only traces of the complex due to the degradation during work-up.

Nonetheless, the formation of the complex could be verified by ESI-MS as represented in Figure 24.

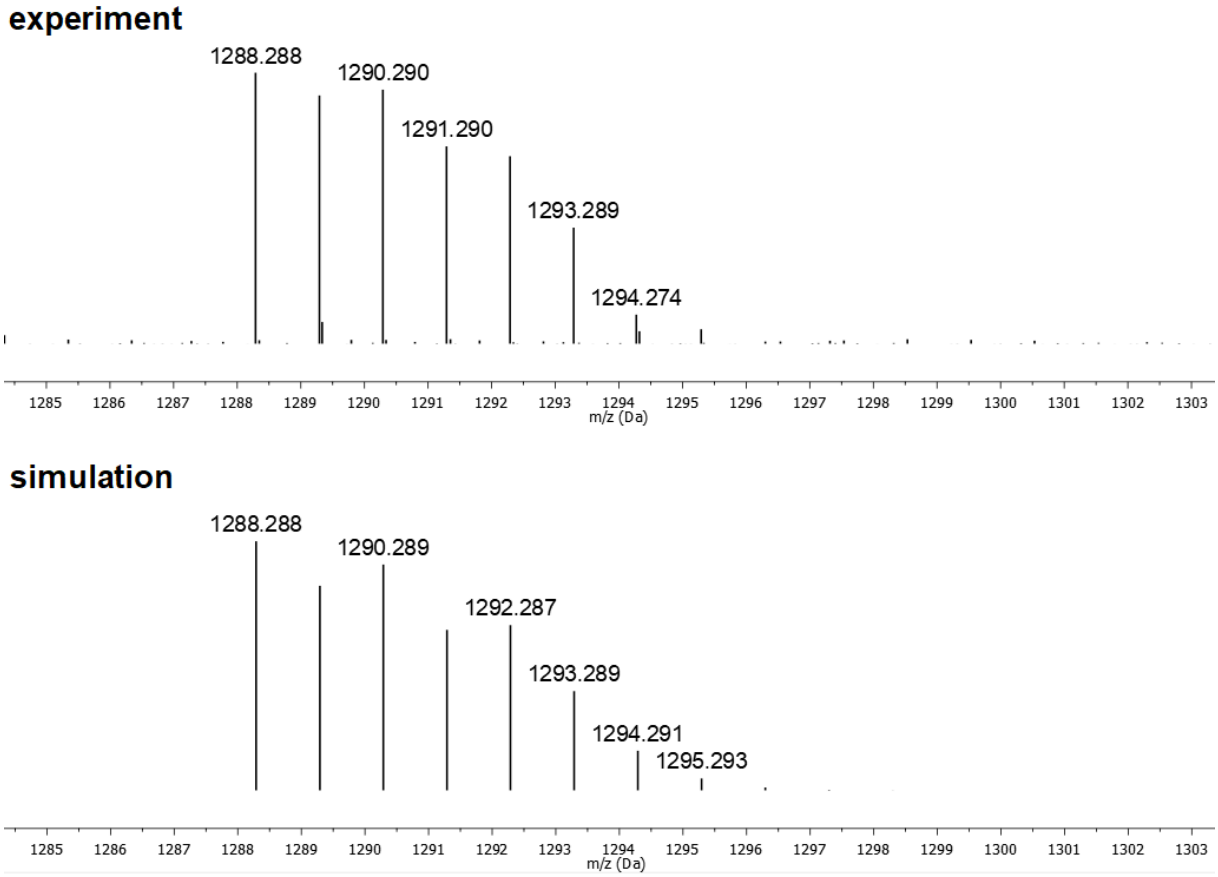

Figure 24: ESI-MS spectrum of the Zn(II)Au(I) complex **121** ($C_{74}H_{52}AuN_4PZn$) – experiment *vs*. simulation.

3.2.3.2 Ru(II)Zn(II)-[2.2]paracyclophane-porphyrin conjugates

Due to the described stability issues for the linear Au(I)-alkyne complex, a different ligand-metal combination is needed and should be applied to the [2.2]paracyclophane-porphyrin scaffold. For the installation of a ruthenium polypyridyl moiety as a photoactive site, a *Suzuki* cross-coupling was used as the first step. $Pd(OAc)_2$ as a palladium source and RuPhos as a ligand in the presence of K_3PO_4 in a mixture of toluene/water (10:1) at 80 °C was chosen to introduce the 2-phenylpyridine residue (Dissertation Daniel Knoll) (Scheme 32).[203] The 4-formyl-16-(4-(pyridine-2-yl)phenyl[2.2]paracyclophane (**122**) was obtained in 11% yield with the result that the aldehyde could be used for the subsequent porphyrin condensation in

5.7% yield. Having the ligand in hand, at first, the coordination of Zn(II) with $Zn(OAc)_2$ was conducted to obtain the Zn(II) analog **123** quantitatively.

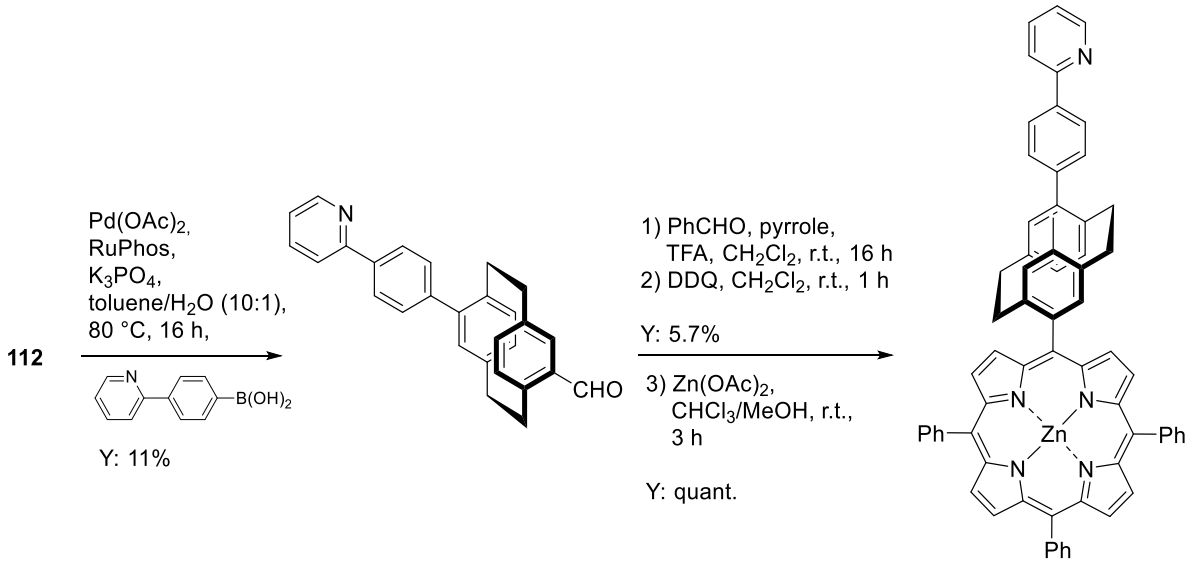

Scheme 32: Synthesis of the Zn(II) complex of the *pseudo-para*-phenyl-pyridyl-[2.2]paracyclophane porphyrin conjugate. **122** was provided by Daniel Knoll.[203]

As the final step, the standard ruthenation procedure following *Braun et al.* enables the cycloruthenation of the remaining phenylpyridine binding site (Scheme 33).[205] According to TLC monitoring, an excess of the Ru(II) salt with 10.0 equivalent was needed since the initial use of 1.00 equivalent almost gave no conversion.

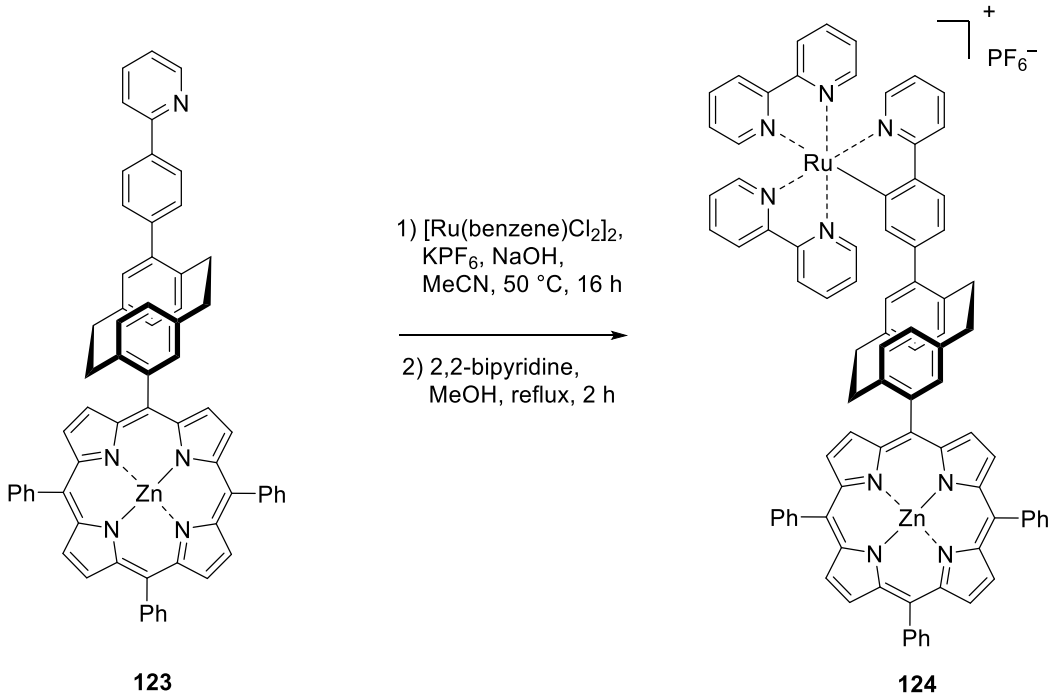

Scheme 33: Synthesis of the first heterobimetallic *pseudo-para*-[2.2]paracyclophane-porphyrin complex containing Zn(II) and Ru(II) **124**.

The obtained crude product was undertaken few purification attempts *via* flash column chromatography and it was proven to be by far more stable than the Au(I)Zn(II) complex **121**. Nevertheless, the charged nature of the PF_6^- salt aggravated a clean separation of the by-products. For HPLC attempts, the solubility of the compound is too low.

However, the characteristic isotope pattern of Ru(II) and Zn(II) coordinated in the [2.2]paracyclophane-porphyrin conjugate can be used to prove the existence of complex **124** unambiguously. For further illustration, the expected ESI-MS spectrum was simulated and compared to the recorded data (Figure 25).

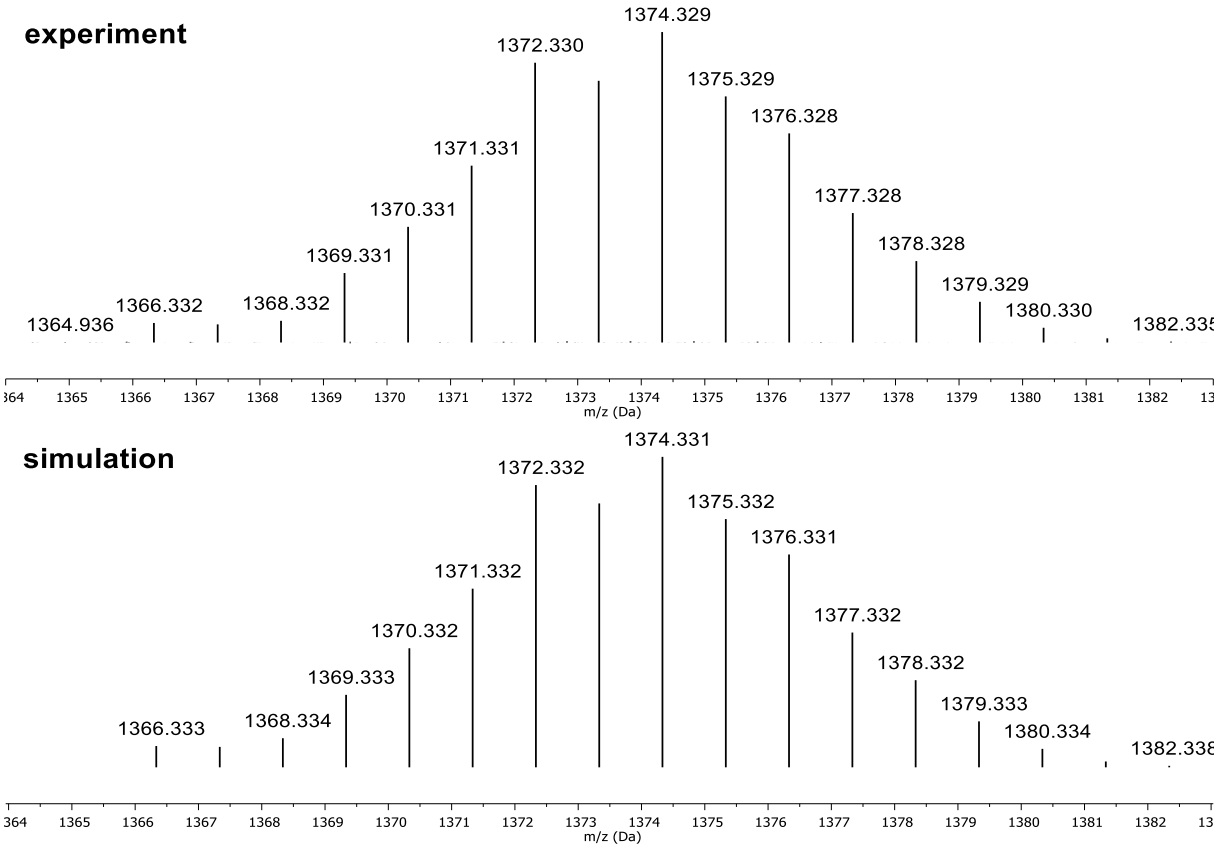

Figure 25: ESI-MS spectrum of the Zn(II)Ru(II) complex **124** ($C_{85}H_{60}N_9ZnRu$) – experiment *vs*. simulation.

Although establishing universally coordinated metal ions without switching the ligands is challenging, introduce the [2.2]paracyclophane scaffold as a rigid linker between two different metal-binding sites was successful. Therefore, the *o*-phenylene linker moiety substituted by two porphyrin subunits reported by *Kobuke et al.* in 1989 and later crystallized by *Osuka et al.* in 1991 is worth reinventing.[175, 206]

3.3 Cofacial *o*-phenylene-bisporphyrin metal complexes

Over the last 50 years, synthetic routes have addressed cofacial bisporphyrins, starting with rather flexible double urea and amide bridged *meso*-connected[207, 208] and *β*-linked[209] sandwich-like structures or later imidazole- and oxo-bridged metalloporphyrins which only demand one linker moiety and one bridging ligand.[210]
Then more rigid linker moieties such as anthracene,[211] bisphenylene,[212] dibenzofuran[213] and xanthene[214] were examined, which were doubly substituted with porphyrin subunits.
Parallel to applying linker systems that intrinsically favor cofacial relationships, *Kobuke et al.* developed the first synthetic route towards *o*-phenylene-bisporphyrins.[206] Even though the benzene moiety exhibits a 60° bite angle between *o*-substituted residues, *Osuka et al.* were able to conduct X-ray diffraction measurements, proving a cofacial arrangement with an average plane distance of 3.43 Å.[175]
The pioneering syntheses described above suffer from quite modest overall yields. The highest literature yield for the overall synthesis of *o*-phenylene linked symmetrical porphyrin dimers is 0.65%.[206] Furthermore, the procedures developed by, e.g., *Therien et al.*[215] and tested as described in section 3.2.1, are not readily generalizable to the coordination of a wide range of different transition metal ions – particularly heterobimetallic combinations. Due to the above-listed drawbacks, a new high yielding, tolerant and robust synthetic methodology is suitable for both homo- and heterobimetallic cofacial bisporphyrin complexes and allows for tunable metal-metal distances, is desirable.

3.3.1 *o*-Formyl-groups as residue functionalization to enable *o*-phenylene-bisporphyrin syntheses

The synthesis route *via* the bromo-porphyrin precursors enables the incorporation of the *o*-formyl-phenylene substitution without the need for a second mixed condensation reaction described in the literature.[175, 206, 216] Therefore, a *Suzuki* cross-coupling reaction with 2-formylphenyl-boronic acid as the coupling partner catalyzed by $Pd(PPh_3)_4$ in the presence of K_3PO_4 as a base in THF under reflux was applied (Scheme 34).[217]

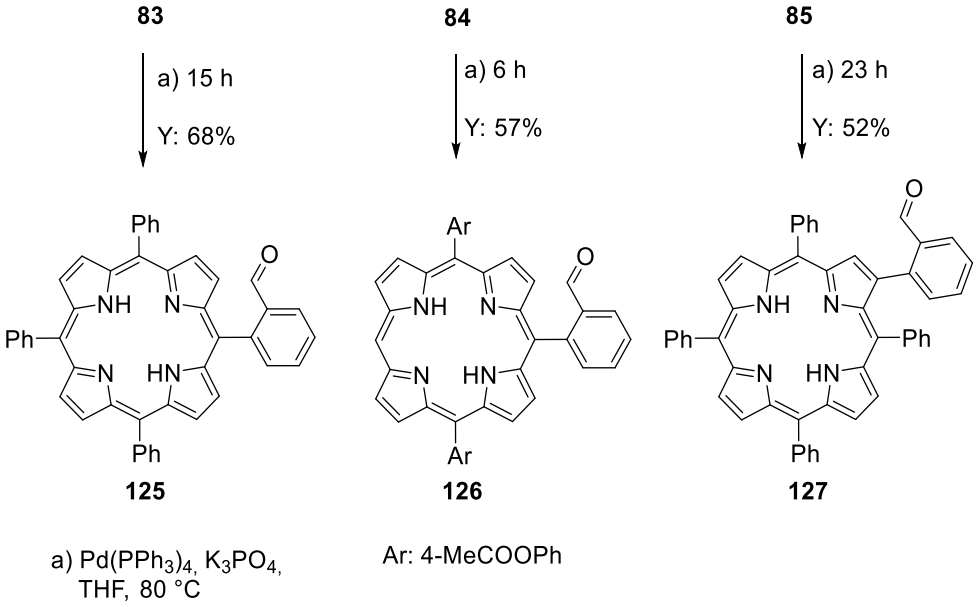

Scheme 34: *Suzuki* cross-coupling reaction to synthesize the 2-formyl-phenyl precursors of the three ligands.

This method makes asymmetric cofacial porphyrin dimers with one free meso-position, as exemplarily shown for **126**, available. On top of that, *β*-bromination of one of the pyrrole carbons allows introducing the linker moiety in *β*-position, which is intrinsically impossible *via* conventional mixed condensation reactions.

This robust methodology provides the above shown monomeric precursors in an overall yield of **125**: 26%, **126**: 12% and **127**: 28%. Single-crystal X-ray diffraction was successfully measured for the 5,15-(4-ethoxycarbonyl-phenyl)-porphyrin **126**, confirming the aldehyde functionality in *o*-position is tilted by 90° concerning the porphyrin core **126**, confirming the aldehyde functionality in *o*-position is tilted by 90° concerning the porphyrin core (Figure 26). This allows space for the incorporation of a second porphyrin moiety by condensation reaction.

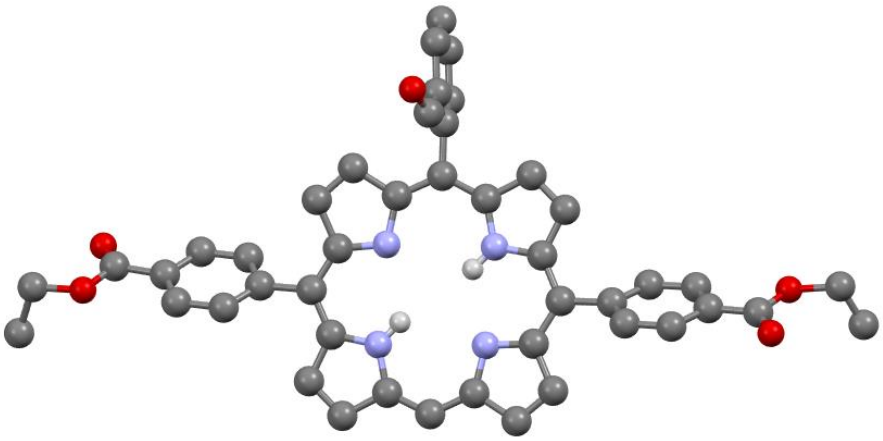

Figure 26: Single-crystal X-ray analysis of compound **126** measured and analyzed by Dr. Martin Nieger.

The aldehyde groups of **125**, **126** and **127** can now participate in the subsequent mixed condensation reaction with pyrrole and benzaldehyde in a ratio of (1:4:3) catalyzed by either TFA or $BF_3 \bullet OEt_2$ (Scheme 35).

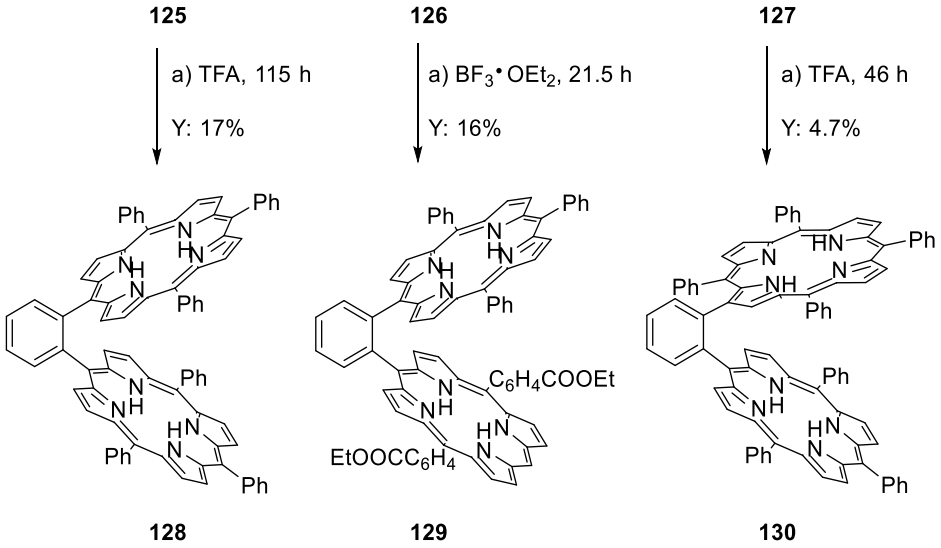

Scheme 35: Concluding mixed condensation reaction to the three cofacial ligands **128**, **129** and **130**.

Decisive is the successive addition of pyrrole and benzaldehyde beyond the theoretical optimal ratio until the reaction progress (consumption of the starting material), monitored by TLC, comes to a standstill. Thus, TPP **32** is formed due to less steric encumbrance and can be separated as the first purple fraction during flash column chromatography on silica gel. These findings underline the assumption that the more sterically hindered porphyrin trimers were not formed following the described methodology.

The final condensation reactions yield the above presented cofacial porphyrin dimers: *o*-phenylene bisporphyrin (OBBP) **128**, ethoxycarbonyl-*o*-phenylene bisporphyrin (EOBBP) **129** and *β-meso-o*-phenylene bisporphyrin (BMOBBP) **130**. For the symmetric OBBP case **128**, the yield can be improved significantly from 0.65%[206] or 0.30%[218] to 4.4% over six steps (i.e., by at least a factor of 6.8). The asymmetric compounds can be synthesized in 1.9% and 1.3% yield *via* only five or three steps. Whereas the concluding mixed condensation of **128** and **129** rank above the yields achieved in the literature, the yield of compound **130** is rather low. The low yield is a sterical issue of the packed *β*-substituted TPP analog and a more complicated purification due to higher basicity originating from the closer stacked porphyrin planes. The high basicity was assumed because the originally red *β-meso* porphyrin stack turned green by loading it on the silica surface of the column. The rather acidic conditions of the silica gel led to the protonation of one of the tertiary amines. The resulting charged nature of the compound influences the π-electron system and manifests in green color.[87]

Note that for the comparable 1,2 biphenylene bridged porphyrin dimer, *Osuka et al.* could show by X-ray crystallography that the molecule comprises a near-parallel, cofacial porphyrin ring arrangement with a dihedral (twist) angle of 6.6° (Figure 27).

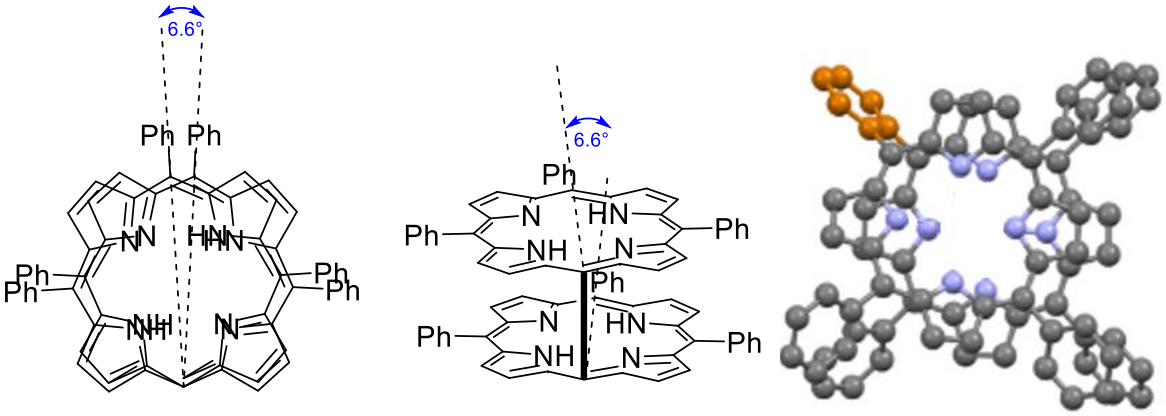

Figure 27: Definition of the dihedral angle of *o*-phenylene-linked porphyrins.

Since no crystal structure could be obtained for X-ray diffraction, no statement on the 3D structure of the ligands **128**, **129** and **130** can be made. For that reason, DFT calculations were carried out, which show similar cofacial benzene-linked porphyrin planes with dihedral angles between the porphyrins by way of the linker benzene hinge of 10.0° (OBBP), 0.1° (EOBBP) and 2.2° (BMOBBP), respectively.

3.3.2 Homobimetallic *o*-phenylene-linked porphyrin complexes

The synthesized ligands were double metalated with six transition metals and two main group elements (Scheme 36) and subsequently investigated using ion mobility spectrometry (IMS) and DFT calculations.

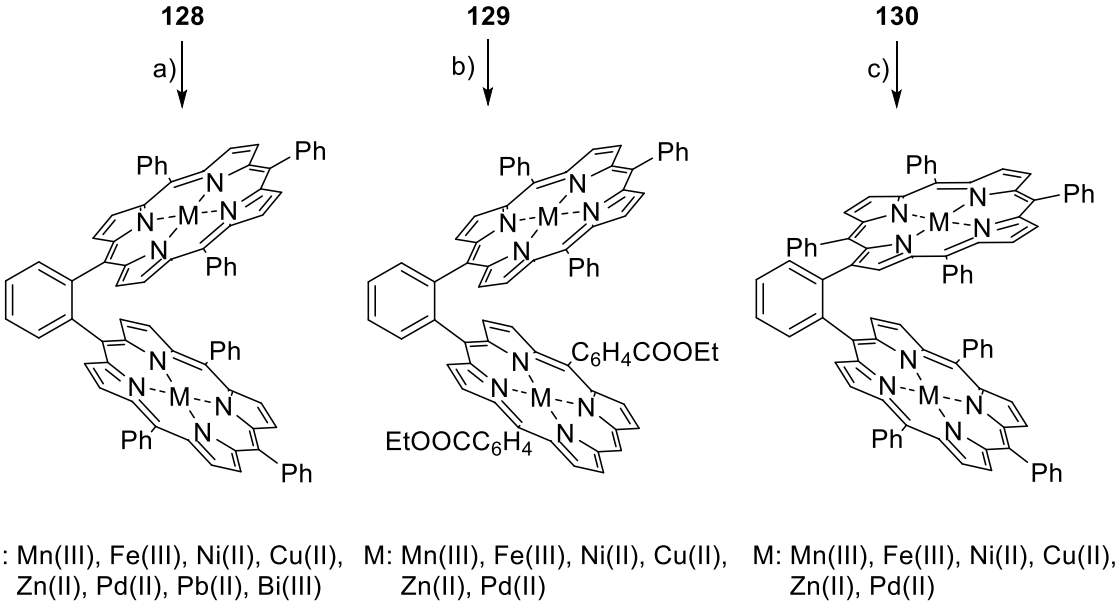

Scheme 36: Porphyrin-based homobimetallic complexes a) (**131**) *Mn(III): $MnCl_2$, DMF, 150 °C, 2h, 86%; (**132**) **Fe(III): $FeBr_2$, HCl, DMF, 140 °C, 1 h, 93%; (**133**) Ni(II): $Ni(acac)_2$, DMF, 100 °C, 19.5 h, 86%; (**134**) Cu(II): $Cu(OAc)_2$, $CHCl_3$/MeOH, 80 °C, 2 h, 93%; (**135**) Zn(II): $Zn(OAc)_2$, $CHCl_3$/MeOH, r.t., 1 h, 72%; (**136**) Pd(II): $PdCl_2$, DMF, 100 °C, 19.5 h, 69%; (**137**) Pb(II): $Pb(OAc)_2$, DMF, 170 °C, 48 h; (**138**) ***Bi(III): $BiBr_3$, DMF, 170 °C, 48 h; b) (**139**) *Mn(III): $MnCl_2$, DMF, 150 °C, 22 h, 73%.; (**140**) **Fe(III): $FeBr_2$, HCl, DMF, 140 °C, 2 h, 93%; (**141**) Ni(II): $Ni(acac)_2$, DMF, 100 °C, 2 h, 96%; (**142**) Cu(II): $Cu(OAc)_2$, $CHCl_3$/MeOH, 80 °C, 1 h, 90%; (**143**) Zn(II): $Zn(OAc)_2$, $CHCl_3$/MeOH, 80 °C, 1 h, 99%; (**144**) Pd(II): $PdCl_2$, DMF, 80 °C, 20 h, 98%; c) (**145**) *Mn(III): $MnCl_2$, DMF, 130 °C, 15.5 h, 79%.; (**146**) **Fe(III): $FeCl_2$, DMF, 150 °C, 14 h, 87%; (**147**) Ni(II): $Ni(acac)_2$, DMF, 150 °C, 5 h, 76%; (**148**) Cu(II): $Cu(OAc)_2$, DMF, 60 °C, 4 h, 93%.; (**149**) Zn(II): $Zn(OAc)_2$, $CHCl_3$/MeOH, r.t., 1 h, 95%; (**150**) Pd(II): $PdCl_2$, DMF, 100 °C, 3 h, 99%. * has been obtained with two coordinated chlorides at the manganese centers; ** has been obtained as μ-oxo complex, ***: has been obtained with two coordinated bromides at the bismuth centers.

In sum, 20 cofacial homobimetallic complexes could be synthesized and characterized by the new method, out of which 18 compounds were literature unknown. Additionally, single-crystals were obtained of the Ni(II) complex **141** shown in Figure 28, representing the first unsymmetrical cofacial benzene-linked metalloporphyrin dimer.

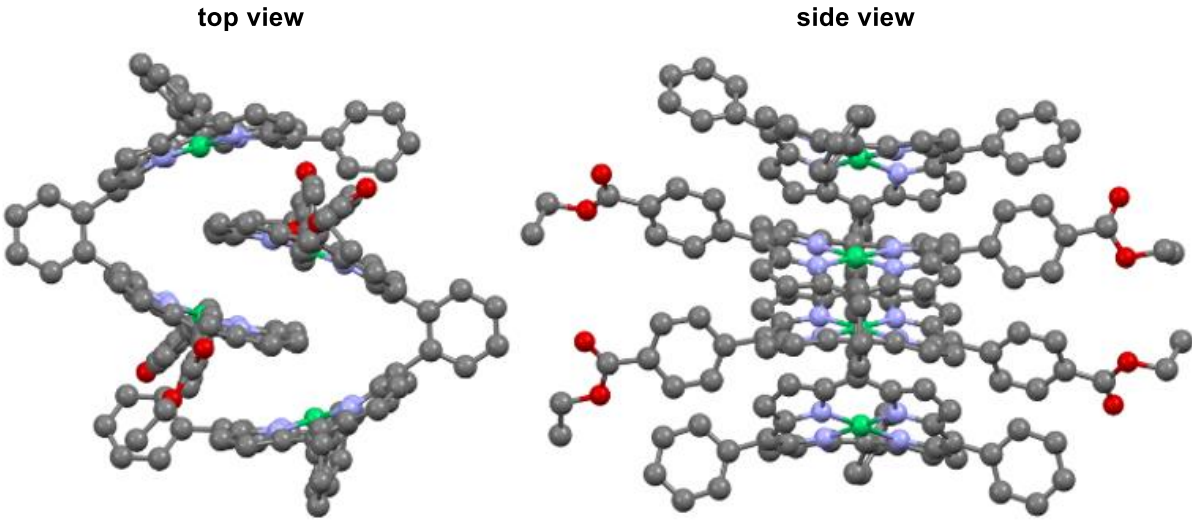

Figure 28: Single-crystal X-ray structure analysis of 2Ni(II)EOBBP **141** measured and analyzed by Dr. Martin Nieger.

The lack of a phenyl ring opposite the backbone of one porphyrin subunit per porphyrin dimer enables the intermolecular π-stacking.

Interestingly, the X-ray diffraction measurement of the single-crystal shows two crystallographic independent but identical molecules in the asymmetric unit. The respective chiral space group is $P2_1$ ("Sohncke space group") but crystallized as a twin containing both enantiomers. **141** was refined as an inversion twin with BASF = 0.38(2) (Hooft's y-parameter) y = 0.39(1)[219]. Therefore, the abundance ratio between the two enantiomers in the measured crystal was approx. 62:38. The unit cell of 24 contains two crystallographic independent molecules with identical chirality in an asymmetric unit (see least-squares fit (L.S.-fit) in section 6.9, which resembles two "Pac-Mans" biting each other). The missing phenyl ring opposite to the backbone of one of the two porphyrins enables this great packing, which disables direct dispersion interactions between the intramolecular porphyrin planes (in contrast to the system by *Osuka et al.*[175]). Fewer sterically demanding peripheral substituents might enable the collapse into a cofacial structure with a significantly strained 1,2-biphenylene link in the crystalline solid. An interdigitated arrangement obtained for **141** can also overcome the difficulties of growing single-crystals of enantiomeric mixtures, which has been problematic in the past. Note, that the interdigitated structure in solid-state does not have to correspond to the situation in liquid (or gas phase), which can be proven later in the more detailed IMS analysis. Due to that, statements regarding the metal-metal distances in the solution cannot be deduced. Additionally, the chiral conformers are only distinguishable in solid-state since the low interconversion barrier leads to averaging the dihedral angles between the porphyrin planes. Nonetheless, all three derivatives are chiral due to their planar chirality based on the unsymmetrical linkage to the linker benzene moiety.

3.3.3 Heterobimetallic *o*-phenylene-linked porphyrin complexes

The following synthetic route was developed as a proof of principle reaction to achieve porphyrin-based transition metal-containing heterobimetallic complexes. As described in section 1.5.3, the tailor-made heterobimetallic complexes, as artificial active site analogs of enzymes, can simplify important information regarding working principles in nature. The developed synthetic approach is tested for its availability for a new facile route to an artificially synthesized carbon monoxide dehydrogenase active site analog containing Ni(II) and Fe(III)-cations. Ensuing to the *Suzuki* cross-coupling reaction, the monomeric porphyrin **125** was

treated with $Ni(acac)_2$ at 150 °C for 4 h to obtain the Ni(II)-complex **151** in 71% yield (Scheme 37).

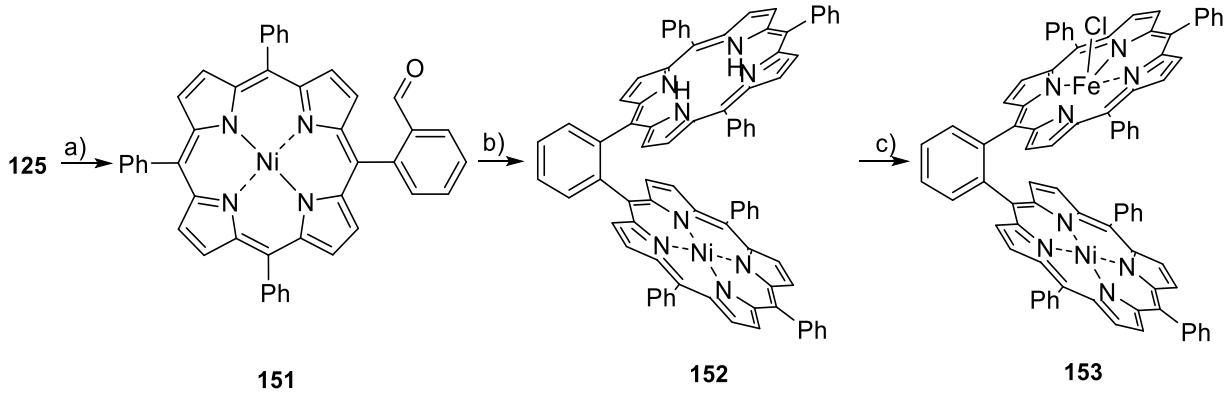

Scheme 37: Synthesis of the artificial carbon monoxide dehydrogenase active site analog (**153**) through a porphyrin building block on the monomeric Ni(II)-containing porphyrin (**151**) and subsequent insertion of Fe(III) in the second porphyrin ring a) $Ni(acac)_2$, DMF, 150 °C, 4 h, 71% b) pyrrole, PhCHO, CH_2Cl_2, TFA, DDQ, r.t., 16 h, 15%, c) $FeCl_2$, DMF, 150 °C, 4 h, 95%.

The coordinated Ni(II)-cation can be proven by the missing NH protons and slightly increased coupling constants of the *β*-protons adjacent to the 2-formyl-benzene residue from ^3J = 4.8 Hz to ^3J = 5.0 Hz as seen in the corresponding ^{1}H NMR-spectra. Through a subsequently performed condensation reaction, the Ni(II)-2H *o*-phenylene-bisporphyrin **152** can then be obtained in a 15% yield. The ring current rising from the *π*-electrons of the Ni(II) containing porphyrin affects the free-base porphyrin in shifting the NH protons to –3.82 ppm, which is typical for cofacially-linked porphyrin dimers. The remaining free-base porphyrin in the complex **152** reacts with $FeCl_2$ in DMF at 150 °C for 4 h to incorporate Fe(III) as the second metal in 95% yield. The overall yield to obtain the first cofacial porphyrin-based heterobimetallic complex **153** is 2.2% starting from pyrrole and benzaldehyde as starting materials. This proves the robustness of the developed synthetic methodology.

Based on the results shown, the protocol was applied to further heterobimetallic combinations. While the Cu(II) complex **154** could be obtained quantitatively using $Cu(OAc)_2$ as a Cu(II) source in a mixture of $CHCl_3$/MeOH at 80 °C (Scheme 38), the commonly applied Pd(II) insertion *via* $PdCl_2$ failed and led to degradation of the porphyrin core. Based on the successful Cu(II) insertion reaction, $Pd(OAc)_2$ was applied and yielded the corresponding Pd(II) complex **155** in 80% yield, indicated by the disappearance of the NH signals in the high-field region of the ^{1}H NMR spectrum. For Pt(II) insertion, $PtCl_2$ had to be used under more forcing conditions employing high temperature or microwave irradiation had to be applied, which can be problematic with functional groups like the formyl-functionality.[220] Therefore, **125** was treated with $PtCl_2$ in benzonitrile under reflux for 1 h. However, near-instant after reaching the reflux conditions, the color changed from red to green, indicating that degradation of the ligand is the main reaction channel.[221] Since the aldehyde-functionality cannot be exposed to elevated

temperatures, reactions in MeCN at 86 °C,[222] dry toluene at 120 °C[223] and chlorobenzene at 140 °C[224] were carried out. While for the first solvent, no conversion was observed after one week. For the two latter, a color change to black was noticed. The corresponding TLC attested product formation indicated an orange spot with a lower R_f value than the starting material. Additionally, significantly fewer by-products were observed in toluene and yielded the product **156** in 32%. Moreover, single-crystals were obtained (Figure 29), proving the tremendous flexibility of porphyrin ligands using coordinating the 5d metal Pt(II) in the same square-planar fashion as can be seen in the previously presented Ni(II) X-ray structure analysis. Furthermore, UV-Vis spectra were recorded from the obtained metal complexes as represented in Scheme 38.

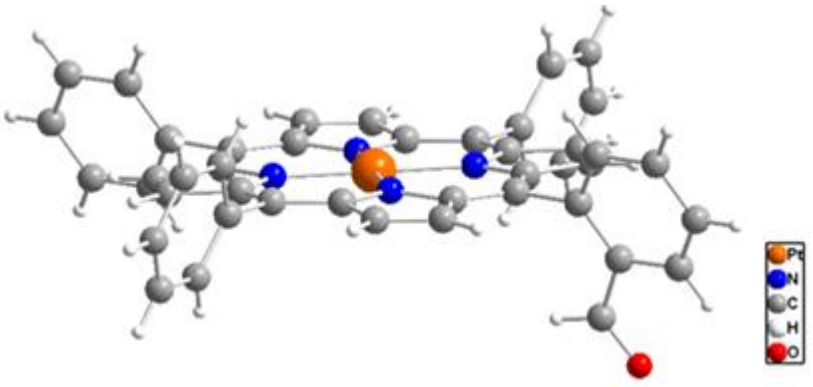

Figure 29. Single-crystal X-ray analysis of Pt(II)-formyl-phenyl-porphyrin **156** measured and analyzed by Dr. Martin Nieger.

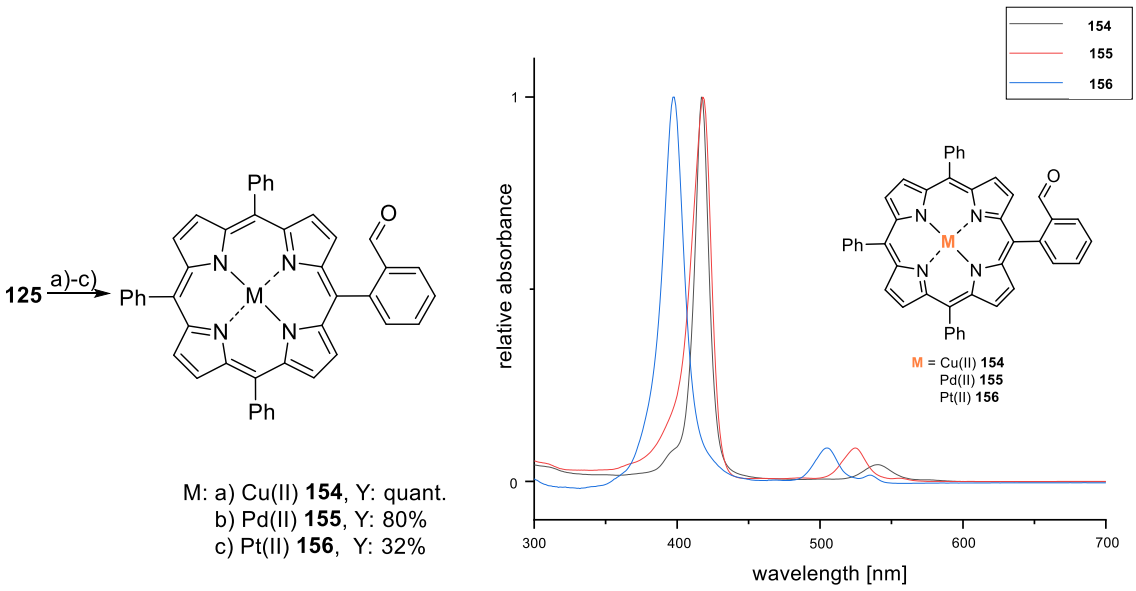

Scheme 38: Synthesis of the Cu(II)-, Pd(II-) and Pt(II)-formyl-phenyl-porphyrin precursors: a) $Cu(OAc)_2$, $CHCl_3$, MeOH, 80 °C, 30 min; b) $Pd(OAc)_2$, $CHCl_3$, MeOH, 80 °C, 5 min; c) $PtCl_2$, toluene, 120 °C, 14 h. Comparison of the UV-Vis absorption bands of **154**, **155** and **156**.

The *Soret*-band of the copper porphyrin **154** is comparably sharp, rising at *circa* 417 nm, causing the red color. The *Soret*-band of the platinum porphyrin is significantly blue-shifted, leading to shiny orange color on a macroscopic scale. Pd(II) as 4d metal ion shows absorption bands that intersects both other *Soret*-bands and thus appear in dark orange.

The difference of the *Soret*-band of a metalloporphyrin *vs*. a free-base porphyrin can be explained by an overlap of the porphyrin's HOMO and the atomic orbitals of their coordinated metal ion. That leads to a larger energy gap between the exited and the ground state and a shorter absorption wavelength.[225] The variation of the size of the in-plane coordinated metal ions is negligible for both Cu(II) and Pd(II) cases, but for the Pt(II) case, a critical value, which seemed to be exceeded, leading to a larger shift, even though the square-planar coordination sphere remains as indicated by the above-depicted X-ray structure. The Q-bands are affected more significantly, originating from the higher perturbations of the respective atomic orbitals for the porphyrins MOs.[225]

According to the procedure described above, the mixed condensation was successful, affording the monometallic ligands (Cu(II)2NH **157**, Y: 15%, Pd(II)2NH **158**, Y: 18%, Pt(II)2NH **159**, Y: 5.0%) (Scheme 39). The addition of TFA is crucial, although it was observed that a too large amount of TFA did not lead to product formation but rather the degradation of the starting material.

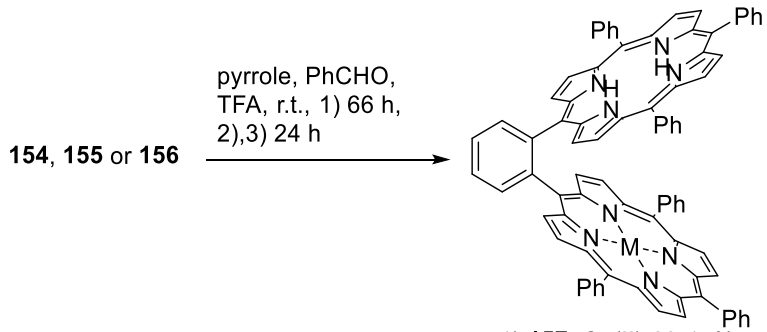

Scheme 39: Mixed condensation reactions to yield the monometallic cofacial porphyrin ligands.

At last, Fe(III) was coordinated in the monometallic ligands by refluxing it with $FeCl_2$ in dry DMF. Besides the commercially available $FeCl_2$, $^{57}FeCl_2$ was synthesized by dissolving ^{57}Fe in concentrated, degassed aqueous HCl for 3 days under sonication (Scheme 40).

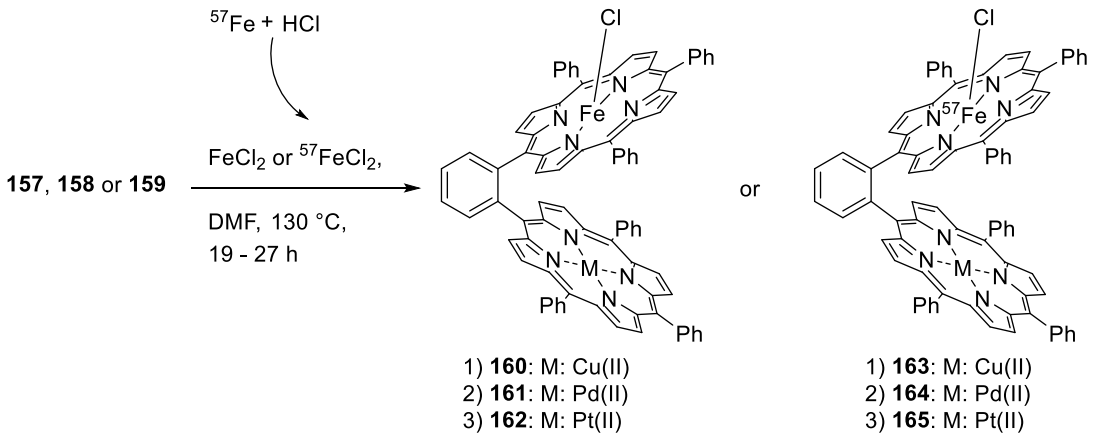

Scheme 40: Fe(III) and ^{57}Fe(III) insertion into the remaining freebase porphyrin, yielding Fe(III)-based heterobimetallic complexes.

The yields could not be determined due to an observed exchange of the ancillary ligand to, e.g., OH^-. The ^{57}Fe complexes were applied in *Mössbauer* spectroscopy and will be discussed in section 3.3.5.

To prove that further heterobimetallic complexes besides Fe(III) can be synthesized, $MnCl_2$ was stirred with the Cu(II)2NH-OBBP **157** in DMF at 150 °C for 2 h to yield the Mn(III)Cu(II) complex **166** in quantitative yield (Scheme 41).

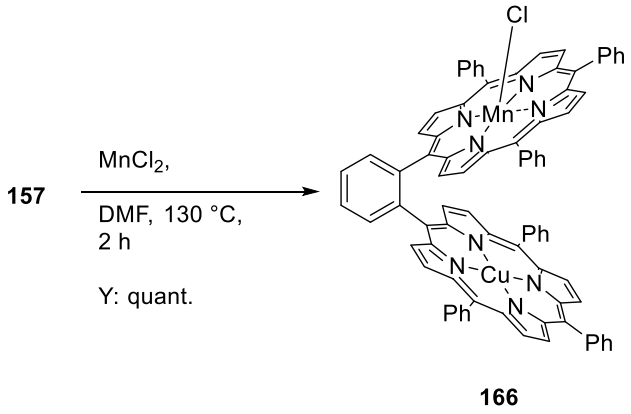

Scheme 41: Synthesis of the heterobimetallic Mn(III)Cu(II)-*o*-phenylene bisporphyrin complex **166**.

In summary, one can expect this protocol to be suitable for many other analogous homo- and heterobimetallic complexes, which can find multiple applications in fields ranging from magnetism/spintronics, catalysis and optical sensors. Furthermore, the impact of cooperative interactions between (different) spatially proximate metal ions is of fundamental interest, e.g., for enzymatic reactivity *in vivo*.

3.3.4 Structure determination and UV-Vis measurements of the OBBP metal-complexes

Whereas the complexes mentioned above have all been well characterized by MS, ^{13}C NMR, ^{1}H NMR, UV-Vis- and IR-spectroscopy, their 3D structure could not be elucidated by X-ray diffraction due to the difficult crystallization of the complexes (except for the dimeric Ni(II) complex, see above). Furthermore, it is to expect that in solid-phase, packing effects and intermolecular interactions significantly disturb the rather delicate balance between π-stacking and *van-der-Waals* attraction of porphyrinic moieties on the one hand and *Coulomb* repulsion of the positively charged metal centers on the other hand. Therefore, a combination of quantum chemical calculations and ion mobility spectrometry (IMS) were done by Erik Karsten Schneider to gain access to at least some structural parameters of the corresponding isolated monocations, such as the average distance of the porphyrin rings. IMS is a gas phase method to determine an ion's collision cross-section (CCS), combined with MS.[226] This method relies on determining the drift time of an ion in an inert collision gas (typically He or N_2) guided by an external electrical field.

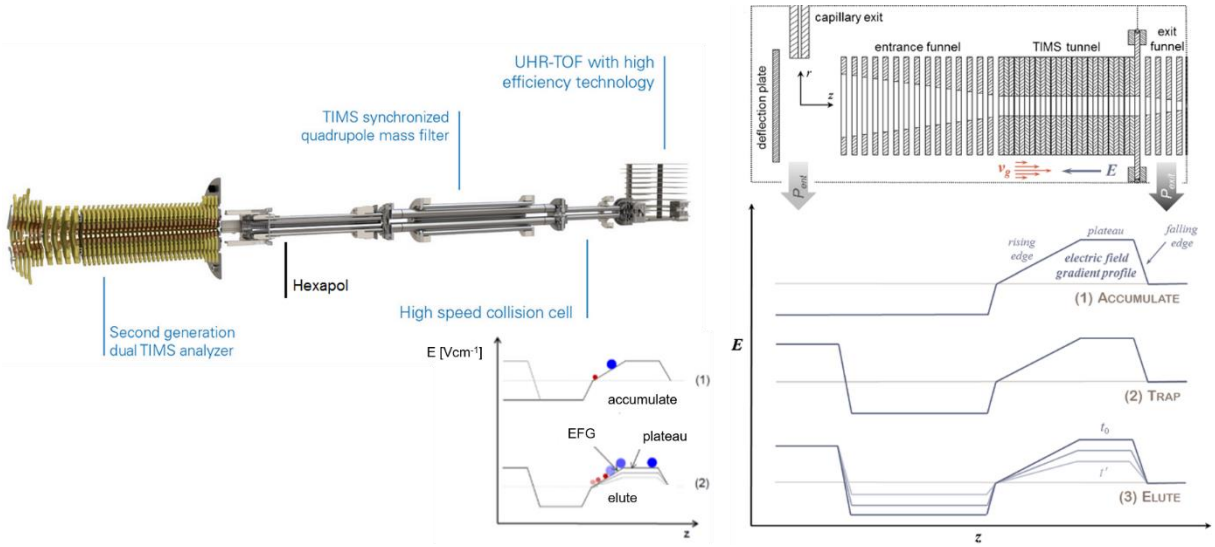

Figure 30: Schematic representation and working principle of an IMS-ToF mass spectrometer.[227-229]

As represented in Figure 30, the previously ionized compounds enter the Trapped Ion Mobility Spectrometry (TIMS) analyzer *via* the capillary exit and get deflected by the deflection plate (top-right). As a result, the charged ions enter the TIMS tunnel accompanied by a static, inert collision gas flow. An adjustable electric field gradient is applied opposite the gas flow, holding the ions fixed along the TIMS tunnel depending on their charge and CCS. During the first period, the ions accumulate (1) in the entrance funnel until the ion count is high enough and the static trap phase (2) starts. By decreasing the electric field gradient, the ions elute (3) at specific

times, with low charged ions with large CCS eluting first (Figure 30, bottom-mid). The downstream quadrupole filter, the collision cell and the ToF analyzer enable the measurement of high-resolution MS on previously separated isomers.

Recent progress improved IMS resolution and raised the method's importance for studies of proteins,[230] polysaccharides,[231] fullerenes[232] and can now provide an additional useful identification parameter in proteomics[233]. To characterize the *o*-phenylene bisporphyrin derivatives, measurements on a high-resolution variant of IMS, the Trapped Ion Mobility Spectrometer (TIMS) coupled with a ToF-mass spectrometer (timsTOF™, *Bruker*) were carried out. The more detailed operational mode of TIMS is reported elsewhere[229]. IMS enables to differentiate between isomers and conformers that differ in CCS by less than 0.5%. Besides isomer separation, measured CCS values can be used to validate structure predictions based on quantum chemical calculations (and collision gas scattering trajectory calculations) and thus obtain a first-order structural assignment by comparing the measurement with the calculated value. Therefore, a DFT-based geometry optimization for each porphyrin complex was performed (*Turbomole* package,[234] *BP-86* functional,[235, 236] *def2-SVP* basis set,[237] *Grimme D3-BJ* dispersion correction[238, 239]. The *Mulliken* algorithm calculated the partial charges and the CCS calculations were conducted with the *IMoS*-package.[240, 241] The coordinates of the 2Zn(II)-dimers **135**, **143** and **149** are reported elsewhere.[242] The optimization was performed for isolated cations without counter ions or solvation effects. Based on these optimized structures, the CCS values were calculated with the trajectory method. All measured CCS values for the covalently linked porphyrin dimers prepared in this study differ by less than 2% from the calculated values and are therefore in good agreement. Furthermore, all measured CCS values for the covalently linked porphyrin dimers prepared in this study differ by only a few percent from the value of $[(H_2TPP)_2+H]^+$. For that reason, the π-stacked TPP dimer fits well as a standard. The structures of non-covalently linked TPP-dimers are known from the literature.[243] Therefore, a scaling factor of 0.94 was determined which has been applied on the CCS and is listed as scaled CCS value. Note that the calculated CCS depends on both geometry and charge distribution as well as the estimated *Lennard-Jones*-parameters of the constituting atoms. The interplay between these factors is rather delicate and deviations of several percent between experimental and absolute theoretical CCS are not unusual. A common strategy to enable a better comparison to theory is to use a calibration molecule and contrast it with a well-studied internal standard with a similar structure in 3D, such as the cofacially stacked TPP dimer $[(H_2TPP)_2+H]^+$.

Table 1: Experimental ^{TIMS}CCS value and their scaled, theoretical counterparts as well as the deviation.

	Measured CCS [Å²]	Scaled CCS [Å²]	Deviation [%]
$[(H_2TPP)_2+H]^+$	354.2	354.2	standard
$[2Zn(II)\text{-}OBBP]^+$	334.9	329.7	1.6
$[2Zn(II)\text{-}EOBBP]^+$	360.5	362.1	-0.4
$[2Zn(II)\text{-}BMOBBP]^+$	352.2	345.6	1.9

Table 2: Experimental ^{TIMS}CCS values of the different porphyrin-dimers. The standard deviation indicated is the result of the two to four independent measurements.

	OBBP	EOBBP	BMOBBP	TPP-Dimer
Central Atoms	$^{TIMS}CCS_{N2}$ [Å²]	$^{TIMS}CCS_{N2}$ [Å²]	$^{TIMS}CCS_{N2}$ [Å²]	$^{TIMS}CCS_{N2}$ [Å²]
$2H_2+H$	339.7 ± 0.2	365.9 ± 1.2	350.3 ± 0.4	354.2 ± 0.5
2Mn(III)+Cl	345.8 ± 0.8	370.3 ± 0.1	357.8 ± 0.1	
2Fe(III)+O	338.1 ± 0.4	362.7 ± 1.3	347.8 ± 0.4	
2Ni(II)	337.5 ± 0.4	362.4 ± 0.6	351.0 ± 0.7	
2Cu(II)	336.1 ± 0.4	363.8 ± 1.1	350.8 ± 0.1	
2Zn(II)	334.9 ± 1.2	360.5 ± 0.7	352.2 ± 0.3	
2Pd(II)	335.5 ± 0.1	361.8 ± 1.9	348.7 ± 1.1	
$Ni(II)H_2+H$	338.0 ± 0.1			
Ni(II)Fe(III)	335.5 ± 1.2			

After applying this scaling factor to the theoretical CCS of $[2Zn(II)\text{-}OBBP]^+$, $[2Zn(II)\text{-}EOBBP]^+$ and $[2Zn(II)\text{-}BMOBBP]^+$, a deviation between theory and experiment of below 2% was reached (see Table 1 for details). Therefore, the found DFT geometries are similar to the actual structures in the gas phase for all investigated dimers.

As the three ligands arrange in the CCS dependence: OBBP < BMOBBP < EOBBP, the complexes with divalent metal centers (Ni(II), Cu(II), Zn(II), Pd(II)) show the same CCS, indicating that the nature of the complexed metal does not significantly influence the 3D structure (Table 2). The CCS of the trivalent Mn(III)-dimers, on the other hand, are systematically larger due to the additional Cl^- located between the respective metal atoms, which pushes the monomers of the calculated ionic structure further apart. The structure of Fe(III)-dimers binding oxygen is analogous as already known for a similar compound in the literature and is further discussed in section 3.3.5.[213]

Based on the DFT optimized structures of the Zn(II)-*o*-phenylene-bisporphyrin with trends validated by TIMS measurements, decreasing metal-to-metal distances from EOBBP **129** (3.276 Å) to OBBP **128** (3.243 Å) to BMOBBP **130** (3.207 Å) were observed (Figure 31). Since the obtained values correspond to the metal-metal separations of gaseous ions at 0 K, the absolute numbers do not necessarily describe the intramolecular metal-center separations in solution or the solid-state. However, it can be assumed that also for condensed phase environments, the trend towards decreasing metal center separation going from EOBBP **129** to BMOBBP **130** will remain unchanged.

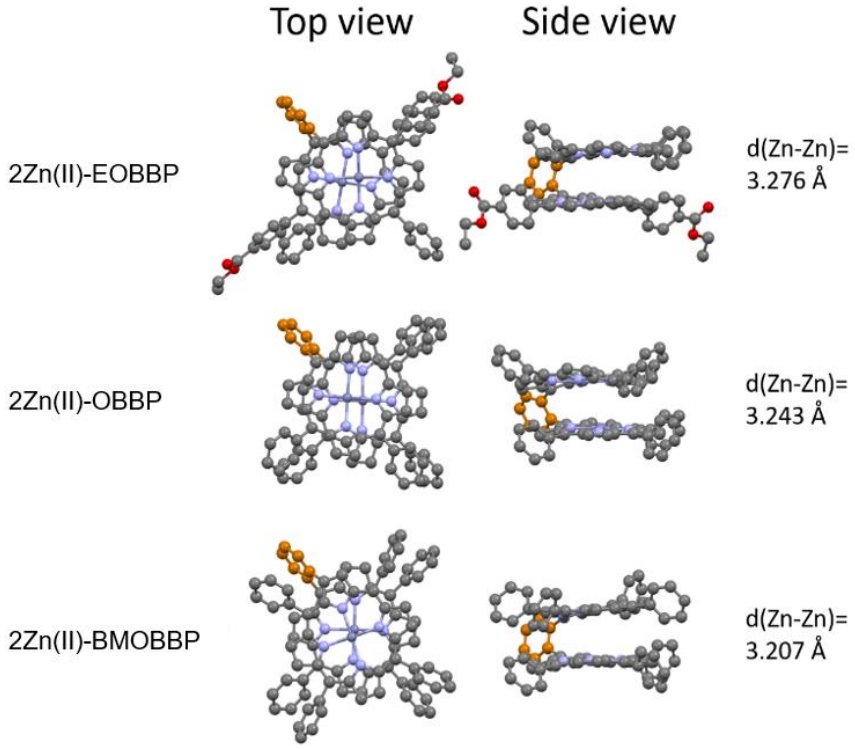

Figure 31: The DFT calculated structures of the 2Zn(II)-dimers in the top (left) and side view (right) with the calculated distance of the two Zn(II) cations in the dimer. The linking phenyl has been colored orange for clarity reasons.

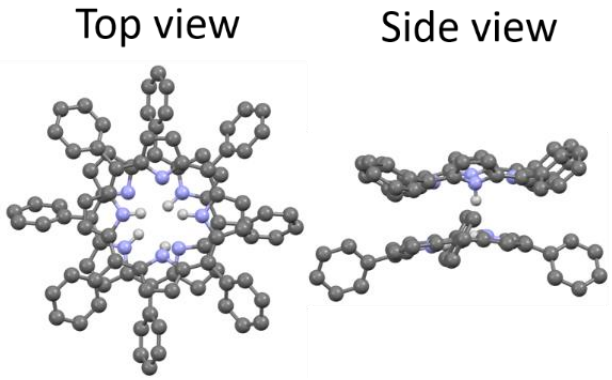

Figure 32: The DFT calculated structure of $[(2HTPP)_2+H]^+$ in top and side view. Only the H-atoms bound to N-atoms have been displayed for clarity reasons.

Interestingly, the sequence correlates with an upcoming shoulder (near 435 nm) in the *Soret*-band region of the UV-Vis spectrum (Figure 33). Furthermore, the UV-Vis spectrum of

[2Zn(II)-BMOBBP] **149** shows a broadened and a slight asymmetric *Soret*-band, which might indicate an additional absorption band.

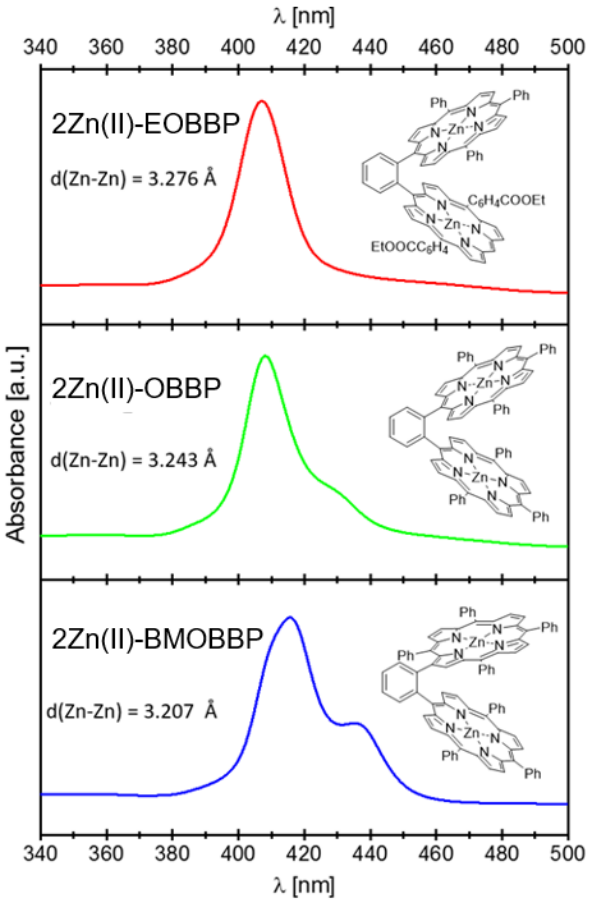

Figure 33: UV-Vis spectra of the different 2Zn(II)-dimers are shown. Both OBBP and BMOBBP show a second absorption band in the *Soret*-region that is red-shifted by roughly 20 nm compared to the band of the highest intensity. Additionally, the most intense band of BMOBBP is red-shifted by about 7 nm compared to OBBP. These shifts (and splittings) can be attributed to different distances between the Zn(II) cations.

These findings can be tentatively assigned to increased spatial π-interaction, stronger coupling between the chromophores as the intermetal separation decreases. Recently, *Jäger et al.* examined the changes in the Q-band absorption region of gaseous dimeric porphyrin ions induced by structural differences.[244] In the case of isolated 2Zn(II)-dimers, analogous shifts of Q-band peak maxima by up to 8 nm were reported.

This goes along with a previous related study by *Takai et al.*, who were able to show that increasing distances between the two monomers of a porphyrin-dimer also increases the reorganization energies associated with electron transfer processes between the chromophores, underlining that the distance can change the properties of porphyrin dimers and presumably higher oligomers as well.[245] Furthermore, *Bolze et al.* have shown that covalently linked dimers of Pd(II)-porphyrins and monomers of Pd(II)-porphyrins can differ drastically in their Q-Band absorption in terms of both wavelength and extinction coefficient (the *Soret*-region was not shown).[246]

The slight decrease of the metal center separation exemplarily for 2Zn(II)-EOBBP **143** and 2Zn(II)-OBBP **135** can be attributed to enhanced attractive interactions between proximal phenyls of the porphyrin dimers (whereas EOBBP lacks one of the corresponding phenyls). As indicated by the X-ray crystal structure, the interdigitated arrangement can, in part, occur in the condensed phase and in addition to that, lead to a median increase in metal-metal distance. Compared to 2Zn(II)-OBBP, the phenyls of the two porphyrin rings of 2Zn(II)-BMOBBP can be better intercalated. Thus, the separation of the metals can be reduced further due to less sterical hindrance. This goes along with the observed basicity in section 3.3.2 of the BMOBBP ligand.

A complementary approach to rigidly clamp two metal ions to each other was presented by *Nocera et al.* by exposing the cofacial Fe(III) dibenzofuran porphyrin to air. A crystal structure analysis of the 2Zn(II) *vs.* the Fe(III)–O–Fe(III) complex attested a Zn(II)–Zn(II) distance of 7.775 Å and the Fe(III)–Fe(III) distance in the μ-oxo complex reduces the distance to 3.504 Å.[213] Since no single-crystal X-ray analysis was possible for the synthesized Fe(III)-*o*-phenylene bisporphyrin derivatives, this complex was analyzed by *Mössbauer* spectroscopy.

3.3.5 Analysis of the ^{57}Fe complexes *via Mössbauer* spectroscopy

Mössbauer spectroscopy is generally used to sense the hyperfine interactions present at the nucleus of the *Mössbauer* active isotopes ^{57}Fe, ^{99}Ru, ^{119}Sn and ^{191}Ir. A recoil-free nuclear resonance of γ-radiation, the so-called *Mössbauer* effect, is the basis of this spectroscopy and was discovered by *Rudolph Mössbauer* in 1957.[247]

A *Mössbauer* spectrometer comprises a source, an absorber containing the sample and a detector. The γ-quanta with the defined energy of 14.4 keV are generated *via* radioactive ^{57}Co cores ($\tau_{1/2}$ = 280 days) necessary to study ^{57}Fe cores. The electron capture, also called ε-decay, converts the ^{57}Co cores into the more stable ^{57}Fe core as a proton to neutron transformation. This way, as depicted in red in Scheme 42, γ-quanta with a suitable wavelength can be generated.

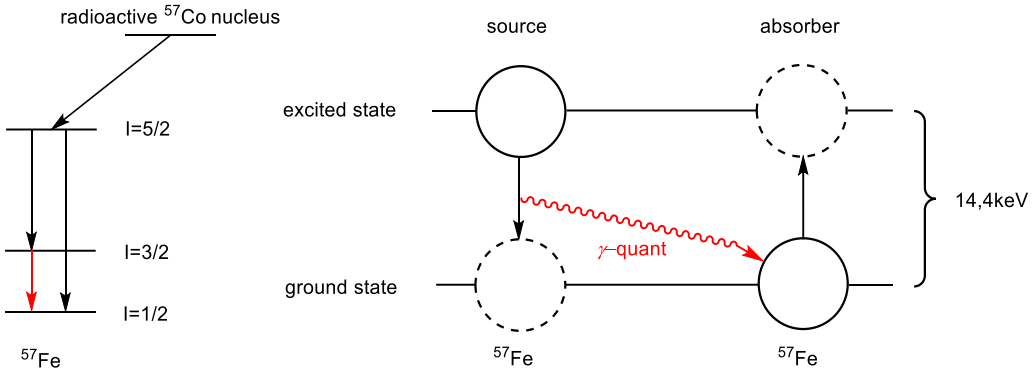

Scheme 42: Working principle of *Mössbauer* spectroscopy for the ^{57}Fe nuclei.

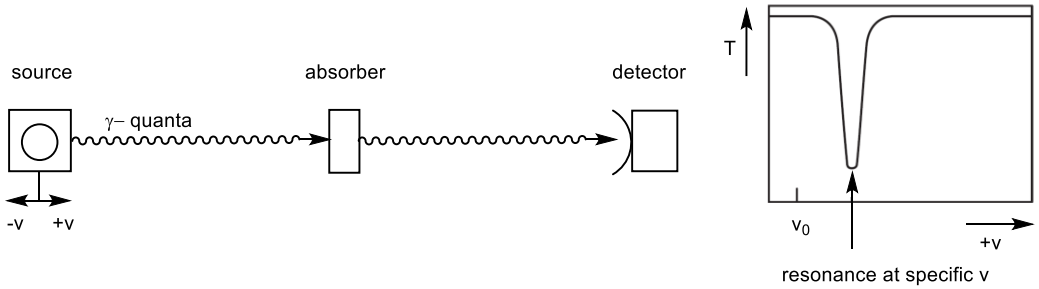

Scheme 43: General arrangement of the relevant units of a *Mössbauer* spectrometer.

The chemical surrounding of each ^{57}Fe core changes the energy of the γ-quantum necessary for resonance to occur by 10^{-8} – 10^{-7} eV. To swipe through this range, the *Doppler* effect is used to fine-tune the energy of the source. Therefore, the source is moved with a velocity of ±10 $^{mm}/_{s}$ to vary the energy of the γ-quantum (1 $^{mm}/_{s}$ equals $5 \cdot 10^{-8}$ eV). In the resulting spectrum, the transmission (T) is plotted against the velocity (v) of the source (proportional to the energy of the photon), as shown in the right part of Scheme 43.[248]

The local electronic environment and the other atoms around the *Mössbauer*-active nucleus can influence its properties and are generally divided into three types of interactions.

The isomer shift describes the electric monopole interaction and is proportional to the s-electron density at the ^{57}Fe nucleus, mainly the electron close to the core. Due to the orbital rearrangement in the excited state, the ground state and the excited state differ in energy. Typical Fe oxidation and spin states are depicted in Scheme 44 (green: less frequently; blue: more frequently observed), allowing a rough assignment of the respective oxidation and spin state and further the valency states, coordination, electronegativity of the ligand as well as the π-acceptor properties of the ligand, based on the isomeric shift range.[249, 250]

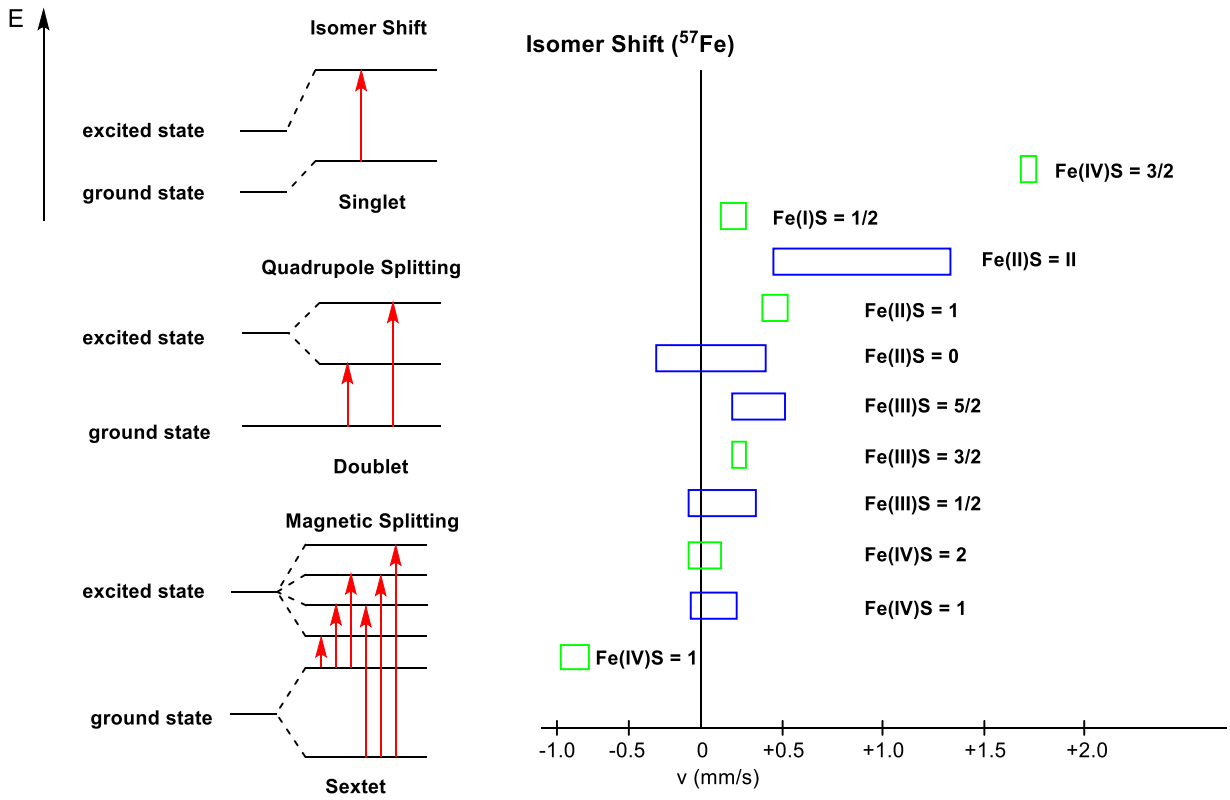

Scheme 44: Isomeric shift, quadrupole splitting and magnetic splitting of a *Mössbauer*-active nucleus + isomeric shift range of ^{57}Fe-nuclei.[250]

A quantum number of I > ½ is necessary for the electric quadrupole splitting since the core needs a non-spherical charge distribution that ends up in a nuclear quadrupole moment. The nuclear quadrupole moment interacts with an asymmetrical electric field and leads to a splitting according to the selection rules ($\Delta m_I = 0, \pm 1$) (quadrupole splitting). As a result, information about symmetry, space symmetry, valency states, coordination and ligand-field splitting can be deduced.

The magnetic hyperfine splitting (*Zeeman* splitting) is caused by an interaction of the magnetic dipole moment of the core and a magnetic field which results in 2I+1 states. The magnetic field can either be applied externally *via* a steady current in a coil or internally by unpaired electrons. Corresponding to the selection rule, six transitions are possible for ^{57}Fe leading to a sextet in the spectrum. As a result, magnetic splitting in the spectra gives information about ferromagnetism, ferrimagnetism and inner magnetic fields' strength. Furthermore, temperature-dependent measurements can determine the *Curie* temperature.[248, 249]

The Fe(III)–*μ*-oxo–Fe(III) *o*-phenylene bisporphyrin complexes **132** were investigated by *Mössbauer* spectroscopy (Figure 34).[250]

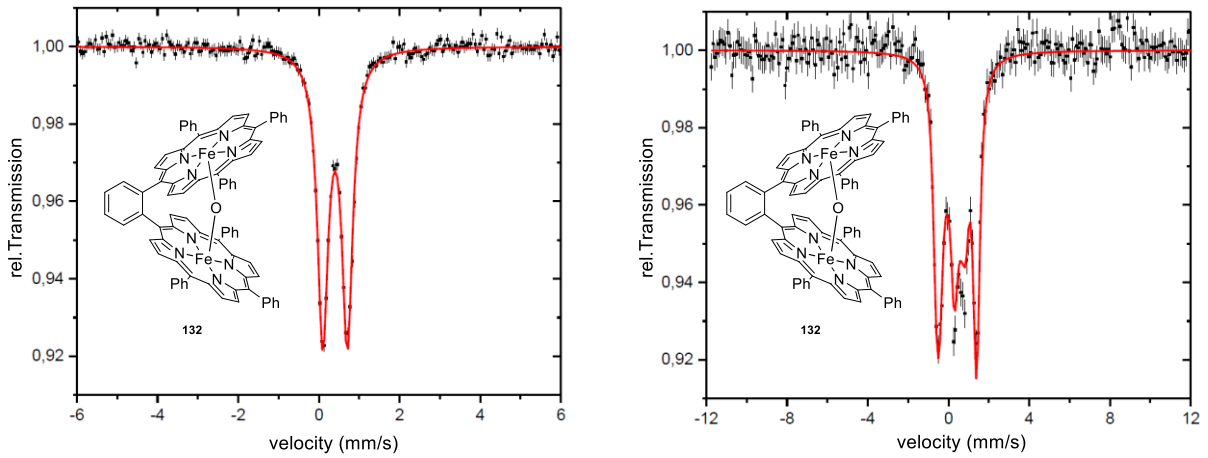

Figure 34: *Mössbauer* spectra of Fe(III)-O–Fe(III) porphyrin **132**; left: 77 K; right: 4.2 K and 5 T.

The left spectrum shows a typical isomeric shift of 0.2 $^{mm}/_{s}$ for a high spin (S = $^{5}/_{2}$) iron(III) component and its small doublet can be interpreted either as a fast occurring relaxation processes or as a diamagnetic compound.[251] Since a diamagnetic high-spin compound contradicts isolated Fe(III) centers, measurements at 4.2 K and a large external field were carried out. A diamagnetic iron species shows the splitting of the signals in the *Mössbauer* spectrum only due to the external magnetic field (Figure 34, right spectrum) since the spin of the diamagnetic compound is 0. The left spectrum was compared to a [octa-ethyl-porphyrin]Fe(II)-complex stabilized at an oxidation state +2 with 2-methylimidazol to guarantee its diamagnetic nature, which was also measured at 77 K, showing a similar doublet shape of the signal.[252] This can be explained by the additional splitting of the excited state of ^{57}Fe (I = $^{3}/_{2}$) evenly into two states. This causes a doublet with a distance depending on the size of the quadrupole splitting.

For the [octamethyltetrabenzoporphyrin]Fe(II) complex also analogs measurements at 4.2 K and 5 T were carried out, which also showed the additional fine splitting similar to the right spectrum of Figure 34.[253]

Taking all three properties that *Mössbauer* spectra can obtain into account, this proves the Fe(III)-*μ*-oxo-Fe(III)OBBP to be diamagnetic and suggests that both high spin iron(III) atoms couple antiparallel leading to a total spin of 0.

These results agree with the measured ^{1}H NMR spectrum that shows rather strong signals in the region of 15 – 12 ppm, instead of signals in 82 – 75 ppm in the ^{1}H NMR spectrum as reported for the pyrrolic protons of high-spin porphyrin-based Fe(III)Cl centers.[254]

As *Mössbauer* spectra of the Fe(III)-EOBBP **140** and BMOBBP **146** showed similar results, the heterobimetallic complexes could not be resolved well enough to gain detailed information to compare distance-dependent effects.

In summary, 20 different homobimetallic species containing the transition metals Mn(III), Fe(III), Ni(II), Cu(II), Zn(II), Pd(II), the main group elements Pb(II), Bi(III) and a selection of five heterobimetallic complexes were prepared and characterized, to give insights into their 3D structures and absorption behaviors.

In contrast, lanthanide and actinides porphyrin complexes are usually not coordinated in a square-planer or square-pyramidal coordination sphere but arranged in a square-antiprismatic manner. Therefore, the 3D structures are affected significantly and a new field of application can be evaluated.

3.3.6 Synthetic approaches towards intramolecular lanthanide complexes

An increased focus on lanthanide complexes arose due to their high coordination number and ability to undergo substitution reactions that provide binding sites for biomolecular coordinations.[255] Since most photosensitizers need to be activated by visible or UV light with poor tissue penetration, lanthanide- or other rare-earth-doped inorganic nanocrystals can circumvent that by acting as (photon-)upconverting nanoparticles (UCNP). Combined with a photosensitizer as the porphyrin scaffold, the UCNP can absorb two or more NIR photons and emit UV-Vis photons to sensitize the spatially close porphyrin subunit.[151, 152] This allows non-invasive NIR irradiation with deep tissue penetration *in vivo* combined with an improved signal-to-noise ratio and detection selectivity because of absent autofluorescence.[152]

As summarized by *Mironov et al*., multiple sandwich-like double-decker porphyrin-lanthanide complexes containing, e.g., La(III), Ce(IV) and Yb(III) are reported in the literature.[256] Since no intramolecular square-antiprismatic coordination of porphyrin metal complexes was literature known, the following two retrosynthetic approaches were examined (Scheme 45). While the upper OBBP approach allows for a rather flexible buildup of the second porphyrin subunit, the *β-meso*-porphyrin dimer provides a square-antiprismatic-like coordination sphere, as depicted in the right part of Scheme 45.

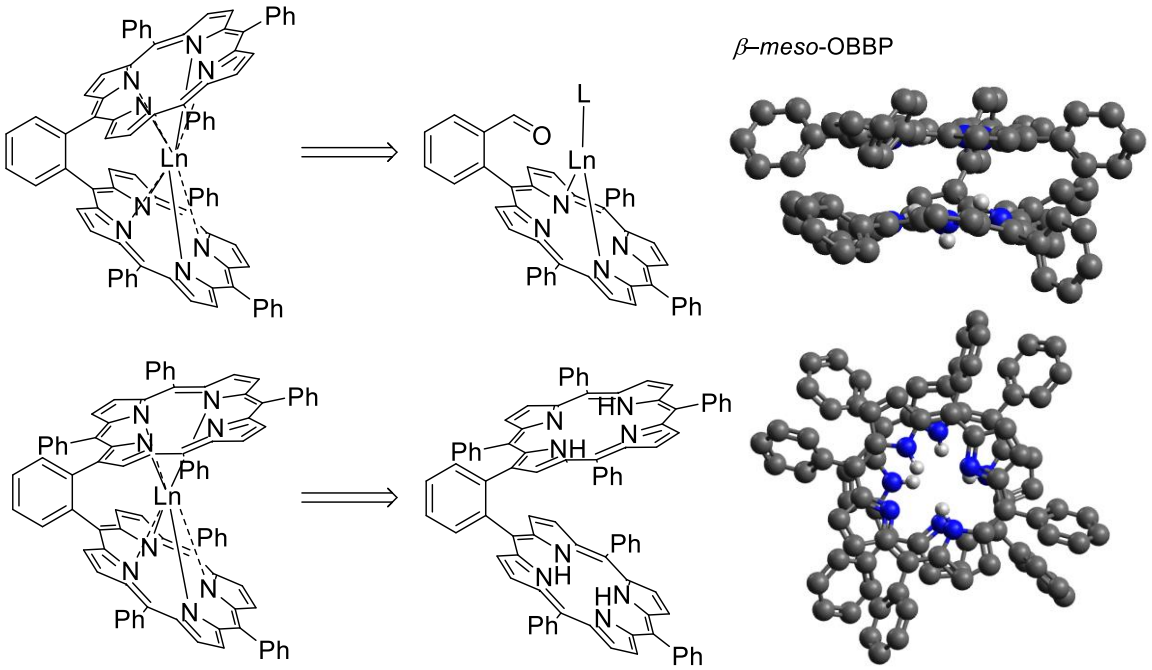

Scheme 45: Left: Retrosynthetic approach towards lanthanide-based sandwich porphyrins. Right: DFT calculation-based molecular structure of the BMOBBP **130**.

At first, the step-by-step approach *via* the monomeric formyl-phenyl porphyrin **168** using $Yb(acac)_3$ **167** as a metal salt was carried out (Scheme 46).

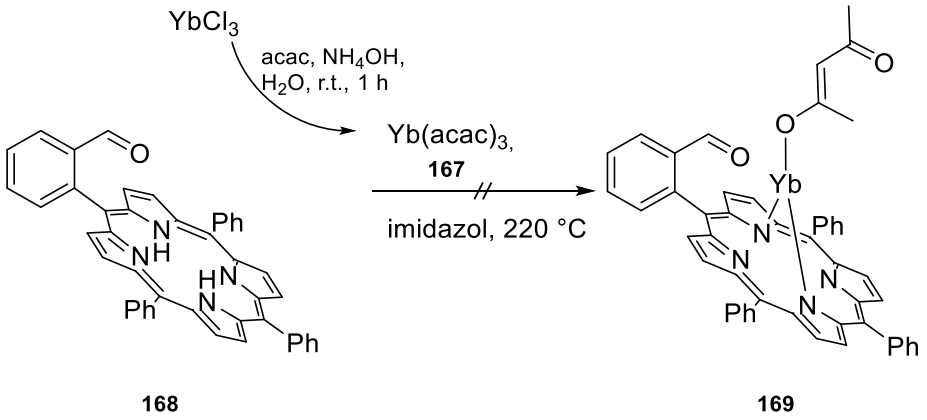

Scheme 46: Coordination of Yb(III) at the stage of the monomeric formyl-phenyl-porphyrin precursor **169**.

Therefore, the $Yb(acac)_3$ **167** was previously synthesized from $YbCl_3$ and applied in the subsequent complexation reaction dissolved in imidazole together with the ligand **168** at 220 °C (Scheme 46). As already found in section 3.3.3, larger metal ions often require the elevated temperature to be coordinated. The conditions to coordinate Ln-ions at this stage are unsuitable for the rather sensitive formyl group and were not further pursued. Additionally, adding the lanthanide chloride salts of La(III), Eu(III), Yb(III) and Lu(III) during the condensation reaction towards the second porphyrin subunit did not yield any desired product.

The *β-meso-o*-phenylene-bisporphyrin **130**, instead, can withstand very harsh conditions and delivers a square-antiprismatic coordination sphere (Scheme 45) so that the prebuilt dimeric ligand was attempted to be coordinated with Ln-ions surrounded by crystal water. None of the attempts using La(III), Ce(III), Sm(II), Eu(III), Tb(III), Yb(III), Lu(III) chloride salts yielded the desired lanthanide complexes as monitored by ESI-MS and only degradation and starting material was observed. One can conclude that the porphyrin planes are too tightly packed onto each other and therefore no intramolecular coordination can take place for the *β-meso*-OBBP case.

Since the DFT calculation described in section 3.3.4 at 0 K already suggests a dihedral angle between the porphyrin subunits of 10.0° for OBBP, the less packed porphyrin dimer was evaluated in lanthanide coordination reactions. Previously dried $Yb(acac)_3$ **167** was used to avoid hydrolysis to the rather unreactive $Yb(OH)_3$.[137]

Stirring the reaction mixture in 1,2,4-trichlorobenzene (+NaH) or imidazole at 220 °C showed the formation of a red spot on TLC (Scheme 47).

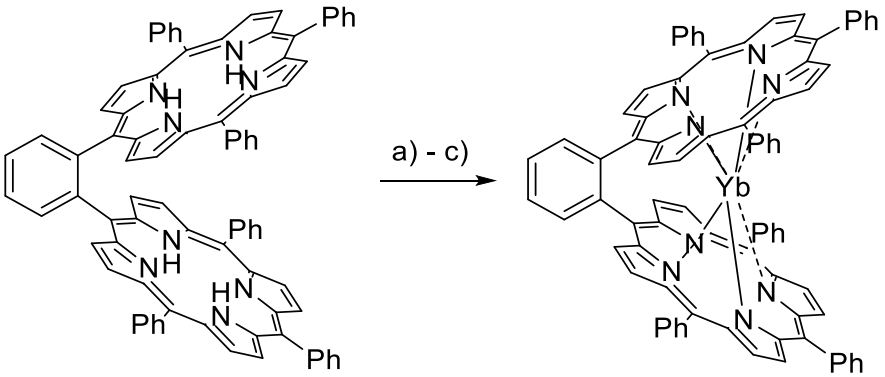

Scheme 47: Insertion approaches of Yb(III) into OBBP **128**. a) $Yb(acac)_3$, 1,2,4-trichlorobenzene, 220 °C, b) $Yb(acac)_3$, imidazole, 220 °C, c) $Yb(acac)_3$, NaH 1,2,4-trichlorobenzene, 220 °C.

An ESI-MS spectrum of this fraction was recorded, showing the M+2H mass of **170**. A deeper study of the remaining peaks containing the Yb-typical isotope pattern can underline well the sitting atop Yb(III) complexes **171** – **173** as represented in Figure 35.

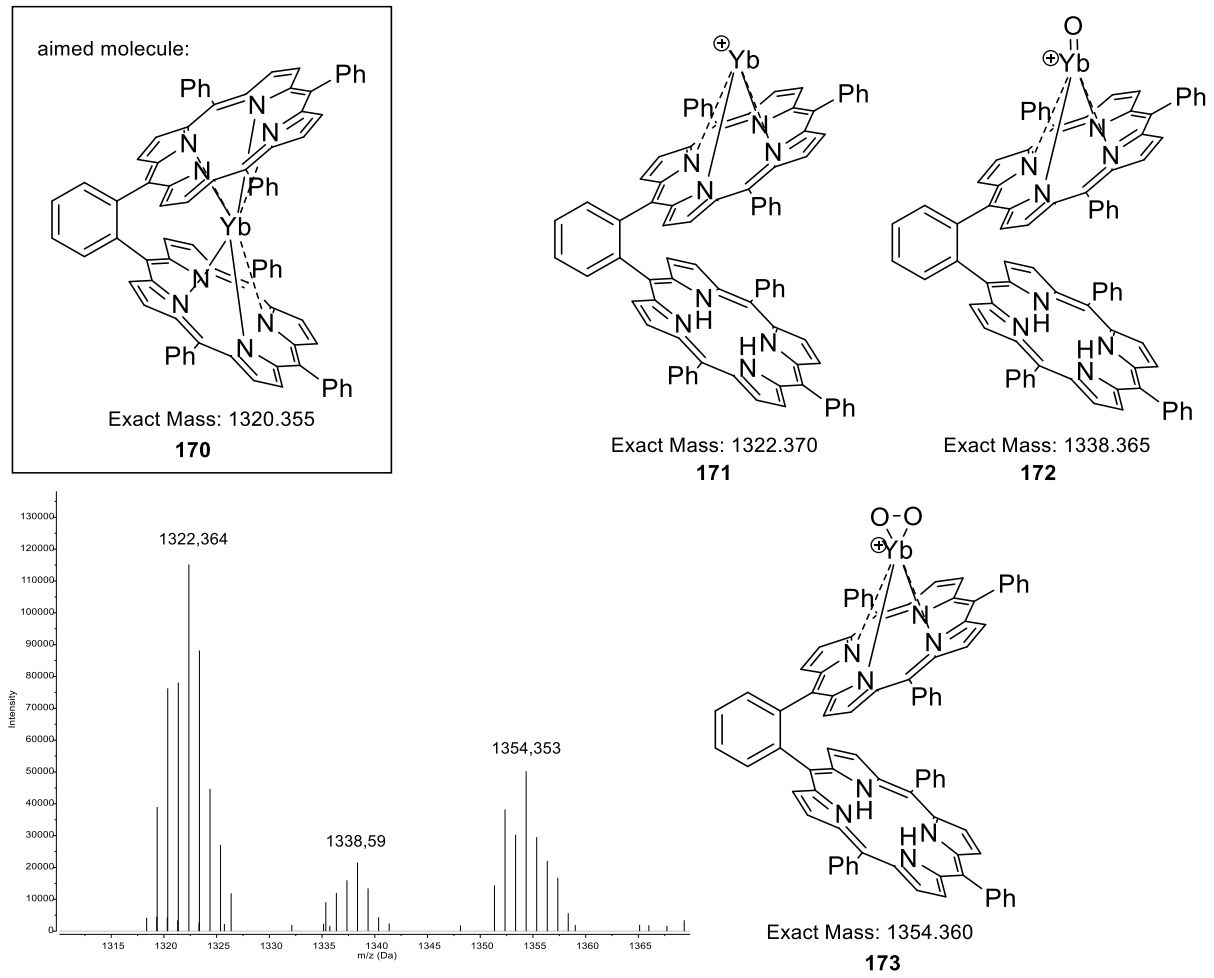

Figure 35: Measured ESI-MS spectrum and the assignment to Yb(III)-based molecular structures **171** – **173**.

Since only fragments of M^+ were found, the higher mass region of the ESI-MS spectrum was investigated further (Figure 35).

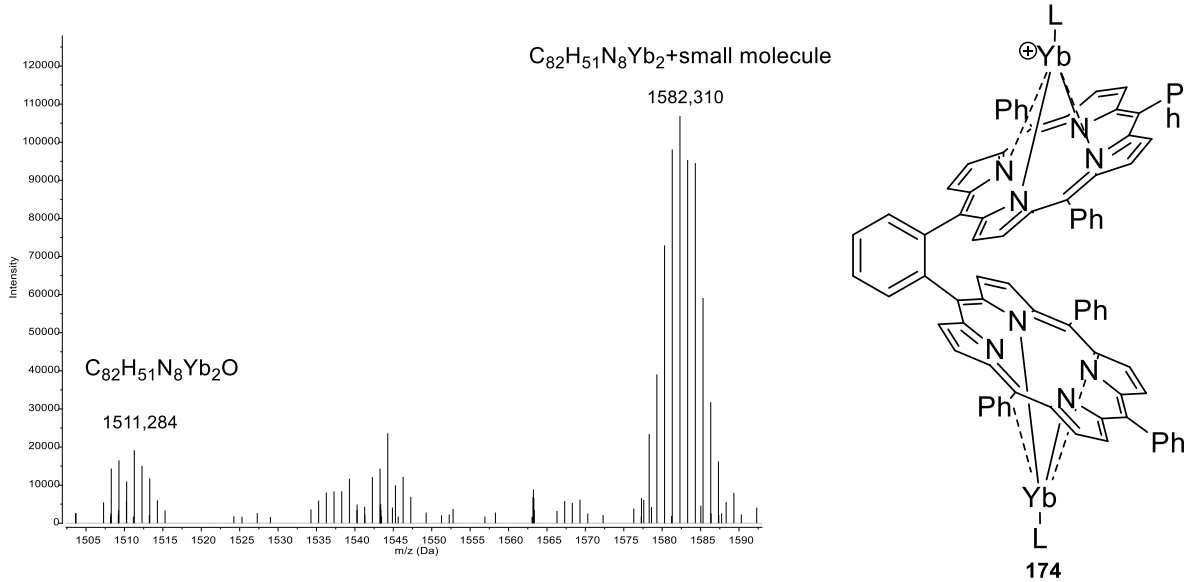

Figure 36: Measured ESI-MS spectrum and assignment to double coordinated Yb(III) porphyrin dimers.

The pattern of the two visible signals can be reasonably explained by adding a second Yb-ion to the sum formula. While the exact mass fits well for the Yb_2O species, the exact molecular formula for the 1582.310 *m/z* peaks cannot be finally determined. Nevertheless, CID experiments could prove that a labile molecular adduct is most likely present due to a less energy demand for the fragmentation.

Even though the structure could only be determined roughly, these complexes fit perfectly to the requirements for a possible novel type of PDT drug. A Yb(III) doped surface of the UCNP could directly coordinate the dimeric porphyrin, as depicted in Figure 37.

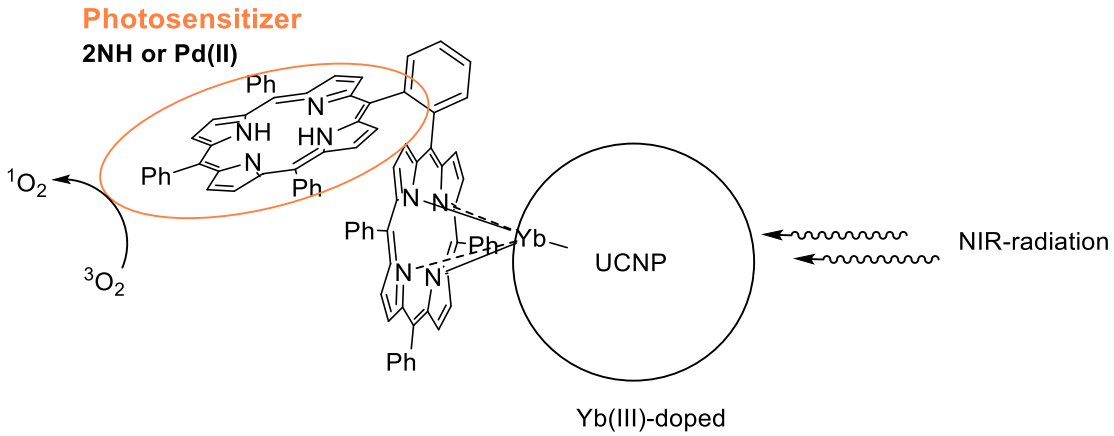

Figure 37: An *via* Yb(III)-coordination connected UCNP-porphyrin-dimer conjugate for photodynamic therapy (PDT).

In principle, NIR-radiation can be upconverted *via* the Yb(III)-doped inorganic crystal, sensitizing the remaining free-base or Pd(II) porphyrin efficiently *via* spatial overlap of the porphyrin subunits to convert $^3O_2$ into the cytotoxic $^1O_2$.

In general, red-shifted absorption bands can not only be achieved by coordinating metal ions but also by slightly adjusting the porphyrin skeleton by varying the attached residues in *meso*-position and by *β*-substitution.

As shortly mentioned in section 3.3.2, trimeric complexes cannot be synthesized following the developed route; therefore, the monomeric porphyrin precursors were further examined.

3.4 Cofacial *o*-phenylene trisporphyrin metal complexes

First attempts to synthesize trimeric porphyrin complexes were already undertaken in 1982 by *Wasielewsk*i *et al.*, who were the first to synthesize a stacked porphyrin trimer comprising coproporphyrin I double-linked *via* ester bridges. However, due to the C_{2h} symmetry of the monomeric porphyrin derivatives, the synthesized trimer was afforded as an inseparable mixture containing three diastereomers.[257] Later on, in the '80s, *Hamilton et al.* and *Seta et al.* found a synthetic route to rather flexible trimeric porphyrins as pigments, which are doubly connected *via* amide bridges – to mimic photosynthetic reaction centers and to synthesize molecular wires.[112, 113, 258] *Chang et al.* adjusted this multistep, linear-sequence strategy by utilizing anthracenes as spacer moieties to fix three porphyrins in a defined spatial arrangement rigidly. For this, 1,8-anthracene dicarbaldehydes were applied as precursors in a two-fold condensation reaction to afford a triple-decker trisporphyrin.[211] *Osuka et al.* extended this reaction procedure by synthesizing 1,3-diphenoxypropane-linked trisporphyrins and enlarging the substrate scope to pentameric porphyrin stacks in cooperation with *Maruyama et al*.[118, 259] Since the molecular planes of the before-mentioned cofacial porphyrin subunits are separated by at least 4.94 Å (anthracene case),[211, 260] an exchange of the linker moiety is necessary to reduce the distance. In the comparable *o*-phenylene-bridged porphyrin dimer case, the average inter-plane distance is reduced to 3.43 Å, as described in more detail in section 6.4.1.[175] X-ray analysis confirms the strong π-interaction of the chromophores, which can compensate the 60° bite angle of the *o*-phenylene-linker for yielding a cofacial arrangement that is well suited for the construction of stacked, trimeric porphyrins.[10]

In 1992 *Osuka et al*. developed a sequential approach beginning with a cross-condensation reaction, which converts a formyl-substituted porphyrin and a monoprotected phthalaldehyde into a dimeric porphyrin. After deprotection followed by a second mixed-condensation reaction, the Z-shaped trisporphyrin was obtained.[261] A complementary synthetic pathway was developed by *Therien et al.*, who transformed the Zn(II) complex of a linear ethynyl-linked alkyl-porphyrin trimer *via* a two-fold Co(II)-mediated [2+2+2] cycloaddition into a Z-shaped trimer.[191]

Both pioneering approaches, however, suffer from a few shortcomings. The procedure of *Osuka et al.* uses rather expensive bis(3-ethyl-4-methyl-1H-pyrrol-2-yl)methane as the basis for all condensation reactions.[175] Additionally, this synthetic approach constrains the fine-tuning of distances because it only allows *meso*-connected porphyrin subunits and limits the incorporation of residues.[242] Similarly, the synthesis route developed by *Therien et al.* does not apply to a wide range of different transition metals – in particular, heterometallic complexes

cannot be synthesized. In the mentioned publication, only reactions on the Zn(II) porphyrin derivatives were reported.[191]

Therefore, a general methodology was developed to synthesize *o*-phenylene linked trisporphyrins as ligands for homo- and heterotrimetallic complexes. The basis for cofacially stacked homo- and heterometallic bisporphyrin complexes has been developed in section 3.3. By adjusting the procedure, analogous trisporphyrin complexes can easily be synthesized.

3.4.1 The *o*-dipyrromethane-phenyl group as residue functionalization to enable *o*-phenylene trisporphyrin syntheses

As for the *o*-phenylene-bisporphyrin **128**, formyl-phenylporphyrin **125** is the starting point for the trimeric porphyrin structure **34** and is easily accessible *via Suzuki* cross-coupling reaction (Scheme 34, 3.3.1). Rather than reacting the aldehyde functionality by mixed condensation to obtain the respective *o*-phenylene-bisporphyrin, as described in section 3.3.2, the formyl-group was instead converted to a porphyrin-bearing dipyrromethane **175**, which serves as the key intermediate (Scheme 48).

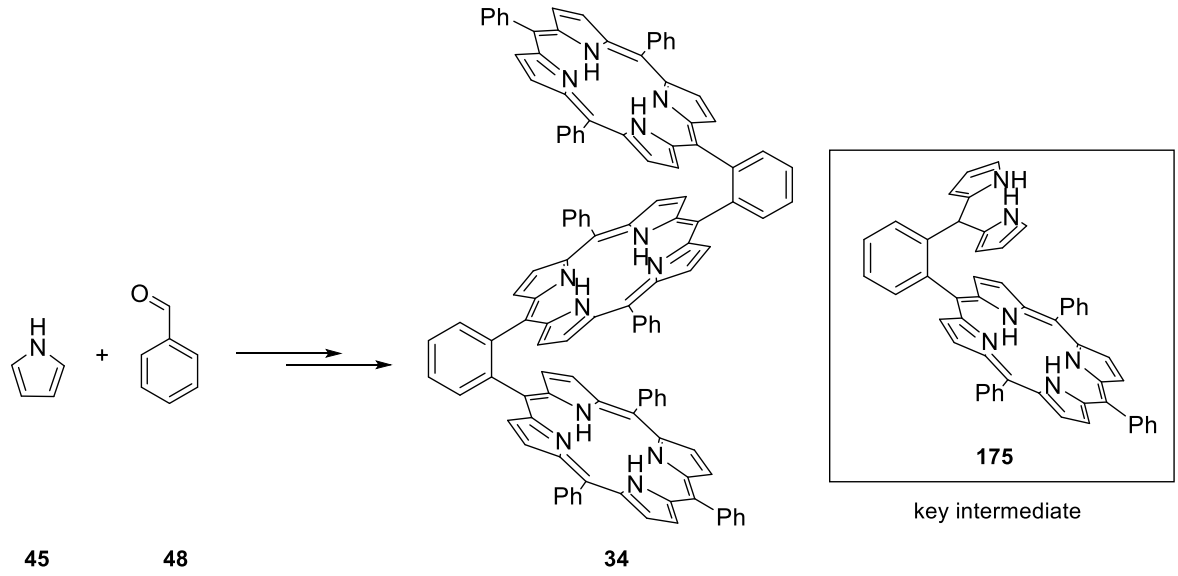

Scheme 48: The general synthesis route towards *o*-phenylene-trisporphyrin **34** starting from pyrrole (**45**) and benzaldehyde (**48**) using the dipyrromethane-phenyl-porphyrin **175** as the key intermediate.

First, *Bein's* strategy, which was employed to synthesize di(1H-pyrrole-2-yl)methane (**57**), was attempted using $InCl_3$ as *Lewis* acid and NaOH as a base. MS could prove the conversion to the desired product, but only as a side product besides the oxidized dipyrromethane.

TFA as a catalyst alongside NEt_3 as a base was explored in the next attempt – a procedure closer to the commonly used conditions in porphyrin chemistry. After 4 h at room temperature and continuously adding TFA, 5-(2-(di(1H-pyrrol-2-yl)methyl)phenyl)-10,15,20-

triphenylporphyrin (**175**) was obtained in 93% yield (Scheme 49). The corresponding NMR spectra were recorded in toluene-d_8 to avoid oxidation and exhibit the nine dipyrromethane protons in the expected region of 6.30 – 4.98 ppm.

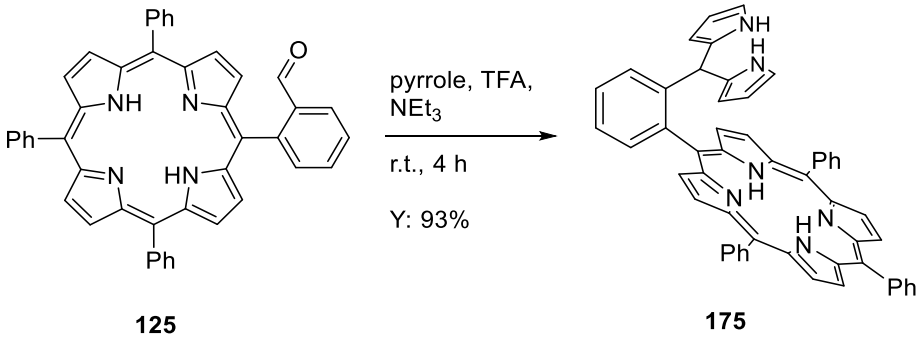

Scheme 49: Synthesis of the"1.5-porphyrin" precursor *via* a TFA catalyzed condensation reaction.

Interestingly, the porphyrin NH signals experience a downfield shift to –2.19 ppm due to additional deshielding from the aromatic pyrrole subunits. This robust procedure provides the "1.5 porphyrins" precursor **175** in an excellent total yield of 28% over six steps.

The dipyrromethane subunit of **175** now takes part in an acid-catalyzed condensation reaction with benzaldehyde in a theoretical ratio of 1:1 (Scheme 50). Surprisingly, by-product **176** was noticed in approaches a) and b), which could not be efficiently separated from **34** even after four consecutive flash column chromatographies on silica gel.

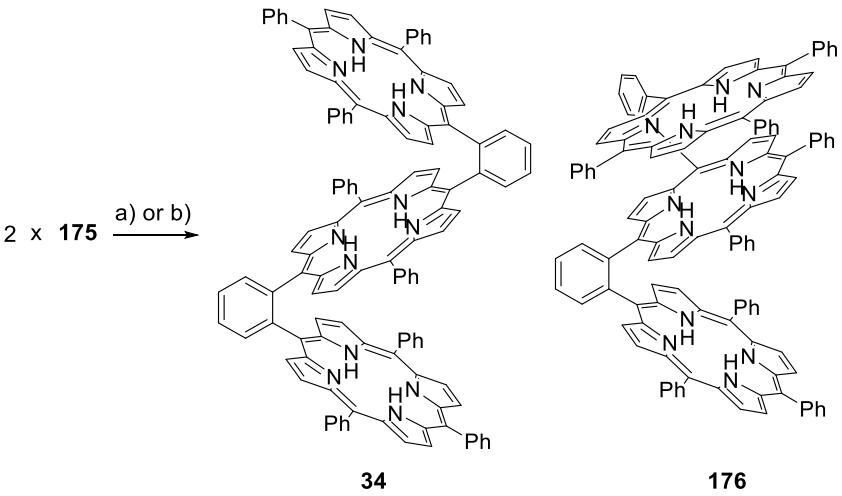

Scheme 50: The condensation reaction of two dipyrromethane-containing porphyrins **175** with benzaldehyde (**48**) yielding two possible isomers of trimeric porphyrin stacks: *trans*-isomer **34** and *cis*-isomer **175**. a) Benzaldehyde (7.22 equiv.), TFA (8.46 equiv.), DDQ (2.10 equiv.), NEt_3, CH_2Cl_2, r.t., 26.5 h, 13%; b) benzaldehyde (2.00 equiv.), $BF_3 \bullet OEt_2$ (2.00 equiv.), DDQ (2.44 equiv.), NEt_3, CH_2Cl_2, r.t., 19 h, 1.9%.

To elucidate the corresponding structure of by-product **176**, the analysis by mass spectrometry alone was not helpful since **34** and **176** are isomers. Since *o*-phenylene-bisporphyrin **128** could be isolated in traces, it became clear that scrambling plays a role in this condensation reaction. Therefore, an IMS spectrum was recorded, showing an additional signal for the single

protonated trimer assigned to the *cis*-isomer **176**. As represented in Figure 38, the molecules synthesized by routes a) and b) show two to three different peaks in their corresponding mobilograms – indicating the presence of multiple (separable) isomeric forms.

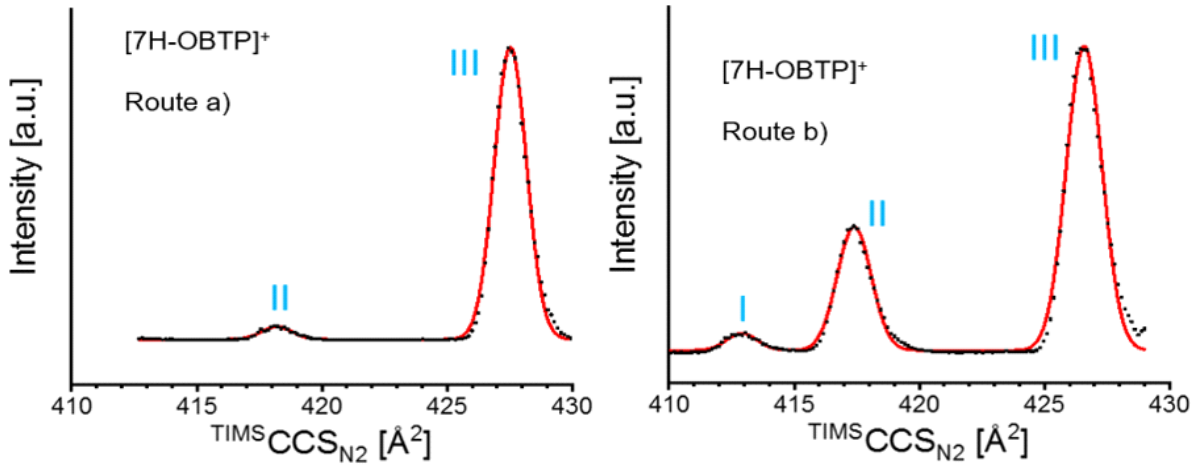

Figure 38: IMS measurements of the isolated porphyrin trimer fraction of the TFA catalyzed route a) and the $BF_3 \bullet OEt_2$ catalyzed route b).

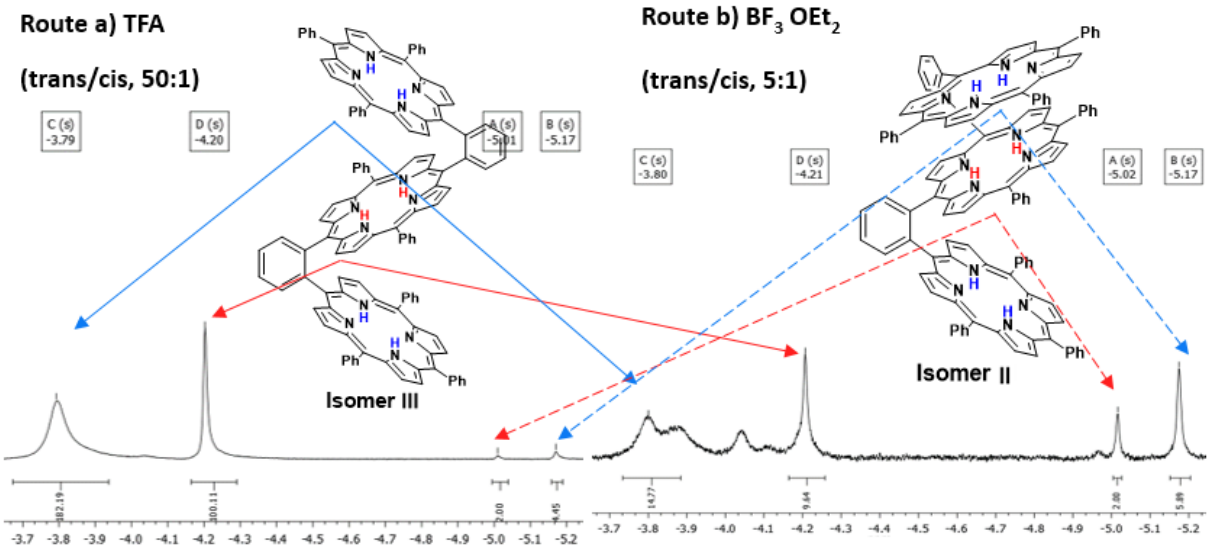

Figure 39: High field of the ^1H NMR spectra of the isolated porphyrin trimer fraction of the TFA catalyzed route a) and the $BF_3 \bullet OEt_2$ catalyzed route b). Isomer III can be assigned to **34** and isomer II can be assigned to **176**.

Four different isomers, namely *cis*- and *trans*-[7H-OBTP]$^+$, each with their two corresponding protonation isomers (protomers), are trivial and can be expected, for which either the inner porphyrin or one of the two outer porphyrins could be protonated. For both syntheses, peak III is the dominant peak in the mobilogram and can be attributed to the *trans*-isomer based on the respective NMR measurements (Figure 39). First DFT calculations with the basis set *Def2-SVP*,[237] the functional *TPSS*[262-264] and the dispersion correction *disp3-BJ*[238, 239] as implemented in the *Turbomole*[265] package were applied to generate the structures and energies

that proposed the *cis*-isomer **176** to be the main species with a larger CCS value (four protomeric forms: *cis*: 433.4 Å; 433.5 Å *vs*. *trans*: 424.0 Å, 423.0 Å) (Table 3)

Table 3: DFT calculations and Molecular Dynamics (MD) simulation of the *cis*- and *trans*-porphyrin trimer.

DFT calculation 0 K (def2-SVP, TPSS, disp3-BJ).

isomer	relative energy [kJ/mol]	Calculated CCS [Å^2]
cis-NH-OBTP-out	0.21	433.4
cis-NH-OBTP-in	0.11	433.5
trans-NH-OBTP-out	0.00	424.0
trans-NH-OBTP-in	0.08	423.0

MD simulation (average CCS over 100 conformers).

isomer	Calculated CCS [Å^2]
cis-NH-OBTP	479.8
trans-NH-OBTP	494.7

Since the low-field region of the ^{1}H NMR spectrum (discussed in the following, Figure 41) shows a dominant symmetric compound and the *trans*-isomer **34** posses a C_2-axis as symmetry element, a Molecular Dynamics (MD) simulation was used to achieve further insights into the 3D structure. While the former DFT calculations aim to calculate the most thermodynamically stable arrangement at 0 K, the MD simulation takes temperature effects into account by averaging the CCS over 100 conformers. As a result, the relative CCS values reverse and for the *trans*-isomer **34,** a by 14.9 Å larger CCS value was obtained than for the *cis*-isomer **176**. Absolut values cannot be considered in this case since no suitable calibration standard could be used as TPP stacks ionize mainly in their monomeric or dimeric forms but not as the respective trimers.

Peaks II and I correspond to the *cis*-isomer **176**, probably in different kinetically locked rotamer or protomer arrangements. The varying intensities of peak II and the absence of peak I in route a) indicate that the two acid catalysts applied for the respective reactions yield the *cis*-isomer in different amounts. Hence, it is conceivable that there may also be catalysts that favor the formation of the *cis*-isomer as the main product.

From the integrated mobilograms, the *trans*/*cis* ratio can be determined to be 25:1 with TFA and 21:(8+1) with $BF_3 \bullet OEt_2$ as the catalyst (Figure 38).

In contrast, the ^{1}H NMR spectra show the ratio of the neutral molecules to be 50:1 and 5:1, respectively. The IMS data might overestimate the *cis*-/*trans*- ratio due to the higher basicity of the *cis*-isomer and, therefore, better ionization *via* protonation. This hypothesis is supported by the increased basicity of the *β-meso*-linked bisporphyrin in section 3.3.2, which also arranges in a twisted shape.

Cis-*o*-phenylene-trisporphyrin **176** is the first conformationally restricted planar chiral porphyrin trimer reported in the literature. Its formation can be enhanced by applying the *Lewis* acid $BF_3 \bullet OEt_2$ as the catalyst. DFT calculations show that the energy of the *cis*-isomer is only 0.14 eV higher than the *trans*-isomer for the geometrically optimized structures at 0 K, which underlines that the isomeric ratio of the condensation reaction is kinetically controlled (see DFT calculation in Table 4 and Figure 40 for details).

Table 4: DFT calculations of the neutral and the H^+ adduct of the trimeric porphyrin ligand.

6H-OBTP	ΔE [eV]	ΔE [kJ/mol]	ΔE [kcal/mol]
cis-6H-OBTP	0.14	14.0	3.34
trans-6H-OBTP	0.00	0.00	0.00

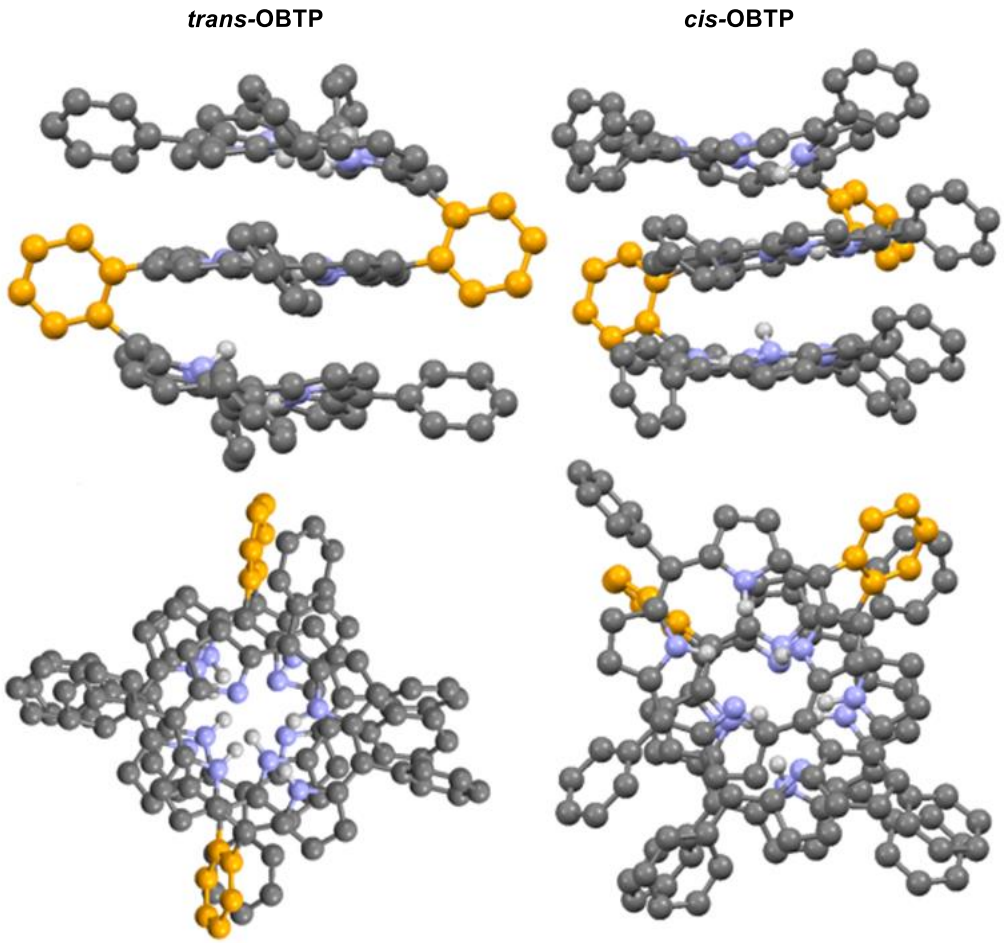

Figure 40: DFT calculations of the *trans*- and *cis*-OBTP compounds represented in top and side view.

The relative energies were collected by subtracting the energy of the lowest-lying isomer from the energy of the respective isomer. The energies shown are the electronic energies without taking corrections into account. Since the TFA catalyzed reaction showed less scrambling, this reaction procedure was further optimized. Compared to the porphyrin dimer case in section 3.3.2, the minimum amount of benzaldehyde necessary to see a conversion while retaining a high acid concentration in previously degassed CH_2Cl_2 represents the optimal reaction condition. Accordingly, the *trans-o*-phenylene trisporphyrin **34** can be obtained in a 13% yield, containing 2% of the respective *cis*-isomer **176** as an inseparable by-product.

trans-6H-OBTP **34** contains a C_2 axis as a symmetry element, leading to a simplified NMR spectrum as indicated in Figure 41.

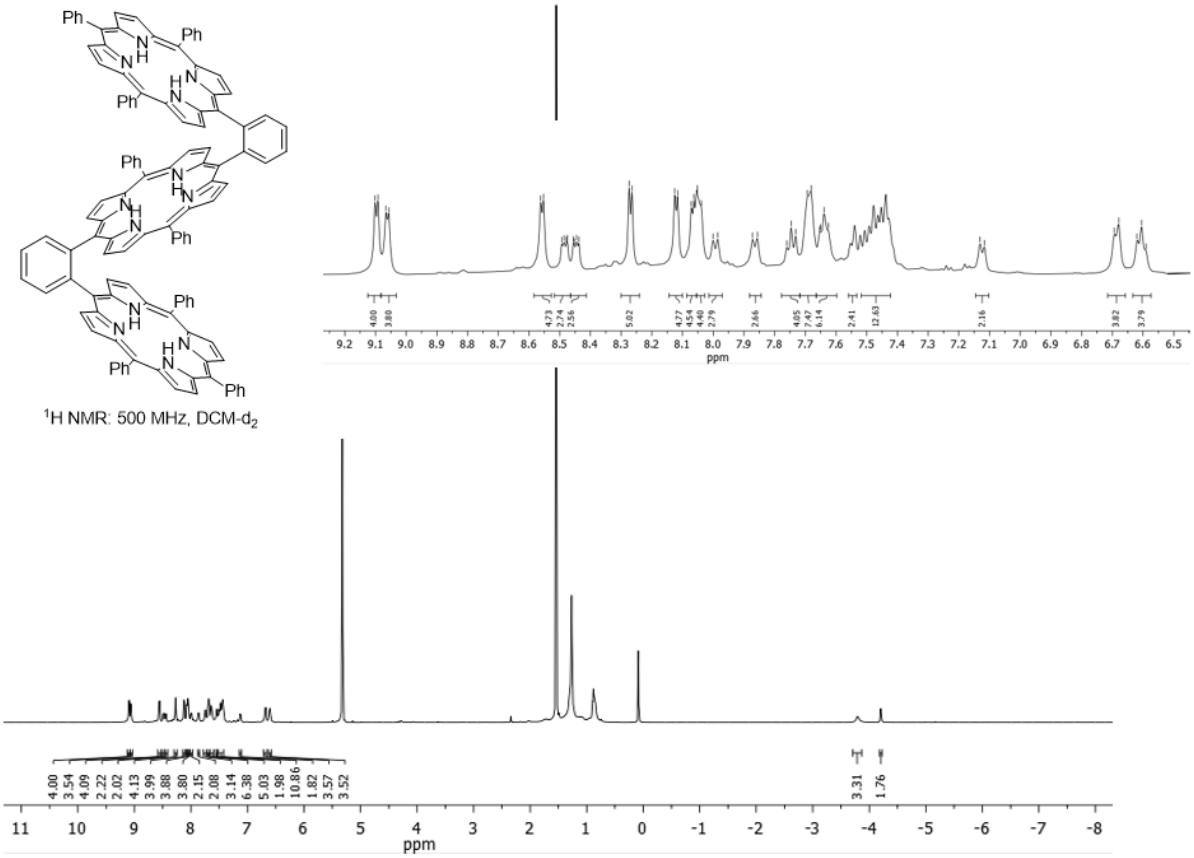

Figure 41: ^{1}H NMR spectrum of the symmetric *trans-o*-phenylene-trisporphyrin **34**.

The downfield shifted NH protons as a broad signal at –3.79 ppm, representing the outer four NH protons. At –4.20 ppm, there is a comparatively sharp singlet that represents the two inner NH protons. In conclusion, the novel synthetic route presents the synthesis of 5,15-bis(2-(10,15,20)-triphenylporphyrinylphenyl)-10,20-diphenylporphyrin (**34**) as the first aryl-based trimeric porphyrin stack, which can be synthesized in seven steps starting from pyrrole and benzaldehyde and in an overall yield of 3.6%.

3.4.2 Homotrimetallic *o*-phenylene-linked trisporphyrin complexes

Next, the as-synthesized free-base ligand **34** with a *trans*/*cis* ratio of 98:2 was triply metalated with six different transition metals (Scheme 51). The resulting metal complexes displayed the same *trans*/*cis* ratio and were systematically analyzed with UV-Vis spectroscopy, IR-spectroscopy, MS and IMS. For the metal coordination, the reaction times had to be only slightly prolonged compared to homobimetallic complexes to achieve complete threefold complexation of the metal ions: Mn(III), Fe(III), Ni(II), Cu(II), Zn(II) and Pd(II) **177** – **182**.[242] However, this does not hold for the 3Ni(II)-OBTP **179** complex since degradation was observed for the former conditions and $Ni(acac)_2$ had to be substituted with $Ni(OAc)_2 \bullet 4\ H_2O$.
The metals in oxidation state +2 have been detected as monocations by MS, whereas for the Mn(III) trimer **177**, mainly two attached chlorides were observed and the Fe(III) complex **178** showed adducts of O and Cl.

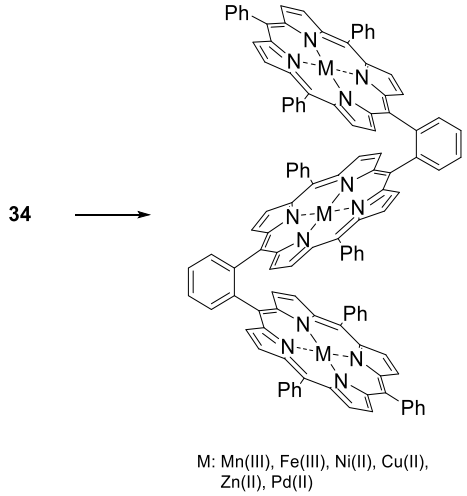

Scheme 51: Cofacial porphyrin-based homotrimetallic complexes a) (**177**) *Mn(III): $MnCl_2$, DMF, 150 °C, 3 h, 86%; (**178**) **Fe(III): $FeBr_2$, HCl, DMF, 140 °C, 3 h, 89%; (**179**) Ni(II): $Ni(OAc)_2 \bullet 4\ H_2O$, $CHCl_3$/MeOH, 100 °C, 17 h, 95%; (**180**) Cu(II): $Cu(OAc)_2$, $CHCl_3$/MeOH, 80 °C, 3 h, 65%; (**181**) Zn(II): $Zn(OAc)_2$, $CHCl_3$/MeOH, r.t., 2 h, 86%; (**182**) Pd(II): $Pd(OAc)_2$, $CHCl_3$/MeOH, 80 °C, 2 h, 84%; * The Mn-trimer was mainly observed with two attached chlorides; **3Fe-OBTP has been detected with adducts of O and Cl. 3Ni-, 3Cu-, 3Zn- and 3Pd-OBTP have been detected as monocations by MS, whereas 3Fe-OBTP has been detected with adducts of O and Cl. The Mn-trimer was mainly observed with two attached chlorides.

Additionally, CID (collision-induced dissociation) spectra of two differently synthesized $[2Ni(II)\text{-}3H\text{-}OBTP]^+$ complexes were measured by Erik Karsten Schneider to make use of the faced enhanced kinetical barrier during the Ni(II) coordination process. In the first approach, the ligand coordination by Ni(II) was not complete since sampling was performed at 50% of the reaction time required for the complete coordination of three metals. In the second approach, the dipyrromethane-bearing Ni(II)porphyrin **183** (see section 3.4.3) was coupled to form a trimer containing two Ni(II) porphyrin subunits and one free base porphyrin subunit. The CID-spectra have been measured using a *Bruker* timsTOF system, which couples high-resolution

ion mobility spectrometry with mass spectrometry (IMS-MS). The fragment spectra of both samples look almost identical as depicted in Figure 42.

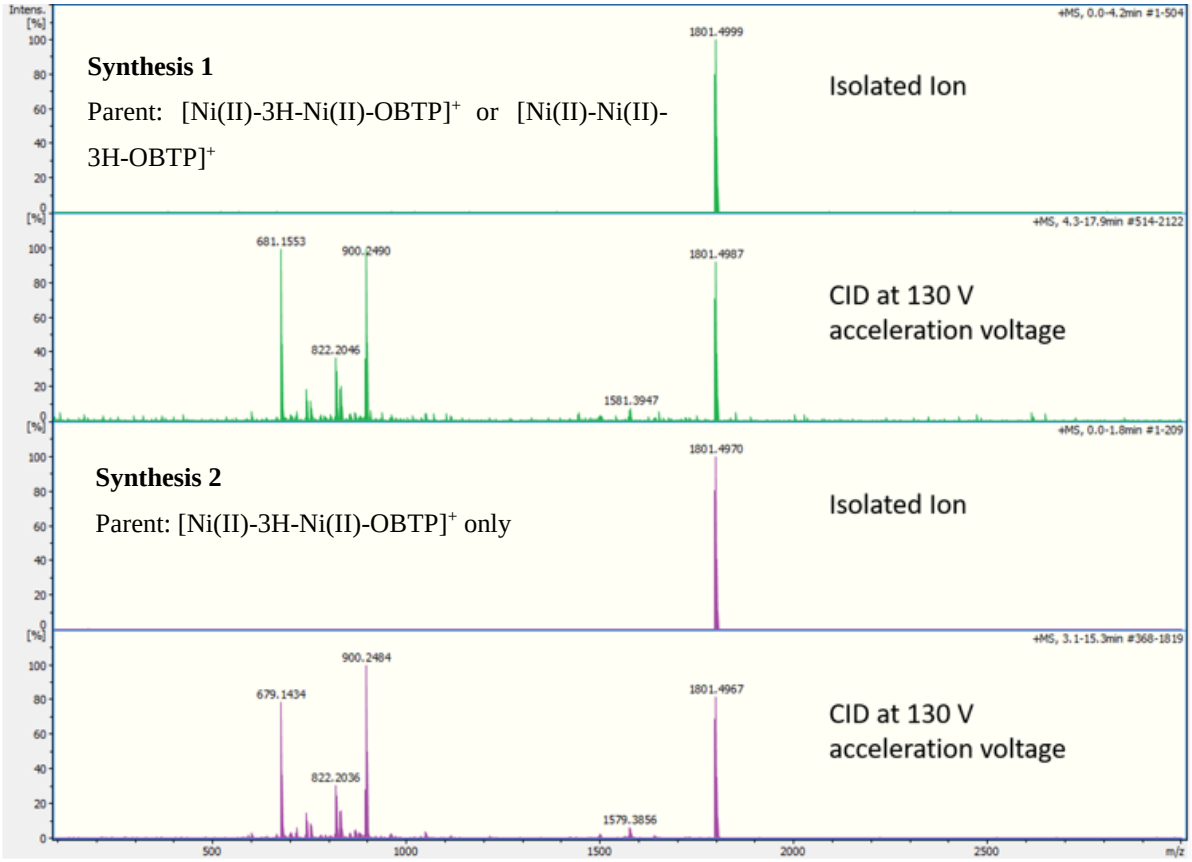

Figure 42: Overview CID spectra: As seen in the spectra, the fragmentation behavior of the two $[2Ni\text{-}3H\text{-}OBTP]^+$ species is almost the same. There are very intense patterns at 679 *m/z* and 900 *m/z* and some minor species between 740 and 850 *m/z*.

In this study, CID has applied to the $[2Ni\text{-}3H\text{-}OBTP]^+$ trimer since the fragmentation pattern of the symmetrical $[Ni\text{-}3H\text{-}Ni\text{-}OBTP]^+$ is expected to be different from that of the asymmetrical $[Ni\text{-}Ni\text{-}3H\text{-}OBTP]^+$. The peak at around 900 *m/z* in the dissociation experiments is visible in the MS spectrum of both synthesis approaches. It can be assigned to the 1.5-mers containing one Ni(II) atom and a differing number of hydrogen atoms due to oxidation and ionization processes, as presented in Figure 43.

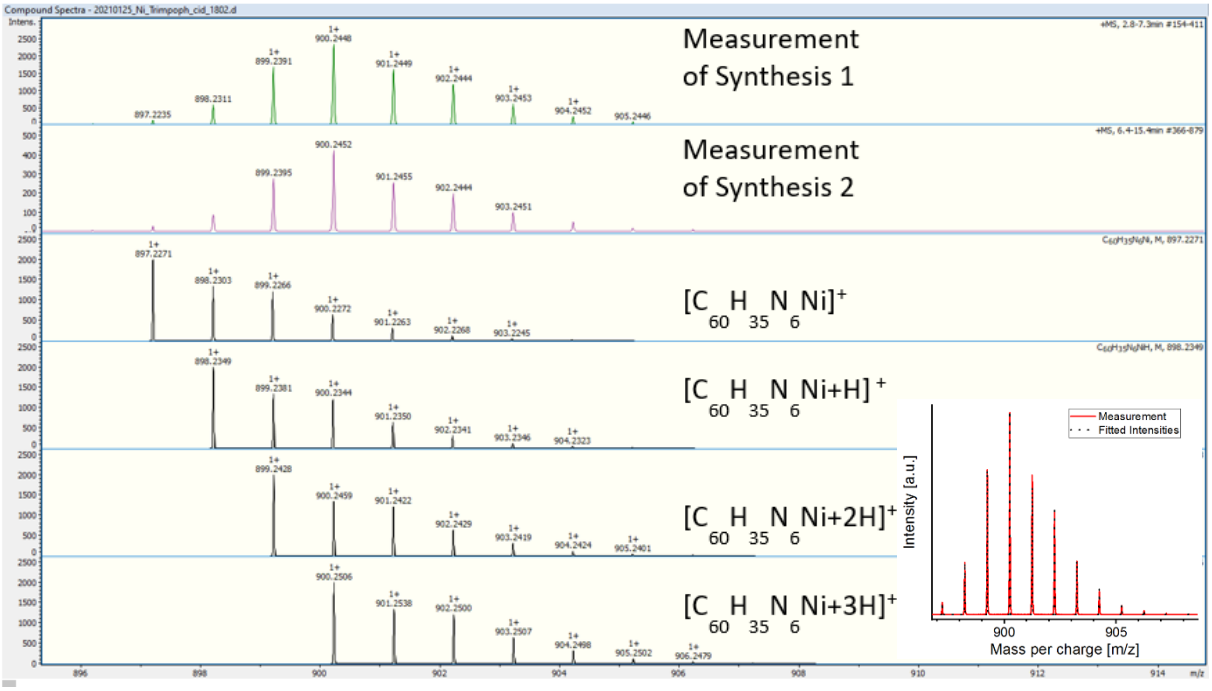

Figure 43: Zoom of the CID measurement of the 2Ni(II)-2NH-trimer presenting the 1.5-mer containing one Ni(II) atom. The figure shows the pattern of the fragments at 900 *m/z* in green (synthesis I) and magenta (synthesis II) and simulated spectra in black. The spectra below show simulations of $[C_{60}H_{35}N_6Ni{+}nH]^+$ (n = 0,…,3) taking scaling factors 1, 3.67, 9.54 and 10.34 into account.

Scaling the pattern of $[C_{60}H_{35}N_6Ni{+}nH]^+$ (n = 0,…,3) species with 1, 3.67, 9.54 and 10.34, respectively, the apparent ratio of the fragments can be roughly estimated to fit the measured data (bottom-right of Figure 43). Instead, the free-base 1.5-mer is absent. This is expected for synthesis II (outer porphyrins nickelated previously) and demonstrates that the same isomer is formed in synthesis I.

The mass spectra and the similarities between the two sets of CID measurements allow for the conclusion that both approaches lead to the same main product: Ni(II) coordinates into each of the two outer porphyrins exclusively. Therefore, these findings follow *Osuka et al.*'s work, which postulated, in 1991, that the outer porphyrin subunits are metalated first.[175]

3.4.3 Heterotrimetallic *o*-phenylene-linked trisporphyrin complexes

To establish porphyrin-based transition metal-containing trimeric heterometallic complexes in a defined manner, a trisporphyrin containing two Ni(II) and one Fe(III) center was built – which may also be thought of as an extended carbon monoxide dehydrogenase active site analog. To circumvent potential oxidation of the porphyrin-dipyrromethane **175,** the Ni(II) cation was inserted after the *Suzuki* cross-coupling reaction in the monomeric formyl-phenyl-porphyrin **125** by treatment with $Ni(OAc)_2 \bullet 4\,H_2O$ at 100 °C for 18.5 h in 93% yield (**52**). The subsequent conversion of the aldehyde group to the dipyrromethane-containing Ni(II)porphyrin **183** was

conducted as described for the free-base analog by doubling the reaction time resulting in a yield of 84%. Apart from the missing porphyrinic NH protons and slightly increased coupling constants (from ^3J = 4.7 to 4.9 Hz), Ni(II) coordination leads to sharpened signals arising from the dipyrromethane subunit in the ^{1}H NMR spectrum. A potential interpretation is that Ni(II) complexation prevents intramolecular hydrogen bonding, which would otherwise occur in the free-base analog **34**. In the following condensation reaction, similar to Scheme 51 but with reduced reaction time, the 2Ni(II)-2H-OBTP **184** was obtained in a 14% yield. To isolate the 2Ni(II)-2H-OBTP species, a work-up comprising three consecutive flash-column chromatography cycles with different solvents, was necessary. The overlapping ring currents of the two adjacent porphyrin planes lead to a significant upfield shift of the NH protons of the inner porphyrin ring to –5.01 ppm.

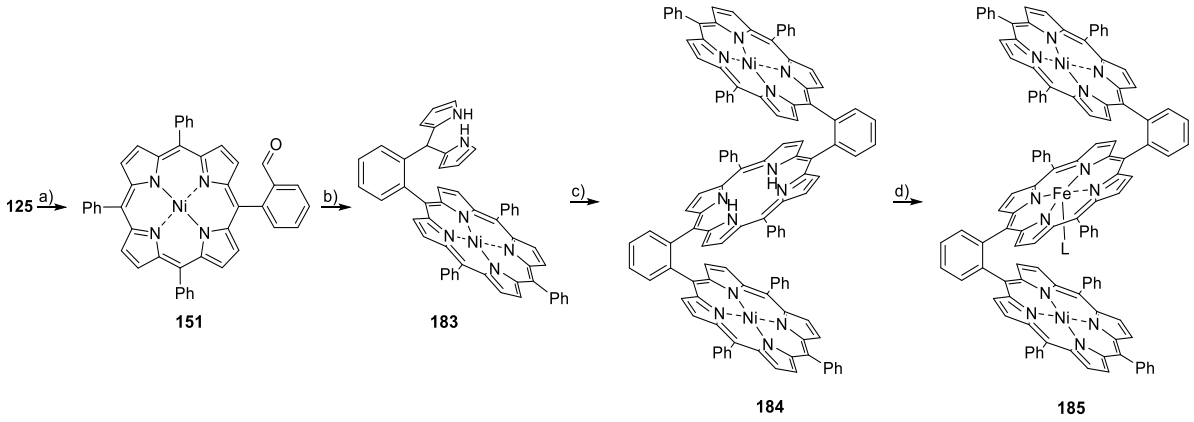

Scheme 52: Synthetic route towards an extended artificial carbon monoxide dehydrogenase active site analog **185** as a proof of principle reaction for several trimeric heterometallic porphyrin complexes. a) $Ni(OAc)_2 \cdot 4\ H_2O$, $CHCl_3$, MeOH, 100 °C, 18.5 h, 93%; b) pyrrole, TFA, NEt_3, r.t., 8 h, 84%; c) benzaldehyde (2.16 equiv.), TFA (3.69 equiv.), NEt_3, CH_2Cl_2, r.t., 3 h, 14%; d) $FeBr_2$, DMF, 150 °C, 2 h, 94%. (Ligand L cannot be determined precisely since MS adducts with several oxygens as dominant counter ions can be assigned in MS).

This demonstrates a significant transformation in the electronic nature of the interior porphyrin subunit, whether the outer porphyrin rings contain metals or are vacant (–4.20 *vs.* –5.01 ppm in the ^{1}H NMR spectra of **34** and **184**). This also shows that the two external Ni(II) containing porphyrins, in spatial proximity to an initially vacant central site, can cooperatively manipulate their electronic properties and thus also the electronic properties of the third metal center.

Furthermore, this underlines the assumed reaction process leading to a threefold Ni(II) complexation of **34** *via* the Ni(II)-NH-Ni(II)-OBTP intermediate, since traces of the signal at –5.01 ppm in the ^{1}H NMR spectrum was observed during the reaction process.[242] Indeed, the reaction time dependence of the ^{1}H NMR signal at –5.01 ppm goes along with the expectation that the outer porphyrin rings are metalated first.

The Fe(III)-2Ni(II)-OBTP **185** represents the first trimeric heterometallic porphyrin complex, obtained in a total yield of 2.3% over nine steps, beginning with pyrrole and benzaldehyde as

starting materials. The interior free-base porphyrin can undergo a reaction with $FeBr_2$ in DMF at 150 °C for 2 h, to coordinate Fe(III) as the third cation in a 74% yield, to afford the triple porphyrin stack bearing two Ni(II) and one Fe(III)-center **185**. This underlines the robustness of the developed synthetic protocol.

Based on the results presented, one can assume this methodology is suitable for another analogous homo- and heterotrimetallic porphyrin complexes. By simply using two different dipyrromethane-bearing porphyrins in a mixed condensation reaction in the presence of an aldehyde followed by a metal insertion, it is possible to synthesize all 18 different perturbative combinations of three different metals (taking point symmetry into account for the *trans*-isomer). In the case of different *meso*-substitutions of the dipyrromethane-containing porphyrins, 27 combinations would result due to the broken point symmetry.

By monitoring the Ni(II) insertion, it can be concluded that the kinetic barrier for the metal insertion into the internal ring is significantly higher and therefore, prebuilt trimeric porphyrin ligands can be converted into defined heterometallic complexes. First tests were performed to see if trimeric porphyrins could serve as a target to deconvolute complex metal salt mixtures through their ability to coordinate different metal ions. This is achieved by stirring the ligand in a metal salt-containing solution in DMF (Scheme 53).

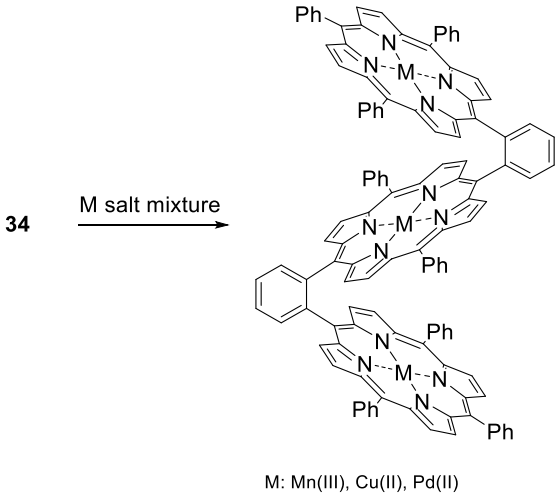

Scheme 53: Cofacial porphyrin-based heterotrimetallic complexes – statistical insertion approach: equimolar solutions of $^{*}MnCl_2$, $CuCl_2$ and $PdCl_2$, DMF, 150 °C, 4 h; * complex has been obtained with a coordinated chloride at the manganese center.

Therefore, the freebase trimeric porphyrin ligand **34** with an equimolar solution of $MnCl_2$, $CuCl_2$ and $PdCl_2$ in DMF was refluxed for 4 h. Besides the heterobimetallic combination of $[Mn+Cu+Cu]^+$, the trimetallic species $[Mn\text{-}Cu\text{-}Pd\text{-}OBTP]^+$ could be identified by the ESI-MS

spectrum (Figure 44). This proves that it is possible to insert all three metal cations into the same ligand through a one-pot reaction.

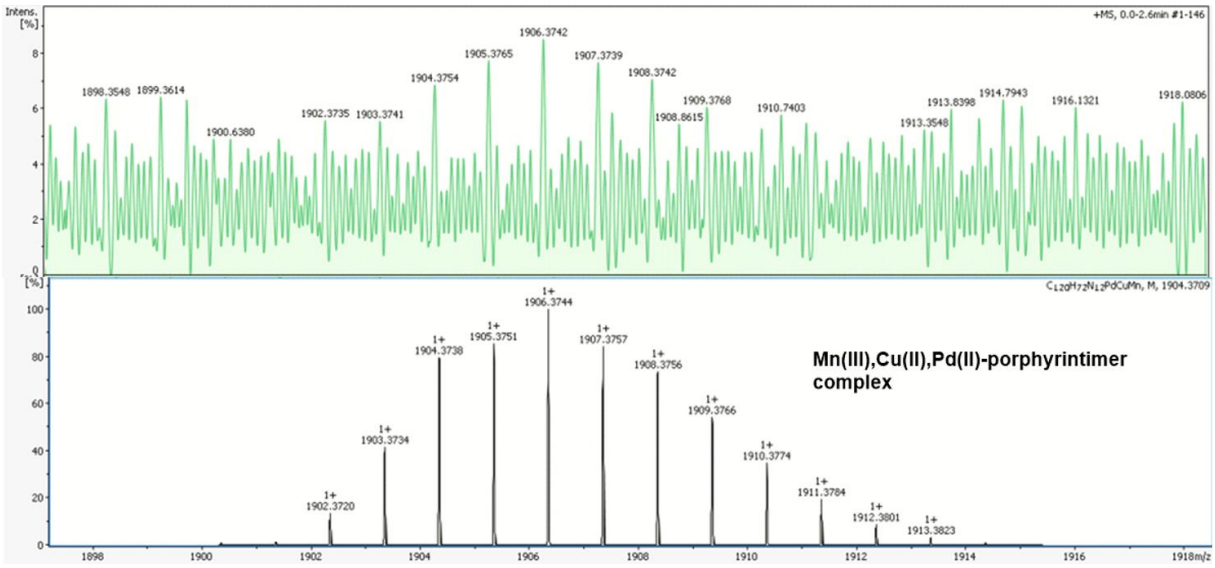

Figure 44: The M^+ peak of the heterotrimetallic Mn(III)Cu(II)Pd(II)-porphyrin trimer complex observed by measuring the crude reaction solution of the statistical insertion of the respective metal salts through a one-pot reaction. Top: measured ESI-MS spectrum, bottom: calculated spectrum.

These early results encourage the research of trimeric porphyrin ligands, as they can be a suitable candidate for application in magnetism/spintronics, catalysis and optical sensors.

3.4.4 Absorption and emission spectra of trimeric metal complexes

In solution, porphyrins display several sharp, intense characteristic bands in their electronic absorption spectra. Therefore, the following measurements were conducted and interpreted by Dr. Sergei Lebedkin to achieve insights into how intramolecular stacking effects change properties compared to the well-known monomeric analogs. Figure 45 compares the absorption of 6H-OBTP **34**, 3Pd(II)-OBTP **182** and Fe(III)-2Ni(II)-OBTP-4O **185** dissolved in CH_2Cl_2, with the absorption of the parent monomeric forms, *i.e.*, of free-base tetraphenylporphyrin 2H-TPP **32** and the respective Pd(II) derivative Pd(II)-TPP **186**.

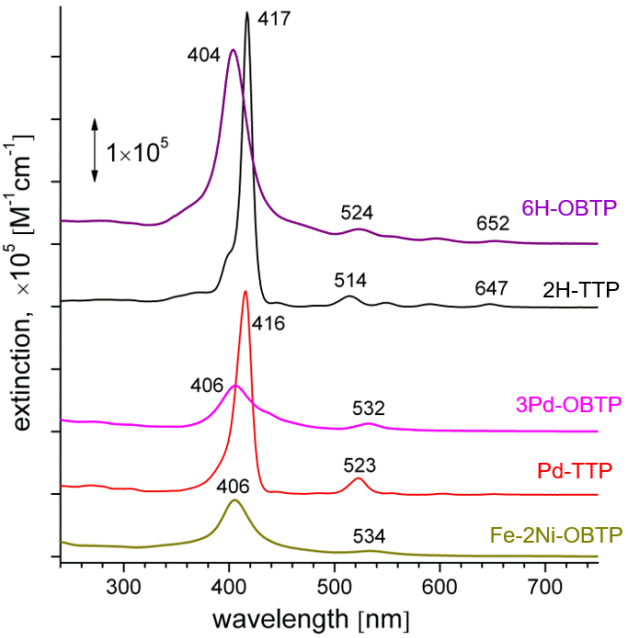

Figure 45: Absorption spectra (vertically shifted for clarity) of trimeric 6H-OBTP **34**, 3Pd-OBTP **182** and Fe-2Ni-OBTP **185** relative to monomeric 2H-TPP **32** and Pd(II)-TPP **186** in CH_2Cl_2. The numbers indicate the positions of the absorption band maxima.

The absorption spectra of the latter monomeric compounds follow the spectra presented in the literature. The extinctions of the *Soret*-band (SB) of 2H-TPP **32** at 417 nm and Pd(II)-TPP **186** at 416 nm were determined as ε(SB) = 4.68 $\times 10^5$ and 3.24 $\times 10^5$ $M^{-1}cm^{-1}$, respectively. This band notably broadens and shifts into the blue region, at 404 nm for OBTP **34** and 406 nm for both trimetallic trisporphyrin cases. The broadening only partly explains the decrease of the extinction in the freebase OBTP trimer **34** (6H-OBTP, ε(SB) = 3.11$\times 10^5$ $M^{-1}cm^{-1}$) *vs*. the monomer (2H-TPP): their *Soret*-band area ratio is 2:1, not 3:1. Such a reduction of the SB oscillator strength has also been observed in dimeric porphyrin cages and has been interpreted as a sign of strong electronic coupling between monomeric chromophore units.[266] This effect is even more apparent in the trimetallic *vs.* monometallic (Pd(II)-TPP) complexes: ε(SB) = 0.73 $\times 10^5$ and 0.90 $\times$ 10^5 $M^{-1}cm^{-1}$ for 3Pd(II)-OBTP **182** and Fe(III)-2Ni(II)-OBTP **185**, respectively and the SB area ratio of 3Pd(II)-OBTP **185** *vs*. Pd(II)-TPP **186** is only ~ 0.6 : 1. In contrast to the *Soret*-band, the Q-band in the green-red spectral region (with four distinct components observed for the free-base monomer and trimer) exhibits a moderate redshift in the trimeric porphyrins, e.g., from 523 nm in Pd(II)-TPP **186** to 532 nm for 3Pd(II)-OBTP **182**. A quantitative comparison of the Q-band oscillator strengths was hindered by band broadening and tailing in the spectra of the trimeric porphyrins and was therefore not conducted. Additionally, photoluminescence spectra of the corresponding air-saturated solutions were recorded and are depicted in Figure 46.

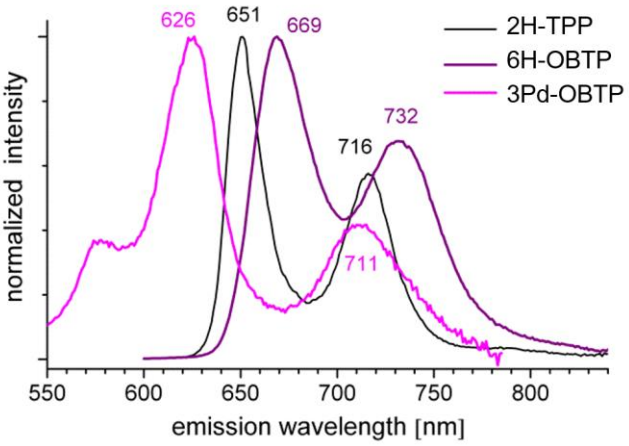

Figure 46: Normalized fluorescence spectra of 6H-OBTP **34** and 3Pd-OBTP **182** relative to monomeric 2H-TPP **32** in CH_2Cl_2 solutions. The excitation wavelengths correspond to the respective positions of the *Soret*-band maxima (see Figure 45).

Similar to compound 2H-TPP **32**, the freebase OBTP trimer **34** emits moderately intense red fluorescence (Figure 46). The major and vibronic emission bands of 6H-OBTP **34** at 669 nm and 732 nm are slightly redshifted and notably broadened than the 2H-TPP analog **32**. The fluorescence intensity moderately decreases in the trimer about the monomer: the emission quantum yield Φ_F, was determined to be 0.022 and 0.047, respectively.

For comparison, Figure 46 also shows the spectrum of weak fluorescence (Φ_F = 0.001) of 3Pd-OBTP **182**. The parent monomer Pd(II)-TPP **186** emits comparatively weak fluorescence (not shown), which peaks at about 610 nm, agreeing with the first observation by *Gouterman et al*.[267] At higher wavelengths, this fluorescence was strongly dominated by a residual impurity of 2H-TPP **32** (~1%) in the sample of Pd(II)-TPP **186**. Finally, no emission could be detected for Fe(III)-2Ni(II)-OBTP **185**, which is in agreement with previous observations for other Ni(II)-containing porphyrins.[268]

3.4.5 Singlet oxygen $^1O_2$ emission using Pd(II) stacks as catalysts

Extending the observed range of the luminescence spectra into the longer-wavelength site, an additional peak at 1275 nm became visible for the Pd(II) porphyrins **186**, **136** and **182** solved in CH_2Cl_2 (Figure 47).

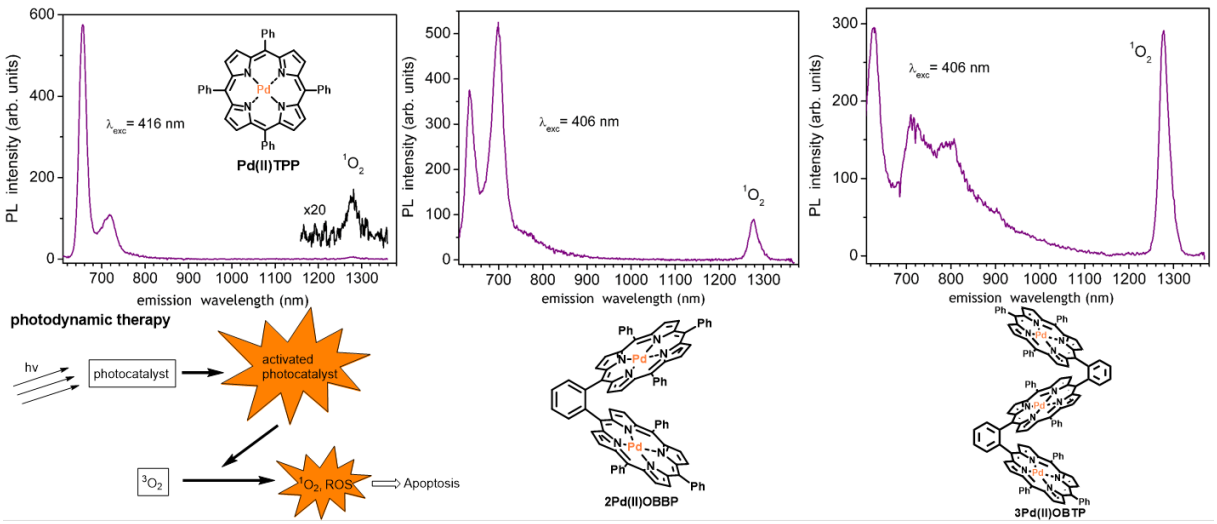

Figure 47: Luminescence spectra of the monomeric-, dimeric- and trimeric-Pd(II) porphyrin complexes **186**, **136** and **182** indicating a non-linear increase of $^1O_2$ emission. Bottom-left: working principle of the photodynamic therapy.

In 1979, *Kasha* and *Khan* first observed a dye-photosensitized 1268 nm emission of the $^1\Delta_g \rightarrow {}^3\Sigma_g$ transition of molecular oxygen in perfluorohexane at room temperature. As they correctly assumed, singlet oxygen emission can be a direct diagnostic tool of its involvement in chemiluminescence, bioluminiescence and other processes.[269] After 24 years, *Photofrin*® as the first photosensitizer for the photodynamic therapy (PDT) for the treatment of bladder cancer, was officially approved in Canada.[270] Since then, many other porphyrin and non-porphyrin photosensitizers have been used in oncology, including the Pd(II)-bacteriochlorine complex known as *Tookad*.[271]

Recently, *Wu et al.* evaluated Pd(II) porphyrins based on their induced $^1O_2$ emission depending on the number of subunits and coordinated metal. In this case, alkyl-bridged 3Pd(II)- are superior to 2Pd(II)- and Pd(II) porphyrin complexes.[272]

The above results can be underlined with the latter findings by studying the $^1O_2$ emission of the monomeric Pd(II) porphyrin complexes **186** with their cofacially stacked dimeric **136** and trimeric **182** analogs. The values obtained must be repeated with defined amounts of the respective porphyrin complexes, but the relative values indicate an increase in singlet oxygen production beyond what would be expected from linear behavior. An increased photosensitization of $^3O_2$ can be explained by the increased lifetime of the exited triplet state of the porphyrin metal complex.[273] Due to the packed cofacial arrangement, other relaxation processes become less likely as the porphyrin planes can effectively shield themselves from the surroundings. O_2 is small enough to be slightly influenced by this effect while maintaining its maximum interaction surface.

Not only transition metals containing porphyrins are under investigation as new drugs for the application in PDT, but also porphyrin derivatives and lanthanide complexes as mentioned in section 3.3.6.

To achieve a bathochromic shift of the absorption band, which favors PDT, porphyrin subunits with different skeletons can be considered, e.g., N-fused porphyrins or N-confused porphyrins.

3.5 Metal complexes of cofacially connected porphyrin derivatives with regular porphyrins

By fusing two adjacent pyrrole rings in the porphyrinoid scaffold, as displayed in N-fused porphyrins, a decrease in the HOMO – LUMO band gap is caused without increasing the number of π-electrons. In this way, optical properties are affected. Compared to traditional porphyrin structures, a bathochromic shift appears and the absorption bands of N-fused porphyrins metal complexes can trespass the 1000 nm benchmark.[73] Additionally, N-fused porphyrins exhibit fluorescence in the NIR region with large Stokes shifts and qualify as small-sized NIR emissive organic compounds applicable in optical communication, bio sensing probes and photovoltaics.[274]

Likewise, N-confused porphyrins show significantly red-shifted *Soret*- and Q-bands, dependent on the respective tautomeric form. The Q-bands in both cases exceed a 700 nm wavelength.[16, 275] The mentioned tautomeric forms of the N-confused porphyrin allow for the coordination of metal ions in different oxidation states as the rather unusual Ag(III) complex for the trianionic ligand[62] and a Ni(II) dianionic N-confused porphyrin[276].

3.5.1 A synthetic pathway towards N-confused-porphyrin based dimeric ligands

The N-confused porphyrins are the bases for the N-fused porphyrins and can be synthesized by substituting the acid catalyst TFA/BF_3 • OEt_2 for methanesulfonic acid ($MeSO_3H$). Following the procedure developed by *Linsey et al*., pyrrole was stirred together with benzaldehyde in the presence of $MeSO_3H$ at room temperature for 30 min in the absence of light to afford **187** in 21% yield (Scheme 54).[277]

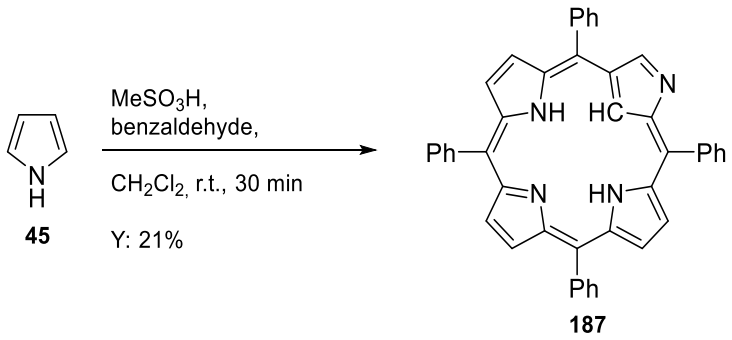

Scheme 54: Synthesis of the TPP-N-confused porphyrin **187**.

The ^{1}H NMR spectrum shows a singlet at 8.77 ppm that can be assigned to the outer proton of the twisted pyrrole ring. Moreover, the high field of the corresponding spectrum exhibits a broad singlet at –2.43 ppm, which can be assigned to the NH protons and a slightly broader

singlet at –4.99 ppm, which can be attributed to the interior CH proton. UV-Vis absorption spectroscopy in CH_2Cl_2 is compared to the regular TPP red-shifted *Soret*-band at 439 nm and the Q-bands at 541 nm, 582 nm and 726 nm.[278, 279] To avoid the intramolecular nucleophilic attack, which would generate the N-fused porphyrin, the N-confused porphyrin was stirred for 5 min with NBS (2.30 equiv.), followed by the immediate removal of the solvent. The reactive dibromo-N-confused porphyrin was purified by flash column chromatography and eluted directly into the AgOTf containing flask to form the stable [5,10,15,20-tetraphenyl-2-aza-3-bromo-21-carbaporphyrin]argentate(III) (Scheme 55).

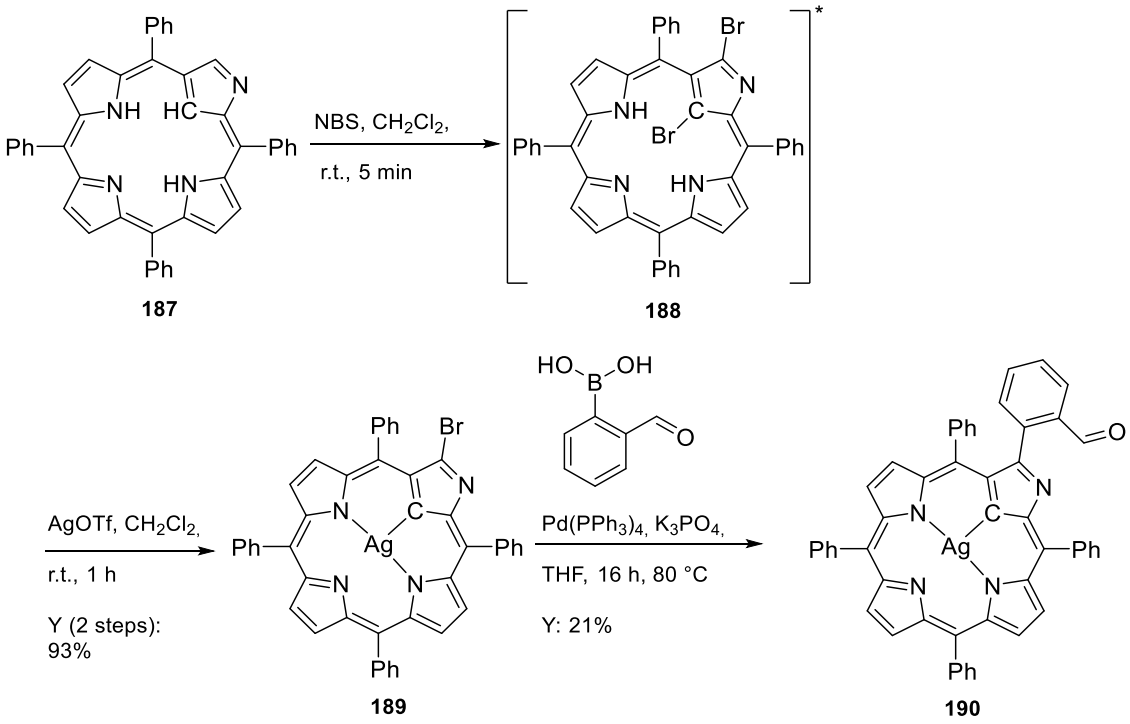

187 188 189 190

Scheme 55: Synthesis of brominated Ag(III) containing the N-confused porphyrin **188** *via* the reactive dibromo intermediate **187** and the subsequent *Suzuki* cross-coupling reaction to yield **190**.

The ^{1}H NMR spectrum of the barley soluble brown solid exhibits the lack of high-field NH and CH protons and the singlet of the proton of the outer twisted pyrrole ring at 8.71 ppm. In accordance, the M^+ peak of $C_{44}H_{27}AgBrN_4$ was found in the ESI-MS spectrum and underlines the Ag(III) coordination. The presence of Ag(II) or Ag(I) coordination would be indicated by a different number of protons in the HRMS spectrum.

The *Suzuki* cross-coupling reaction as described in Scheme 55 yielded the formyl-phenyl N-confused porphyrin analog and the success of this reaction could be proven by HRMS. Unfortunately, the solubility decreased to the extent that neither proper ^{1}H NMR spectroscopy, nor a subsequent condensation reaction was possible. An Ag(III) decomplexation reaction with $NaBH_4$ in THF/EtOH can most likely overcome the solubility issues and might also increase the yield if performed before the *Suzuki* cross-coupling reaction.[280]

These problems did not arise for the N-fused porphyrin and were subsequently studied to a deeper extent.

3.5.2 A synthetic pathway towards N-fused-porphyrin based dimeric ligands

Therefore, N-confused-tetraphenylporphyrin **187** was used as the starting point of the synthesis to convert it into the reactive dibromo species **188**. After work-up, **188** was dissolved in pyridine and stirred for 1 h at r.t. to promote the ring fusion to a [5,5,5] fused tri-pentacyclic ring and obtain the bromo-N-fused porphyrin **191** in 53% yield over two steps (Scheme 56).

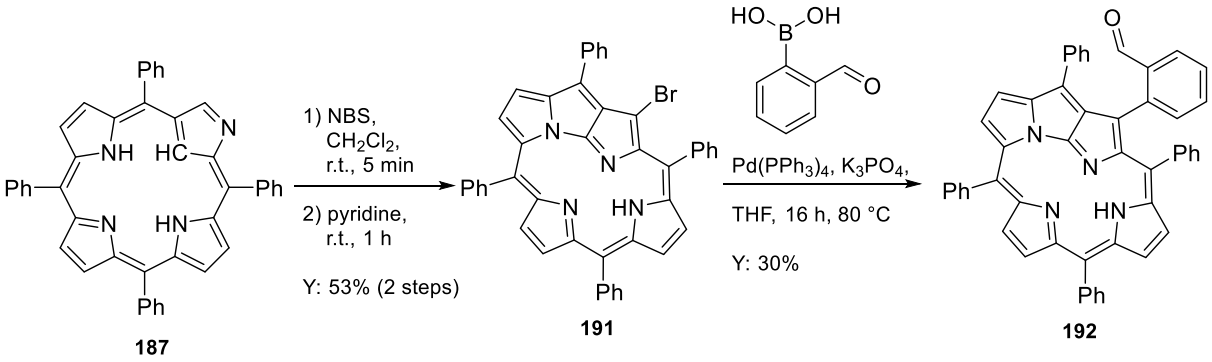

Scheme 56: Synthetic route towards the formyl-phenyl-N-fused-porphyrin precursor **192**.

^{1}H NMR spectroscopy showed doublets in the 7 – 8 ppm region with slightly increased coupling constants compared to the regular porphyrin scaffold (4.6 Hz, diphenylporphyrin) to 5.1 Hz, caused by its slightly bent structure.[279] Subsequently, **191** was subjected to a *Suzuki* cross-coupling reaction, as previously reported, to yield the formyl-phenyl-N-fused porphyrin **192** in 30% yield. The corresponding ^{1}H NMR spectrum was measured in $CDCl_3$ and displayed broad signals for the pyrrolic protons. To test if stacking effects lead to the signal broadening, pyridine was added in a ratio of 1:10. The broad signals narrowed to strong signals due to longer T_2 times (Scheme 57).[281]

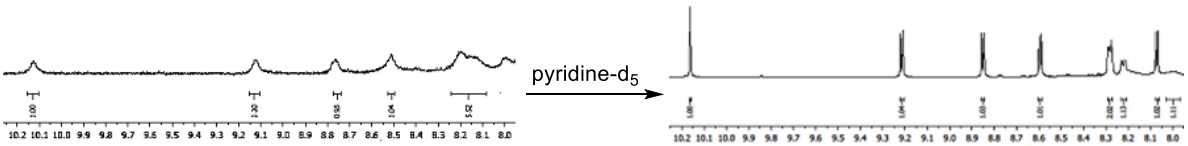

Scheme 57: Downfield region of the ^{1}H NMR spectrum of **192** before and after adding pyridine-d_5.

The successful *Suzuki* cross-coupling reaction can be confirmed with the singlet signal of the aldehyde group at 10.16 ppm. Furthermore, the broad singlet at 8.00 ppm can be assigned to the NH proton arising not in the upfield but the downfield region for the N-fused derivative.
In the following reaction, conditions were screened to improve the limited yield of 30%. Neither ligands reported for sterically demanding *Suzuki* cross-coupling reactions (Figure 48), nor

freeze-pump-thaw technique, higher concentration or Cs_2CO_3 as a base, improved the yield.[282-284]

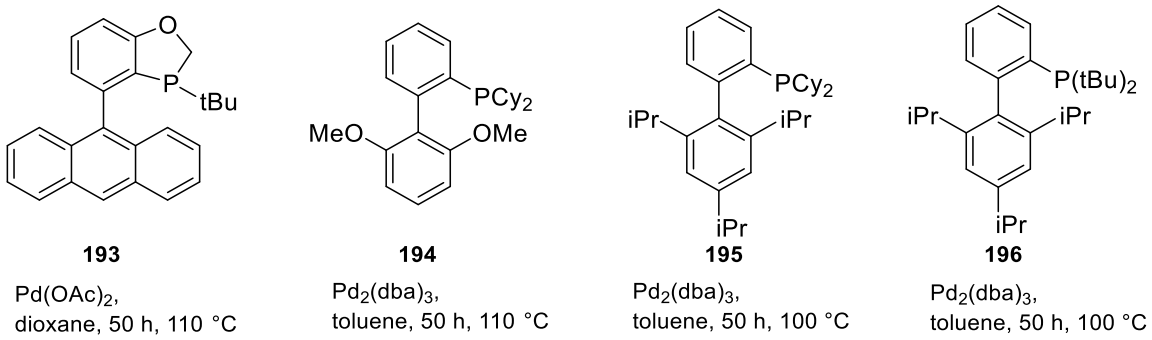

193 **194** **195** **196**

$Pd(OAc)_2$, dioxane, 50 h, 110 °C

$Pd_2(dba)_3$, toluene, 50 h, 110 °C

$Pd_2(dba)_3$, toluene, 50 h, 100 °C

$Pd_2(dba)_3$, toluene, 50 h, 100 °C

Figure 48: Screened Ligands **193** – **196** for *Suzuki* cross-coupling reactions with sterically demanding substituents.

The main side-product can be assigned to the defunctionalized phenyl-derivative of the N-fused porphyrin and can be removed by the subsequent flash column chromatography on silica gel. Therefore, the moderate yield of 30% was satisfactory for this crowded halogen center. Furthermore, the aldehyde functionality was investigated in the subsequent condensation reaction to synthesize the novel cofacial N-fused-porphyrin-based dimeric ligand **197**.

3.5.3 Synthesis of the N-fused *o*-phenylene porphyrin derivative dimer

To a degassed solution of CH_2Cl_2 and formyl-phenyl-N-fused-porphyrin **192**, pyrrole (**45**), benzaldehyde (**48**) and TFA as acid catalysts were added dropwise over 19 h to guarantee a steady buildup of the N-fused porphyrin-dimer **197** (Scheme 58). This also generates TPP **32** as a side product, which can be removed in the following purification steps to obtain the cofacial dimer as a red solid in a 22% yield. Therefore, a novel synthetic route towards the N-fused-porphyrin - porphyrin dimer **197** in a total yield of 1.1% over five steps, starting from pyrrole (**45**) and benzaldehyde (**48**), has been designed.

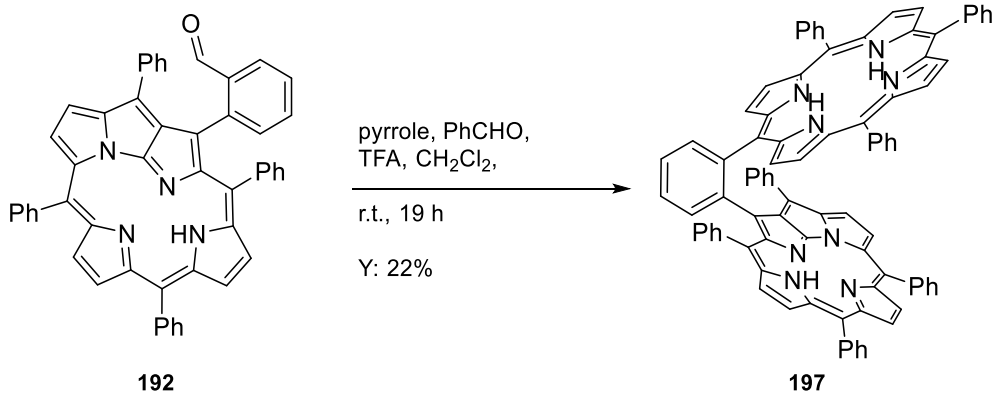

192 **197**

Scheme 58: The mixed condensation reaction of the first cofacial N-fused-porphyrin - porphyrin dimeric ligand **197**.

The ^{1}H NMR spectrum shows similar line broadening due to stacking effects, but this can be circumvented by adding pyridine-d_5. In this case, the optimal amount of added pyridine-d_5 was screened. As depicted in Figure 49 and Figure 50, the pyrrolic/aromatic protons and the NH protons condense into sharper signals depending on the ratio of CD_2Cl_2/pyridine-d_5. The same explanation brought forward in section 3.5.2 is valid for the dimeric case. The effect for the NH protons is even more drastic since they experience line broadening already due to exchange effects because of the two equivalent tautomeric forms.

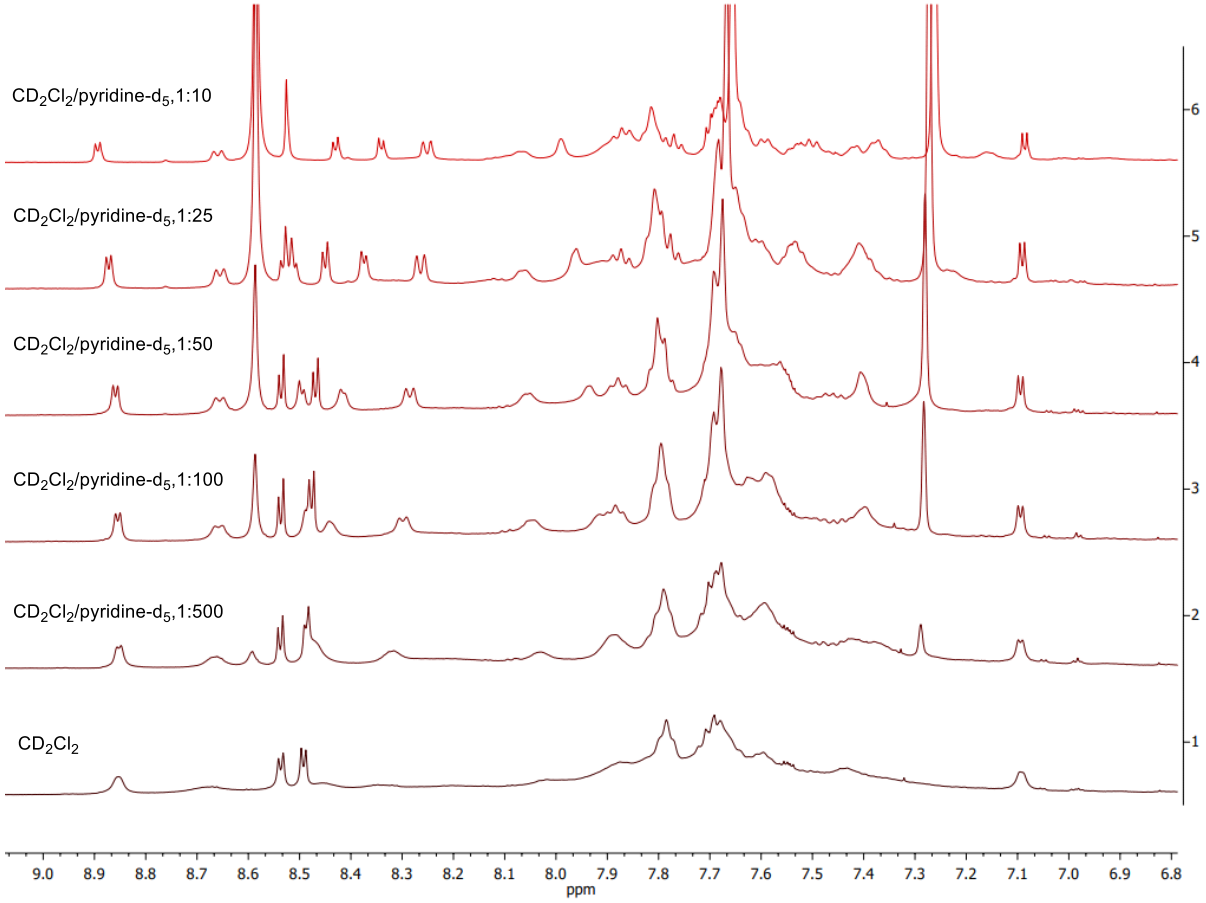

Figure 49: Downfield region of the ^{1}H NMR spectra of the cofacial ligand **197** – screening of CD_2Cl_2 / pyridine-d_5 ratio for strong signals.

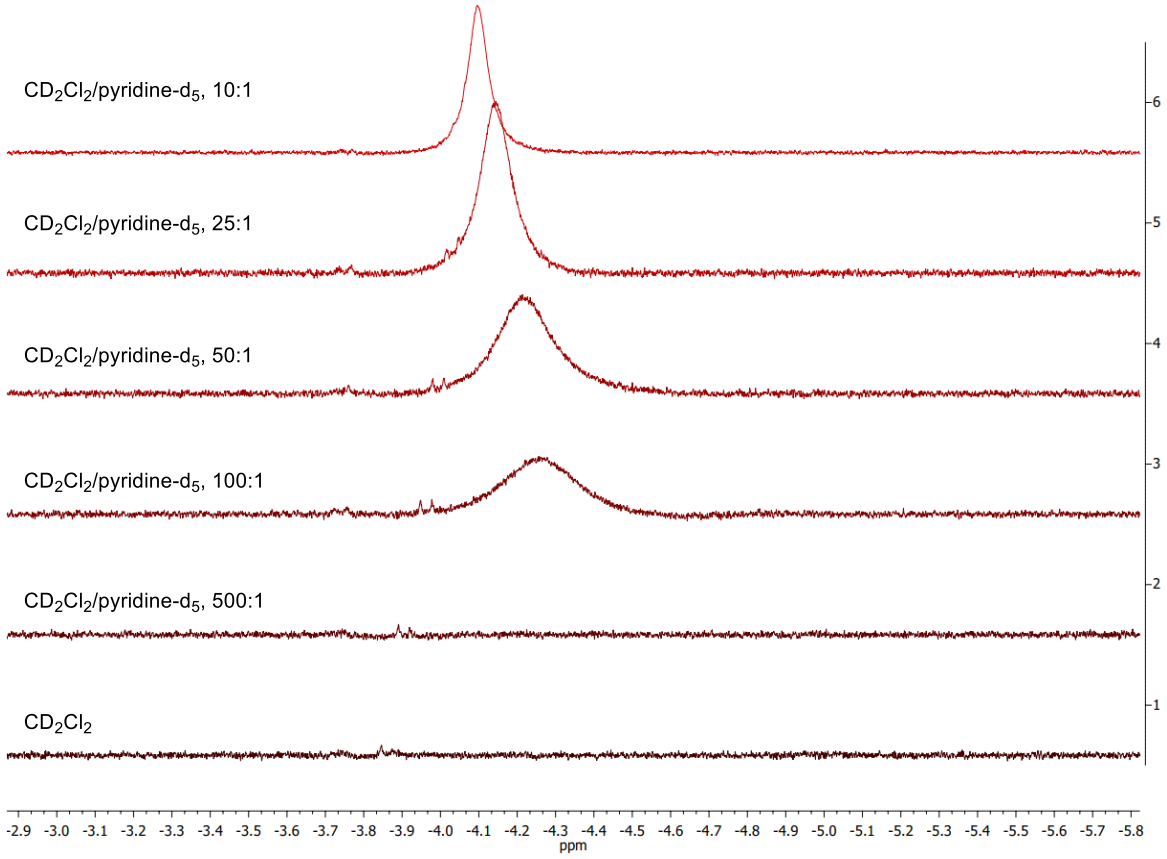

Figure 50: Upfield region of the ^{1}H NMR spectra of the cofacial ligand **197** – screening of CD_2Cl_2 / pyridine-d_5 ratio for strong signals.

The solubility of the monomeric and the dimeric N-fused porphyrins is significantly higher than for the Ag(III)-N-confused analogs. The concluding statement of section 3.5.1 is for that reason even more promising and encourages examining the free-base analogs in the concluding mixed condensation, affording the N-confused-porphyrin - porphyrin dimers.

The original idea behind synthesizing a ligand containing an N-fused- / N-confused-porphyrin stacked cofacially with a regular porphyrin subunit was to bring the same two metals in different oxidation states in spatial proximity.

3.5.4 N-fused-porphyrin - porphyrin metal complexes

Therefore, metal complexation reactions were investigated on the N-fused-tetraphenylporphyrin **198** as a test substrate, obtained as a side-product of the *Suzuki* cross-coupling reaction, as depicted in Scheme 56. The most prominent N-fused porphyrin complexes, which exhibit different oxidation states in the N-fused porphyrin core in comparison to the regular porphyrin core, are Mn(I), Mn(III), Re(I) and Re(II)/Re(V). By extending the reaction time of the procedure developed by *Furuta et al.*, the below presented Mn(I) and Re(I)

complexes **199** and **200** were synthesized in 78% and 76% yield, respectively (Scheme 59).[74, 285, 286]

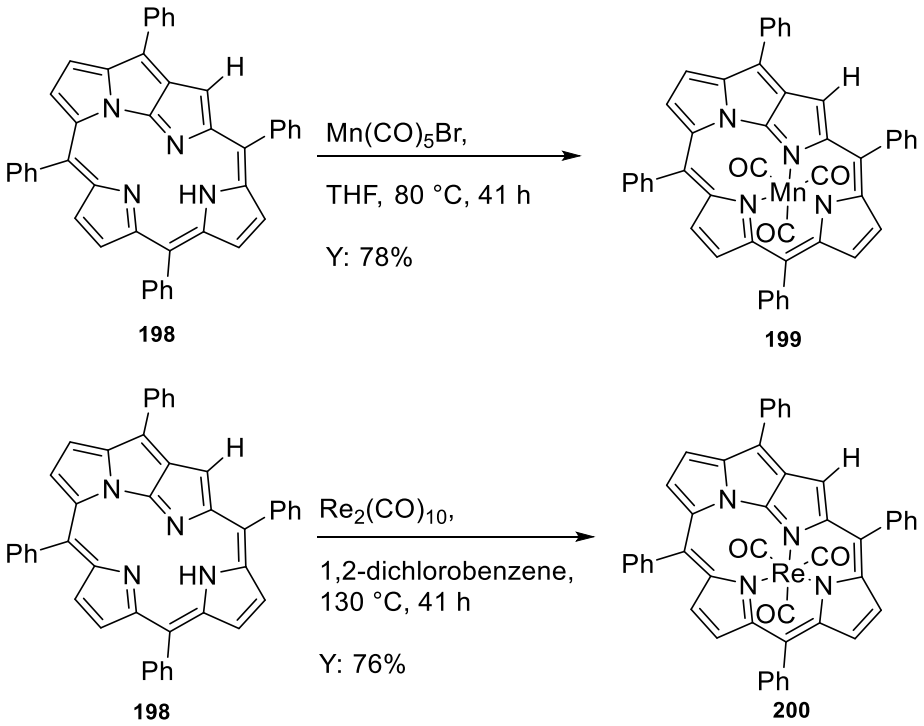

Scheme 59: Mn(I) and Re(I) complexation into TPP-N-fused porphyrin **198**.

According to a report by *Lindner* and *Dreher*, Mn(I)-carbonyl complexes attached to thiol-groups were analyzed *via* ^{1}H NMR spectroscopy and exhibited strong signals.[287] For the more common Mn(II) and Mn(III) complexes, as well as for the Re(II) and Re(III) complexes, a significant line broadening due to paramagnetic effects is expected. Thus, both complexes were analyzed by NMR spectroscopy. The spectra showed strong signals without a singlet that could be assigned to the NH proton in the low-field region of the ^{1}H NMR spectrum.

The adjusted protocol was subsequently applied to the cofacial N-fused porphyrin - porphyrin dimer **197** (Scheme 60).

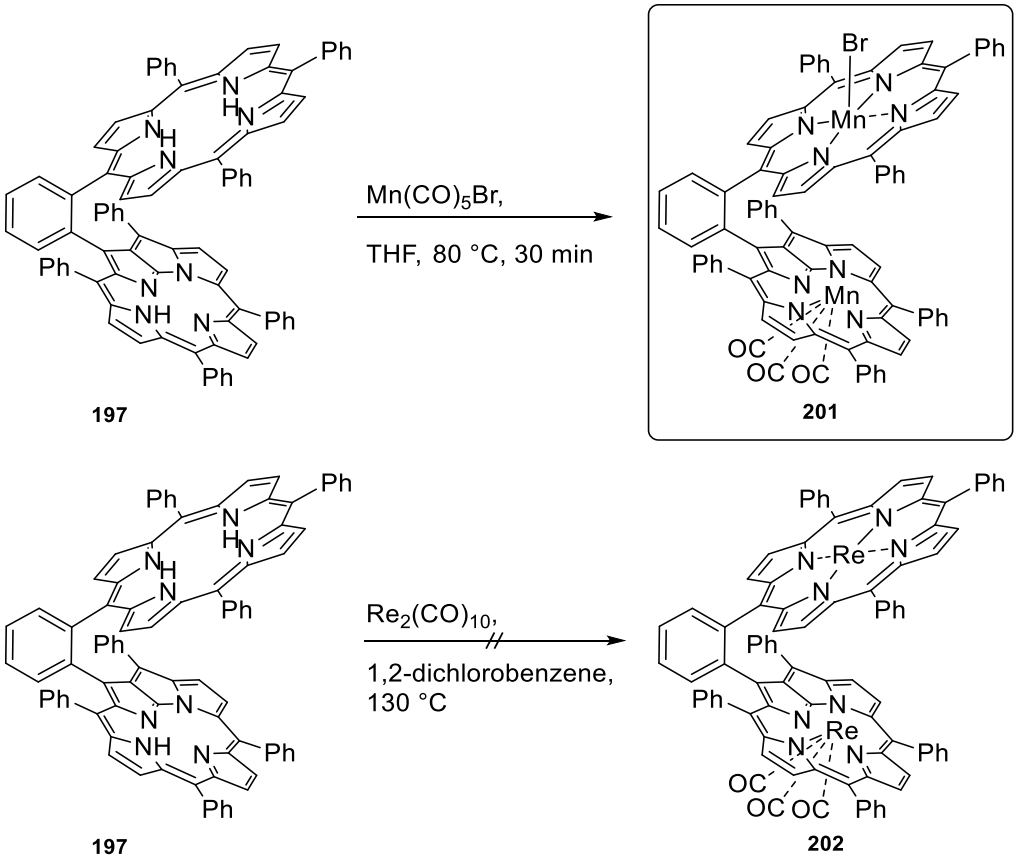

Scheme 60: Mn- and Re-ion coordination into the cofacial N-fused-porphyrin - porphyrin dimeric ligands **197**.

After stirring the N-fused porphyrin dimer, **197** in THF in the presence of the Mn(I) source and K_2CO_3 for 4 days, only partially metalated product was obtained. While monitoring the reaction progress *via* TLC, a few new spots on the TLC could be observed after 30 min, which corresponds to the reaction time reported by *Naruta et al.* Therefore, the solvent was removed after 30 min and the crude product was purified *via* flash column chromatography on silica gel, isolating a brownish solid.

The isolated fraction did not contain enough substance to analyze the compound properly *via* NMR spectroscopy or UV-Vis absorption spectroscopy. Therefore, the product was investigated by mass spectrometry and CID measurements. In parallel, DFT calculations were carried out to understand the 3D structure of the analyzed compound in its ionized form (Figure 51).

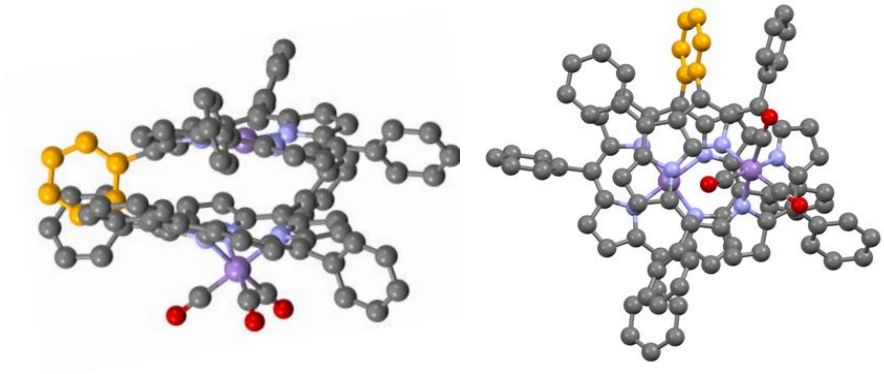

Figure 51: The structure of the Mn(I)Mn(III) complex **201** calculated with DFT. Side view and top view.

In the crystal structure, described by *Furuta et al.*, the Mn(I) center is sitting atop of the monomeric N-fused porphyrin plane and binds the three CO ligands facially. The Mn(III) center can be coordinated in-plane as shown by the crystal structure obtained for the Mn(III)-μ-oxo-Mn(III) complex **38** in section 1.2. DFT calculations suggest both mentioned 3D arrangements for the dimeric analog.

The HRMS of the Mn(I)-N-fused porphyrin-Mn(III)-porphyrin complex **201** was measured *via* ESI-MS and further CID measurements could prove the three coordinative Mn(I)-CO bonds. The three Mn(I)-CO bonds break simultaneously by increasing the acceleration voltage, indicating the facial arrangement as predicted by the DFT calculation in Figure 51. By applying 24 V, the half-life-period of the conversion from $Mn(I)(CO)_3$ to $Mn(I)(CO)_0$ is reached (Figure 52).

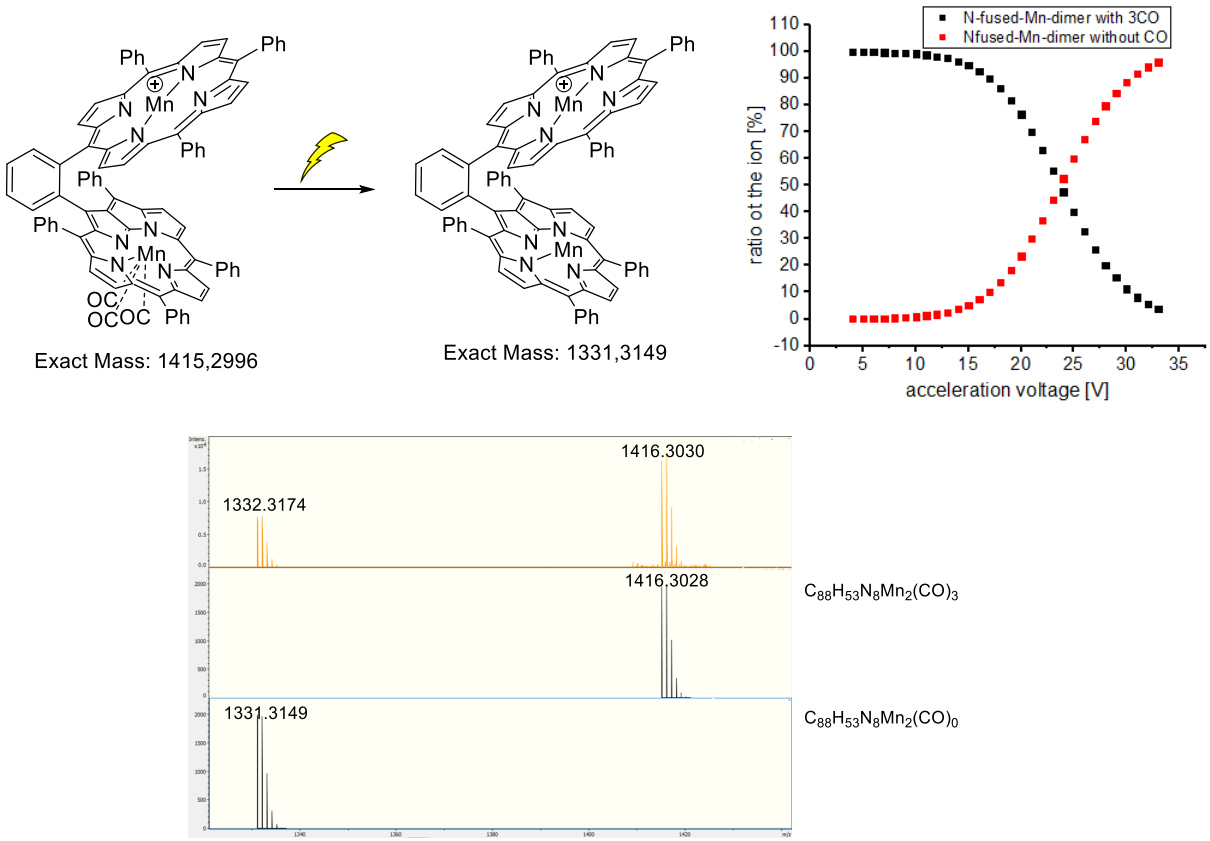

Figure 52: CID measurements to evaluate the coordination sphere of the Mn(I) center.

To increase the yield, the monomeric N-fused-porphyrin precursor **192** should be coordinated with Mn(I) before the subsequent mixed condensation reaction. The half-metalated complex can afterward be treated with $MnCl_2$ at elevated temperature as described in section 3.3.3 to achieve complete Mn(III) coordination for the regular porphyrin subunit. It might circumvent the Mn(I)-2NH-complex as the main by-product since the applied conditions were too mild for an efficient Mn(III) coordination in a regular porphyrin plane.

The respective Re(I)-N-fused-porphyrin-Re(II)-porphyrin complexes were not obtained with the depicted conditions in Scheme 60. However, the step-by-step metal insertion also seems to be promising in this case.

As the porphyrin ligands have been modified to adjust metal-metal distances, stabilize different oxidation states, or enable trimeric complexes, all neutral metal complexes suffer from a low solubility in aqueous solution and are difficult to ionize. Therefore, the ligands were sulfonated in the following steps to introduce a negative charge, enabling the analysis of ions in the gas phase and making the compounds water-soluble.

3.6 Ligand modification: Sulfonated *o*-phenylene bisporphyrin metal complexes

Porphyrin-based compounds *in vivo* have to be water-soluble to be functional in organisms. In 1888, the X-ray analysis of Heme b, a cofactor, which plays a crucial role in O_2 transportation in red blood cells, revealed the importance of water-soluble porphyrins in nature. Artificially induced water solubility can be implemented by incorporating charged substituents like sulfonates, carboxylates, phosphates, hydroxyl or amino groups.[288, 289]

In the following, sulfonate groups were introduced because of their applicability for various subsequent measurements in the gas phase.[243, 290, 291]

For that reason, the *o*-phenylene bisporphyrin **128** was dissolved in 98% H_2SO_4, while an immediate color change from red to green was observed and stirred at 100 °C for 14 h.[292] The subsequent work-up had to be modified from the protocol proposed by *Dong et al*. since neutralizing with NaOH as a base yielded the respective 6Na(I)-salt of the sulfonated dimer, which can barely be removed from the sample afterward. Instead, a 7 M methanolic ammonia solution was poured dropwise into the reaction mixture until a color change back to red was observed. After removal of the solvent and extraction with EtOH, 1,2-phenylene-bis-5-(10,15,20-(4-trisulfonicacidphenylporphyrin) (OBBPS, **203**) was obtained (Scheme 61).

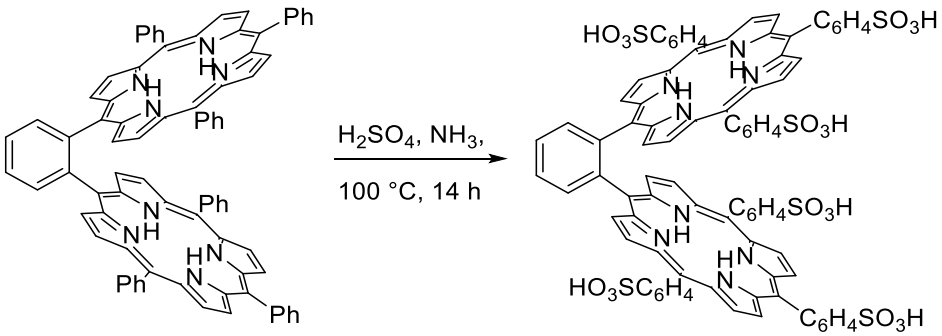

128 **203**

Scheme 61: 6-Fold sulfonation of OBBP **128** using H_2SO_4 as the sulfonating agent.

The obtained sulfonated porphyrin dimer exhibits the opposite solubility properties contradictory to OBBP **128**. While the molecule is insoluble in large amounts of EtOH, the solubility increases from MeOH to water. A methanolic instead of an aqueous ammonia solution had to be used to avoid the distillation to remove H_2O. The obtained sulfonated OBBPS **203** was analyzed by Erik Karsten Schneider *via* ESI-MS in the negative mode, as depicted in Figure 53. Depending on the H^+ concentration of the sample, differing amounts of H^+ are attached to the sulfonate groups.

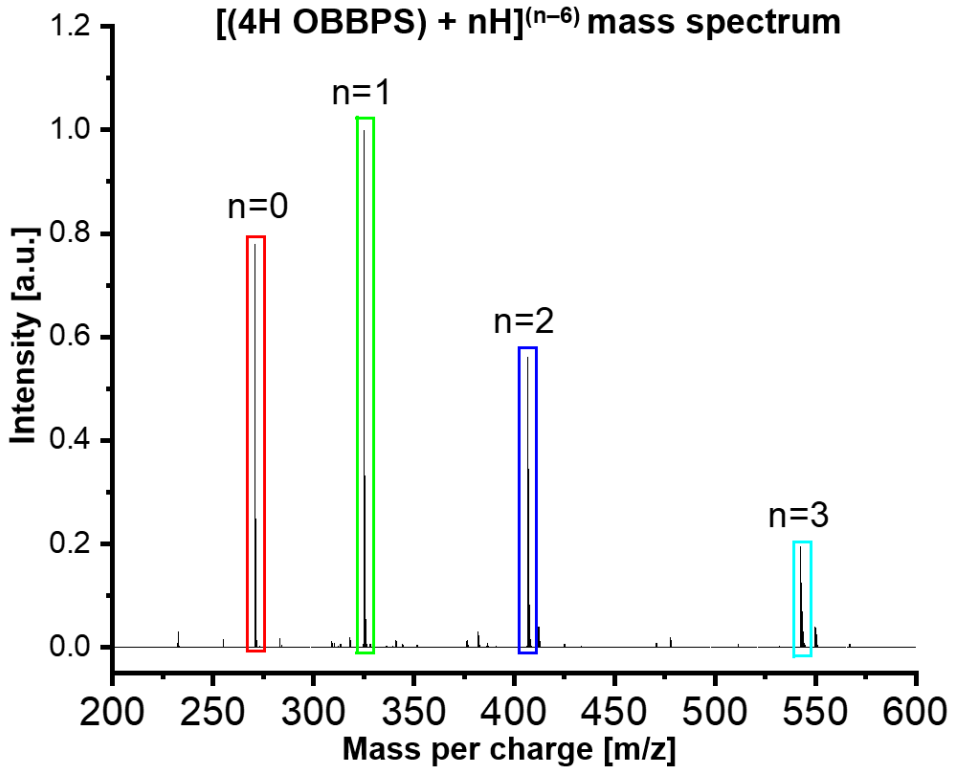

Figure 53: Negative-mode ESI-MS spectrum of the OBBPS ligand **203**.

Due to the promising results of the Pd(II) complexes in terms of $^1O_2$ emission (section 3.4.5) and the report by *Fülling et al.*, the corresponding Pd(II) complex was synthesized.[293]

To obtain the corresponding Pd(II) complex, the established protocol using $PdCl_2$ as the Pd(II) source was applied first (section 3.3.2). Interestingly, the Pd(II) seemed to avoid the coordination in a square-planar fashion into the porphyrin planes and instead interacts with the sulfonates joining the ligands intermolecularly. Thus, the partially deprotonated sulfonate groups were protonated by dropwise addition of 38% aqueous HCl solution to the methanolic reaction mixture until the color switches from red to green. Subsequently, $PdCl_2$ was added and the reaction mixture was stirred at 60 °C for 12 h (Scheme 62).

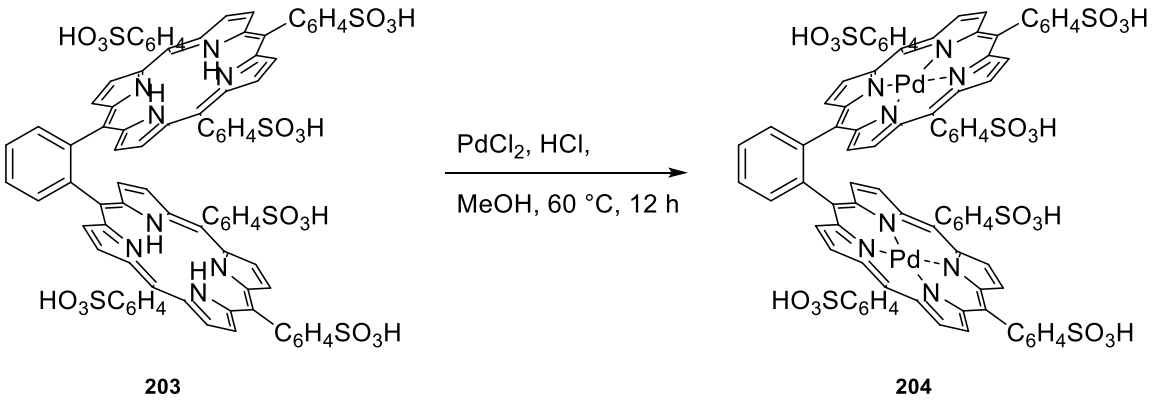

Scheme 62: The Pd(II) insertion into the sulfonated OBBPS ligand **203**.

The reaction progress can be monitored by a color change back to red, indicating removing the additional protonated tertiary amines of the porphyrin core by Pd(II). After removing the solvent under reduced pressure, the residue was recrystallized from EtOH to collect 2Pd(II)OBBPS **204**. Three iterations were necessary to purely obtain the 2Pd(II) complex after removal of the solvent without NH_4OH and Pd-salt impurities.

3.6.1 Photodissociation spectroscopy

Having negatively charged ions in hand, the compounds can be investigated *via* photodissociation and photoelectron spectroscopy in the gas phase.

The law of *Lambert-Beer* describes light absorption in the condensed phases. The value for the extinction can be obtained as the logarithmic ratio between the intensity of the irradiated light and the intensity after passing through the sample. These factors depend on the concentration c, path length d and the extinction coefficient ε.[294]

$$E = \log\left(\frac{\Phi_0}{\Phi}\right) = \epsilon \cdot c \cdot d \qquad \text{(II)}$$

In the gas phase, the concentration of particles is by order of magnitudes lower, so that it is not sufficient to measure absorption. A valid alternative to observe an interaction with light and particles represents photodissociation processes. This process can be understood as fragmentation of a molecule or an ion induced by irradiation with light. Such a process is only possible if the system can absorb a photon, i.e., an excited state populated by the interaction with the photon. These decay processes are used in photodissociation spectroscopy, which investigates ions in the gas phase. The recording of the spectrum is based on the detection of the ions at different excitation wavelengths. For this purpose, a mass filter separates intact ions from dissociated ions after being exposed to light. The comparison of the resulting mass spectrum with a reference spectrum without exposure to laser light enables the calculation of the absorption bands of the studied ions.

The sulfonated OBBPS **203** was measured and analyzed by Manuel Link as described below Figure 54.

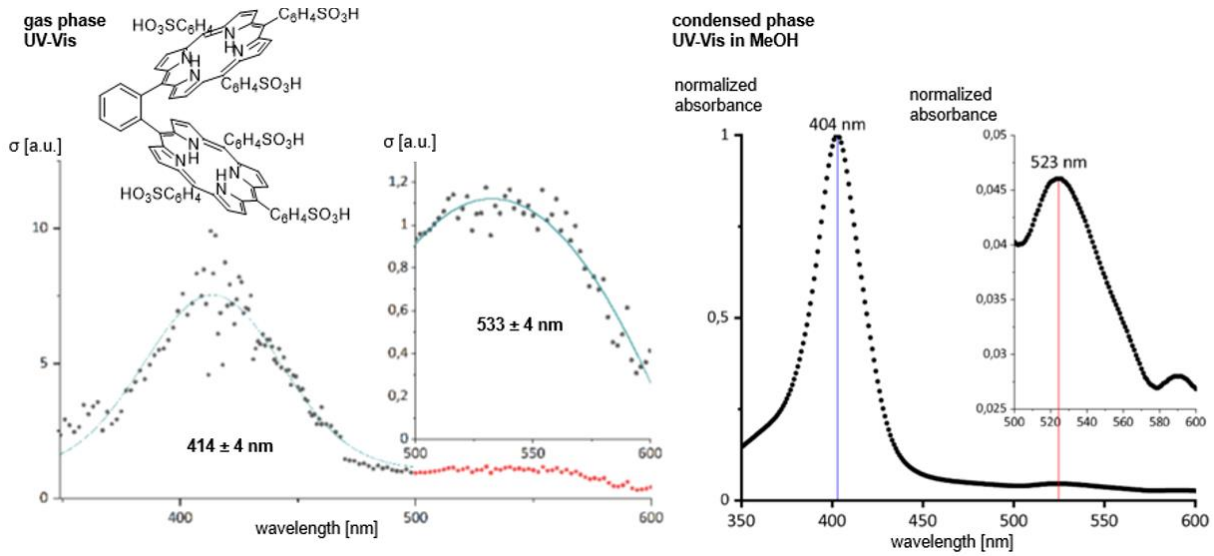

Figure 54: Photodissociation spectroscopy – gas-phase UV-Vis of the $OBBPS^{5-}$ *vs.* condensed phase UV-Vis spectra of the neutral OBBPS **203**.[295]

Only the ion signal of the $OBBPS^{5-}$ was large enough to measure photodissociation spectroscopy and is therefore discussed in the following. Based on the spectrum, a maximum of the *Soret*-band at 414 ± 4 nm and a maximum of the Q-band at 533 ± 4 nm can be seen. A distinctive feature of the $OBBPS^{5-}$ ion is that the Q-band appears as the shoulder of the *Soret*-band and is broadened compared to the monomer.[295] For comparison, a condensed phase spectrum of OBBPS **203** in MeOH is shown in Figure 54. The maximum of the *Soret*-band in the condensed phase is at 404 nm and the Q-band is only weakly pronounced, showing a maximum at 524 nm. Both bands are blue-shifted to a similar extent in solution ($\Delta\lambda_{Soret\text{-band}}$ = 10 nm, $\Delta\lambda_{Q\text{-band}}$ = 10 nm). This could be explained by the interaction with solvent molecules in the condensed phase. For the respective Pd(II) complex **204**, shifts are also expected but might differ depending on the solubility of the metal complex.

3.6.2 Photoelectron spectroscopy

Furthermore, photoelectron spectroscopy was conducted with the free-base OBBPS **203**. Photoelectron spectroscopy observes emerging photoelectrons due to the interaction of light with the ions. Conclusions about their bonding situation can then be drawn from their kinetic energy. The analyzed ions are irradiated in a high vacuum with monochromatic light, usually generated by a laser. The expulsion of the electrons is based on the photoelectric effect: in case that the energy of the incident photons is equal to or greater than the binding energy of the electron, the electron can be released from the ion.[296] In addition to that, the kinetic energy can be calculated back.

$$E_{kin} = h\nu - E_{bind} \qquad \text{(III)}$$

The binding energy, which the electron just needs to be released, can be investigated with a photoelectron spectrum. If, in addition, a spectrum with higher excitation energy is used to prove that electrons with higher binding energy also exist, then the kinetic energy of the slowest electrons can be used to determine the barrier according to the formula depicted below, which defines the repulsive *Coulomb* barrier (RCB).

$$RCB = h\nu - E_{bind,max} \qquad \text{(IV)}$$

An intuitive explanation for the RCB is based on the micro-reversibility of reactions. Looking at the approach of an electron to an anion, an electrostatic repulsion of the negative charges can be observed, which is inversely proportional to the distance. This electrostatic repulsion represents a barrier that an electron must overcome before forming a stable anion with an additional charge through a binding interaction. The ejection of photoelectrons now represents the exact reverse of this process and describes the barrier that must be considered. The energy required to remove an electron from a multi-anion result from the sum of the binding energy and the height of the RCB. In practice, this is done by extrapolating the edge of the signal of the slowest electrons onto the x-axis. [297, 298]

The photoelectron spectrum of $OBBPS^{6-}$ is represented in Figure 55 and gives information about the stability, the RCB and the electron affinity of the molecule.

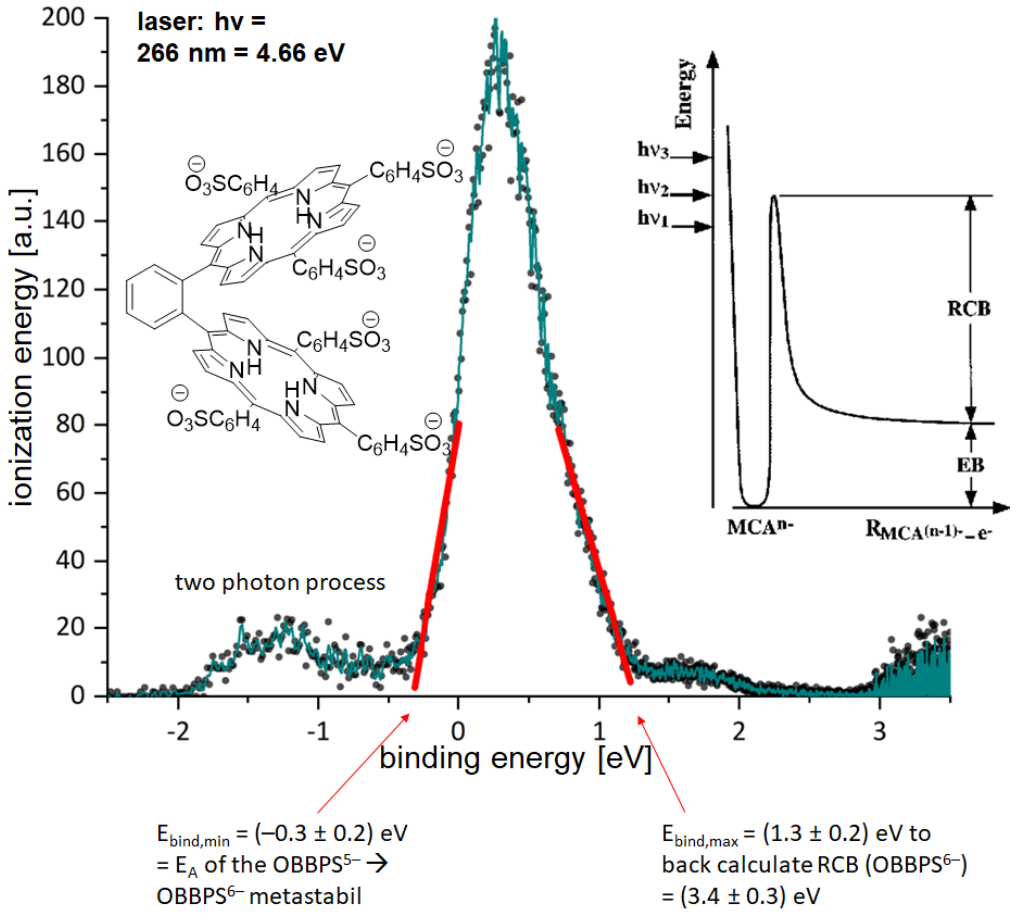

Figure 55: Photoelectron spectrum of the $OBBPS^{6-}$ anion and an illustrated explanation of the RCB.[295]

By extrapolating the edges of the spectrum towards lower energies, the $E_{bind,min}$ = (−0.3 ± 0.2) eV, which is equivalent to the electron affinity (E_A) of the $OBBPS^{5-}$, indicates that the $OBBPS^{6-}$ is metastable. Additionally, extrapolating the edges to higher binding energies allows to deduce $E_{bind,max}$ = (1.3 ± 0.2) eV and back calculating of RCB ($OBBPS^{6-}$) = (3.4 ± 0.3) eV. The signal at lower E_{bind} arises from two-photon processes and, therefore, cannot deduce information from these points of view.[295]

For the 2Pd(II)OBBPS complexes, preliminary results show a dramatic change of the electronic environment due to the Pd(II) coordination.

4 Conclusion and Outlook

Many biochemical processes in nature are strongly dependent on highly specific multimetallic reaction centers. Over thousands of years, they have evolved to catalyze, e.g., the reduction of CO_2 – the most central chemical conversion to accomplish life conditions as we find on earth. However, the research about interactions of spatially coupled metal centers is still in its infancy. This work provided synthetic tools to synthesize tailor-made homo- and heteromultimetallic rigid arrangements, precisely adjusting the metal-metal distances. The rough adjustments were made by adapting the tetrahedral angle given by the selected backbone or the connectivity to the linker moiety. The introduction of different residues to the *meso*- and *β*-position of each porphyrin subunit allows for sterical fine-tuning and modified electronical and physical properties. Advancements of the protocol paved the way towards cofacial heterotrimeric complexes and asymmetrical porphyrin derivative-based complexes capable of stabilizing different oxidation states of the same metal. The resulting complexes were investigated to examine *inter alia* cooperative effects using ^{1}H NMR, ^{13}C NMR, IR, MS, X-ray diffraction, UV-Vis, luminescence, *Mössbauer*, photodissociation, photoelectron, high-resolution CID and IMS measurements, which were contrasted with DFT calculations.

4.1 Varying the backbone of angled porphyrin dimeric metal complexes

First different rigid backbones were considered to be tested to vary the metal-metal distances. Even though single internal alkynes between two porphyrin subunits could not be transformed into angular systems – double internal alkyne bridged porphyrin dimers could be converted into the [2,5-thiophene-bridged porphyrin]-dizinc(II) complex **94** (Figure 56).

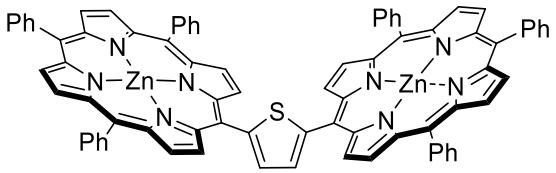

94

Figure 56: Molecular structure of [2,5-thiophene-bridged porphyrin]-dizinc(II) **94**.

By using reactive monomeric porphyrin precursors instead of the unreactive alkyne-joined porphyrin dimers, the homobimetallic 2Ni(II)- and the heterobimetallic Ni(II)-Zn(II) amino-connected porphyrin complexes were synthesized starting from pyrrole (**45**) and benzaldehyde (**48**). While the former is affordable in an overall yield of 4.4% over eight steps *via* a crucial

S_NAr substitution reaction, the latter was synthesized in a 17% yield *via* six steps having a *Buchwald-Hartwig* cross-coupling reaction the decisive step (Figure 57).

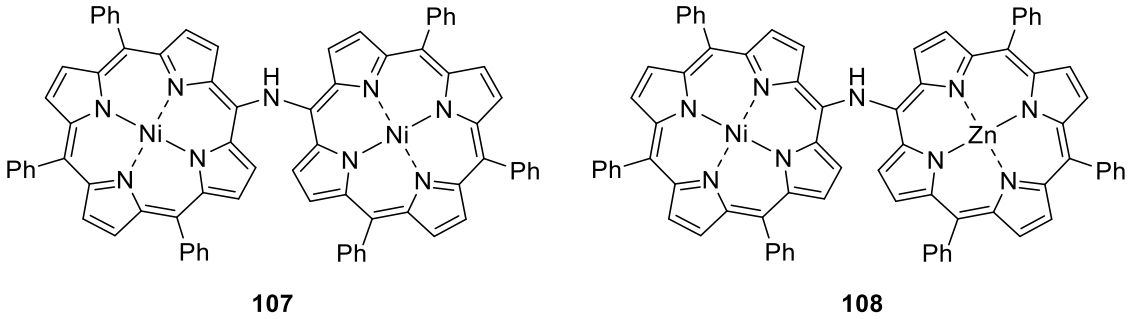

Figure 57: Molecular structures of 2Ni(II)- and Ni(II)Zn(II)-N-connected dimeric porphyrin complex **107** and **108**.

UV-Vis absorption spectroscopy showed a significant band broadening of the dimeric complexes compared to their monomeric analogs, regardless of the coordinated metal ions. Since the introduced angles between the porphyrin planes of 148° and 108°, respectively, do not enforce a π-stacking large enough to observe spatial coupling between the metal ions, the [2.2]paracyclophane (**109**) was considered to be investigated as a backbone. In terms of this research, a *pseudo-ortho* Zn(II)-Au(I)- as well as a *pseudo-para* Zn(II)-Ru(II)-complex could be synthesized, of which in the former, the metal centers lean toward each other (Figure 58).

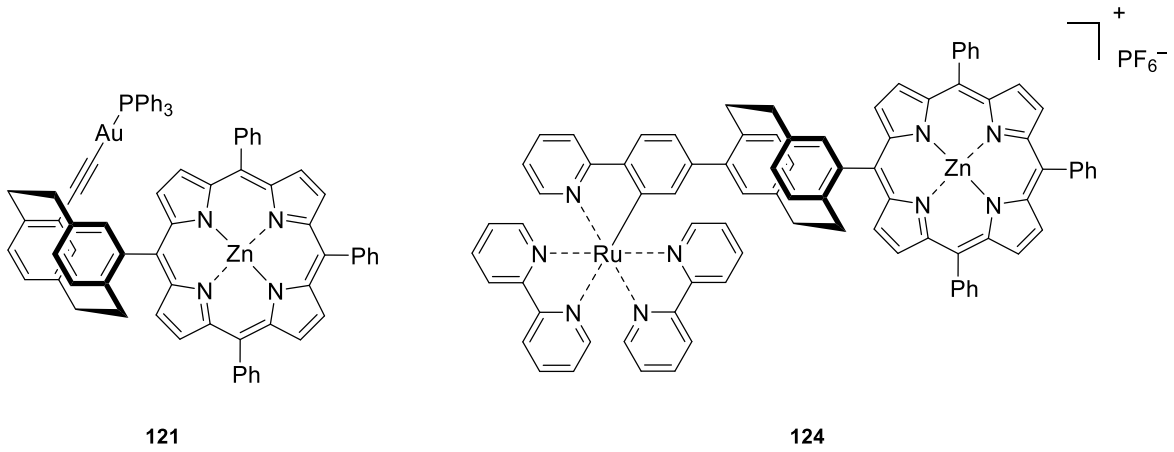

Figure 58: Molecular structure of *pseudo-ortho* Zn(II)Au(I)- and *pseudo-para* Zn(II)Ru(II)-[2.2]paracyclophane-porphyrin conjugates **121** and **124**.

As investigated by *Bräse et al*., the *pseudo-meta*, - *ortho* and -*geminal* substitution pattern should be applicable for the latter complex.[299] Since there are stability issues only for the Zn(II)-Au(I) complex, the Zn(II)-Ru(II) complex can be studied in more detail concerning rising distance-depending cooperative effects between the metal centers, e.g., by UV-Vis or luminescence spectroscopy. Since the porphyrin Fe(III) complexes are also accessible using the developed protocol, *Mössbauer* spectroscopy of the heterobimetallic complexes can be interesting. In regular porphyrins, the stability of an Fe(III) center is usually superior to that of

its Fe(II) analog, so that the second coordination site can be used to coordinate Fe(II) in a square-planar fashion, as reported, e.g., by *Deng et al.* for an Fe(II) biphenyl-2,2'-diyl complex with NHC ligation.[300] Through-space Fe(II)–Fe(III) interactions might be observed in *Mössbauer* spectra.

Since the *o*-phenylene-moiety is the most studied backbone for cofacial porphyrin complexes, the focus in the following was directed to adjusting the metal-metal distances through the connectivity to the backbone and the *meso*-substituents.

4.2 Cofacial *o*-phenylene-bisporphyrin metal complexes

A new synthesis route for both homo- and heterobimetallic porphyrin complexes was developed. The protocol allows the synthesis of aryl-based *meso*-*meso* and *β*-*meso*-linked porphyrins with an optional phenyl residue on one of the porphyrin subunits **128** – **130** (Figure 59).

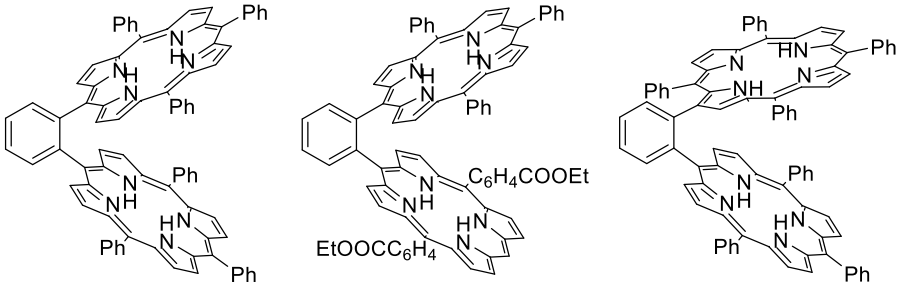

Figure 59: Molecular structure of the three different dimeric cofacial ligand systems **128** – **130**.

Where comparisons with literature can be drawn, the developed methodology generally provides higher yields, such as a factor of 6.8 for the well-known symmetric porphyrin dimer **128**. Based on this improved accessibility, 20 different homobimetallic species containing the transition metals Mn(III), Fe(III), Ni(II), Cu(II), Zn(II), Pd(II) and the main group elements Pb(II) and Bi(III) have been synthesized. In the case of Fe(III), heterobimetallic species with Ni(II), Cu(II), Pd(II) and Pt(II) were prepared – additionally, an Mn(III)-Cu(II) complex was synthesized (Figure 60).

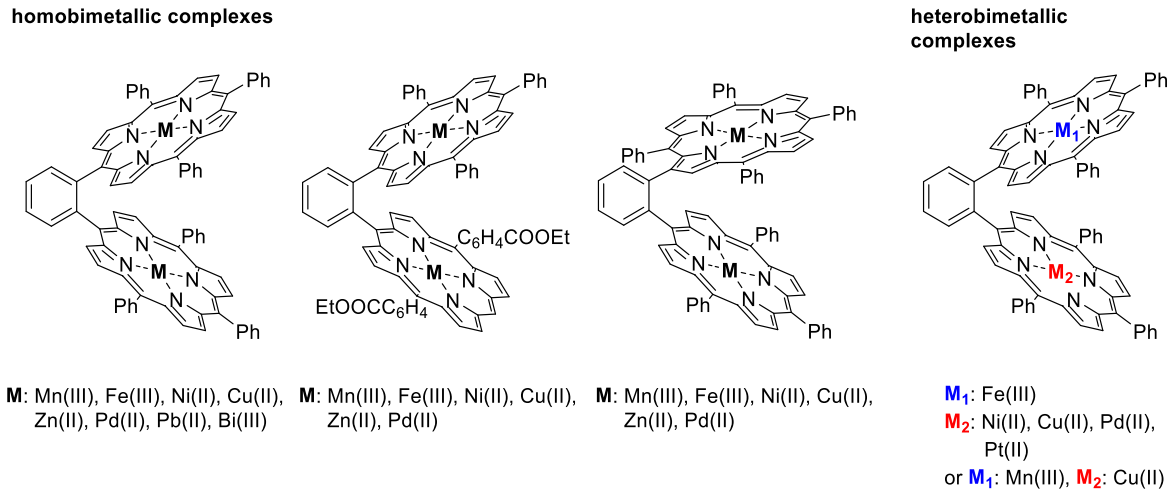

Figure 60: Molecular structures of the synthesized homo- and heterobimetallic complexes.

The isolated species were characterized through ^{1}H NMR, ^{13}C NMR, UV-Vis, IR, MS and high-resolution IMS measurements, contrasted with DFT calculations. For a set of three different bimetallic Zn(II) complexes, it could be shown that metal-metal distances differ systematically with the ligand (due to steric effects) and were able to be correlated with a trend visible in the *Soret*-band shifts and splitting. Furthermore, an unsymmetrical 2Ni(II) complex **141** could be crystallized in the form of a twin containing both planar-chiral enantiomers. This represents the first single-crystal X-ray structure of an unsymmetrical cofacial benzene-linked porphyrin dimer (Figure 61).

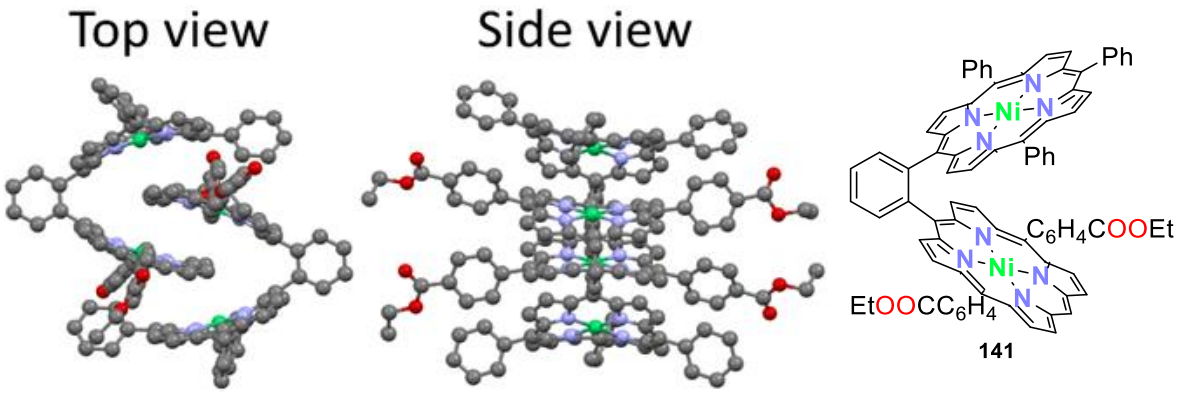

Figure 61: X-ray crystal structure of the 2Ni(II)EOBBP **141**.

The Fe(III) complexes were synthesized using a ^{57}Fe enriched chloride salt to perform *Mössbauer* spectroscopy. It could be proven that the dimeric Fe(III) centers are connected *via* a μ-oxo bridge coupling antiparallel to form a diamagnetic complex (Figure 62).

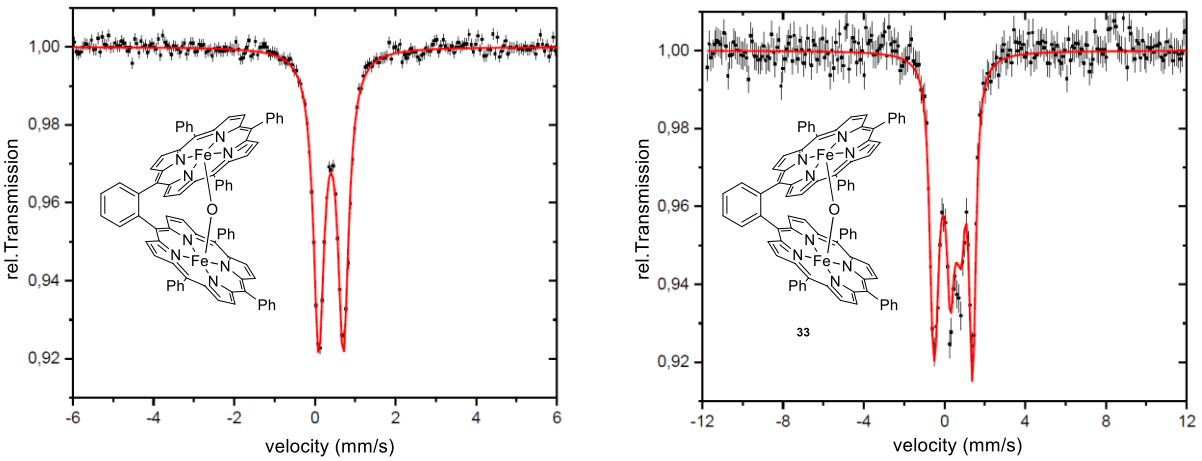

Figure 62: *Mössbauer* spectra of the antiparallel coupled diamagnetic Fe(III)-O–Fe(III) porphyrin complex. left: 77 K; right: 4.2 K and 5 T.

From these points of view, heterobimetallic complexes ought to be studied to evaluate possible through-space spin couplings. Therefore, the Fe(III) complexes containing different sized diamagnetic metal centers such as Ni(II), Pd(II) and Pt(II) as the second cation could be investigated to their affected isotope shifts. The paramagnetic analogs Cu(II) center, on the other hand, could influence the quadrupole and magnetic splitting of the Fe(III) core. As described in section 1.2, Mn(III)–O–Mn(III) centers can be obtained by exposing Mn(III)TPP monomers to air. The analog Mn(III)–O–Fe(III) center within the OBBP ligand is likely to exhibit intramolecular spin coupling *via* the covalent μ-oxo bridge. The interaction between the $^{5}/_{2}$ spin of the high-spin Fe(III) and the 2 spins of the high-spin Mn(III) center could couple antiparallel to a resulting total spin of ½ spin or parallel to a total spin of $^{9}/_{2}$.

Even though the respective lanthanide complexes could not be prepared by straightforward metal insertion, Yb(III) complexes were observed in which the metal sits on either one or both porphyrin subunits. The complexes perfectly meet the requirements for a novel type of PDT drug. A possible Yb(III) doped surface of (photon-)upconverting nanoparticles UCNP could directly coordinate the dimeric porphyrin (Figure 63).

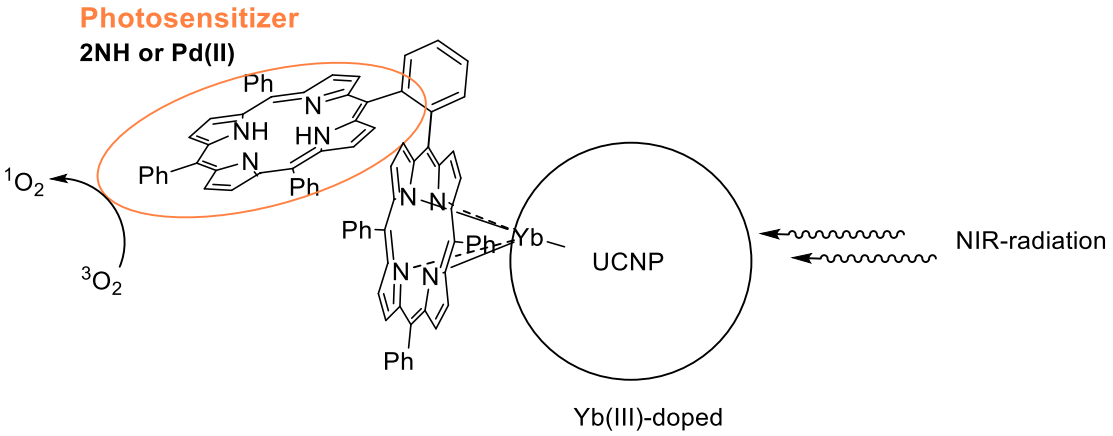

Figure 63: Yb(III)-based UCNP-porphyrin-dimer conjugate for photodynamic therapy (PDT).

In principle, NIR-radiation can be upconverted *via* the Yb(III)-doped inorganic crystal, sensitizing efficiently the remaining free-base porphyrin *via* spatial overlap of the porphyrin subunits to convert $^3O_2$ into the cytotoxic $^1O_2$.

4.3 Cofacial *o*-phenylene-trisporphyrin metal complexes

A straightforward novel synthesis route for homo- and heterotrimetallic trisporphyrin complexes have been established. The developed protocol enables the synthesis of the first aryl-based *trans*-*o*-phenylene trisporphyrin **34**, which has been prepared in an overall yield of 3.6% in seven steps starting from pyrrole (**45**) and benzaldehyde (**48**) (Scheme 63).

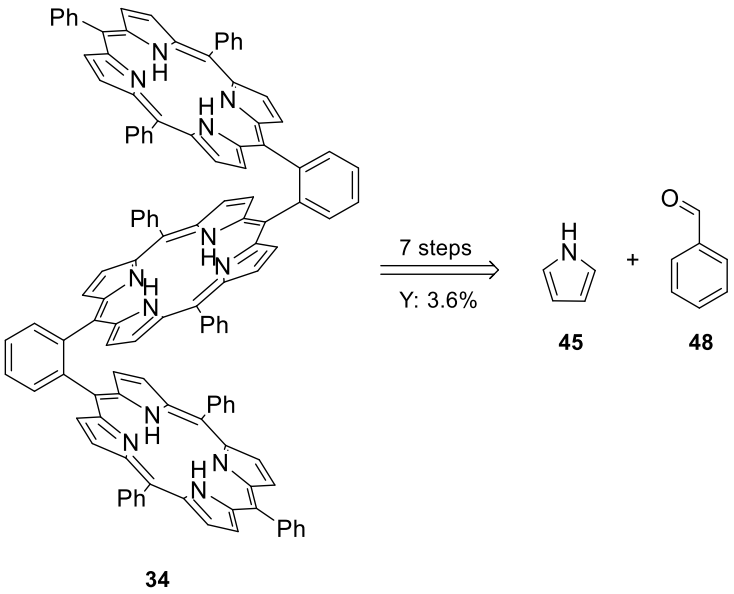

Scheme 63: Retrosynthetic pathway to synthesize the *o*-phenylene-trisporphyrin (OBTP) **34** starting from pyrrole (**45**) and benzaldehyde (**48**).

The synthesis also allows the *cis*-isomer to be studied as the first conformationally restricted planar-chiral trisporphyrin and the synthesized ratio to be adapted towards the *cis*-isomer by changing the acid catalyst from TFA to $BF_3 \bullet OEt_2$. The molecular structures of the two isomers and their ratio could be determined by IMS going in hand with DFT calculations and verified by ^{1}H NMR spectroscopy.

The *o*-phenylene linked freebase trisporphyrin ligand was used as the basis for the synthesis of homotrimetallic Mn(III)-, Fe(III)-, Ni(II)-, Cu(II)-, Zn(II)- and Pd(II)- complexes. An analogous procedure was also used to prepare the defined Ni(II)Fe(III)Ni(II)- heterometallic complex in an overall yield of 2.3% over nine steps (beginning with pyrrole and benzaldehyde) highlighting the robustness of the synthetic protocol (Figure 64).[301]

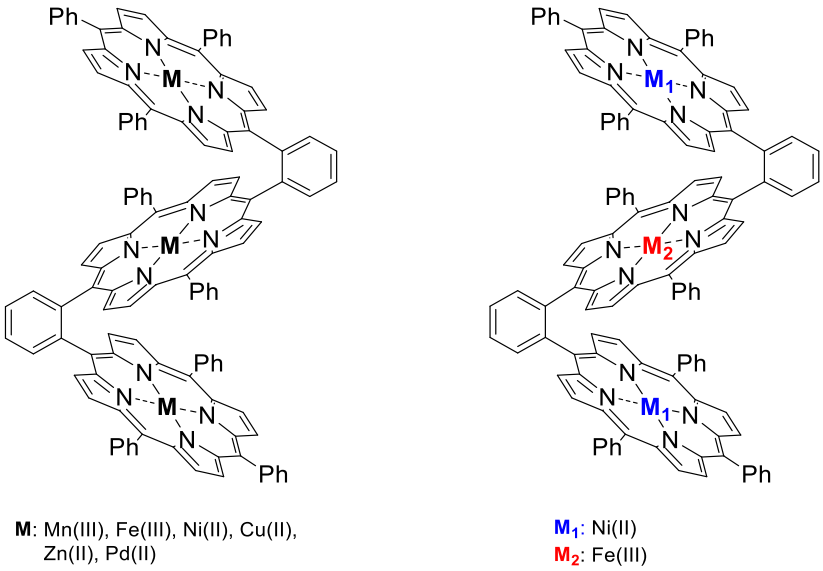

Figure 64: Molecular structures of the homo- and heterotrimetallic porphyrin complexes.

The molecular species were characterized using ^{1}H NMR, UV-Vis, luminescence, IR, MS, CID and high-resolution IMS measurements. The respective luminescence spectra of the Pd(II) monomer-, dimer- and trimer-derivatives showed a significant increase in $^{1}O_2$ emission at a wavelength of 1275 nm, giving rise to future experiments as a promising photodynamic therapy drug (Figure 65).

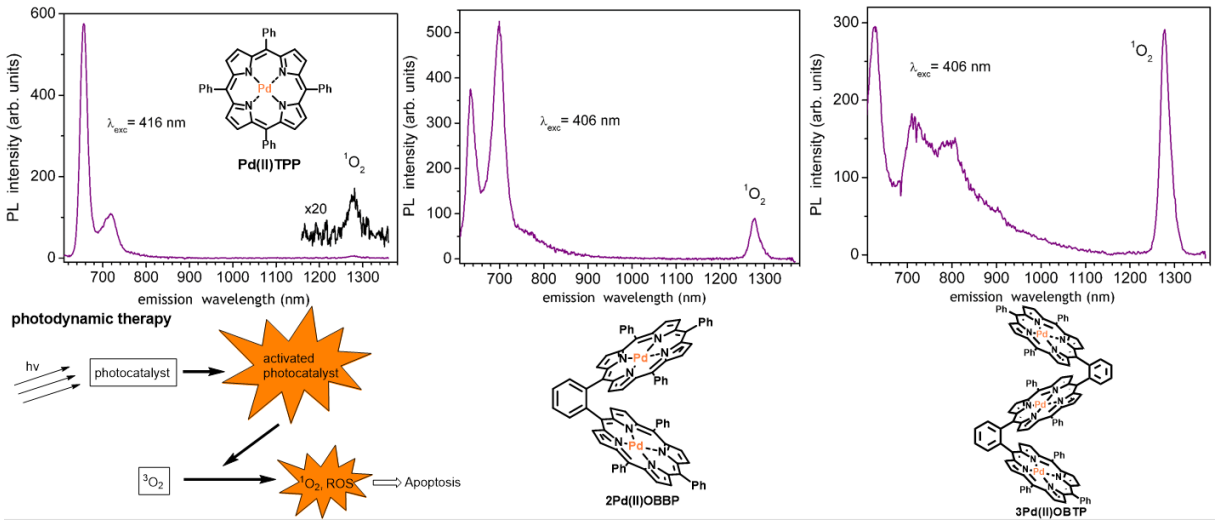

Figure 65: Luminescence spectra of the monomeric-, dimeric-, trimeric-Pd(II) porphyrin complexes indicating a non-linear increase of $^{1}O_2$ emission.

Therefore, quantitative measurements have to be carried out to be able to make more than semi-quantitative comparisons. Indirect quantification of $^{1}O_2$ production can be performed using, e.g., the dichlorofluorescein (DCFH) method. Therefore, the reactive oxygen species (ROS) can be detected using a probe for the non-fluorescent 2',7'-dichlorofluorescein diacetate (DCFH-DA). Under white light irradiation, ROS generated by the photosensitizer rapidly

oxidizes DCFH to emissive 2',7'-dichlorodihydrofluorescein (DCF) with a fluorescence peak at 522 nm and can thus be quantified.[272]

Studies of Ni(II) insertion kinetics suggest that it is possible to control the metalation order *via* the central porphyrin ring's characteristic steric and electronic environment. Correspondingly, the uses of the ligand as a selective complexation probe for dissolved metal ions was explored. To test whether the kinetical restriction is large enough to coordinate three different metals one-pot, the freebase trimeric porphyrin ligand was refluxed in DMF with an equimolar solution of $MnCl_2$, $CuCl_2$ and $PdCl_2$ for 4 h (Scheme 64). As a preliminary result, the trimetallic [Mn-Cu-Pd-OBTP]$^+$ species could be detected in the mass spectrum of a crude mixture. This was the first prove that porphyrin trimers can enable the deconvolution of complex metal salt mixtures.

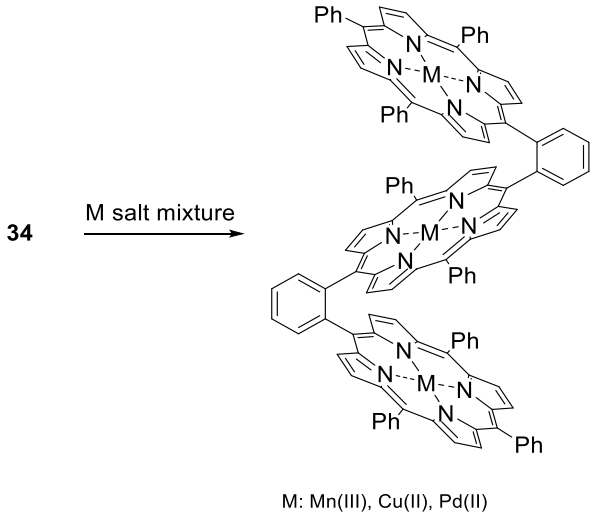

Scheme 64: Cofacial porphyrin-based heterotrimetallic complexes – statistical insertion approach.

In general, this idea can be expanded by the synthesis of porphyrin pentamers. For this purpose, a doubly *trans*-substituted *o*-phenylene-dipyrromethane porphyrin precursor could undergo a two-fold condensation reaction with two equivalent of *o*-phenylene-dipyrromethane porphyrin **175**. A pentameric metal complex will likely face a drastically reduced solubility and can therefore only be investigated by, e.g., mass spectrometry in crude mixtures.

Since the developed synthetic tools provide dimeric and trimeric ligands, they were applied to N-confused and N-fused porphyrin derivatives.

4.4 Metal complexes of cofacially connected porphyrin derivatives with regular porphyrins

A synthesis route for the first cofacially connected N-fused porphyrin with a regular porphyrin *via* an *o*-phenylene moiety was established with a total yield of 1.1% over five steps starting from pyrrole (**45**) and benzaldehyde (**48**) (Scheme 65). Stacking effects depending on the

pyridine concentration present were studied by ^{1}H NMR and the respective Mn(I)-Mn(III) tris-carbonyl-complex **201** could be synthesized using $Mn(CO)_5Br$ as a Mn(I) source.

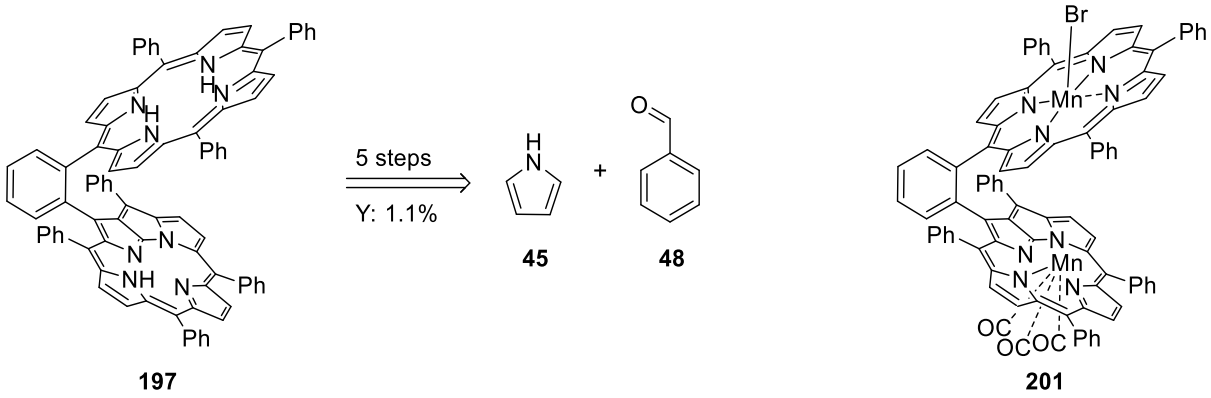

Scheme 65: Retrosynthesis of the first cofacially connected N-fused porphyrin with a regular porphyrin *via* an *o*-phenylene moiety.

The HRMS of the Mn(I)-N-fused porphyrin- Mn(III)-porphyrin complex was obtained *via* ESI-MS and CID measurements could prove the three coordinative Mn(I)–CO bonds. The three Mn(I)–CO bonds break simultaneously by increasing the acceleration voltage, indicating the facial arrangement predicted by the DFT calculation in Figure 66.

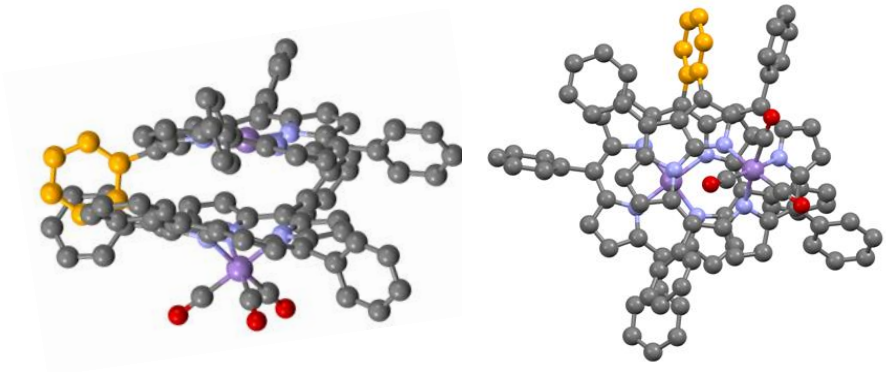

Figure 66: DFT calculations of the Mn(I)Mn(III)porphyrin complex **201**.

At an applied voltage of about 24 V, the half-life period of the conversion from $Mn(I)(CO)_3$ to $Mn(I)(CO)_0$ is reached.

As proof of principle, the Re(I) coordination into N-fused porphyrins showed a high yielding and clean reaction, encouraging the test of the mentioned dimeric complexes in more detail. Since Re(II) complexes are known to be stabilized in regular porphyrin cores, as described by *Collman et al*., this may provide an analog to show that in addition to the M(I)-M(III) centers, M(I)-M(II) centers can also be synthesized *via* the developed protocol.[302] Since Re-ions are stable even in oxidation states such as Re(V), further oxidation can be tested later.[303]

Furthermore, the route towards the [*o*-formyl-phenyl-N-confused-TPP]-silver(III) **190** was achieved, but the subsequent condensation reaction could not be further investigated due to solubility issues. *Ishizuka et al.* reported a reductive decomplexation reaction of the Ag(III)

complex using $NaBH_4$ in 70% yield, which is supposed to increase the solubility significantly.[280] Subsequent condensation reactions analogs to the N-fused derivative can provide a cofacial N-confused-porphyrin - porphyrin dimer capable of stabilizing different metals in differing oxidation states in a square-planar fashion. At a later stage, e.g., an Ag(I) source can be used to coordinate an Ag(II) in the regular porphyrin[304] and Ag(III) in the N-confused porphyrin, respectively[62]. Thus, an excess of the Ag(I) is required since apart from coordination, it is consumed as an oxidation reagent to yield the thermodynamically stable product.[280]

Solubility and ionization issues were not tackled besides ligand modifications to adjust metal-metal distances, stabilize different oxidation states, or enable trimeric complexes.

4.5 Ligand modification: Sulfonated *o*-phenylene bisporphyrin metal complexes

The *o*-phenylene bisporphyrin ligand could be sulfonated 6-fold in the respective *p*-position of the phenyl residues. By avoiding alkaline bases, the up to 6-fold negatively charged sulfonated dimeric porphyrin ligand could be observed in ESI-MS measurements (Figure 67).

Furthermore, two Pd(II) ions could be inserted into the ligand and the complex was subsequently isolated by recrystallization from EtOH.

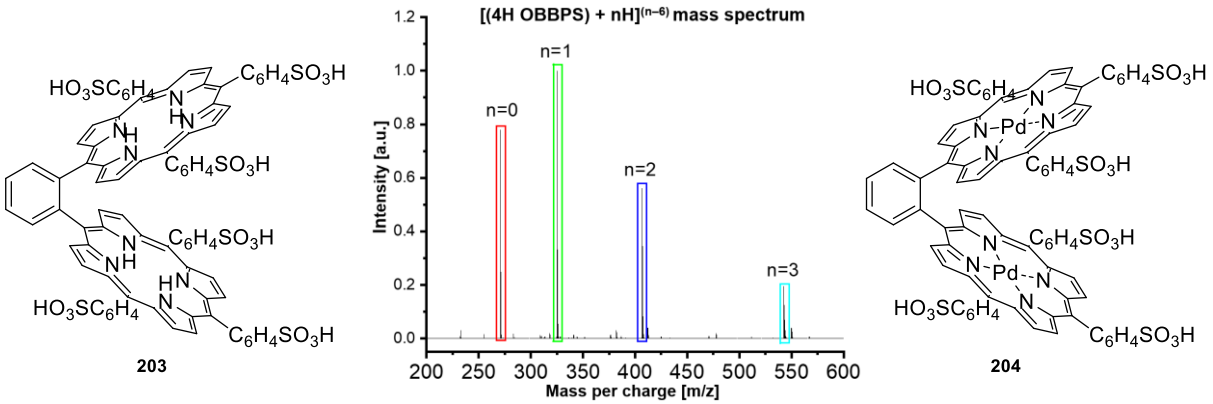

Figure 67: Negative-mode ESI-MS spectrum of the OBBPS ligand **203**.

The free-base ligand was investigated by photodissociation and photoelectron spectroscopy in the gas phase. The interaction between the sulfonated porphyrin dimer **203** and the solvent molecules in condensed phase results in a hypsochromic shift of the *Soret*-band and the Q-bands by 10 nm each. Furthermore, the 6-times negatively charged OBBPS could be characterized as a metastable compound with an RCB energy of 3.4 ± 0.3 eV.

For the photoelectron spectroscopy, first results show that the coordinated metal ions lead to a significant change of the electronic environment. Furthermore photodissociation spectroscopy of the respective metal complexes could lead to a different absorption behavior. Metalated porphyrin derivatives tend to be less soluble and therefore the absorption bands in the gas phase can change dramatically. Especially the comparison between the two can lead to valuable information.

Testing of sulfonated trimeric porphyrin ligands and their metal complexes derivatives can be used to deduce even more insightful information about solubility and stacking effects affecting absorption and electronical properties of porphyrins in the condensed phase compared to the gas phase.

Moreover, the sulfonation protocol can be applied on the trimeric Pd(II) complex **182** to make the compound water-soluble – a decisive property of a potential photodynamic therapy drug.

5 R-SF_4CN – The polar SF_5 group (ETH Zurich)

5.1 Theoretical background

Due to its high electronegativity, paired with low polarizability and small size, fluorine has remarkable physicochemical properties and takes up an exposed position in the periodic table. The exceptional properties of the element are also transferred to fluorinated organic compounds. For that reason, fluorinated materials play a key role in the context of functional molecules in the field of optoelectronic materials,[305] pharmaceuticals,[306-308] herbicides and fungicides[309, 310]. Fluorinated compounds have a unique composition of properties, such as the link between lipophilicity and polarity. They shape our everyday life in an often unrecognized way in the form of modern high-performance materials. The use of *Teflon*,[311] *Gore-Tex* membranes, [312] fluorinated fuel tanks or perfluorinated alkanes, which can effectively slow down the oxidative metabolism of drugs *via* cytochrome P450 monooxygenase, are just a few outstanding examples[313]. Fluorine has for long been regarded as an element for military and special purposes. Until the accidental discovery of fludrocortisone as part of the investigation of halogenated cortisol derivatives in the 1950s, the remarkable influence of the substituent on pharmacological properties was shown for the first time.[314] In 1970, only 2% of the authorized drugs in the market contained at least one fluorine substituent.[315] In 2007, however, the number of approved, fluorinated drugs was estimated at around 20%[316] and is now on the way to reaching the share of 30%.[317]

Besides simple fluoride substitutions, fluorides' unique properties were frequently introduced in the form of trifluoromethane or pentafluorosulfanyl groups. The essential property of the pentafluorosulfanyl group is its square pyramidal morphology in contrast to the tetrahedral geometry of trifluoromethyl groups. The spatial arrangement of pentafluorosulfanyl groups enlarges the rotation barrier, increasing interaction with binding pockets *in vivo*.[318]

Furthermore, the SF_5 group excels due to an, e.g., increased hydrolytic stability, a greater *van-der-Waals* volume and a higher electronegativity and lipophilicity than the CF_3- group. Especially the latter is a curse and a savior at the same time since potential drug candidates in an organism all need to be water-soluble to an extent.[319]

The first organic compound containing an SF_5-group was reported in 1950 by *Silvey* and *Cady* in their synthesis of trifluoromethyl sulfur pentafluoride.[320] A decade later, *Sheppard et al.* described the first synthesis of an aryl sulfanyl pentafluoride.[321] Since then, synthetic methodologies to introduce the SF_5-group have become available and were summed up by

Zanda et al. in 2012[322] and later by *Welch et al*. in 2015[318]. Access to SF_5 substituted aryl derivatives is primarily accomplished through a few methods, such as treating thiophenols with fluorine gas or the chlorofluorination of aryl disulfides with KF and Cl_2 give chlorotetrafluorosulfanyl benzene derivatives ($ArSF_4Cl$), which can be fluorinated to the SF_5 analogs in the last step.[323, 324]

The surprisingly specific synthetic reaction towards an SF_4X system suggests the applicability of other tetrafluoro-λ^6-sulfanyl groups containing a substituent with more prominent properties than a chloride. To circumvent the low water solubility of the SF_5 group, the 6th coordination site could be substituted to a more polar carbonitrile group.

5.2 Main part

Before studying as a visiting researcher at ETH Zurich, Dr. David Rombach worked independently on this topic and conceived the respective experiments. His former results indicated a successful one-pot procedure to the first organic SF_4CN-group starting from an aromatic disulfide **205** (Scheme 66).

First hints about the existence of the SF_4CN-group were obtained after a reaction with ^{13}C-KCN under oxidative conditions in the presence of NBu_4Cl and XeF_2. The ^{13}C mass matching to the molecular formula of **207** was detected for the first time.

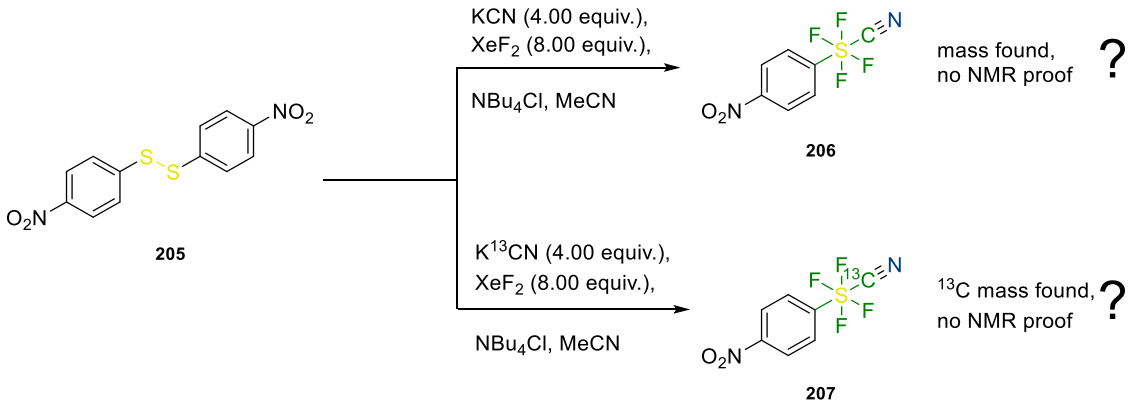

Scheme 66: Preliminary results of the conversion of an aromatic disulfide into the first organic *trans*-SF_4CN group.

A control experiment using ^{12}C-KCN showed the corresponding differences in the mass spectrum. Therefore, it was assumed that a CN group had been introduced initially. Furthermore, a preliminary reaction screening was conducted by Dr. David Rombach, using relative gas chromatography-mass spectrometry (GC-MS) to determine yields and an analysis of the side-products encountered.

Based on the mentioned studies, this work aims for a one-step protocol converting sulfur precursors into tetrafluoro-λ^6-sulfanyl carbonitrile groups, a hydrophilic alternative to the well-established pentafluorosulfanyl group. Therefore, variable reaction conditions were investigated for 1,2-bis(4-nitrophenyl)disulfane (**205**), 1-nitro-4-thiocyanatobenzene (**208**), trifluoro(4-nitrophenyl)-λ^4-sulfane (**209**) and chlorotetrafluoro(4-nitrophenyl)-λ^6-sulfane (**210**) were investigated under the supervision of Dr. David Rombach (Scheme 67).

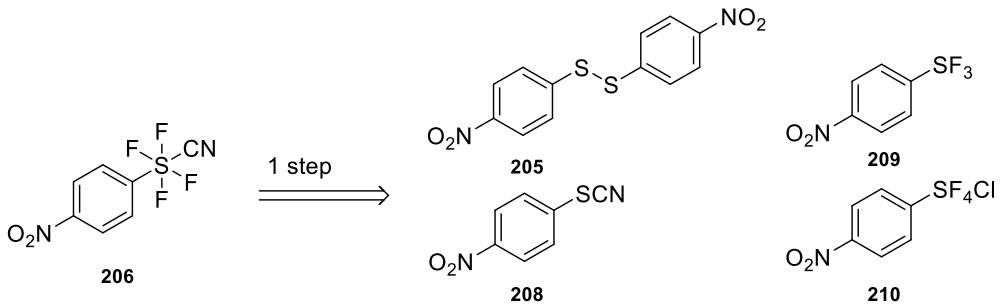

Scheme 67: Retrosynthetic approach yielding the *trans*-SF_4CN group using **205**, **208** – **210** as a starting material.

Reaction products were mainly evaluated by ^{19}F NMR spectroscopy and GC-MS. According to the literature, it was assumed that the $S(VI)F_4$ species should have resonances in the low field region of the ^{19}F NMR spectra.[325] Therefore, all unknown species were evaluated, arising as a singlet (for the *trans*-SF_4 case) or split into three signals with an AM_2X spin system (for the *cis*-SF_4 case). With the literature known signal sets as described in the below-presented Table 5, NO_2-Ph-SF_4Cl was carefully considered as a role model, keeping in mind that the π-back-bonding property of the introduced nitrile-group can dramatically alter the electronic environment of the fluoride substituents.[325]

Table 5: ^{19}F NMR chemical shifts [ppm] and coupling constants [Hz] measured in $CDCl_3$ in a 6:1 mixture of *trans*-NO_2-Ph-SF_4Cl and *cis*-NO_2-Ph-SF_4Cl.[325]

^{19}F NMR chemical shifts [ppm]	Multiplicity and *J* [Hz]	Compound
135.5	s, –	*trans*-NO_2-Ph-SF_4Cl
159.8	td, 163.7, 153.3	*cis*-NO_2-Ph-SF_4Cl
101.3	dd, 163.7, 83.2	
67.3	dt, 153.5, 83.5	

GC-MS experiments were undertaken in the case of a promising ^{19}F NMR spectrum and high-resolution mass spectrometry was conducted to characterize the sample further.

For the screening of the possible formation of NO_2-Ph-SF_4CN **206**, the above presented *p*-substituted nitro-compounds **205**, **208** – **210** were screened to provide the aimed SF_4CN group on different stages. The NO_2-group was chosen because of the simplified handling of a rather melting late compound, its commercial availability for the disulfide case, its resistance against oxidation and the ability to be reduced to the amine derivative later. Phenyl sulfur chlorotetrafluoride has a boiling point of 80 °C / 20 mmHg. In comparison to that, the NO_2 analog melts at 130 – 131 °C.[324] Additionally, subsequent functionalization *via* the NO_2 group is expected to be beneficial for future applications.

5.2.1 Disulfide – a commercially available reduced sulfur source

The first experiments showed fluorinated sulfuric compounds bearing nitriles after the disulfide's oxidation reactions with KCN, N-base and XeF_2 (Scheme 66). At that point, the HRMS of a molecule with the molecular formula $C_7H_4F_4N_2O_2S$ was consistent with the NO_2-Ph-SF_4CN analog **206**. After optimizing the reaction conditions for this compound, more detailed NMR studies were possible and the HRMS results could be assigned to the 4-nitrobenzene-(N-(trifluoromethyl)sulfinimidic fluoride) (NO_2-Ph-$SFNCF_3$, imine) **215** and not to the initially presumed SF_4CN isomer **206**. This can be underlined with the rearrangement for SF_5CN gas reported by *Willner* and *Vorobev et al.*[326, 327]

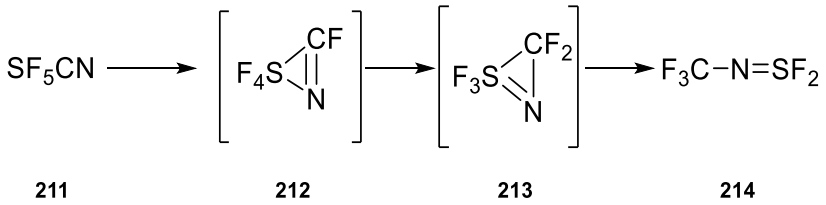

Scheme 68: Rearrangement taking place while storing SF_5CN gas.

Furthermore, this goes along with the additional found HRMS found for $C_8H_4O_2N_3F_7S$ in the reaction mixture, representing the 4-nitrobenzene-((N-(trifluoromethyl)sulfinimidic)$_2$ fluoride) (NO_2-Ph-$SF(NCF_3)_2$, diimine) **216**.

Concludingly, the rearrangement can be attributed to the thermodynamically favored buildup of the short formal S–N double bond at the former reduced sulfuric center. However, it is expected that the ionic formulation as S^+–N^- contributes significantly, as reported in the theoretical charge density study by *Stalke et al.*[328] The remaining challenge is to circumvent rearrangement reactions to form a stable S–CN bond.

As the discovered novel NO_2-Ph-$SFNCF_3$ **215** represents an unknown structural motive, this route was taken to investigate the electronic properties, stability and subsequent substitution reactions of **215**.

5.2.1.1 Unexpected product formation: the N-(trifluoromethyl)sulfinimidic fluoride derivatives

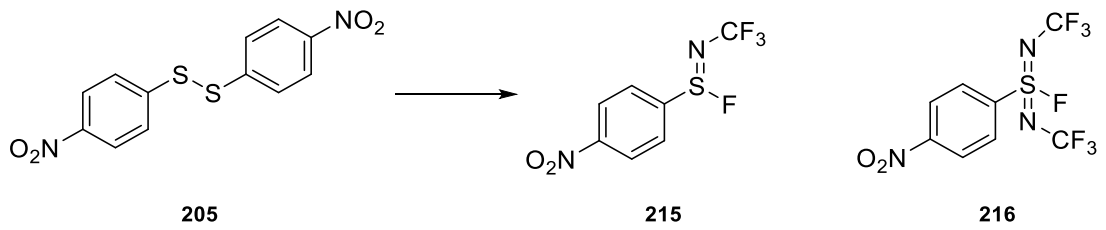

205 215 216

Scheme 69: NO_2-Ph-$SFNCF_3$ **215** and NO_2-Ph-$SF(NCF_3)_2$ **216** as the unexpected compounds formed instead of the aimed NO_2-Ph-SF_4CN **206**.

After attributing the found HRMS to the above-represented reaction products **215** and **216** (Scheme 69), the two quartets at 76.2 and 76.1 ppm belong to two isomers of the imine **215** and the two heptets at 70.6 and 70.3 ppm belong to the diimine **216**.

They can be assigned by a 2D ^{19}F ^{19}F-COSY spectrum and are following the GC-MS results. Nevertheless, the exact nature of the imine cannot be proven unambiguously (Figure 68).

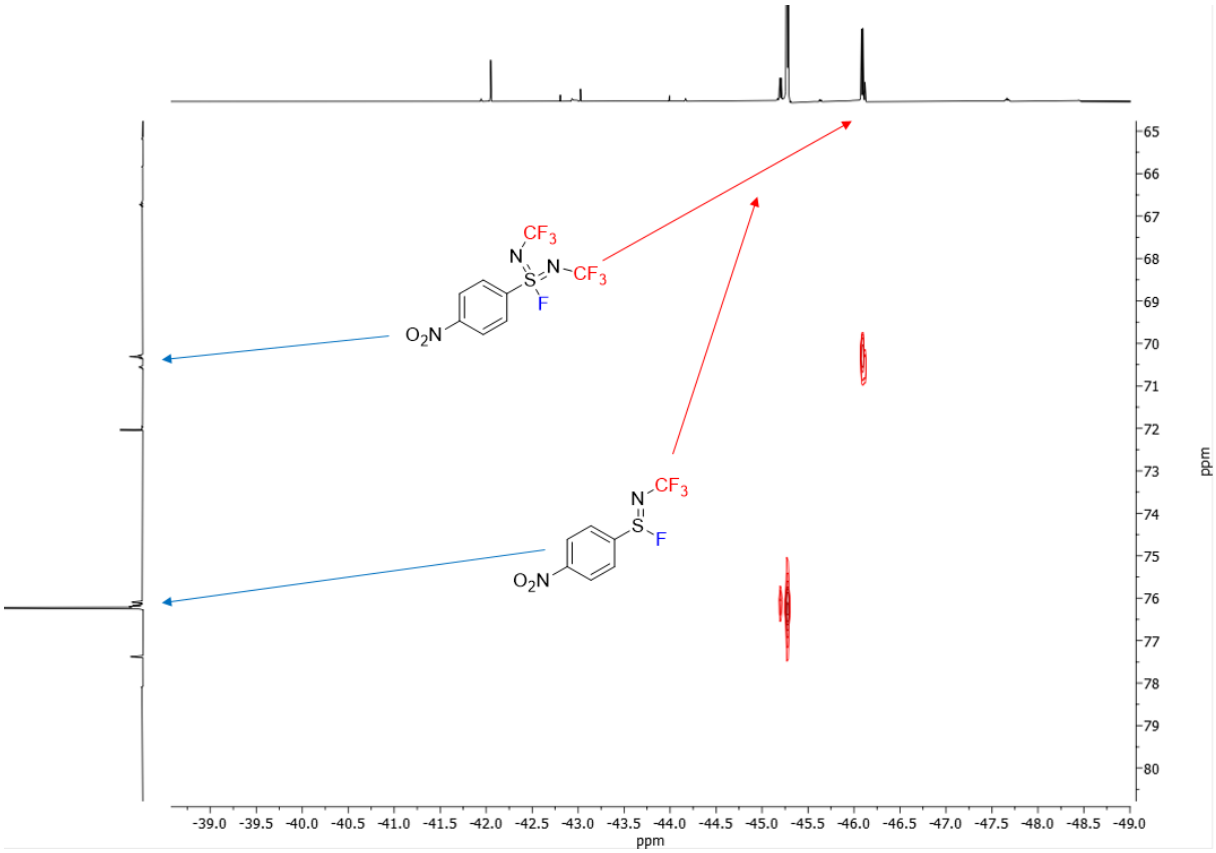

Figure 68: ^{19}F ^{19}F-COSY spectrum with an assignment of the cross-peaks to the imine **215** and diimine **216**.

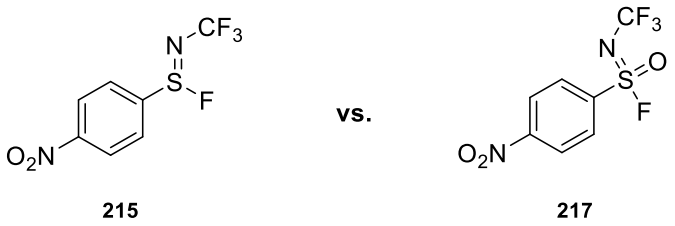

215 **217**

Figure 69: Structural evidence – 4-nitrobenzene-(N-(trifluoromethyl)sulfinimidic fluoride) **215** *vs.* 4-nitrobenzene-(N-(trifluoromethyl)sulfonimidic fluoride) **217**.

The ^{19}F NMR peaks and the HRMS results fit to two possible structures: the 4-nitrobenzene-(N-(trifluoromethyl)sulfinimidic fluoride) **215** and the 4-nitrobenzene-(N-(trifluoromethyl)sulfonimidic fluoride) **217** (Figure 69). Considering a formal S–N double bond, for the *trans*- and the *cis*-imine different coupling constants are expected, which are not present in the ^{19}F spectra depicted in Figure 70. Having an equilibrium of the S(IV) and S(VI) compounds **215** and **217** present, the signal sets are unlikely in a window of 0.2 ppm of the respective ^{19}F NMR spectra. Therefore, the signals rather show rotational isomers around the sulfuric center.

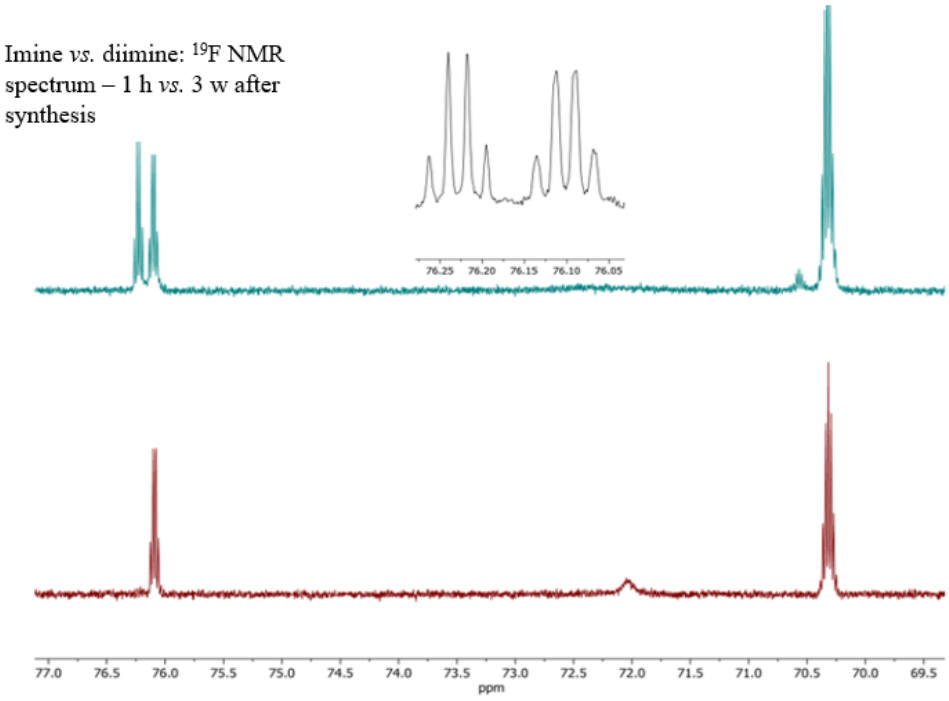

Figure 70*:* ^{19}F spectrum of the imine **215** or **217** and the diimine **216** – dynamic conversion of the isomers: 1 h *vs.* 3 weeks after the synthesis in a $CDCl_3$ solution.

The indications for having either a S(IV) or a S(VI) center present are contrasted in the following:

Pro S(IV): Reactions were conducted strictly under N_2 atmosphere and the NMR tubes were prepared and sealed in a glovebox. The HRMS measurements instead were carried out under air, which could have led to post-synthetical oxidation. Leaving the NMR under air for three weeks accumulates a signal at 76.1 ppm – however, the addition of H_2O_2 after the synthesis

does not affect the integral at 76.2 ppm and results in no buildup of the signal at 76.1 ppm. The GC-MS spectrum shows two separated peaks, for which no mass spectrum shows the M^+ of the NO_2-Ph-$SFONCF_3$ **217**, but only as a fragment of the NO_2-Ph-$SF(NCF_3)_2$ **216**.

Pro S(VI): Even under inert conditions, the *in situ* presence of HF in the reaction mixture can react with the SiO_2 of the glass tube yielding SiF_4 and H_2O as a possible oxygen source. Generally, deducting structure information based on the ^{19}F NMR chemical shift due to similarity to related compounds has to be done with care. The NO_2-Ph-SF_3 species **209** gives two signal sets in the ^{19}F NMR spectrum: one doublet at 60.9 ppm and one triplet at –45.1 ppm.[325] This shows that electronic environments strongly depend on the exact orbital overlap of each system. The signal sets in Figure 70 separated by 5.5 ppm by no means exclude the assignment to a S(IV) and a S(VI) species.

Nevertheless, due to its resistance against oxidation and the fact that the reaction was conducted under glovebox conditions, it is more likely, that the S(IV) is present. However, a single-crystal X-ray analysis is required to confirm this structure.

5.2.1.2 Reaction optimization

Regardless of the exact nature of the imine, a systematic screening of the reaction conditions was conducted to increase the yield for the imine **215** and the diimine **216**. Thereby, the chemical shifts must be considered with an error bar of ±0.3 ppm since they were measured on different NMR spectrometers without using an internal standard (Table 6).[329]

Table 6: ^{19}F NMR chemical shifts [ppm] and coupling constants [Hz] measured in $CDCl_3$ for $PhSF_5$ **218**, $NO_2PhSFNCF_3$ **215** and $NO_2PhSF(NCF_3)_2$ **216**.

^{19}F NMR chemical shifts [ppm]	Multiplicity and *J* [Hz]	Compound
84.5	p, 147.8	$PhSF_5$
61.9	d, 147.8	
76.2, 76.1	q, 8.4	$NO_2PhSFNCF_3$
–45.2, –45.3	d, 8.8	
70.6, 70.3	h, 8.4	$NO_2PhSF(NCF_3)_2$
–46.1	d, 8.5	

The integral of the respective two signal sets have been summed up in Table 7 since a fast conversion between them was observed and precise time control is impractical.

Table 7: Optimization of the reaction shown in Scheme 69: Yields were given with relation to 2.00 equiv. of the disulfide based on the analyzed samples taken after stirring at r.t. for 24 h, *: upscale reaction: 20 mg disulfide, the yields of the reaction were calculated based on ^{19}F NMR measurements with the following parameter set: o_1p: 100 ppm, range: 300 ppm, d_1 time: 10 s, focusing on the following compounds.

Entry	XeF_2 (equiv.)	KCN (equiv.)	NEt_4Cl (equiv.)	CsF (equiv.)	MeCN-d_3 [mL]	Imine **215**	Diimine **216**
concentration screening							
1	12.0	4.00	0.60	-	0.50	15%	16%
2	12.0	4.00	0.60	-	1.00	5%	–
3	12.0	4.00	0.60	-	0.25	16%	13%
4	12.0	4.00	0.60	-	0.13	15%	23%
5	12.0	4.00	0.60	-	0.06	18%	32%
KCN and NEt_4Cl screening							
6	12.0	4.00	0.60	-	0.25	34%	6%
7	12.0	2.00	0.60	-	0.25	16%	13%
8	12.0	8.00	0.60	-	0.25	16%	1%
9	12.0	12.0	0.60	-	0.25	6%	4%
10	12.0	2.00	2.40	-	0.25	14%	17%
11	12.0	8.00	1.20	-	0.25	11%	25%
12*	12.0	4.00	0.60	-	0.50	7%	23%
XeF_2 and CsF tests							
13	16.0	4.00	0.60	-	0.25	15%	13%
14*	12.0	4.00	0.20	2.00	0.25	30%	32%

While conducting the reaction screening, large fluctuations in the yield were observed even for the marginal deviation of the reaction procedure. Especially the time in solution before the XeF_2 was added and the rate of the addition of the oxidation agent is crucial. Even visually, a color change from colorless to yellow was observed when KCN was added to the disulfide. The green marked entries are the best conditions and represent the best yields achieved by reproducing the reaction six times each. The average yield of the reproduced condition of entry 6, it is 32 ± 8% for the imine **215 –** for the entry 14* it is 22 ± 8% for the diimine **216**

5.2.1.3 Analysis of the occurring by-products

To gain further insight into the reactions, GC-MS spectra were recorded and are exemplarily represented for the reaction conditions of entry 4 in Figure 71.

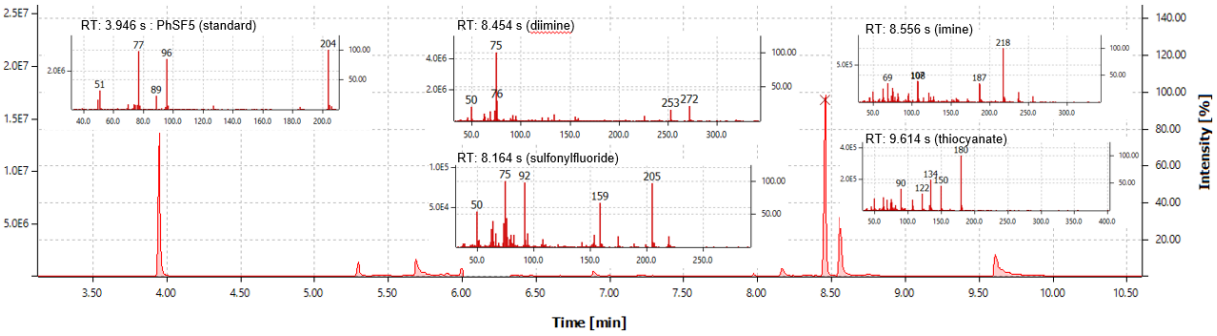

Figure 71: Analysis of the by-products *via* GC-MS of the reaction to be optimized.

The conclusion deduced from the GC-MS spectra allows only semi-quantitative estimations of the reaction products, even though $PhSF_5$ **218** (RT: 3.946 s) was used as an internal standard. Also, NMR spectroscopy does not deliver accurate numbers due to a crowded ^{1}H NMR spectrum in the $H_{aromatic}$ region and too large differences in the offsets for the relevant peaks of other fluorinated compounds in the ^{19}F NMR spectra. Additionally, compounds sensitive to water, air or heat do not survive the GC column and therefore cannot be represented in the spectrum shown above.

NO_2-Ph-SCN **208** as a by-product could be proven by comparing the NMR spectra with the spectra of the compound known from the literature.[330] To test whether NO_2-Ph-SCN **208** is an intermediate of the reaction as proposed for the internal conversion of SF_5CN **211** to CF_3-NSF_2 **214** or a dead-end by-product, a similar reaction protocol was applied, using the thiocyanate **208** instead of the disulfide **205** and no external addition of KCN (Scheme 70, Table 8).

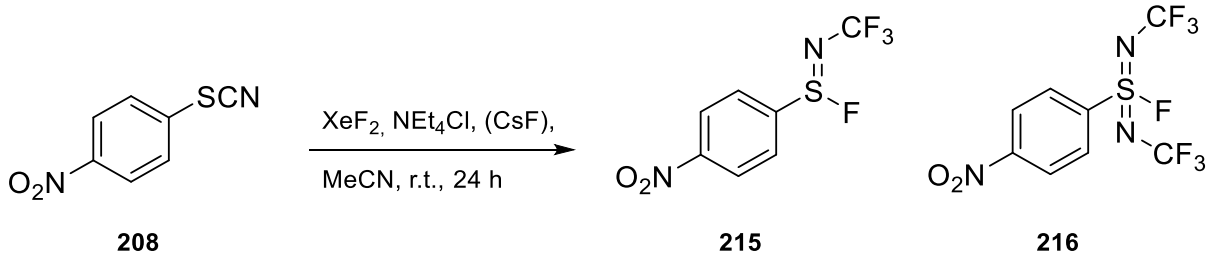

Scheme 70: NO_2-Ph-SCN **208** instead of the previously NO_2-Ph-S-S-Ph-NO_2 **205** as a starting material being converted to NO_2-Ph-$SFNCF_3$ **215** and NO_2-Ph-$SF(NCF_3)_2$ **216**.

Table 8: NO_2-Ph-SCN **208** as a starting material converted to NO_2-Ph-$SFNCF_3$ **215** and NO_2-Ph-$SF(NCF_3)_2$ **216** without the need for additional KCN. Yields are based on the analyzed samples taken after stirring at r.t. for 24 h.

Entry	XeF_2 (equiv.)	KCN (equiv.)	NEt_4Cl (equiv.)	CsF (equiv.)	MeCN-d_3 [mL]	Imine **215**	Diimine **216**
1	7.00	–	0.60	–	0.50	–	3%
2	7.00	–	0.60	2.00	0.50	2%	5%

It can be demonstrated that NO_2-Ph-SCN **208** can be converted to $NO_2PhSFNCF_3$ **215** and $NO_2PhSF(NCF_3)_2$ **216**. The main reaction pathway needs to be conclusively proven as the yields dropped dramatically.

Besides the NO_2-Ph-SCN **208**, the hydrolysis product 4-nitrobenzenesulfonyl fluoride (NO_2-Ph-SO_2F) was observed *via* GC-MS. It can be assumed that NO_2-Ph-SO_2F, plays no role in the way to the final product. Generally, all approaches conducted under air showed the products only in traces and increased conversion to NO_2-Ph-SO_2. For that reason, this can be considered to be a dead-end that should be avoided.

According to the signals of the GC-MS at RT: 8.454 min, the M^+ of the NO_2-Ph-$SF(NCF_3)_2$ **216** and a more dominant peak that can be assigned to the species NO_2-Ph-$SFNCF_3$ **215** at RT: 8.556 min.

Furthermore, it can be assumed that NO_2-Ph-SF_3 **209** could also be a key intermediate, as proposed by *Umemoto et al.*[324] or by *Janzen et al.*[331] for the reaction to give Ar-Ph-SF_4Cl **210** (Scheme 71 and Scheme 72).

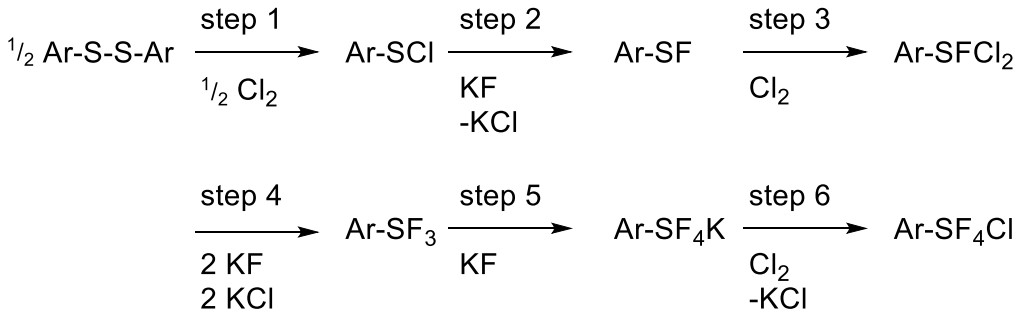

Scheme 71: The reaction mechanism for the ionic intermediate-based conversion of an aryl disulfide to an Ar-SF_4Cl compound as proposed by *Umemoto et al*.[324]

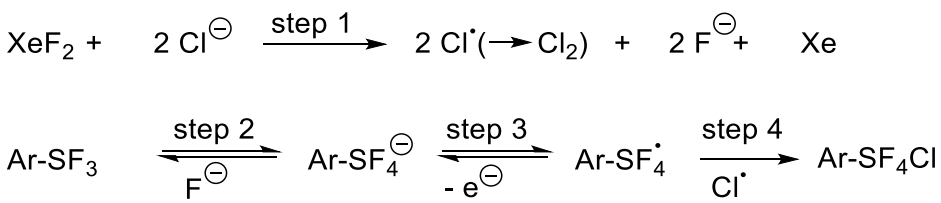

Scheme 72: The reaction mechanism for the radical intermediate-based conversion of an Ar-SF_3 to an Ar-SF_4Cl compound as proposed by *Janzen et al.*[331]

To apply the mechanisms above onto the developed system, step 5 (Scheme 71) and step 4 (Scheme 72) must be replaced by an attack of a CN-anion or CN-radical. The subsequent isomerization reaction, investigated by *Willner* and *Vorobev et al.*[326, 327] and represented in Scheme 68, occurs at a late stage at the SF_5CN core. Therefore, the highly unstable S(IV) species **209** was applied under less oxidative conditions (Table 9).

Table 9: NO_2-Ph-SF_3 **209** as highly sensitive starting material that can be converted into the imine **215** and the diimine **216**. The yield is based on the analyzed samples taken after stirring at r.t. for 24 h.

Entry	XeF_2 (equiv.)	KCN (equiv.)	NEt_4Cl (equiv.)	CsF (equiv.)	MeCN-d_3 (equiv.)	Imine **215**	Diimine **216**
1	2.00	16.0	0.10	–	0.50	4%	2%

Since NO_2-Ph-SF_3 **209** is far more sensitive to water and air than other sulfur fluorides such as NO_2-Ph-SF_4Cl **210** and the product of hydrolysis NO_2-Ph-SO_2F, the developed reaction procedure applied is not robust enough to provide reproducible data. Nevertheless, it has been demonstrated that NO_2-Ph-SF_3 **209** can also be transformed to NO_2-Ph-$SFNCF_3$ **215** and NO_2-Ph-$SF(NCF_3)_2$ **216**.

NO_2-Ph-SF_4Cl **210**, on the other hand, is known to be highly kinetically stable; therefore, great efforts were made to successfully substitute the λ^6-Cl with a λ^6-F to obtain the SF_5-species. To afford the pentafluorosulfanyl group, conditions such as HF, ZnF or SbF_2/SbF_5, neat, 120 °C,[332] AgF, neat, 120 °C,[333] Ag_2CO_3, CH_2Cl_2, r.t.,[334] IF_5, neat, r.t.,[335] HgO/HF, neat, –30 °C to r.t.,[336] or more recently $AgBF_4$, MeCN, r.t.[337] had to be applied according to the literature. For this reason, simple $CN^- – Cl^-$ substitution was not considered for the synthesis of the imine **215** or diimine **216** but was investigated in other approaches below.

5.2.1.4 Stability tests

Stability tests were performed in NMR tubes, with the compounds dissolved in MeCN-d_3 and the following solutions were added.

Using *n*-pentane and CH_2Cl_2 NO_2-Ph-$SFNCF_3$ **215** and NO_2-Ph-$SF(NCF_3)_2$ **216** can be extracted from the MeCN solution and remain stable in solution. While *n*-pentane affords the product mixture without salt contaminations, CH_2Cl_2 partially dissolves the NEt_4Cl of the reaction mixture.

Both **215** and **216** can be stored in a MeCN solution for 21 days without degradation. Additionally, both species are stable in water. Exposing the two compounds to 1M aqueous HCl

solution leads to rapid degradation of the diimine **216** – the imine **215** shows no degradation after 11 days. Storing the samples in a saturated aqueous K_2CO_3 solution leads to a color change from colorless to dark yellow, but only minor degradation after 20 min. After 10 days the imine **215** can only be found in traces while the diimine **216** is no longer present.
The rather stable compounds encouraged further tests, in which the fluoride was replaced in a SuFEx reaction with different nucleophiles (5.2.5.1).

5.2.2 Thiocyanate – the prebuilt SCN precursor

As demonstrated in 5.2.1, controlled fluorination reactions of rather simple sulfur precursors can enable novel structural motives as shown for the N-(trifluoromethyl)sulfinimidic fluoride derivatives. Encouraged by that, the tetrafluoro(4-nitrophenyl)-λ^6-sulfanecarbonitrile (**206**) is in the following pursued.
Based on the knowledge gained through the by-product analysis in section 5.2.1.3, it was decided to synthesize the thiocyanate first in the next approach to react it under fluorinating conditions. To a solution of the respective aryl-disulfides in MeCN were added TMSCN and *Selectfluor* were added and stirred at 80 °C for 4 h (Scheme 73).[330]

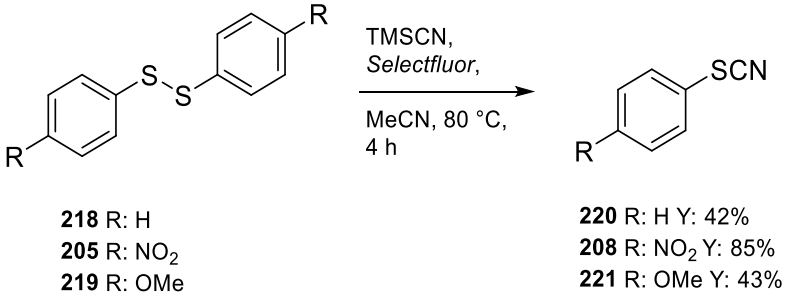

Scheme 73: The thiocyanate syntheses using aryl-disulfides as starting materials.

In the following, only NO_2-Ph-SCN **208** was used to handle solids in the glovebox. In the hope that the S–CN bond would be preserved, the optimized conditions for the disulfide case were applied (section 5.2.1.2) without adding KCN. However, this approach did not lead to success. The experiment showed that the rearrangement leading to the NO_2-Ph-$SFNCF_3$ **215** and the NO_2-Ph-$SF(NCF_3)_2$ **216** could occur after the S–CN bond is already formed.

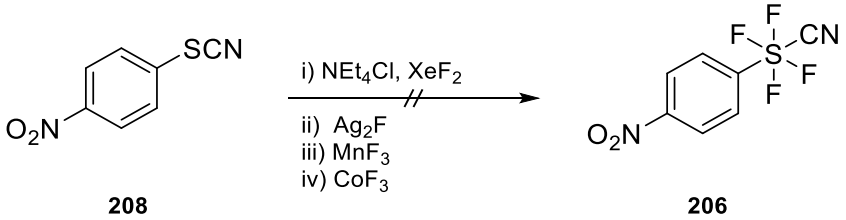

Scheme 74: Approaches to fluorinate the sulfur of the thiocyanate-group of NO_2-Ph-SCN **208**.

As described in Scheme 74, more powerful fluorinating AgF_2,[331] MnF_3 or CoF_3 under neat conditions at 150 °C or in *n*-heptane solution at room temperature were tested. The addition of AgF_2 mainly results in degradation products, indicated by an increase of the signals in the high field of the ^{19}F NMR spectrum. Generally, this can be tentatively assigned to fluorinated carbons rather than fluorinated sulfur compounds. Additionally, NO_2-Ph-SO_2F and dominantly NO_2-Ph-SOF were observed for the MnF_3 and CoF_3 reactions, even though the NMR spectra were measured in *Teflon*-based inlets. This indicates that traces of oxygen or water are sufficient to form the more stable hydrolysis products while the oxidation state of the sulfur center is maintained or S(VI) is formed.

Since the above-mentioned transition metal fluorides have the potential to fluorinate even alkanes, MnF_3, for instance, can convert aromatic hydrocarbons,[338] cyclobutenes[339] and fullerenes[340] while CoF_3 can fluorinate, e.g., propane,[341] the selected reaction conditions can be considered as too harsh.

Since the previously introduced S–CN bond can undergo a rearrangement, NO_2-Ph-SF_3 **209** was investigated as a sterically more hindered precursor for the future SF_4CN-group.

5.2.3 SF_3-group – the highly reactive S(IV) precursor

NO_2-Ph-SF_3 **209** was synthesized according to the procedure developed by *Janzen et al.* as described in Scheme 75.

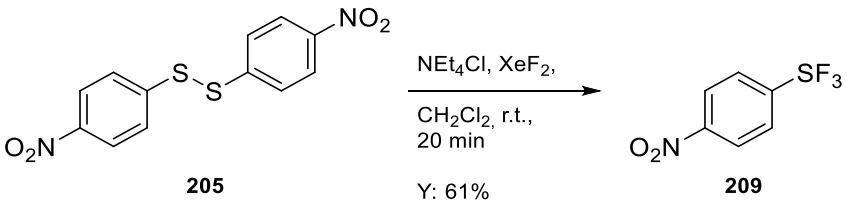

Scheme 75: Synthesis of NO_2-Ph-SF_3 **209** using NO_2-Ph-SS-Ph-NO_2 **205** as a starting material.

The S(IV) species NO_2-Ph-SF_3 **209** was proven to be highly sensitive to oxygen and water – exposing the solid to air leads to rapid smoke evolution and formation of the hydrolysis products NO_2-Ph-SO_2F and NO_2-Ph-SOF, as indicated by subsequent ^{19}F NMR measurements. Therefore, the following experiments were conducted in a glovebox or in air-tight PFA vials, which were reopened in the glovebox.

Applying the developed conditions using KCN, NEt_4Cl and XeF_2 to NO_2-Ph-SF_3 as starting material yielded minor NO_2-Ph-$SFNCF_3$ **215** and NO_2-Ph-$SF(NCF_3)_2$ **216**, in addition to the hydrolysis products NO_2-Ph-SO_2F and NO_2-Ph-SOF (Scheme 76). This indicates that at the

stage of NO_2-Ph-SF_3 **209**, the nucleophilic attack of the CN-anion can still take place but is accompanied by the undesired rearrangement.

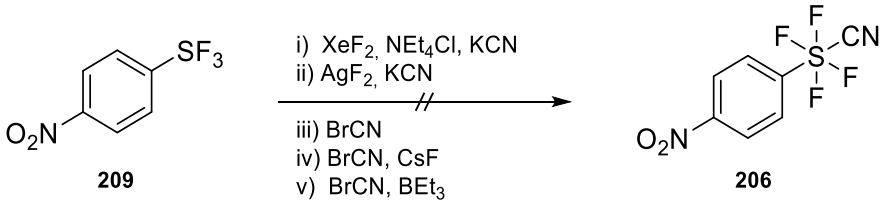

Scheme 76: Reaction screening using NO_2-Ph-SF_3 **209** as a starting material.

For this reason, the AgF_2 was tested as an alternative to XeF_2 without the chloride catalyst. Again only degradation and hydrolysis occur already at room temperature in MeCN in the glovebox. Additionally, BrCN was tested as a CN-source accompanied by the catalytically required halogens described by *Janzen et al.*,[331] tested with additives like CsF as a fluoride source and BEt_3 as a radical initiator. Neither neat nor in MeCN at room temperature nor at 40 °C, the reaction was successful. Mainly, the loss of the SF_3 group or hydrolysis products were observed. Nevertheless, the attack and the subsequent rearrangement of a nucleophilic nitrile at the S(IV) center can occur twice. Based on these findings, the following approaches use the kinetically hindered 6-times coordinated S(VI) center of NO_2-Ph-SF_4Cl **210** to achieve a chloride substitution reaction and avoid rearrangement.

5.2.4 SF_4Cl-group – the kinetically stable S(VI) source

NO_2-Ph-SF_4Cl **210** was synthesized according to *Janzen et al.* as described in Scheme 77.

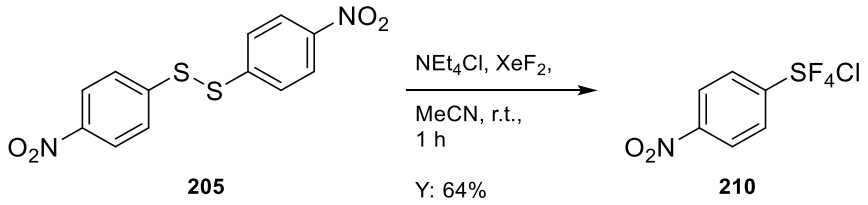

Scheme 77: Synthesis of NO_2-Ph-SF_4Cl **210** using NO_2-Ph-SS-Ph-NO_2 **205** as a starting material.

The packed S(VI) center and the electron-deficient nature of the compound makes the NO_2-Ph-SF_4Cl **210** a surprisingly stable compound compared to other derivatives reported by *Umemoto* and *Togni et al.*[324, 342] No hydrolysis was observed after 40 h in solution outside the glovebox. Instead, a rearrangement from the *trans*-isomer to the *cis*- isomer in MeCN can be observed,[331] which can be reduced by storage in non-polar solvents as $CHCl_3$, CH_2Cl_2 and *n*-pentane as reported by *Janzen et al.* Additionally, NO_2-Ph-SF_4Cl **210** can be extracted from a MeCN solution with *n*-pentane.[342]

5.2.4.1 Ionic approach

First, different *Lewis* acids were screened to selectively abstract the chloride and stabilize the resulting cationic SF_4^+ intermediate (Scheme 78).[343] Therefore, cyanide sources such as KCN and TMSCN (better soluble in MeCN and toluene) were tested. Converting NO_2-Ph-SF_4Cl **210** in MeCN or toluene in the presence of $B(C_6F_6)_3$, $AlBr_3$ or $GaCl_3$ at room temperature showed slow conversion to the SF_5-species. For the neat reaction of $B(C_6F_6)_3$ and KCN at 130 °C, only NO_2-Ph-SF_5 and NO_2-Ph-SO_2F could be detected in the low field of the ^{19}F NMR spectrum.

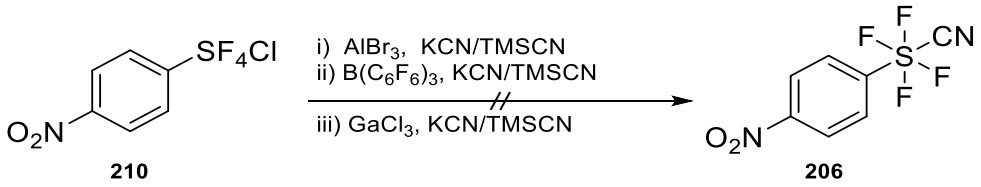

210 206

Scheme 78: Reaction screening using NO_2-Ph-SF_4Cl **210** as a starting material *via* an ionic intermediate, using a *Lewis* acid.

The exchange of the λ^6-chloride substitution for the fifth fluoride of the pentafluorosulfanyl group was the subject of investigation for a long time. Harsh conditions had to be applied, as mentioned earlier in section 5.2.1.3. Nevertheless, *Shibata et al.* recently succeeded found a convenient way to substitute the chloride by using $AgBF_4$ as a fluoride source and thermodynamically impetus at once.[337] Based on these results, metal salt-based CN^- analogs like $KB(CN)_4$ and $Zn(CN)_2$ were screened (Scheme 79).

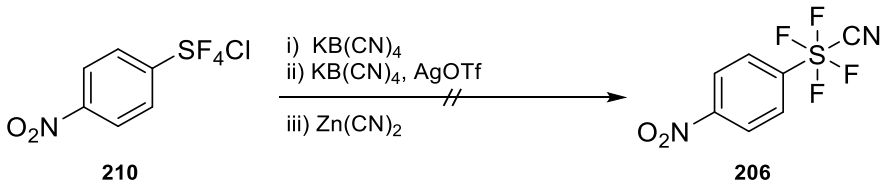

210 206

Scheme 79: Reaction screening using NO_2-Ph-SF_4Cl **210** as starting material in an ionic, salt-based approach.

The reaction of NO_2-Ph-SF_4Cl **210** with $Zn(CN)_2$ in *n*-heptane led to the reduction product NO_2-Ph-SF_3 **209**, which can explain an eventual formation of dicyanogen. This stands following the literature, attesting a strongly oxidizing effect on the hexavalent sulfur(VI) element of Ar-SF_4Cl derivatives.[324] $KB(CN)_4$ and AgOTf in CH_2Cl_2 or MeCN should form the CN^- analog of $AgBF_4$, efficiently enabling the Cl^- to F^- substitution. While no conversion was observed in MeCN, reduction to NO_2-Ph-SF_3 **209** occurred in CH_2Cl_2 and a few other new signals appeared in the ^{19}F NMR spectra that could not be assigned yet. The GC-MS, however, showed no evidence of the product. Additionally, liquid crystals were used as solvents, but neither the 1-butyl-3-methylimidazolium tetrafluoroborate nor the 1,3-di-cyclohexyl imidazolium tetrafluoroborate-based salt yielded the desired product, but only NO_2-Ph-SF_3 **209**. Adding

AgOTf to increase the thermodynamically driving force by eventual AgCl precipitation led to the solidification of the liquid crystal and was therefore not practicable.

Since the route *via* ionic intermediates is not feasible for S–CN bond formation, various complementary radical approaches were tested. *Shreeve et al.* were the first to investigate the light-driven photolysis of CF_3SF_4Cl as a CF_3SF_4 transfer reagent.[344] *Welch et al.* later pursued a radical reaction to post functionalize SF_4Cl-residues with alkynes initiated by BEt_3[345] and later *Shibata et al.* showed that alkenes could also be installed initiated by irradiation.[346]

5.2.4.2 Radical approach

Initially, AIBN was applied as a radical initiator to generate the NO_2-Ph-SF_4-radical and start the radical chain reaction in the presence of a cyanide sources like Tos-CN or N-cyano-succinimide in MeCN at 70 °C. That led to traces to *iso*-butyronitrile adducts at the SF_4 center, underlining the findings of previously listed literature that chloride substitution is enforced *via* a radical pathway. Additionally, calculations could prove that the CN sources cannot close the radical reaction cycle due to too high thermodynamical stability.

Instead, subsequent approaches aimed to harness the nitrile group of the AIBN itself. *Janzen et al.* investigated the decay of AIBN in the presence of O_2 by ESR/Spin trapping.[347] Additionally, *Fu et al.* proposed a pathway in which AIBN is converted to acetone and CN-anions in the presence of O_2 and a base, which can initiate aerobic oxidative coupling of primary amines to imines and cyanation. In the process, the general pathways for AIBN-initiated autoxidation are described as depicted in Scheme 80.[348]

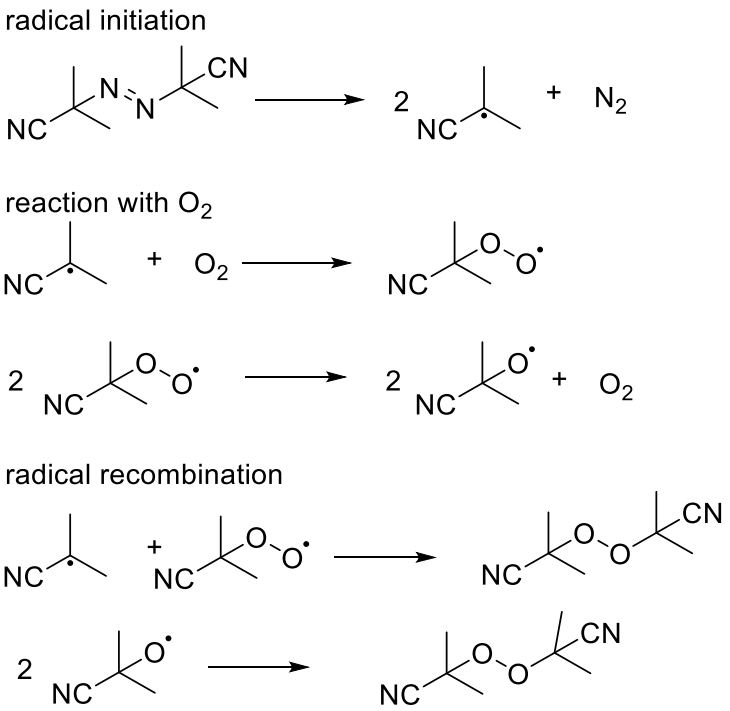

Scheme 80: AIBN radical reaction in the presence of O_2.[348]

NO_2-Ph-SF_4Cl **210** and AIBN were dissolved in dry MeCN in a glovebox. Before the reaction was heated to above 50 °C, the atmosphere was changed to O_2 with a constant O_2 balloon overpressure. The elevated temperature was required for the fragmentation of AIBN. The reaction mixture was analyzed by NMR spectroscopy. In the beginning, four literature unknown signals in the low field looked promising and may be attributed to the expected resonance of the *trans*-substituted SF_4 group (**B**: 72.1, **F**: 60.6, **G**: 58.9, **H**: 52.7 ppm) (Figure 72).[325]

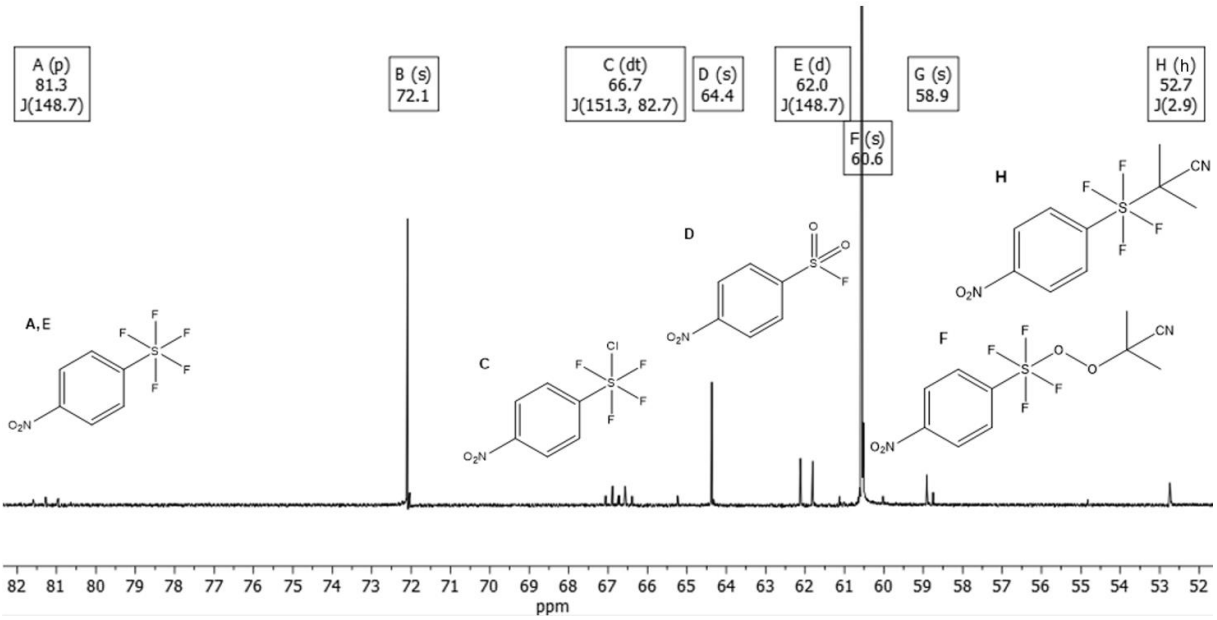

Figure 72: Part of the low-field ^{19}F NMR spectrum of the reaction of NO_2-Ph-SF_4Cl **210** with AIBN in the presence of O_2 and the respective assignment of the peaks to molecular structures.

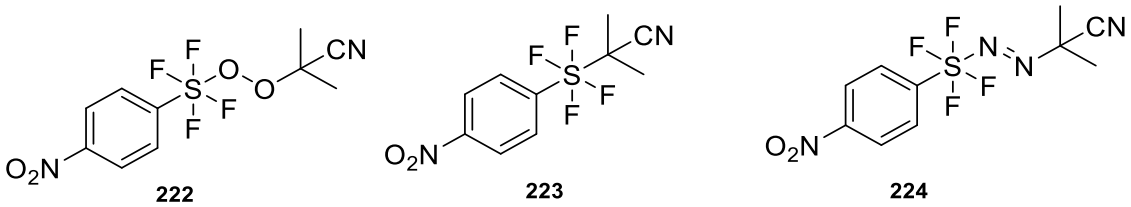

Figure 73: AIBN-based reaction products **222** – **224** of the reaction of NO_2-Ph-SF_4Cl **210** with AIBN in the presence of O_2.

It could be shown that the signals at 72.1 ppm (**B**) and 58.9 ppm (**G**) also arise after photolysis experiments of NO_2-Ph-SF_4Cl **210** under inert gas in MeCN, which is why they were not considered further. The coupling constant of the heptet at 52.7 ppm (**H**) of 2.9 Hz can be assigned to the $^4J_{FH}$ coupling between the methyl protons of the *iso*-butyronitrile adduct and the *trans*-substituted SF_4 group of **223** (Figure 73). This can be proven by a ^1H ^{19}F COSY NMR experiment and the 1D ^1H signal at 2.05 ppm showing the same coupling constant. Additionally, this product could be isolated *via* flash column chromatography on silica gel and the HRMS proved the molecular formula.

The nature of the molecule behind the dominant peak at 60.6 ppm initially remained unclear, as no cross-peaks between the SF_4-group and aliphatic protons could be found and no pentet was visible in the ^{13}C spectrum. Isolation of the molecule by flash column chromatography on silica gel and subsequent ^1H NMR measurement showed evidence of six methyl protons as a singlet at 1.76 ppm, objecting to the presumption that the ^{19}F signal could be attributed to the aimed SF_4CN-group. Measuring MS spectra of the isolated compound gave the HRMS of the azo-compound **224** shown above and not the peroxide-analog **222** as the reported autoxidation of AIBN might suggest (Scheme 80). However, no correlation between a ^{15}N and a ^{19}F of the SF_4-group was found when ^{15}N ^{19}F HSQC spectra were measured. Fortunately, a single-crystal X-ray structure could be obtained, which underlines the results of the 2D NMR spectrum showing the SF_4-peroxide analog **F**, **222** as the main product in this fraction (Figure 74). The peroxide is not stable enough under the ionization conditions of the conducted EI measurements to obtain the HRMS. On top of that, it is not expected to ionize as easily as the azo compound **224**. Therefore, the NO_2-Ph-$SF_4OOC(CH_3)_2CN$ **222** can be seen as the obtained product, besides minor impurities of the azo-compound **224**.

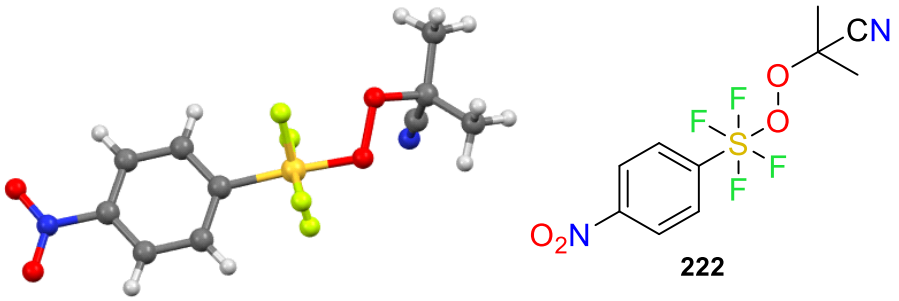

Figure 74: Single-crystal X-ray structure of NO_2-Ph$SF_4OOC(CH_3)_2CN$ **222**.

Even though the aimed tetrafluoro-λ^6-sulfanyl carbonitrile group could not be installed *via* this approach, the novel SF_4-peroxide motive is worth to be investigated in more detail.

In the following, the conditions for the functionalization were optimized under O_2- and N_2-atmosphere (Scheme 81). A clear trend was visible while performing the reaction at different temperatures under air. While no conversion was observed at room temperature, the ratio from the peroxide adduct **222** to the IBN-adduct **223** shifted increasingly at elevated temperatures (Table 10).

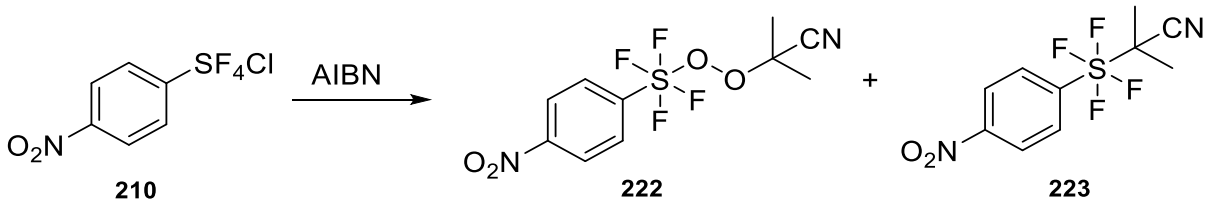

Scheme 81: Reaction screening of the AIBN-based radical reaction with NO_2-Ph-SF_4Cl as the starting material.

Table 10: NO_2-Ph-SF_4Cl AIBN reaction – temperature screening. The yields are based on the analyzed samples taken after stirring for 24 h.

Entry	AIBN (equiv.)	MeCN [mL]	T [°C]	Peroxide-adduct **222**	IBN-adduct **223**
1	2.50	0.50	25	–	–
2	2.50	0.50	50	5%	–
3	2.50	0.50	70	3%	1%
4	2.50	0.50	90	<1%	4%

Irradiation of the sample under exclusion of O_2 with an Hg vapor lamp with a Pyrex cut-off or an uranium glass cut-off yielded only the IBN adduct **223**. Was the sample exposed to air, the peroxide compound **222** was formed. The summary of all entries of the reaction optimization is listed in the experimental part 6.8.

No products were formed when the reaction was carried out under O_2 and in solvents capable of quenching radicals, such as THF or DMF. Carrying out the reaction in non-polar solvents such as *n*-hexane and toluene yielded the products in reduced yields (Table 11).

Table 11: NO_2-Ph-SF_4Cl **210** AIBN reaction – solvent screening. The yields are based on the analyzed samples taken after stirring for 24 h. *: The reaction was carried out under an O_2 atmosphere.

Entry	AIBN (equiv.)	MeCN [mL]	T [°C]	Solvent	Peroxide-adduct **222**	IBN-adduct **223**
5*	2.50	0.50	70	*n*-hexane	6%	–
6*	2.50	0.50	70	toluene	3%	2%
7*	2.50	0.50	70	THF	–	–
8*	2.50	0.50	50	CH_2Cl_2	<1%	–
9*	2.50	0.50	70	$CHCl_3$	1%	1%
10*	2.50	0.50	70	DMF	–	–

Screening the overall concentration under O_2 suggests that the optimal conditions are at moderate dilution to ensure proper mixing at relatively high concentrations (Table 12)

Table 12: NO_2-Ph-SF_4Cl AIBN reaction – overall concentration screening. *: The reaction was carried out under an O_2 atmosphere.

Entry	AIBN (equiv.)	MeCN [mL]	T [°C]	Peroxide-adduct **222**	IBN-adduct **223**
11*	5.00	0.25	70	20%	<1%
12*	5.00	0.50	70	12%	4%
13*	5.00	0.13	70	3%	5%
14*	5.00	1.00	70	2%	5%

Despite the optimization results shown above, the reaction with NO_2-Ph-SF_4Cl **210** and AIBN remains highly temperature-dependent and is strongly dependent on the (O_2) atmosphere. Entry 11*, the approach with the best yields under most stable conditions, was reproduced ten times to calculate an average value of 8% ±2% for the NO_2-Ph-$OOC(CH_3)_2CN$ **222** and 2% ±1% for the NO_2-Ph-$C(CH_3)CN$ **223** using the chosen reaction set up.

Adding BEt_3 as an additional radical initiator or *tert*-butyl peroxide as an additive, no product formation occurred.

In summary, the use of the S(VI) source NO_2-Ph-SF_4Cl **210** as a precursor on the way to the SF_4CN group seems to be the most promising approach since the SF_4-radical is a rather stable intermediate but should be reactive enough to form the future S–CN bond (Scheme 82). Additionally, the already formed SF_4-core should prevent kinetic rearrangements that cannot be avoided in disulfide-, thiocyanate- and SF_3-precursors. The already developed chemistry of the SF_4Cl compound is versatile and can provide useful knowledge, e.g., for the conversion of pre-functionalized molecules to the final CN-functionality.[349]

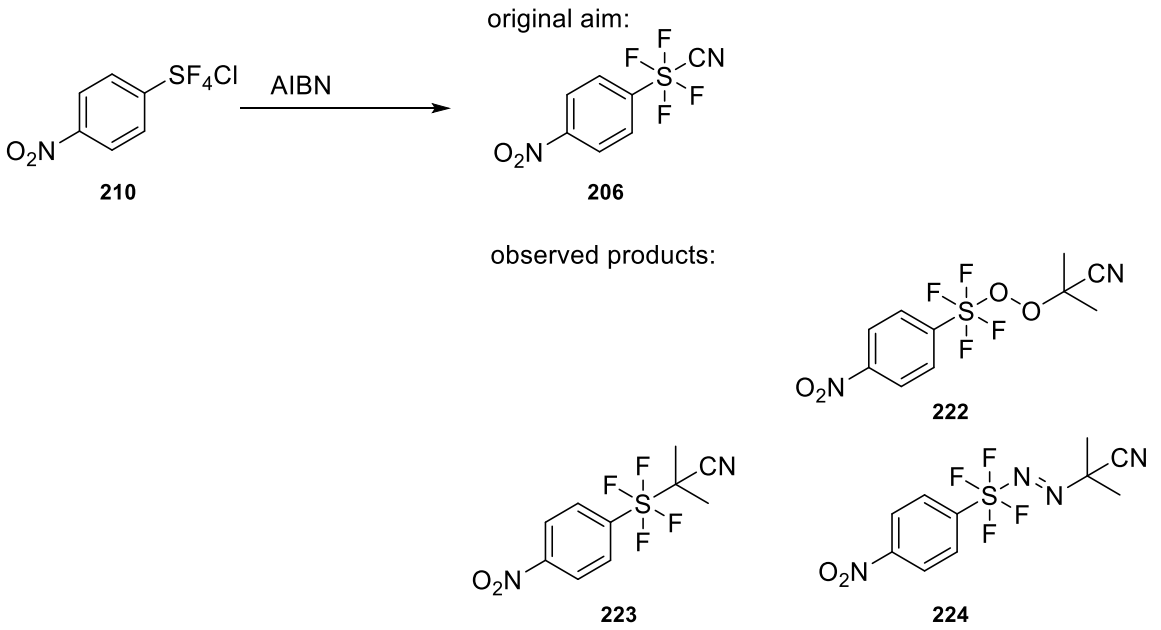

Scheme 82: AIBN-based radical reactions starting with NO_2-Ph-SF_4Cl **210** – original aim **206** and reaction outcome **222** – **224**.

5.2.5 N-(trifluoromethyl)sulfinimidic fluoride applied in SuFEx reactions

NO_2-Ph-$SFNCF_3$ **215** and NO_2-Ph-$SF(NCF_3)_2$ **216** exhibit stability under neutral and acidic conditions, while suffering in the basic milieu. The substitution of fluoride by different nucleophiles provided many lead structures and was therefore further investigated starting from the model substrates **215** and **216**.

The idea aims to apply the conditions of the classical Sulfonyl Fluoride Exchange (SuFEx) approach, as brought back into focus by *Sharpless et al*. in 2014 for the sulfonyl-fluoride analogs,[350] to the N-(trifluoromethyl)sulfinimidic fluoride species **215** and **216**. Originally, the first promising properties of sulfonyl-fluorides were reported by *Steinkopf et al.* in 1927,[351] followed by *Hyatt et al*., who demonstrated their reactivity when treated with N-nucleophiles,[352] before these promising results faded. Since *Sharpless* has adopted this underestimated tool, applicable in biorthogonal reactions, this reaction is discussed in the field of controllable ligation chemistry for small molecules, polymers and biomolecules. The SuFEx reaction can be considered the future of CuAAC and thus the future of click-chemistry.[353]

‘‘On my thoughts about the future of click chemistry, probably the best are for SuFEx, not for CuAAC. After all, CuAAC is a pretty brutally, single-minded business, but SuFEx is another beast entirely, which I sense holds the most ´magic` in the future I see for click chemistry.[….]” (*Barry S. Sharpless*).[350]

Since it can be assumed that the S(IV) species NO_2-Ph-$SFNCF_3$ **215** and the S(VI) species NO_2-Ph-$SF(NCF_3)_2$ **216** also undergo a fluoride exchange reaction, an excess of N- and O-

nucleophiles was added to the crude mixture of the fluorination reaction, to avoid immediate oxidation due to the presence of XeF_2.

5.2.5.1 Screening of different N- and O-nucleophiles

After a successful substitution reaction, it can be expected that the low field signal rising for the ^{19}FS in the ^{19}F NMR spectrum vanishes and the signal of the C^{19}F$_3$ in the high field of the spectrum shifts slightly and collapses to a singlet due to the absence of the fluoride. While no promising new signal could be obtained for pyrrolidine, EtOH and phenol as nucleophiles, fluorinated compounds were applied to have an NMR probe that splits the CF_3 singlet. First, 2-fluoroaniline was applied and indeed a doublet at –42.0 ppm with 0.9 Hz coupling constant over seven covalent bonds appeared in the ^{19}F NMR spectrum, even though in fewer amounts. The same reaction was carried out with water added in traces to activate the aniline derivative and a ^{19}F NMR spectrum was recorded after 5 min (Figure 75).

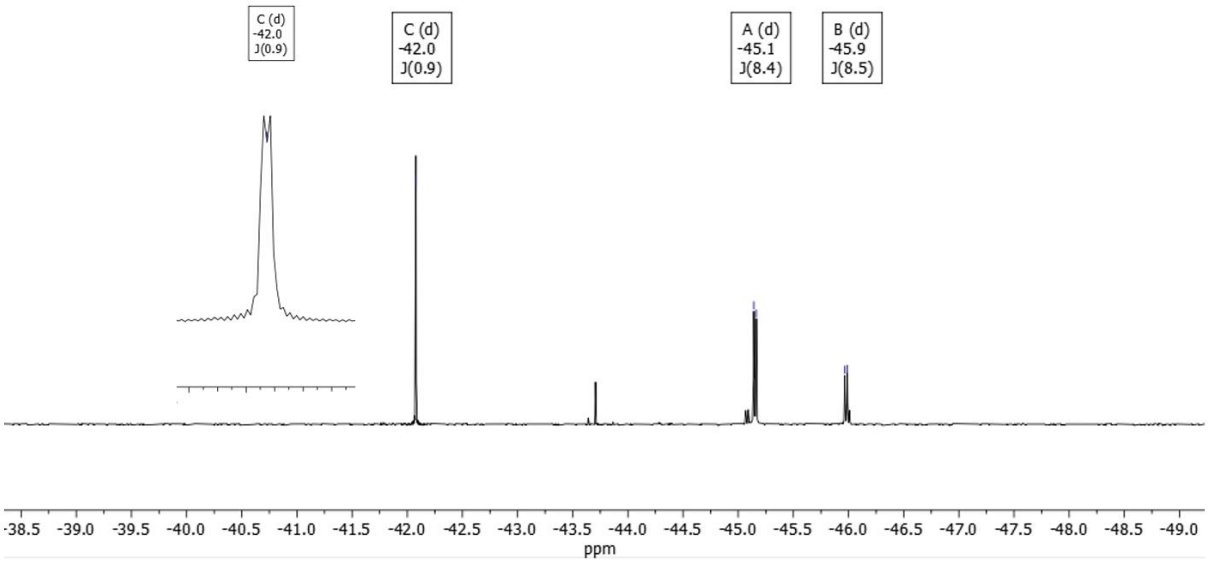

Figure 75: Part of the high-field of the ^{19}F NMR spectrum representing the conversion of imine- **215** and diimine **216** (–45.1 and –45.9 ppm) and a rising doublet at –42.0 ppm that can be assigned to the SuFEx product **225**.

The emerging doublet at –42.0 ppm with a coupling constant of 0.9 Hz can be assigned to the CF_3 group shifted by substituting the SF-fluoride. Additionally, the coupling constant of 0.9 Hz reflects the scalar $^7J_{FF}$ coupling of CF_3 and F. To finally prove that this coupling raises from a rather long-range coupling over seven bonds, 2,6-difluoroaniline was applied and the substitution product showed a triplet at –41.8 ppm with a 1.3 Hz coupling constant. Unfortunately, the N-nucleophile products are not stable and degrade within hours in the

reaction solution, not even extraction with *n*-pentane after 10 min saved the product from degradation.

The basicity of the amines used is too high, so a subsequent nucleophilic addition at the CF_3 carbon takes place and destabilizes the product. This can be underlined by an emerging signal at –151.5 ppm – typical for alkyl fluorides.[325]

Therefore, the less nucleophilic and basic O-nucleophiles were retested below using fluorinated compounds for easier identification in the ^{19}F NMR spectrum. To cover both aliphatic nucleophiles and aromatic nucleophiles, 2-fluoroethanol and 2,6-difluorophenol were investigated in a SuFEx reaction.

First, 2-fluoroethanol was tested by using an excess of the nucleophile (50.0 equiv.) (Scheme 83).

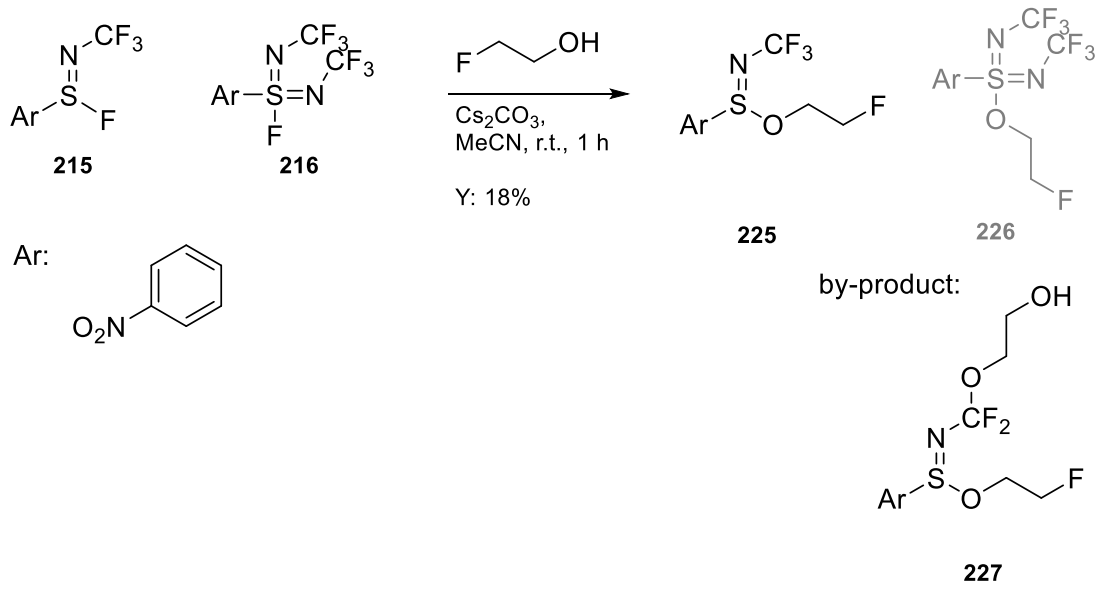

Scheme 83: SuFEx reaction starting from the imine **215** and the diimine **216** – 2-fluoroethanol as an O-nucleophile.

According to the literature, since no conversions were observed for the EtOH and phenol nucleophile in previous experiments, Cs_2CO_3 (10.0 equiv.) was added as a base.[354] The reaction mixture immediately turned from colorless to yellow and after 2 h, a doublet arose at –44.3 ppm in the ^{19}F NMR spectrum with a coupling constant of 0.9 Hz. In contrast to the N-nucleophile reaction products, the doublet did not vanish with time but remained in solution at the same intensity after 20 h. Subsequent flash column chromatography on silica gel afforded the SuFEx product of the S(IV) imine **215** with a substituted fluoride to form the 2-fluoroethoxy species **225**. The S(VI) diimino derivative **226** could neither be detected in solution nor as a column fraction, even though the starting material was completely converted at the end of the reaction. Presumably, a degradation of the diimine **216** is the dominant reaction channel leading to the by-product **227**, since the reactive center consists of an electrophilic S(VI) center in

combination with an electron-deficient aromatic ring and two trifluoroiminyl groups, which may represent vulnerabilities. An attack of aniline at the carbon center of an iminyl carbon trifluoride was already reported.[355] Emerging singlets can underline the consumption by a subsequent degradation of this packed center in the high field of the ^{19}F NMR spectrum in the range of –40 ppm – –60 ppm and at resonances < –100 ppm.

Consistent with this theory, the barely separable by-product **227** indicates a second nucleophilic attack at the electrophilic CF_3 carbon center. In the case of the S(IV) species, the core remains stable, yielding the substitution mentioned above product **225** (Scheme 83).

Since no conversion was observed without the addition of a base, it can be concluded that avoiding too reactive nucleophiles in the reaction may prevent the second nucleophilic attack at the CF_3 center. In the following approach, Cs_2CO_3 was added slowly over time, while the conversion of the starting material was monitored. This reduced the by-product **227** to less than 5% of the overall yield and gave NO_2-Ph-S(NCF_3)(OC_2H_4F) **225** in 18% yield with a one-pot reaction using NO_2-Ph-S-S-Ph-NO_2 **205** as the starting material.

Figure 76 shows the ^{1}H NMR spectrum of the isolated product **225**, indicating restricted rotation around the SO bond, resulting in a geminal $^2J_{FH}$ coupling besides the $^3J_{FH}$ and $^4J_{FH}$ couplings. Additionally, the CH_2F protons are further split into four signal sets.

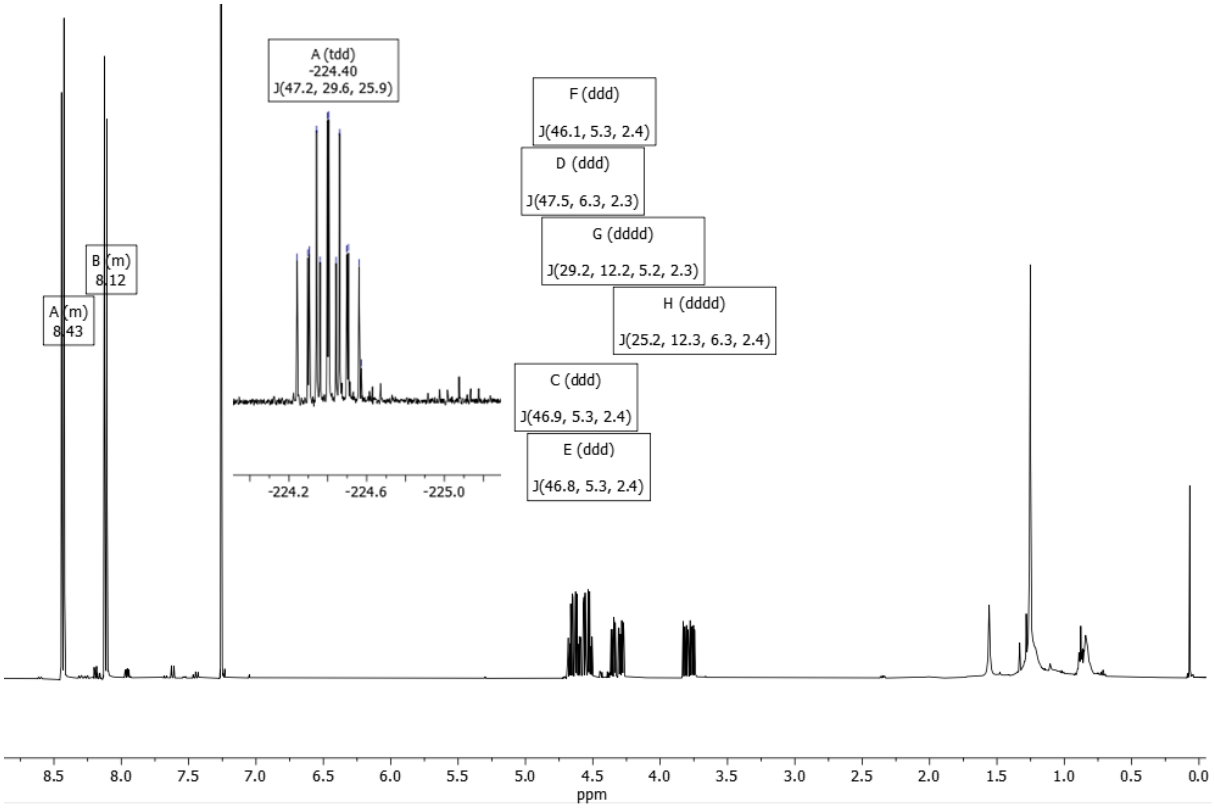

Figure 76: ^{1}H NMR product spectrum of **225** with a zoom of the relevant part of the ^{19}F NMR spectrum after the successful SuFEx reaction with 2-fluoroethanol as the nucleophile.

The extract of the high field of the ^{19}F NMR spectrum shows the iminyl-CF_3 group together with the resonance of the 2-fluoroethoxy substitution at –225 ppm.

This reaction procedure was also applied with 2,6-difluorophenol as a nucleophile that yielded three rotamers indicated by three triplets at –43.7, –44.0 and –44.1 ppm with the coupling constants of 3.8 Hz that are also stable over more than 2 weeks.

In summary, appliying the SuFEx reaction to the novel N-(trifluoromethyl)sulfinimidic fluoride scaffold yields the substitution products for both N-nucleophiles and O-nucleophiles. In the reactions containing N-nucleophiles, a rapid buildup of the product was observed without a base, but subsequent degradation occurred. In contrast, the O-nucleophiles applied in a SuFEx reaction show less reactivity and must be activated *via* a base. The resulting products are stable in solution for days and can be isolated by flash column chromatography on silica gel. No SuFEx product could be observed for the NO_2-Ph-$SF(NCF_3)_2$ **216**, only degradation.

5.2.6 Vinyl-azide-SF_5

In addition to the development of more polar-SF_5-groups, this work addresses the use of prebuilt SF_5-precursors to form SF_5-group containing heterocycles. Triisopropyl((pentafluoro-λ^6-sulfanyl)ethynyl)silane (TIPS-SF_5, **228**) is a rather cheap, commercially available precursor for different heterocycles, as demonstrated by *Rombach et al.* by the hydroamination of SF_5-C≡C-TIPS. The presented method combines the *in-situ* deprotection by a fluoride source with a sequential one-pot hydroamination of SF_5-acetylene, thus circumventing toxic gases in the laboratories. Based on this, Dr. David Rombach and Jonas Wenzel deduced the idea of replacing the amine with $TMSN_3$ and applied the conditions depicted in Scheme 84 to obtain the (E)-(2-azidovinyl)pentafluoro-λ^6-sulfane (SF_5-vinyl-N_3) **229**. First spectroscopical data indicated the evidence of the SF_5-vinyl-N_3 **229** – the final proof of the molecular structure kept pending and is pursued in this work.

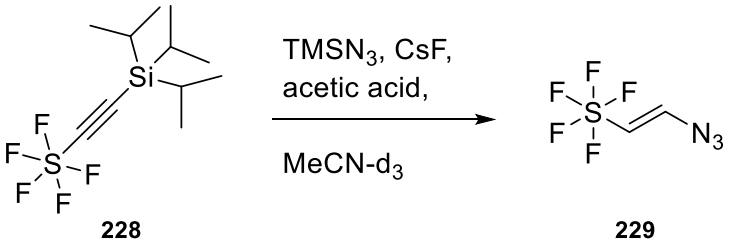

Scheme 84: Synthesis of SF_5-vinyl-N_3 **229** starting from SF_5-acetylene-TIPS **228**.

Using the N_3-anion as a nucleophile in a hydroamination reaction transforms the TIPS-SF_5 **228** into a new species, as indicated in the ^{19}F NMR spectra of the crude reaction mixture presented below. Significantly, one can see the anisotropic effect originating from the alkyne group,

leading to higher shielding at the axial fluoride of the pentafluorosulfanyl-group in comparison to the equatorial fluorides.[356] This effect is expected to have vanished for the alkene case and therefore underlines the presence of SF_5-vinyl-N_3 **229**.[357]

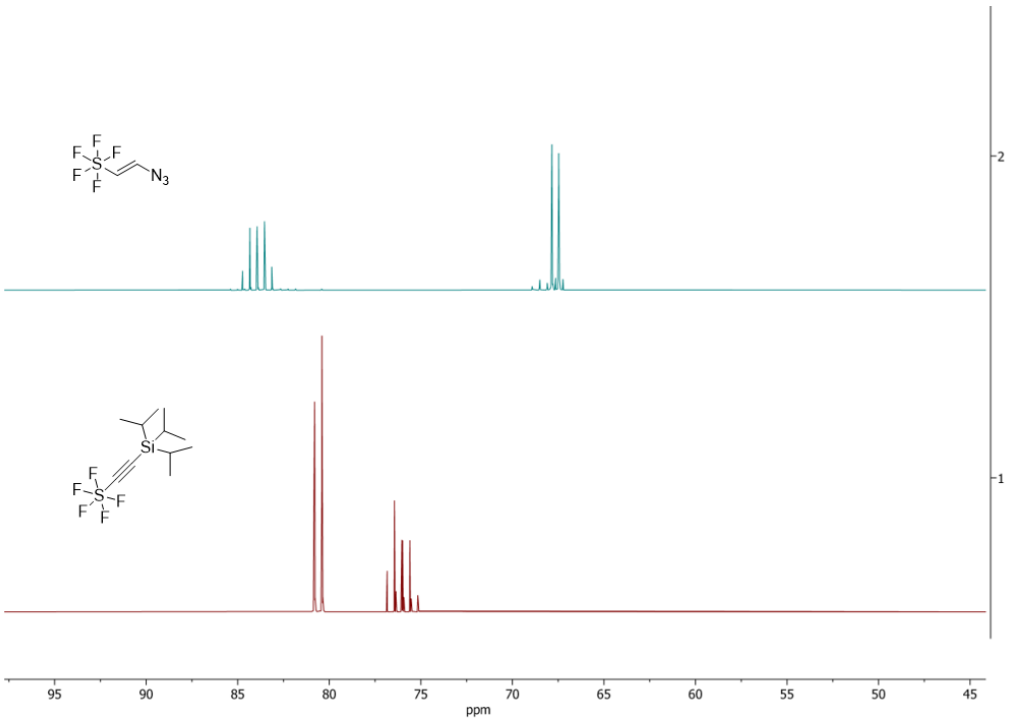

Figure 77: ^{19}F NMR spectra to monitor the conversion of SF_5-acetylene-TIPS **228** to SF_5-vinyl-N_3 **229**.

However, final characterization remained difficult because the suspected vinyl-azide decomposes on both silica gel and deactivated Al_2O_3 (MeOH/NEt_3, 1:1), hindering the isolation of the product. Similarly, no successful HRMS measurements could be performed, probably due to the low boiling point of the compound. Nevertheless, the reaction conditions were optimized based on NMR spectroscopy concerning the evolving product.

Due to the distinguishable ^1H and ^{19}F NMR signals, yields could be calculated from crude NMR spectra using benzotrifluoride as the internal standard. As expected, lowering the reaction temperature decreased the conversion per time to about half. After a reaction time of 5 min, the conversion can be estimated to be 50% at room temperature and 25% at –18 °C and 0 °C.

Table 13: SF_5-acetylene-TIPS **228** as the starting material for a one-pot reaction to the SF_5-vinyl-azide **229**. Yields are based on ^1H and ^{19}F NMR and the analyzed samples were taken after stirring for 1.5 h.

Entry	SF_5-TIPS (equiv.)	CsF (equiv.)	Acetic acid (equiv.)	TMS-N_3 (equiv.)	MeCN-d_3 [mL]	T [°C]	t [h]	SF_5-vinyl-azide **229**
1	1.00	1.00	1.40	1.70	0.25	–18	1.5	85%, 82%
2	1.00	1.00	1.40	1.70	0.25	0	1.5	70%, 71%
3	1.00	1.00	1.40	1.70	0.25	25	1.5	76%, 78%
4	1.00	1.00	–	1.70	0.25	25	1.5	44%, 50%
5	1.00	–	1.40	1.70	0.25	25	1.5	–, –

After 1.5 h, the full conversion could be obtained, regardless of the reaction temperature, as listed in the Table 13 above. Running the hydroazidation without the addition of acetic acid at room temperature slows down the reaction dramatically. After 1.5 h, a yield of less than 50% was obtained because full conversion did not occur. The same result was observed for the reaction without CsF as a deprotecting agent. No conversion could be observed after 1.5 h. Therefore, the mixture was heated to 60 °C and stirred for a further 16 h, which led to a yield of 10%.

Because of the rather clean reaction, direct conversion to a more stable product was aimed to ensure proper evidence of the (E)-(2-azidovinyl)pentafluoro-λ^6-sulfane precursor. Preliminary indications of an *in situ* reactivity of the SF_5-vinyl-N_3 **229** without a definitive structural proof were noticed by Dr. David Rombach and Dr. Kun Zhang.

Therefore, the vinyl-azide **229** was applied under different reaction conditions by adding the respective reagents to the mixture at room temperature after 1.5 h.

A simple addition of ethyl 3-oxobutanoate as 1,3-dicarbonyl yielded the 1,2,3 triazole in an overall yield of 40%, containing the *trans*- **230** or the *cis*- isomer **231**. A cross-peak in the HMBC between 2.52 ppm (s, CH_3) and 139.9 ppm (m, NCH*C*HSF_5), indicates that the *trans*-triazole **230** is more likely present. X-ray diffraction measurement or a well-resolved NOESY spectrum is required for unambiguous proof. In addition, the work on vinyl-azide–acetylene coupling reactions by *Nulwala et al.* emphasizes the formation of the *trans*-product.[358]

These findings support the existence of the vinyl-azide after the first step. As suggested in the work of *Narasaka et al.*, the addition of $Mn(OAc)_3$ was tested to support the radical pathway ending up with a pyrrole species.[359] The N_2 extrusion was not observed, but the triazole **230** or **231** could be obtained in a slightly better yield of 49% (Scheme 85).

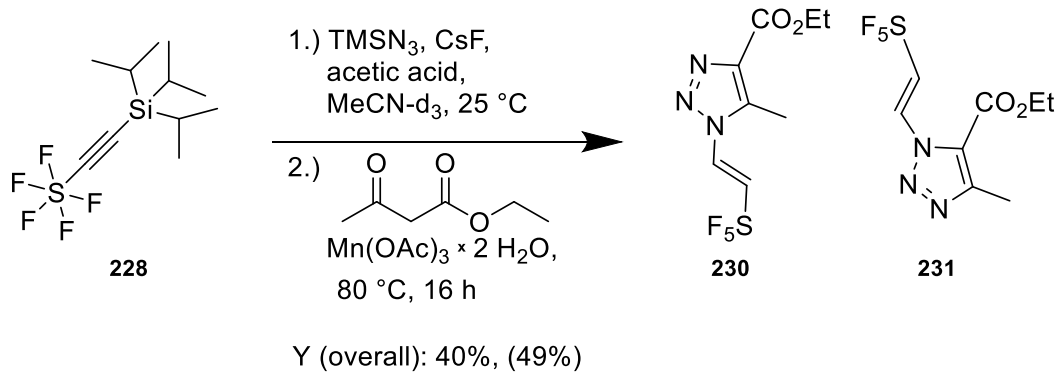

Scheme 85: One-pot synthesis of the SF_5-vinyl-triazoles **230** or **231** using ethyl 3-oxobutanoate as 1,3 dicarbonyl.

To prove the tolerance of this reaction, further 1,3-dicarbonyls such as the pentane-2,4-dione, the dimethyl malonate as a 1,3-dicarboxylic ester or the 4,4-dimethoxybutan-2-one as a 3-oxobutanal precursor were tested

While the diester and the 3-oxobutanal analog showed no conversion after 16 h, the acetylacetone reacted in the same manner as the ethyl 3-oxobutanoate to yield 1,2,3-triazole **232** or **233** with a carbonyl residue (Scheme 86).

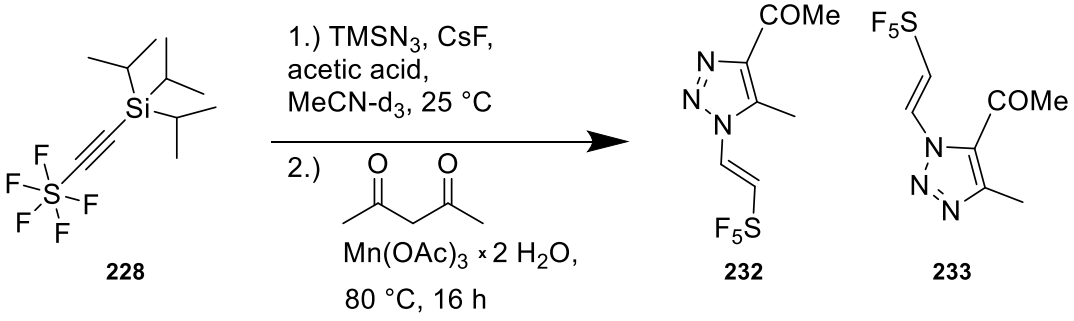

Scheme 86: One-pot synthesis of the SF_5-vinyl-triazole **232** or **233** using pentane-2,4-dione as 1,3 dicarbonyl catalyzed by $Mn(OAc)_3$.

HRMS can be found for both products of the two cycloaddition reactions, confirming the existence of the (E)-(2-azidovinyl)pentafluoro-λ^6-sulfane (**229**) as the reaction precursor. Affordable starting from the commercially available SF_5-acetylene-TIPS **228** after silyl-group deprotection and addition of TMS-N_3.

5.3 Conclusion

Fluorine fascinated many generations of chemists because of its ambivalence between the extreme inertness of the fluoride anion and the extreme reactivity of fluorine gas and many other compounds.[360] Fluorine-containing molecules already shape our everyday life in the form of, e.g., the *Teflon*[311] pan in the kitchen, the *Gore-Tex*[312] membrane in hiking boots or as *Atorvastatin*,[361] a drug against high cholesterol levels. Nevertheless, synthetic methods to install fluorine-based functional groups, in addition to fluorides and trifluoromethane groups, are limited. So far, only the pentafluorosulfanyl group shows a significant increase of impact, e.g., in drug discovery.

For this reason, this work endeavors novel methodologies towards unknown fluorine-based functional groups.

Herein, novel N-(trifluoromethyl)sulfinimidic fluoride derivatives were observed in the reaction of 1,2-bis(4-nitrophenyl)disulfane (**205**) in a XeF_2-driven fluorination reaction in the presence of KCN and NEt_4Cl in MeCN. Optimized conditions increased the yields of the imine **215** and the diimine **216** to up to 34% and 32%.

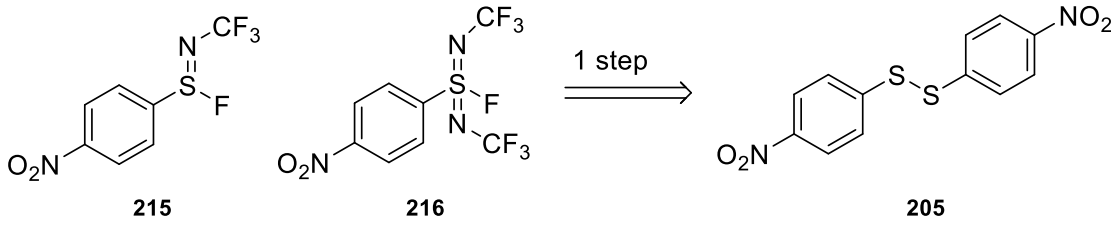

Scheme 87: Retrosynthesis of the N-(trifluoromethyl)sulfinimidic fluoride derivatives **215** and **216** starting from the disulfide **205**.

Subsequently, the reaction mixture was employed in a SuFEx reaction modeled after the protocol for sulfonyl fluorides developed by *Sharpless et al.* 2-Fluoroethanol as an O-nucleophile successfully promoted fluoride exchange and afforded the respective substitution product **225** in 18% yield.

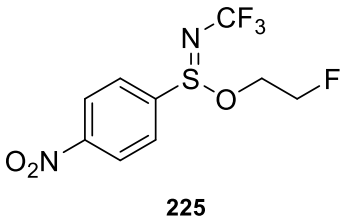

Figure 78: Substitution product **225**, obtained after the first SuFEx reaction at an N-(trifluoromethyl)sulfinimidic fluoride scaffold with 2-fluroethanol.

Furthermore, novel *trans*-substituted SF_4 groups were observed in the radical reaction of NO_2-Ph-SF_4Cl and AIBN under an O_2 atmosphere. After optimizing the reaction conditions, NO_2-

Ph-SF_4-OO-IBN **222** and NO_2-Ph-SF_4-IBN **223** could be isolated in up to 20% and 5% yields. In the case of **222**, the first crystal structure of an SF_4-peroxide was obtained.

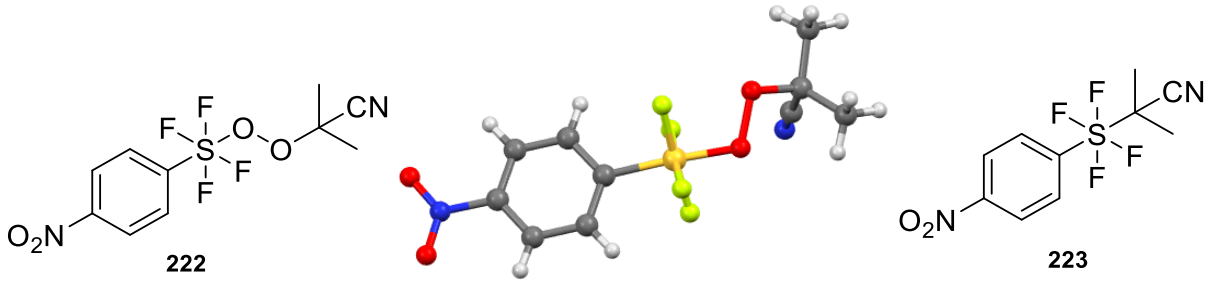

Figure 79: Reaction products **222** and **223** after the radical reaction of AIBN and NO_2-Ph-SF_4Cl **210** under O_2 atmosphere. Central: single-crystal X-ray structure of NO_2-Ph$SF_4OOC(CH_3)_2CN$ **222**.

Besides the development of more polar SF_5-groups, prebuilt SF_5-precursors were used to synthesize SF_5-group containing heterocycles. Thereby, TIPS-SF_5 **228** was deprotected by a fluoride source and subsequently trapped with an N_3-anion in the presence of AcOH. The reaction mixture could be employed in one-pot cycloadditions with different 1,3-dicarbonyls to obtain the SF_5-containing triazoles **230** and **232**.

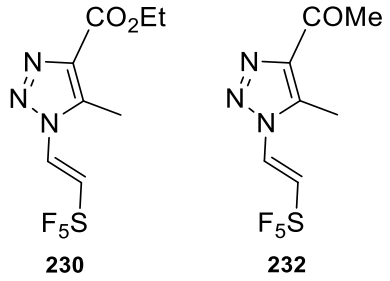

Figure 80: Cycloaddition products **230** and **232** of the one-pot synthesis starting with SF_5-acetylene-TIPS **228** and TMS-N_3.

6 Experimental Section

6.1 General information

6.1.1 Methods and analytics

During the preparation of reactions containing air- or moist-sensitive reagents, the glassware was previously dried with either a heat gun or a gas burner. These reactions were carried out under conventional *Schlenk*-technique, using argon as an inert gas, liquids were transferred *via* plastic syringes and V2A-steel cannulas.[362] Solids were used in pulverized form. For running reactions at low temperature, flat *Dewar* flasks of the company *Isotherm* were used for cooling, using the following frigorific mixtures:

0 °C: ice/H_2O
–18 °C: NaCl/ice/H_2O
–78 °C: isopropanol/dry ice

The used solvent mixtures were volumetrically measured. Solvents were removed under reduced pressure using rotary evaporators with a 40 °C water bath.

6.1.2 Solvents and chemicals

Solvents of *p.a.* (pro analysis) quality were commercially purchased at *Acros Organics, Sigma-Aldrich, Fisher Scientific, or Alpha Aesar* and used without further purification. Absolute solvents were used in the following listed standard procedure and stored under inert gas or commercially purchased.

Acetone was purchased as an absolute solvent at *Fisher Scientific*.

Chloroform was purchased as an absolute solvent at *Acros Organics*.

Dichloroethane was purchased as an absolute solvent at *Alpha Aesar*.

Dichloromethane was purchased in *p.a.* quality and dried over two columns as part of the MBRAUN SPS 800 system.

Dimethylsulfoxide	was purchased as an absolute solvent at *Acros Organics*.
Dimethylformamide	was purchased as an absolute solvent at *Acros Organics*.
Ethyl acetate	was purchased as an absolute solvent at *Acros Organics*.
Methanol	was purchased as an absolute solvent at *Acros Organics*.
2-Methoxyethanol	was purchased as an absolute solvent at *Acros Organics*.
Propionic acid	was purchased as an absolute solvent at *Sigma-Aldrich.*
Pyridine	was purchased as an absolute solvent at *Fisher Scientific*.
Pyrrole	was purchased as an absolute solvent at *Sigma-Aldrich* and distilled before use.
Tetrahydrofurane	was purchased in *p.a.* quality and dried over two columns in the MBRAUN SPS 800 system.
Triethylamine	was purchased as an absolute solvent at *Sigma-Aldrich.*
Toluene	was purchased in *p.a.* quality and dried over two columns as part of the MBRAUN SPS 800 system.
o-Xylene	was purchased as an absolute solvent at *Sigma-Aldrich.*
p-Xylene	was purchased as an absolute solvent at *Sigma-Aldrich.*

6.1.3 Devices and analytical Instruments

Nuclear magnetic resonance spectroscopy (NMR):

The NMR-spectra were recorded on the following devices: ^{1}H- and ^{13}C- NMR spectra were recorded on *Bruker Avance* (300 MHz, 400 MHz), *Bruker* DRX (500 MHz) and at ETH Zürich on *Bruker Avance* (400 MHz, 500 MHz, 600 MHz) spectrometers in the solvents indicated. All spectra were recorded at room temperature. As solvents were used: chloroform-d_1 ($CDCl_3$), dichloromethane-d_2 or THF-d_8 purchased at *Eurisotop*. The chemical shift δ is expressed in parts per million (ppm) and referenced to the residual solvent peaks of chloroform (^{1}H: δ = 7.26 ppm; ^{13}C: δ = 77.16 ppm), dichloromethane (^{1}H: δ = 5.32 ppm; ^{13}C: δ = 54.00 ppm), tetrahydrofuran (^{1}H: δ = 3.58 ppm; ^{13}C: δ = 67.57 ppm) and toluene-d_8 (^{1}H: δ = 7.09 ppm; ^{13}C: δ = 137.86 ppm).[363, 364] For ^{19}F spectra at ETH Zürich no internal standard was used as reference. The recorded spectra were evaluated by 1st order. For centrosymmetric signals, it's the median point, for multipletts the range of the signal was listed. For characterization of the multiplicity the abbreviation s = singlet, d = doublet, t = triplet, q = quartet, p = pentet, m = multiplet, dd = doublet of doublets, td = triplet of doublets ddd = doublet of doublets of doublets and so forth were used. Coupling constants were sorted by absolute values expressed in Hertz (Hz). The number of bonds between the coupling counterparts was expressed as indices as ^{n}J. The assignment of the signals *via* ^{1}H NMR spectra was based on the multiplicity and the chemical shift by using the following abbreviations: $H_{pyrrole}$ = proton of the pyrrolic subunit of the porphyrin ring, $H_{aromatic}$ = proton of the aryl-residues in *meso*-position, $H_{paracyclophane}$ = proton of the aromatic ring of [2.2]paracyclophane and H_{bridge} = proton of the ethylene bridge of [2.2]paracyclophane. In the course of the assignment of the aromatic proton signals of the residues in *meso*-position, the porphyrin residue was allocated to the highest value. The assignment of the signals *via* ^{13}C NMR spectra was based on the chemical shift and the multiplicity obtained *via* DEPT 90- and DEPT 135-spectra (DEPT = distortionless enhancement by polarization transfer) or by phase edited HSQC (heteronuclear single quantum coherence) and are described as follows: + = primary or tertiary C-atom (positive DEPT- or HSQC-signal), – = secondary C-atom (negative signal) and C_q = quaternary C-atom (no signal). Common solvent and solvent impurity signals as followed were not explicitly listed: in $CDCl_3$: ^{1}H NMR 1.55 (H_2O), 1.25 (H grease), 0.84 – 0.87 (H grease), 0.07 (silicon grease) ppm; ^{13}C NMR 29.7 (H grease), 1.20 (silicon grease) ppm; DCM-d_2: ^{1}H NMR 1.52 (H_2O), 1.29 (H grease), 0.84 – 0.90 (H grease), 0.09 (silicon grease) ppm; ^{13}C NMR 30.1 (H grease), 1.2

(silicon grease) ppm; THF-d_8: ^{1}H NMR 10.84 (THF-d_8 impurity), 3.26 (THF-d_8 impurity), 2.50 (THF-d_8 impurity), 2.49 (H_2O), 1.29 (H grease), 0.85 – 0.91 (H grease), 0.11 (silicon grease) ppm; ^{13}C NMR 29.9 ppm (H grease) 1.2 (silicon grease) ppm. In low resolution, the signals were listed based on the ^{1}H-broadband-decoupled ^{13}C NMR spectra without phases.

Infrared spectroscopy (IR):

IR spectra were recorded on an FT-IR *Bruker* Alpha P spectrometer. All samples were measured by the ATR technique (attenuated total reflection) ranging from 3600 cm^{-1} to 500 cm^{-1}. The positions of the absorption bands are given in wavenumbers $\tilde{\nu}$ in cm^{-1}. The signal intensity was listed and characterized as followed (T = transmission): vs = very strong (0 – 10% T), s = strong (10 – 40% T), m = middle (40 – 70% T), w = weak (70 – 90% T), vw = very weak (90 – 100% T).

Mass spectrometry (MS):

Mass spectra were measured either by FAB-MS (Fast Atom Bombardment) recorded on a *Finnigan MAT 95* with *m*-nitrobenzyl alcohol (3-NBA) like matrix, by EI-MS (electron ionization) recorded on *Finnigan MAT 95* or by ESI-MS (electron spray ionization) recorded on a *Thermo Scientific Q Exactive Plus* or a *Bruker timsTOF*™.

For the *o*-phenylene bisporphyrins and trisporphyrins, the mass spectra and ion mobility spectra, the porphyrins were dissolved in a 1:2 mixture of CH_2Cl_2 and DMF. A capillary voltage of up to 6 kV was necessary to ionize the neutral porphyrins (2Ni(II), 2Cu(II), 2Zn(II), 2Pd(II)). For the already charged 2Mn(III), 2Fe(III) and the free base porphyrins, a voltage of 2.5 kV was sufficient. The used source pressure was 1.3 bar and the dry gas temperature was 200 °C.

At ETH Zurich, the mass spectra were measured by either EI-MS recorded on a *Thermo scientific Q Exactive GC Orbitrap* with a direct probe or by ESI-MS and recorded on a *Bruker Daltonics maXis ESI-QTOF*.

In general, the molecular peak $[M]^+$ or $[M+H]^+$ and the characteristic fragmentation peaks $[M – fragment]^+$ or $[fragment]^+$ were given, as far as they were significant, as the mass-to-charge ratio (*m/z*) with their intensity relative to the basic signal (100%). Under HRMS, the

molecular mass was determined, whereby "calc." represents the theoretical value of the exact mass and "found" represents the obtained value in the spectra.

UV-Vis spectroscopy (UV-Vis):

All UV-Vis spectra were recorded on a *Specord 50 Plus* made by the company *Q Analytik Jena*. Before the measurement, the samples were dissolved in CH_2Cl_2, MeOH or $CHCl_3$ filled in glass cuvettes with a layer thickness of 0.1 cm or 0.5 cm.

Analytical thin-layer chromatography (TLC):

TLC was carried out on *Merck* silica gel coated aluminum plates (silica 60, F_{254}). Solvent mixtures were measured volumetrically. If an assignment was not possible under daylight, fluorescence quenching under UV light was used at λ = 254 nm or λ = 365 nm *via* a UV lamp *UV-6 S/L* purchased at *Hereolab* or λ = 395 nm *via* a UV flashlight *Veetop Schwarzlicht UV* purchased by *QVQ EU*.

Column chromatography:

If not stated otherwise, the crude products were purified *via* flash column chromatography using *p.a.* solvents as described after *Still et al.*[365] Silica gel 60 (0.040 × 0.063 mm, *Geduran*®, *Merck*) was used as a stationary phase. Alternatively, aluminum oxide 150 basic (particle size: 70% between 0.063 – 0.200 mm, *Sigma Aldrich*) *Brockmann* activity III (6% H_2O (w/w)) was used.

Analytical balance:

Weight measurements were done on an *HR-250A* purchased at *A&D Company*.
Minimum weight: 10 mg, maximum weight: 252 g, calibrated value: 1 mg.

X-ray diffraction analysis

The single-crystal X-ray diffraction studies were carried out by Dr. Martin Nieger at the University of Helsinki on a *Bruker* D8 Venture diffractometer with Photon II detector at 123(2) K using Cu-K$_\alpha$ radiation (λ = 1.54178 Å). Dual space methods SHELXT[366] were used for structure solution and refinement was carried out using SHELXL-2014 (full-matrix least-squares on F^2).[366] Alternatively, a Kappa-CCD-X-ray diffractometer produced by *Bruker-Nonius* at 123(2) K using Mo-K$_\alpha$-radiation (λ = 0.71073 Å)

Computing details: Data collection: *APEX3*[367]; cell refinement: *APEX3*[367]; data reduction: *SAINT*[367]; program used to solve structure: *SHELXT*[366]; program used to refine structure: *SHELXL2014*/7[368]; software used to prepare material for publication: *publCIF*[369].

The single-crystal X-ray diffraction studies were carried out by Dr. Nils Trapp at the Eidgenössische Technische Hochschule Zurich on an *XtaLAB* Synergy, *Dualflex*, *Pilatus* 300 K diffractometer. The crystal was kept at 100.0 ±1 K during data collection. Using *Olex2*,[370] the structure was solved with the *SHELXT*[366] structure solution program using intrinsic phasing and refined with the *SHELXL*[371] refinement package using least-squares minimization.

Synthesis and Characterization of the Synthesized Compounds

6.2 Synthesis of the porphyrin precursors

6.2.1 Syntheses of monomeric *meso*- and residue-substituted porphyrin precursors

Di(1*H*-pyrrol-2-yl)methane (**57**) was synthesized according to a previous publication of the *Bräse* group.[372]

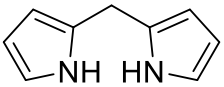

Under an argon atmosphere, paraformaldehyde (1.59 g, 53.1 mmol, 1.00 equiv.) was added to freshly distilled pyrrole (340 mL, 330 g, 4.92 mol, 92.7 equiv.) and the resulting suspension was stirred for 10 min at 55 °C. Then $InCl_3$ (1.16 g, 5.25 mmol, 0.10 equiv.) was added and the reaction mixture was stirred for 3 h at 55 °C. After cooling to room temperature, powdered NaOH (7.02 g, 176 mmol, 3.31 equiv.) was added and stirred for 1 h. The reaction mixture was filtered and pyrrole was removed under reduced pressure. The crude product was purified by flash column chromatography on silica gel (*c*Hex/EtOAc, 10:1 to 2:1) to afford the title compound **57** as a colorless crystalline solid (5.05 g, 34.5 mmol, 65%). ***R*f** (*c*Hex/EtOAc, 2:1) = 0.57. – **^{1}H NMR** (400 MHz, $CDCl_3$): δ = 7.67 (bs, 2H, N*H*), 6.62 (td, ^3J = 2.7, 1.6 Hz, 2H), 6.18 (q, ^3J = 2.9 Hz, 2H), 6.03 – 6.09 (m, 2H), 3.94 (s, 2H, CH_2) ppm. – **^{13}C NMR** (101 MHz, $CDCl_3$): δ = 129.2 (C_q), 117.5 (+, CH), 108.4 (+, CH), 106.6 (+, CH), 26.4 (–, *C*H_2) ppm. – **IR** (ATR): $\tilde{\nu}$ = 3325, 1561, 1439, 1422, 1327, 1244, 1181, 1119, 1108, 1095, 1024, 960, 884, 806, 798, 747, 720, 683, 666, 625, 599, 585, 496, 469 cm^{-1}. – **MS** (EI, 70 eV, 20 °C): *m/z* (%) =146.1 (100) $[M]^+$, 118.1 (12), 80.1 (30), 67.1 (18). – **HRMS** ($C_{10}H_{10}O_3$): calc.: 146.0844, found: 146.0844.

Additional information on the reaction details of previously obtained results is available *via* the Chemotion repository:

https://dx.doi.org/10.14272/reaction/SA-FUHFF-UHFFFADPSC-PBTPREHATA-UHFFFADPSC-NUHFF-NUHFF-NUHFF-ZZZ.4

Additional information on the analysis of the target compound for previously obtained results is available *via* the Chemotion repository:

https://dx.doi.org/10.14272/PBTPREHATAFBEN-UHFFFAOYSA-N.1

Ethyl-4-formylbenzoate (**81^{aldehyde}**) was synthesized according to a previous publication of our group.[372]

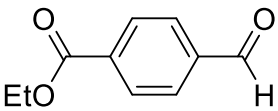

4-Formylbenzoic acid (7.93 g, 52.8 mmol, 1.00 equiv.) was dissolved in DMF (197 mL). Subsequently, K_2CO_3 (14.1 g, 102 mmol,

1.94 equiv.) and iodoethane (10.8 mL, 20.9 g, 134 mmol, 2.54 equiv.) were added. The reaction mixture was stirred for 3 h at room temperature and quenched with H_2O (250 mL). The aqueous phase was extracted with Et_2O (2 × 200 mL). The combined organic phases were washed with brine (2 × 200 mL), dried over $MgSO_4$ and filtered. The solvent was removed under reduced pressure. The crude product was purified by flash column chromatography on silica gel (*c*Hex/EtOAc, 6:1) to afford the title compound **81**$^{\textbf{aldehyde}}$ as a colorless, crystalline solid (7.98 g, 44.8 mmol, 85%).

***R*f** (*c*Hex/EtOAc, 6:1) = 0.60. – **^{1}H NMR** (400 MHz, $CDCl_3$): δ = 10.06 (s, 1H, OC*H*), 8.16 (d, ^3J = 8.5 Hz, 2H, $H_{aromatic}$), 7.91 (d, ^3J = 8.5 Hz, 2H, $H_{aromatic}$), 4.38 (q, ^3J = 7.1 Hz, 2H, CH_2), 1.38 (t, ^3J = 7.1 Hz, 3H, CH_3) ppm. – **^{13}C NMR** (101 MHz, $CDCl_3$): δ = 191.7 (+, O*C*H), 165.6 (C_q, *C*OO), 139.2 (C_q), 135.5 (C_q), 130.2 (+, *C*H), 129.5 (+, *C*H), 61.6 (–, *C*H_2), 14.3 (+, *C*H_3) ppm. – **IR** (ATR): $\tilde{\nu}$ = 2924, 2854, 1701, 1577, 1503, 1448, 1367, 1272, 1200, 1172, 1103, 1017, 854, 818, 758, 733, 690, 630, 461 cm^{-1}. – **MS** (EI, 70 eV, 20 °C): *m/z* (%) =178 (44) $[M]^+$, 149 (24) $[M–CO]^+$, 133 (100) $[M–C_2H_5O]^+$, 105 (18) $[M–CO_2C_2H_5]^+$. – **HRMS** ($C_{10}H_{10}O_3$): calc.: 178.0630, found: 178.0630.

Additional information on the reaction details of previously obtained results is available *via* the Chemotion repository:

https://dx.doi.org/10.14272/reaction/SA-FUHFF-UHFFFADPSC-BHYVHYPBRY-UHFFFADPSC-NUHFF-NUHFF-NUHFF-ZZZ

Additional information on the analysis of the target compound for previously obtained results is available *via* the Chemotion repository:

https://dx.doi.org/10.14272/BHYVHYPBRYOMGC-UHFFFAOYSA-N.1

5,15-Diphenylporphyrin (**80**)[373]

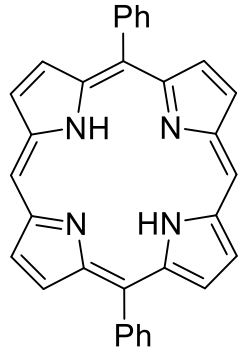

Under an argon atmosphere, di(1*H*-pyrrol-2-yl)methane (**57**) (2.87 g, 19.6 mmol, 2.00 equiv.) and benzaldehyde (**48**) (2.1 mL, 2.15 g, 20.3 mmol, 2.05 equiv.) were dissolved in CH_2Cl_2 (3.67 L). A stream of argon was passed through the mixture for 15 min to remove dissolved oxygen. Then, dropwise added trifluoroacetic acid (0.92 mL, 1.36 g, 11.9 mmol, 1.21 equiv.). The mixture was stirred for 18 h in the dark. Afterward, first triethylamine (30 mL) and then DDQ (5.40 g, 23.8 mmol, 2.42 equiv.) were added and the mixture was stirred for 1 h. The crude mixture was concentrated under reduced pressure and filtered through a short layer of silica gel eluting with CH_2Cl_2. A final thorough wash with MeOH afforded the title compound **80** as a crystalline purple solid (2.87 g, 6.18 mmol, 63%).

***R*f** (CH_2Cl_2/*c*Hex, 1:1) = 0.48. – **^{1}H NMR** (400 MHz, $CDCl_3$): δ = 10.32 (s, 2H, H_{meso}), 9.40 (d, ^3J = 4.6 Hz, 4H, $H_{pyrrole}$), 9.10 (d, ^3J = 4.6 Hz, 4H, $H_{pyrrole}$), 8.32 – 8.25 (m, 4H, $H_{aromatic}$), 7.85 – 7.79 (m, 6H, $H_{aromatic}$), –3.11 (bs, 2H, N*H*) ppm. – **^{13}C NMR** (101 MHz, $CDCl_3$): δ = 147.3 (C_q), 145.4 (C_q), 141.5 (C_q), 135.0 (+, CH), 131.8 (+, CH), 131.2 (+, CH), 127.9 (+, CH), 127.1 (+, CH), 119.3 (C_q), 105.4 (+, CH) ppm. – **UV-Vis** ($CHCl_3$): λ_{max} (rel. absorption) = 407 (5.44), 503 (4.23), 537 (3.70), 575 (3.74), 630 (3.18) nm. – **IR** (ATR): $\tilde{\nu}$ = 3050, 1578, 1532, 1482, 1438, 1406, 1324, 1237, 1196, 1145, 1051, 1000, 985, 972, 955, 851, 784, 745, 717, 688, 649, 558, 500, 432, 414, 396 cm^{-1}. – **MS** (ESI): *m/z* (%) = 463 (100) $[M+H]^+$. – **HRMS** ($C_{32}H_{23}N_4$): calc.: 463.1917, found: 463.1900.

Additional information on the reaction details is available *via* the Chemotion repository: https://dx.doi.org/10.14272/reaction/SA-FUHFF-UHFFFADPSC-FNNOEKVUXX-UHFFFADPSC-NUHFF-NZWZG-NUHFF-ZZZ

Additional information on the analysis of the target compound is available *via* the Chemotion repository:

https://dx.doi.org/10.14272/FNNOEKVUXXVPAI-DUVOQLPESA-N.1

5,15-Diethoxycarbonylphenylporphyrin (**81**)[373]

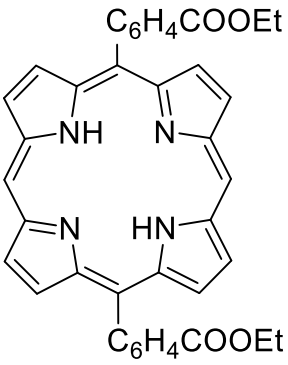

Under an argon atmosphere, di(1*H*-pyrrol-2-yl)methane (**57**) (600 mg, 4.10 mmol, 2.00 equiv.) and 4-ethoxycarbonylbenzaldehyde **81^{aldehyde}** (713 mg, 4.00 mmol, 1.95 equiv.) were dissolved in $CHCl_3$ (800 mL). A stream of argon was passed through the mixture for 15 min to remove dissolved oxygen. Then, trifluoroacetic acid (0.31 mL, 459 mg, 4.02 mmol, 2.01 equiv.) was added dropwise. The mixture was stirred for 18 h in the dark. Afterward, first NEt_3 (1.8 mL) and then *p*-chloranile (2.70 g, 11.9 mmol, 5.95 equiv.) were added and the mixture was refluxed for 1.5 h. The crude mixture was concentrated under reduced pressure, filtered through a short layer of silica gel eluting with CH_2Cl_2 and purified by flash chromatography on silica gel (CH_2Cl_2/EtOAc, 100:0 →100:1). A final thorough wash with MeOH afforded the title compound **81** as a purple solid (664 mg, 1.09 mmol, 53%).

***R*f** (*c*Hex/EtOAc, 4:1) = 0.52. – **^{1}H NMR** (400 MHz, $CDCl_3$): δ = 10.36 (s, 2H, H_{meso}), 9.43 (d, ^3J = 4.6 Hz, 4H, $H_{pyrrole}$), 9.05 (d, ^3J = 4.6 Hz, 4H, $H_{pyrrole}$), 8.51 (d, ^3J = 8.1 Hz, 4H, $H_{aromatic}$), 8.37 (d, ^3J = 8.1 Hz, 4H, $H_{aromatic}$). 4.63 (q, ^3J = 7.2 Hz, 4H, COCH_2), 1.58 (t, ^3J = 7.1 Hz, 6H, CH_2CH_3), –3.12 (bs, 2H, N*H*) ppm. – **^{13}C NMR** (101 MHz, $CDCl_3$): δ = 167.0 (C_q), 146.9 (C_q, *C*OOEt), 146.2 (C_q), 145.5 (C_q), 135.0 (+, CH), 132.2 (+, CH), 131.0 (+, CH), 130.1 (+, CH),

128.3 (+, CH), 118.1 (C_q), 105.8 (+, CH), 61.5 (–, $COCH_2$), 14.7 (+, CH_2CH_3) ppm. – **UV-Vis** ($CHCl_3$): λ_{max} (rel. absorption) = 405 (5.27), 504 (4.22), 539 (3.85), 576 (3.74), 631 (3.33) nm. – **IR** (ATR): $\tilde{\nu}$ = 3484, 3276, 2976, 1703, 1602, 1437, 1398, 1363, 1305, 1268, 1239, 1194, 1173, 1096, 1051, 1017, 986, 971, 952, 900, 868, 843, 812, 792, 752, 736, 723, 691, 520, 489, 435, 411 cm^{-1}. – **MS** (FAB, 3-NBA): *m/z* (%) = 607 (100) $[M+H]^+$. – **HRMS** ($C_{38}H_{31}O_4N_4$): calc.: 607.2340, found: 607.2340.

Additional information on the reaction details of previously obtained results is available *via* the Chemotion repository:

https://dx.doi.org/10.14272/reaction/SA-FUHFF-UHFFFADPSC-QKHPYPUCYC-UHFFFADPSC-NUHFF-NHYOA-NUHFF-ZZZ

Additional information on the analysis of the target compound for previously obtained results is available *via* the Chemotion repository:

https://dx.doi.org/10.14272/QKHPYPUCYCZMQU-WTFXTOSCSA-N.1

5,10,15-Triphenylporphyrin (**82**)[373]

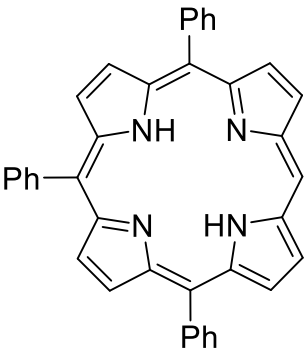

Under an argon atmosphere, 5,15-diphenylporphyrin (**80**) (1.26 g, 2.70 mmol, 1.00 equiv.) was dissolved in dry THF (600 mL) and cooled to 0 °C. Subsequently, 1.9M phenyllithium in butyl ether (13.6 mL, 2.52 g, 25.9 mmol, 13.3 equiv.) was added. The reaction mixture was stirred at room temperature for 30 min and then quenched with H_2O (3.5 mL). After stirring for 10 min, DDQ (650 mg, 2.86 mmol, 2.00 equiv.) was added and stirred for a further 15 min. The solvent was removed under reduced pressure and filtered through a short layer of silica gel eluting with CH_2Cl_2. A final thorough wash with MeOH afforded the title compound **82** as a purple solid (1.38 g, 2.56 mmol, 95%).

***R*f** (CH_2Cl_2/*c*Hex, 1:1) = 0.47. – **^{1}H NMR** (400 MHz, $CDCl_3$): δ = 10.22 (s, 1H, H_{meso}), 9.34 (d, ^3J = 4.6 Hz, 2H, $H_{pyrrole}$), 9.04 (d, ^3J = 4.6 Hz, 2H, $H_{pyrrole}$), 8.93 (d, ^3J = 4.8 Hz, 2H, $H_{pyrrole}$), 8.90 (d, ^3J = 4.8 Hz, 2H, $H_{pyrrole}$), 8.30 – 8.21 (m, 6H, $H_{aromatic}$), 7.84 – 7.73 (m, 9H, $H_{aromatic}$). – 2.98 (bs, 2H, N*H*) ppm. – **^{13}C NMR** (101 MHz, $CDCl_3$): δ = 142.7 (C_q), 141.9 (C_q), 134.8 (+, CH), 134.6 (+, CH), 131.6 (+, CH), 131.4 (+, CH), 130.8 (+, CH), 127.9 (+, CH), 127.0 (+, CH), 126.7 (+, CH), 120.7 (C_q), 119.8 (C_q), 104.9 (+, CH) ppm. – **UV-Vis** ($CHCl_3$): λ_{max} (rel. Absorption) = 413 (2.83), 509 (0.41), 543 (0.12), 583 (0.12), 638 (0.05) nm. – **IR** (ATR): $\tilde{\nu}$ = 2330, 1592, 1555, 1471, 1438, 1405, 1341, 1220, 1191, 1150, 1065, 1051, 1031, 1000, 977,

959, 854, 794, 784, 745, 726, 701, 654, 638, 555, 512, 494 cm^{-1}. – **MS** (FAB, 3-NBA): *m/z* (%) = 539 (100) $[M+H]^+$. – **HRMS** ($C_{38}H_{27}N_4$): calc.: 539.2236, found: 539.2234.

Additional information on the reaction details is available *via* the Chemotion repository: https://dx.doi.org/10.14272/reaction/SA-FUHFF-UHFFFADPSC-ONZNTVWSXS-UHFFFADPSC-NUHFF-NBVCV-NUHFF-ZZZ

Additional information on the analysis of the target compound is available *via* the Chemotion repository: https://dx.doi.org/10.14272/ONZNTVWSXSVUHQ-WIYWIPGRSA-N.1

5-Bromo-10,15,20-triphenylporphyrin (**83**)[373]

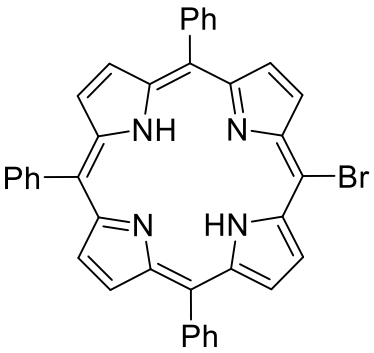

5,10,15-Triphenylporphyrin (**82**) (648 mg, 1.20 mmol, 1.00 equiv.) was dissolved in CH_2Cl_2 (128 mL). The solution was cooled to 0 °C and NBS (225 mg, 1.26 mmol, 1.05 equiv.) was added. The resulting mixture was stirred for 3 h while warming up to room temperature. After removing the solvent under reduced pressure, the crude product was recrystallized (CH_2Cl_2/MeOH) to afford the title compound **83** (723 mg, 1.17 mmol, 97%) as a crystalline purple solid.

***R*f** (CH_2Cl_2/*c*Hex, 1:1) = 0.66. – **^{1}H NMR** (400 MHz, $CDCl_3$): δ = 9.67 (d, ^3J = 4.8 Hz, 2H, $H_{pyrrole}$), 8.91 (d, ^3J = 4.9 Hz, 2H, $H_{pyrrole}$), 8.80 (s, 4H, $H_{pyrrole}$), 8.23 – 8.15 (m, 6H, $H_{aromatic}$), 7.83 – 7.71 (m, 9H, $H_{aromatic}$), –2.14 (bs, 2H, N*H*) ppm. – **^{13}C NMR** (101 MHz, $CDCl_3$): δ = 142.0 (C_q), 141.9 (C_q), 134.7 (+, CH), 134.6 (+, CH), 128.0 (+, CH), 128.0 (+, CH), 121.1 (C_q), 120.9 (C_q), 103.0 (C_q) ppm. – **UV-Vis** ($CHCl_3$): λ_{max} (rel. absorption) = 418 (5.34), 518 (4.22), 553 (3.93), 595 (3.70), 652 (3.61) nm. – **IR** (ATR): $\tilde{\nu}$ = 1594, 1469, 1439, 1341, 1216, 1176, 1071, 1000, 979, 963, 843, 793, 743, 718, 697, 633, 554, 517, 418 cm^{-1}. – **MS** (ESI): *m/z* (%) = 617/618/619/620 (100/43/99/41) $[M+H]^+$. – **HRMS** ($C_{38}H_{26}N_4{}^{79}Br$): calc.: 617.1335, found: 617.1323.

Additional information on the reaction details is available *via* the Chemotion repository: https://dx.doi.org/10.14272/reaction/SA-FUHFF-UHFFFADPSC-SSDAPHKBPY-UHFFFADPSC-NUHFF-NCEIP-NUHFF-ZZZ

Additional information on the analysis of the target compound is available *via* the Chemotion repository: https://dx.doi.org/10.14272/SSDAPHKBPYAYKP-YVFGNCJRSA-N.1

5-Bromo-10,20-diethoxycarbonylphenylporphyrin (**84**)[373]

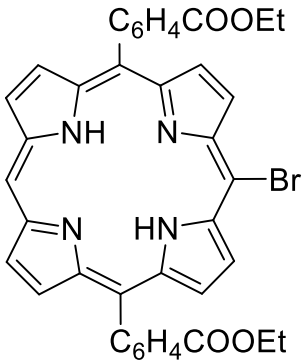

5,15-Diethoxycarbonylphenylporphyrin (**81**) (509 mg, 839 µmol, 1.00 equiv.) was dissolved in CH_2Cl_2 (210 mL) and pyridine (0.23 mL, 221 mg, 9.87 equiv.) was added. The reaction mixture was cooled to 0 °C and NBS (164 mg, 921 mmol, 1.10 equiv.) was added. The resulting mixture was stirred for 20 min at this temperature. After removing the solvent under reduced pressure, the crude product was purified by flash column chromatography on silica gel (CH_2Cl_2) to afford the title compound **84** (345 mg, 503 µmol, 60%) a purple solid. ***R*f** (*c*Hex/EtOAc, 4:1) = 0.55. – **^{1}H NMR** (400 MHz, $CDCl_3$): δ = 10.04 (s, 1H, H_{meso}), 9.69 (d, ^3J = 4.8 Hz, 2H, $H_{pyrrole}$), 9.19 (d, ^3J = 4.6 Hz, 2H, $H_{pyrrole}$), 8.85 (dd, J = 4.8 Hz, 1.1 Hz, 4H, $H_{pyrrole}$), 8.48 (d, ^3J = 8.2 Hz, 4H, $H_{aromatic}$), 8.23 (d, ^3J = 8.2 Hz, 4H, $H_{aromatic}$). 4.63 (q, ^3J = 7.2 Hz, 4H, COC*H*$_2$), 1.59 (t, ^3J = 7.2 Hz, 6H, CH_2CH_3), –3.14 (bs, 2H, N*H*) ppm. –**^{13}C NMR** (101 MHz, $CDCl_3$): δ = 166.9 (C_q, *C*OOEt), 146.0 (C_q), 134.7 (+, CH), 133.0 (+, CH), 132.1 (+, CH), 131.7 (+, CH), 131.5 (+, CH), 130.2 (+, CH), 128.2 (+, CH), 119.1 (C_q), 105.9 (+, CH), 104.2 (C_q), 61.5 (–, CO*C*H$_2$), 14.7 (+, CH$_2$*C*H$_3$) ppm. – **UV-Vis** (CH_2Cl_2): λ_{max} (rel. absorption) = 231 (0.38), 306 (0.18), 373 (0.36), 416 (3.38), 512 (0.22), 546 (0.08), 588 (0.07), 644 (0.03). – **IR** (ATR): $\tilde{\nu}$ = 3475, 3303, 2983, 2945, 2917, 1708, 1605, 1398, 1363, 1265, 1256, 1190, 1173, 1109, 1096, 1047, 1021, 993, 983, 973, 955, 873, 850, 790, 781, 752, 731, 703, 690, 630, 493 cm^{-1}. – **MS** (ESI): *m/z* (%) = 685.1 (93) $[M+H]^+$, 686.1 (40) $[M+H]^+$, 687.1 (100) $[M+H]^+$, 688.1 (40) $[M+H]^+$. – **HRMS** ($C_{38}H_{30}BrN_4O_4$): calc.: 685.1450, found: 685.1445.

Additional information on the reaction details is available *via* the Chemotion repository: https://dx.doi.org/10.14272/reaction/SA-FUHFF-UHFFFADPSC-OMAOSJQEKB-UHFFFADPSC-NUHFF-NYLSX-NUHFF-ZZZ

Additional information on the analysis of the target compound is available *via* the Chemotion repository: https://dx.doi.org/10.14272/OMAOSJQEKBZBDX-UGXFXZPKSA-N.1

6.2.2 Synthesis of the monomeric *β*-substituted porphyrin precursors

2-Bromo-5,10,15,20-tetraphenylporphyrin (**85**)[374]

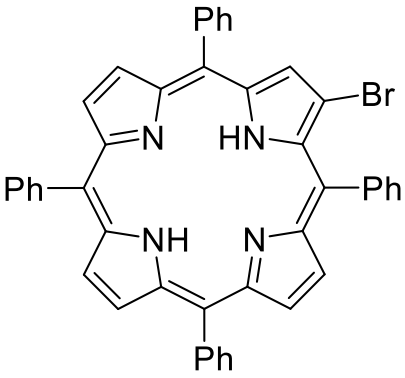

Tetraphenylporphyrin **32** (358 mg, 582 µmol, 1.00 equiv.) was dissolved in CH_2Cl_2 (200 mL) and heated to reflux. Then, pyridine (6 mL) and NBS (362 mg, 2.03 mmol, 3.49 equiv.) dissolved in CH_2Cl_2 (100 mL) were slowly added. After 8 h, the reaction was quenched with 20 mL acetone. The solvent was removed under reduced pressure and the crude product was filtered through a small layer of silica gel eluting with CH_2Cl_2. The resulting crude product was purified by flash column chromatography on silica gel (*c*Hex/CH_2Cl_2, 2:1) to afford the title compound **85** (217 mg, 312 µmol, 54%) a purple solid.

***R*f** (*c*Hex/EtOAc, 4:1) = 0.61. – **^{1}H NMR** (400 MHz, $CDCl_3$): δ = 8.96 – 8.90 (m, 3H, $H_{pyrrole}$), 8.90 – 8.86 (m, 1H, $H_{pyrrole}$), 8.86 – 8.82 (m, 1H, $H_{pyrrole}$), 8.81 – 8.76 (m, 2H, $H_{pyrrole}$), 8.25 – 8.19 (m, 6H, $H_{aromatic}$), 8.14 – 8.09 (m, 2H, $H_{aromatic}$), 7.84 – 7.71 (m, 12H, $H_{aromatic}$), –2.81 (bs, 2H, N*H*) ppm. – **^{13}C NMR** (101 MHz, $CDCl_3$): δ = 142.2 (C_q), 141.8 (C_q), 140.9 (C_q), 138.2 (+, CH), 134.7 (+, CH), 134.7 (+, CH), 134.7 (+, CH), 134.6 (+, CH), 134.5 (+, CH), 134.0 (+, CH), 133.7 (+, CH), 129.7 (+, CH), 129.0 (+, CH), 128.4 (+, CH), 128.1 (+, CH), 128.0 (+, CH), 127.1 (+, CH), .127.0 (+, CH), .127.0 (+, CH), 126.9 (+, CH), 126.9 (+, CH). 120.9 (C_q), 120.4 (C_q), 120.2 (C_q), 119.7 (C_q) ppm. – **UV-Vis** (CH_2Cl_2): λ_{max} (rel. absorption) = 217 (0.19), 420 (3.08), 517 (0.17), 551 (0.05), 592 (0.05), 648 (0.04). – **IR** (ATR): $\tilde{\nu}$ = 2918, 2850, 1740, 1592, 1465, 1441, 1346, 1239, 1177, 1145, 1071, 1023, 1000, 975, 963, 829, 796, 722, 698, 671, 657, 640, 619, 557, 524 cm^{-1}. – **MS** (ESI): *m/z* (%) = 693.2 (95) $[M+H]^+$, 694.2 (59) $[M+H]^+$, 695.2 (100) $[M+H]^+$, 696.2 (43) $[M+H]^+$. – **HRMS** ($C_{44}H_{30}BrN_4$): calc.: 693.1654, found: 693.1633.

Additional information on the reaction details is available *via* the Chemotion repository: https://dx.doi.org/10.14272/reaction/SA-FUHFF-UHFFFADPSC-PUHJRVJBTV-UHFFFADPSC-NUHFF-NNFZG-NUHFF-ZZZ

Additional information on the analysis of the target compound is available *via* the Chemotion repository: https://dx.doi.org/10.14272/PUHJRVJBTVWPFU-FGSSQFOESA-N.1

6.2.3 Synthesis of the metal-containing monomeric porphyrin precursors

[5-Bromo-10,15,20-triphenylporphyrin]-nickel(II) (**86**)[178]

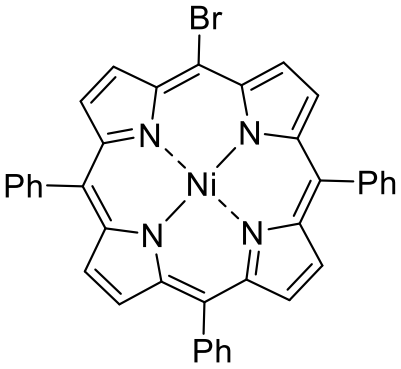

5-Bromo-10,15,20-triphenylporphyrin (**83**) (500 mg, 810 µmol, 1.00 equiv.) and $Ni(acac)_2$ (1.04 g, 4.02 mmol, 5.00 equiv.) were dissolved in $CHCl_3$ (100 mL) and stirred at 96 °C for 18 h in a pressure vial. The mixture was cooled to room temperature, the solvent was removed under reduced pressure and the residue was thoroughly washed with H_2O (5 × 50 mL) and extracted with $CHCl_3$ (5 × 50 mL). The combined organic phases were dried over Na_2SO_4, filtered and the solvent was removed under reduced pressure to yield the title compound **86** as a purple solid (530 mg, 786 µmol, 97%).

***R*f** (CH_2Cl_2/*c*Hex, 1:1) = 0.68. – **^{1}H NMR** (400 MHz, $CDCl_3$): δ = 9.51 (d, ^3J = 5.1 Hz, 2H, $H_{pyrrole}$), 8.79 (d, ^3J = 5.0 Hz, 2H, $H_{pyrrole}$), 8.70 – 8.66 (m, 4H, $H_{pyrrole}$), 8.00 – 7.95 (m, 6H, $H_{aromatic}$), 7.74 – 7.63 (m, 9H, $H_{aromatic}$) ppm. – **^{13}C NMR** (101 MHz, $CDCl_3$): δ = 143.1 (C_q), 142.9 (C_q), 142.5 (C_q), 140.8 (C_q), 140.7 (C_q), 140.6 (C_q), 133.8 (+, CH), 133.5 (+, CH), 133.3 (+, CH), 132.7 (+, CH), 128.1 (+, CH), 127.0 (+, CH) ppm. – **IR** (ATR): $\tilde{\nu}$ = 2916, 2848, 1590, 1510, 1390, 1258, 1071, 1004, 792, 748, 697 (w, ν-CBr) cm^{-1}. – **MS** (FAB, 3-NBA**)**: *m/z* (%) = 672 (65) $[M]^+$, 613 (39), 307 (38), 154 (100), 136 (61). – **HRMS** ($C_{38}H_{23}N_4{}^{79}Br_1{}^{58}Ni_1$): calc.: 672.0460, found:672.0458.

[5-Brom-10,15,20-triphenylporphyrin]-zinc(II) (**87**)[177]

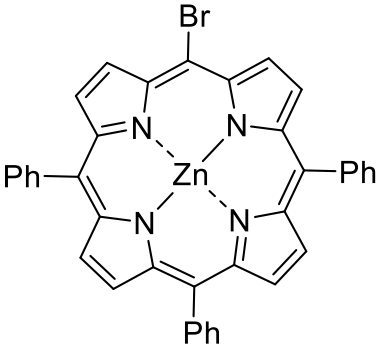

5-Bromo-10,15,20-triphenylporphyrin (**83**) (224 mg, 360 µmol, 1.00 equiv.) and $Zn(OAc)_2$ (151 mg, 830 µmol, 2.00 equiv.) were dissolved in a mixture of $CHCl_3$ and MeOH (6:1, 70 mL) and stirred at room temperature for 14.5 h. Subsequently, the reaction mixture was washed with a saturated $NaHCO_3$ solution (5 × 30 mL), dried over Na_2SO_4, filtered and the solvent removed under reduced pressure to afford the title compound **87** as a purple solid (253 mg, 370 µmol, 92%).

***R*f** (CH_2Cl_2/*c*Hex, 3:2) = 0.48. – **^{1}H NMR** (300 MHz, $CDCl_3$): δ = 9.77 (d, ^3J = 4.7 Hz, 2H $H_{pyrrole}$), 8.99 (d, ^3J = 4.7 Hz, 2H, $H_{pyrrole}$), 8.90 – 8.87 (m, 4H, $H_{pyrrole}$), 8.23 – 8.14 (m, 6H,

$H_{aromatic}$), 7.82 – 7.69 (m, 9H, $H_{aromatic}$) ppm. The analytical data is in accordance with the literature.[177]

[2-Bromo-5,10,15,20-tetraphenylporphyrin]-zinc(II) (**88**)[374]

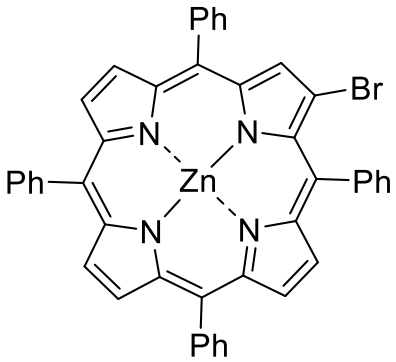

2-Bromo-5,10,15,20-tetraphenylporphyrin (**85**) (160 mg, 230 µmol, 1.00 equiv.) and $Zn(OAc)_2$ (95.4 mg, 520 µmol, 2.26 equiv.) were dissolved in a mixture of $CHCl_3$ and MeOH (10:1, 44 mL) and stirred at room temperature for 14.5 h. Subsequently, the reaction mixture was washed with saturated $NaHCO_3$ solution (2 × 50 mL), H_2O (1 × 50 mL), dried over Na_2SO_4 and the solvent was removed under reduced pressure to afford the title compound **88** as a purple solid (166 mg, 219 µmol, 95%). ***R*f** (CH_2Cl_2/*n*-pentane, 1:1) = 0.52 – **^{1}H NMR** (400 MHz, $CDCl_3$): δ = 9.07 (s, 1H), 8.96 – 8.82 (m, 6H), 8.23 – 8.16 (m, 6H), 8.09 – 8.05 (m, 2H), 7.81 – 7.67 (m, 12H) ppm. – **^{13}C NMR** (101 MHz, $CDCl_3$): δ = 150.2 (C_q), 149.8 (C_q), 149.6 (C_q), 149.2 (C_q), 146.8 (C_q), 142.0 (C_q), 141.5 (C_q), 141.4 (C_q), 140.6 (C_q), 135.8 (+, CH), 133.4 (+, CH), 133.3 (+, CH), 131.8 (+, CH), 131.4 (+, CH), 131.3 (+, CH), 130.8 (+, CH), 127.0 (+, CH), 126.7 (+, CH), 126.6 (+, CH), 125.7 (+, CH), 125.6 (+, CH), 125.6 (+, CH), 120.8 (C_q), 120.0 (C_q), 119.2 (C_q), 118.4 (C_q) ppm. – **HRMS** (ESI) ($C_{44}H_{27}BrN_4Zn$): calc.: 754.0711, found. 754.0702.

[5-Trimethylsilylethynyl-10,15,20-triphenylporphyrin]-nickel(II) (**89^{TMS}**)[182]

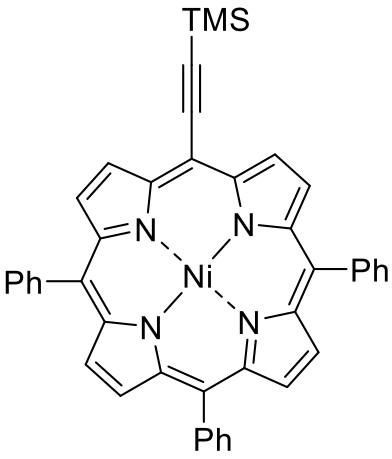

To a deoxygenated solution of [5-bromo-10,15,20-triphenylporphyrin]-nickel(II) (**86**) (65.0 mg, 96.0 µmol, 1.00 equiv.) in dry THF (23 mL) and NEt_3 (23 mL) were added $Pd(PPh_3)_2Cl_2$ (13.3 mg, 19.0 µmol, 0.20 equiv.), CuI (5.5 mg, 29.0 µmol, 0.30 equiv.) and TMS-acetylene (0.14 mL, 94.3 mg, 960 µmol, 10.0 equiv.). The reaction mixture was stirred at reflux for 19.5 h. Subsequently, the solvent was removed under reduced pressure. The residue was redissolved in CH_2Cl_2 (30 mL), washed with H_2O (3 × 20 mL), dried over Na_2SO_4, filtered and removed the solvent under reduced pressure. The

crude product was purified by flash chromatography on silica gel (CH_2Cl_2/*c*Hex, 1:5 → 1:2) to afford the title compound **89^{TMS}** as a purple solid (49.0 mg, 71.0 µmol, 74%).

***R*$_f$** (CH_2Cl_2/*c*Hex, 3:1) = 0.65. – **^{1}H NMR** (400 MHz, $CDCl_3$): δ = 9.51 (d, ^3J = 4.9 Hz, 2H, $H_{pyrrole}$), 8.79 (d, ^3J = 4.9 Hz, 2H, $H_{pyrrole}$), 8.69 – 8.64 (m, 4H, $H_{pyrrole}$), 8.03 – 7.95 (m, 6H, $H_{aromatic}$), 7.74 – 7.63 (m, 9H, $H_{aromatic}$), 0.55 (s, 9H, Si(C*H*$_3$)$_3$) ppm. – **^{13}C NMR** (101 MHz, $CDCl_3$): δ = 145.3, 143.4, 142.7, 142.6 140.8, 140.8, 133.8, 133.7, 133.1, 132.5, 132.2, 131.8, 128.0, 127.1, 127.0, 0.41 (3C, (*C*H$_3$)Si) ppm. – **IR** (ATR): $\tilde{\nu}$ = 2957, 2147, 2067, 1351, 1248, 1070, 1007, 840, 796, 755, 700, 645 cm^{-1}. – **MS** (FAB, 3-NBA): *m/z* (%) = 690 (94)[M]$^+$, 618 (13) [M–TMS]$^+$, 614 (15), 155 (23), 147 (57), 136 (25), 97 (19). – **HRMS** ($C_{43}H_{32}N_4{}^{58}Ni_1{}^{28}Si_1$): calc.: 690.1750, found: 690.1747.

[5-Trimethylsilylethynyl-10,20-diphenylporphyrin]-zinc(II) (**90^{TMS}**)[182]

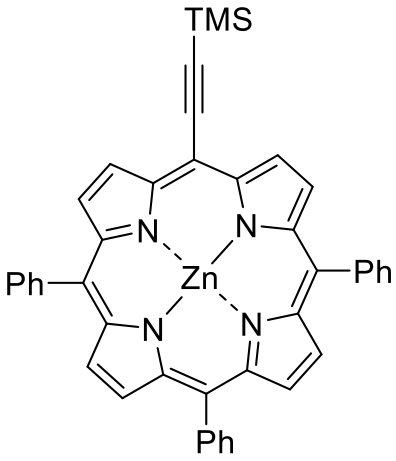

To a deoxygenated solution of [5-bromo-10,15,20-triphenylporphyrin]-zinc(II) (**87**) (160 mg, 235 µmol, 1.00 equiv.) in dry THF (16 mL) and NEt_3 (16 mL) were added $Pd(PPh_3)_2Cl_2$ (33.0 mg, 47.0 µmol, 0.20 equiv.), CuI (13.4 mg, 71.0 µmol, 0.30 equiv.) and TMS-acetylene (335 µL, 231 mg, 2.35 mmol, 10.0 equiv.). The reaction mixture was stirred at reflux for 21 h. Subsequently, the solvent was removed under reduced pressure. The residue was redissolved in CH_2Cl_2 (50 mL), washed with H_2O (3 × 30 mL), dried over Na_2SO_4, filtered and the solvent was removed under reduced pressure. The crude product was purified by flash chromatography on silica gel (CH_2Cl_2/*c*Hex, 1:5 → 1:2) to afford the title compound **90^{TMS}** as a purple solid (128 mg, 180 µmol, 77%).

***R*$_f$** (*c*Hex/CH_2Cl_2, 3:2) = 0.50. – **^{1}H NMR** (400 MHz, $CDCl_3$): δ = 9.76 (d, ^3J = 4.6 Hz, 2H, $H_{pyrrole}$), 8.98 (d, ^3J = 4.6 Hz, 2H, $H_{pyrrole}$), 8.89 – 8.86 (m, 4H, $H_{pyrrole}$), 8.23 – 8.14 (m, 6H, $H_{aromatic}$), 7.81 – 7.70 (m, 9H, $H_{aromatic}$), 0.61 (s, 9H, Si(C*H*$_3$)$_3$ ppm. – **^{13}C NMR** (101 MHz, $CDCl_3$): δ = 152.8 (C_q), 150.7 (C_q), 150.1 (C_q), 150.0 (C_q), 134.6 (+, CH), 134.4 (+, CH), 132.4 (+, CH), 132.0 (+, CH), 131.2 (+, CH), 127.8 (+, CH), 126.8 (+, CH), 126.7 (+, CH), 0.54 (+, 3 × (*C*H$_3$)Si)) ppm. The analytical data is in accordance with the literature.[182]

[2-Trimethylsilylethynyl-5,10,15,20-tetraphenylporphyrin]-zinc(II) (**91^{TMS}**)[215]

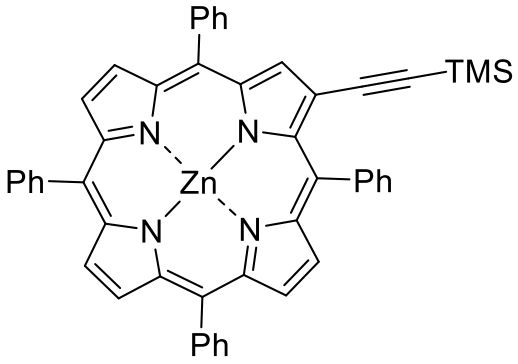

To a deoxygenated solution of [2-Bromo-5,10,15,20-tetraphenylporphyrin]-zinc(II) (**88**) (101 mg, 133 µmol, 1.00 equiv.) in dry NEt_3 (40 mL) and DMF (4 mL) were added $Pd(PPh_3)_2Cl_2$ (33.5 mg, 47.7 µmol, 0.36 equiv.) CuI (6.9 mg, 36.2 µmol, 0.27 equiv.) and TMS-acetylene (1.13 mL, 0.8 mg, 795 µmol, 5.98 equiv.). The reaction mixture was stirred at reflux for 5 h and the solvent was removed under reduced pressure. The crude product was purified by flash column chromatography on silica gel (CH_2Cl_2/*c*Hex, 2:3) to afford the title compound **91^{TMS}** as a red solid (66.4 mg, 85.8 µmol, 64%).

***R*$_f$** (CH_2Cl_2/*c*Hex, 2:3) = 0.43. – **^{1}H NMR** (300 MHz, $CDCl_3$): δ = 9.21 (s, 1H, $H_{pyrrole}$), 8.94 – 8.84 (m, 6H, $H_{pyrrole}$), 8.23 – 8.15 (m, 8H, $H_{aromatic}$), 7.83 – 7.72 (m, 12H, $H_{aromatic}$). 1.43 (s, 9H, H_{TMS}) ppm. The data is in accordance with the literature.[215] **HRMS** (ESI) ($C_{49}H_{36}N_4SiZn$): calc.: 772.2001, found. 772.1989.

[5-Ethynyl-10,15,20-triphenylporphyrin]-nickel(II) (**89**)[182]

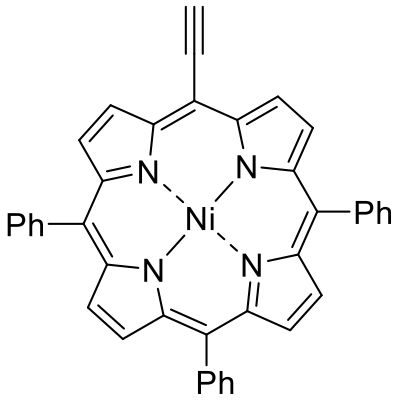

To a solution of [5-trimethylsilylethynyl-10,15,20-triphenylporphyrin]-nickel(II) (**89^{TMS}**) (828 mg, 1.20 mmol, 1.00 equiv.) in CH_2Cl_2 (300 mL), 1 M TBAF in THF (2.6 mL, 519 mg, 2.40 mmol, 3.00 equiv.) was added and the reaction was stirred at room temperature for 6.5 h. MeOH (20 mL) was added and the solvent was removed under reduced pressure. The residue was redissolved in CH_2Cl_2 (200 mL), washed thoroughly with H_2O (5 × 200 mL), dried over Na_2SO_4 and the solvent was removed under reduced pressure to afford the title compound **XX** as a purple solid (697 mg, 1.13 mmol, 94%).

***R*$_f$** (*c*Hex/CH_2Cl_2, 3:1) = 0.54. – **^{1}H NMR** (400 MHz, $CDCl_3$): δ = 9.53 (d, ^3J = 4.9 Hz, 2H, $H_{pyrrole}$), 8.81 (d, ^3J = 4.9 Hz, 2H, $H_{pyrrole}$), 8.71 – 8.65 (m, 4H, $H_{pyrrole}$), 8.03 – 7.95 (m, 6H, $H_{aromatic}$), 7.74 – 7.62 (m, 9H, $H_{aromatic}$), 4.06 (s, 1H, CC*H*) ppm. – **^{13}C NMR** (101 MHz, $CDCl_3$): δ = 145.3 (C_q), 143.4 (C_q), 142.7 (C_q), 142.6 (C_q), 140.7 (C_q), 133.8 (+, CH), 133.4 (+, CH), 132.6 (+, CH), 132.3 (+, CH), 131.7 (+, CH), 128.0 (+, CH), 127.1 (+, CH), 127.0 (+, CH),

120.8 (C_q), 119.9 (C_q) ppm. – **IR** (ATR): $\tilde{\nu}$ = 3269, 2918, 2849, 1597, 1439, 1349, 1070, 1004, 793, 699, 612 cm^{-1}. – **MS** (FAB, 3-NBA): *m/z* (%) = 619 (100) $[M]^+$, 542 (20), 507 (18), 154 (46), 136 (42), 95 (57). – **HRMS** ($C_{40}H_{25}N_4{}^{58}Ni_1$): calc.: 619.1433, found: 619.1430.

[5-Ethynyl-10,15,20-triphenylporphyrine]-zinc(II) (**90**)[182]

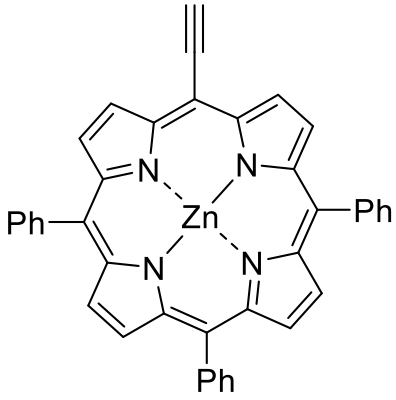

To a solution of [5-trimethylsilylethynyl-10,15,20-triphenylporphyrin]-zinc(II) (**90**^{TMS}) (128 mg, 180 µmol, 1.00 equiv.) in CH_2Cl_2 (65 mL), 1 M TBAF in THF (1.5 mL, 320 mg, 1.48 mmol, 8.00 equiv.) was added and the reaction was stirred at room temperature for 17 h. MeOH (15 mL) was added and the solvent was removed under reduced pressure. The residue was redissolved in CH_2Cl_2 (50 mL), washed thoroughly with H_2O (5 × 30 mL), dried over Na_2SO_4 and the solvent was removed under reduced pressure to afford the title compound **90** as a purple solid (113 mg, 180 µmol, 99%).

***R*f** (*c*Hex/CH_2Cl_2, 3:2) = 0.35. – **^{1}H NMR** (300 MHz, $CDCl_3$): δ = 9.77 (d, ^3J = 4.7 Hz, 2H, $H_{pyrrole}$), 8.99 (d, ^3J = 4.7 Hz, 2H, $H_{pyrrole}$), 8.88 – 8.85 (m, 4H, $H_{pyrrole}$), 8.22 – 8.15 (m, 6H, $H_{aromatic}$), 7.81 – 7.70 (m, 9H, $H_{aromatic}$), 4.17 (s, 1H, CC*H*) ppm. – **^{13}C NMR** (101 MHz, $CDCl_3$): δ = 150.1, 150.0, 134.6, 134.5, 134.4, 132.0, 131.9, 131.1, 128.6, 128.4, 127.7, 126.8, 126.6 ppm. The analytical data is in accordance with the literature.[182]

[2-Ethynyl-5,10,15,20-tetraphenylporphyrin]-zinc(II) (**91**)[215]

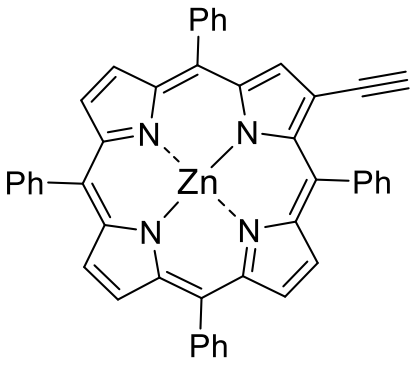

To a solution of [2-Trimethylsilylethynyl-5,10,15,20-tetraphenylporphyrin]-zinc(II) (**91**^{TMS}) (300 mg, 430 µmol, 1.00 equiv.) in CH_2Cl_2 (200 mL), 1 M TBAF in THF (0.86 mL, 593 mg, 860 µmol, 2.00 equiv.) was added and the reaction was stirred at room temperature for 1.5 h. MeOH (20 mL) was added and the solvent was removed under reduced pressure. The residue was redissolved in $CHCl_3$ (200 mL), thoroughly washed with H_2O (3 × 200 mL), dried over Na_2SO_4 and the solvent was removed under reduced pressure. The crude product was purified by flash

column chromatography on silica gel (CH_2Cl_2/*c*Hex, 1:2) to afford the title compound **91** as a red solid (153 mg, 218 µmol, 51%).

***R*f** (CH_2Cl_2/*c*Hex, 1:2) = 0.38. – **^{1}H NMR** (500 MHz, $CDCl_3$): δ = 9.23 (s, 1H, $H_{pyrrole}$), 8.95 – 8.91 (m, 4H, $H_{pyrrole}$), 8.91 – 8.88 (m, 2H, $H_{pyrrole}$), 8.23 – 8.18 (m, 6H, $H_{aromatic}$), 8.11 – 8.08 (m, 2H, $H_{aromatic}$), 7.80 – 7.72 (m, 10H, $H_{aromatic}$), 7.67 – 7.62 (m, 2H, $H_{aromatic}$), 3.29 (s, 1H, H_{alkyne}) ppm. – **^{13}C NMR** (126 MHz, $CDCl_3$): δ = 151.0 (C_q), 150.9 (C_q), 148.1 (C_q), 148.0 (C_q), 142.7 (C_q), 142.7 (C_q), 142.6 (C_q), 139.6 (C_q), 134.5 (+, CH), 134.1 (+, CH), 132.6 (+, CH), 132.5 (+, CH), 132.5 (+, CH), 132.4 (+, CH), 132.0 (+, CH), 128.1 (+, CH), 127.8 (+, CH), 127.7 (+, CH), 126.8 (+, CH), 126.8 (+, CH), 126.5 (+, CH), 124.7 (C_q), 121.6 (C_q), 121.3 (C_q), 121.3 (C_q), 121.2 (C_q). 85.5 (C_q, 1C, C_{alkyne}), 27.1 (CH, 1C, C_{alkyne}) ppm. – **IR** (ATR): $\tilde{\nu}$ = 2955, 2922, 2853, 1598, 1441, 1339, 1065, 1004, 994, 847, 800, 796, 747, 721, 697, 663, 598, 446, 433, 419, 404 cm^{-1}. **HRMS** (ESI) ($C_{46}H_{28}N_4Zn$): calc.: 700.1605, found. 700.1654.

6.3 Varying the backbone of angled dimeric porphyrin metal complexes

6.3.1 Synthesis and functionalization of alkyne-linked porphyrin dimers

1,2-Bis(10,15,20-triphenylporphyrin-5-yl)ethyne-dizink(II) (**92**)[375]

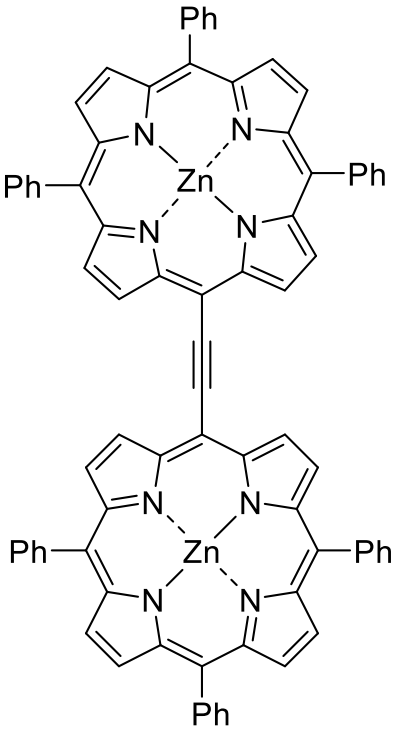

A Schlenk-tube was charged with [5-ethynyl-10,15,20-triphenylporphyrin]-zinc(II) (**90**) (180 mg, 290 µmol, 1.00 equiv.), [5-brom-10,15,20-triphenylporphyrin]-zinc(II) (196 mg, 290 µmol, 1.00 equiv.) (**87**), $AsPh_3$ (42.3 mg, 140 µmol, 1.20 equiv.) were dissolved in dry THF (40 mL) and dry NEt_3 (4 mL). The reaction mixture was degassed by three freeze-pump-thaw cycles. Subsequently, Pd_2dba_3 (52.4 mg, 57.2 µmol, 0.19 equiv.) was added. The reaction mixture was stirred at 60 °C for 16 h and the solvent was removed under reduced pressure. The residue was redissolved in CH_2Cl_2 (100 mL), washed with saturated NH_4Cl solution (3 × 50 mL), the combined organic phases were dried over Na_2SO_4, filtered and the solvent was removed under reduced pressure. The crude product was purified by flash column chromatography on silica gel (THF/*c*Hex, 1:10 to 1:2) to afford the title compound **92** as a purple solid (139 mg, 110 µmol, 40%).

***R*f** (*c*Hex/THF, 3:1) = 0.58. – **^{1}H NMR** (300 MHz, THF-d_8): δ = 10.47 (d, ^3J = 4.6 Hz,4H, $H_{pyrrole}$), 9.19 (d, ^3J = 4.6 Hz, 4H, $H_{pyrrole}$), 8.93 – 8.88 (m, 8H, $H_{pyrrole}$), 8.34 – 8.27 (m, 8H, $H_{aromatic}$), 8.25 – 8.19 (m, 4H, $H_{aromatic}$), 7.83 – 7.72 (m, 18H, $H_{aromatic}$) ppm. – **^{13}C NMR** (101 MHz, THF-d_8): δ = 154.5 (C_q), 151.8 (C_q), 151.0 (C_q), 150.8 (C_q), 144.3 (C_q), 144.2 (C_q), 135.5 (+, CH), 135.4 (+, CH), 133.8 (+, CH), 132.8 (+, CH), 132.4 (+, CH), 131.3 (+, CH), 128.5 (+, CH), 127.5 (+, CH), 127.4 (+, CH), 124.5 (+, CH), 123.3 (C_q) ppm. – **IR** (ATR): $\tilde{\nu}$ = 2921, 2137, 1596, 1486, 1439, 1339, 1204, 1004, 793, 700 cm^{-1}. – **HRMS** (ESI): ($C_{78}H_{46}N_8{}^{64}Zn_2$): calc.: 1222.243, found: 1222.240.[376]

[1-(10,15,20-Triphenylporphyrin-5-yl)-4-(10,15,20-triphenylporphyrin-5-yl)buta-1,3-diyne]-dizinc(II) (**93**)[185, 377]

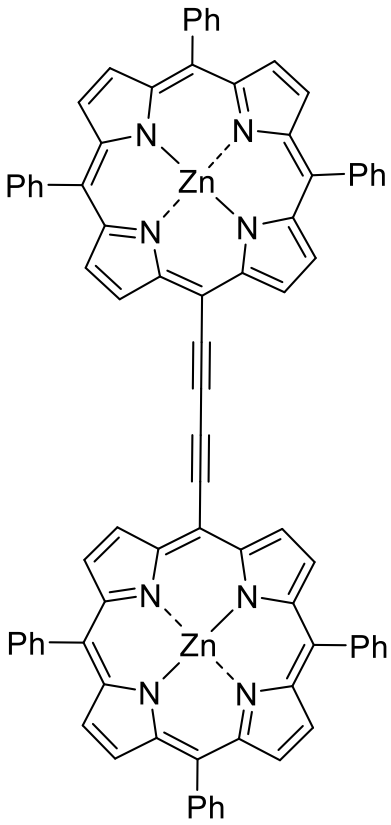

To a solution of [5-ethynyl-10,15,20-triphenylporphyrin]-zinc(II) (**90**) (100 mg, 160 µmol, 1.00 equiv.) in pyridine (16 mL) $Cu(OAc)_2 \cdot H_2O$ (158 mg, 790 µmol, 4.95 equiv.) was added and stirred at 50 °C for 42 h. Subsequently, the solvent was removed under reduced pressure and the residue was purified by flash column chromatography on silica gel (THF/*c*Hex, 1:3 to 1:1). The product was then recrystallized (CH_2Cl_2/MeOH) to afford the title compound **93** as a purple solid (87.0 mg, 70.0 µmol, 87%).

***R*f** (*c*Hex/THF, 3:1) = 0.54. – **^{1}H NMR** (400 MHz, THF-d_8): δ = 9.95 (d, ^3J = 4.6 Hz,4H, $H_{pyrrole}$), 9.00 (d, ^3J = 4.6 Hz, 4H, $H_{pyrrole}$), 8.79 – 8.75 (m, 8H, $H_{pyrrole}$), 8.26 – 8.21 (m, 8H, $H_{aromatic}$), 8.20 – 8.16 (m, 4$H_{aromatic}$), 7.82 – 7.72 (m, 18H, $H_{aromatic}$) ppm. – **^{13}C NMR** (101 MHz, THF-d_8): δ = 154.5 (C_q), 151.8 (C_q), 151.0 (C_q), 150.8 (C_q), 144.3 (C_q), 144.2 (C_q), 135.5 (+, CH), 135.4 (+, CH), 133.8 (+, CH), 132.8 (+, CH), 132.4 (+, CH), 131.3 (+, CH), 128.5 (+, CH), 127.5 (+, CH), 127.4 (+, CH), 123.3 (C_q), 108.6 (C_q) ppm. – **IR** (ATR): $\tilde{\nu}$ = 1595, 1484, 1439, 1338, 1208, 1063, 1003, 993, 792, 749, 699 cm^{-1}. – **HRMS** (ESI) ($C_{78}H_{46}N_8{}^{64}Zn_2$): calc.: 1246.243, found: 1246.241.

[1,2-Bis(5,10,15,20-triphenylporphyrin-2-yl)ethyne]-dizinc(II) (**100**)[183, 184]

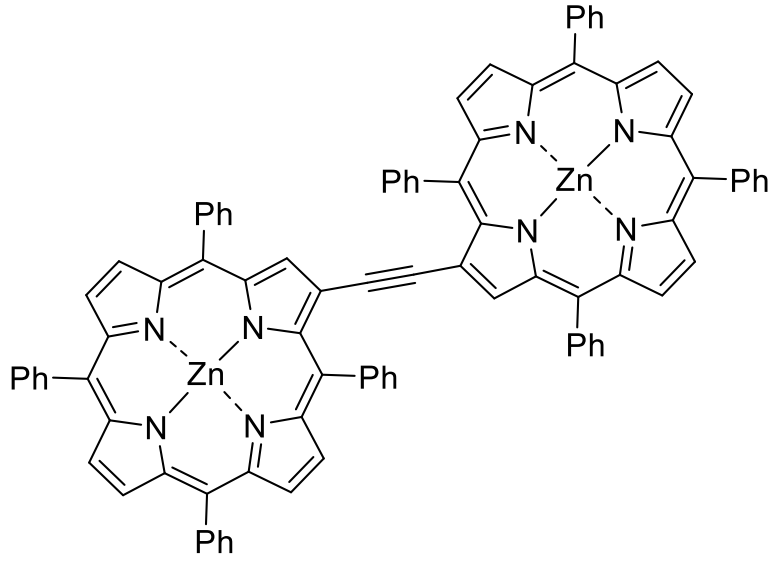

A Schlenk-tube was charged under an argon atmosphere with [2-ethynyl -5,10,15,20-tetraphenylporphyrin]-zinc(II) (**91**) (19.6 mg, 28.0 µmol, 1.00 equiv.), [2-bromo-5,10,15,20-tetraphenylporphyrin]-zinc(II) (**88**) (21.2 mg, 28.0 µmol, 1.00 equiv.), Pd_2dba_3 (5.1 mg,

5.58 µmol, 0.20 equiv.) and $AsPh_3$ (10.3 mg, 33.6 µmol, 1.20 equiv.). Subsequently, degassed THF (2.4 mL) and NEt_3 (12 mL) were added and the solution was stirred at 40 °C for 16 h. The reaction mixture was quenched with H_2O (30 mL), the organic phase extracted with $CHCl_3$ (50 mL), washed with saturated NH_4Cl solution (2 × 50 mL) and dried over Na_2SO_4. After filtration, the solvent was removed under reduced pressure. The crude product was purified by flash column chromatography on silica gel (THF/*c*Hex, 1:6) to afford the title compound **100** as a red solid (12.5 mg, 9.07 µmol, 35%).

***R*f** (THF/*c*Hex, 1:7) = 0.39. – **^{1}H NMR** (500 MHz, $CDCl_3$): δ = 9.02 – 8.76 (m, 13H, $H_{pyrrole}$), 8.69 – 8.66 (m, 1H, $H_{pyrrole}$), 8.44 – 8.33 (m, 3H, $H_{aromatic}$), 8.27 – 8.14 (m, 13H, $H_{aromatic}$), 8.04 – 7.96 (m, 4H, $H_{aromatic}$), 7.82 – 7.68 (m, 16H, $H_{aromatic}$). 7.48 – 7.39 (m, 4H, $H_{aromatic}$) ppm. – **^{13}C NMR** (126 MHz, $CDCl_3$): δ = 134.7, 134.7, 134.6, 132.4, 132.3, 132.2, 127.0, 126.8, 126.7, 126.7 ppm, signal set is not complete due to a poor solubility. – **UV-Vis** (CH_2Cl_2): λ_{max} (rel. absorption) = 218 (0.44), 271 (0.16), 423 (1.02), 482 (0.21), 560 (0.12), 608 (0.10) nm. – **IR** (ATR): $\tilde{\nu}$ = 2919, 2850, 1612, 1595, 1574, 1448, 1439, 1336, 1278, 1191, 1176, 1156, 1112, 1095, 1068, 1001, 992, 922, 877, 793, 749, 721, 696, 662, 620, 550, 526, 476, 433, 391 cm^{-1}. – **HRMS** (ESI) ($C_{90}H_{54}N_4Zn_2$): calc.: 1374.3054, found: 1374.3039.

1,2-(10,15,20-triphenylporphyrin-5-yl-[10,15,20-triphenylporphyrin-5-yl]-nickel(II))ethane (**101**) [375]

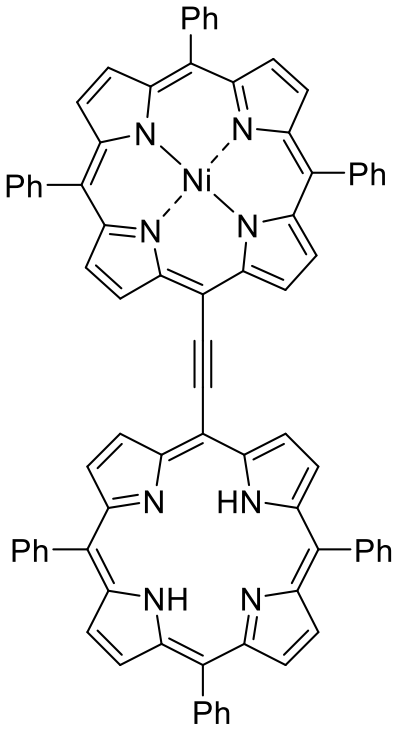

A Schlenk-tube was charged under an argon atmosphere with [5-ethynyl-10,15,20-triphenylporphyrin]-nickel(II) (**89**) (100 mg, 160 µmol, 1.00 equiv.), 5-bromo-10,15,20-triphenylporphyrin (**83**) (123 mg, 192 µmol, 1.20 equiv.), Pd_2dba_3 (29.3 mg, 32.0 µmol, 0.20 equiv.) and $AsPh_3$ (58.8 mg, 192 µmol, 1.20 equiv.). Subsequently, the degassed solvent mixture consisting of THF (5 mL) and NEt_3 (50 mL) was added and the solution was stirred at 60 °C for 16.5 h. The reaction mixture was quenched with H_2O (30 mL), the organic phase extracted with $CHCl_3$ (50 mL), washed with saturated NH_4Cl solution (2 × 50 mL) and dried over Na_2SO_4. After filtration, the solvent was removed under reduced pressure. The crude product was purified by flash

column chromatography on silica gel (THF/*c*Hex, 1:5) to afford the title compound **101** as a purple solid (50.1 mg, 43.3 µmol, 27%).

***R*f** (*c*Hex/CH_2Cl_2, 3:2) = 0.35. – **^{1}H NMR** could not be measured since the product could not be completely separated from dibenzylidene acetone. – **HRMS** (ESI): ($C_{78}H_{48}N_8Ni_2H$): calc.:1155.3434 found: 1155.3432.

6.3.2 Syntheses of thiophene-linked porphyrin dimers

2,5-Bis(10,15,20-triphenylporphyrin-5-yl)thiophene-dizinc(II) (**94**)[186]

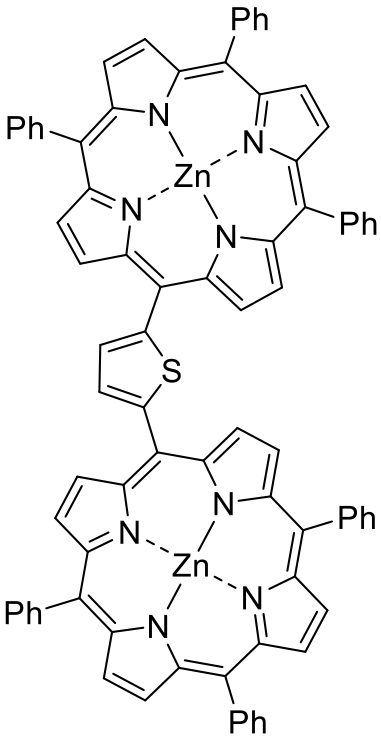

To a solution of [1-(10,15,20-triphenylporphyrin-5-yl)-4-(10,15,20-triphenylporphyrin-5-yl)buta-1,3-diyn]-dizinc(II) (**93**) (11.0 mg, 8.83 µmol, 1.00 equiv.) in *p*-xylene (5 mL) and 2-methoxyethanol (5 mL) $Na_2S \cdot 9H_2O$ (80.0 mg, 330 µmol, 11.6 equiv.) was added and the reaction mixture was stirred at 130 °C for 87 h. Subsequently, the solvent was removed under reduced pressure. The crude product was purified by flash column chromatography on silica gel (THF/*c*Hex, 1:5 →1:4) to afford the title compound **94** as a purple solid (5.2 mg, 4.06 µmol, 46%).

***R*f** (*c*Hex/THF, 3:1) = 0.54. – **^{1}H NMR** (400 MHz, THF-d_8): δ = 9.71 (d, ^3J = 4.6 Hz, 4H, $H_{pyrrole}$), 9.04 (d, ^3J = 4.6 Hz, 4H, $H_{pyrrole}$), 8.88 – 8.84 (m, 8H, $H_{pyrrole}$), 8.34 (s, 2H, $H_{thiophene}$) 8.29 – 8.24 (m, 8H, $H_{aromatic}$), 8.24 – 8.19 (m, 4$H_{aromatic}$), 7.82 – 7.78 (m, 12H, $H_{aromatic}$), 7.78 – 7.74 (m, 6H, $H_{aromatic}$) ppm. – **^{13}C NMR** (101 MHz, THF-d_8): δ = 152.4 (C_q), 151.4 (C_q), 151.1 (C_q), 147.9 (C_q), 144.6 (C_q), 135.6 (+, CH), 135.5 (+, CH), 133.2 (+, CH), 133.0 (+, CH), 132.6 (+, CH), 132.5 (+, CH), 132.4 (+, CH), 128.4 (+, CH), 127.4 (+, CH), 127.4 (+, CH), 122.6 (C_q), 122.2 (C_q), 112.0 (C_q) ppm. – **IR** (ATR): $\tilde{\nu}$ = 3281, 2922, 2852, 1710, 1621, 1539, 1467, 1295, 1133, 1049, 934, 719, 606 cm^{-1}. – **HRMS** (*nano*-ESI) ($C_{80}H_{48}N_8S^{64}Zn_2$): calc.: 1280.231, found: 1280.277.

6.3.3 N-joined porphyrin dimers

[5-Amino-10,15,20-triphenylporphyrin]-nickel(II) (**103**)[378]

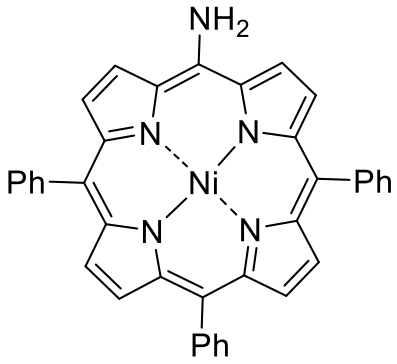

5,10,15-Triphenylporphyrin (**82)** (99.5 mg, 185 µmol, 1.00 equiv.) was dissolved under an argon atmosphere in a mixture of CH_2Cl_2 (8 mL) and MeCN (3 mL). A solution of I_2 (40.0 mg, 158 µmol, 0.85 equiv.) in CH_2Cl_2 (3 mL) was added. The resulting solution was stirred at room temperature in the dark. After 30 min, a suspension of $AgNO_2$ (52.5 mg, 341 µmol, 1.84 equiv.) in MeCN (3 mL) was added. The resulting mixture was stirred at room temperature for 30 min. Then, insoluble silver salts were filtered off and the solvent was removed under reduced pressure. The crude product was dissolved in toluene (10 mL) and $Ni(acac)_2$ (194 mg, 755 µmol, 4.08 equiv.) was added. The resulting mixture was stirred at 110 °C for 14 h. After the mixture was cooled to room temperature, it was passed through a short layer of silica gel eluting with CH_2Cl_2. The solvents were removed under reduced pressure. The residue was dissolved in a mixture of CH_2Cl_2 (15 mL) and MeOH (15 mL). After adding 10% Pd/C (36.0 mg) to the solution, $NaBH_4$ (49.9 mg, 1.32 mmol, 7.13 equiv.) was slowly added under an argon atmosphere. The resulting suspension was stirred at room temperature for 10 min and residual Pd/C was filtered off using a short celite pad eluting with CH_2Cl_2. The crude product was purified by flash column chromatography on silica gel (CH_2Cl_2/*c*Hex, 1:1) to afford the title compound **103** as a purple solid (92.6 mg, 152 µmol, 82%).

***R*f** (CH_2Cl_2/*c*Hex, 1:1) = 0.26. – **^{1}H NMR** (400 MHz, THF-d_8): δ = 9.05 (d, ^3J = 4.9 Hz, 2H, $H_{pyrrole}$), 8.30 (d, ^3J = 4.9 Hz, 2H, $H_{pyrrole}$), 8.26 (d, ^3J = 4.8 Hz, 2H, $H_{pyrrole}$), 8.22 (d, ^3J = 4.8 Hz, 2H, $H_{pyrrole}$), 7.91 – 7.83 (m, 6H, $H_{aromatic}$), 7.64 – 7.58 (m, 9H, $H_{aromatic}$), 7.35 (bs, 2H, NH_2) ppm. – **^{13}C NMR** (101 MHz, THF-d_8): δ = 146.2 (C_q), 142.4 (C_q), 141.9 (C_q), 141.6 (C_q), 134.6 (+, CH), 134.3 (+, CH), 133.1 (+, CH), 130.9 (+, CH), 128.9 (+, CH), 128.4 (+, CH), 128.2 (+, CH), 128.0 (+, CH), 127.9 (+, CH), 125.5 (+, CH), 119.7 (C_q) ppm. – **UV-Vis** (CH_2Cl_2): λ_{max} (rel. absorption) = 423 (1.00), 534 (0.06), 599 (0.05). – **IR** (ATR): $\tilde{\nu}$ = 2961, 2918, 2850, 1592, 1497, 1456, 1439, 1364, 1354, 1259, 1069, 1016, 1007, 793, 749, 697, 666, 401, 387 cm^{-1}. – **HRMS** (ESI) ($C_{38}H_{25}N_5Ni$) calc.: 609.1463, found: 609.1454. The analytical data is in accordance with the literature.[378]

5-Chloro-10,15,20-triphenylporphyrin (**104**)[165]

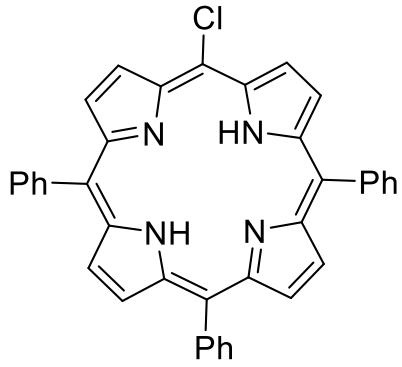

5,10,15-Triphenylporphyrin (**82**) (200 mg, 372 µmol, 1.00 equiv.) was dissolved in acetic acid (36 mL). Then, 30% H_2O_2 (0.36 mL, 522 mg, 15.4 mmol, 41.3 equiv.) and NaCl (43.5 mg, 744 µmol, 2.00 equiv.) were added to the mixture and was stirred at 60 °C for 4 h. The crude product precipitated as black solid, collected by filtration and washed with H_2O (50 mL). The crude product was purified by flash column chromatography on silica gel (CH_2Cl_2/*c*Hex, 1:1) to afford the title compound **104** (83.1 mg, 145 µmol, 39%) as a purple solid (83.1 mg, 145 µmol, 39%).

***R*f** (CH_2Cl_2/ *c*Hex, 1:1) = 0.58. – **^{1}H NMR** (400 MHz, $CDCl_3$): δ = 9.66 (d, ^3J = 4.8 Hz, 2H, $H_{pyrrole}$), 8.93 (d, ^3J = 4.8 Hz, 2H, $H_{pyrrole}$), 8.83 (s, 4H, $H_{pyrrole}$), 8.24 – 8.18 (m, 6H, $H_{aromatic}$), 7.84 – 7.72 (m, 9H, $H_{aromatic}$). –2.68 (bs, 2H, NH) ppm. – **^{13}C NMR** (101 MHz, $CDCl_3$): δ = 142.1 (C_q), 141.9 (C_q), 134.7 (+, CH), 134.6 (+, CH), 132.5 – 131.1 (bs, C_q, 8C), 128.0 (+, CH), 128.0 (+, CH), 126.9 (+, CH), 126.9 (+, CH), 120.9 (C_q), 120.9 (C_q), 112.3 (C_q) ppm. – **UV-Vis** (CH_2Cl_2): λ_{max} (rel. absorption) = 419 (3.31), 517 (0.20), 552 (0.10), 595 (0.06), 652 (0.05) nm. – **IR** (ATR): $\tilde{\nu}$ = 3316, 2921, 2851, 1591, 1557, 1469, 1439, 1356, 1343, 1225, 1072, 1016, 1001, 979, 965, 790, 783, 756, 747, 717, 698, 667, 657, 637, 630, 619, 582, 554, 534, 520, 501, 486, 407, 384, 375 cm^{-1}. – **HRMS** (ESI) ($C_{38}H_{25}ClN_4$): calc.: 572.1768, found: 572.1751.

[5-Chloro-10,15,20-triphenylporphyrin]-nickel(II) (**105**)[178]

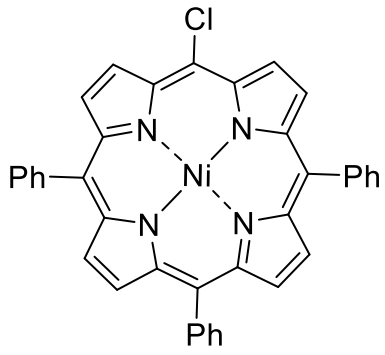

5-Chloro-10,15,20-triphenylporphyrin (**104**) (27.0 mg, 47.1 µmol, 1.00 equiv.) and $Ni(acac)_2$ (47.6 mg, 185 µmol, 3.92 equiv.) were dissolved in DMF (16 mL) and stirred at 100 °C for 2 h. The mixture was cooled to room temperature and the solvent was removed under reduced pressure. The crude product was purified by flash column chromatography on silica gel (CH_2Cl_2/*c*Hex, 1:2) to afford the title compound **105** as a red solid (21.8 mg, 34.6 µmol, 73%).

***R*f** (CH_2Cl_2/*c*Hex, 1:1) = 0.72. – **^{1}H NMR** (300 MHz, $CDCl_3$): δ = 9.49 (d, ^3J = 5.00 Hz, 2H, $H_{pyrrole}$), 8.80 (d, ^3J = 5.00 Hz, 2H, $H_{pyrrole}$), 8.69 (s, 4H, $H_{pyrrole}$), 8.03 – 7.91 (m, 6H, $H_{aromatic}$),

7.74 – 7.68 (m, 9H, $H_{aromatic}$) ppm. The analytical data is in accordance with the literature. – **UV-Vis** (CH_2Cl_2): λ_{max} (rel. absorption) = 217 (0.72), 295 (0.25), 414 (3.53), 530 (0.31) nm. – **IR** (ATR): $\tilde{\nu}$ = 2918, 2849, 1459, 1438, 1356, 1334, 1312, 1072, 1064, 1003, 994, 901, 790, 749, 732, 714, 697, 667, 653, 636, 619, 605, 558, 530, 506, 497, 484, 473, 462, 438, 416, 412, 404, 395, 387 cm^{-1}. – **HRMS** (ESI) ($C_{38}H_{23}ClN_4Ni$): calc.: 628.0965, found: 628.0941. The analytical data is in accordance with the literature.

[5-Chloro-10,15,20-triphenylporphyrin]-zinc(II) (**106**)[378]

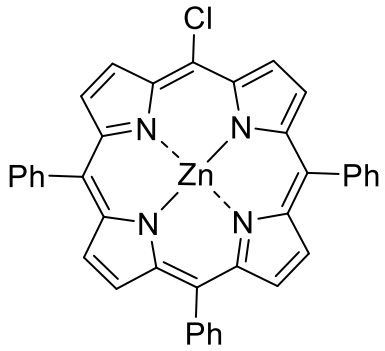

5-Chloro-10,15,20-triphenylporphyrin (**82**) (8.8 mg, 15.4 µmol, 1.00 equiv.) and $Zn(OAc)_2$ (5.65 mg, 30.8 µmol, 2.00 equiv.) were dissolved in a mixture of $CHCl_3$ (6 mL) and MeOH (0.6 mL) and stirred at room temperature for 16 h. Subsequently, the reaction mixture was washed with a saturated $NaHCO_3$ solution (5 × 15 mL), dried over Na_2SO_4, filtered and removed the solvent under reduced pressure to afford the title compound **106** (9.8 mg, 15.4 µmol, quant.) as a purple solid.

– **^{1}H NMR** (300 MHz, $CDCl_3$): δ = 9.76 – 9.61 (m, 2H, $H_{pyrrole}$), 9.05 – 8.93 (m, 2H, $H_{pyrrole}$), 8.93 – 8.80 (m, 4H, $H_{pyrrole}$), 8.29 – 8.10 (m, 6H, $H_{aromatic}$), 7.87 – 7.67 (m, 9H, $H_{aromatic}$) ppm. The analytical data follow the literature.[177, 378] [177, 378] [177, 378] [177, 378] [177, 377] [177, 376] [177, 376] [177, 376] [177, 376]

[Bis(10,15,20-triphenylporphyrin-5-yl)amine]-dinickel(II) (**107**)[378]

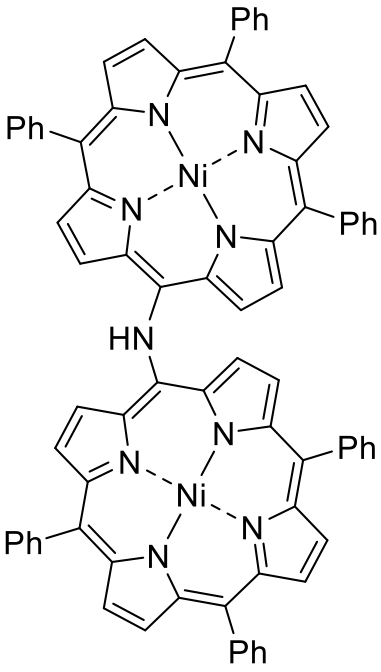

[5-Chloro-10,15,20-triphenylporphyrin]-nickel(II) (**105**) (18.0 mg, 28.6 µmol, 1.00 equiv.), [5-amino-10,15,20-triphenylporphyrin]-nickel(II) (**103**) (17.5 mg, 28.6 µmol, 1.00 equiv.) and NaH (60% in mineral oil) (3.4 mg, 143 µmol, 5.00 equiv.) were placed in a *Schlenk* tube and purged with argon. DMF (5 mL) was added and stirred at 60 °C for 2.5 h. The solvent was removed under reduced pressure and the crude product was purified by flash column chromatography on silica gel (CH_2Cl_2/*c*Hex, 1:2 → 1:1) to afford the title compound **107** as a purple solid (16.4 mg, 13.6 µmol, 48%).

***R*f** (CH_2Cl_2/*c*Hex, 1:1) = 0.67. – **^{1}H NMR** (400 MHz, THF-d_8): δ =11.44 (s, 1H, NH), 8.98 (d, ^3J =5.0 Hz, 4H, $H_{pyrrole}$), 8.49 (d, ^3J =5.0 Hz, 4H, $H_{pyrrole}$), 8.46 (d, ^3J =5.0 Hz, 4H, $H_{pyrrole}$), 8.26 (d, ^3J = 5.0 Hz, 4H, $H_{pyrrole}$), 7.97 – 7.92 (m, 4H, $H_{aromatic}$), 7.83 – 7.78 (m, 8H, $H_{aromatic}$), 7.68 – 7.64 (m, 6H, $H_{aromatic}$), 7.58 – 7.49 (m, 12H, $H_{aromatic}$) ppm. – **^{13}C NMR** (101 MHz, THF-d_8): δ = 144.7 (C_q), 143.0 (C_q), 142.1 (C_q), 141.8 (C_q), 141.1 (C_q), 134.6 (+, CH), 134.4 (+, CH), 133.2 (+, CH), 132.2 (+, CH), 132.0 (+, CH), 129.8 (+, CH), 129.1 (+, CH), 128.6 (+, CH), 128.0 (+, CH), 127.8 (+, CH), 119.8 (C_q) ppm. – **UV-Vis** (CH_2Cl_2): λ_{max} (rel. absorption) = 217 (0.45), 291 (0.17), 413 (0.78), 441 (0.54), 625 (0.10) nm. – **IR** (ATR): $\tilde{\nu}$ = 3373, 2953, 2919, 2850, 1490, 1460, 1439, 1381, 1371, 1351, 1315, 1259, 1231, 1217, 1205, 1174, 1088, 1072, 1048, 1033, 1001, 953, 800, 792, 773, 749, 727, 713, 697, 670, 636, 622, 560, 548, 518, 506, 500, 463, 397, 385 cm^{-1}. – **HRMS** (ESI) ($C_{76}H_{47}N_9Ni_2$): calc.: 1201.2661, found: 1201.2574.

([10,15,20-Triphenylporphyrin-5-yl]-nickel(II)-[10,15,20-triphenylporphyrin-5-yl]-zinc(II))amine (**108**)[196]

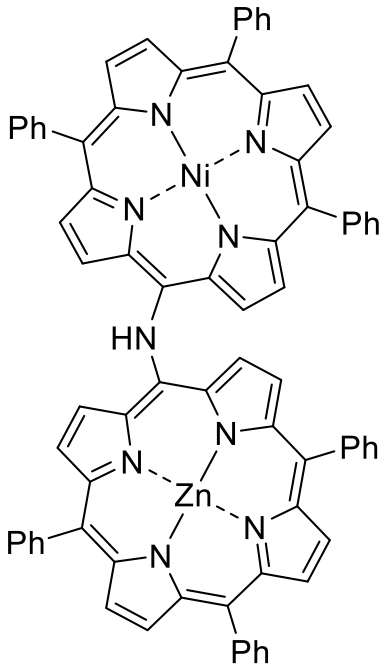

A Schlenk tube was charged under an argon atmosphere with [5-bromo-10,15,20-triphenylporphyrin]-zinc(II) (**87**) (33.2 mg, 48.8 µmol, 1.00 equiv.), [5-amino-10,15,20-triphenylporphyrin]-nickel(II) (**103**) (36.1 mg, 59.1 µmol, 1.21 equiv.), $Pd(OAc)_2$ (3.8 mg, 16.9 µmol, 0.35 equiv.), DPEPhos (4.9 mg, 9.10 µmol, 0.19 equiv.) and Cs_2CO_3 (379 mg, 1.16 mmol, 23.8 equiv.). THF (3 mL) was added and the resulting reaction mixture was stirred at 68 °C for 14 h. After cooling to room temperature, the reaction mixture was concentrated under reduced pressure, extracted with EtOAc (30 mL), washed with brine (3 × 30 mL) and dried over Na_2SO_4. The crude product was purified by flash column chromatography on silica gel (CH_2Cl_2/*c*Hex, 1:2) to afford the title compound **108** as a purple solid (19.0 mg, 15.7 µmol, 55%).

***R*f** (CH_2Cl_2/*c*Hex, 1:1) = 0.32. – **^{1}H NMR** (400 MHz, THF-d_8): δ = 11.69 (s, 1H, NH), 9.25 (d, ^3J = 4.6 Hz, 2H, $H_{pyrrole}$), 9.00 (d, ^3J = 4.9 Hz, 2H, $H_{pyrrole}$), 8.70 (s, 4H, $H_{pyrrole}$), 8.50 (d, ^3J = 4.6 Hz, 2H, $H_{pyrrole}$), 8.40 – 8.34 (m, 4H, $H_{pyrrrole}$), 8.17 – 8.12 (m, 2H, $H_{aromatic}$), 8.09 – 8.04 (m, 4H, $H_{aromatic}$), 8.03 (d, ^3J = 4.9 Hz, 2H, $H_{pyrrole}$), 7.96 – 7.91 (m, 2H, $H_{aromatic}$), 7.79 – 7.74 (m, 4H, $H_{aromatic}$), 7.74 – 7.69 (m, 3H, $H_{aromatic}$), 7.68 – 7.57 (m, 9H, $H_{aromatic}$), 7.52 – 7.44 (m, 6H, $H_{aromatic}$) ppm. – **^{13}C NMR** (101 MHz, THF-d_8): δ = 151.8 (C_q), 151.1 (C_q), 150.9 (C_q), 150.2 (C_q), 145.2 (C_q), 144.4 (C_q), 142.2 (C_q), 142.2 (C_q), 142.0 (C_q), 141.2 (+, CH), 138.9 (C_q), 134.6 (+, CH), 134.3 (+, CH), 133.1 (+, CH), 132.7 (+, CH), 132.5 (+, CH), 132.1 (+, CH), 131.6 (+, CH), 130.4 (+, CH), 129.8 (+, CH), 129.6 (+, CH), 128.4 (+, CH), 128.2 (+, CH), 128.1 (+, CH), 128.1 (+, CH), 127.8 (+, CH), 127.4 (+, CH), 127.2 (+, CH), 121.6 (C_q), 119.6 (C_q) ppm. – **UV-Vis** (CH_2Cl_2): λ_{max} (rel. absorption) = 217 (0.35), 299 (0.18), 317 (0.18), 422 (0.70), 546 (0.15), 645 (0.12) nm. – **IR** (ATR): $\tilde{\nu}$ = 3053, 2915, 2853, 1545, 1485, 1465, 1441, 1405, 1334, 1128, 1069, 1048, 1035, 1003, 979, 959, 953, 790, 752, 742, 718, 700, 449, 435, 429, 411, 399, 382 cm^{-1}. – **HRMS** (ESI) ($C_{76}H_{47}N_9NiZn$): calc.: 1207.2599, found: 1207.2544.

6.3.4 [2.2]Paracyclophane porphyrin conjugates

4-Bromo-16-(10,15,20-triphenylporphyrin-5-yl)[2.2]paracyclophane (**113^{NH}**)[83]

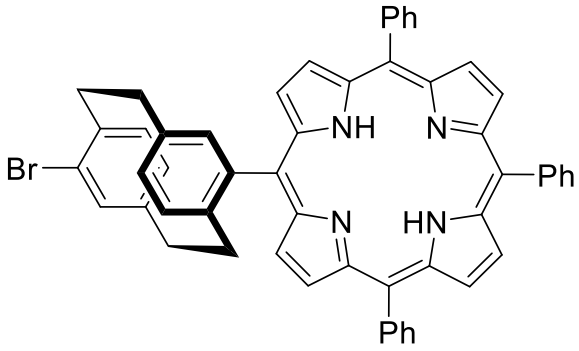

Under an argon atmosphere, 4-bromo-16-formyl[2.2]paracyclophane (**112**) (314 mg, 996 µmol, 1.00 equiv.) was dissolved in dry CH_2Cl_2 (1.0 L). A stream of argon was passed through the mixture for 15 min to remove dissolved oxygen. Subsequently, freshly distilled benzaldehyde (202 µL, 211 mg, 1.99 mmol, 2.00 equiv.) and 5-phenyldipyrromethane (442 mg, 1.99 mmol, 2.00 equiv.) were added. After 5 min, TFA (77 µL, 114 mg, 1.00 mmol, 1.08 equiv.) was added. The mixture was stirred for 14.5 h in the dark. DDQ (560 mg, 2.47 mmol, 2.48 equiv.) was added and the mixture was stirred for 1 h. Then, NEt_3 (10 mL) was added and the crude mixture was concentrated under reduced pressure. The crude product was filtered through a short layer of silica gel eluting with CH_2Cl_2 and purified by flash column chromatography on silica gel (CH_2Cl_2/*c*Hex, 3:5) to afford the title compound **113^{NH}** as a purple solid (40.6 mg, 49.2 µmol, 4.9%).

***R*$_f$** (CH_2Cl_2/*c*Hex, 1:1) = 0.40. – **^{1}H NMR** (400 MHz, $CDCl_3$): δ = 10.08 (d, ^3J = 4.8 Hz, 1H, $H_{pyrrole}$), 9.16 (d, ^3J = 4.8 Hz, 1H, $H_{pyrrole}$), 8.90 – 8.84 (m, 4H, $H_{pyrrole}$), 8.71 (d, ^3J = 4.9 Hz, 1H, $H_{pyrrole}$), 8.68 (d, ^3J = 4.9 Hz, 1H, $H_{pyrrole}$), 8.45 – 8.36 (m, 2H, $H_{aromatic}$), 8.35 – 8.29 (m, 1H, $H_{aromatic}$), 8.21 – 8.16 (m, 1H, $H_{aromatic}$), 8.16 – 8.09 (m, 1H, $H_{aromatic}$), 8.02 – 7.98 (m, 1H, $H_{aromatic}$), 7.95 (d, ^4J = 1.8 Hz, 1H, $H_{paracyclophane}$), 7.83 – 7.72 (m, 9H, $H_{aromatic}$), 7.47 (dd, J = 7.8, 1.8 Hz, 1H, $H_{paracyclophane}$), 7.24 (d, ^3J = 8.0 Hz, 1H, $H_{paracyclophane}$), 6.98 (d, ^4J = 1.8 Hz, 1H, $H_{paracyclophane}$), 6.89 (d, ^3J = 7.8 Hz, 1H, $H_{paracyclophane}$), 6.70 (dd, J = 8.0, 1.7 Hz, 1H, $H_{paracyclophane}$), 3.84 – 3.73 (m, 1H, H_{bridge}), 3.73 – 3.61 (m, 1H, H_{bridge}), 3.41 – 3.25 (m, 2H, H_{bridge}), 3.08 –2.99 (m, 1H, H_{bridge}), 2.66 – 2.55 (m, 1H, H_{bridge}), 2.43 – 2.33 (m, 1H, H_{bridge}), 2.21 – 2.10 (m, 1H, H_{bridge}), –2.64 (bs, 2H, NH) ppm. – **^{13}C NMR** (101 MHz, $CDCl_3$): δ = 145.2 (C_q), 142.8 (C_q), 142.7 (C_q), 142.5 (C_q), 142.0 (C_q), 140.5 (C_q), 139.3 (C_q), 138.7 (C_q), 137.5 (+, CH), 136.3 (+, CH), 134.7 (+, CH), 134.4 (+, CH), 133.9 (+, CH), 129.9 (+, CH), 129.7 (+, CH), 127.9 (+, CH), 127.8 (+, CH), 126.9 (+, CH), 126.8 c, 126.7 (+, CH), 120.4 (C_q), 120.3 (C_q), 119.8 (C_q), 119.1 (C_q), 35.5 (–, CH_2), 34.8 (–, CH_2), 34.6 (–, CH_2), 34.4 (–, CH_2) ppm. – **UV-Vis** (CH_2Cl_2): λ_{max} (rel. absorption) = 288 (0.19), 420 (3.11), 519 (0.21), 555 (0.14), 594 (0.07), 650 (0.07) nm. – **IR** (ATR): $\tilde{\nu}$ = 3308, 2953, 2918, 2856, 1466, 1439, 1346, 1027, 963,

798, 724, 698, 669, 659, 642, 518 cm^{-1}. – **HRMS** (ESI) ($C_{54}H_{40}BrN_4$): calc.: 823.2436, found: 823.2397.

4-Bromo-16-(10,15,20-triphenylporphyrin-5-yl)zinc(II) [2.2]paracyclophane (**113**)[379]

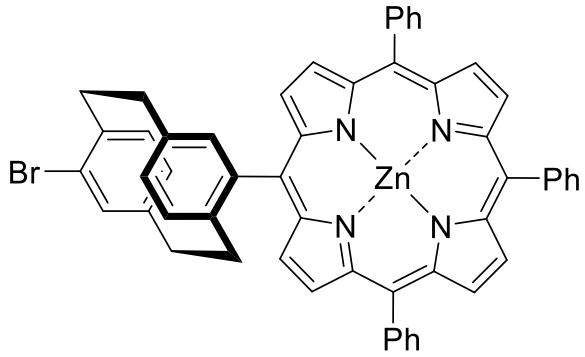

4-Bromo-16-(10,15,20-triphenylporphyrin-5-yl)[2.2]paracyclophane (**113^{NH}**) (22.4 mg, 27 µmol, 1.00 equiv.) and $Zn(OAc)_2$ (9.9 mg, 54.0 µmol, 2.00 equiv.) were dissolved in a mixture of $CHCl_3$ and MeOH (9:1, 20 mL). The reaction mixture was stirred for 2.5 h at room temperature. Subsequently, the solvent was evaporated under reduced pressure. The crude product was redissolved in CH_2Cl_2 (30 mL) and thoroughly washed with H_2O (3 × 50 mL). The combined organic phases were dried over Na_2SO_4, filtered and the solvent removed under reduced pressure to afford the title compound **113** as a purple solid (25.1 mg, 28.3 µmol, quant.).

***R*f** (CH_2Cl_2/*c*Hex, 1:2) = 0.36. – **^{1}H NMR** (500 MHz, $CDCl_3$): δ = 10.18 (d, ^3J = 4.6 Hz, 1H, $H_{pyrrole}$), 9.25 (d, ^3J = 4.6 Hz, 1H, $H_{pyrrole}$), 8.99 – 8.96 (m, 2H, $H_{pyrrole}$), 8.94 (d, ^3J = 4.6 Hz, 1H, $H_{pyrrole}$), 8.92 (d, ^3J = 4.6 Hz, 1H, $H_{pyrrole}$), 8.81 – 8.79 (m, 2H, $H_{pyrrole}$), 8.43 – 8.38 (m, 1H, $H_{aromatic}$), 8.38 – 8.34 (m, 1H, $H_{aromatic}$), 8.31 – 8.27 (m, 1H, $H_{aromatic}$), 8.26 – 8.21 (m, 1H, $H_{aromatic}$), 8.21 – 8.17 (m, 1H, $H_{aromatic}$), 8.06 – 8.03 (m, 1H, $H_{aromatic}$), 7.91 (d, ^4J = 1.8 Hz, 1H, $H_{paracyclophane}$), 7.84 – 7.80 (m, 2H, $H_{aromatic}$), 7.81 – 7.72 (m, 6H, $H_{aromatic}$), 7.71 – 7.65 (m, 1H, $H_{aromatic}$), 7.42 (dd, J = 7.8, 1.8 Hz, 1H, $H_{paracyclophane}$), 7.22 (d, ^3J = 8.0 Hz, 1H, $H_{paracyclophane}$), 6.94 (d, ^4J = 1.7 Hz, 1H, $H_{paracyclophane}$), 6.86 (d, ^3J = 7.9 Hz, 1H, $H_{paracyclophane}$), 6.73 (dd, J = 8.0, 1.7 Hz, 1H, $H_{paracyclophane}$), 3.80 – 3.73 (m, 1H, H_{bridge}), 3.68 – 3.61 (m, 1H, H_{bridge}), 3.36 – 3.23 (m, 2H, H_{bridge}), 3.08 – 3.00 (m, 1H, H_{bridge}), 2.64 – 2.56 (m, 1H, H_{bridge}), 2.44 – 2.36 (m, 1H, H_{bridge}), 2.17 – 2.09 (m, 1H, H_{bridge}) ppm. – **^{13}C NMR** (126 MHz, $CDCl_3$): δ = 152.6 (C_q), 150.3 (C_q), 150.3 (C_q), 150.3 (C_q), 150.2 (C_q), 150.1 (C_q), 150.1 (C_q), 149.9 (C_q), 149.9 (C_q), 145.0 (C_q), 143.3 (C_q), 143.1 (C_q), 143.0 (C_q), 141.4 (C_q), 139.3 (C_q), 138.3 (C_q), 137.4 (+, CH), 136.4 (+, CH), 134.7 (+, CH), 134.6 (+, CH), 134.6 (+, CH), 134.5 (+, CH), 134.5 (+, CH), 134.1 (+, CH), 133.9 (+, CH), 133.0 (+, CH), 132.6 (+, CH), 132.3 (+, CH), 132.2 (+, CH), 132.1 (+, CH), 132.0 (+, CH), 132.0 (+, CH), 131.9 (+, CH), 129.8 (+, CH), 129.6 (+, CH), 127.7 (+, CH), 127.6 (+, CH), 127.6 (+, CH), 126.9 (+, CH), 126.7 (+, CH), 126.7 (+, CH), 126.6 (+, CH), 126.6 (+, CH), 126.6 (+, CH), 121.2 (C_q), 121.2 (C_q), 121.2 (C_q), 120.7 (C_q),

120.2 (C_q), 35.4 (–, CH_2), 34.9 (–, CH_2), 34.6 (–, CH_2), 34.5 (–, CH_2) ppm. – **UV-Vis** (CH_2Cl_2): λ_{max} (rel. absorption) = 310 (0.13), 349 (0.09), 423 (3.07), 551 (0.16), 590 (0.03) nm. – **IR** (ATR): $\tilde{\nu}$ = 2953, 2921, 2849, 1656, 1599, 1438, 1337, 1200, 1067, 1034, 1001, 993, 795, 751, 718, 701, 662, 435 cm^{-1}. – **HRMS** (ESI) ($C_{54}H_{37}BrN_4Zn$): calc.: 884.1493, found: 884.1462.

4-Trimethylsilylethynyl-12-(10,15,20-triphenylporphyrin-5'-yl)[2.2]paracyclophane (**117^{NH}**)[83]

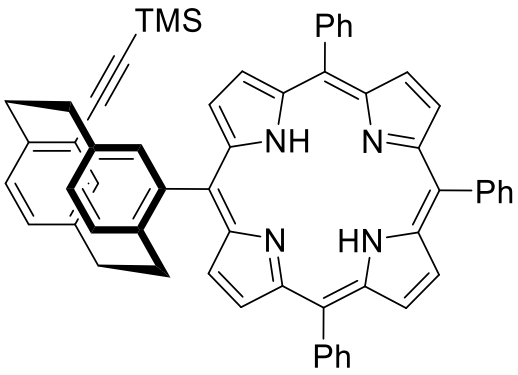

Under an argon atmosphere, 4-formyl-12-trimethylsilylethynyl[2.2]paracyclophane (**116**) (300 mg, 902 µmol, 1.00 equiv.) was dissolved in dry CH_2Cl_2 (400 mL). A stream of argon was passed through the mixture for 15 min to remove dissolved oxygen. Subsequently, freshly distilled benzaldehyde (275 µL, 287 mg, 2.70 mmol, 3.00 equiv.) and pyrrole (250 µL, 242 mg, 3.61 mmol, 4.00 equiv.) were added. After 5 min, TFA (85 µL, 125 mg, 1.09 mmol, 1.22 equiv.) was added. The mixture was stirred for 15 h in the dark. DDQ (494 mg, 2.18 mmol, 2.42 equiv.) was added and stirred for a further 1 h. Then, NEt_3 (5 mL) was added and the crude mixture was concentrated under reduced pressure. The crude product was filtered through a short layer of silica gel eluting with CH_2Cl_2 and purified by flash column chromatography on silica gel (CH_2Cl_2/*c*Hex, 1:2) to afford the title compound **117^{NH}** as a purple solid (23.1 mg, 27.5 µmol, 2.6%).

***R*$_f$** (*c*Hex/CH_2Cl_2, 2:1) = 0.36. – **^{1}H NMR** (400 MHz, $CDCl_3$): δ = 10.64 (d, ^3J = 4.9 Hz, 1H, $H_{pyrrole}$), 9.15 (d, ^3J = 4.7 Hz, 1H, $H_{pyrrole}$), 8.91 (d, ^3J = 4.7 Hz, 1H, $H_{pyrrole}$), 8.89 – 8.85 (m, 2H, $H_{pyrrole}$), 8.84 (d, ^3J = 4.8 Hz, 1H, $H_{pyrrole}$), 8.66 (d, ^3J = 4.8 Hz, 1H, $H_{pyrrole}$), 8.58 (d, ^3J = 4.8 Hz, 1H, $H_{pyrrole}$), 8.48 – 8.42 (m, 1H, $H_{aromatic}$), 8.41 – 8.36 (m, 1H, $H_{aromatic}$), 8.36 – 8.29 (m, 1H, $H_{aromatic}$), 8.26 – 8.08 (m, 3H, $H_{aromatic}$), 8.02 (d, ^3J = 7.6 Hz, 1H, $H_{aromatic}$), 7.88 – 7.64 (m, 9H, $H_{aromatic}$), 7.04 (d, ^4J = 7.6 Hz, 1H, $H_{paracyclophane}$), 7.00 (d, ^3J = 7.8 Hz, 1H, $H_{aromatic}$), 6.98 – 6.90 (m, 2H, $H_{paracyclophane}$), 6.81 (dd, J = 7.9, 1.8 Hz, 1H, $H_{paracyclophane}$), 4.03 (dd, J = 13.4, 9.1 Hz, 1H, H_{bridge}), 3.66 – 3.46 (m, 2H, H_{bridge}), 3.20 – 3.06 (m, 1H, H_{bridge}), 2.91 – 2.80 (m, 1H, H_{bridge}), 2.64 – 2.53 (m, 1H, H_{bridge}), 2.34 – 2.23 (m, 1H, H_{bridge}), 1.94 – 1.83 (m, 1H, H_{bridge}), 1.44 (s, 9H, Si(C*H*$_3$)), –2.65 (bs, 2H, NH) ppm. – **^{13}C NMR** (101 MHz, $CDCl_3$): δ = 145.4 (C_q), 144.2 (C_q), 142.8 (C_q), 142.6 (C_q), 142.1 (C_q), 140.1 (C_q), 139.5 (C_q), 138.5 (C_q), 135.1 (+, CH), 134.6 (+, CH), 134.1 (+, CH), 133.9 (+, CH), 133.6 (+, CH), 133.3 (+, CH),

127.8 (+, CH), 126.9 (+, CH), 126.7 (+, CH), 123.4 (C_q), 120.3 (C_q), 120.1 (C_q), 119.7 (C_q), 119.2 (C_q), 105.0 (C_q), 101.0 (C_q), 43.6 (35.6 (–, CH_2), 35.2 (–, CH_2), 34.2 (–, CH_2), 33.4 (–, CH_2), 0.42 (+, CH_3, Si(*C*H_3)$_3$) ppm. – **UV-Vis** (CH_2Cl_2): (rel. absorption) = 280 (0.18), 423 (2.93), 519 (0.14), 556 (0.09), 594 (0.04), 650 (0.04) nm. – **IR** (ATR): $\tilde{\nu}$ = 3310, 2919, 2847, 2140, 1468, 1441, 1401, 1347, 1248, 1001, 966, 875, 840, 798, 727, 700, 659, 643, 500 cm^{-1}. – **HRMS** (ESI) ($C_{59}H_{48}N_4Si$): calc.: 841.3726, found: 841.3712.

4-Trimethylsilylethynyl-12-(10,15,20-triphenylporphyrin-5-yl)zinc(II) [2.2]paracyclophane (**117**)[379]

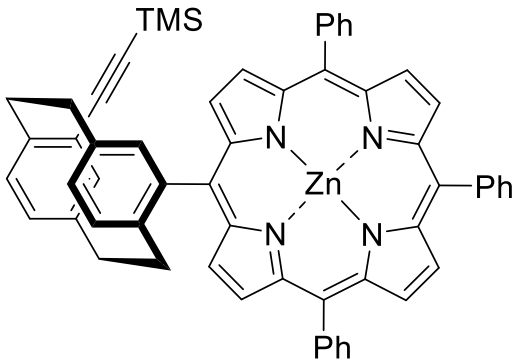

4-Trimethylsilylethynyl-12-(10,15,20-triphenylporphyrin-5-yl)[2.2]paracyclophane (**117^{NH}**) (23.1 mg, 24.4 µmol, 1.00 equiv.) and $Zn(OAc)_2$ (9.91 mg, 54.0 µmol, 2.00 equiv.) were dissolved in a mixture of $CHCl_3$ and MeOH (9:1, 20 mL). The reaction mixture was stirred for 3 h at room temperature and the solvent was removed under reduced pressure. The crude product was redissolved in CH_2Cl_2 (50 mL) and thoroughly washed with H_2O (3 × 50 mL). The combined organic phases were dried over Na_2SO_4, filtered and the solvent removed under reduced pressure to afford the title compound **117** as a purple solid (22.1 mg, 24.4 µmol, quant.).

***R*$_f$** (*c*Hex/CH_2Cl_2, 2:1) = 0.40. **^{1}H NMR** (500 MHz, $CDCl_3$): δ = 10.72 (d, ^3J = 4.7 Hz, 1H, $H_{pyrrole}$), 9.26 (d, ^3J = 4.7 Hz, 1H, $H_{pyrrole}$), 9.04 (d, ^3J = 4.7 Hz, 1H, $H_{pyrrole}$), 8.99 (d, ^3J = 4.6 Hz, 1H, $H_{pyrrole}$), 8.96 (d, ^3J = 4.6 Hz, 1H, $H_{pyrrole}$), 8.93 (d, ^3J = 4.6 Hz, 1H, $H_{pyrrole}$), 8.79 (d, ^3J = 4.7 Hz, 1H, $H_{pyrrole}$), 8.74 (d, ^3J = 4.7 Hz, 1H, $H_{pyrrole}$), 8.45 – 8.42 (m, 1H, $H_{aromatic}$), 8.38 – 8.35 (m, 1H, $H_{aromatic}$), 8.32 – 8.28 (m, 1H, $H_{aromatic}$), 8.25 – 8.21 (m, 1H, $H_{aromatic}$), 8.21 – 8.18 (m, 1H, $H_{aromatic}$), 8.08 (d, ^4J = 1.6 Hz, 1H, $H_{paracyclophane}$), 8.07 – 8.04 (m, 1H, $H_{aromatic}$), 7.87 – 7.80 (m, 2H, $H_{aromatic}$), 7.80 – 7.73 (m, 6H, $H_{aromatic}$), 7.71 – 7.66 (m, 1H, $H_{aromatic}$), 7.13 (d, ^4J = 1.6 Hz, 1H, $H_{paracyclophane}$), 7.01 (d, ^3J = 7.8 Hz, 1H, $H_{paracyclophane}$), 6.96 (d, ^3J = 7.7 Hz, 1H, $H_{paracyclophane}$), 6.91 (dd, J = 7.9, 1.8 Hz, 1H, $H_{paracyclophane}$), 6.82 (dd, J = 7.9, 1.8 Hz, 1H, $H_{paracyclophane}$), 4.04 (dd, J = 13.6, 9.1 Hz, 1H, H_{bridge}), 3.61 (dd, J = 13.9, 9.8 Hz, 1H, H_{bridge}), 3.55 – 3.47 (m, 1H, H_{bridge}), 3.18 – 3.09 (m, 1H, H_{bridge}), 2.88 (ddd, J = 13.6, 10.6, 5.4 Hz, 1H, H_{bridge}), 2.61 (ddd, J = 13.3, 10.6, 2.6 Hz, 1H, H_{bridge}), 2.24 (ddd, J = 13.4, 10.2, 2.7 Hz, 1H, H_{bridge}), 1.99 (ddd, J = 13.3, 10.2, 5.4 Hz, 1H, H_{bridge}), 0.46 (s, 9H, Si(CH_3)) ppm.

– **^{13}C NMR** (126 MHz, $CDCl_3$): δ = 152.6 (C_q), 150.4 (C_q), 150.3 (C_q), 150.1 (C_q), 150.1 (C_q), 150.1 (C_q), 149.9 (C_q), 149.9 (C_q), 145.1 (C_q), 144.2 (C_q), 143.3 (C_q), 143.1 (C_q), 143.0 (C_q), 140.2 (C_q), 140.0 (C_q), 138.2 (C_q), 135.5 (+, CH), 135.1 (+, CH), 134.7 (+, CH), 134.6 (+, CH), 134.6 (+, CH), 134.5 (+, CH), 134.3 (+, CH), 134.0 (+, CH), 133.7 (+, CH), 133.3 (+, CH), 132.7 (+, CH), 132.7 (+, CH), 132.2 (+, CH), 131.9 (+, CH), 131.9 (+, CH), 131.7 (+, CH), 127.6 (+, CH), 127.6 (+, CH), 126.8 (+, CH), 126.7 (+, CH), 126.7 (+, CH), 126.6 (+, CH), 126.6 (C_q), 123.5 (C_q), 121.2 (C_q), 121.1 (C_q), 120.7 (C_q), 120.4 (C_q), 105.0 (C_q), 100.9 (C_q), 35.6 (–, CH_2), 35.2 (–, CH_2), 34.3 (–, CH_2), 33.4 (–, CH_2) ppm. – **UV-Vis** (CH_2Cl_2): λ_{max} (rel. absorption) = 282 (0.11), 310 (0.10), 424 (2.56), 551 (0.11), 590 (0.03) nm. – **IR** (ATR): $\tilde{\nu}$ = 2952, 2918, 2847, 2140, 1596, 1485, 1470, 1439, 1402, 1337, 1261, 1247, 1204, 1176, 1068, 1003, 994, 979, 943, 904, 881, 871, 839, 795, 749, 728, 718, 698, 660, 643, 622, 567, 548, 520, 499, 433 cm^{-1}. – **HRMS** (ESI) ($C_{59}H_{46}N_4SiZn$): calc.: 902.2783, found: 902.2770.

4-Ethynyl-12-(10,15,20-triphenylporphyrin-5'-yl)zinc(II) [2.2]paracyclophane (**120**)[215]

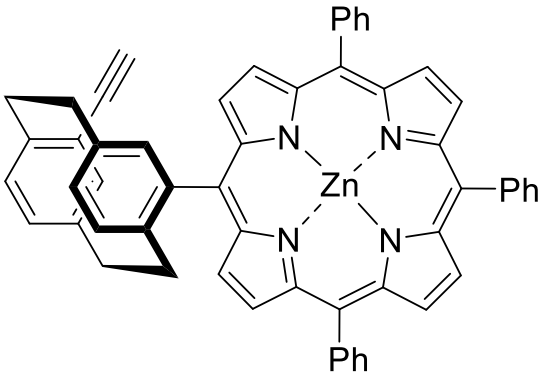

To a solution of 4-trimethylsilylethynyl-12-(10,15,20-triphenylporphyrin-5-yl)zinc(II) [2.2]paracyclophane (**117**) (19.9 mg, 22.0 µmol, 1.00 equiv.) in CH_2Cl_2 (10 mL), 1 M TBAF in THF (44 µL, 9.5 mg, 44.0 µmol, 2.00 equiv.) was added and the reaction was stirred at room temperature for 1.5 h. MeOH (5 mL) was added and the solvent was removed under reduced pressure. The residue was redissolved in CH_2Cl_2 (30 mL) and thoroughly washed with H_2O (3 × 50 mL). The combined organic phases were dried over Na_2SO_4 and the solvent was removed under reduced pressure to afford the title compound **120** as a purple solid (18.2 mg, 21.9 µmol, 99%).

***R*$_f$** (*c*Hex/CH_2Cl_2, 2:1) = 0.36. – **^{1}H NMR** (300 MHz, $CDCl_3$): δ = 10.69 (d, ^3J = 4.8 Hz, 1H, $H_{pyrrole}$), 9.22 (d, ^3J = 4.7 Hz, 1H, $H_{pyrrole}$), 9.03 – 8.86 (m, 4H, $H_{pyrrole}$), 8.76 (d, ^3J = 4.8 Hz, 1H, $H_{pyrrole}$), 8.68 (d, ^3J = 4.8 Hz, 1H, $H_{pyrrole}$), 8.48 – 8.41 (m, 1H, $H_{aromatic}$), 8.40 – 8.34 (m, 1H, $H_{aromatic}$), 8.34 – 8.26 (m, 1H, $H_{aromatic}$), 8.26 – 8.13 (m, 3H, $H_{aromatic}$), 8.12 – 8.06 (m, 1H, $H_{paracyclophane}$), 8.06 –7.96 (m, 1H, $H_{aromatic}$), 7.90 – 7.61 (m, 10H, $H_{aromatic}$), 7.21 – 7.16 (m, 1H, $H_{paracyclophane}$), 7.02 (d, ^3J = 7.8 Hz, 1H, $H_{paracyclophane}$), 6.98 – 6.80 (m, 1H, $H_{paracyclophane}$), 4.11 – 3.96 (m, 1H, H_{bridge}), 3.90 (s, 1H, H_{alkyne}), 3.68 – 3.42 (m, 2H, H_{bridge}), 3.22 – 3.06 (m, 1H, H_{bridge}), 2.93 – 2.78 (m, 1H, H_{bridge}), 2.69 – 2.54 (m, 1H, H_{bridge}), 2.2.6 – 2.11 (m, 1H, H_{bridge}),

2.06 – 1.94 (m, 1H, H_{bridge}) ppm. – **^{13}C NMR** (126 MHz, $CDCl_3$): δ = l50.4 (C_q), 150.1 (C_q), 149.9 (C_q), 145.2 (C_q), 144.2 (C_q), 143.3 (C_q), 143.1 (C_q), 140.2 (C_q), 135.1 (+, CH), 134.6 (+, CH), 134.4 (+, CH), 134.1 (+, CH), 133.7 (+, CH), 133.5 (+, CH), 132.7 (+, CH), 132.1 (+, CH), 131.9 (+, CH), 131.6 (+, CH), 127.6 (+, CH), 126.7 (+, CH), 122.5 (C_q), 121.2 (C_q), 120.6 (C_q), 120.2 (C_q), 83.6 (+, CH, C_{alkyne}), 35.5 (–, CH_2), 35.1 (–, CH_2), 34.3 (–, CH_2), 33.5 (–, CH_2) ppm.

6.3.5 Syntheses of heterobimetallic [2.2]paracyclophane-porphyrin conjugates

(4-Ethynyl)gold(I)-triphenylphosphane-12-(10,15,20-triphenylporphyrin-5'-yl)zinc(II) [2.2]paracyclophane (**121**)[204]

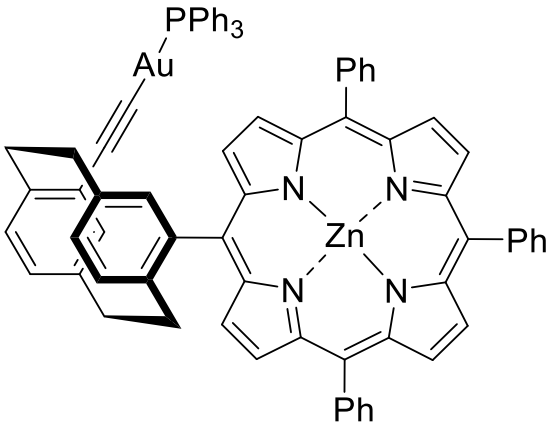

To a mixture of MeOH/CH_2Cl_2, 1:1 (5 mL) containing alkyne-Zn(II)-porphyrin **120** (25.1 mg, 30.0 µmol, 1.00 equiv.) and KOH (1.7 mg, 30.0 µmol, 1.00 equiv.), Ph_3PAuCl (13.4 mg, 27.0 µmol, 0.90 µmol) was added while stirring. After 20 h at room temperature, the suspension was filtered and washed with MeOH (2 × 5 mL) and Et_2O (2 × 5 mL). The solvent was removed under reduced pressure and the crude product of **121** was analyzed *via* ESI-MS.

HRMS (ESI) ($C_{74}H_{52}N_4PZnAu$): calc.: 1288.288, found: 1288.288.

4-(10,15,20-triphenylporphyrin-5-yl)-16-(4-(2'-pyridyl)phenyl)[2.2]paracyclophane (**123^{NH}**)[83]

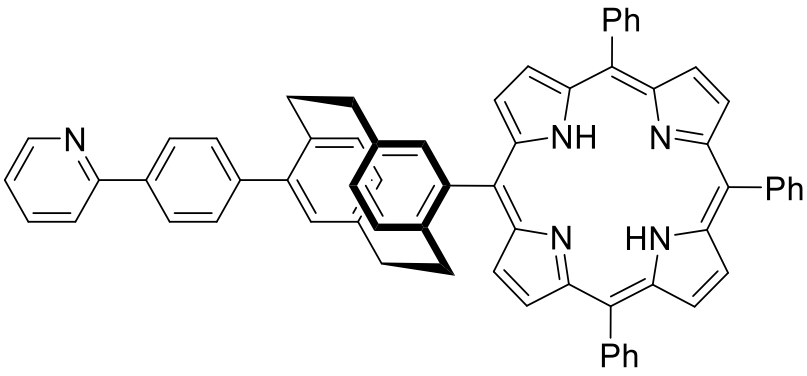

Under an argon atmosphere 4-formyl-16-(4-(2'-pyridyl)phenyl)[2.2]-paracyclophane (**122**) (300 mg, 771 µmol, 1.00 equiv.) was dissolved in dry CH_2Cl_2 (350 mL). A stream of argon was passed through the mixture for 15 min to remove dissolved oxygen.

Subsequently, freshly distilled benzaldehyde (258 µL, 287 mg, 2.31 mmol, 3.00 equiv.) and pyrrole (213 µL, 207 mg, 3.08 mmol, 4.00 equiv.) were added. After 5 min, TFA (72 µL, 106 mg, 933 µmol, 1.22 equiv.) was added. The mixture was stirred for 14 h in the dark. DDQ (424 mg, 1.87 mmol, 2.44 equiv.) was added and stirred for a further 1 h. Then, NEt_3 (10 mL) was added and the crude mixture was concentrated under reduced pressure. The crude product was filtered through a short layer of silica gel eluting with CH_2Cl_2 and purified by flash column chromatography on silica gel (*c*Hex/EtOAc, 4:1) to afford the title compound **123^{NH}** (39.7 mg, 44.2 µmol, 5.7%) as purple solid.

***R*$_f$** (*c*Hex/EtOAc, 4:1) = 0.44. – **^{1}H NMR** (500 MHz, $CDCl_3$): δ = 10.20 (d, ^3J = 4.7 Hz, 1H, $H_{pyrrole}$), 9.22 (d, ^3J = 4.7 Hz, 1H, $H_{pyrrole}$), 8.91 – 8.88 (m, 2H, $H_{pyrrole}$), 8.87 (d, ^3J = 4.8 Hz, 1H, $H_{pyrrole}$), 8.84 (d, ^3J = 4.7 Hz, 1H, $H_{pyrrole}$), 8.81 – 8.79 (m, 1H, $H_{pyridyl}$), 8.78 (d, ^3J = 4.9 Hz, 1H, $H_{pyrrole}$), 8.74 (d, ^3J = 4.8 Hz, 1H, $H_{pyrrole}$), 8.45 (bs, 1H, $H_{aromatic}$), 8.43 – 8.39 (m, 1H, $H_{aromatic}$), 8.36 – 8.31 (m, 1H, $H_{aromatic}$) 8.27 – 8.22 (m, 2H, $H_{aromatic}$), 8.22 – 8.19 (m, 1H, $H_{aromatic}$), 8.19 – 8.13 (m, 1H, $H_{aromatic}$), 8.06 – 8.01 (m, 1H, $H_{aromatic}$), 8.01 – 7.99 (m, 1H, $H_{aromatic}$), 7.90 – 7.82 (m, 6H, $H_{aromatic}$), 7.82 – 7.73 (m, 6H, $H_{aromatic}$), 7.72 –7.66 (m, 1H, $H_{aromatic}$), 7.36 (d, ^3J = 7.9 Hz, 1H $H_{paracyclophane}$), 7.30 (ddd, J = 7.3, 4.8, 1.2 Hz, 1H, $H_{paracyclophane}$), 7.06 (d, ^4J = 1.8 Hz, 1H, $H_{paracyclophane}$), 7.00 (d, ^3J = 7.8 Hz, 1H, $H_{paracyclophane}$), 6.89 (dd, J = 8.0, 1.7 Hz, 1H, $H_{paracyclophane}$), 6.85 (dd, ^3J = 7.9, 1.8 Hz, 1H, $H_{paracyclophane}$), 3.63 (m, 1H, $H_{paracyclophane}$), 3.53 (ddd, J = 13.9, 10.2, 2.6 Hz 1H, $H_{paracyclophane}$), 3.39 (ddd, J = 13.4, 10.2, 2.6 Hz 1H, $H_{paracyclophane}$), 3.24 – 3.19 (m, 1H, $H_{paracyclophane}$), 3.14 (ddd, J = 13.9, 10.2, 2.6 Hz 1H, $H_{paracyclophane}$), 2.77 (ddd, J = 13.4, 10.6, 5.1 Hz 1H, $H_{paracyclophane}$), 2.46 (ddd, J = 13.5, 10.4, 2.8 Hz 1H, $H_{paracyclophane}$), 2.32 (ddd, J = 14.2, 10.5, 5.1 Hz, 1H, $H_{paracyclophane}$), – 2.59 (bs, 2H, NH) ppm. – **^{13}C NMR** (126 MHz, $CDCl_3$): δ = 157.4 (C_q), 150.0 (+, CH), 144.9 (C_q), 142.8 (C_q), 142.8 (C_q), 142.6 (C_q), 142.1 (C_q), 142.1 (C_q), 140.7 (C_q), 140.2 (C_q), 138.9 (C_q), 138.3 (C_q), 137.7 (C_q), 137.0 (+, CH), 134.7 (+, CH), 134.6 (+, CH), 134.5 (+, CH), 134.2 (+, CH), 132.5 (+, CH), 130.8 (+, CH), 130.6 (+, CH), 130.1 (+, CH), 127.9 (+, CH), 127.9 (+, CH), 127.8 (+, CH), 127.4 (+, CH), 126.9 (+, CH), 126.8 (+, CH), 126.7 (+, CH), 122.3 (+, CH), 120.8 (+, CH), 120.4 (C_q), 120.3 (C_q), 119.8 (C_q), 119.4 (C_q), 35.6 (–, CH_2), 34.7 (–, CH_2, 2C), 33.4 (–, CH_2) ppm. – **UV-Vis** (CH_2Cl_2): λ_{max} (rel. absorption) = 289 (0.13), 422 (3.02), 456 (0.13), 519 (0.15), 555 (0.09), 594 (0.05), 650 (0.05) nm. – **IR** (ATR): $\tilde{\nu}$ = 2963, 2918, 2849, 1706, 1585, 1463, 1432, 1264, 870, 805, 802, 783, 727, 700, 493, 402 cm^{-1}. – **HRMS** (ESI) ($C_{54}H_{40}BrN_4$): calc.: 897.3831, found: 897.4224.

4-[(10,15,20-triphenylporphyrin-5-yl)]zinc(II)-16-(4-(2'-pyridyl)phenyl)[2.2]paracyclophane (**123**)[379]

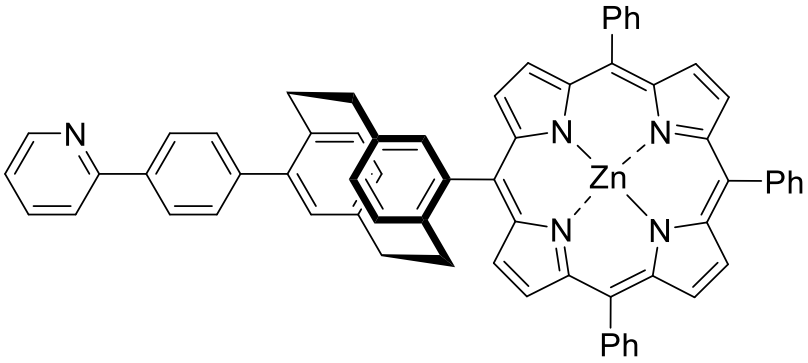

4-(10,15,20-triphenylporphyrin-5-yl)-16-(4-(2'-pyridyl)phenyl)[2.2]paracyclophane (**123^{NH}**) (30.4 mg, 33.9 µmol, 1.00 equiv.) and $Zn(OAc)_2$ (22.1 mg, 120 µmol, 2.00 equiv.) were dissolved in a mixture of $CHCl_3$ and MeOH (10:1, 33 mL). The reaction mixture was stirred for 3 h at room temperature and the solvent was removed under reduced pressure. The crude product was redissolved in CH_2Cl_2 (50 mL) and thoroughly washed with H_2O (3 × 50 mL). The combined organic phases were dried over Na_2SO_4, filtered and the solvent was removed under reduced pressure to afford the title compound **123** as a purple solid (32.8 mg, 34.1 µmol, quant.).

***R*f** (*c*Hex/EtOAc, 4:1) = 0.50. – **^{1}H NMR** (500 MHz, $CDCl_3$): δ = 10.30 (d, ^3J = 4.6 Hz, 1H, $H_{pyrrole}$), 9.31 (d, ^3J = 4.5 Hz, 1H, $H_{pyrrole}$), 9.00 (d, ^3J = 4.6 1H, $H_{pyrrole}$), 8.99 (d, ^3J = 4.6 Hz, 1H, $H_{pyrrole}$), 8.96 (d, ^3J = 4.6 Hz, 1H, $H_{pyrrole}$), 8.94 (d, ^3J = 4.6 Hz, 1H, $H_{pyrrole}$), 8.91 (d, ^3J = 4.6 Hz, 1H, $H_{pyrrole}$), 8.84 (d, ^3J = 4.6 Hz, 1H, $H_{pyrrole}$), 8.69 – 8.67 (m, 1H, $H_{aromatic}$), 8.44 – 8.40 (m, 1H, $H_{aromatic}$), 8.39 – 8.36 (m, 1H, $H_{aromatic}$), 8.31 – 8.27 (m, 1H, $H_{aromatic}$), 8.26 – 8.22 (m, 1H, $H_{aromatic}$), 8.22 – 8.18 (m, 1H, $H_{aromatic}$), 8.18 – 8.15 (m, 2H, $H_{aromatic}$), 8.07 – 8.03 (m, 1H, $H_{aromatic}$), 7.95 (d, ^4J = 1.7 Hz, 1H, $H_{paracyclophane}$), 7.86 – 7.73 (m, 12H, $H_{aromatic}$), 7.71 – 7.66 (m, 1H, $H_{aromatic}$), 7.94 (d, ^3J = 7.9 Hz, 1H, $H_{paracyclophane}$), 7.29 – 7.26 (m, 1H, $H_{paracyclophane}$), 7.03 (d, ^4J = 1.9 Hz, 1H, $H_{paracyclophane}$), 6.98 (d, ^3J = 7.9 Hz, 1H, $H_{paracyclophane}$), 6.89 (dd, J = 8.0, 1.8 Hz, 1H, $H_{paracyclophane}$), 6.85 (d, J = 7.9, 1.7 Hz, 1H, $H_{paracyclophane}$), 3.60 (ddd, J = 14.2, 10.2, 5.9 Hz, 1H, H_{bridge}), 3.51 (ddd, J = 13.9, 10.1, 2.6 Hz, 1H, H_{bridge}), 3.37 (ddd, J = 13.4, 10.2, 2.6 Hz, 1H, H_{bridge}), 3.22 – 3.10 (m, 2H, H_{bridge}), 2.75 (ddd, J = 13.6, 10.6, 5.5 Hz, 1H, H_{bridge}), 2.48 (ddd, J = 13.5, 10.4, 2.7 Hz, 1H, H_{bridge}), 2.27 (ddd, J = 14.1, 10.5, 5.4 Hz, 1H, H_{bridge}) ppm. – **^{13}C NMR** (126 MHz, $CDCl_3$): δ = 157.4, 152.6, 150.3, 150.3, 150.2, 150.1, 150.1, 150.1, 150.0, 149.9 (+, CH), 144.7, 143.3, 143.1, 143.0, 142.7, 142.1, 140.9, 140.6, 138.5, 138.2, 137.6, 137.0 (+, CH), 137.0 (+, CH), 134.7 (+, CH), 134.6 (+, CH), 134.6 (+, CH), 134.5 (+, CH), 134.5 (+, CH), 134.5 (+, CH), 134.0 (C_q), 133.2 (+, CH), 130.0 (+, CH), 132.5 (+, CH), 132.4 (+, CH), 132.2 (+, CH), 132.0 (+, CH), 132.0 (+, CH), 132.0 (+, CH), 131.9 (+, CH), 130.6 (+, CH), 130.5 (+, CH), 130.1 (+, CH), 127.7 (+,

CH), 127.6 (+, CH), 127.6 (+, CH), 127.4 (+, CH), 126.8 (+, CH), 126.7 (+, CH), 126.7 (+, CH), 126.7 (+, CH), 126.6 (+, CH), 126.6 (+, CH), 122.3 (+, CH), 121.2 (C_q), 121.2 (C_q), 120.8 (C_q), 120.8 (+, CH), 120.5 (C_q), 35.6 (–, CH_2), 34.8 (–, CH_2, 2C), 33.4 (–, CH_2) ppm. – **UV-Vis** (CH_2Cl_2): λ_{max} (rel. absorption) = 302 (0.09), 423 (2.68), 551 (0.12), 590 (0.03) nm. – **IR** (ATR): $\tilde{\nu}$ = 3050, 3024, 2953, 2918, 2867, 2849, 2793, 1592, 1466, 1434, 1336, 1201, 1067, 1001, 992, 965, 907, 795, 785, 749, 728, 718, 701, 660, 647, 622, 432, 408 cm^{-1}. – **HRMS** (ESI) ($C_{65}H_{45}N_5Zn$): calc.: 959.2966, found: 959.3000.

4-[(10,15,20-Triphenylporphyrin-5-yl)]zinc(II)-16-(4-(bis(2,2ˈ-bipyridyl)4-(2ˈ-pyridyl)phenyl)ruthenium(II)[2.2]paracyclophane (**124**)[205]

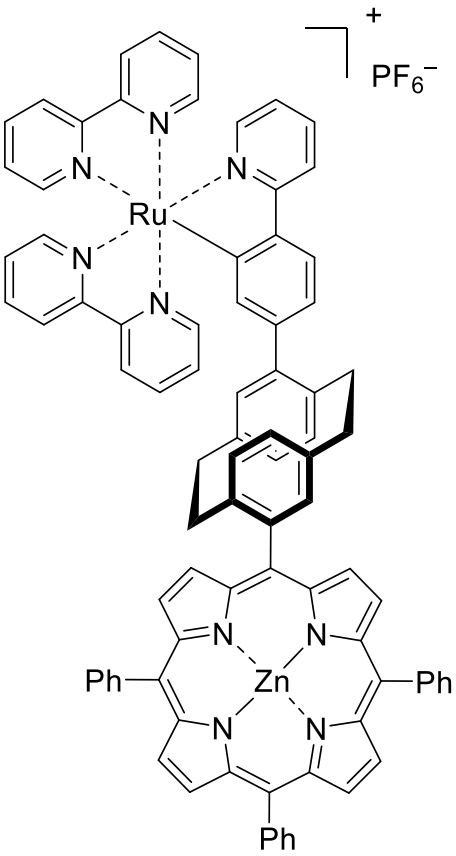

Under an argon atmosphere, a crimp vial was charged with pyridyl-phenyl-Zn(II)porphyrin **123** (21.8 mg, 22.6 mmol, 1.00 equiv.), benzeneruthenium(II) chloride dimer (56.7 mg, 454 µmol, 20.0 equiv.), KPF_6 (83.5 g, 454 µmol, 20.0 equiv.) and NaOH (36.3 mg, 907 µmol, 40.0 equiv.). The reaction mixture was stirred at room temperature in MeCN (5 mL). After 16 h, the solvent was removed under reduced pressure. Dry, degassed MeOH and 2-phenylpyridine (70.8 mg, 45.4 mmol, 20.0 equiv.) were added and stirred at reflux for 2 h. Afterward, the solvent was removed and the crude product of **123** was analyzed *via* ESI-MS.

HRMS (ESI) ($C_{85}H_{60}N_9ZnRu$): calc.: 1372.331, found: 1372.330.

6.4 Cofacial *o*-phenylene-bisporphyrin metal complexes

6.4.1 *o*-Formyl-groups as residue functionalization to enable *o*-phenylene-bisporphyrin syntheses

5-(2-Formylphenyl)-10,15,20-triphenylporphyrin (**125**)[88]

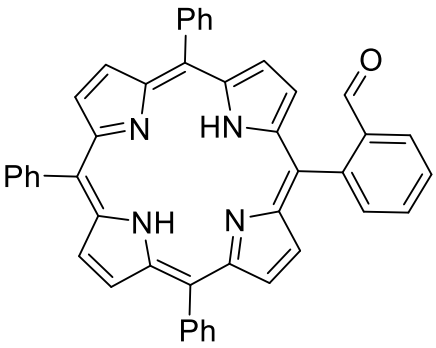

Under an argon atmosphere, 5-bromo-10,15,20-triphenylporphyrin (**83**) (181 mg, 293 µmol, 1.00 equiv.), 2-(formylphenyl)boronic acid (526 mg, 3.51 mmol, 12.0 equiv.), tetrakis(triphenylphosphine)palladium(0) (81.1 mg, 70.2 µmol, 0.24 equiv.) and tripotassium phosphate (1.55 g, 7.32 mmol, 25.0 equiv.) were dissolved in dry THF (250 mL). The mixture was stirred for 15 h at 80 °C. The solvent was removed under reduced pressure and redissolved in CH_2Cl_2 (100 mL). The organic phase was washed with H_2O (3 × 250 mL), dried over Na_2SO_4, filtered and removed the solvent under reduced pressure. The crude product was purified by flash column chromatography on silica gel (1:1, CH_2Cl_2/*n*-pentane) to afford the title compound (**125**) as a purple solid (128 mg, 200 µmol, 68%).

***R*f** (*c*Hex/EtOAc, 4:1) = 0.64. – **^{1}H NMR** (400 MHz, $CDCl_3$): δ = 9.52 (s, 1H, C*H*O), 8.93 – 8.86 (m, 6H, $H_{pyrrole}$), 8.67 (d, ^3J = 4.8 Hz, 2H), 8.46 – 8.41 (m, 1H, $H_{aromatic}$), 8.29 – 8.20 (m, 7H, $H_{aromatic}$), 7.99 – 7.90 (m, 2H, $H_{aromatic}$), 7.83 – 7.73 (m, 9H, $H_{aromatic}$), –2.67 (bs, 2H, N*H*) ppm. – **^{13}C NMR** (101 MHz, $CDCl_3$): δ = 191.2 (+, *C*HO), 145.6 (C_q), 142.1 (C_q), 142.0 (C_q), 138.2 (C_q), 135.8 (+, CH), 134.7 (+, CH), 134.7 (+, CH), 131.5 (+, CH), 129.1 (+, CH), 128.0 (+, CH), 127.0 (+, CH), 126.9 (+, CH), 126.3 (+, CH), 121.1 (C_q), 120.9 (C_q), 114.1 (C_q) ppm. – **UV-Vis** (CH_2Cl_2): λ_{max} (rel. absorption) = 243 (0.33), 372 (0.40), 418 (3.19), 516 (0.28), 551 (0.11), 591 (0.08), 647 (0.05) nm. – **IR (ATR)**: $\tilde{\nu}$ = 415, 518, 557, 574, 620, 642, 657, 663, 680, 696, 707, 724, 748, 786, 800, 915, 963, 980, 1000, 1058, 1071, 1157, 1176, 1184, 1193, 1214, 1220, 1349, 1383, 1439, 1470, 1592, 1694 (ν-CO), 1810, 1952, 2728, 2822, 2919, 3021, 3051, 3129, 3320 cm^{-1}. – **MS** (FAB, 3-NBA): *m/z* (%) = 642.2 (100) $[M]^+$, 419.3 (92). – **HRMS** ($C_{45}H_{31}O_1N_4$): calc.: 643.2498, found: 643.2497.

Additional information on the reaction details is available *via* the Chemotion repository: https://dx.doi.org/10.14272/reaction/SA-FUHFF-UHFFFADPSC-IXMWRMWFCF-UHFFFADPSC-NUHFF-NAGQZ-NUHFF-ZZZ

Additional information on the analysis of the target compound is available *via* the Chemotion repository https://dx.doi.org/10.14272/IXMWRMWFCFDTKE-HIXPDHBDSA-N.1

5-(2-Formylphenyl)-10,20-diethoxycarbonylphenylporphyrin (**126**)[88]

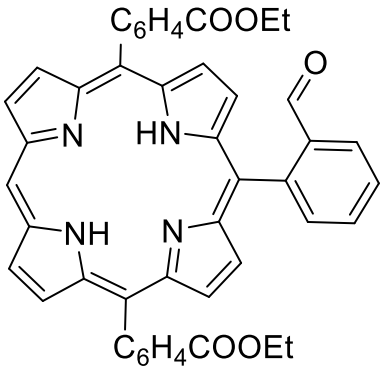

Under an argon atmosphere, 5-bromo-10,20-diethoxycarbonylphenylporphyrin (**84**) (104 mg, 152 µmol, 1.00 equiv.), 2-(formylphenyl)boronic acid (262 mg, 1.75 mmol, 11.5 equiv.), tetrakis(triphenylphosphine)palladium(0) (20.3 mg, 44 µmol, 0.12 equiv.) and tripotassium phosphate (808 mg, 381 µmol, 25.0 equiv.) were dissolved in dry THF (40 mL). The mixture was stirred for 6 h at 80 °C. The solvent was removed under reduced pressure and the residue was redissolved in CH_2Cl_2 (100 mL). The organic phase was washed with H_2O (3 × 100 mL), dried over Na_2SO_4, filtered and removed the solvent under reduced pressure. The crude product was purified by flash column chromatography on silica gel (CH_2Cl_2) to afford the title compound **126** as a purple solid (61.2 mg, 86.1 µmol, 57%).

***R*f** (*c*Hex/EtOAc, 4:1) = 0.42. – **^{1}H NMR** (400 MHz, $CDCl_3$): δ = 10.29 (s, 1H, H_{meso}), 9.46 (s, 1H, C*H*O), 9.38 (d, ^3J = 4.7 Hz, 2H, $H_{pyrrole}$), 8.99 (d, ^3J = 4.6 Hz, 2H, $H_{pyrrole}$), 8.87 (d, ^3J = 4.8 Hz, 2H, $H_{pyrrole}$), 8.71 (d, ^3J = 4.8 Hz, 2H, $H_{pyrrole}$), 8.52 – 8.46 (m, 4H, $H_{aromatic}$), 8.44 – 8.40 (m, 1H, $H_{aromatic}$), 8.37 – 8.30 (m, 4H, $H_{aromatic}$), 8.25– 8.21 (m, 1H, $H_{aromatic}$), 8.00 – 7.90 (m, 2H, $H_{aromatic}$), 4.60 (q, ^3J = 7.1 Hz, 4H, COC*H*$_2$), 1.57 (t, ^3J = 7.2 Hz, 6H, CH_2CH_3), –2.94 (bs, 2H, N*H*) ppm. – **^{13}C NMR** (101 MHz, $CDCl_3$): δ = 191.0 (+, *C*HO), 167.0 (*C*OOEt), 146.2 (C_q), 145.6 (C_q), 138.2 (C_q), 135.7 (+, CH), 134.8 (+, CH), 134.8 (+, CH), 132.2 (+, CH), 131.5 (+, CH), 131.4 (+, CH), 130.2 (C_q), 129.3 (+, CH), 128.3 (+, CH), 128.2 (+, CH), 126.4 (+, CH), 119.2 (C_q), 115.1 (C_q), 106.0 (C_q), 61.5 (–, CO*C*H$_2$), 14.7 (+, CH_2CH_3) ppm. – **UV-Vis** (CH_2Cl_2): λ_{max} (rel. absorption) = 234 (0.65), 296 (0.26), 304 (0.26), 369 (0.52), 413 (3.22), 415 (3.26), 510 (0.32), 545 (0.11), 584 (0.10), 639 (0.04). – **IR** (ATR): $\tilde{\nu}$ = 3295, 2975, 2962, 2745, 1711, 1697, 1604, 1594, 1401, 1364, 1262, 1191, 1176, 1157, 1095, 1054, 1020, 993, 977, 963, 955, 868, 847, 819, 795, 782, 758, 724, 704, 691, 670, 635, 577, 558, 523, 511, 496, 469, 455, 441, 397, 385 cm–1. – **MS** (FAB, 3-NBA): *m/z* (%) = 710.2 (85) $[M]^+$, 711.3 (100) $[M+H]^+$, 712.3 (70). – **HRMS** ($C_{45}H_{35}O_5N_4$): calc.: 711.2607, found: 711.2609.

Additional information on the reaction details is available *via* the Chemotion repository: https://dx.doi.org/10.14272/reaction/SA-FUHFF-UHFFFADPSC-GJXVXQKLCL-UHFFFADPSC-NUHFF-NPXAD-NUHFF-ZZZ

Additional information on the analysis of the target compound is available *via* the Chemotion repository: https://dx.doi.org/10.14272/GJXVXQKLCLKLLN-NVZKTODFSA-N.1

2-(2-Formylphenyl)-5,10,15,20-tetraphenylporphyrin (**127**)[88]

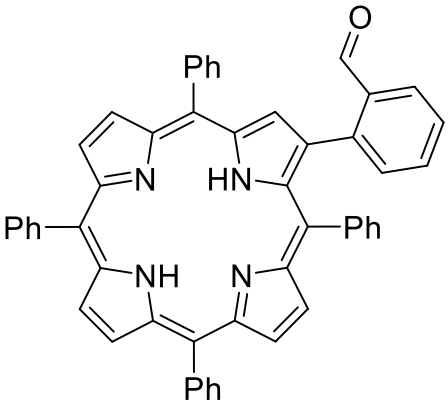

Under an argon atmosphere, 2-bromo-5,10,15,20-tetraphenylporphyrin (**85**) (200 mg, 288 µmol, 1.00 equiv.), 2-(formylphenyl)boronic acid (518 mg, 3.46 mmol, 12.0 equiv.), tetrakis(triphenylphosphine)-palladium(0) (80.0 mg, 69.2 µmol, 0.24 equiv.) and tripotassium phosphate (1.53 g, 7.20 mmol, 25.0 equiv.) were dissolved in dry THF (120 mL). The mixture was stirred for 23 h at 80 °C. The solvent was removed under reduced pressure and the residue was redissolved in CH_2Cl_2 (100 mL). The organic phase was consecutively washed with H_2O (3 × 100 mL), dried over Na_2SO_4, filtered and removed the solvent under reduced pressure. The crude product was purified by flash column chromatography on silica gel (CH_2Cl_2/*n*-pentane, 1:1) to afford the title compound **127** as a purple solid (108 mg, 150 µmol, 52%).

***R*f** = 0.25 (CH_2Cl_2/*n*-pentane, 1:1). – **^{1}H NMR** (400 MHz, THF-d_8): δ = 9.82 (s, 1H, C*H*O), 8.89 – 8.83 (m, 2H, $H_{pyrrole}$), 8.82 – 8.78 (m, 2H, $H_{pyrrole}$), 8.75 (d, ^3J = 4.8 Hz, 1H, $H_{pyrrole}$), 8.72 (s, 1H, $H_{pyrrole}$), 8.62 (d, ^3J = 4.9 Hz, 1H, $H_{pyrrole}$), 8.29 – 8.15 (m, 6H, $H_{aromatic}$), 7.82 – 7.74 (m, 8H, $H_{aromatic}$), 7.74 – 7.70 (m, 3H, $H_{aromatic}$), 7.66 (dd, *J* = 7.9, 1.5 Hz, 1H, $H_{aromatic}$), 7.52 (dd, *J* = 7.6, 1.3 Hz, 1H, $H_{aromatic}$), 7.43 (td, *J* = 7.5, 1.5 Hz, 1H, $H_{aromatic}$), 7.34 – 7.28 (m, 1H, $H_{aromatic}$), 7.28 – 7.17 (m, 2H, $H_{aromatic}$), 7.17 – 7.10 (m, 1H, $H_{aromatic}$), –2.54 (bs, 2H, N*H*) ppm. – **^{13}C NMR** (101 MHz, THF-d_8): δ = 191.5 (+, *C*HO), 167.0 (C_q), 143.5 (C_q), 143.4 (C_q), 143.0 (C_q), 141.3 (C_q), 136.4 (+, CH), 135.8 (+, CH), 135.6 (+, CH), 135.4 (+, CH), 133.4 (+, CH), 133.3 (+, CH), 128.9 (+, CH), 128.7 (+, CH), 128.1 (+, CH), 127.9 (+, CH), 127.8 (+, CH), 127.4 (+, CH), 122.0 (C_q), 121.6 (C_q), 121.3 (C_q), 121.1 (C_q) ppm. – **UV-Vis** (CH_2Cl_2): λ_{max} (rel. absorption) = 218 (0.56), 310 (0.29), 375 (0.52), 421 (3.22), 519 (0.38), 533 (0.13), 594 (0.10), 650 (0.07) nm. – **IR** (ATR): $\tilde{\nu}$ = 2917, 2849, 1690, 1595, 1469, 1439, 1388, 1347, 1261, 1194, 1177, 1146, 1096, 1071, 1030, 1000, 980, 963, 823, 798, 756, 724, 713, 697, 671, 657, 635, 619, 569, 558, 513 cm^{-1}. – **MS** (ESI): *m/z* (%) = 718.3 (4) $[M]^+$, 719.3 (100) $[M+H]^+$, 720.3 (55) $[M+H]^+$, 721.3 (15) $[M+H]^+$. – **HRMS** ($C_{51}H_{35}N_4O$): calc.: 719.2811, found: 719.2770.

Additional information on the reaction details is available *via* the Chemotion repository: https://dx.doi.org/10.14272/reaction/SA-FUHFF-UHFFFADPSC-KXWSDZYAKU-UHFFFADPSC-NUHFF-NTVBH-NUHFF-ZZZ

Additional information on the analysis of the target compound is available *via* the Chemotion repository: https://dx.doi.org/10.14272/KXWSDZYAKUDZPF-ROVQYOBGSA-N.1

6.4.2 Cofacial bisporphyrin ligands

1,2-Phenylene-bis-5-(10,15,20-triphenylporphyrin) (**128**)[83]

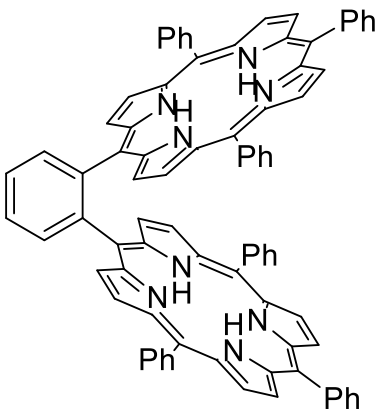

Under an argon atmosphere 5-(2-formylphenyl)-10,15,20-triphenylporphyrin (**125**) (100 mg, 156 µmol, 1.00 equiv.) was dissolved in dry CH_2Cl_2 (80 mL). A stream of argon was passed through the mixture for 15 min to remove dissolved oxygen. Subsequently, freshly distilled benzaldehyde (145 µL, 151 mg, 1.42 mmol, 9.15 equiv.) and pyrrole (153 µL, 148 mg, 2.20 mmol, 14.2 equiv.) were added. After 5 min, TFA (12.9 µL, 19.1 mg, 168 µmol, 1.08 equiv.) was added. The mixture was stirred for 115 h in the dark. DDQ (105 mg, 2.20 mmol, 14.2 equiv.) was added and stirred for a further 1 h. Then, NEt_3 (5 mL) was added and the crude mixture was concentrated under reduced pressure. The mixture was filtered through a short layer of silica gel eluting with CH_2Cl_2 and purified by flash column chromatography on silica gel (1 × CH_2Cl_2/*n*-pentane, 1:1, 1 × CH_2Cl_2/*n*-pentane, 2:1) to afford the title compound **128** as a purple solid (30.6 mg, 26.6 µmol, 17%).

***R*f** (CH_2Cl_2/*n*-pentane, 1:1) = 0.63. – **^{1}H NMR** (500 MHz, THF-d_8): δ = 9.28 (d, ^3J = 4.7 Hz, 4H, $H_{pyrrole}$), 8.87 (dd, J = 5.7, 3.4 Hz, 2H, $H_{aromatic}$), 8.39 – 8.28 (m, 14H, 12$H_{pyrrole}$, 2$H_{aromatic}$), 8.03 – 7.97 (m, 2H $H_{aromatic}$), 7.80 (d, ^3J = 7.3 Hz, 4H, $H_{aromatic}$), 7.74 – 7.69 (m, 4H, $H_{aromatic}$), 7.68 – 7.52 (m, 14H), $H_{aromatic}$, 7.50 – 7.40 (m, 6H, $H_{aromatic}$), –3.82 (bs, 4H, N*H*) ppm. – **^{13}C NMR** (126 MHz, THF-d_8): δ = 146.7 (C_q), 143.1 (C_q), 143.1 (C_q), 135.5 (+, CH), 135.2 (+, CH), 135.1 (+, CH), 135.0 (+, CH), 128.4 (C_q), 128.2 (C_q), 127.5 (+, CH), 127.5 (+, CH), 127.4 (+, CH), 120.6 (C_q), 120.2 (C_q), 119.1 (C_q) ppm. – **UV-Vis** (CH_2Cl_2): λ_{max} (rel. absorption) = 218 (0.24), 409 (1.33), 419 (1.48), 520 (0.12), 552 (0.06), 594 (0.05), 649 (0.03) nm. – **IR** (ATR): $\tilde{\nu}$ = 3313, 2921, 2846, 1714, 1693, 1595, 1470, 1439, 1349, 1071, 1033, 1001, 980, 965, 798, 749, 727, 700 cm^{-1}. – **HRMS** (ESI) ($H_5C_{82}H_{50}N_8$): calc.: 1151.4544, found: 1151.4598.

Additional information on the reaction details is available *via* the Chemotion repository: https://dx.doi.org/10.14272/reaction/SA-FUHFF-UHFFFADPSC-GCDCSJMXKZ-UHFFFADPSC-NUHFF-NWDCB-NUHFF-ZZZ

Additional information on the analysis of the target compound is available *via* the Chemotion repository: https://dx.doi.org/10.14272/GCDCSJMXKZHSKI-XZDYDVNVSA-N.1

1,2-Phenylene-(5-(10,20-*para*-diethoxycarbonylphenylporphyrin),5-(10,15,20-triphenylporphyrin)) (**129**)[83]

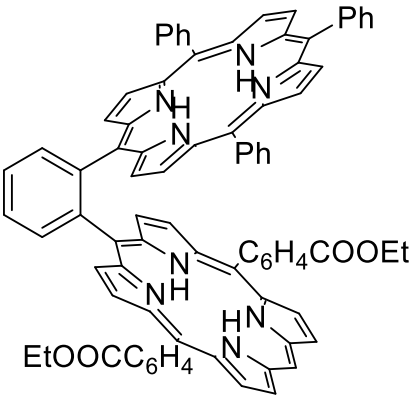

Under an argon atmosphere, 5-(2-formylphenyl)-10,20-diethoxycarbonylphenylporphyrin (**126**) (72.0 mg, 101 µmol, 1.00 equiv.) was dissolved in dry CH_2Cl_2 (20 mL). A stream of argon was passed through the mixture for 15 min to remove dissolved oxygen. Subsequently, freshly distilled benzaldehyde (41 µL, 42.1 mg, 397 µmol, 3.93 equiv.) and pyrrole (42 µL, 41.1 mg, 613 µmol, 6.07 equiv.) were added and stirred. After 5 min, $BF_3 \cdot OEt_2$ (44 µL, 49.7 mg, 350 µmol, 3.47 equiv.) was added. The mixture was stirred for 21.5 h in the dark. DDQ (50.7 mg, 223 µmol, 2.21 equiv.) was added and stirred for a further 1 h. The crude mixture was concentrated under reduced pressure, filtered through a short layer of silica gel eluting with (CH_2Cl_2/EtOAc, 100:1) and purified three times by flash column chromatography on silica gel (CH_2Cl_2) to afford the title compound **129** as a purple solid (19.6 mg, 16.1 µmol, 16%).

***R*f** (CH_2Cl_2) = 0.54. – **^{1}H NMR** (500 MHz, THF-d_8): δ = 9.41 – 9.34 (m, 4H, $H_{pyrrole}$), 8.94 (dd, J = 7.3, 1.9 Hz, 1H, $H_{aromatic}$), 8.84 (dd, J = 7.5, 1.6 Hz, 1H, $1H_{aromatic}$), 8.46 – 8.40 (m, 2H, $H_{aromatic}$), 8.39 – 8.28 (m, 10H, $H_{aromatic}$), 8.20 (d, ^3J = 4.7 Hz, 2H, $H_{pyrrole}$), 8.15 – 8.10 (m, 2H, $H_{aromatic}$), 7.91 – 7.84 (m, 3H, $H_{aromatic}$), 7.83 – 7.74 (m, 5H, $H_{aromatic}$), 7.73 – 7.68 (m, 2H, $H_{aromatic}$), 7.63 – 7.57 (m, 4H, $H_{aromatic}$), 7.52 – 7.42 (m, 3H, $H_{aromatic}$), 7.43 – 7.36 (m, 3H, $H_{aromatic}$), 7.19 – 7.09 (m, 1H, $H_{aromatic}$), 7.02 – 6.80 (m, 1H, $H_{aromatic}$) 4.62 (qt, J = 7.5, 3.9 Hz, 4H, COC*H*$_2$), 1.61 (t, ^3J = 7.2 Hz, 6H, CH_2CH_3). –3.70 (bs, 2H, N*H*), –4.75 (bs, 2H, N*H*) ppm. – **^{13}C NMR** (126 MHz, $CDCl_3$): δ = 167.0 (C_q, *C*OOEt), 146.2 (C_q), 145.7 (C_q), 145.5 (C_q), 141.9 (C_q), 134.8 (+, CH), 134.6 (+, CH), 134.5 (+, CH), 134.5 (+, CH), 134.3 (+, CH), 134.2 (+, CH), 134.2 (+, CH), 129.7 (+, CH), 127.9 (+, CH), 127.9 (+, CH), 127.6 (+, CH), 127.5 (+, CH), 127.3 (+, CH), 127.2 (+, CH), 126.6 (+, CH), 126.6 (+, CH), 126.4 (+, CH), 119.8 (C_q), 119.5 (C_q), 118.0 (C_q), 117.3 (C_q), 61.5 (–, CO*C*H$_2$), 14.8, (+, CH$_2$*C*H$_3$) ppm. – **UV-Vis** (CH_2Cl_2): λ_{max} (rel. absorption) = 231 (0.38), 299 (0.26), 406 (3.17), 521 (0.21), 561 (0.07), 595 (0.07), 653 (0.03) nm. – **IR** (ATR): $\tilde{\nu}$ = 2953, 2919, 2850, 1713, 1660, 1632, 1605, 1554, 1463, 1441, 1401, 1377, 1366, 1349, 1306, 1264, 1176, 1154, 1098, 1054, 1021, 1000, 992, 979, 963, 958, 851, 793, 754, 722, 701, 663, 636 cm^{-1}. – **HRMS** (ESI) ($H_5C_{82}H_{54}N_8O_4$): calc.: 1219.4654, found: 1219.4662.

Additional information on the reaction details is available *via* the Chemotion repository: https://dx.doi.org/10.14272/reaction/SA-FUHFF-UHFFFADPSC-KSCHWMPABP-UHFFFADPSC-NUHFF-NCLAH-NUHFF-ZZZ.1

Additional information on the analysis of the target compound is available *via* the Chemotion repository: https://dx.doi.org/10.14272/KSCHWMPABPZXSS-WAZFGYTESA-N.2

1,2-Phenylene-(2-(5,10,15,20-tetraphenylporphyrin),5-(10,15,20-triphenylporphyrin)) (**130**)[83]

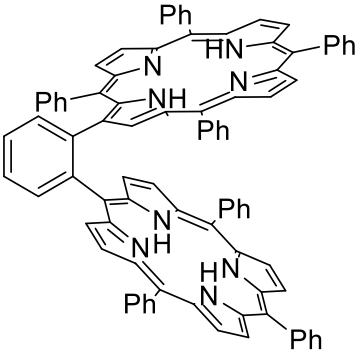

Under an argon atmosphere 2-(2-formylphenyl)-5,10,15,20-tetraphenylporphyrin (**127**) (50.0 mg, 69.6 µmol, 1.00 equiv.) was dissolved in dry CH_2Cl_2 (30 mL). A stream of argon was passed through the mixture for 15 min to remove dissolved oxygen. Subsequently, freshly distilled benzaldehyde (65 µL, 67.4 mg, 635 µmol, 9.13 equiv.) and pyrrole (68 µL, 65.7 mg, 979 µmol, 14.1 equiv.) were added and stirred. After 5 min, TFA (17 µL, 25.5 mg, 224 µmol, 3.21 equiv.) was added. The mixture was stirred for 46 h in the dark. DDQ (17.4 mg, 76.7 µmol, 1.10 equiv.) was added and stirred for a further 1 h. The crude mixture was concentrated under reduced pressure, filtered through a short layer of silica gel eluting with CH_2Cl_2 and purified by flash column chromatography on silica gel (1 × CH_2Cl_2/*n*-pentane, 1:1 – 1 × CH_2Cl_2/*n*-pentane, 2:1, 1 × CH_2Cl_2/*n*-pentane, 3:1) to afford the title compound **130** as a red solid (4.0 mg, 3.26 µmol, 4.7%).

***R*f** (CH_2Cl_2/*n*-pentane, 3:2) = 0.55. – **^{1}H NMR** (500 MHz, THF-d_8/pyridine-d_5, 1:1): δ = 9.48 (bs, 1H, $H_{pyrrole}$), 8.99 (bs, 1H, $H_{pyrrole}$), 8.88 (bs, 1H, $H_{pyrrole}$), 8.78 (bs, 1H, $H_{pyrrole}$), 8.73 (bs, 1H, $H_{pyrrole}$), 8,68 (bs, 1H, $H_{pyrrole}$), 8.66 – 8.59 (m, 6H), 8.59 – 8.54 (m, 2H), 8.26 (bs, 1H), 8.23 (d, ^3J = 4.9 Hz, 1H, $H_{pyrrole}$), 8.15 (dd, J = 7.2, 1.8 Hz, 2H, $H_{aromatic}$), 8.13 – 8.07 (m, 3H,), 8.05 – 7.95 (m, 2H), 7.90 – 7.82 (m, 7H, $H_{aromatic}$), 7.80 – 7.67 (m, 10H, $H_{aromatic}$), 7.64 – 7.50 (m, 8H), 7.50 – 7.39 (m, 4H, $H_{aromatic}$), 7.29 (bs, 1H), 5.94 (t, ^3J = 7.5 Hz, 1H), –2.58 (bs, 2H, N*H*), –2.95 (bs, 2H, N*H*) ppm. – **^{13}C NMR** (126 MHz, THF-d_8 + pyridine-d_5): δ = 143.6 (C_q), 143.4 (C_q), 143.2 (C_q), 142.7 (C_q), 141.7 (C_q), 141.6 (C_q), 135.9 (+, CH), 135.8 (+, CH), 135.5 (+, CH), 135.4 (+, CH), 129.1 (+, CH), 128.7 (+, CH), 128.6 (+, CH), 128.3 (+, CH), 127.7 (+, CH), 127.6 (+, CH), 127.4 (+, CH), 126.6 (+, CH), 125.5 (+, CH), 124.9 (+, CH), 121,8 (C_q), 121.1 (C_q), 120.9 (C_q), 120.9 (C_q), 120.5 (C_q), 120.4 (C_q) ppm. – **UV-Vis** (CH_2Cl_2): λ_{max} (rel. absorption) =16), 417 (1.17), 436 (0.68), 521 (0.10), 555 (0.05), 596 (0.03), 651 (0.02) nm. – **IR** (ATR): $\tilde{\nu}$ = 3313, 2956, 2919, 2868, 2850, 1683, 1598, 1465, 1439, 1349, 1259, 1177, 1092, 1071, 1052, 1028, 1020, 1001, 982, 965, 798, 747, 727, 700, 669, 659, 639, 620, 591, 585, 572, 561, 554, 540, 520, 510, 503, 493, 483, 469, 424, 415, 394, 380 cm^{-1}. – **HRMS** (ESI) ($H_5C_{88}H_{54}N_8$): calc.: 1227.4857, found: 1227.4876.

Additional information on the reaction details is available *via* the Chemotion repository: https://dx.doi.org/10.14272/reaction/SA-FUHFF-UHFFFADPSC-CRQVKDBVTV-UHFFFADPSC-NUHFF-NOQOQ-NUHFF-ZZZ

Additional information on the analysis of the target compound is available *via* the Chemotion repository: https://dx.doi.org/10.14272/CRQVKDBVTVUHKQ-OMBJQYCLSA-N.1

6.4.3 Homobimetallic *o*-phenylene-linked porphyrin complexes

[1,2-Phenylene-bis-5-(10,15,20-triphenylporphyrin)]-dimanganese(III)-dichloride (**131**)[380]

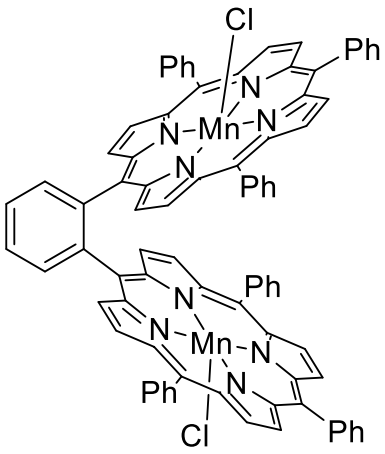

1,2-Phenylene-bis-5-(10,15,20-triphenyporphyrin) (**128**) (1.0 mg, 0.87 µmol, 1.00 equiv.) and $MnCl_2$ (1.1 mg, 8.74 µmol, 10.1 equiv.) were dissolved in DMF (1 mL). The reaction mixture was stirred for 15 h at 150 °C. Afterward, the solvent was removed under reduced pressure. The crude product was purified by flash column chromatography on silica gel (CH_2Cl_2/MeOH, 10:1) to afford the title compound **131** as a brown solid (1.0 mg, 0.75 µmol, 86%).

***R*f** (CH_2Cl_2/MeOH, 9:1) = 0.55. – **UV-Vis** (CH_2Cl_2): λ_{max} (rel. absorption) = 222 (2.35), 336 (0.02), 418 (0.12), 473 (0.06), 606 (0.01). – **IR** (ATR): $\tilde{\nu}$ = 3350, 2955, 2921, 2851, 1725, 1451, 1259, 1091, 1074, 1055, 1014, 799, 701 cm^{-1}. – **HRMS** (ESI) ($Mn_2ClC_{82}H_{50}N_8$): calc.: 1291.2602, found: 1291.2617.

Additional information on the reaction details is available *via* the Chemotion repository: https://dx.doi.org/10.14272/reaction/SA-FUHFF-UHFFFADPSC-WGEQYAUFPW-UHFFFADPSC-NUHFF-LJEXN-NUHFF-ZZZ

Additional information on the analysis of the target compound is available *via* the Chemotion repository: https://dx.doi.org/10.14272/WGEQYAUFPWFRFW-PBDMMGFFSA-L.1

[1,2-Phenylene-bis-5-(10,15,20-triphenylporphyrin)]-*µ*-oxo-diiron(III) (**132**)[7]

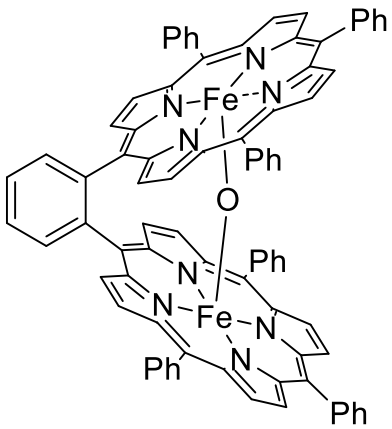

1,2-Phenylene-bis-5-(10,15,20-triphenyporphyrin) (**128**) (3.0 mg, 2.61 µmol, 1.00 equiv.) and $FeBr_2$ (5.2 mg, 24.1 µmol, 9.24 equiv.) were dissolved in DMF (3 mL). The reaction mixture was stirred for 1 h at 140 °C. Afterward, the solvent was removed under reduced pressure. The crude product was diluted with $CHCl_3$ (30 mL) and washed with 1 M aqueous HCl (3 × 20 mL), saturated aqueous $NaHCO_3$ solution (3 × 20 mL) and H_2O (3 × 20 mL). The combined

organic phases were dried over Na_2SO_4, filtered and the solvent was removed under reduced pressure. The crude product was purified by flash column chromatography on silica gel (CH_2Cl_2/MeOH, 10:1) to afford the title compound **132** as a brown solid (3.1 mg, 2.43 µmol, 93%).

***R*f** (CH_2Cl_2/MeOH, 9:1). = 0.54. – **UV-Vis** (CH_2Cl_2): λ_{max} (rel. absorption) = 218 (0.24), 363 (0.25), 410 (1.33), 419 (1.48), 520 (0.12), 552 (0.06), 594 (0.05), 649 (0.03) nm. – IR (ATR): $\tilde{\nu}$ = 3350, 2955, 2921, 2851, 1725, 1451, 1259, 1091, 1074, 1055, 1014, 799, 701 cm^{-1}. – **HRMS** (ESI) ($Fe_2OC_{82}H_{50}N_8$): calc.: 1274.2807, found: 1274.2840.

Additional information on the reaction details is available *via* the Chemotion repository: https://dx.doi.org/10.14272/reaction/SA-FUHFF-UHFFFADPSC-FPUPSGZDLX-UHFFFADPSC-NUHFF-NVIHC-NUHFF-ZZZ

Additional information on the analysis of the target compound is available *via* the Chemotion repository: https://dx.doi.org/10.14272/FPUPSGZDLXQFJX-LKHNKGCCSA-N

[1,2-Phenylene-bis-5-(10,15,20-triphenylporphyrin)]-dinickel(II) (**133**)[178]

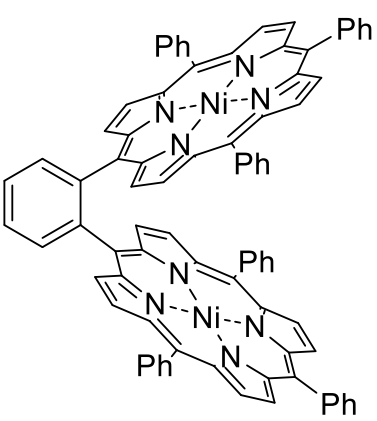

1,2-Phenylene-bis-5-(10,15,20-triphenyporphyrin) (**128**) (1.9 mg, 1.65 µmol, 1.00 equiv.) and $Ni(acac)_2$ (3.3 mg, 12.8 µmol, 7.76 equiv.) were dissolved in DMF (3 mL). Subsequently, the reaction mixture was stirred for 19.5 at 100 °C. Afterward, the solvent was removed under reduced pressure. The crude product was purified by flash column chromatography on silica gel (CH_2Cl_2/*n*-pentane, 1:1) to afford the title compound **133** as a purple solid (1.8 mg, 1.42 µmol, 86%).

***R*f** (CH_2Cl_2/*n*-pentane, 1:2) = 0.66. – **^{1}H NMR** (500 MHz, THF-d_8): δ = 8.91 (^3J = 4.9 Hz, 4H, $H_{pyrrole}$), 8.74 (dd, J = 5.7, 3.4 Hz, 2H, $H_{aromatic}$), 8.28 – 8.22 (m, 12H, $H_{pyrrole}$), 8.21 (dd, J = 5.4, 3.6 Hz, 2H, $H_{aromatic}$), 7.81 – 7.57 (m, 8H, $H_{aromatic}$), 7.58 – 7.19 (m, 22H, $H_{aromatic}$) ppm. – **^{13}C NMR** (126 MHz, THF-d_8): δ = 144.1 (C_q), 143.6 (C_q), 143.1 (C_q), 142.9 (C_q), 142.7 (C_q), 141.9 (C_q), 141.8 (C_q), 135.5 (+, CH), 135.4 (+, CH), 134.4 (C_q), 133.2 (+, CH), 132.4 (+, CH), 132.2 (+, CH), 132.1 (+, CH), 128.5 (C_q), 127.7 (+, CH), 119.1 (C_q) ppm. – **UV-Vis** (CH_2Cl_2): λ_{max} (rel. absorption) = 218 (0.15), 295 (0.06), 325 (0.04), 405 (0.60), 536 (0.04) nm. – **IR** (ATR): $\tilde{\nu}$ = 3293, 3063, 2917, 2871, 2849, 1659, 1598, 1550, 1465, 1441, 1351, 1075, 1004, 796, 752, 700 cm^{-1}. – **HRMS** (ESI) ($Ni_2C_{82}H_{50}N_8$): calc.: 1264.2853, found: 1264.2882.

Additional information on the reaction details is available *via* the Chemotion repository: https://dx.doi.org/10.14272/reaction/SA-FUHFF-UHFFFADPSC-SNXKMNZEFG-UHFFFADPSC-NUHFF-NCDDW-NUHFF-ZZZ

Additional information on the analysis of the target compound is available *via* the Chemotion repository: https://dx.doi.org/10.14272/SNXKMNZEFGGYRK-IGJFLPGISA-N.1

[1,2-Phenylene-bis-5-(10,15,20-triphenylporphyrin)]-dicopper(II) (**134**)[381]

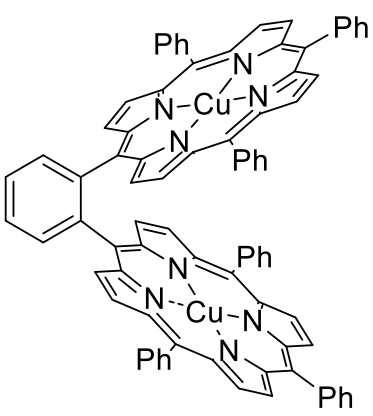

1,2-Phenylene-bis-5-(10,15,20-triphenyporphyrin) (**128**) (3.00 mg, 2.61 µmol, 1.00 equiv.) and $Cu(OAc)_2$ (1.70 mg, 9.36 µmol, 3.60 equiv.) were dissolved in a mixture of $CHCl_3$ and MeOH (10:1, 2.2 mL). The reaction mixture was stirred for 2 h at 80 °C. Subsequently, the solvent was removed under reduced pressure. The crude product was purified by flash column chromatography on silica gel (CH_2Cl_2/*n*-pentane, 1:1) to afford the title compound **134** as a red solid (3.1 mg, 2.43 µmol, 93%).

***R*f** (CH_2Cl_2/*n*-pentane, 1:2) = 0.69. – **UV-Vis** (CH_2Cl_2): λ_{max} (rel. absorption) = 219 (0.57), 302 (0.19), 405 (3.02), 547 (0.14) nm. – **IR** (ATR): $\tilde{\nu}$ = 3293, 3063, 2917, 2871, 2849, 1659, 1598, 1550, 1465, 1441, 1351, 1075, 1004, 796, 752, 700 cm^{-1}. – **HRMS** (ESI) ($Cu_2C_{82}H_{50}N_8$): calc.: 1274.2753, found: 1274.2784.

Additional information on the reaction details is available *via* the Chemotion repository: https://dx.doi.org/10.14272/reaction/SA-FUHFF-UHFFFADPSC-HGYDNOGDZH-UHFFFADPSC-NUHFF-NCDDW-NUHFF-ZZZ

Additional information on the analysis of the target compound is available *via* the Chemotion repository: https://dx.doi.org/10.14272/HGYDNOGDZHKGHX-IGJFLPGISA-N.1

[1,2-Phenylene-bis-5-(10,15,20-triphenylporphyrin)]-dizinc(II) (**135**)[379]

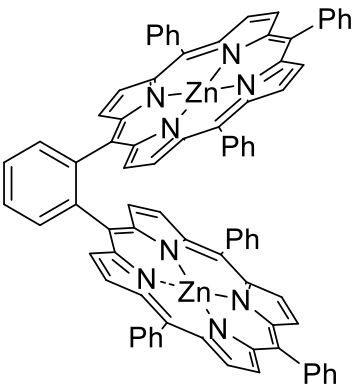

1,2-Phenylene-bis-5-(10,15,20-triphenyporphyrin) (**128**) (3.00 mg, 2.61 µmol, 1.00 equiv.) and $Zn(OAc)_2$ (1.31 mg, 10.4 µmol, 4.00 equiv.) were dissolved in a mixture of $CHCl_3$ and MeOH (10:1, 3.3 mL). The reaction mixture was stirred for 1 h at room temperature. Subsequently, the solvent was removed under reduced pressure. The crude product was purified by flash column chromatography on silica gel (CH_2Cl_2/*c*Hex, 1:1) to afford the title compound **135** as a purple solid (2.40 mg, 1.88 µmol, 72%).

***R*f** (CH_2Cl_2/*n*-pentane, 1:1) = 0.63. – **^{1}H NMR** (500 MHz, THF-d_8): δ = 9.57 (^3J = 4.7 Hz, 4H, $H_{pyrrole}$), 8.68 (dd, J = 5.7, 3.4 Hz, 2H, $H_{aromatic}$), 8.56 (^3J = 4.6 Hz, 4H, $H_{pyrrole}$), 8.45 – 8.41 (m, 8H, $H_{pyrrole}$), 8.21 (dd, J = 5.6, 3.6 Hz, 2H, $H_{aromatic}$), 8.00 – 7.96 (m, 2H, $H_{aromatic}$), 7.89 – 7.86 (m, 4H, $H_{aromatic}$), 7.80 – 7.76 (m, 4H, $H_{aromatic}$), 7.74 – 7.67 (m, 8H, $H_{aromatic}$), 7.65 – 7.60 (m, 6H, $H_{aromatic}$), 7.59 – 7.54 (m, 4H, $H_{aromatic}$), 7.48 – 7.43 (m, 2H, $H_{aromatic}$) ppm. – **^{13}C NMR** (126 MHz, THF-d_8): δ = 151.7 (C_q), 150.5 (C_q), 150.3 (C_q), 150.2 (C_q), 144.5 (C_q), 144.4 (C_q), 136.3 (+, CH), 135.5 (+, CH), 135.4 (+, CH), 135.2 (+, CH), 133.9 (C_q), 131.7 (+, CH), 131.6 (+, CH), 131.4 (+, CH), 128.1 (C_q), 127.3 (+, CH), 127.2 (+, CH), 127.1 (+, CH), 120.9 (C_q) ppm. – **UV-Vis** (CH_2Cl_2): λ_{max} (rel. absorption) = 218 (0.26), 316 (0.14), 357 (0.13), 409 (1.51), 430 (0.50), 559 (0.08) nm. – **IR** (ATR): $\tilde{\nu}$ = 2953, 2918, 2850, 1596, 1523, 1485, 1460, 1441, 1412, 1377, 1366, 1337, 1261, 1225, 1203, 1176, 1156, 1069, 1001, 993, 965, 912, 878, 841, 795, 755, 727, 717, 703, 669, 662, 620 cm^{-1}. – **HRMS** (ESI) ($Zn_2C_{82}H_{50}N_8$): calc.: 1278.2718, found: 1278.2724.

Additional information on the reaction details is available *via* the Chemotion repository: https://dx.doi.org/10.14272/reaction/SA-FUHFF-UHFFFADPSC-QXJPAKPAHZ-UHFFFADPSC-NUHFF-NCDDW-NUHFF-ZZZ

Additional information on the analysis of the target compound is available *via* the Chemotion repository: https://dx.doi.org/10.14272/QXJPAKPAHZFTEB-IGJFLPGISA-N.1

[1,2-Phenylene-bis-5-(10,15,20-triphenylporphyrin)]-dipalladium(II) (**136**)[382]

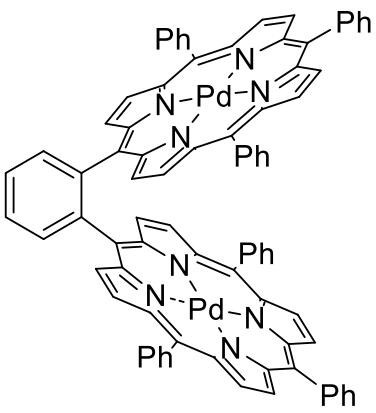

1,2-Phenylene-bis-5-(10,15,20-triphenyporphyrin) (**128**) (1.1 mg, 0.96 µmol, 1.00 equiv.) and $PdCl_2$ (1.4 mg, 7.89 µmol, 8.14 equiv.) were dissolved in DMF (3 mL). The reaction mixture was stirred for 19.5 h at 100 °C. Subsequently, the solvent was removed under reduced pressure. The crude product was purified by flash column chromatography on silica gel (CH_2Cl_2/*n*-pentane, 1:1) to afford the title compound **136** as a red-purple solid (0.90 mg, 0.66 µmol, 69%).

***R*f** (CH_2Cl_2/*n*-pentane, 1:2) = 0.61. – **^{1}H NMR** (500 MHz, THF-d_8): δ = 8.96 (dd, J = 5.6, 3.4 Hz, 2H, $H_{aromatic}$), 8.82 (d, ^3J = 4.9 Hz, 4H, $H_{pyrrole}$), 8.35 (dd, J = 5.4, 3.7 Hz, 2H, $H_{aromatic}$), 8.33 (d, ^3J = 4.9 Hz, 4H, $H_{pyrrole}$), 8.16 (d, ^3J = 4.8 Hz, 4H, $H_{pyrrole}$), 7.98 – 7.94 (m, 2H, $H_{aromatic}$), 7.90 (d, ^3J = 4.9 Hz, 4H, $H_{pyrrole}$), 7.79 – 7.76 (m, 2H, $H_{aromatic}$), 7.69 – 7.58 (m, 10H, $H_{aromatic}$), 7.58 – 7.53 (m, 4H, $H_{aromatic}$), 7.50 –7.45 (m, 8H, $H_{aromatic}$), 6.74 (dd, J = 7.4, 1.4 Hz, 4H, $H_{aromatic}$) ppm. – **^{13}C NMR** (126 MHz, THF-d_8): δ = 141.5 (C_q), 135.1 (+, CH), 134.7 (+, CH), 134.5 (+, CH), 133.2 (+, CH), 130.9 (+, CH), 130.6 (+, CH), 130.1 (+, CH), 127.4 (+, CH), 127.3 (+, CH), 110.5 (C_q) ppm (not complete due to a small amount of substance). – **UV-Vis** (CH_2Cl_2): λ_{max} (rel. absorption) = 218 (0.11), 274 (0.04), 309 (0.03), 406 (0.28), 531 (0.02) nm. – **IR** (ATR): $\tilde{\nu}$ = 3027, 2959, 2914, 2851, 2166, 1717, 1659, 1595, 1448, 1350, 1262, 1077, 1009, 798, 749, 705 cm^{-1}. – **HRMS** (ESI) ($Pd_2C_{82}H_{50}N_8$): calc.: 1360.2259, found: 1360.2267.

Additional information on the reaction details is available *via* the Chemotion repository: https://dx.doi.org/10.14272/reaction/SA-FUHFF-UHFFFADPSC-XSSRUEVVUK-UHFFFADPSC-NUHFF-NCDDW-NUHFF-ZZZ

Additional information on the analysis of the target compound is available *via* the Chemotion repository: https://dx.doi.org/10.14272/XSSRUEVVUKKETO-IGJFLPGISA-N.1

[1,2-Phenyl-bis-5-(10,15,20-triphenylporphyrin))]-dilead(II) (**137**)[383]

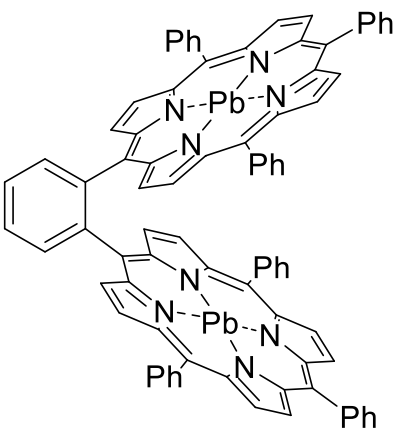

A crimp vial was charged with 1,2-phenylene-bis-5-(10,15,20-triphenylporphyrin) (**128**) (3.0 mg, 2.6 µmol, 1.00 equiv.) and $Pb(OAc)_2$ (31.7 mg, 119 µmol, 45.6 equiv.) under an argon atmosphere. Dry DMF (2 mL) was added and the resulting solution was stirred at 170 °C for 48 h. Subsequently, the solvent was removed under reduced pressure and the crude product was dissolved in CH_2Cl_2 and washed with H_2O (3 × 5 mL). The crude product was purified by flash column chromatography on silica gel (CH_2Cl_2/*n*-pentane, 2:1) to afford the title compound **137** in 95% purity as a brown solid (2.1 mg, 1.34 µmol, 52%).

***R*f** (CH_2Cl_2/*n*-pentane, 1:1) = 0.55. – **^{1}H NMR** (500 MHz, CD_2Cl_2): δ = 9.32 (d, ^3J = 4.6 Hz, 4H, $H_{pyrrole}$), 9.07 (dd, J = 5.7, 3.4 Hz, $2H_{aromatic}$), 8.51 (d, ^3J = 4.5 Hz, 4H, $H_{pyrrole}$), 8.46 (d, ^3J = 4.5 Hz, 4H, $H_{pyrrole}$), 8.43 (dd, J = 5.4, 3.6 Hz, 3H, $H_{aromatic}$), 8.25 (d, ^3J = 4.5 Hz, 4H, $H_{pyrrole}$), 7.72 – 7.66 (m, 7H, $H_{aromatic}$), 7.64 – 7.51 (m, 22H, $H_{aromatic}$) ppm. – **^{13}C NMR** (500 MHz, CD_2Cl_2): δ = 149.3 (C_q), 148.8 (C_q), 148.6 (C_q), 148.0 (C_q), 143.0 (+, CH), 142.7 (+, CH), 133.3 (+, CH), 132.5 (+, CH), 131.9 (+, CH) 131.7 (+, CH), 130.7 (+, CH), 128.1 (+, CH), 127.8 (+, CH), 126.8 (+, CH), 121.8 (C_q), 121.2 (C_q) ppm. – **UV-Vis** (CH_2Cl_2): λ_{max} (rel. absorption) = 223 (0.149), 251 (0.0578), 263 (0.0530), 267 (0.0531), 333 (0.0422), 417 (0.0987), 443 (0.0414), 466 (0.0596) nm. – **IR** (ATR): $\tilde{\nu}$ = 2953, 2922, 2851, 1684, 1465, 1441, 1377, 1327, 1261, 1200, 1176, 1069, 1010, 1001, 986, 966, 795, 751, 727, 717, 701 cm^{-1}. – **HRMS** (ESI) ($C_{82}H_{50}N_8Pb_2$) calc.: 1562.369, found 1562.371.

[1,2-Phenyl-bis-5-(10,15,20-triphenylporphyrin))]-dibismut(III)-dibromide (**138**)[384]

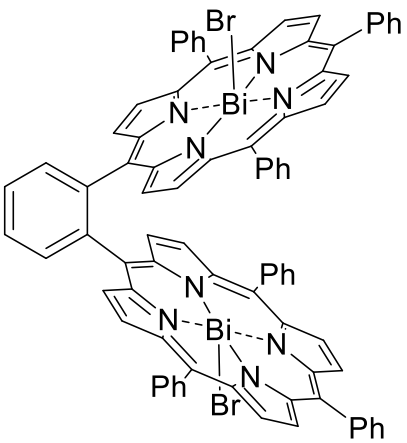

A crimp vial was charged with 1,2-phenylene-bis-5-(10,15,20-triphenylporphyrin) (**128**) (3.00 mg, 2.6 µmol, 1.00 equiv.) and $BiBr_3$ (23.4 mg, 52.2 µmol, 20.0 equiv.) under an argon atmosphere. Dry DMF (1.8 mL) was added and the resulting solution was stirred at 170 °C for 48 h. The solvent was removed under reduced pressure. The crude product was purified by flash column chromatography on

silica gel (CH_2Cl_2/MeOH, 50:1) to afford the title compound **138** in 95% purity as a green solid (0.9 mg, 0.57 µmol, 22%).

***R*f** (CH_2Cl_2/MeOH, 50:1) = 0.52. – **^{1}H NMR** (500 MHz, CD_2Cl_2): δ = 9.64 (d, J = 4.7 Hz, 4H, $H_{pyrrole}$), 8.96 (d, J = 4.7 Hz, 4H, $H_{aromatic}$), 8.82 – 8.75 (m, 4H, $H_{pyrrole}$, 8.67 (d, J = 4.6 Hz, 4H, $H_{pyrrole}$), 8.40 – 8.35 (m, 4H, $H_{pyrrole}$), 8.06 – 8.00 (m, 8H, $H_{aromatic}$), 7.89 – 7.83 (m, 10H, $H_{aromatic}$), 7.66 – 7.57 (m, 6H, $H_{aromatic}$), 7.56 – 7.46 (m, 6H, $H_{aromatic}$) ppm. – **UV-Vis** (CH_2Cl_2): λ_{max} (rel. absorption) = 223 (0.19), 253 (0.08), 298 (0.04), 330 (0.05), 361 (0.05), 386 (0.04), 407 (0.05), 471 (0.09) nm. – **IR** (ATR): $\tilde{\nu}$ = 2955, 2914, 2868, 1740, 1667, 1646, 1493, 1459, 1377, 1363, 1312, 1262, 1247, 1207, 1186, 1159, 1079, 1001, 965, 894, 799, 739, 703, 663, 646, 605, 484 cm^{-1}. – **HRMS** (ESI) ($C_{82}H_{50}Bi_2N_9O_3$) calc.: 1626.364, found: 1626.361 $[M+(NO_3)_2]^+$.

[1,2-Phenylene-(5-(10,20-*para*-diethoxycarbonylphenylporphyrin),5-(10,15,20-triphenylporphyrin))]-dimanganese(III)-dichloride (**139**)[380]

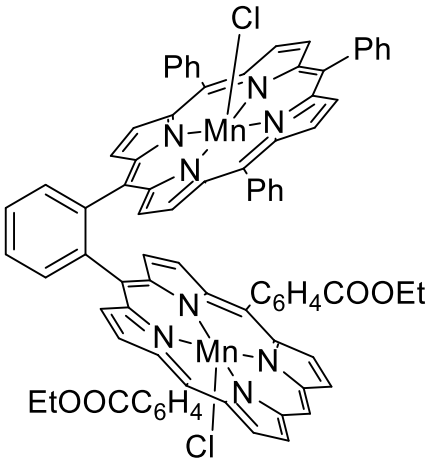

1,2-Phenylene-(5-(10,20-*para*-diethoxycarbonylphenylporphyrin),5-(10,15,20-triphenylporphyrin)) (**129**) (1.2 mg, 0.98 µmol, 1.00 equiv.) and $MnCl_2$ (0.7 mg, 5.56 µmol, 5.68 equiv.) were dissolved in DMF (1 mL). The reaction mixture was stirred for 22 h at 150 °C. Subsequently the solvent was evaporated under reduced pressure. The crude product was purified by flash column chromatography on silica gel (CH_2Cl_2/MeOH, 10:1) to afford the title compound **139** as a brown solid (1.0 mg, 0.72 µmol, 73%).

***R*f** (CH_2Cl_2/MeOH, 90:10) = 0.55. – **UV-Vis** (CH_2Cl_2): λ_{max} (rel. absorption) = 232 (0.16), 345 (0.12), 378 (0.14), 471 (0.17), 578 (0.02), 616 (0.02) nm. – **IR** (ATR): $\tilde{\nu}$ = 2919, 2850, 1713, 1460, 1441, 1375, 1366, 1340, 1269, 1203, 1176, 1098, 1071, 1009, 796, 754, 734, 714, 703, 664, 455, 384 cm^{-1}. – **HRMS** (ESI) ($Mn_2ClC_{82}H_{54}N_8O_4$): calc.: 1359.2712, found: 1359.2752.

Additional information on the reaction details is available *via* the Chemotion repository: https://dx.doi.org/10.14272/reaction/SA-FUHFF-UHFFFADPSC-DYSYYPJZFG-UHFFFADPSC-NUHFF-JPGMY-NUHFF-ZZZ

Additional information on the analysis of the target compound is available *via* the Chemotion repository: https://dx.doi.org/10.14272/DYSYYPJZFGJYMY-OOBAMIPXSA-J.1

[1,2-Phenylene-(5-(10,20-*para*-diethoxycarbonylphenylporphyrin),5-(10,15,20-triphenylporphyrin))]-μ-oxo-diiron(III) (**140**)[385]

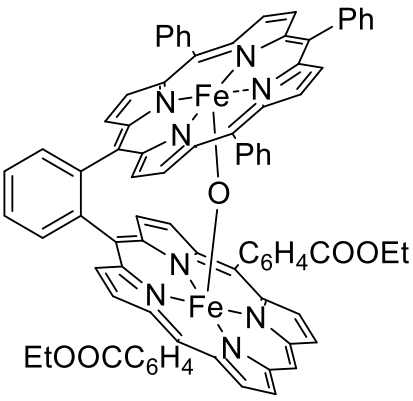

1,2-Phenylene-(5-(10,20-para-diethoxycarbonyl-phenylporphyrin),5-(10,15,20-triphenylporphyrin)) (**129**) (3.7 mg, 3.03 µmol, 1.00 equiv.) and $FeBr_2$ (6.0 mg, 27.8 µmol, 9.23 equiv.) were dissolved in DMF (3 mL). The reaction mixture was stirred for 2 h at 140 °C. Subsequently, the solvent was removed under reduced pressure. The crude product was diluted with $CHCl_3$ (30 mL) and washed with 1 M aqueous HCl (3 × 20 mL), saturated aqueous $NaHCO_3$ solution (3 × 20 mL) and H_2O (3 × 20 mL). The combined organic phases were dried over Na_2SO_4, filtered and the solvent removed under reduced pressure. The crude product was purified by flash column chromatography on silica gel (CH_2Cl_2/MeOH, 10:1) to afford the title compound **140** as a brown solid (3.8 mg, 2.83 µmol, 93%).

***R*f** (CH_2Cl_2/MeOH, 9:1) = 0.64. – **UV-Vis** (CH_2Cl_2): λ_{max} (rel. absorption) = 218 (0.40), 321 (0.32), 407 (0.88), 560 (0.06) nm. – **IR** (ATR): $\tilde{\nu}$ 2919, 2850, 1715, 1605, 1441, 1265, 1176, 1099, 1069, 1010, 992, 795, 756, 715, 701 cm^{-1}. – **HRMS** (ESI) ($Fe_2OC_{82}H_{54}N_8O_4$): calc.: 1342.2916, found: 1342.2940.

Additional information on the reaction details is available *via* the Chemotion repository: https://dx.doi.org/10.14272/reaction/SA-FUHFF-UHFFFADPSC-JZZVMMDSKU-UHFFFADPSC-NUHFF-LJYNX-NUHFF-ZZZ

Additional information on the analysis of the target compound is available *via* the Chemotion repository: https://dx.doi.org/10.14272/JZZVMMDSKUEMHK-IJEKNQBHSA-L

[1,2-Phenylene-(5-(10,20-*para*-diethoxycarbonylphenylporphyrin),5-(10,15,20-triphenylporphyrin))]-dinickel(II) (**141**)[178]

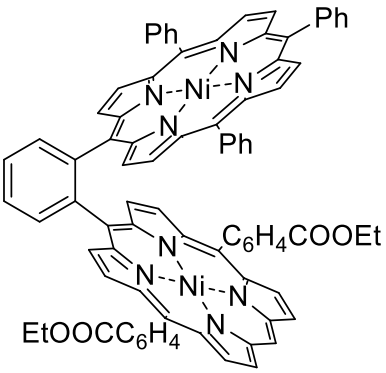

1,2-Phenylene-(5-(10,20-*para*-diethoxycarbonylphenyl-porphyrin),5-(10,15,20-triphenylporphyrin)) (**129**) (2.0 mg, 1.64 µmol, 1.00 equiv.) and $Ni(acac)_2$ (1.8 mg, 7.00 µmol, 4.27 equiv.) were dissolved in DMF (2 mL). The reaction mixture was stirred for 2 h at 100 °C. Subsequently, the solvent was removed under reduced pressure. The crude product was purified by flash column chromatography on silica gel ($CHCl_3$) to afford the title compound **141** as a purple solid (2.1 mg, 1.58 µmol, 96%).

***R*f** (CH_2Cl_2) = 0.73. – **^{1}H NMR** (500 MHz, $CDCl_3$): δ = 9.16 (bs, 2H, $H_{pyrrole}$), 8.99 (bs, 1H, $H_{pyrrole}$), 8.94 (d, ^3J = 4.8 Hz, 3H, $H_{pyrrole}$), 8.73 (dd, J = 7.6, 1.63 Hz, 2H, $H_{aromatic}$), 8.56 (bs, 4H), 8.27 – 8.21 (m, 4H), 8.14 (d, ^3J = 4.8 Hz, 4H, $H_{pyrrole}$), 7.76 (bs, 2H), 7.67 – 7.57 (bs, 4H), 7.57 – 7.35 (m, 10H), 6.71 (bs, 1H), 6.41 (bs, 3H), 5.79 (bs, 2H), 5.34 (bs, 2H), 4.71 (bs, 4H, C*H*$_2$), 1.70 (bs, 6H, C*H*$_3$) ppm. – **^{13}C NMR** (126 MHz, $CDCl_3$): δ = 167.1 (C_q, *C*OO), 145.8 (C_q), 142.9 (C_q), 140.6 (C_q), 133.9 (+, CH), 133.5 (+, CH), 132.5 (+, CH), 130.3 (+, CH), 129.6 (+, CH), 127.6 (C_q), 127.0 (+, CH), 126.9 (+, CH), 125.8 (+, CH), 124.3 (+, CH), 61.5 (–, CH_2), 14.8 (+, CH_3) ppm. – **UV-Vis** (CH_2Cl_2): λ_{max} (rel. absorption) = 223 (2.46), 326 (0.05), 401 (0.74), 534 (0.05) nm. – **IR** (ATR): $\tilde{\nu}$ = 3048, 2917, 2854, 1720, 1604, 1458, 1442, 1353, 1268, 1111, 1096, 1075, 1004, 789, 752, 698 cm^{-1}. – **HRMS** (ESI) ($Ni_2C_{82}H_{54}N_8O_4$): calc.: 1332.2963, found: 1332.3040.

Additional information on the reaction details is available *via* the Chemotion repository: https://dx.doi.org/10.14272/reaction/SA-FUHFF-UHFFFADPSC-VSSZQPPDIO-UHFFFADPSC-NUHFF-LREIQ-NUHFF-ZZZ

Additional information on the analysis of the target compound is available *via* the Chemotion repository: https://dx.doi.org/10.14272/VSSZQPPDIOMEAK-VEGFVYEWSA-L.1

[1,2-Phenylene-(5-(10,20-*para*-diethoxycarbonylphenylporphyrin),5-(10,15,20-triphenylporphyrin))]-dicopper(II)) (**142**)[381]

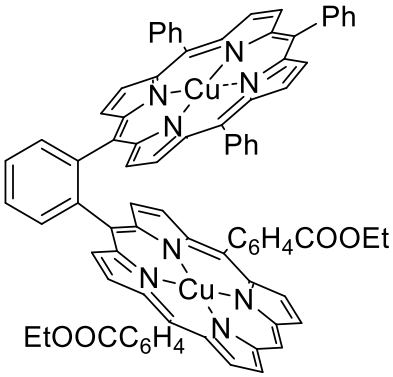

1,2-Phenylene-(5-(10,20-*para*-diethoxycarbonylphenylporphyrin-10,15,20-triphenylporphyrin)) (**129**) (1.0 mg, 0.82 µmol, 1.00 equiv.) and $Cu(OAc)_2$ (1.2 mg, 6.61 µmol, 8.06 equiv.) were dissolved in a mixture of $CHCl_3$ and MeOH (10:1, 2.1 mL). The reaction mixture was stirred for 1 h at 80 °C. Subsequently, the solvent was removed under reduced pressure. The crude product was purified by flash column chromatography on silica gel ($CHCl_3$) to afford the title compound **142** as a red solid (1.0 mg, 0.74 µmol, 90%).

***R*f** (CH_2Cl_2) = 0.66. – **UV-Vis** (CH_2Cl_2): λ_{max} (rel. absorption) = 219 (0.59), 305 (0.21), 404 (2.76), 546 (0.13) nm. – **IR** (ATR): $\tilde{\nu}$ = 2949, 2917, 2849, 1715, 1604, 1458, 1439, 1344, 1264, 1204, 1174, 1154, 1096, 1068, 1027, 1014, 996, 790, 751, 728, 714, 700, 663, 647, 402 cm^{-1}. – **HRMS** (ESI) ($Cu_2C_{82}H_{54}N_8O_4$): calc.: 1342.2863, found: 1342.2922.

Additional information on the reaction details is available *via* the Chemotion repository: https://dx.doi.org/10.14272/reaction/SA-FUHFF-UHFFFADPSC-OSSDKDCBOY-UHFFFADPSC-NUHFF-LREIQ-NUHFF-ZZZ

Additional information on the analysis of the target compound is available *via* the Chemotion repository: https://dx.doi.org/10.14272/OSSDKDCBOYMDHQ-VEGFVYEWSA-L.1

[1,2-Phenylene-(5-(10,20-*para*-diethoxycarbonylphenylporphyrin),5-(10,15,20-triphenylporphyrin))]-dizinc(II) (**143**)[379]

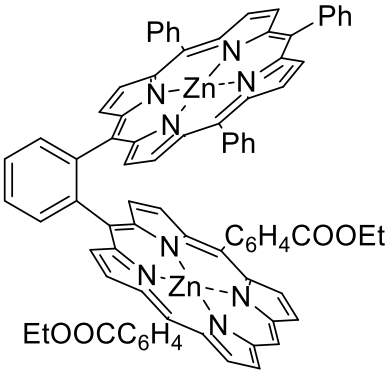

1,2-Phenylene-(5-(10,20-*para*-diethoxycarbonylphenylporphyrin),5-(10,15,20-triphenylporphyrin)) (**129**) (2.2 mg, 1.80 µmol, 1.00 equiv.) and $Zn(OAc)_2$ (3.6 mg, 19.6 µmol, 10.9 equiv.) were dissolved in a mixture of $CHCl_3$ and MeOH (10:1, 2.2 mL). The reaction mixture was stirred for 1 h at 80 °C. Subsequently, the solvent was removed under reduced pressure. The crude product was purified by flash column chromatography on silica gel (CH_2Cl_2/*n*-pentane, 1:1) to afford the title compound **143** as a purple solid (2.4 mg, 1.78 µmol, 99%).

***R*f** (CH_2Cl_2/*n*-pentane, 1:1) = 0.33. – **^{1}H NMR** (500 MHz, $CDCl_3$): δ = 9.38 (d, ^3J = 4.6 Hz, 2H, $H_{pyrrole}$), 9.37 (d, ^3J = 4.6 Hz, 2H, $H_{pyrrole}$), 8.95 – 8.89 (m, 2H, $H_{aromatic}$), 8.47 (d, ^3J = 4.6 Hz, 2H, $H_{pyrrole}$), 8.39 – 8.30 (m, 9H), 8.27 (dd, J = 7.6, 1.9 Hz, 4H, $H_{aromatic}$), 8.17 – 7.86 (m, 1H), 7.84 – 7.69 (m, 6H, $H_{aromatic}$), 7.69 – 7.56 (m, 6H, $H_{aromatic}$), 7.53 – 7.35 (m, 5H, $H_{aromatic}$), 7.26 – 7.22 (m, 4H, $H_{aromatic}$), 7.19 – 7.00 (m, 1H), 4.66 (qt, J = 7.2, 3.7 Hz, 4H, C*H*$_2$), 1.64 (t, ^3J = 7.2, 6H, C*H*$_3$) ppm. – **^{13}C NMR** (126 MHz, $CDCl_3$): δ = 167.1 (C_q, *C*OO), 150.0 (C_q), 149.6 (C_q), 149.3 (C_q), 149.1 (C_q), 148.8 (C_q), 147.1 (C_q), 146.4 (C_q), 142.5 (C_q), 134.3 (+, CH), 134.3 (+, CH), 133.7 (+, CH), 132.9 (+, CH), 132.7 (+, CH), 131.3 (+, CH), 131.2 (+, CH), 130.7 (+, CH), 130.1 (+, CH), 129.5 (C_q), 127.7 (+, CH), 127.7 (+, CH), 127.4 (+, CH), 127.2 (+, CH), 126.5 (+, CH), 120.5 (C_q), 120.2 (C_q), 119.1 (C_q), 61.5 (–, CH_2), 14.8 (+, CH_3) ppm. – **UV-Vis** (CH_2Cl_2): λ_{max} (rel. absorption) = 218 (0.18), 316 (0.10), 358 (0.08), 408 (1.42), 557 (0.07) nm. – **IR** (ATR): $\tilde{\nu}$ = 2927, 2857, 1720, 1434, 1418, 1275, 1101, 992, 875, 839, 792, 618 cm^{-1}. – **HRMS** (ESI) ($Zn_2C_{82}H_{54}N_8O_4$): calc.: 1346.2828, found: 1346.2866.

Additional information on the reaction details is available *via* the Chemotion repository: https://dx.doi.org/10.14272/reaction/SA-FUHFF-UHFFFADPSC-WVKIULBYJF-UHFFFADPSC-NUHFF-LREIQ-NUHFF-ZZZ

Additional information on the analysis of the target compound is available *via* the Chemotion repository: https://dx.doi.org/10.14272/WVKIULBYJFBQGD-VEGFVYEWSA-L.1

[1,2-Phenylene-(5-(10,20-*para*-diethoxycarbonylphenylporphyrin),5-(10,15,20-triphenylporphyrin))]-dipalladium(II) (**144**)[382]

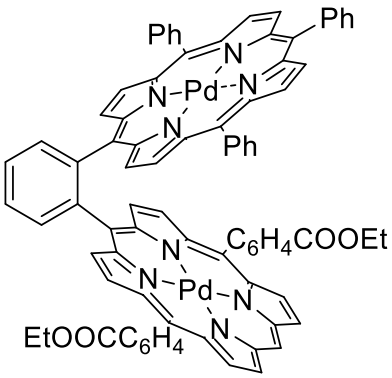

1,2-Phenylene-(5-(10,20-*para*-diethoxycarbonylphenylporphyrin),5-(10,15,20-triphenylporphyrin)) (**129**) (2.0 mg, 1.64 µmol, 1.00 equiv.) and $PdCl_2$ (1.5 mg, 8.45 µmol, 5.16 equiv.) were dissolved in DMF (2 mL). The reaction mixture was stirred for 20 h at 80 °C. Subsequently, the solvent was removed under reduced pressure. The crude product was purified by flash column chromatography on silica gel (CH_2Cl_2/*n*-pentane, 1:1) to afford the title compound **144** as a purple solid (2.3 mg, 1.61 µmol, 98%).

***R*f** (CH_2Cl_2) = 0.73. – **^{1}H NMR** (500 MHz, $CDCl_3$): δ = 8.95 (d, ^3J = 4.9 Hz, 2H, $H_{pyrrole}$), 8.92 – 8.88 (m, 1H, $H_{aromatic}$), 8.89 (d, ^3J = 4.8 Hz, 2H, $H_{pyrrole}$), 8.88 – 8.84 (m, 2H, $H_{aromatic}$), 8.33 (d, ^3J = 4.8 Hz, 2H, $H_{pyrrole}$), 8.32 – 8.26 (m, 6H), 8.22 (dd, J = 7.8, 1.9 Hz, 2H, $H_{aromatic}$), 8.19 (d, ^3J = 4.8 Hz, 2H, $H_{pyrrole}$), 8.04 (d, ^3J = 4.9 Hz, 2H, $H_{pyrrole}$), 8.02 (d, ^3J = 4.9 Hz, 2H, $H_{pyrrole}$), 7.97 – 7.92 (m, 1H), 7.69 – 7.61 (m, 6H), 7.60 – 7.51 (m, 7H), 7.51– 7.46 (m, 3H), 7.06 (dd, J = 7.7, 1.8 Hz, 2H, $H_{aromatic}$), 6.97 – 6.93 (m, 2H, $H_{aromatic}$), 4.62 (qt, ^3J = 6.9, 3.6 Hz, 4H, CH_2), 1.61 (t, ^3J = 7.2 Hz, 6H, CH_3) ppm. – **^{13}C NMR** (126 MHz, $CDCl_3$): δ =134.1 (+, CH), 133.9 (+, CH), 133.8 (+, CH), 133.6 (+, CH), 133.4 (+, CH), 131.3 (+, CH), 130.9 (+, CH), 130.2 (+, CH), 129.7 (+, CH), 127.7(+, CH), 126.6 (+, CH), 126.5 (+, CH), 123.0 (C_q), 120.7 (C_q) ppm. – **UV-Vis** (CH_2Cl_2): λ_{max} (rel. absorption) = 223 (2.35), 277 (0.02), 404 (0.29), 529 (0.02) nm. – **IR** (ATR): $\tilde{\nu}$ = 2952, 2922, 2851, 1672, 1657, 1412, 1099, 875, 671, 618, 584, 572, 526, 445, 392 cm^{-1}. – **HRMS** (ESI) ($Pd_2C_{82}H_{54}N_8O_4$): calc.: 1428.2369, found: 1428.2448.

Additional information on the reaction details is available *via* the Chemotion repository: https://dx.doi.org/10.14272/reaction/SA-FUHFF-UHFFFADPSC-SGZVALPMXJ-UHFFFADPSC-NUHFF-LREIQ-NUHFF-ZZZ

Additional information on the analysis of the target compound is available *via* the Chemotion repository: https://dx.doi.org/10.14272/SGZVALPMXJPJGD-VEGFVYEWSA-L.1

[1,2-Phenylene-(2-(5,10,15,20-tetraphenylporphyrin),5-(10,15,20-triphenylporphyrin))]-dimanganese(III)-dichloride (**145**)[380]

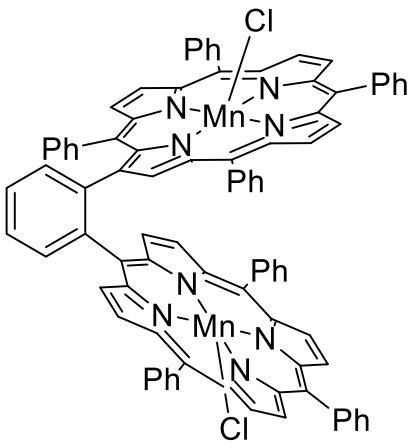

1,2-Phenylene-(2-(5,10,15,20-tetraphenylporphyrin),5-(10,15,20-triphenyporphyrin)) (**130**) (1.0 mg, 0.81 µmol, 1.00 equiv.) and $MnCl_2$ (1.4 mg, 7.89 µmol, 9.74 equiv.) were dissolved in DMF (1 mL). The reaction mixture was stirred for 15.5 h at 130 °C. Subsequently, the solvent was removed under reduced pressure. The crude product was purified by flash column chromatography on silica gel (CH_2Cl_2/MeOH, 19:1) to afford the title compound **145** as a brown solid (0.9 mg, 0.64 µmol, 79%).

***R*f** (CH_2Cl_2/MeOH, 9:1) = 0.58. – **UV-Vis** (CH_2Cl_2): λ_{max} (rel. absorption) = 226 (3.64), 346 (0.72), 382 (0.90), 401 (0.80), 473 (1.08), 579 (0.17), 614 (0.14) nm. – **IR** (ATR): $\tilde{\nu}$ = 2952, 2919, 2851, 1458, 1441, 1377, 1340, 1256, 1094, 1074, 1041, 1013, 875, 800, 752, 718, 701, 683, 667, 663, 619, 581, 569, 560, 527, 453 cm^{-1}. – **HRMS** (ESI) ($Mn_2ClC_{88}H_{54}N_8$): calc.: 1367.2915, found: 1367.2961.

Additional information on the reaction details is available *via* the Chemotion repository: https://dx.doi.org/10.14272/reaction/SA-FUHFF-UHFFFADPSC-YNHSRIYWLO-UHFFFADPSC-NUHFF-LIEHO-NUHFF-ZZZ

Additional information on the analysis of the target compound is available *via* the Chemotion repository: https://dx.doi.org/10.14272/YNHSRIYWLOEFKN-NDIBZSDSSA-L

[1,2-Phenylene-(2-(5,10,15,20-tetraphenylporphyrin),5-(10,15,20-triphenylporphyrin))]-*µ*-oxo-diiron(III) (**146**)[385]

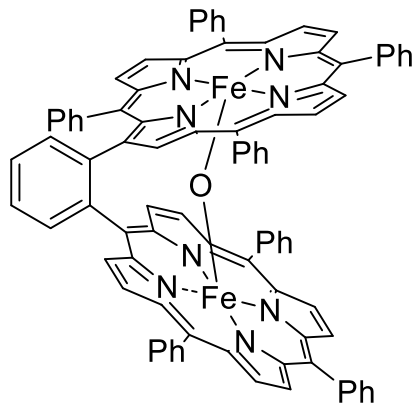

1,2-Phenylene-(2-(5,10,15,20-tetraphenylporphyrin),5-(10,15,20-triphenyporphyrin)) (**130**) (0.3 mg, 0.24 µmol, 1.00 equiv.) and $FeCl_2$ (0,7 mg, 5.52 µmol, 23.0 equiv.) were dissolved in DMF (0.5 mL). The reaction mixture was stirred for 14 h at 150 °C. Subsequently, the solvent was removed under reduced pressure. The crude product was purified by flash column chromatography on silica gel (CH_2Cl_2/MeOH, 19:1) to afford the title compound **146** as a brown solid (0.3 mg, 0.21 µmol, 87%).

***R*f** (CH_2Cl_2/MeOH, 9:1) = 0.54. – **UV-Vis** (CH_2Cl_2): λ_{max} (rel. absorption) = 217 (0.51), 256 (0.34), 322 (0.37), 413 (1.08), 581 (0.08), 630 (0.04) nm. – **IR** (ATR): $\tilde{\nu}$ = 2952, 2922, 2851, 1708, 1598, 1458, 1442, 1377, 1337, 1072, 1003, 994, 871, 798, 752, 720, 701, 660, 514, 510, 463, 433 cm^{-1}. – **HRMS** (ESI) ($Fe_2OC_{88}H_{54}N_8$): calc.: 1350.3120, found: 1350.305.

Additional information on the reaction details is available *via* the Chemotion repository: https://dx.doi.org/10.14272/reaction/SA-FUHFF-UHFFFADPSC-OOXACMCOHF-UHFFFADPSC-NUHFF-NIQCL-NUHFF-ZZZ

Additional information on the analysis of the target compound is available *via* the Chemotion repository: https://dx.doi.org/10.14272/OOXACMCOHFJPIU-PWNOKTKGSA-N

[1,2-Phenylene-(2-(5,10,15,20-tetraphenylporphyrin),5-(10,15,20-triphenylporphyrin))]-dinickel(II) (**147**)[178]

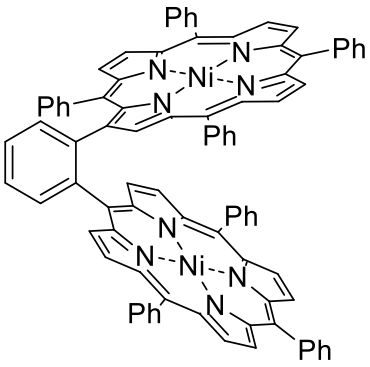

1,2-Phenylene-(2-(5,10,15,20-tetraphenylporphyrin),5-(10,15,20-triphenylporphyrin)) (**130**) (1.2 mg, 0.98 µmol, 1.00 equiv.) and $Ni(acac)_2$ (2.1 mg, 8.17 µmol, 8.34 equiv.) were dissolved in DMF (2 mL). The reaction mixture was stirred for 5 h at 150 °C. Subsequently, the solvent was removed under reduced pressure. The crude product was purified by flash chromatography on silica gel (CH_2Cl_2/*n*-pentane, 2:1) to afford the title compound **147** as a red solid (1.0 mg, 0.75 µmol, 76%).

***R*f** (CH_2Cl_2/*n*-pentane, 1:2) = 0.65. – **^{1}H NMR** (500 MHz, THF-d_8): δ = 9.28 (d, ^3J = 5.0 Hz, 1H, $H_{pyrrole}$), 8.91 (d, ^3J = 5.0 Hz, 1H, $H_{pyrrole}$), 8.79 (d, ^3J = 5.0 Hz, 1H, $H_{pyrrole}$), 8.74 (d, ^3J = 5.0 Hz, 1H, $H_{pyrrole}$), 8.71 (d, ^3J = 4.9 Hz, 1H, $H_{pyrrole}$), 8.60 (d, ^3J = 4.9 Hz, 1H, $H_{pyrrole}$), 8.51 (d, ^3J = 4.9 Hz, 1H, $H_{pyrrole}$), 8.50 – 8.46 (m, 2H, $H_{pyrrole}$), 8.45 – 8.41 (m, 2H), 8.40 (dd, J = 7.7, 1.3 Hz, 1H, $H_{aromatic}$), 8.26 (t, ^3J = 4.9 Hz, 2H, $H_{pyrrole}$), 8.21 – 8.00 (m, 2H), 7.98 (d, ^3J = 4.9 Hz, 1H, $H_{pyrrole}$), 7.90 (d, ^3J = 7.34 Hz, 4H, $H_{aromatic}$), 7.88 – 7.71 (m, 7H), 7.71 – 7.64 (m, 3H), 7.64 – 7.47 (m, 14H), 7.44 (td, J = 7.35, 1.76 Hz, 1H, $H_{aromatic}$), 7.26 – 7.18 (m, 2H), 7.09 (s, 1H), 6.55 (tt, J = 7.57, 1.31 Hz, 1H), 6.43 – 6.01 (m, 2H), 5.96 – 5.57 (m, 2H) ppm. – **^{13}C NMR** (126 MHz, THF-d_8): δ = 145.4 (C_q), 143.4 (C_q), 143.0 (C_q), 142.7 (C_q), 140.7 (C_q), 140.2 (C_q), 137.4 (+, CH), 136.1 (+, CH), 135.4 (+, CH), 134.7 (+, CH), 134.6 (+, CH), 134.5 (+, CH), 132.9 (+, CH), 132.8 (+, CH), 132.6 (+, CH), 132.4 (+, CH), 128.7 (+, CH), 128.2 (+, CH), 127.9 (+, CH), 127.8 (+, CH), 127.4 (+, CH), 127.1 (+, CH), 126.1 (+, CH), 119.3 (C_q) ppm. – **UV-Vis** (CH_2Cl_2): λ_{max} (rel. absorption) = 226 (3.64), 346 (0.72), 382 (0.90), 401 (0.80), 473

(1.08), 579 (0.17), 614 (0.14) nm. – **IR** (ATR): $\tilde{\nu}$ = 2953, 2922, 2850, 2325, 2164, 1088, 1007, 616, 547, 453 cm^{-1}. – **HRMS** (ESI) ($Ni_2C_{88}H_{54}N_8$): calc.: 1340.3169, found: 1340.3175.

Additional information on the reaction details is available *via* the Chemotion repository: https://dx.doi.org/10.14272/reaction/SA-FUHFF-UHFFFADPSC-AIOYFZDBUI-UHFFFADPSC-NUHFF-NOTDD-NUHFF-ZZZ

Additional information on the analysis of the target compound is available *via* the Chemotion repository: https://dx.doi.org/10.14272/AIOYFZDBUIGAAQ-OLRUKZAISA-N.1

[1,2-Phenylene-(2-(5,10,15,20-tetraphenylporphyrin),5-(10,15,20-triphenylporphyrin))]-dicopper(II) (**148**)[381]

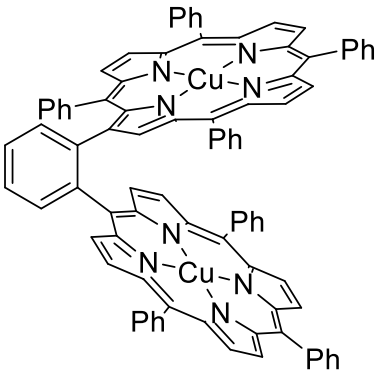

1,2-Phenylene-(2-(5,10,15,20-tetraphenylporphyrin),5-(10,15,20-triphenylporphyrin)) (**130**) (0.3 mg, 0.24 µmol, 1.00 equiv.) and $Cu(OAc)_2$ (0.8 mg, 3.71 µmol, 15.5 equiv.) were dissolved in DMF (0.5 mL). The reaction mixture was stirred for 4 h at 60 °C. Subsequently, the solvent was evaporated under reduced pressure. The crude product was purified by flash column chromatography on silica gel (CH_2Cl_2/*n*-pentane, 2:1) to afford the title compound **148** as a red solid (0.3 mg, 0.22 µmol, 93%).

***R*f** (CH_2Cl_2/*n*-pentane, 1:2) = 0.66. – **UV-Vis** (CH_2Cl_2): λ_{max} (rel. absorption) = 218 (1.37), 309 (0.44), 413 (3.91), 431 (2.90), 544 (0.53) nm. – **IR** (ATR): $\tilde{\nu}$ = 2962, 2922, 2851, 2183, 1460, 1436, 1340, 1264, 1075, 1006, 798, 749, 717, 704, 666, 630, 558, 517 cm^{-1}. – **HRMS** (ESI) ($Cu_2C_{88}H_{54}N_8$): calc.: 1350.3069, found: 1350.3105.

Additional information on the reaction details is available *via* the Chemotion repository: https://dx.doi.org/10.14272/reaction/SA-FUHFF-UHFFFADPSC-FCHGNDMBSH-UHFFFADPSC-NUHFF-NOTDD-NUHFF-ZZZ

Additional information on the analysis of the target compound is available *via* the Chemotion repository: https://dx.doi.org/10.14272/FCHGNDMBSHCUEK-OLRUKZAISA-N.1

[1,2-Phenylene-(2-(5,10,15,20-tetraphenylporphyrin),5-(10,15,20-triphenylporphyrin))]-dizinc(II) (**149**)[379]

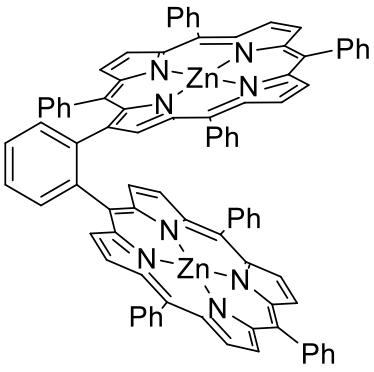

1,2-Phenylene-(2-(5,10,15,20-tetraphenylporphyrin),5-10,15,20-triphenylporphyrin)) (**130**) (2.0 mg, 1.63 µmol, 1.00 equiv.) and $Zn(OAc)_2$ (1.2 mg, 6.54 µmol, 4.01 equiv.) were dissolved in a mixture of $CHCl_3$ and MeOH (10:1, 2.1 mL). The reaction mixture was stirred for 30 min at 60 °C. Subsequently, the solvent was removed under reduced pressure. The crude product was purified by flash column chromatography on silica gel (CH_2Cl_2/*n*-pentane, 2:1) to afford the title compound **149** as a purple solid (2.1 mg, 1.55 µmol, 95%).

***R*f** (CH_2Cl_2/*n*-pentane, 1:2) = 0.52. – **^{1}H NMR** (500 MHz, CD_2Cl_2): δ = 9.50 (bs, 1H, $H_{pyrrole}$), 8.99 (bs, 1H, $H_{pyrrole}$), 8.91 (bs, 1H, $H_{pyrrole}$), 8.88 (bs, 1H, $H_{pyrrole}$), 8.79 (bs, 1H, $H_{pyrrole}$), 8.74 (d, ^3J = 4.8 Hz, 1H, $H_{pyrrole}$), 8.71 (d, ^3J = 4.9 Hz, 1H, $H_{pyrrole}$), 8.70 (d, ^3J = 4.6 Hz, 1H, $H_{pyrrole}$), 8.68 (bs, 1H) 8.64 (d, ^3J = 4.6 Hz, 2H, $H_{pyrrole}$), 8.58 (bs, 2H), 8.52 (m, 1H), 8.39 (d, ^3J = 4.8 Hz, 1H, $H_{pyrrole}$), 8.34 (bs, 1H), 8.22 – 8,14 (m, 2H), 8.14 – 7.96 (m, 6H), 7.96 – 7.88 (m, 2H, $H_{aromatic}$), 7.88 – 7.83 (m, 3H, $H_{aromatic}$), 7.83 – 7.77 (m, 3H, $H_{aromatic}$), 7.77 – 7.73 (m, 2H, $H_{aromatic}$), 7.73 – 7.68 (m, 4H, $H_{aromatic}$), 7.68 – 7.62 (m, 1H, $H_{aromatic}$), 7.61 (dt, *J* = 7.55, 1.43 Hz, 1H, $H_{aromatic}$), 7.56 (m, 4H), 7.52 – 7.45 (m, 3H), 7.45 – 7.38 (m, 1H), 7.35 (bs, 1H), 7.08 (bs, 1H), 6.39 (tt, *J* = 7.7, 1.3 Hz, 1H), 5.37 – 5.34 (m, 1H), 5.08 (bs, 1H), 4.76 (bs, 1H) ppm. – **^{13}C NMR** (126 MHz, CD_2Cl_2): δ = 150.5 (C_q), 150.3 (C_q), 150.1 (C_q), 141.6 (C_q), 135.0 (+, CH), 134.7 (+, CH), 133.3 (+, CH), 131.6 (+, CH), 131.2 (+, CH), 130.3 (+, CH), 127.1 (+, CH), 126.9 (+, CH), 126.6 (+, CH), 124.2 (+, CH), 122.9 (C_q) ppm. – **UV-Vis** (CH_2Cl_2): λ_{max} (rel. absorption) = 224 (0.07), 302 (0.06), 354 (0.05), 417 (0.81), 436 (0.36), 553 (0.06), 589 (0.01) nm. – **IR** (ATR): $\tilde{\nu}$ = 2952, 2919, 2850, 1647, 1598, 1458, 1439, 1337, 1259, 1092, 1068, 1001, 992, 795, 742, 730, 720, 700, 671, 660, 650, 569, 527, 432, 401, 394, 377 cm^{-1}. – **HRMS** (ESI) ($Zn_2C_{88}H_{54}N_8$): calc.: 1354.3034, found: 1354.3033.

Additional information on the reaction details is available *via* the Chemotion repository: https://dx.doi.org/10.14272/reaction/SA-FUHFF-UHFFFADPSC-CCIAYANZDW-UHFFFADPSC-NUHFF-NOTDD-NUHFF-ZZZ

Additional information on the analysis of the target compound is available *via* the Chemotion repository: https://dx.doi.org/10.14272/CCIAYANZDWKSEV-OLRUKZAISA-N.1

[1,2-Phenylene-(2-(5,10,15,20-tetraphenylporphyrin),5-(10,15,20-triphenylporphyrin))]-dipalladium(II) (**150**)[382]

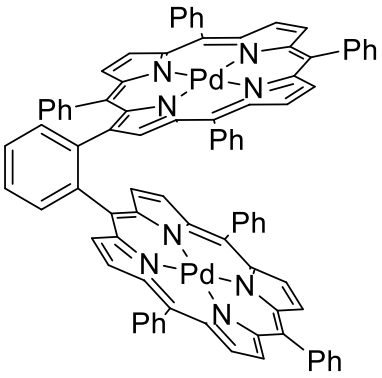

1,2-Phenylene-(2-(5,10,15,20-tetraphenylporphyrin),5-(10,15,20-triphenyporphyrin)) (**130**) (1.2 mg, 0.98 µmol, 1.00 equiv.) and $PdCl_2$ (3.2 mg, 18.0 µmol, 18.4 equiv.) were dissolved in DMF (1.5 mL). The reaction mixture was stirred for 3 h at 100 °C. Subsequently, the solvent removed under reduced pressure. The crude product was purified by flash column chromatography on silica gel (CH_2Cl_2/*n*-pentane, 2:1) to afford the title compound **150** as a red solid (1.4 mg, 0.97 µmol, 99%).

***R*f** (CH_2Cl_2/*n*-pentane, 1:2) = 0.63. – **^{1}H NMR** (500 MHz, THF-d_8): δ = 9.40 (d, ^3J = 5.0 Hz, 1H, $H_{pyrrole}$), 8.96 (d, ^3J = 5.1 Hz, 1H, $H_{pyrrole}$), 8.83 (d, ^3J = 5.0 Hz, 1H, $H_{pyrrole}$), 8.81 – 8.77 (m, 1H, $H_{pyrrole}$), 8.75 (d, ^3J = 4.8 Hz, 1H, $H_{pyrrole}$), 8.61 (t, ^3J = 4.7 Hz, 2H, $H_{pyrrole}$), 8.60 (d, ^3J = 4.9 Hz, 1H, $H_{pyrrole}$), 8.57 (dd, J = 7.3, 5.0 Hz, 2H, $H_{aromatic}$), 8.54 – 8.50 (m, 2H), 8.46 (d, ^3J = 4.8 Hz, 1H, $H_{pyrrole}$), 8.44 – 8.27 (m, 1H), 8.25 (d, ^3J = 5.1 Hz, 1H, $H_{pyrrole}$), 8.23 – 8.20 (m, 1H), 8.11 – 8.03 (m, 2H), 8.03 – 7.92 (m, 4H), 7.91 – 7.85 (m, 1H), 7.84 – 7.79 (m, 5H), 7.78 – 7.69 (m, 10H), 7.68 – 7.63 (m, 1H), 7.63 – 7.49 (m, 6H), 7.49 – 7.41 (m, 2H), 7.41 – 7.32 (m, 1H), 7.32 – 7.25 (m, 1H), 7.25 – 7.01 (m, 2H), 6.59 (tt, J = 7.6, 1.2 Hz, 1H, $H_{aromatic}$), 4.83 – 4.69 (m, 1H), 4.24 – 4.15 (m, 1H) ppm. – **^{13}C NMR** (126 MHz, THF-d_8): δ = 144.7 (C_q), 143.9 (C_q), 143.0 (C_q), 142.9 (C_q), 142.8 (C_q), 142.6 (C_q), 142.5 (C_q), 142.5 (C_q), 142.4 (C_q), 142.4 (C_q), 142.3 (C_q), 142.1 (C_q), 139.7 (C_q), 137.0 (C_q), 135.4 (+, CH), 135.1 (+, CH), 134.9 (+, CH), 133.0 (C_q), 132.9 (C_q), 131.7 (+, CH), 131.6 (+, CH), 131.4 (+, CH), 131.2 (+, CH), 131.2 (+, CH), 130.9 (+, CH), 130.7 (+, CH), 129.1 (+, CH), 128.8 (+, CH), 128.8 (+, CH), 128.7 (+, CH), 128.4 (+, CH), 128.2 (+, CH), 128.1 (+, CH), 127.8 (+, CH), 127.6 (+, CH), 127.5 (+, CH), 127.1 (+, CH), 126.1 (+, CH), 124.9 (+, CH), 123.3 (C_q), 122.7 (C_q), 122.5 (C_q), 122.3 (C_q), 121.9 (C_q), 121.0 (C_q) ppm. – **UV-Vis** (CH_2Cl_2): λ_{max} (rel. absorption) = 219 (0.91), 270 (0.40), 308 (0.26), 413 (3.51), 528 (0.53), 559 (0.08) nm. – **IR** (ATR): $\tilde{\nu}$ = 2946, 2927, 2900, 2146, 2040, 1983, 1919, 1016, 943, 860, 666, 647, 612, 517, 463, 418 cm^{-1}. – **HRMS** (ESI) ($Ni_2C_{88}H_{54}N_8$): calc.: 1436.2574, found: 1436.2627.

Additional information on the reaction details is available *via* the Chemotion repository: https://dx.doi.org/10.14272/reaction/SA-FUHFF-UHFFFADPSC-YIJXPKHLVV-UHFFFADPSC-NUHFF-NOTDD-NUHFF-ZZZ

Additional information on the analysis of the target compound is available *via* the Chemotion repository: https://dx.doi.org/10.14272/YIJXPKHLVVHSSI-OLRUKZAISA-N.1

6.4.4 Heterobimetallic *o*-phenylene-linked porphyrin complexes

[5-(2-Formylphenyl)-10,15,20-triphenylporphyrin]-nickel(II) (**151**)[178]

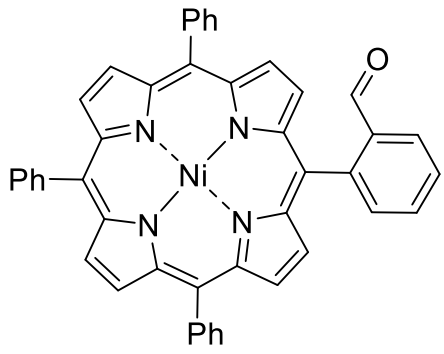

5-(2-Formylphenyl)-10,15,20-triphenylporphyrin (**125**) (40.0 mg, 62.2 µmol, 1.00 equiv.) and $Ni(acac)_2$ (56.9 mg, 310 µmol, 5.00 equiv.) were dissolved in DMF (15 mL). The reaction mixture was stirred for 4 h at 150 °C. The solvent was removed under reduced pressure. The crude product was purified by flash column chromatography on silica gel (CH_2Cl_2/*n*-pentane, 1:1) to afford the title compound **151** as a purple solid (31.1 mg, 44.5 µmol, 71%).

***R*f** (CH_2Cl_2/n-pentane, 1:1) = 0.44. – **^{1}H NMR** (500 MHz, $CDCl_3$): δ = 9.34 (s, 1H, CHO), 8.78 – 8.73 (m, 6H, $H_{pyrrole}$), 8.54 (d, 3J = 4.9 Hz, 2H, $H_{pyrrole}$), 8.35 – 8.31 (m, 1$H_{aromatic}$), 8.13 – 8.09 (m, 1H, $H_{aromatic}$), 8.05 – 7.97 (m, 6H, H), 7.89 – 7.84 (m, 2H, $H_{aromatic}$), 7.74 – 7.65 (m, 9H, $H_{aromatic}$) ppm. – **^{13}C NMR** (126 MHz, $CDCl_3$) : δ = 191.1 (+, CHO), 144.3 (C_q), 143.2 ($_{Cq}$), 143.1 (C_q), 142.9 (C_q), 140.8 (C_q), 137.6 (C_q), 135.0 (C_q), 133.9 (+, CH), 133.8 (+, CH), 133.1 (+, CH), 132.7 (+, CH), 132.6 (+, CH), 131.8 (+, CH), 131.7 (+, CH), 129.1 (+, CH), 128.0 (+, CH), 128.0 (+, CH), 127.1 (+, CH), 127.0 (+, CH), 126.3 (+, CH), 119.7 (C_q), 119.7 (C_q), 113.3 (C_q) ppm. – **UV-Vis** (CH_2Cl_2): λ_{ma}x (rel. absorption) = 217 (0.33), 294 (0.22), 291 (0.11), 416 (1.70), 528 (0.13) nm. – **IR** (ATR): $\tilde{\nu}$ = 3053, 3019, 2952, 2921, 2854, 1691, 1592, 1438, 1350, 1196, 1072, 1006, 792, 745, 708, 697 cm^{-1} – **HRMS** (ESI) ($C_{45}H_{28}N_4NiO$): calc.: 698.1617, found: 698.1614.

Additional information on the reaction details is available *via* the Chemotion repository: https://dx.doi.org/10.14272/reaction/SA-FUHFF-UHFFFADPSC-PNJCQSRZVF-UHFFFADPSC-NUHFF-MVQBS-NUHFF-ZZZ.1

Additional information on the analysis of the target compound is available *via* the Chemotion repository: https://dx.doi.org/10.14272/PNJCQSRZVFLATK-RORYYHOOSA-

1,2-Phenylene-([5-(10,15,20-triphenylporphyrin)]-nickel(II),5-(10,15,20-triphenylporphyrin)) (**152**)[83]

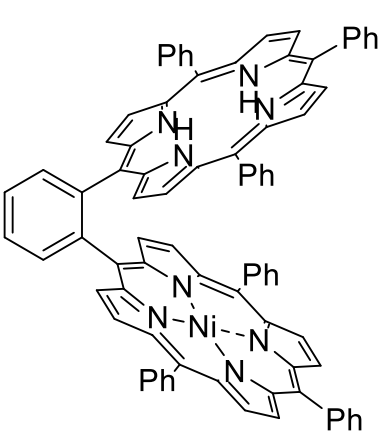

Under an argon atmosphere, [5-(2-formylphenyl)-10,15,20-triphenylporphyrin]-nickel(II) (**151**) (27.6 mg, 39.5 µmol, 1.00 equiv.) was dissolved in dry CH_2Cl_2 (20 mL). A stream of argon was passed through the mixture for 15 min to remove dissolved oxygen. Subsequently, freshly distilled benzaldehyde (16 µL, 16.9 mg, 159 µmol, 4.03 equiv.) and pyrrole (17 µL, 16.4 mg, 252 µmol, 6.38 equiv.) were added. After 5 min, TFA (2.2 µL, 3.19 mg, 28 µmol, 0.71 equiv.) was added. The mixture was stirred for 16 h in the dark. DDQ (21.7 mg, 95.6 µmol, 2.42 equiv.) was added and stirred for 1 h. The crude mixture was then concentrated under reduced pressure, filtered through a short layer of silica gel eluting with CH_2Cl_2 and purified by flash column chromatography on silica gel (1 × CH_2Cl_2/*n*-pentane, 1:1, 1 × CH_2Cl_2/*n*-pentane, 2:1) to afford the title compound **152** as a red solid (7.3 mg, 6.04 µmol, 15%).

***R*f** (CH_2Cl_2/*n*-pentane, 1:1) = 0.73. – **^{1}H NMR** (500 MHz, THF-d_8): δ = 9.11 (d, ^3J = 4.9 Hz, 2H, $H_{pyrrole}$), 8.98 (dd, J = 7.8, 1.4 Hz, 1H, $H_{aromatic}$), 8.96 – 8.92 (m, 1H, $H_{pyrrole}$), 8.66 (dd, J = 7.5, 1.4 Hz, 1H, $H_{aromatic}$), 8.43 (d, ^3J = 4.9 Hz, 2H, $H_{pyrrole}$), 8.38 (d, ^3J = 4.7 Hz, 2H, $H_{pyrrole}$), 8.31 (td, J = 7.7, 1.4 Hz, 1H, $H_{aromatic}$), 8.26 – 8.18 (m, 5H, $H_{aromatic}$), 8.16 (d, ^3J = 4.8 Hz, 2H, $H_{pyrrole}$), 8.10 (d, ^3J = 4.8 Hz, 2H, $H_{pyrrole}$), 8.07 – 8.03 (m, 1H, $H_{aromatic}$), 7.79 – 7.72 (m, 4H), 7.72 – 7.66 (m, 3H), 7.66 – 7.61 (m, 3H), 7.61 – 7.55 (m, 8H), 7.53 – 7.47 (m, 4H), 7.47 – 7.34 (m, 5H), 7.34 – 7.25 (m, 3H), –3.82 (bs, 2H, NH) ppm. – **^{13}C NMR** (126 MHz, THF-d_8): δ = 145.8 (C_q), 145.0 (C_q), 143.9 (C_q), 143.2 (C_q), 143.0 (C_q), 143.0 (C_q), 142.8 (C_q), 142.5 (C_q), 142.2 (C_q), 141.7 (C_q), 135.4 (+, CH), 135.2 (+, CH), 135.0 (+, CH), 135.0 (+, CH), 134.4 (+, CH), 134.4 (+, CH), 133.4 (+, CH), 132.1 (+, CH), 131.9 (+, CH), 131.8 (+, CH), 130.3 (+, CH), 129.9 (+, CH), 128.8 (+, CH), 128.5 (+, CH), 128.5 (+, CH), 128.4 (+, CH), 128.4 (+, CH), 128.3 (+, CH), 128.1 (+, CH), 127.6 (+, CH), 127.5 (+, CH), 127.4 (+, CH), 120.7 (C_q), 120.2 (C_q), 119.4 (C_q), 119.0 (C_q), 118.7 (C_q), 118.1 (C_q) ppm. **– UV-Vis** (CH_2Cl_2): λ_{max} (rel. absorption) = 217 (0.51), 294 (0.22), 406 (2.01), 524 (0.11), 593 (0.03), 651 (0.03) nm – **IR** (ATR): $\tilde{\nu}$ = 3323, 3316, 3312, 2956, 2929, 2891, 1759, 1723, 1441, 1367, 1347, 1187, 1061, 1035, 1006, 963, 924, 881, 844, 701, 561 cm^{-1}. – **HRMS** (ESI) ($NiC_{82}H_{53}N_8$): calc.: 1207.3741, found: 1207.3728.

Additional information on the reaction details is available *via* the Chemotion repository: https://dx.doi.org/10.14272/reaction/SA-FUHFF-UHFFFADPSC-QYFQNSKAHG-UHFFFADPSC-NUHFF-NZLTO-NUHFF-ZZZ

Additional information on the analysis of the target compound is available *via* the Chemotion repository: https://dx.doi.org/10.14272/QYFQNSKAHGLVQL-XRTKQMIRSA-N.1

1,2-Phenylene-([5-(10,15,20-triphenylporphyrin)]-iron(III)-chloride,[5-(10,15,20-triphenylporphyrin)]-nickel(II)) (**153**)[385]

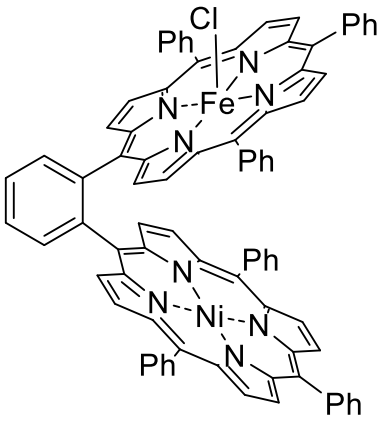

1,2-Phenylene-([5-(10,15,20-triphenylporphyrin)]-nickel(II),5-(10,15,20-triphenylporphyrin)) (**152**) (2.00 mg, 1.66 µmol, 1.00 equiv.) and $FeCl_2$ (1.6 mg, 12.6 µmol, 7.60 equiv.) were dissolved in DMF (2 mL). The reaction mixture was stirred for 4 h at 150 °C. Subsequently, the solvent was removed under reduced pressure. The crude product was purified by flash column chromatography on silica gel (CH_2Cl_2/MeOH, 20:1) to afford the title compound **153** as a brownish-red solid (2.0 mg, 1.58 µmol, 95%).

***R*f** (CH_2Cl_2/MeOH, 20:1) = 0.49. – **UV-Vis** (CH_2Cl_2): λ_{max} (rel. absorption) = 217 (0.28), 294 (0.22), 408 (0.65), 532 (0.08) nm. – **IR** (ATR): $\tilde{\nu}$ = 3329, 2958, 2890, 1754, 1718, 1366, 1351, 1186, 1120, 1060, 1035, 963, 924, 843, 798, 751, 700, 561, 551, 520, 412 cm^{-1}. – **HRMS** (ESI) ($NiFeC_{82}H_{50}N_8$): calc.: 1260.2906, found: 1260.2859.

Additional information on the reaction details is available *via* the Chemotion repository: https://dx.doi.org/10.14272/reaction/SA-FUHFF-UHFFFADPSC-BUROBQJXUQ-UHFFFADPSC-NUHFF-MVIHC-NUHFF-ZZZ
Additional information on the analysis of the target compound is available *via* the Chemotion repository: https://dx.doi.org/10.14272/BUROBQJXUQHYNS-LKHNKGCCSA-M.1

6.4.5 ^{57}Fe complexes for *Mössbauer* spectroscopy

[5-(2-Formylphenyl)-10,15,20-triphenylporphyrin]copper(II) (**154**)[381]

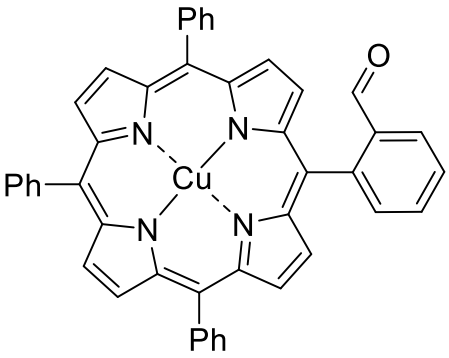

$Cu(OAc)_2$ (44.7 mg, 250 µmol, 4.00 equiv.) and 5-(2-formylphenyl)-10,15,20-triphenylporphyrin (**125**) (40.0 mg, 62.2 µmol, 1.00 equiv.) were dissolved in a mixture of $CHCl_3$ and MeOH (10:1, 11 mL). The reaction mixture was heated to 80 °C for 30 min and the solvent was removed under reduced pressure. The crude product was purified by flash column chromatography on silica gel (CH_2Cl_2/*n*-pentane, 1:1) to afford the title compound **154** as a purple solid (46.0 mg, 65.3 µmol, quant.).

***R*f** = 0.50 (CH_2Cl_2/*n*-pentane, 1:1). – **UV-Vis** (CH_2Cl_2): λ_{max} (rel. absorption) = 342 (0.02), 361 (0.02), 417 (1.04), 470 (0.01), 502 (0.01), 540 (0.05) nm.– **IR** (ATR): $\tilde{\nu}$ = 3309, 3301, 3285, 3234, 3223, 2955, 2915, 2868, 2850, 1730, 1696, 1595, 1490, 1459, 1442, 1418, 1377, 1366, 1346, 1309, 1288, 1262, 1235, 1220, 1196, 1177, 1096, 1075, 1047, 1024, 1001, 994, 972, 945, 918, 885, 878, 860, 843, 817, 800, 756, 741, 718, 697, 663, 645, 633, 578, 561, 552, 547, 528, 499, 490, 484, 472, 443, 398, 381 cm^{-1}. – **HRMS** (ESI) ($C_{45}H_{28}CuN_4O$): calc.: 703.1559, found: 703.1548.

[5-(2-Formylphenyl)-10,15,20-triphenylporphyrin]palladium(II) (**155**)[386]

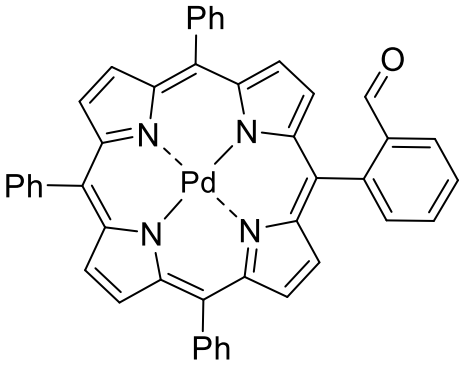

$Pd(OAc)_2$ (30.7 mg, 140 µmol, 4.00 equiv.) and [5-(2-formylphenyl)-10,15,20-triphenylporphyrin (**125**) (22.3 mg, 34.7 µmol, 1.00 equiv.) were dissolved in a mixture of $CHCl_3$ and MeOH (6:1, 7 mL). The reaction mixture was stirred at 80 °C for 5 min. Subsequently, the solvent was removed under reduced pressure. The crude product was purified by flash column chromatography on silica gel (CH_2Cl_2/*n*-pentane, 1:1) to afford the title compound **155** as a purple-red solid (23.3 mg, 31.2 µmol, 80%).

***R*f** = 0.25 (CH_2Cl_2/*n*-pentane, 1:2). – **^{1}H NMR** (500 MHz, $CDCl_3$): δ = 9.44 (s, 1H, C*H*O), 8.87 – 8.82 (m, 6H, $H_{pyrrole}$), 8.63 (d, ^3J = 4.9 Hz, 2H, $H_{pyrrole}$), 8.43 – 8.39 (m, 1H, $H_{aromatic}$), 8.24 – 8.14 (m, 7H, $H_{aromatic}$), 7.96 – 7.88 (m, 2H, $H_{aromatic}$), 7.81 – 7.70 (m, 9H, $H_{aromatic}$) ppm. – **^{13}C NMR** (126 MHz, $CDCl_3$): δ = 191.1 (+, CH, C*H*O), 145.2 (C_q), 142.1 (C_q), 142.0 (C_q), 141.7(C_q), 141.6 (C_q), 137.9 (C_q), 135.4 (+, CH), 132.0 (+, CH), 131.6 (+, CH), 131.5 (+, CH), 130.5 (+, CH), 129.2 (+, CH), 128.0 (+, CH), 127.0 (+, CH), 126.9 (+, CH), 126.6 (+, CH), 122.5 (C_q), 122.4 (C_q), 115.9 (C_q) ppm. – **UV-Vis** (CH_2Cl_2): λ_{max} (rel. absorption) = 266 (0.11), 273 (0.11), 329 (0.03), 418 (0.85), 463 (0.01), 525 (0.07), 556 (0.01) nm. – **IR** (ATR): $\tilde{\nu}$ = 2953, 2917, 2868, 2850, 1776, 1730, 1697, 1670, 1653, 1626, 1595, 1558, 1540, 1507, 1492, 1459, 1417, 1377, 1366, 1353, 1310, 1286, 1261, 1220, 1210, 1196, 1180, 1096, 1079, 1047, 1013, 970, 880, 860, 799, 748, 741, 714, 698, 667, 645, 630, 619, 603, 598, 577, 565, 557, 551, 538, 531, 526, 509, 501, 490, 467, 450, 443, 435, 424, 407, 399, 391, 380 cm^{-1}. – **HRMS** (ESI) ($C_{45}H_{28}N_4OPd$): calc.: 746.1298, found: 746.1305.

[5-(2-Formylphenyl)-10,15,20-triphenylporphyrin]platinum(II) (**156**)[223]

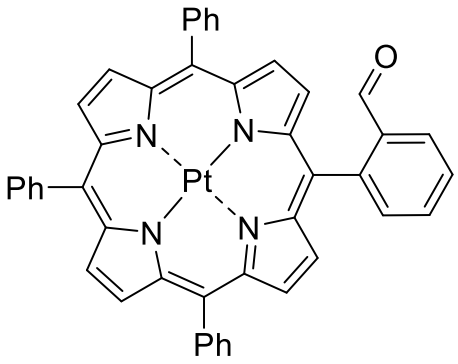

$PtCl_2$ (74.6 mg, 280 µmol 4.50 equiv.) and 5-(2-formylphenyl)-10,15,20-triphenylporphyrin (**125**) (41.0 g, 63.8 µmol, 1.00 equiv.) were dissolved in dry toluene (11 mL). A stream of argon was passed through the mixture for 15 min to remove dissolved oxygen. The reaction mixture was stirred at 120 °C for 14 h. Subsequently, the solvent was removed under reduced pressure. The crude product was purified by flash column chromatography on silica gel (CH_2Cl_2/*n*-pentane 1:1) to afford the title compound **155** as a purple-red solid (17.3 mg, 20.7 µmol, 32%).

***R*f** = 0.25 (CH_2Cl_2/*n*-pentane 1:2). – **^{1}H NMR** (500 MHz, $CDCl_3$): δ = 9.48 (s, 1H, C*H*O), 8.81 – 8.75 (m, 6H, $H_{pyrrole}$), 8.58 (d, ^3J = 5.0 Hz, 2H, $H_{pyrrole}$), 8.42 – 8.38 (m, 1H, $H_{aromatic}$), 8.24 – 8.12 (m, 7H, $H_{aromatic}$), 7.96 – 7.88 (m, 2H, $H_{aromatic}$), 7.80 – 7.70 (m, 9H, $H_{aromatic}$) ppm. – **^{13}C NMR** (126 MHz, $CDCl_3$): δ = 191.1 (+, CH, CHO), 144.7 (C_q), 141.4 (C_q), 141.3 (C_q), 141.2 (C_q), 141.0 (C_q), 140.9 (C_q), 137.8 (C_q), 135.2 (+, CH), 134.1 (+, CH), 134.0 (+, CH), 131.8 (+, CH), 131.3 (+, CH), 131.2 (+, CH), 130.2 (+, CH), 129.2 (+, CH), 128.1 (+, CH), 127.1 (+, CH), 127.0 (+, CH), 126.4 (+, CH), 123.1 (C_q), 123.0 (C_q), 116.6 (C_q) ppm. – **UV-Vis** (CH_2Cl_2): λ_{max} (rel. absorption) = 268 (0.04), 275 (0.04), 405 (0.29), 512 (0.03) nm. – **IR** (ATR): $\tilde{\nu}$ = 2953, 2918, 2868, 2850, 1776, 1731, 1714, 1669, 1653, 1595, 1560, 1547, 1541, 1531, 1507, 1493, 1482, 1459, 1377, 1364, 1306, 1261, 1220, 1196, 1180, 1096, 1081, 1058, 1045, 1018, 970, 935, 881, 861, 846, 800, 769, 748, 738, 720, 701, 663, 652, 643, 635, 616, 603, 595, 578, 569, 557, 537, 520, 499, 490, 482, 473, 466, 458, 445, 435, 422, 409, 391, 378 cm^{-1}. – **HRMS** (ESI) ($C_{45}H_{28}N_4OPt$): calc.: 835.1911, found: 835.1868.

[1,2-Bis(5,10,15-triphenylporphyrin)phenylene]copper(II) (**157**)[83]

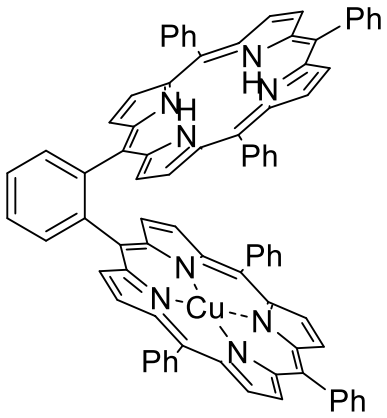

[5-(2-Formylphenyl)-10,15,20-triphenylporphyrin]copper(II) (**154**) (28.8 mg, 55.3 μmol, 1.00 equiv.) was dissolved in dry toluene (60 mL). A stream of argon was passed through the mixture for 15 min to remove dissolved oxygen. After the addition of benzaldehyde (25.3 mg, 280 μmol, 5.00 equiv.), pyrrole (24.6 mg, 370 μmol, 7.00 equiv.) and TFA (3.19 mg, 22.4 μmol, 0.40 equiv.), the reaction mixture was stirred for 66 h at room temperature. After monitoring the reaction progress, the second portion of benzaldehyde (25.3 mg, 280 μmol, 5.00 equiv.), pyrrole (24.6 mg, 370 μmol, 7.00 equiv.) and TFA (3.19 mg, 22.4 μmol, 0.40 equiv.) was added and the reaction mixture was stirred for further 24 h at room temperature. DDQ (30.6 mg, 135 μmol, 2.42 equiv.) was added. After 30 min, NEt_3 (1 mL) was added and the solvent was removed under reduced pressure. The resulting crude product was filtered through a short layer of silica gel eluting with CH_2Cl_2. The solvent was removed under reduced pressure and the crude product was purified by flash column chromatography on silica gel (CH_2Cl_2/*n*-pentane, 1:2) to afford the title compound **157** as a purple solid (10.0 mg, 8.24 μmol, 15%).

***R*f** (CH_2Cl_2/*n*-pentane 1:2) = 0.30.– **UV-Vis** (CH_2Cl_2): λ_{max} (rel. absorption) = 267 (0.04), 276 (0.04), 321 (0.01), 406 (0.23), 522 (0.01), 550 (0.01) nm. – **IR** (ATR): $\tilde{\nu}$ = 2955, 2922, 2853, 1460, 1378, 1259, 1096, 1020, 798 cm^{-1}. – **HRMS** (ESI) ($C_{82}H_{53}CuN_8^+$): calc.: 1212.3689, found: 1212.3663.

[1,2-Bis(5,10,15-triphenylporphyrin)phenylene]palladium(II) (**158**)[83]

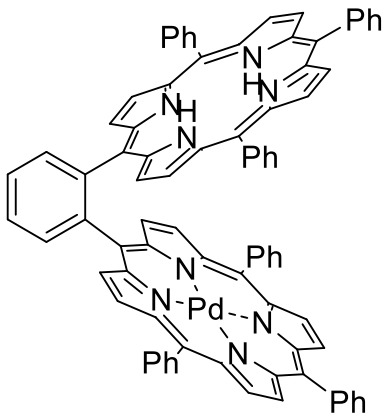

[5-(2-Formylphenyl)-10,15,20-triphenylporphyrin] palladium(II) (**155**) (19.3 mg, 25.8 μmol, 1.00 equiv.) was dissolved in dry toluene (30 mL). A stream of argon was passed through the mixture for 15 min to remove dissolved oxygen. After the addition of benzaldehyde (16.9 mg, 160 μmol, 6.00 equiv.), pyrrole (16.4 mg, 240 mol, 6.00 equiv.) and TFA (3.19 mg, 22.4 μmol, 0.40 equiv.), the reaction mixture was stirred for 67 h at room temperature. After monitoring the reaction progress, the second portion of benzaldehyde (16.9 mg, 160 μmol, 9.00 equiv.), pyrrole (16.4 mg, 240 μmol, 9.00 equiv.) and TFA (3.19 mg, 22.4 μmol, 0.40 equiv.) was added and the reaction mixture was stirred for further 24 h at room

temperature. DDQ (14.2 mg, 62.6 μmol, 2.42 equiv.) was added. After 30 min, NEt_3 (1 mL) was added and the solvent was removed under reduced pressure. The resulting crude product was filtered through a short layer of silica gel eluting with CH_2Cl_2. The solvent was removed under reduced pressure and the crude product was purified by flash column chromatography on silica gel (CH_2Cl_2/*n*-pentane 1:2) to afford the title compound **158** as a purple-red solid (5.10 mg, 4.06 μmol, 18%).

R_f (CH_2Cl_2/*n*-pentane 1:1) = 0.40. – **^{1}H NMR** (500 MHz, THF-d_8): δ = 9.15 (d, ^3J = 4.9 Hz, 2 H, $H_{pyrrole}$), 9.12 – 9.08 (m, 2H, $H_{pyrrole}$), 8.93 – 8.90 (m, 1H, $H_{aromatic}$), 8.89 – 8.86 (m, 1H, $H_{aromatic}$), 8.39 – 8.30 (m, 6H, $H_{pyrrole}$), 8.30 – 8.24 (m, 4H, $H_{pyrrole}$), 8.22 – 8.16 (m, 4H, 2$H_{pyrrole}$, 2H_{ar}), 8.03 – 7.99 (m, 2H, $H_{aromatic}$), 7.99 – 7.97 (m, 2H, $H_{aromatic}$), 7. 74 – 7.63 (m, 10H, $H_{aromatic}$), 7.63 – 7.47 (m, 16H, $H_{aromatic}$), –3.96 (s, 2H, N*H*) ppm. – **UV-Vis** (CH_2Cl_2): λ_{max} (rel. absorption) = 275 (0.06), 323 (0.02), 325 (0.02), 407 (0.23), 530 (0.02) nm. – **IR** (ATR): $\tilde{\nu}$ = 2919, 1375, 1350, 1262, 1071, 1013, 976, 965, 796, 749, 739, 730, 714, 701, 666, 659, 652, 618, 555, 526, 518, 509, 494, 375 cm^{-1}. – **HRMS** (ESI) ($C_{82}H_{53}PdN_8^+$): calc.: 1255.3423, found: 1255.3444.

[1,2-Bis(5,10,15-triphenylporphyrin)phenylene]platinum(II) (**159**)[83]

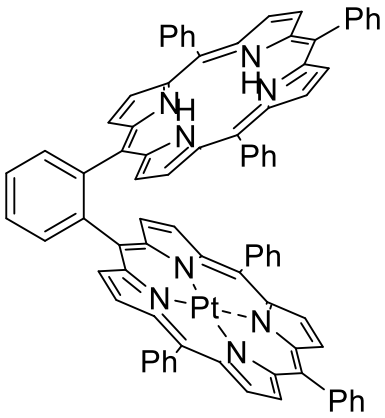

[5-(2-Formylphenyl)-10,15,20-triphenylporphyrin] platinum(II) (**156**) (21.8 mg, 26.1 μmol, 1.00 equiv.) was dissolved in dry toluene (30 mL). A stream of argon was passed through the mixture for 15 min to remove dissolved oxygen. After the addition of benzaldehyde (16.9 mg, 160 μmol, 6.00 equiv.), pyrrole (16.4 mg, 240 μmol, 9.00 equiv.) and TFA (3.19 mg, 22.4 μmol, 0.40 equiv.), the reaction mixture was stirred for 16 h at room temperature. After monitoring the reaction progress, benzaldehyde (16.9 mg, 160 μmol, 6.00 equiv.), pyrrole (16.4 mg, 240 μmol, 9.00 equiv.) and TFA (3.19 mg, 22.4 μmol, 0.40 equiv.) were added again and the reaction mixture was stirred for further 24 h at room temperature. DDQ (14.3 mg, 63.0 μmol, 2.42 equiv.) was added. After 30 min, NEt_3 (1 mL) was added and the solvent was removed under reduced pressure. The resulting crude product was filtered through a short layer of silica gel eluting with CH_2Cl_2. The solvent was removed under reduced pressure and the crude product was purified by flash column chromatography on silica gel (CH_2Cl_2/*n*-pentane 1:2 → 1:1) to afford the title compound **159** as a purple-red solid (1.9 mg, 1.41 μmol, 5%).

R_f (CH_2Cl_2/*n*-pentane 1:1) = 0.40. – **^{1}H NMR** (500 MHz, $CDCl_3$): δ = 9.15 – 9.11 (m, 4H, $H_{pyrrole}$), 8.83 – 8.80 (m, 1H, $H_{aromatic}$), 8.80 - 8.77 (m, 1H, $H_{aromatic}$), 8.44 – 8.40 (m, 2H, $H_{pyrrole}$), 8.40 – 8.35 (m, 2H, $H_{pyrrole}$), 8.34 – 8.23 (m, 10H, 8$H_{pyrrole}$, 2$H_{aromatic}$), 8.05 – 8.00 (m, 1H, H_{ar}), 8.00 – 7.95 (m, 1H, $H_{aromatic}$), 7.81 – 7.74 (m, 2H, $H_{aromatic}$), 7.74 – 7.63 (m, 8H, $H_{aromatic}$), 7.63 – 7.55 (m, 9H, $H_{aromatic}$), 7.55 – 7.48 (m, 4H, $H_{aromatic}$), 7.48 – 7.42 (m, 3H, $H_{aromatic}$), 7.42 – 7.37 (m, 2H, $H_{aromatic}$), –3.86 (s, 2H, N*H*) ppm. – **UV-Vis** (CH_2Cl_2): λ_{max} (rel. absorption) = 275 (0.08), 323 (0.02), 398 (0.54), 521 (0.03) nm. – **IR** (ATR): $\tilde{\nu}$ = 2921, 2853, 1725, 1458, 1439, 1375, 1356, 1315, 1264, 1218, 1208, 1177, 1156, 1119, 1102, 1072, 1017, 1001, 980, 966, 922, 909, 902, 894, 875, 853, 839, 796, 749, 739, 713, 701, 676, 666, 659, 647, 639, 632, 620, 611, 599, 572, 561, 541, 531, 523, 516, 503, 497, 486, 470, 453, 446, 439, 419, 408, 397, 385cm^{-1}. – **HRMS** (ESI) ($C_{82}H_{53}PtN_8^+$): calc.: 1344.4014, found: 1344.4022.

[1,2-Bis(5,10,15-triphenylporphyrin)phenylene]copper(II)-iron(III)-chloride (**160**)[385]

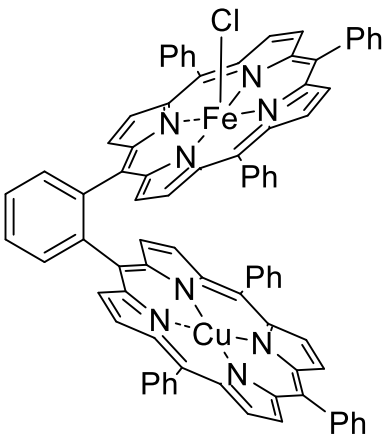

A crimp vial was charged with [1,2-bis(5,10,15-triphenylporphyrin)phenylene]copper(II) (**157**) (0.5 mg, 0.41 µmol, 1.00 equiv.), $FeCl_2$ (0.2 mg, 1.58 µmol, 4.00 equiv.) and DMF (0.5 mL). The reaction mixture was stirred at 150 °C for 20 h. The solvent was removed under reduced pressure. The crude product was purified by flash column chromatography on silica gel (CH_2Cl_2/MeOH, 1:0 → 19:1) to afford the title compound **160** as a brown solid. The yield could not be determined due to the presence of several ancillary ligands.

***R*$_f$** (CH_2Cl_2/MeOH, 20:1) = 0.26. – **UV-Vis** (CH_2Cl_2): λ_{max} (rel. absorption) = 276 (0.03), 300 (0.02), 323 (0.02), 327 (0.02), 410 (0.22), 547 (0.01) nm. – **IR** (ATR): $\tilde{\nu}$ = 2952, 2921, 2851, 1711, 1598, 1577, 1538, 148, 1456, 1442, 1377, 1344, 1245, 1220, 1203, 1174, 1126, 1099, 1071, 1018, 1003, 996, 976, 945, 890, 877, 846, 833, 820, 798, 754, 717, 701, 662, 652, 630, 616, 611, 588, 577, 564, 543, 521, 493, 473, 466, 448, 433, 424, 408, 392, 380 cm^{-1}. – **HRMS** (ESI) ($C_{82}H_{50}CuFeN_8^+$): calc.: 1265.2798, found: 1265.2798.

[1,2-Bis(5,10,15-triphenylporphyrin)phenylene]iron(III)-paladium(II) (**161**)[385]

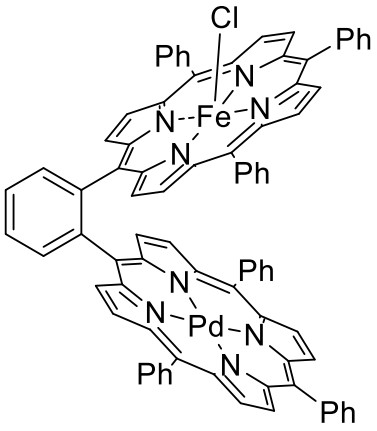

A crimp vial was charged with [1,2-bis(5,10,15-triphenylporphyrin)phenylene]palladium(II) (**158**) (0.5 mg, 0.4 μmol, 1.00 equiv.), $FeCl_2$ (0.2 mg, 1.58 μmol, 4.00 equiv.) and DMF (0.5 mL). The reaction mixture was stirred at 150 °C for 20 h. Subsequently, the solvent was removed under reduced pressure. The crude product was purified by flash column chromatography on silica gel (CH_2Cl_2/MeOH, 1:0 → 19:1) to afford the title compound **161** as a brown solid. The yield could not be determined due to the presence of several ancillary ligands.

***R*f** (CH_2Cl_2/MeOH, 20:1) = 0.20. – **UV-Vis** (CH_2Cl_2): λ_{max} (rel. absorption) = 321 (0.02), 332 (0.02), 347 (0.03), 415 (0.1), 471 (0.01), 527 (0.02) nm. – **IR** (ATR): $\tilde{\nu}$ = 2952, 2922, 2868, 2853, 1711, 1635, 1606, 1601, 1575, 1570, 1557, 1548, 1538, 1531, 1516, 1456, 1417, 1405, 1375, 1169, 1119, 1074, 1051, 1016, 972, 939, 897, 885, 870, 864, 854, 844, 832, 817, 799, 756, 735, 714, 703, 683, 674, 662, 653, 645, 633, 616, 606, 594, 588, 577, 557, 543, 533, 526, 507, 500, 492, 480, 470, 462, 449, 439, 431, 409, 398, 388, 380 cm^{-1}. – **HRMS** (ESI) ($C_{82}H_{50}FeN_8Pd^+$): calc.: 1308.2537, found: 1308.2551.

[1,2-Bis(5,10,15-triphenylporphyrin)phenylene]iron(III)-platinum(II) (**162**)[385]

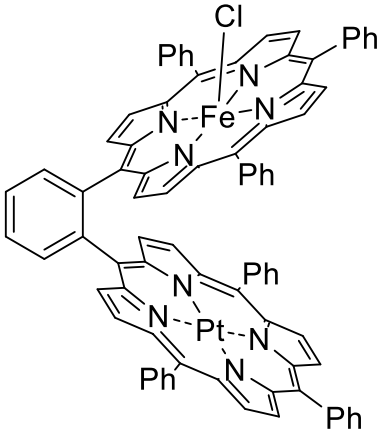

A crimp vial was charged with [1,2-bis(5,10,15-triphenylporphyrin)phenylene]platinum(II) (**159**) (0.5 mg, 0.40 μmol, 1.00 equiv.), $FeCl_2$ (0.2 mg, 1.58 μmol, 4.00 equiv.) and DMF (0.5 mL). The reaction mixture was stirred at 150 °C for 20 h. Subsequently, the solvent was removed under reduced pressure. The crude product was purified by flash column chromatography on silica gel (CH_2Cl_2/MeOH, 1:0 → 19:1) to afford the title compound **162** as a brown solid. The yield could not be determined due to inaccuracies of the ancillary ligand.

***R*f** (CH_2Cl_2/MeOH, 20:1) = 0.35. – **UV-Vis** (CH_2Cl_2): λ_{max} (rel. absorption) = 275 (0.20), 321 (0.05), 401 (0.24), 516 (0.03) nm. – **IR** (ATR): $\tilde{\nu}$ = 1050, 1040, 1017, 1003, 993, 976, 963, 946, 483, 463, 456, 499, 438, 429, 416, 407, 398, 390, 381 cm^{-1}. – **HRMS** (ESI) ($C_{82}H_{50}FeN_8Pt^+$): calc.: 1397.3150, found: 1397.2952.

[1,2-Bis(5,10,15-triphenylporphyrin)phenylene]^{57}iron(III)-nickel(II) (**153**$^{\boldsymbol{möss}}$)[385]

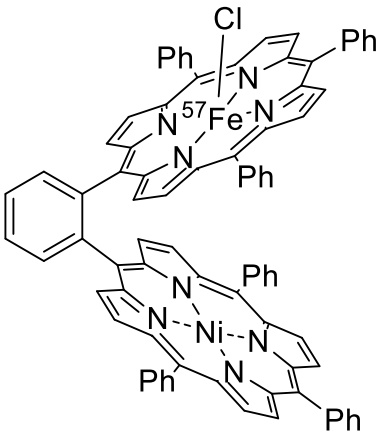

A crimp vial was charged with [1,2-bis(5,10,15-triphenylporphyrin)phenylene]nickel(II) (**151**) (2.00 mg, 1.66 µmol, 1.00 equiv.), $FeCl_2$ (1.6 mg, 12.6 µmol, 7.63 equiv.), $^{57}FeCl_2$ (1.6 mg, 12.5 µmol, 7.58 equiv.) and DMF (2 mL). The reaction mixture was stirred at 150 °C for 4 h. Subsequently, the solvent was removed under reduced pressure. The crude product was purified by flash column chromatography on silica gel (CH_2Cl_2/MeOH, 1:0 → 99:1) to afford the title compound **153**$^{\boldsymbol{möss}}$ as a brown solid. The yield could not be determined due to inaccuracies of the ancillary ligand.

$\boldsymbol{R_f}$ (CH_2Cl_2/MeOH, 20:1) = 0.49. – **HRMS** (ESI) ($C_{82}H_{50}Cu^{57}FeN_8^+$) calc.: 1260.286, found: 1260.285.

[1,2-Bis(5,10,15-triphenylporphyrin)phenylene]^{57}iron(III)-copper(II) (**163**)[385]

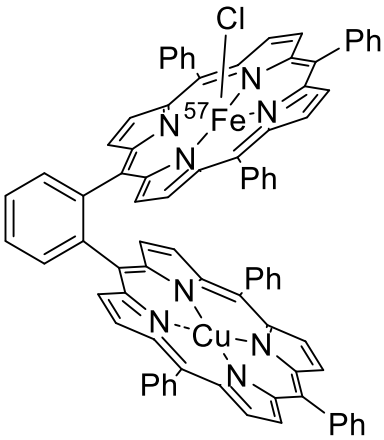

A crimp vial was charged with [1,2-bis(5,10,15-triphenylporphyrin)phenylene]copper(II) (**157**) (5.00 mg, 4.10 µmol, 1.00 equiv.), $FeCl_2$ (0.6 mg, 5.05 µmol, 1.00 equiv.), $^{57}FeCl_2$ (1.5 mg, 11.8 µmol, 3.00 equiv.) and DMF (4.5 mL). The reaction mixture was stirred at 150 °C for 24 h. Subsequently, the solvent was removed under reduced pressure. The crude product was purified by flash column chromatography on silica gel (CH_2Cl_2/MeOH, 1:0 → 19:1) to afford the title compound **163** as a brown solid. The yield could not be determined due to inaccuracies of the ancillary ligand.

$\boldsymbol{R_f}$ (CH_2Cl_2/MeOH, 20:1) = 0.26. – **HRMS** (ESI) ($C_{82}H_{50}Ni^{57}FeN_8^+$): calc.: 1262.9568, found: 1266.2815.

[1,2-Bis(5,10,15-triphenylporphyrin)phenylene]^{57}iron(III)-palladium(II) (**164**)[385]

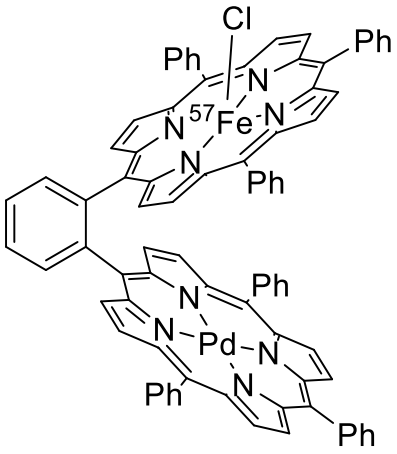

A crimp vial was charged with [1,2-bis(5,10,15-triphenylporphyrin)phenylene]palladium(II) (**158**) (2.00 mg, 1.59 μmol, 1.00 equiv.), $FeCl_2$ (0.3 mg, 2.34 μmol, 1.00 equiv.), $^{57}FeCl_2$ (0.6 mg, 4.72 μmol, 3.00 equiv.) and DMF (1,8 mL). The reaction mixture was stirred at 150 °C for 24 h. Subsequently, the solvent was removed under reduced pressure. The crude product was purified by flash column chromatography (CH_2Cl_2/MeOH, 1:0 → 49:1) to afford the title compound **164** as a brown solid. The exact yield was not determined due to inaccuracies of the ancillary ligand but ranked in >70%.

***R*f** (CH_2Cl_2/MeOH, 20:1) = 0.20. – **HRMS** (ESI) ($C_{82}H_{50}{}^{57}FeN_8Pd^+$): calc.: 1309.2542, found: 1309.2568.

[1,2-Bis(5,10,15-triphenylporphyrin)phenylene]^{57}iron(III)-platinum(II) (**165**)[385]

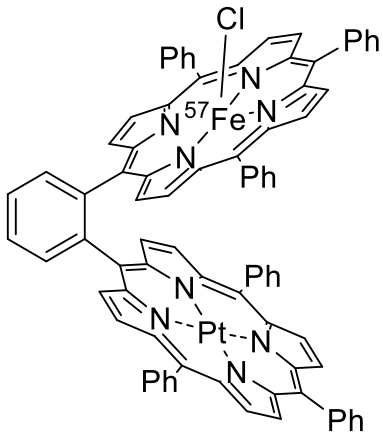

A vial was charged with [1,2-bis(5,10,15-triphenylporphyrin)phenylene]platinum(II) (**159**) (1.50 mg, 1.12 μmol, 1.00 equiv.), $FeCl_2$ (0.2 mg, 1.58 μmol, 1.00 equiv.), $^{57}FeCl_2$ (0.7 mg, 5.61 μmol, 3.00 equiv.) and DMF (2 mL). The reaction mixture was stirred at 150 °C for 24 h. Subsequently, the solvent was removed under reduced pressure. The crude product was purified by flash column chromatography on silica gel (CH_2Cl_2/MeOH, 1:0 → 99:1) to afford the title compound (**165**) as a brown solid. The yield could not be determined due to inaccuracies of the ancillary ligand.

***R*f** (CH_2Cl_2/MeOH, 20:1) = 0.35. – **HRMS** (ESI) ($C_{82}H_{50}{}^{57}FeN_8Pt^+$) calc.: 1398.3155, found: 1398.3002.

1,2-Phenylene-([5-(10,15,20-triphenylporphyrin)]-manganese(III),[5-(10,15,20-triphenylporphyrin)]copper(II)-chlorid) (**166**)[380]

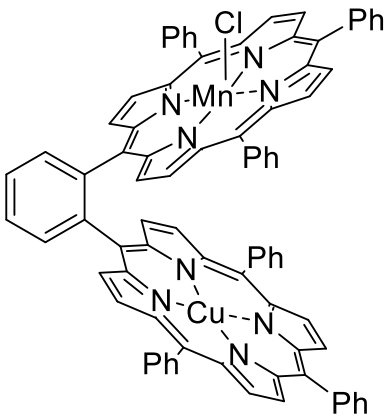

[1,2-Bis(5,10,15-triphenylporphyrin)phenylene]copper(II) (**157**) (1.5 mg, 1.24 µmol, 1.00 equiv.) and $MnCl_2$ (1.00 mg, 7.95 µmol, 6.41 equiv.) were dissolved in DMF (1 mL) and stirred for 2 h at 150 °C. Subsequently, the solvent was removed under reduced pressure. The crude product was purified by flash column chromatography on silica gel (CH_2Cl_2/MeOH, 19:1) to afford the title compound **166** as a brown solid (1.6 mg, 1.24 µmol, quant.).

HRMS (ESI) ($C_{82}H_{52}ClCuMnN_8^+$) calc.: 1301.268, found: 1301.252.

6.4.6 Synthetic approaches towards intramolecular lanthanide complexes

Ytterbium(III) acetylacetonate (**167**)[137]

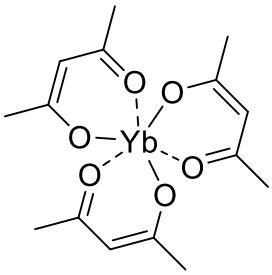

$YtCl_2$ (506 mg, 1.25 mmol, 1.00 equiv.) was dissolved in H_2O (2.0 mL). After the addition of acetylacetone (390 µL, 380 mg, 3.81 mmol, 3.10 equiv.) and 25% aqueos ammonia solution (250 µL, 227 mg, 6.46 mmol, 3.10 equiv.), the reaction mixture was stirred for 1 h before it was cooled to 0 °C. Filtration, washing with H_2O and removal of the solvent under reduced pressure gave the title compound **167** as a white solid. **UV-Vis** (CH_2Cl_2): λ_{max} (rel. absorption) = 275 (0.19) nm. **IR** (ATR): $\tilde{\nu}$ = 1584, 1517, 1449, 1445, 1384, 1361, 1265, 1190, 1014, 922, 790, 769, 761, 727, 720, 705, 681, 656, 611, 591, 581, 564, 535, 507, 493, 483, 466, 459, 452, 439, 399, 377 cm^{-1}.

[1,2-Phenylene-bis-5-(10,15,20-triphenyporphyrin)]-ytterbium(III) **171** / [1,2-Phenylene-bis-5-(10,15,20-triphenyporphyrin)]-diytterbium(III) **174**[137]

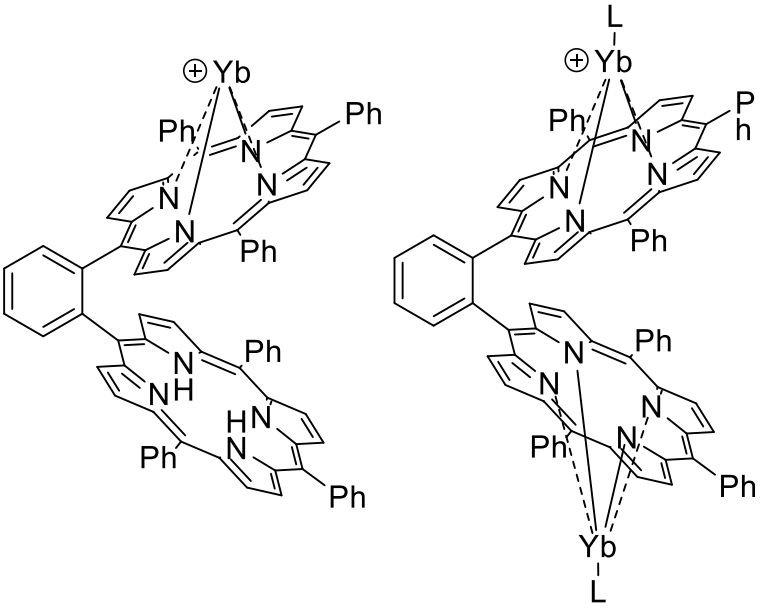

1,2-Phenylene-bis-5-(10,15,20-triphenyporphyrin) (**128**) (2.0 mg, 1.74 µmol, 1.00 equiv.) and $Yb(acac)_3$ **167** (3.3 mg, 7.02 µmol, 4.00 equiv.) were dissolved in 1,2,4-trichlorobenzene (1 mL). Subsequently, the reaction mixture was stirred for 7.5 at 220 °C. Afterward, the solvent was removed under reduced pressure. The crude product was purified by flash column chromatography on silica gel (CH_2Cl_2/MeOH, 100:0 → 100:1) to afford the title compounds **171** and **174** as red solids

***R*f** (CH_2Cl_2/MeOH, 20:1) = 0.30. – **HRMS** (ESI) ($C_{82}H_{52}N_8Yb$): calc.: 1322.370, found: 1322.364, 1338.359 and ($C_{82}H_{50}N_8Yb_2OH$): calc.: 1511.296, found: 1511.284, 1582.310.

6.5 Cofacial *o*-phenylene trisporphyrin metal complexes

6.5.1 The *o*-dipyrromethane-phenyl group as residue functionalization to enable *o*-phenylene trisporphyrin syntheses

5-(2-(Di(1H-pyrrol-2-yl)methyl)phenyl)-10,15,20-triphenylporphyrin (**175**) [387]

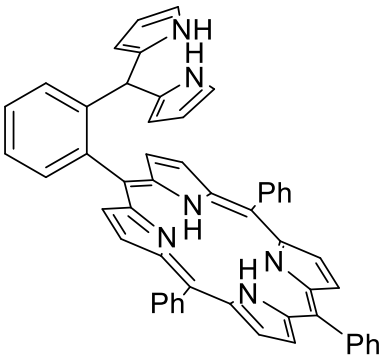

Under an argon atmosphere, 5-(2-formylphenyl)-10,15,20-triphenylporphyrin (**125**) (60.0 mg, 93,3 µmol, 1.00 equiv.) was dissolved in pyrrole (6.5 mL, 6288 mg, 93.7 mmol, 1004 equiv.). A stream of argon was passed through the mixture for 15 min to remove dissolved oxygen. Then, TFA (24.7 mL, 36.5 g, 338 µmol, 3.62 equiv.) was added dropwise. The mixture was stirred for 4 h in the dark. Afterward, triethylamine (0.5 mL) was added and stirred for 15 min. Subsequently, the solvent was removed under reduced pressure in the absence of air. The crude product was purified by flash column chromatography on silica gel (toluene) to afford the title compound **175** as a purple solid (66.0 mg, 87.2 µmol, 93%).

***R*f** (toluene) = 0.58. – **^{1}H NMR** (500 MHz, toluene-d_8): δ = 8.88 – 8.83 (m, 4H, $H_{pyrrole}$), 8.79 (d, ^{3}J = 4.7 Hz, 2H, $H_{pyrrole}$), 8.66 (d, ^{3}J = 4.8 Hz, 2H, $H_{pyrrole}$), 8.13 – 8.04 (m, 6H, $H_{aromatic}$), 7.95 (dd. J = 7.5, 1.4 Hz, 1H, $H_{aromatic}$), 7.69 (dd, J = 8.1, 1.4 Hz, 1H, $H_{aromatic}$), 7.53 – 7.42 (m, 10H, $H_{aromatic}$), 7.34 (td, J = 7.5, 1.4 Hz, 1H, $H_{aromatic}$), 6.30 (bs, 2H, $NH_{dipyrromethane}$), 6.04 (dd, J = 6.5, 2.8 Hz, 2H, $H_{dipyrromethane}$), 5.93 – 5.85 (m, 4H, $H_{dipyrromethane}$), 4.98 (s, 1H, $H_{dipyrromethane}$), –2.19 (bs, 2H, NH) ppm. – **^{13}C NMR** (126 MHz, toluene-d_8) : δ = 145.9 (C_q), 143.3 (C_q), 143.1 (C_q), 141.6 (C_q), 134.0 (C_q), 135.3 (+, CH), 135.3 (+, CH), 135.2 (+, CH), 134.5 (+, CH), 132.8 (C_q), 129.6 (+, CH), 128.6 (+, CH), 128.5 (+, CH), 128.3 (+, CH), 128.2 (+, CH), 127.3 (+, CH), 127.3 (+, CH), 126.0 (+, CH), 121.2 (C_q), 121.0 (C_q), 118.6 (+, CH), 116.7 (+, CH), 42.4 (+, CH) ppm. – **UV-Vis** (CH_2Cl_2): λ_{max} (rel. absorption) = 217 (0.21), 298 (0.07), 419 (1.61), 482 (0.02), 516 (0.08), 550 (0.04), 590 (0.03), 646 (0.02) nm. – **IR (ATR)**: $\tilde{\nu}$ = 3410, 3309, 3050, 3017, 2919, 2847, 1691, 1595, 1554, 1469, 1439, 1400, 1347, 1213, 1176, 1153, 1111, 1069, 1054, 1030, 1000, 979, 965, 798, 748, 720, 698, 656, 640, 463, 452, 439, 425, 416, 398, 382 cm^{-1}. – **MS** (ESI): *m/z* (%) = 759.3 (33) $[M+H]^+$, 643.2 (100). – **HRMS** (ESI) ($C_{53}H_{38}N_6$): calc.: 759.3236, found: 759.3225.

Additional information on the reaction details is available *via* the Chemotion repository: https://dx.doi.org/10.14272/reaction/SA-FUHFF-UHFFFADPSC-FJGPNDURHC-UHFFFADPSC-NUHFF-NXVFY-NUHFF-ZZZ

Additional information on the analysis of the target compound is available *via* the Chemotion repository:

https://dx.doi.org/10.14272/FJGPNDURHCLNNX-IIFGQYIMSA-N.1

6.5.2 Synthesis of free-base cofacial porphyrintrimer ligands

5,15-Bis(2-(10,15,20)-triphenylporphyrinylphenyl)-10,20-diphenylporphyrin (**34**)[373]

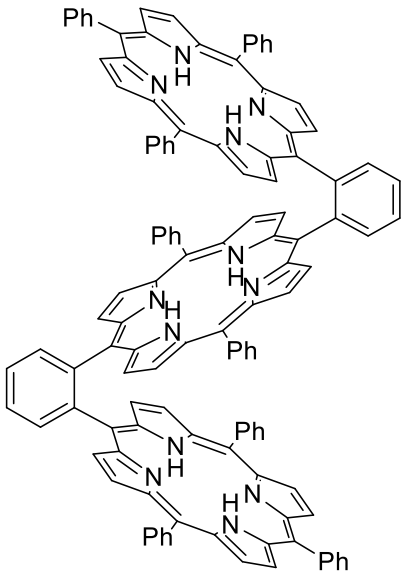

Route A:

Under an argon atmosphere, 5-(2-(di(1H-pyrrole-2-yl)methyl)phenyl)-10,15,20-triphenylporphyrin (**175**) (150 mg, 198 µmol, 2.00 equiv.) was dissolved in CH_2Cl_2, (60 mL) previously degassed by three freeze-pump-thaw-cycles. Subsequently, in sum, benzaldehyde (73.0 µL, 75.9 mg, 715 µmol, 7.22 equiv.) and TFA (64.6 µL, 95.6 mg, 1.18 mmol, 8.46 equiv.) were added within 26.5 h while stirring the mixture in the dark until all starting material was consumed. Afterward, DDQ (47.2 mg, 208 µmol, 2.10 equiv.) was added and stirred for 1 h under air, whereas oxygen suppored oxidation. Then, NEt_3 (5 mL) was added and the crude mixture was concentrated under reduced pressure, filtered through a short layer of silica gel eluting with CH_2Cl_2 + 1% NEt_3 and purified by flash column chromatography on silica gel (1 × CH_2Cl_2/*n*-pentane, 1:1 + 1% NEt_3); (1 × toluene/*c*Hex, 5:1) to afford the title compound **34** as a purple solid (22.2 mg, 13.2 µmol, 13%).

Route B:

The reaction procedure of route A was adapted using the following conditions: benzaldehyde (2.00 equiv.), $BF_3 \cdot OEt_2$ (2.00 equiv.), DDQ (2.44 equiv.), NEt_3, CH_2Cl_2, room temperature 19 h. The title compound **34** was obtained as a purple solid (3.2 mg, 1.9 µmol, 1.9%).

***R*f** (CH_2Cl_2) = 0.60. – **^{1}H NMR** (500 MHz, CD_2Cl_2): δ = 9.10 (d, ^3J = 4.8 Hz, 4H, $H_{pyrrole}$), 9.06 (d, ^3J = 4.8 Hz, 4H, $H_{pyrrole}$), 8.56 (d, ^3J = 4.8 Hz, 4H, $H_{pyrrole}$), 8.48 (dd, J = 6.5, 2.9 Hz, 2H, $H_{linker\text{-}benzene}$), 8.48 (dd, J = 6.3, 2.9 Hz, 2H, $H_{linker\text{-}benzene}$), 8.27 (d, ^3J = 4.8 Hz, 4H, $H_{pyrrole}$), 8.12 (d, ^3J = 4.8 Hz, 4H, $H_{pyrrole}$), 8.07 (d, ^3J = 4.7 Hz, 4H, $H_{pyrrole}$), 8.06 – 8.02 (m, 4H, $H_{aromatic}$), 7.99 (d, ^3J = 7.6 Hz, 2H, $H_{aromatic}$), 7.86 (d, ^3J = 7.8 Hz, 2H, $H_{aromatic}$), 7.75 (t, ^3J = 7.4 Hz, 3H, $H_{aromatic}$), 7.72 – 7.67 (m, 6H, $H_{aromatic}$), 7.66 – 7.60 (m, 5H, $H_{aromatic}$), 7.56 – 7.53 (m, 2H, $H_{aromatic}$), 7.53 – 7.41 (m, 10H, $H_{aromatic}$), 7.12 (d, ^3J = 7.3 Hz, 2H, $H_{aromatic}$), 6.73 – 6.65 (m, 4H, $H_{aromatic}$), 6.65 – 6.56 (m, 4H, $H_{aromatic}$), –3.79 (bs, 4H, NH_{out}), –4.20 (bs, 2H, NH_{in}) ppm. – **^{13}C NMR** (126 MHz, CD_2Cl_2) : δ = 144.9 (C_q), 144.7 (C_q), 142.5 (C_q), 142.1 (C_q), 142.1 (C_q), 136.9

(C_q), 136.5 (C_q), 135.3 (+, CH), 135.0 (+, CH), 134.8 (+, CH), 134.8 (+, CH), 134.4 (+, CH), 134.3 (+, CH), 132.5 – 128.9 (m, C_q), 128.1 (+, CH), 127.8 (+, CH), 127.6 (+, CH), 127.2 (+, CH), 127.2 (+, CH), 127.2 (+, CH), 126.8 (+, CH), 126.6 (+, CH), 120.3 (C_q), 119.8 (C_q), 119.6 (C_q), 119.2 (C_q), 118.9 (C_q) ppm. – **UV-Vis** (CH_2Cl_2): λ_{max} (rel. absorption) = 288 (3.12), 404 (4.14), 522 (3.01), 549 (2.72), 596 (2.59), 651 (2.34) nm. – **IR (ATR)**: $\tilde{\nu}$ = 2953, 2919, 2854, 1666, 1596, 1468, 1439, 1349, 1259, 1181, 1153, 1088, 1072, 1031, 967, 800, 798, 749, 730, 703, 577, 511, 418, 397 cm^{-1}. – **HRMS** (ESI) ($C_{120}H_{78}N_{12}H$): calc.: 1687.6551, found: 1687.6552.

Additional information on the reaction details is available *via* the Chemotion repository: https://dx.doi.org/10.14272/reaction/SA-FUHFF-UHFFFADPSC-MGTQLOOLBA-UHFFFADPSC-NUHFF-NZPNZ-NUHFF-ZZZ

Additional information on the analysis of the target compound is available *via* the Chemotion repository: https://dx.doi.org/10.14272/MGTQLOOLBARGGW-FOTJXGMTSA-N.1

6.5.3 Homotrimetallic *o*-phenylene-linked trisporphyrin complexes

5,15-Bis(2-(10,15,20)-triphenylporphyrinylphenyl)-10,20-diphenylporphyrin-trichloro-trimanganese(III) (**177**)[380]

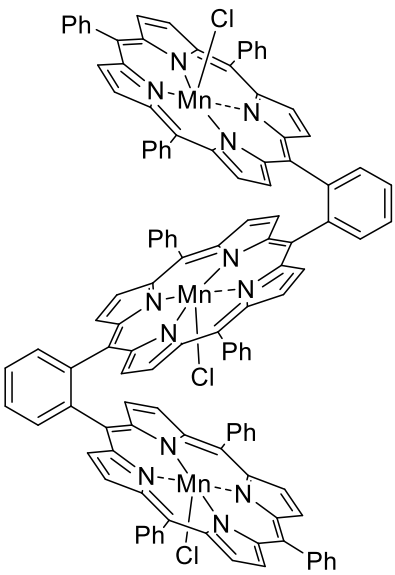

5,15-Bis(2-(10,15,20)-triphenylporphyrinylphenyl)-10,20-diphenylporphyrin (**34**) (2.5 mg, 1.48 µmol, 1.00 equiv.) and $MnCl_2$ (1.9 mg, 15.1 µmol, 10.2 equiv.) were dissolved in DMF (2 mL). The reaction mixture was stirred for 3 h at 150 °C, changing its color from brown to green. Subsequently, the solvent was removed under reduced pressure. The crude product was purified by flash column chromatography on silica gel (CH_2Cl_2/MeOH, 10:1) to afford the title compound **177** as a brown solid (2.5 mg, 12.8 µmol, 86%).

R_f (CH_2Cl_2/MeOH, 19:1) = 0.27. – **UV-Vis** (CH_2Cl_2): λ_{max} (rel. absorption) = 226 (2.93), 279 (0.80), 408 (1.20), 476 (0.52), 595 (0.11), 725 (0.01), 783 (0.01), 888 (0.02) nm. – **IR (ATR)**: $\tilde{\nu}$ = 2953, 2921, 2851, 1724, 1649, 1596, 1541, 1487, 1460, 1441, 1401, 1375, 1341, 1300, 1261, 1221, 1203, 1179, 1156, 1072, 1030, 1010, 982, 966, 887, 875, 850, 799, 754, 714, 703, 664, 649, 619, 606, 591, 577, 560, 538, 521, 499, 493, 479, 466, 453, 428, 419, 408, 397, 384 cm^{-1}. – **HRMS** (ESI) ($C_{120}H_{72}N_{12}Cl_2Mn_3$): calc.: 1915.3521, found: 1915.3550.

Additional information on the reaction details is available *via* the Chemotion repository: https://dx.doi.org/10.14272/reaction/SA-FUHFF-UHFFFADPSC-BZKSZHYSBV-UHFFFADPSC-NUHFF-KKQLC-NUHFF-ZZZ

Additional information on the analysis of the target compound is available *via* the Chemotion repository: https://dx.doi.org/10.14272/BZKSZHYSBVPMTQ-PAOGYPPFSA-K.1

5,15-Bis(2-(10,15,20)-triphenylporphyrinylphenyl)-10,20-diphenylporphyrin-chloro-oxo-triiron(III) (**178**)[7]

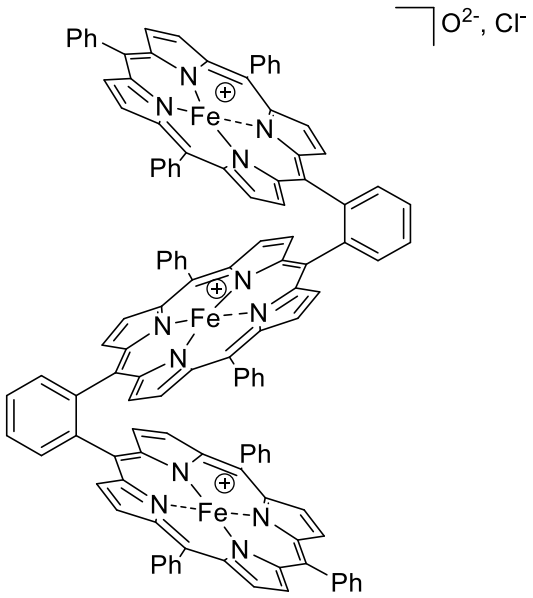

5,15-Bis(2-(10,15,20)-triphenylporphyrinylphenyl)-10,20-diphenylporphyrin (**34**) (2.5 mg, 1.48 µmol, 1.00 equiv.) and $FeBr_2$ (3.2 mg, 14.8 µmol, 10.2 equiv.) were dissolved in DMF (2 mL). The reaction mixture was stirred for 3 h at 150 °C, changing its color from brown to dark brown. Subsequently, the solvent was removed under reduced pressure. The crude product was dissolved in CH_2Cl_2 (20 mL) and washed with 1 M aqueous HCl solution (3 × 20 mL), dried over Na_2SO_4, filtered and removed the solvent under reduced pressure. The obtained crude product was purified by flash column chromatography on silica gel (CH_2Cl_2/MeOH, 10:1) to afford the title compound **178** as a brown solid (2.5mg, 1.32 µmol, 89%).

***R*f** (CH_2Cl_2/MeOH, 19:1) = 0.20. – **UV-Vis** (CH_2Cl_2): λ_{max} (rel. absorption) = 226 (2.82), 284 (0.44), 374 (0.98), 411 (1.33), 518 (0.22), 670 (0.05), 698 (0.05) nm. **IR (ATR)**: $\tilde{\nu}$ = 2953, 2919, 2851, 1721, 1717, 1669, 1596, 1460, 1441, 1415, 1397, 1377, 1366, 1334, 1261, 1200, 1176, 1157, 1101, 1071, 1035, 1018, 1001, 994, 922, 894, 880, 850, 833, 798, 752, 718, 701, 660, 650, 620, 598, 588, 568, 538, 521, 501, 490, 467, 450, 433, 405, 392, 382 cm^{-1}. – **HRMS** (ESI) ($C_{120}H_{72}N_{12}Fe_3OCl$): calc.: 1900.372, found: 1900.375.

Additional information on the reaction details of previously obtained results is available *via* the Chemotion repository:
https://www.chemotion-repository.net/inchikey/reaction/SA-FUHFF-UHFFFADPSC-XADYGZHEUS-UHFFFADPSC-NUHFF-NBPXK-NUHFF-ZZZ

Additional information on the analysis of the target compound for previously obtained results is available *via* the Chemotion repository:
https://dx.doi.org/10.14272/XADYGZHEUSBXDW-SMDKEBRUSA-N

5,15-Bis(2-(10,15,20)-triphenylporphyrinylphenyl)-10,20-diphenylporphyrin-trinickel(II) (**179**)[388]

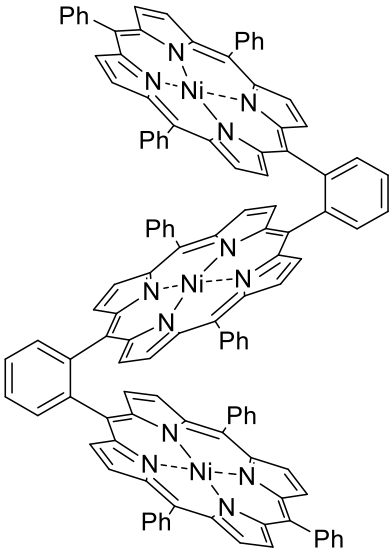

5,15-Bis(2-(10,15,20)-triphenylporphyrinylphenyl)-10,20-diphenylporphyrin (**34**) (2.2 mg, 1.30 µmol, 1.00 equiv.) and $Ni(OAc)_2 \cdot 4\ H_2O$ (3.1mg, 12.5 µmol, 9.62 equiv.) were dissolved in a mixture of $CHCl_3$ and MeOH (10:1, 2.2 mL). The reaction mixture was stirred for 17 h at 100 °C, changing its color from brown to red. Subsequently, the solvent was removed under reduced pressure. The crude product was purified by flash column chromatography on silica gel ($CHCl_3$) to afford the title compound **179** as a red solid (2.3 mg, 1.24 µmol, 95%).

***R*f** (CH_2Cl_2/*n*-pentane, 1:2) = 0.28. – **^{1}H NMR** (500 MHz, CD_2Cl_2): δ = 8.85 (d, ^3J = 5.0 Hz, 4H, $H_{pyrrole}$), 8.77 (dd, J = 7.7, 1.4 Hz, 2H, $H_{linker\text{-}benzene}$), 8.40 (d, ^3J = 4.9 Hz, 4H, $H_{pyrrole}$), 8.27 (d, ^3J = 4.8 Hz, 4H, $H_{pyrrole}$), 8.23 (d, ^3J = 4.8 Hz, 4H, $H_{pyrrole}$), 8.20 (d, ^3J = 4.9 Hz, 4H, $H_{pyrrole}$), 8.10 (dd, J = 7.6, 1.6 Hz, 2H, $H_{linker\text{-}benzene}$), 7.98 (dd, J = 7.7, 1.6 Hz, 2H, $H_{linker\text{-}benzene}$), 7.94 (td, J = 7.7, 1.4 Hz, 2H, $H_{linker\text{-}benzene}$), 7.62 (d, ^3J = 4.9 Hz, 4H, $H_{pyrrole}$), 7.61 – 7.58 (m, 4H, $H_{aromatic}$), 7.57 – 7.35 (m, 28H, $H_{aromatic}$), 7.31 – 7.26 (m, 4H, $H_{aromatic}$), 6.62 – 6.58 (m, 4H, $H_{aromatic}$) ppm. — **UV-Vis** (CH_2Cl_2): λ_{max} (rel. absorption) = 0.93 (219), 272 (0.20), 322 (0.10), 400 (1.20), 536 (0.09) nm. – **IR (ATR)**: $\tilde{\nu}$ = 2955, 2919, 2850, 1657, 1632, 1598, 1490, 1459, 1441, 1411, 1375, 1367, 1350, 1313, 1259, 1203, 1177, 1156, 1072, 1004, 866, 796, 751, 711, 701, 669, 650, 564, 558, 524, 499, 494, 477, 465, 432, 398 cm^{-1}. – **HRMS** (ESI) ($C_{120}H_{72}N_{12}Ni_3$): calc.: 1854.4063, found: 1854.4030.

Additional information on the reaction details is available *via* the Chemotion repository: https://dx.doi.org/10.14272/reaction/SA-FUHFF-UHFFFADPSC-YTMDZVLVQK-UHFFFADPSC-NUHFF-NBPXK-NUHFF-ZZZ

Additional information on the analysis of the target compound is available *via* the Chemotion repository: https://dx.doi.org/10.14272/YTMDZVLVQKEENN-SMDKEBRUSA-N.1

5,15-Bis(2-(10,15,20)-triphenylporphyrinylphenyl)-10,20-diphenylporphyrin-tricopper(II) (**180**)[381]

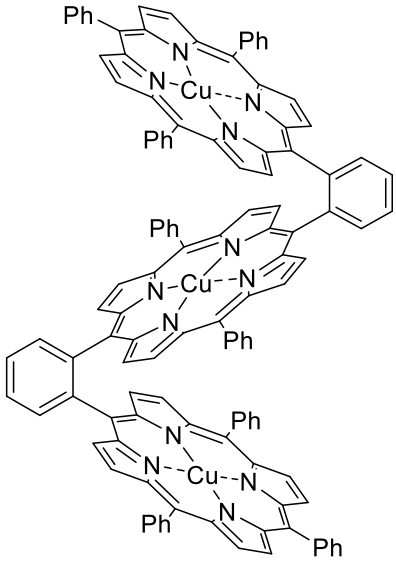

5,15-Bis(2-(10,15,20)-triphenylporphyrinylphenyl)-10,20-diphenylporphyrin (**34**) (2.2 mg, 1.30 µmol, 1.00 equiv.) and $Cu(OAc)_2$ (1.5mg, 6.26 µmol, 5.58 equiv.) were dissolved in a mixture of $CHCl_3$ and MeOH (10:1, 3.3 mL). The reaction mixture was stirred for 3 h at 80 °C, changing its color from brown to red. Subsequently, the solvent was removed under reduced pressure. The crude product was purified by flash column chromatography on silica gel ($CHCl_3$) to afford the title compound **180** as a red solid (1.8 mg, 9.61 µmol, 65%). ***R*f** (CH_2Cl_2/*n*-pentane, 1:2) = 0.32. – **UV-Vis** (CH_2Cl_2): λ_{max} (rel. absorption) = 218 (0.80), 273 (0.14), 309 (0.08), 402 (0.95), 545 (0.06), 735 (0.01) nm. – **IR (ATR)**: $\tilde{\nu}$ = 2958, 2918, 2850, 1659, 1630, 1595, 1459, 1439, 1377, 1344, 1259, 1203, 1177, 1156, 1089, 1077, 1018, 1003, 932, 924, 914, 902, 863, 798, 747, 731, 715, 701, 663, 565, 520, 499, 480, 460, 448, 428, 399, 391, 384 cm^{-1}. – **HRMS** (ESI) ($C_{120}H_{72}N_{12}Cu_3$): calc.: 1869.3891, found: 1869.3902.

Additional information on the reaction details is available *via* the Chemotion repository: https://dx.doi.org/10.14272/reaction/SA-FUHFF-UHFFFADPSC-COBWACPMXF-UHFFFADPSC-NUHFF-NBPXK-NUHFF-ZZZ

Additional information on the analysis of the target compound is available *via* the Chemotion repository: https://dx.doi.org/10.14272/COBWACPMXFSUCI-SMDKEBRUSA-N.1

5,15-Bis(2-(10,15,20)-triphenylporphyrinylphenyl)-10,20-diphenylporphyrin-trizinc(II) (**181**)[379]

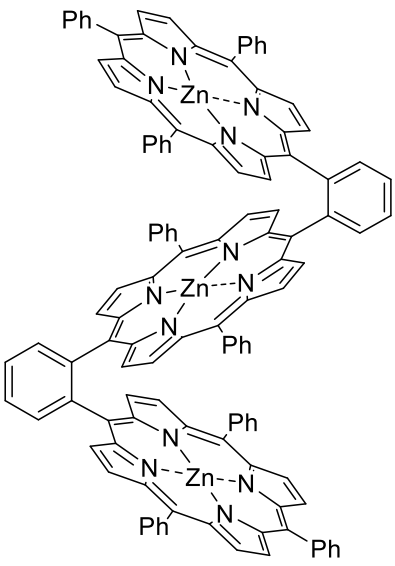

5,15-Bis(2-(10,15,20)-triphenylporphyrinylphenyl)-10,20-diphenylporphyrin (**34**) (2.2 mg, 1.30 µmol, 1.00 equiv.) and $Zn(OAc)_2$ (1.5 mg, 6.18 µmol, 6.27 equiv.) were dissolved in a mixture of $CHCl_3$ and MeOH (10:1, 3.3 mL). The reaction mixture was stirred for 2 h at room temperature changing its color from brown to purple-red. Subsequently, the solvent was removed under reduced pressure. The crude product was purified by flash column chromatography on silica gel ($CHCl_3$) to afford the title compound **181** as a red solid (2.1 mg, 1.12 µmol, 86%).

***R*f** (CH_2Cl_2/*n*-pentane, 1:1) = 0.50. – **^{1}H NMR** (500 MHz, CD_2Cl_2): δ = 9.23 (d, ^3J = 4.7 Hz, 4H, $H_{pyrrole}$), 9.19 (d, ^3J = 4.7 Hz, 4H, $H_{pyrrole}$), 8.62 (d, ^3J = 4.7 Hz, 4H, $H_{pyrrole}$), 8.55 – 8.53 (m, 2H, $H_{linker\text{-}benzene}$), 8.43 – 8.37 (m, 2H, $H_{aromatic}$) 8.40 (d, ^3J = 4.7 Hz, 4H, $H_{pyrrole}$), 8.16 (d, ^3J = 4.9 Hz, 4H, $H_{pyrrole}$), 8.15 (d, ^3J = 4.8 Hz, 4H, $H_{pyrrole}$), 8.06 (pd, J = 7.5, 1.7 Hz, 4H, $H_{linker\text{-}benzene}$), 7.95 (d, ^3J = 7.5 Hz, 2H, $H_{linker\text{-}benzene}$), 7.90 – 7.85 (m, 2H, $H_{aromatic}$), 7.77 – 7.72 (m, 4H, $H_{aromatic}$), 7.70 – 7.57 (m, 8H, $H_{aromatic}$), 7.54 – 7.49 (m, 12H, $H_{aromatic}$), 7.43 – 7.39 (m, 2H, $H_{aromatic}$), 6.94 – 6.89 (m, 2H, $H_{aromatic}$), 6.88 – 6.83 (m, 4H, $H_{aromatic}$), 6.83 – 6.76 (m, 4H, $H_{aromatic}$) ppm. – **UV-Vis** (CH_2Cl_2): λ_{max} (rel. absorption) = 219 (0.78), 273 (0.15), 315 (0.10), 356 (0.09), 411 (0.90), 558 (0.06) nm. – **IR (ATR)**: $\tilde{\nu}$ = 2953, 2921, 2851, 1655, 1632, 1596, 1523, 1459, 1441, 1411, 1377, 1337, 1315, 1261, 1203, 1177, 1156, 1094, 1069, 1010, 1001, 993, 922, 878, 843, 793, 752, 717, 701, 670, 660, 647, 524, 487, 448, 429, 415, 407, 395, 384 cm^{-1}. – **HRMS** (ESI) ($C_{120}H_{72}N_{12}Zn_3$): calc.: 1872.3877, found: 1872.3910.

Additional information on the reaction details is available *via* the Chemotion repository: https://dx.doi.org/10.14272/reaction/SA-FUHFF-UHFFFADPSC-JDNBAWBPMP-UHFFFADPSC-NUHFF-NBPXK-NUHFF-ZZZ

Additional information on the analysis of the target compound is available *via* the Chemotion repository: https://dx.doi.org/10.14272/JDNBAWBPMPRJFN-SMDKEBRUSA-N.1

5,15-Bis(2-(10,15,20)-triphenylporphyrinylphenyl)-10,20-diphenylporphyrin-tripalladium(II) (**182**)[382]

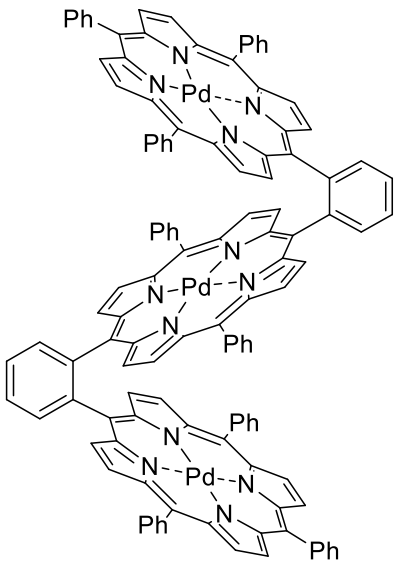

5,15-Bis(2-(10,15,20)-triphenylporphyrinylphenyl)-10,20-diphenylporphyrin (**34**) (2.2 mg, 1.30 µmol, 1.00 equiv.) and $Pd(OAc)_2$ (4.0 mg, 17.8 µmol, 13.7 equiv.) were dissolved in a mixture of $CHCl_3$ and MeOH (10:1, 3.3 mL). The reaction mixture was stirred for 2 h at 80 °C, changing its color from brown to orange. Subsequently, the solvent was removed under reduced pressure. The crude product was purified by flash column chromatography on silica gel ($CHCl_3$) to afford the title compound **182** as a red solid (2.2 mg, 1.10 µmol, 84%).

***R*f** (CH_2Cl_2/*n*-pentane, 1:2) = 0.24. – **^{1}H NMR** (500 MHz, CD_2Cl_2): δ = 9.07 (d, ^3J = 5.0 Hz, 4H, $H_{pyrrole}$), 9.03 (d, ^3J = 5.0 Hz, 4H, $H_{pyrrole}$), 8.50 (d, ^3J = 4.9 Hz, 4H, $H_{pyrrole}$), 8.46 – 8.43 (m, 2H, $H_{linker\text{-}benzene}$), 8.42 – 8.39 (m, 2H, $H_{linker\text{-}benzene}$), 8.16 (d, ^3J = 4.9 Hz, 4H, $H_{pyrrole}$), 8.14 (d, ^3J = 5.0 Hz, 4H, $H_{pyrrole}$), 8.06 – 8.03 (m, 4H, $H_{linker\text{-}benzene}$), 8.02 (d, ^3J = 5.0 Hz, 4H, $H_{pyrrole}$), 7.98 – 7.95 (m, 2H, $H_{aromatic}$), 7.75 – 7.72 (m, 2H, $H_{aromatic}$), 7.71 (dt, *J* = 7.5, 1.4 Hz, 2H, $H_{aromatic}$), 7.69 – 7.66 (m, 2H, $H_{aromatic}$), 7.65 – 7.58 (m, 6H, $H_{aromatic}$), 7.57 – 7.52 (m, 2H, $H_{aromatic}$), 7.50 – 7.47 (m, 4H, $H_{aromatic}$), 7.46 – 7.38 (m, 10H, $H_{aromatic}$), 7.19 (dd, *J* = 7.4, 1.4 Hz, 2H, $H_{aromatic}$), 6.57 (d, ^3J = 7.3 Hz, 4H, $H_{aromatic}$), 6.50 (dd, *J* = 7.3, 1.7 Hz, 4H, $H_{aromatic}$) ppm.– **UV-Vis** (CH_2Cl_2): λ_{max} (rel. absorption) = 218 (0.44), 273 (0.07), 309 (0.02), 406 (0.19), 529 (0.02) nm. – **IR (ATR)**: $\tilde{\nu}$ = 2955, 2922, 2853, 1660, 1598, 1538, 1460, 1442, 1378, 1351, 1310, 1261, 1078, 1013, 970, 868, 795, 751, 724, 711, 703, 664, 533, 404, 385 cm^{-1}. – **HRMS** (ESI) ($C_{120}H_{72}N_{12}Pd_3$): calc.: 1998.3107, found: 1998.3202.

Additional information on the reaction details is available *via* the Chemotion repository: https://dx.doi.org/10.14272/reaction/SA-FUHFF-UHFFFADPSC-WGFBNGVGII-UHFFFADPSC-NUHFF-NBPXK-NUHFF-ZZZ

Additional information on the analysis of the target compound is available *via* the Chemotion repository: https://dx.doi.org/10.14272/WGFBNGVGIIZZAE-SMDKEBRUSA-N/CHMO0000593

6.5.4 Heterotrimetallic *o*-phenylene-linked porphyrin complexes

[5-(2-(Di(1H-pyrrol-2-yl)methyl)phenyl)-10,15,20-triphenylporphyrin]-nickel(II) (**183**)[387]

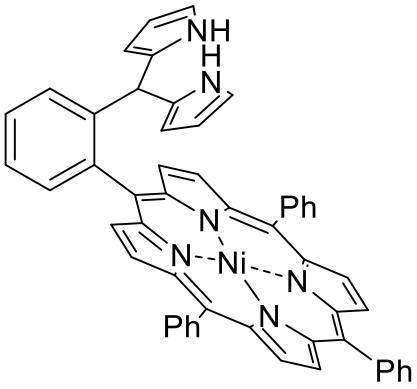

Under an argon atmosphere, [5-(2-formylphenyl)-10,15,20-triphenylporphyrin]-nickel(II) (**161**) (180 mg, 258 µmol, 1.00 equiv.) was dissolved in freshly distilled pyrrole (15 mL, 14.5 mg, 216 mmol, 838 equiv.). TFA (64 µL, 94.3 mg, 827 µmol, 3.21 equiv.) was added dropwise. The reaction mixture was stirred for 8 h at room temperature and the solvent was removed under reduced pressure. The crude product was purified by flash column chromatography on silica gel (toluene) to afford the title compound **183** as a red solid (177 mg, 218 µmol, 84%). ***R*f** (toluene) = 0.65. – **^{1}H NMR** (500 MHz, toluene-d$_8$): δ = 8.79 – 8.76 (m, 4H, H$_{pyrrole}$), 8.72 (d, ^{3}J = 4.9 Hz, 2H, H$_{pyrrole}$), 8.60 (d, ^{3}J = 4.9 Hz, 2H, H$_{pyrrole}$), 7.96 – 7.86 (m, 6H, H$_{pyrrole}$), 7.80 (dd, J = 7.5, 1.4 Hz, 1H, H$_{aromatic}$), 7.61 (dd, J = 8.0, 1.3 Hz, 1H, H$_{aromatic}$), 7.45 – 7.35 (m, 10H, H$_{aromatic}$), 7.27 (td, J = 7.5, 1.4 Hz, 1H, H$_{aromatic}$), 6.39 (bs, 2H, NH$_{dipyrromethane}$), 6.02 (dd, J = 6.4, 2.8 Hz, 2H, H$_{dipyrromethane}$), 5.92 – 5.90 (m, 2H, H$_{dipyrromethane}$), 5.85 – 5.82 (m, 2H, H$_{dipyrromethane}$), 4.87 (s, 1H, H$_{dipyrromethane}$) ppm. – **^{13}C NMR** (126 MHz, toluene-d$_8$) : δ = 145.3 (C$_q$), 144.1 (C$_q$), 144.0 (C$_q$), 143.9 (C$_q$), 143.9 (C$_q$), 142.2 (C$_q$), 142.1 (C$_q$), 140.4 (C$_q$), 134.4 (+, CH), 134.2 (+, CH), 132.9 (+, CH), 132.9 (+, CH), 132.8 (+, CH), 132.7 (+, CH), 132.6 (+, CH), 132.6 (+, CH), 129.7 (+, CH), 129.6 (+, CH), 129.4 (+, CH), 129.1 (+, CH), 128.6 (+, CH), 128.3 (+, CH), 127.5 (+, CH), 127.4 (+, CH), 126.0 (+, CH), 125.8 (+, CH), 120.2 (C$_q$), 120.1 (C$_q$), 117.9 (C$_q$), 116.8 (C$_q$), 109.1 (+, CH), 107.8 (+, CH), 42.1 (+, CH) ppm. – **UV-Vis** (CH_2Cl_2): λ_{max} (rel. absorption) = 218 (0.48), 288 (0.12), 317 (0.08), 326 (0.08), 415 (1.91), 528 (0.14) nm. – **IR (ATR)**: $\tilde{\nu}$ = 2952, 2921, 2851, 1694, 1596, 1456, 1439, 1374, 1350, 1275, 1203, 1174, 1071, 1004, 795, 751, 711, 700, 666, 654, 560, 524, 509, 466 cm^{-1}. – **HRMS** (ESI) ($C_{53}H_{36}N_6NiH$) calc.: 815.2433, found: 815.2328.

Additional information on the reaction details is available *via* the Chemotion repository: https://dx.doi.org/10.14272/reaction/SA-FUHFF-UHFFFADPSC-RADSWVOTYL-UHFFFADPSC-NUHFF-NJAQL-NUHFF-ZZZ

Additional information on the analysis of the target compound is available *via* the Chemotion repository: https://dx.doi.org/10.14272/RADSWVOTYLGRBW-QURYMOASSA-N.1

6.5.5 Heterotrimetallic *o*-phenylene-linked porphyrin complexes

5,15-Bis(2-(10,15,20)-triphenylporphyrinylphenyl)-10,20-diphenylporphyrin-dinickel(II) (**184**)[373]

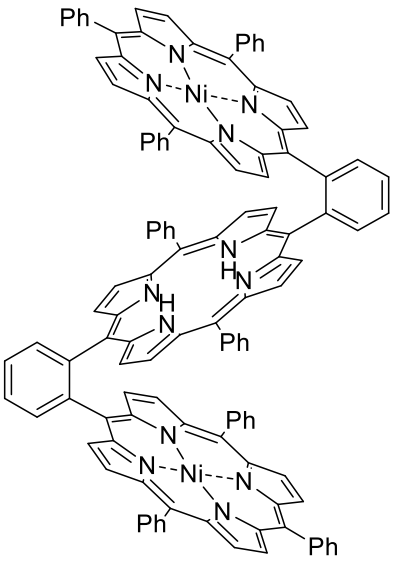

Under an argon atmosphere, [5-(2-(di(1H-pyrrole-2-yl)methyl)phenyl)-10,15,20-triphenylporphyrin]-nickel(II) (74 mg, 90.7 µmol, 2.00 equiv.) (**183**) was dissolved in CH_2Cl_2, (40 mL) previously degassed by three freeze-pump-thaw cycles. Subsequently, benzaldehyde (10.0 µL, 10.4 mg, 98.0 µmol, 2.16 equiv.) and TFA (12.9 µL, 19.1 mg, 111 mmol, 3.69 equiv.) were added over 4 h while stirring the mixture in the dark until all starting material was consumed. Afterward, DDQ (25.0 mg, 110 µmol, 2.43 equiv.) was added and stirred for 1 h under air, whereas the presence of oxygen additionally supports the oxidation. Then, NEt_3 (2.0 mL) was added and the crude mixture was concentrated under reduced pressure, filtered through a short layer of silica gel eluting with CH_2Cl_2 + 1% NEt_3 and purified by flash column chromatography on silica gel (1 × toluene/*c*Hex, 4:1 → 7:1; 1 × CH_2Cl_2/*n*-pentane 1:1, 1 × CH_2Cl_2/*n*-pentane 1:2) to afford the title compound **184** as a red solid (11.5 mg, 6.38 µmol, 14%).

***R*f** (CH_2Cl_2/*n*-pentane, 1:1) = 0.55. – **^{1}H NMR** (500 MHz, CD_2Cl_2): δ = 8.98 (d, ^3J = 4.9 Hz, $4H_{pyrrole}$), 8.87 (dd, ^3J = 7.9, 1.4 Hz, 2H, $H_{aromatic}$), 8.77 (d, ^3J = 5.0 Hz, 2H, $H_{pyrrole}$), 8.57 (d, ^3J = 4.9 Hz, 2H, $H_{pyrrole}$), 8.54 (d, ^3J = 4.9 Hz, 4H, $H_{pyrrole}$), 8.22 (d, ^3J = 4.9 Hz, 4H, $H_{pyrrole}$), 8.21 – 8.16 (m, 5H, $H_{aromatic}$), 8.15 – 8.13 (m, 8H, $H_{pyrrole}$), 8.05 – 7.99 (m, 6H, $H_{aromatic}$), 7.90 (dd, ^3J = 5.6, 3.5 Hz, 2H, $H_{aromatic}$), 7.81 (d, ^3J = 4.3 Hz, 4H, $H_{aromatic}$), 7.74 – 7.70 (m, 4H, $H_{aromatic}$) 7.63 (d, ^3J = 4.7 Hz, 4H, $H_{aromatic}$), 7.60 – 7.57 (m, 5H, $H_{aromatic}$), 7.53 – 7.47 (m, 12H, $H_{aromatic}$), 6.89 (d, ^3J = 7.1 Hz, 4H, $H_{aromatic}$), –5.02 (bs, 2H, NH) ppm. – **^{1}H NMR** (400 MHz, $CDCl_3$): δ = 8.96 (d, ^3J = 4.9 Hz, 4H, $H_{pyrrole}$), 8.86 (d, ^3J = 7.5 Hz, 2H, $H_{aromatic}$), 8.52 (d, ^3J = 4.8 Hz, 4H, $H_{pyrrole}$), 8.23 (d, ^3J = 4.9 Hz, 4H, $H_{pyrrole}$), 8.18 – 8.14 (m, 8H, $H_{pyrrole}$), 8.12 (d, ^3J = 7.5 Hz, 4H, $H_{aromatic}$), 7.96 (t, 2H, $H_{aromatic}$), 7.81 (d, ^3J = 4.8 Hz, 4H, $H_{pyrrole}$), 7.74 – 7.66 (m, 2H, $H_{aromatic}$) 7.63 – 7.55 (m, 10H, $H_{aromatic}$), 7.53 – 7.39 (m, 18H, $H_{aromatic}$), 7.40 – 7.30 (m, 6H, $H_{aromatic}$), 6.93 (d, ^3J = 7.2 Hz, 4H, $H_{aromatic}$), –4.85 (bs, 2H, NH) ppm.– **UV-Vis** (CH_2Cl_2): λ_{max} (rel. absorption) = 276 (0.10), 313 (0.01), 348 (0.02), 417 (0.10), 535 (0.04), 606 (0.04) nm. – **IR (ATR)**: $\tilde{\nu}$ = 2958, 2922, 2853, 1591, 1572, 1472, 1439, 1422, 1375, 1317, 1264,

1221, 1017, 769, 742, 701, 686, 613 cm^{-1}. – **HRMS** (ESI) ($C_{120}H_{74}N_{12}Ni_2H$) calc.: 1799.4945, found: 1799.4969.

Additional information on the reaction details is available *via* the Chemotion repository: https://dx.doi.org/10.14272/reaction/SA-FUHFF-UHFFFADPSC-QOZSKCCXEX-UHFFFADPSC-NUHFF-NOKPY-NUHFF-ZZZ

Additional information on the analysis of the target compound is available *via* the Chemotion repository: https://dx.doi.org/10.14272/QOZSKCCXEXNQRL-DAZOZZHLSA-N.1

5,15-Bis(2-(10,15,20)-triphenylporphyrinylphenyl)-10,20-diphenylporphyrin-dinickel(II)-tetraoxo-iron(III) (**185**)[7]

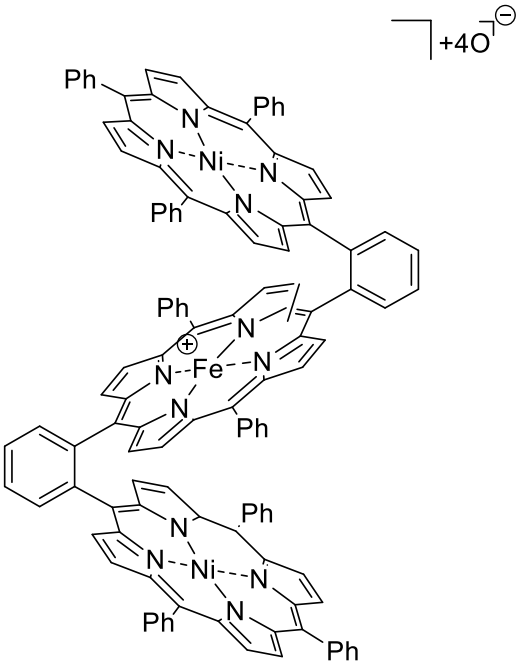

5,15-Bis(2-(10,15,20)-triphenylporphyrinylphenyl)-10,20-diphenylporphyrin (**184**) (2.0 mg, 1.11 µmol, 1.00 equiv.) and $FeBr_2$ (2.4 mg, 1.11 µmol, 10.0 equiv.) were dissolved in DMF (2 mL). The reaction mixture was stirred for 2.5 h at 150 °C, changing its color from brown to dark brown. Subsequently, the solvent was removed under reduced pressure. The crude product was purified by flash column chromatography on silica gel ($CHCl_3$ to $CHCl_3$/MeOH, 1:0 → 10:1) to afford the title compound **185** as a brown solid (2.0 mg, 1.03 µmol, 94%).

***R*f** (CH_2Cl_2/MeOH, 19:1) = 0.37. – **UV-Vis** (CH_2Cl_2): λ_{max} (rel. absorption) = 307 (0.19), 408 (0.34), 539 (0.09), 699 (0.07) nm. – **IR (ATR)**: $\tilde{\nu}$ = 3361, 2955, 2922, 2867, 2854, 1737, 1660, 1636, 1463, 1378, 1259, 1191, 1079, 1007, 967, 795, 754, 704 cm^{-1}. – **HRMS** (ESI) ($C_{120}H_{72}N_{12}Fe_3O_4$) calc.: 1918.3960, found: 1918.3866.

Additional information on the reaction details is available *via* the Chemotion repository: https://dx.doi.org/10.14272/reaction/SA-FUHFF-UHFFFADPSC-KBKATLUIZN-UHFFFADPSC-NUHFF-NBPXK-NUHFF-ZZZ

Additional information on the analysis of the target compound is available *via* the Chemotion repository: https://dx.doi.org/10.14272/KBKATLUIZNVPGD-SMDKEBRUSA-N

6.6 Metal complexes of cofacially connected porphyrin derivatives with regular porphyrins

6.6.1 A synthetic pathway towards N-confused-porphyrin based dimeric ligands

5,10,15,20-Tetraphenyl-2-aza-21-carbaporphyrin (**187**)[15]

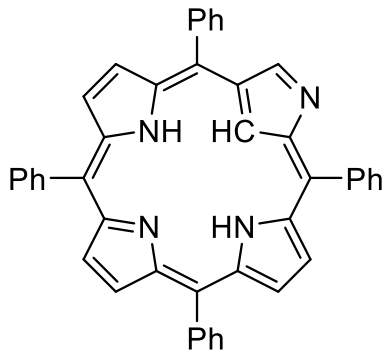

Benzaldehyde (1.88 mL, 1.97 g, 18.6 mmol, 1.00 equiv.) and pyrrole (1.28 mL, 1.24 g, 18.6 mmol, 1.00 equiv.) were dissolved in degassed CH_2Cl_2 (1.8 L). Methansulfonic acid (0.84 mL, 1.25 g, 13.0 mmol, 0.75 equiv.) was added and the reaction mixture was stirred under the exclusion of light for 30 min at room temperature. DDQ (6.30 g, 27.8 mmol, 1.50 equiv.) was added and the reaction mixture was stirred for 2 h at room temperature before NEt_3 (6 mL) was added. The crude product was purified by flash column chromatography on silica gel (CH_2Cl_2/MeOH, 97:3), "Brockmann activity III" basic alumina (*c*Hex/ CH_2Cl_2, 3:1, 1% NEt_3) and on silica gel (CH_2Cl_2/MeOH, 99:1 → 98.5:1.5). The title compound **187** was obtained as a purple solid (654 mg, 1.06 mmol, 29%). ***R*f** (CH_2Cl_2/MeOH, 50:1) = 0.71. – **^{1}H NMR** (400 MHz, $CDCl_3$): δ = 8.99 (d, ^3J = 4.9, 1H, $H_{pyrrole}$), 8.92 (d, ^3J = 4.9, 1H, $H_{pyrrole}$), 8.77 (s, 1H, $H_{confused,outer}$), 8.62 (d, ^3J = 4.9, 1H, $H_{pyrrole}$), 8.63 – 8.55 (m, 3H, $H_{pyrrole}$), 8.39 – 8.35 (m, 4H, $H_{aromatic}$), 8.19 – 8.15 (m, 4H, $H_{aromatic}$), 7.87 – 7.74 (m, 12H, $H_{aromatic}$), – 2.43 (bs, 2H, N*H*), –4.99 (s, 1H, $H_{confused,inner}$) ppm, impurities: 1.30 – 1.27 (m, H grease), 0.91 – 0.83 (m, H grease), 0.10 (s, silicon grease). – **^{13}C NMR** (126 MHz, toluene-d_8) : δ = 157.4 (C_q), 156.4 (C_q), 156.1 (C_q), 149.6 (C_q), 141.9 (C_q), 140.5 (C_q), 140.0 (C_q), 139.8 (C_q), 139.8 (C_q), 137.3 (+, CH), 137.0 (+, CH), 135.2 (+, CH), 134.8 (+, CH), 134.7 (+, CH), 134.7 (+, CH), 134.2 (+, CH), 128.5 (+, CH), 128.5 (+, CH), 128.2 (+, CH), 128.0 (+, CH), 127.9 (+, CH), 127.8 (+, CH), 127.6 (+, CH), 127.1 (+, CH), 127.1 (+, CH), 126.5 (+, CH), 125.7 (+, CH), 125.2 (+, CH), 119.2 (C_q), 117.6 (C_q) ppm. – **HRMS** (ESI) ($C_{44}H_{31}N_4^+$): calc.: 615.25, found: 615.253.

[5,10,15,20-Tetraphenyl-2-aza-3-bromo-21-carbaporphyrin]argentate(III) (**189**)[280]

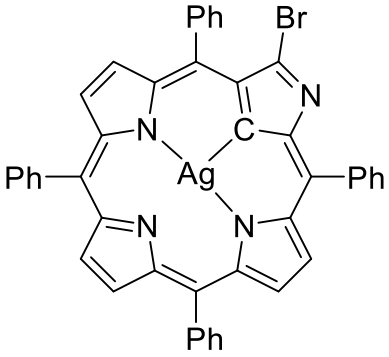

5,10,15,20-Tetraphenyl-2-aza-carbaporphyrin (**187**) (50.0 mg, 81.3 µmol, 1.00 equiv.) was dissolved in CH_2Cl_2 (20 mL) and NBS (33.3 mg, 187 mmol, 2.30 equiv.) was added. The reaction mixture was stirred for 5 min before the solvent was removed under reduced pressure. The crude product was purified by flash column chromatography on silica gel (CH_2Cl_2/MeOH, 1:0 → 99:1). The green fraction was directly added to a flask with silver trifluoromethanesulfonate (418 mg, 1.63 mmol, 20.0 equiv.) and stirred for 1 h at room temperature. The crude product was washed with H_2O (3 × 20 mL) and dried over Na_2SO_4. After purification by flash column chromatography on silica gel (CH_2Cl_2/MeOH, 1:0 → 99:1) the title compound **189** was obtained as a brown solid (60.5 mg, 75.8 mmol, 93%).

^{1}H NMR (400 MHz, $CDCl_3$): δ = 8.81 (m, 1H, $H_{pyrrole}$), 8.67 – 8.58 (m, 5H, $H_{pyrrole}$), 8.13 – 8.06 (m, 6H, $H_{aromatic}$), 7.96 – 7.94 (m, 2H, $H_{aromatic}$), 7.73 – 7.69 (m, 12H, $H_{aromatic}$) ppm. The analytical data is in accordance with the literature.[280] – **HRMS** (ESI) ($C_{44}H_{27}AgBrN_4^+$) calc.: 797.05, found: 797.046.

[5,10,15,20-Tetraphenyl-3-bromo-21-carba-2-(2-formylphenyl)porphyrin]argentate(III) (**189**)[88]

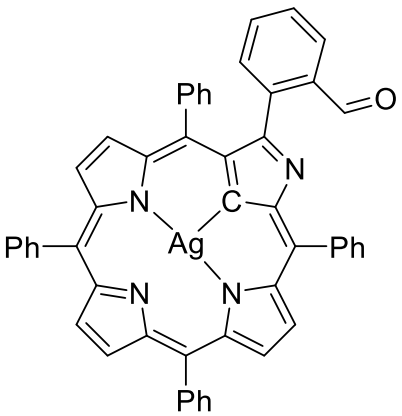

[5,10,15,20-Tetraphenyl-2-aza-3-bromo-21-carbaporphyrin]argentate(III) (**189**), (13.0 mg, 162 µmol, 1.00 equiv.), 2-(formylphenyl)boronic acid (293 mg, 1.95 mmol, 12.0 equiv.), K_2CO_3 (864 mg, 4.07 mmol, 25.0 equiv.) and tetrakis(triphenylphosphine)palladium(0) (45.2 mg, 39.1 µmol, 0.24 equiv.) were dissolved in dry THF (9 mL) and stirred for 14 h at 80 °C. CH_2Cl_2 (10 mL) was added and the organic phase was washed with H_2O (3 × 10 mL), dried over Na_2SO_4, filtered and the solvent removed under reduced pressure. The crude product was purified by flash column chromatography on silica gel (CH_2Cl_2/MeOH, 99:1 → 97:3) to afford the title compound **189** as a brown solid (2.8 mg, 3.40 µmol, 21%). – NMR spectroscopy was not possible due to the poor solubility of the product.

HRMS (ESI) ($C_{51}H_{32}AgN_4O^+$) calc.: 823.16, found: 823.304.

6.6.2 The synthetic pathway towards N-fused-porphyrin based dimeric ligands

19-Bromo-3,8,13,16-tetraphenyl-4,7-imino-2,17-methano-9,12-nitrilo[1,3]diazacyclohexadecino[2,1,16-*cd*]pyrrolizine (**191**)[18]

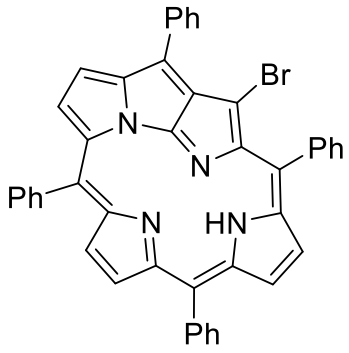

5,10,15,20-Tetraphenyl-2-aza-21-carbaporphyrin (**187**) (42.0 mg, 68.3 µmol, 1.00 equiv.) was dissolved in CH_2Cl_2 (20 mL) and NBS (28.0 mg, 157 µmol, 2.30 equiv.) was added. The reaction mixture was stirred for 5 min. Subsequently, the solvent was removed under reduced pressure. The residue was purified by flash column chromatography on silica gel (CH_2Cl_2/MeOH, 99:1) and the solvent was removed under reduced pressure. The residue was redissolved in pyridine (10 mL) and stirred for 8 h at room temperature. The solvent was removed under reduced pressure and purification by flash column chromatography (CH_2Cl_2/MeOH, 98:2), afforded the title compound **191** as a red solid (24.9 mg, 36.0 µmol, 53%).

***R*f** (CH_2Cl_2 /MeOH, 25:1) = 0.56. – **^{1}H NMR** (400 MHz, $CDCl_3$): δ = 8.97 (d, ^3J = 5.1 Hz, 1H, $H_{pyrrole}$), 8.62 (d, ^3J = 5.1 Hz, 1H, $H_{pyrrole}$), 8.55 (m, 2H, $H_{pyrrole}$), 8.34 (bs, N*H*), 8.07 – 8.03 (m, 5H, $H_{aromatic}$), 8.00 – 7.97 (m, 3H, $H_{aromatic}$), 7.96 – 7.95 (m, 1H, $H_{aromatic}$), 7.75 – 7.65 (m, 11H, $H_{aromatic}$), 7.55-7.58 (m, 2H, $H_{pyrrole}$) ppm. – **^{13}C NMR** (500 MHz, DCM-d_2): δ = 150.6 (C_q), 146.8 (C_q), 139.0 (+, CH), 137.5 (C_q), 136.9 (C_q), 134.5 (+, CH), 133.4 (+, CH), 133.2 (+, CH), 132.7 (+, CH), 132.2 (+, CH), 130.3 (+, CH), 129.2 (+, CH), 129.2 (+, CH), 128.6 (+, CH), 128.1 (+, CH), 128.0 (+, CH), 127.8 (+, CH), 127.3 (+, CH), 124.6 (+, CH), 120.4 (+, CH) ppm. – **UV-Vis** (CH_2Cl_2): λ_{max} (rel. absorption) = 279 (0.04), 373 (0.03), 424 (0.03), 450 (0.03), 465 (0.03), 497 (0.03), 543 (0.02) nm. – **IR** (ATR): $\tilde{\nu}$ = 3054, 3029, 2953, 2924, 2851, 1775, 1706, 1594, 1574, 1531, 1465, 1441, 1391, 1356, 1264, 1228, 1204, 1177, 1154, 1072, 1044, 1018, 1001, 958, 919, 881, 846, 827, 799, 786, 752, 728, 698, 662, 647, 626, 598, 571, 557, 544, 530, 404 cm^{-1}. – **MS** (EI, 70 eV, 30 °C), *m/z* (%): 691.149 (94.26) $[M+H]^+$, 693.147 (100) $[M+H]^+$. – **HRMS** (ESI) ($C_{44}H_{28}BrN_4^+$) calc.: 691.15, found: 691.148. The analytical data is in accordance with the literature.

19-Formylphenyl-3,8,13,16-tetraphenyl-4,7-imino-2,17-methano-9,12-nitrilo[1,3]diazacyclohexadecino[2,1,16-*cd*]pyrrolizine (**192**)[88]

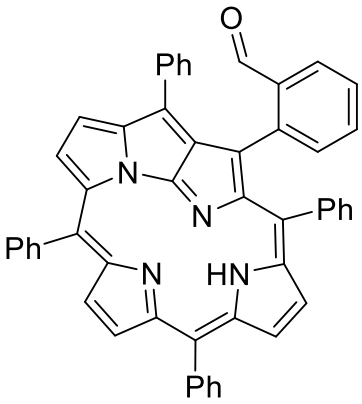

Under an argon atmosphere, 19-bromo-3,8,13,16-tetraphenyl-4,7-imino-2,17-methano-9,12-nitrilo[1,3]diazacyclohexadecino [2,1,16-*cd*]pyrrolizine (**191**) (20.0 mg, 28.9 µmol, 1.00 equiv.), 2-(formylphenyl)boronic acid (52.0 mg, 347 µmol, 120 equiv.), K_2CO_3 (153 mg, 723 µmol, 15.0 equiv.) and $Pd(PPh_3)_4$ (8.02 mg, 6.94 µmol, 0.24 equiv.) were dissolved in THF (6 mL) that has been degassed by three freeze-pump-thaw cycles. After 20.5 h at 80 °C, the solvent was removed under reduced pressure and redissolved in CH_2Cl_2 (5 mL). The organic phase was washed with H_2O (3 × 10 mL), dried over Na_2SO_4, filtered and the solvent removed under reduced pressure. The crude product was purified by flash column chromatography on silica gel (CH_2Cl_2/MeOH, 98:2) to afford the title compound **192** as a red solid (4.80 mg, 6.70 µmol, 23%).

***R*f** (CH_2Cl_2/MeOH, 50:1) = 0.50. ***R*f** (toluene/EtOAc 10:1) = 0.44. – **^{1}H NMR** (500 MHz, $CDCl_3$, 1 M HCl, (50:1)): δ = 10.16 (s, 1H, C*H*O), 9.21 (d, ^3J = 5.0 Hz, 1H, $H_{pyrrole}$), 8.85 (d, ^3J = 5.0 Hz, 1H, $H_{pyrrole}$), 8.59 (d, ^3J = 5.0 Hz, 1H, $H_{pyrrole}$), 8.29 – 8.27 (m, 2H, $H_{pyrrole}$), 8.22 (d, ^3J = 7.5 Hz, 1H, $H_{aromatic}$), 8.07 (d, ^3J = 5.0 Hz, 1H, $H_{pyrrole}$), 8.00 (bs, 1H, N*H*), 7.84 – 7.80 (m, 5H, $H_{aromatic}$), 7.80 – 7.71 (m, 5H, $H_{aromatic}$), 7.70 – 7.61 (m, 4H, $H_{aromatic}$), 8 H between 7.60 – 7.32 ppm could not be assigned due to aqueous HCl-based and toluene signals overlap. – **^{1}H NMR** (400 MHz, $CDCl_3$): δ = 9.88 (bs, 1H, C*H*O), 9.04 (bs, 1H, $H_{pyrrole}$), 8.68 (bs, 1H, $H_{pyrrole}$), 8.17 – 7.96 (m, 7H, $H_{pyrrole}$), 7.81 – 7.63 (m, 12H, $H_{pyrrole}$), 7.49 – 7.40 (m, 2H, $H_{aromatic}$), 7.49 – 7.40 (m, 8H, $H_{aromatic}$).The N*H* signal is overlaid by the signals. – **^{13}C NMR** (500 MHz, CD_2Cl_2): δ =192.2, 158.0, 154.6, 153.3, 150.7, 149.4, 147.8, 147.0, 146.9, 142.2, 142.2, 139.6, 137.9, 137.5, 137.0, 135.6, 135.4, 135.0, 134.8, 134.7, 134.3, 134.3, 133.9, 133.7, 133.6, 133.5, 133.3, 133.0, 132.7, 131.7, 130.2, 129.8, 129.6, 129.3, 129.2, 128.8, 128.7, 128.4, 128.3, 128.2), 128.1, 127.7, 127.6), 126.7, 125.7, 125.4, 125.2, 125.1, 120.4, 120.0, 119.5, 110.3 ppm. – **UV-Vis** (CH_2Cl_2): λ_{max} (rel. absorption) = 294 (0.11), 357 (0.18), 499 (0.22), 545 (0.17), 646 (0.03), 702 (0.02) nm. – **IR** (ATR): $\tilde{\nu}$ = 3054, 2953, 2922, 2853, 1687, 1664, 1595, 1574, 1528, 1479, 1452, 1441, 1421, 1391, 1368, 1358, 1336, 1264, 1244, 1231, 1196, 1179, 1156, 1071, 1001, 959, 826, 785, 734, 698, 660, 643, 632, 618, 608, 577, 558, 541, 520 cm^{-1}. – **HRMS** (ESI) ($C_{51}H_{33}N_4O^+$) calc.: 717.26, found: 717.264.

6.6.3 Synthesis of cofacially connected N-fused-porphyrin - porphyrin ligands

N-fused-tetraphenylporphyrin-triphenylporphyrin **197**[301]

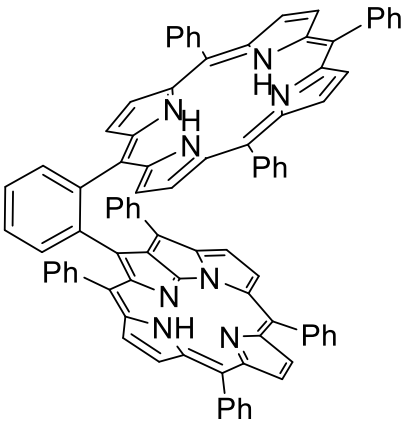

Under an argon atmosphere, a crimp vial was charged with formylphenyl-N-fused-TPP **192** (64.0 mg, 89.2 µmol, 1.00 equiv.) and dissolved in CH_2Cl_2 (20 mL). Pyrrole (51.0 µL, 49.3 mg, 735 µmol, 8.23 equiv.), benzaldehyde (56.0 µL, 58.2 mg, 548 µmol, 6.15 equiv.) and TFA (12.7 µL, 18.9 mg, 166 µmol, 1.86 equiv.) were all added dropwise while stirring for 19 h at room temperature. Afterward, DDQ (20.3 mg, 89.0 µmol, 1.00 equiv.) was added and stirred for 1 h under air. Then, NEt_3 (0.5 mL) was added and the solvent was removed under reduced pressure. The crude product was purified three times by flash column chromatography on silica gel (CH_2Cl_2/MeOH, 9:1), (toluene/EtOAc, 7:1→ 5:1), (CH_2Cl_2/MeOH, 93:7) to afford the title compound **197** as a red solid (23.8 mg, 19.0 µmol, 22%).

***R*f** (CH_2Cl_2/MeOH, 97:3 + 1% NEt_3) = 0.45. – **^{1}H NMR** (500 MHz, CD_2Cl_2 + pyridine-d_5, 1:1): δ = 8.87 (d, J = 4.6 Hz, 2H, $H_{pyrrole}$), 8.66 (d, *J* = 7.7 Hz, 2H, $H_{aromatic}$), 8.53 (d, *J* = 4.6 Hz, 2H, $H_{pyrrole}$), 8.51 (d, *J* = 4.7 Hz, 2H, $H_{pyrrole}$), 8.45 (d, *J* = 4.5 Hz, 2H, $H_{pyrrole}$), 8.42 – 8.18 (m, XXH), 8.37 (d, *J* = 4.6 Hz, 2H, $H_{aromatic}$), 8.26 (d, *J* = 7.5 Hz, 2H, $H_{aromatic}$), 8.17 – 8.10 (m, 2H), 8.10 – 8.02 (m, 4H), 8.01 – 7.90 (m, 9H), 7.90 – 7.85 (m, 6H), 7.84 – 7.75 (m, 18H), 7.57 – 7.47 (12H), 7.45 – 7.34 (m, 10H), 7.25 – 7.18 (m, 4H), 7.09 (d, *J* = 4.7 Hz, 2H, $H_{pyrrole}$), 7.09 (d, *J* = 4.7 Hz, 1H, $H_{pyrrole}$). –4.14 (bs, 2H, NH) ppm. – **^{13}C NMR** (126 MHz, CD_2Cl_2 + pyridine-d_5, 1:1) δ = 146.0, 144.4, 142.5, 142.2, 141.9, 136.9, 134.6, 133.4, 132.0, 129.8, 128.7, 128.1, 127.9, 127.7, 127.4, 127.1, 127.0, 126.5, 125.5, 124.6, 119.9, 119.3 ppm. The ^{13}C NMR peak list only represents the distinguishable signals and therewith can only be used as a foot-print like spectrum for comparison. – **UV-Vis** (CH_2Cl_2): λ_{max} (rel. absorption) = 218 (0.06), 309 (0.05), 420 (0.23), 508 (0.04), 550 (0.03), 652 (0.01) nm. – **IR** (ATR): $\tilde{\nu}$ = 2955, 2921, 2851, 1455, 1441, 1374, 1259, 1173, 1086, 1072, 1014, 966, 878, 798, 752, 722, 698, 663, 407, 399, 390 cm^{-1}. – **HRMS** ($C_{88}H_{56}N_8H$) calc.: 1225.4706, found: 1225.4663.

6.6.4 N-fused-porphyrin-based metal complexes

N-fused-tetraphenylporphyrin **198**[88]

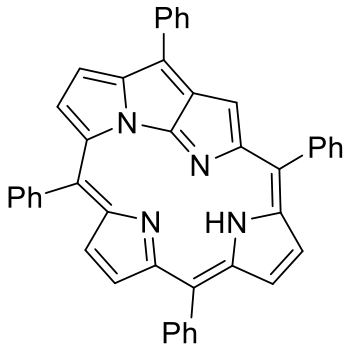

Under an argon atmosphere, a crimp vial was charged with Br-N-fused-TPP **191** (319 mg, 452 µmol, 1.00 equiv.), $Pd(PPh_3)_4$ (135 mg, 904 µmol, 2.00 equiv.), K_2CO_3 (879 mg, 4.14 mmol, 9.15 equiv.) and 2-formylphenyl-boronic acid (2.59 g, 7.01 mmol, 15.5 equiv.) and dissolved in dry THF (18 mL). The reaction mixture was stirred at 110 °C for 20 min. The solvent was removed under reduced pressure, redissolved in CH_2Cl_2 (10 mL) and washed with H_2O (3 × 20 mL). The crude product was purified by flash column chromatography on silica gel (CH_2Cl_2/MeOH, 50:1) to afford the title compound **198** as a red solid (31.9 mg, 52.1 mmol, 10%), representing the side-product of the *Suzuki* cross-coupling reaction.

***R*f** = (CH_2Cl_2/MeOH, 50:1) = 0.50. – **^{1}H NMR** (500 MHz, CD_2Cl_2): δ = 9.31 (s, 1H, $H_{pyrrole}$), 9.18 (d, J = 5.1 Hz, 1H, $H_{pyrrole}$), 8.76 (d, J = 6.9 Hz, 2H, $H_{aromatic}$), 8.61 (d, J = 5.1 Hz, 1H, $H_{pyrrole}$), 8.43 – 8.39 (m, 3H, $H_{aromatic}$), 8.10 – 8.05 (m, 6H, 2H $H_{pyrrole}$; 4H, $H_{aromatic}$), 7.98 (s, 1H N*H*), 7.72 – 7.68 (m, 10H, $H_{aromatic}$), 7.61 (s, 3H, $H_{pyrrole}$) ppm. – **^{13}C NMR** (500 MHz, CD_2Cl_2): δ = 153.0 (C_q), 151.8 (C_q), 146.1 (C_q), 140.2, 140.1, 139.1, 138.6, 138.5, 137.8, 137.2, 135.7, 134.7, 134.3, 133.9, 133.6, 133.3, 131.6, 131.2, 130.9, 130.4, 129.9, 129.7, 129.4, 128.9, 128.7, 128.3, 128.0, 127.3, 124.9, 124.4, 120.4, 110.9 ppm. – **UV-Vis** (CH_2Cl_2): λ_{max} (rel. absorption) = 227 (0.14), 289 (0.11), 364 (0.18), 497 (0.22), 545 (0.15), 647 (0.03), 703 (0.02) nm. – **IR** (ATR): $\tilde{\nu}$ = 3058, 2924, 1687, 1664, 1592, 1477, 1453, 1439, 1392, 1360, 1334, 1241, 1176, 1145, 1010, 1001, 788, 717, 696, 541 cm^{-1}. – HR**MS** (ESI) ($C_{44}H_{29}N_4$) calc.: 613.239, found: 613.238.

N-fused-tetraphenylporphyrin-manganese(I)tricarbonyl (**199**)[389]

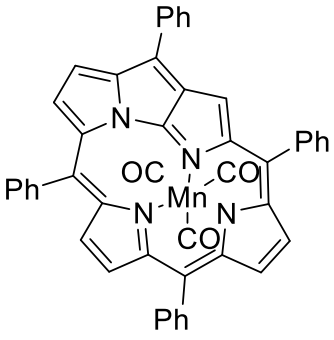

Under an argon atmosphere, a crimp vial was charged with N-fused-TPP **198** (10.0 mg, 16.0 µmol, 1.00 equiv.), $Mn(CO)_5Br$ (3.1 mg, 11.3 µmol, 0.71 equiv.) and K_2CO_3 (6.77 mg, 49.0 µmol, 3.07 equiv.) and dissolved in dry THF (2 mL). After 41 h at 80 °C, the solvent was removed under reduced pressure. The crude product was purified by flash column

chromatography on silica gel (CH_2Cl_2/*c*Hex, 2:1) to afford the title compound **199** as a red solid (8.2 mg, 12.0 µmol, 76%).

***R*f** (CH_2Cl_2/*n*-pentane, 1:3) = 0.55. – **^{1}H NMR** (500 MHz, CD_2Cl_2): δ = 9.39 (s, 1H, $H_{pyrrole}$), 9.24 (d, ^3J = 5.2 Hz, 1H, $H_{pyrrole}$), 8.75 (d, ^3J = 6.9 Hz, 2H, $H_{aromatic}$), 8.72 (d, ^3J = 5.1 Hz, 1H, $H_{pyrrole}$), 8.27 – 8.23 (m, 2H, $H_{aromatic}$), 8.07 (d, J = 7.5 Hz, 2H, $H_{aromatic}$), 7.93 – 7.88 (m, 3H, $H_{pyrrole}$, 2$H_{aromatic}$), 7.85 – 7.74 (m, 8H, $H_{aromatic}$), 7.67 – 7.62 (m, 3H, $H_{aromatic}$), 7.59 (d, *J* = 4.4 Hz, 1H, $H_{pyrrole}$), 7.56 – 7.52 (m, 1H, $H_{aromatic}$), 7.48 (d, *J* = 4.8 Hz, 1H, $H_{pyrrole}$), 7.37 (d, *J* = 4.4 Hz, 1H, $H_{pyrrole}$) ppm. – **^{13}C NMR** (500 MHz, CD_2Cl_2): δ = 165.20 (C_q), 159.18 (C_q), 154.69 (C_q), 153.85 (C_q), 153.75 (C_q), 149.06 (C_q), 145.34 (C_q), 143.21 (C_q), 138.60 (+, CH), 138.52 (+, CH), 137.93 (+, CH), 135.85 (+, CH), 135.62 (+, CH), 135.09 (+, CH), 133.02 (+, CH), 132.86 (+, CH), 132.38 (+, CH), 130.65 (+, CH), 130.14 (+, CH), 129.76 (+, CH), 129.23 (+, CH), 128.48 (+, CH), 128.26 (+, CH), 128.05 (+, CH), 127.63 (+, CH), 127.46 (+, CH), 126.85 (+, CH), 124.99 (+, CH), 120.90 (+, CH), 118.79 (+, CH), 112.01 (C_q), 111.66 (C_q) ppm. The NMR data is in accordance with the literature.[389] – **UV-Vis** (CH_2Cl_2): λ_{max} (rel. absorption) = 232 (0.08), 278 (0.05), 312 (0.05), 325 (0.04), 353 (0.04), 497 (0.04) nm. – **IR** (ATR): $\tilde{\nu}$ = 2953, 2922, 2851, 2010, 1919, 1740, 1683, 1462, 1266, 1137, 1020 cm^{-1}.

<u>N-fused-tetraphenylporphyrin-rhenium(I)tricarbonyl</u> (**200**)[390, 391]

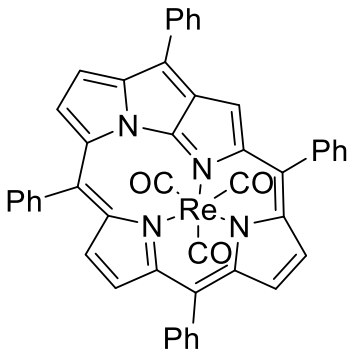

Under an argon atmosphere, a crimp vial was charged with N-fused-TPP **198** (5.20 mg, 8.30 µmol, 1.00 equiv.) and $Re(CO)_{10}$ (2.9 mg, 4.50 µmol, 0.54 equiv.) and dissolved in dry 1,2 dichlorobenzene (5 mL) and stirred at 130 °C for 41 h. The solvent was removed under reduced pressure and the crude product was purified by flash column chromatography on silica gel (CH_2Cl_2/*c*Hex, 1:1) to afford the title compound **200** as a red solid (5.1 mg, 6.28 µmol, 76%).

***R*f** (CH_2Cl_2/*n*-pentane, 1:2) = 0.59. – **^{1}H NMR** (500 MHz, CD_2Cl_2): δ = 9.32 (s, 1H, $H_{pyrrole}$), 9.29 (d, J = 5.2 Hz, 1H, $H_{pyrrole}$), 8.79 (d, J = 5.1 Hz, 1H, $H_{pyrrole}$), 8.75 – 8.71 (m, 2H, $H_{aromatic}$), 8.24 – 8.19 (m, 2H, $H_{pyrrole}$), 8.07 – 8.02 (m, 2H, $H_{pyrrole}$), 7.86 – 7.73 (m, 11H, $H_{aromatic}$), 7.66 – 7.59 (m, 4H, $H_{aromatic}$), 7.48 (d, J = 4.4 Hz, 1H, $H_{aromatic}$), 7.34 (d, J = 4.8 Hz, 1H, $H_{aromatic}$), 7.24 (d, J = 4.4 Hz, 1H, $H_{aromatic}$) ppm. – **^{13}C NMR** (500 MHz, CD_2Cl_2): δ = 164.3 (C_q), 158.1 (C_q), 154.5 (C_q), 154.1 (C_q), 150.2 (C_q), 145.4 (C_q), 143.7 (C_q), 138.7 (C_q), 138.3 (C_q), 138.2 (C_q), 137.4 (C_q), 135.4 (C_q), 133.5 (C_q), 132.9 (+, CH), 132.1 (+, CH), 131.9 (+, CH), 130.4 (+, CH), 130.0 (+, CH), 129.9 (+, CH), 129.1 (+, CH), 129.0 (+, CH), 128.8 (+, CH), 128.1 (+,

CH), 126.4 (+, CH), 124.0 (+, CH), 122.0 (+, CH), 120.0 (C_q), 112.9 (C_q), 112.5 (C_q) ppm. The NMR data is in accordance with the literature.[390, 391] – **UV-Vis** (CH_2Cl_2): λ_{max} (rel. absorption) = 270 (0.06), 359 (0.07), 494 (0.07) nm. – **IR** (ATR): $\tilde{\nu}$ = 2953, 2921, 2868, 2853, 2003, 1897, 1459, 1377, 1363, 1186, 1081, 966 cm^{-1}.

[N-fused-tetraphenylporphyrin]Mn(I)-tricarbonyl-[triphenylporphyrin]Mn(III)-bromide (**201**)[389]

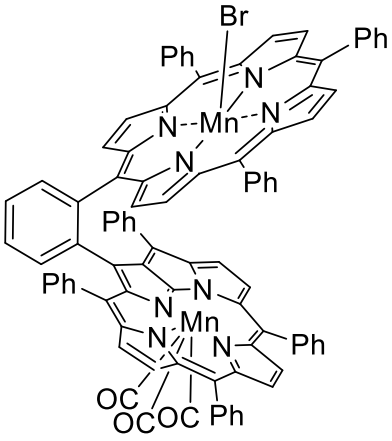

Under an argon atmosphere, a crimp vial was charged with N-fused-tetraphenylporphyrin-triphenylporphyrin (**197**) (1.00 mg, 0.82 µmol, 1.00 equiv.), $Mn(CO)_5Br$ (0.5 mg, 1.82 µmol, 2.22 equiv.) and K_2CO_3 (0.7 mg, 4.90 µmol, 6.00 equiv.) and dissolved in dry THF (0.2 mL). The resulting mixture was stirred at 80 °C for 30 min. Subsequently, the solvent was removed under reduced pressure and the crude product was purified by flash column chromatography on silica gel (CH_2Cl_2/MeOH, 1:0 → 96:4) to afford the title compound **201** as a brown solid. The yield could not be determined due to the small amount isolated.

HRMS (ESI) ($C_{91}H_{53}N_8O_3Mn_2H$) calc.: 1416.3028, found: 1416.3028. **CID**: [M–CO] 1388.3079, [M–2CO] 1359.3098, [M–3CO] 1331.3149.

6.7 Synthesis of sulfonated *o*-phenylene bisporphyrins

1,2-Phenylene-bis-5-(10,15,20-(4-trisulfonicacidphenylporphyrin)) (**203**)[392]

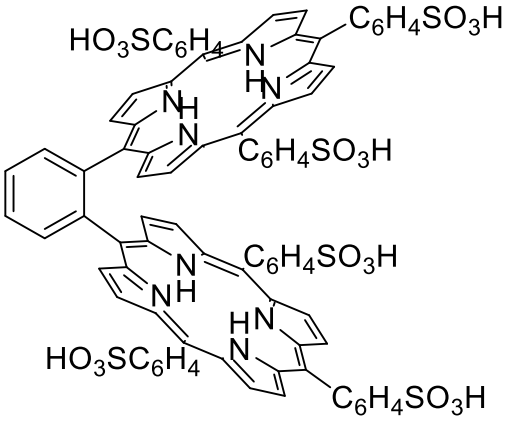

1,2-Phenylene-bis-5-(10,15,20-triphenylporphyrin) (**128**) (1.0 mg, 0.87 µmol, 1.00 equiv.) was dissolved in 98% H_2SO_4 (1 mL) and stirred at 100 °C for 14 h. Subsequently, a 7 M ammonia solution in MeOH was added while cooling the reaction mixture to 0 °C, until the color changed from green to red. The solvent was removed under reduced pressure and the crude product was extracted with ethanol (30 mL) to afford the title compound **203** as purple solid. The yield could not be determined due to undefined adducts attached to the sulfonate groups.

HRMS (ESI, –) ($C_{82}H_{54}N_8O_{18}S_6$): calc.: 1630.1880, ions found: M^{3-}: calc.: 542.7232, found: 542.7156, M^{4-}: calc.: 406.5397, found: 406.5341, M^{5-}: calc.: 325.0303, found: 325.0259, M^{6-}: calc.: 270.6907, found: 270.6871.

[1,2- Phenylene -bis-5-(10,15,20-(4-trisulfonicacidphenylporphyrin))]-dipalladium(II) (**204**)[382]

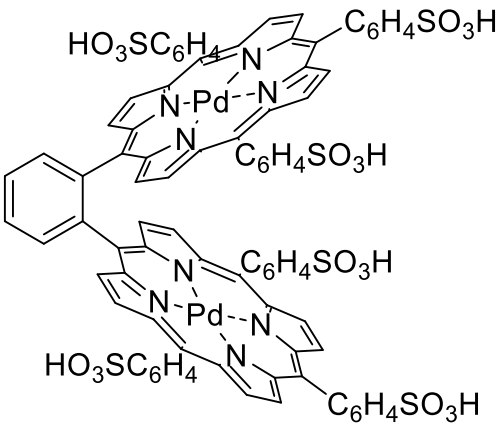

1,2- Phenylene -bis-5-(10,15,20 (4-trisulfonicacidphenylporphyrin)) (**203**) (0.3 mg, 0.26 µmol, 1.00 equiv.) was dissolved in MeOH (0.3 mL) and 38% HCl solution in H_2O (0.1 mL) was added until the color changed from red to green. Afterward, $PdCl_2$ (0.2 mg, 1.13 µmol, 4.33 equiv.) was added and stirred at 60 °C for 12 h while the color of the reaction mixture changed from green to red. The solvent was removed under reduced pressure, the residue was redissolved in boiling EtOH (10 mL), cooled to 0 °C and filtered the precipitate. This was repeated three times, before the solvent was removed under reduced pressure to afford the title compound **204** as purple solid. The yield could not be determined due to undefined adducts attached to the sulfonate groups.

HRMS (ESI, –) ($C_{82}H_{50}N_8O_{18}Pd_2S_6$): calc.: 1837.9637, ions found: M^{6-}: calc.: 305.6534, found: 305.6496, M^{5-}: calc.: 366.9855, found: 366.9815, $M^{4-}Na$: calc.: 464.4792, found: 464.4732.

6.8 Experimental section ETH Zurich

6.8.1 Potential precursors for the SF_4CN-group synthesis

p-Substituted-thiocyanatobenzene derivatives (R-Ph-SCN)[330]

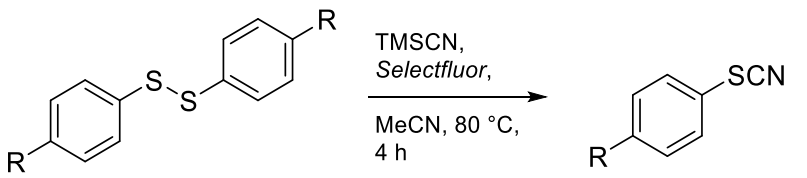

218 R: H
205 R: NO_2
219 R: OMe

220 R: H Y: 42%
208 R: NO_2 Y: 85%
221 R: OMe Y: 43%

General procedure:

A mixture of the disulfide (**218**, **205** and **219**), TMSCN and *Selectfluor* was added to MeCN (6 mL). The mixture was stirred at 80 °C for 4 h under reflux. After completion of the reaction, the mixture was cooled to room temperature and extracted with EtOAc (3 × 10 mL). The organic layer was concentrated and the resulting crude product was further purified by silica gel column chromatography to provide R-Ph-SCN as a colorless solid or oil.

220 R: H: disulfide (150 mg, 687 µmol, 1.00 equiv.), TMSCN (275 µL, 204 mg, 2.06 mmol, 3.00 equiv.), *Selectfluor* (487 mg, 1.37 mmol, 2.00 equiv.), column (1:40, EtOAc/*n*-hexane) Ph-SCN (78 mg, 577 µmol, 42% based on 2.00 equiv. sulfide), oil.

^{1}H NMR (400 MHz, $CDCl_3$):

7.56 – 7.50 (m, 2H, $H_{m\text{-aromatic}}$), 7.47 – 7.38 (m, 3H, $H_{o,p\text{-aromatic}}$) ppm.

The NMR data are following the literature.[330]

208 R: NO_2: disulfide (150 mg, 486 mmol, 1.00 equiv.), TMSCN (194 µL, 145 mg, 1.46 mmol, 3.00 equiv.), *Selectfluor* (344 mg, 972 µmol, 2.00 equiv.), column (1:10, EtOAc/*n*-hexane) NO_2-Ph-SCN (148 mg, 822 µmol, 85% based on 2.00 equiv. sulfide), solid.

^{1}H NMR (400 MHz, $CDCl_3$):

8.34 – 8.27 (m, 2H, $H_{aromatic}$), 7.70 – 7.64 (m, 2H, $H_{aromatic}$) ppm.

^{13}C NMR (101 MHz, $CDCl_3$):

147.5 (s, C_q, S*C*N), 133.5 (s, C_q, *C*NO_2), 128.9 (s, CH, $C_{aromatic}$), 125.3 (s, CH, $C_{aromatic}$), 108.2 (s, C_q, *C*SCN) ppm.

The NMR data are following the literature.[330]

221 R: OMe: disulfide (150 mg, 539 mmol, 1.00 equiv.), TMSCN (217 µL, 160 mg 1.62 mmol, 3.00 equiv.), *Selectfluor* (381 mg, 1.08 mmol, 2.00 equiv.), column (1:10, EtOAc/*n*-hexane) MeO-Ph-SCN (76 mg, 460 µmol, 43% based on 2.00 equiv. sulfide), oil.

^{1}H NMR (400 MHz, $CDCl_3$):

7.53 – 7.48 (m, 2H, $H_{aromatic}$), 6.97 – 6.92 (m, 2H, $H_{aromatic}$), 3.83 (s, 3H, OCH_3) ppm.

The NMR data are following the literature.[330]

Trifluoro(4-nitrophenyl)-λ^4-sulfane (NO_2-Ph-SF_3, **209**)

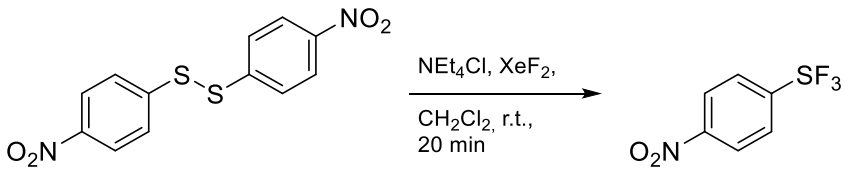

205 **209**

General procedure:

In a glovebox, a plastic 15 mL Falcon tube was charged with the commercially available 1,2-bis(4-nitrophenyl)disulfane **205** (40 mg, 129 µmol, 1.00 equiv.) and NEt_4Cl (1.0 mg, 6.04 µmol, 0.05 equiv.) together with the a stirring bar. The mixture was dissolved in dry CH_2Cl_2 (1.0 mL) and mixed intensively. While stirring, XeF_2 (102 mg, 602 µmol, 4.67 equiv.) was added, the reaction tube was sealed and mixed again. In the first 10 min, a color change from colorless to yellow was observed. After 20 min the cap was removed carefully because the Xenon gas formation led to overpressure. The same procedure was carried out in four more reaction tubes since upscaling in the falcon tube led to lower yields.

The reaction mixtures were combined and CH_2Cl_2 was removed under reduced pressure *via* an external cold trap outside of the glovebox.

Then, the remaining slurry mixture was extracted with *n*-pentane (6 × 4 mL) and the solvent was again removed *via* an external cold trap. NO_2-Ph-SF_3 **209** could be afforded as a pale-yellow solid (165 mg, 781 µmol, 61%).

^{1}H NMR (400 MHz, CD_3CN):

δ = 8.44 (d, $^3J_{HH}$ = 9.1 Hz, 2H, $H_{aromatic}$), 8.21 (d, $^3J_{HH}$ = 9.0 Hz, 2H, $H_{aromatic}$) ppm.

^{19}F NMR (376 MHz, CD_3CN):

δ = 60.9 (d, $^2J_{FF}$ = 70.1 Hz, 2H, SF_2F), –45.1 (d, $^2J_{FF}$ = 70.1 Hz, 2H, SFF$_2$) ppm.

The NMR data are following the literature.[393]

Chlorotetrafluoro(4-nitrophenyl)-λ^6-sulfane (NO_2-Ph-SF_4Cl, **210**)[331]

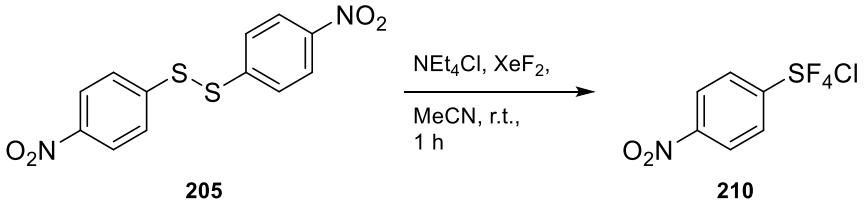

205 **210**

General procedure

In a glovebox, a plastic 50 mL Falcon tube was charged with the commercially available 1,2-bis(4-nitrophenyl)disulfane **205** (60 mg, 194 µmol, 1.00 equiv.) and NEt_4Cl (60 mg, 362 µmol, 1.87 equiv.) together with the stirring bar. The mixture was dissolved in 1.5 mL dry MeCN and mixed intensively. While stirring, XeF_2 (408 mg, 2.41 mmol, 12.4 equiv.) was added, the reaction tube was sealed and mixed again. In the first 10 min, a color change from colorless to yellow and back to colorless was observed. After 1 h, the cap was removed carefully because of the overpressure due to Xenon gas formation. The same procedure was carried out for four more reaction tubes since upscaling in the falcon tube leads to lower yields.

The reaction mixtures were combined and MeCN was removed under reduced pressure *via* an external cold trap outside of the glovebox.

Then, the remaining slurry mixture was extracted with *n*-pentane (6 × 8 mL) and the solvent was again distilled off *via* an external cold trap. NO_2-Ph-SF_4Cl **210** could be afforded as a *cis*/*trans* mixture (1:14) as a colorless solid (330 mg, 1.24 mmol, 64%).

^{1}H NMR (500 MHz, $CDCl_3$):

trans-isomer: 8.35 – 8.30 (m, $2H_{aromatic}$), 7.97 – 7.93 (m, $H_{aromatic}$) ppm.

cis-isomer: δ = 8.49 – 8.46 (m, $2H_{aromatic}$), 8.10 – 8.07 (m, $2H_{aromatic}$) ppm.

^{19}F NMR (471 MHz, $CDCl_3$):

trans-isomer: 135.5 (s, 4H, SF_4Cl) ppm.

cis-isomer: δ = 159.8 (td, $^2J_{FF}$ = 163.7, 153.7 Hz, 1H, SFF$_3$Cl), 101.3 (dd, $^2J_{FF}$ = 163.7, 83.4 Hz, 2H, SF_2F$_2$Cl), 67.3 td, $^2J_{FF}$ = 153.7, 83.4 Hz, 1H, SFF$_3$Cl) ppm.

by-products: NO_2-Ph-SF_5: 81.1 (p, $^2J_{FF}$ = 150.5 Hz, 1H, SFF$_4$), 62.7 (d, $^2J_{FF}$ = 150.8 Hz, 4H, SFF_4); NO_2-Ph-SO_2F: 66.2 (s, 1H) ppm.

^{13}C NMR (126 MHz, $CDCl_3$):

trans-isomer: 159.4 (p, $^3J_{CF}$ = 20.5 Hz, $1C_q$, *C*SF_4Cl), 149.2 (s, C_q, NO_2*C*), 127.6 (p, $^4J_{CF}$ = 4.8 Hz, 2CH, *C*HCSF_4Cl), 124.2 (s, 2CH, NO_2C*C*H) ppm.

cis-isomer: cannot be resolved completely.

The NMR data are following the literature.[331]

6.8.2 N-(trifluoromethyl)sulfinimidic fluorido derivatives

NO_2-Ph-$SNCF_3F$ and NO_2-PH-$S(NCF_3)_2F$ **215** and **216**

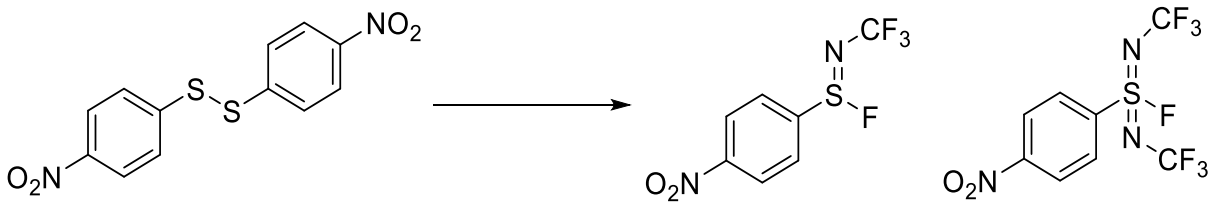

205 **215** **216**

General procedure:

In a glovebox, a plastic Eppendorf vial was charged with NO_2-Ph-S-S-Ph-NO_2 **205** (10 mg, 32.4 µmol, 1.00 equiv.), KCN, NEt_4Cl and CsF together with the smallest string bar. It was dissolved in dry MeCN-d_3 while an orange color arose and mixed intensively. While stirring, XeF_2 was added, accompanied by a color change from red to slightly yellow to colorless was observed. The reaction was stirred for 24 h at room temperature in the glovebox.

The product can be extracted with *n*-pentane, but the subsequent flash column chromatography on silica gel led to degradation on the column surface.

General standardization protocol:

A stock solution containing $PhSF_5$ (6.62 mg, 4.44 µl, 32.4 µmol, 1.00 equiv.) per 100 µL dry MeCN-d_3 was freshly made to avoid evaporation of $PhSF_5$. 100 µL was transferred into the reaction mixture and well mixed. The reaction mixture was filtered over a syringe filter.

GC/MS: 50 µL of the mixture was transferred into a GC/MS Vial and filled with 200 µL MeCN-h_3.

NMR: The rest of the reaction mixture was transferred into an NMR tube and was filled with dry MeCN-d_3 to guarantee proper NMR measurements.

Table 14: Reaction optimization: Yields are based on the analyzed samples taken after stirring for 24 h and were given in relation to 2.00 equiv. of the disulfide **205**, *: upscale reaction: 20 mg disulfide, the reaction yields of the reaction were calculated based on ^{19}F NMR measurements with the following parameter set: o_1p: 100 ppm, range: 300 ppm, d_1 time: 10 s, focusing on the following compounds.

Entry	XeF_2 (equiv.)	KCN (equiv.)	NEt_4Cl (equiv.)	CsF (equiv.)	MeCN-d_3 [mL]	Imine **215**	Diimine **216**
concentration screening							
1	12.0	4.00	0.60	-	0.50	15%	16%
2	12.0	4.00	0.60	-	1.00	5%	–
3	12.0	4.00	0.60	-	0.25	16%	13%
4	12.0	4.00	0.60	-	0.13	15%	23%
5	12.0	4.00	0.60	-	0.06	18%	32%
KCN and NEt_4Cl screening							
6	12.0	4.00	0.60	-	0.25	34%	6%
7	12.0	2.00	0.60	-	0.25	16%	13%
8	12.0	8.00	0.60	-	0.25	16%	1%
9	12.0	12.0	0.60	-	0.25	6%	4%
10	12.0	2.00	2.40	-	0.25	14%	17%
11	12.0	8.00	1.20	-	0.25	11%	25%
12*	12.0	4.00	0.60	-	0.50	7%	23%
XeF_2 and CsF tests							
13	16.0	4.00	0.60	-	0.25	15%	13%
14*	12.0	4.00	0.20	2.00	0.25	30%	32%

Characterization in solution:

NO_2-Ph-$SNCF_3F$ or NO_2-Ph-$SNOCF_3F$ **215** *vs*. **217**

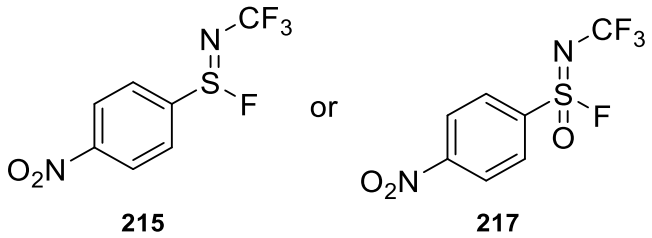

215 **217**

^{19}F NMR (565 MHz, CD_3CN):

Compound 1: δ = 76.1 (q, $^4J_{FF}$ = 8.5 Hz, 1F, *F*S), –45.2 (d, $^4J_{FF}$ = 8.5 Hz, 3F, C*F*$_3$N) ppm.

Compound 2: δ = 76.2 (q, $^4J_{FF}$ = 8.5 Hz, 1F, *F*S), –45.3 (d, $^4J_{FF}$ = 8.5 Hz, 3F, C*F*$_3$N) ppm.

^{19}F ^{19}F-COSY NMR (565 MHz, CD_3CN):

Cross-peak: 76.1 and –45.2 ppm.

Cross-peak: 76.2 and –45.3 ppm.

GC-MS:

RT: 8.454 s: MS [m/z]: 272 ($ArSFONCF_3$), 253, 226, 75, 50.

RT: 8.556 s: MS [m/z]: 256 ($ArSFNCF_3$), 238 ($ArSHNCF_3$)), 218, 187, 108, 107, 69.

HRMS (EI, +):

S(IV) compound ($C_7H_4O_2N_2F_4S$): calc.: 255.9924, found: 255.9926.

S(VI) compound ($C_7H_4O_3N_2F_4S$): calc.: 271.9879, found: 271.9874.

NO_2-Ph-$S(NCF_3)_2F$ **216**

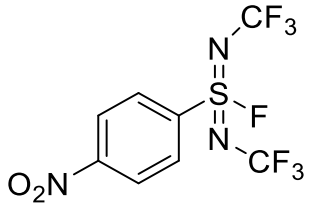

^{19}F NMR (565 MHz, CD_3CN):

Compound 1: δ = 70.6 (h, $^4J_{FF}$ = 8.5 Hz, 1F, *F*S), –46.1 (d, $^4J_{FF}$ = 8.6 Hz, 3F, (C*F*$_3$)$_2$N) ppm.

Compound 2: δ = 70.3 (h, $^4J_{FF}$ = 8.5 Hz, 1F, *F*S), –46.1 (d, $^4J_{FF}$ = 8.4 Hz, 3F, (C*F*$_3$)$_2$N) ppm.

^{19}F ^{19}F-COSY NMR (565 MHz, CD_3CN):

Cross-peak: 70.6 and –46.1 ppm.

Cross-peak: 70.3 and –46.1 ppm.

GC-MS:

RT: 8.454 s: MS [m/z]: 339 ($ArSF(NCF_3)_2$), 320 ($ArS(NCF_3)_2$), 272 ($ArSFONCF_3$), 253 ($ArSONCF_3$), 226, 75, 50.

HRMS (EI, +):

S(VI) compound ($C_8H_4O_2N_3F_7S$): calc.: 338.9907, found: 338.9905.

Two signal sets arise because of constrained rotation around the sulfuric center.

6.8.3 SF_4Cl-group – Cl substitution reactions towards the SF_4CN-group

NO_2-Ph-SF_4(OO/NN)-IBN **222** – **224**

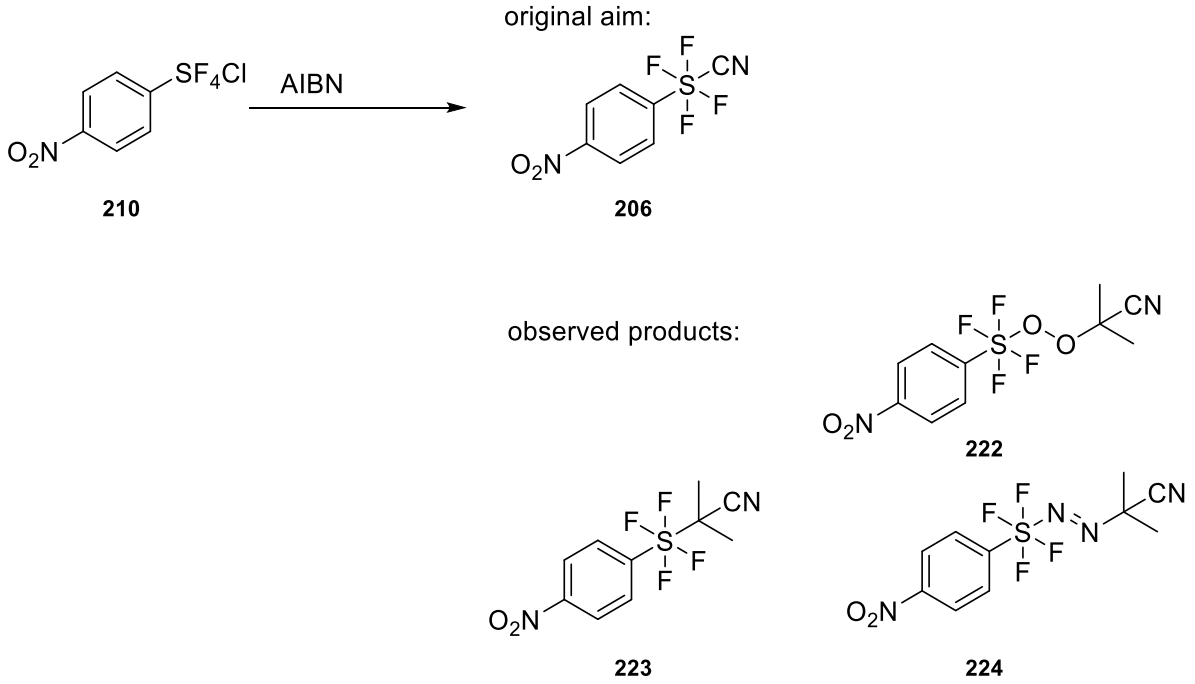

210 **206** **222** **223** **224**

General procedure:

In a glovebox, a 1 mL sealed tube was charged with NO_2-Ph-SF_4Cl **210** (5.00 mg, 18.8 µL, 1.00 equiv.) and a variable amount of AIBN. The reaction mixture was stirred outside the glovebox for 4 h at a defined temperature. The mixture was dissolved in a variable volume of MeCN-d_3.

General standardization protocol:

A stock solution containing $PhSF_5$ (1.92 mg, 1.28 µL, 9.40 µmol, 0.5 equiv.) per 100 µL dry MeCN-d_3 was freshly made to avoid evaporation of $PhSF_5$. 100 µL was transferred into the reaction mixture and well mixed. The reaction mixture was filtered with a syringe filter, if necessary.

NMR: The reaction mixture was transferred into an NMR tube and was filled with dry MeCN-d_3 to guarantee proper NMR measurements.

Reaction optimization:

Table 15: Reaction optimization for the AIBN-based radical Cl^- to CN^- substitution reaction. The yields are based on the analyzed samples taken after stirring for 24 h. If not stated otherwise, a full conversion of the starting material was obtained. *: The reaction was carried out under an O_2 atmosphere. An O_2 balloon was tightly connected to a cannula, which was stabbed through the vial cap of the reaction vessel.

Entry	AIBN	MeCN-d_3 [ml]	T [°C]	addition	Peroxide-adduct **222**	IBN-adduct **223**	conversion
concentration screening							
1*	5.00	0.25	70		10%	4%	
2*	5.00	0.50	70		12%	4%	
3*	5.00	0.13	70		3%	5%	
4*	5.00	1.00	70		2%	5%	
AIBN screening							
5*	10.0	0.50	70		6%	4%	72%
6*	1.25	0.50	70		11%	–	93%
7*	2.50	0.50	70		12%	1%	95%
T screening							
8*	5.00	0.50	50		3%	4%	98%
9*	5.00	0.50	90		11%	4%	
10*	2.50	0.50	70		12%	1%	95%
solvent screening							
11*	2.50	0.50	70	solvent: hexane	6%	–	
12*	2.50	0.50	70	solvent: toluene	3%	2%	
13*	2.50	0.50	70	solvent: THF	–	–	81%
14*	2.50	0.50	50	solvent: CH_2Cl_2	<1%	–	
15*	2.50	0.50	70	solvent: $CHCl_3$	1%	1%	
16*	2.50	0.50	70	solvent: DMF	–	–	
T screening without O_2							
17	2.50	0.50	25		–	–	
18	2.50	0.50	50		5%	–	
19	2.50	0.50	70		3%	1%	
20	2.50	0.50	90		<1%	4%	
additive screening							
21*	5.00	0.50	25	BEt_3 5.00 equiv.	<1%	–	97%
22*	5.00	0.50	50	BEt_3 5.00 equiv.	<1%	–	98%
23	2.50	0.50	50	BEt_3 10.0 equiv.	–	–	72%
best conditions							
24*	2.50	0.50	70		20%	<1%	79%
25*	2.50	0.50	70		17%	–	

Characterization:

2-Methyl-2-((tetrafluoro(4-nitrophenyl)-λ^6-sulfaneyl)peroxy)propanenitrile

(NO_2-Ph-SF_4(OO)-IBN, **222**)

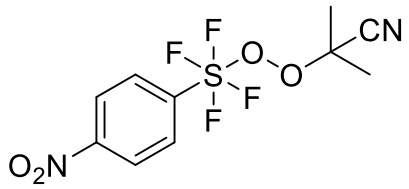

^{1}H NMR (400 MHz, $CDCl_3$):

δ = 8.32 (d, $^3J_{HH}$ = 8.9 Hz, 2H, $H_{aromatic}$), 8.00 – 7.96 (m, 2H, $H_{aromatic}$), 1.76 (s, 6H, (CH_3)C) ppm.

^{19}F NMR (377 MHz, $CDCl_3$):

δ = 60.6 (s, 4F, SF_4) ppm.

^{13}C NMR (126 MHz, $CDCl_3$):

δ = 159.1 (p, $^2J_{CF}$ = 21.1 Hz, 1C_q, *C*SF_4C(CH_3), 149.0 (s, 1C_q, NO_2*C*), 127.8 (s, 1CH, $C_{aromatic}$), 124.1 (s, 1CH, $C_{aromatic}$), 118.8 (s, 1C_q, *C*N), 77.9 (s, 1C_q, $C_q(CH_3)_2$), 25.0 (s, 2C_q, C(*C*$H_3)_2$) ppm.

2-Methyl-2-(tetrafluoro(4-nitrophenyl)-λ^6-sulfanyl)propanenitrile (NO_2-Ph-SF_4-IBN, **223**)

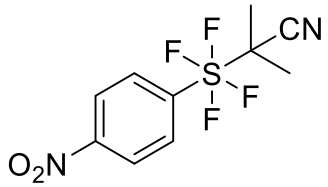

^{1}H NMR (400 MHz, $CDCl_3$):

δ = 8.27 (d, $^3J_{HH}$ = 8.9 Hz, 2H, $H_{aromatic}$), 8.00 – 7.96 (m, 2H, $H_{aromatic}$), 2.05 (p, $^4J_{FH}$ = 3.0 Hz, 6H, (CH_3)C) ppm.

^{19}F NMR (377 MHz, $CDCl_3$):

δ = 54.2 (h, $^4J_{FH}$ = 2.9 Hz 4F, SF_4) ppm.

^{13}C NMR too less substance to resolve all peaks.

HRMS (EI, +):

calc.: 298.0394, found: 298.0393.

(E)-2-Methyl-2-((tetrafluoro(4-nitrophenyl)-λ^6-sulfaneyl)diazenyl)propanenitrile

(NO_2-Ph-SF_4(NN)-IBN, **224**)

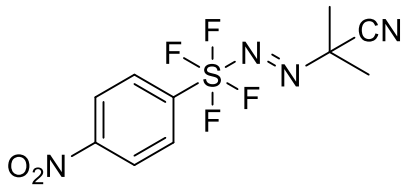

HRMS (EI, +):

M^+ not found, fragments found: $C_7H_4F_2N_2O_2S^+$ calc.: 280.0532, found: 280.0527 ([M–NO_2]$^\bullet$.

6.8.4 One-pot SuFEx reactions starting with N-(trifluoromethyl)sulfinimidic fluoride derivatives

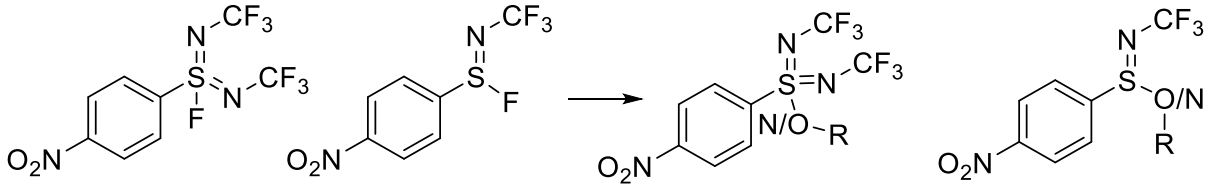

General procedure:

After 24 h reaction time, the conversion of the disulfide to the imine and the diimine was checked *via* ^{19}F NMR spectroscopy. Based on the amount of the disulfide, N- and O-nucleophiles (50.0 equiv.) were added. In the case of the N-nucleophiles, water was added and Cs_2CO_3 (7.50 equiv.) was added for the O-nucleophiles.

N-nucleophiles: pyrrolidine, 2-fluoroaniline, 2,6-difluoroaniline.

O-nucleophiles: EtOH, phenol, 2,6-difluorphenol, 2-fluorethanol.

Defined protocol for the SuFEx reaction with 2-fluoroethanol:

NO_2-Ph-S(NCF_3)(OC_2H_4F) **225**

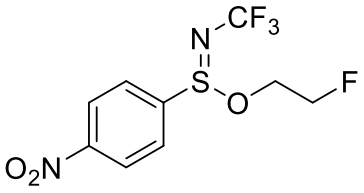

After 24 h reaction time of the disulfide **205** (100 mg, 325 µmol, 1.00 equiv.), which was converted to the imine **215** and the diimine **216**, 2-fluoroethanol (945 µL, 1.04 g, 16.3 mmol) and Cs_2CO_3 (793 mg, 2.44 mmol, 7.50 equiv.) were added in three portions over 15 min intervals were added. After 1 h, the reaction mixture was extracted with *n*-pentane (5 x 2 mL), the solvent evaporated and the crude product purified *via* flash column chromatography on silica gel, using *n*-hexane/CH_2Cl_2 (5:2) as an eluent. The title compound **225** was obtained as colorless solid (18.0 mg, 60.0 µmol, 18%), contaminated with the by-product **227** by <5%.

by-product:

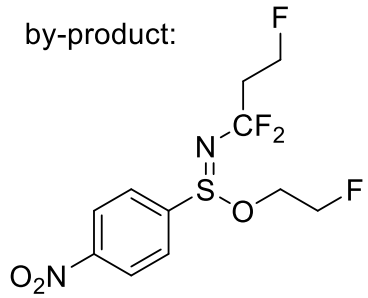

The amount of the by-product **227** increases with the amount of the base which is used.

^{1}H NMR (600 MHz, $CDCl_3$):

δ = 8.45 – 8.42 (m, 2H$_{aromatic}$), 8.14 – 8.10 (m, 2H$_{aromatic}$), 4.62 (ddd, 46.9, 5.3, 2.4 Hz, OCH_2CH_2F), 4.61 (ddd, *J* = 47.5, 6.3, 2.3 Hz, 1H, OCH_2CH_2F), 4.58 (ddd, *J* = 46.8, 5.3, 2.4 Hz, 1H, OCH_2CH_2F), 4.55 (ddd, *J* = 46.1, 5.3, 2.4 Hz, OCH_2CH_2F), 4.32 (dddd, *J* = 29.2, 12.2, 5.2, 2.3 Hz, 1H, OCH_2), 3.79 (dddd, *J* = 25.2, 12.3, 6.3, 2.4 Hz, 1H, OCH_2) ppm. OCH_2CH_2F protons split additional to the geminal splitting due to constrained rotation. By 4.70 – 4.67 + 4.60 – 4.58 (m, 2H, $FCH_2CH_2CF_2$), 4.45 – 4.43 + 4.39 – 4.37 (m, 2H, NCF_2CH_2) ppm can be assigned to the above-mentioned by-product.

^{19}F NMR (565 MHz, $CDCl_3$):

–44.5 (d, $^{7}J_{FF}$ = 0.9 Hz, CF_3N), – 224.4 (*J* = 47.2, 29.5, 25.8, 1F, FCH_2) –225.1 (tt, *J* = 47.2, 28.1 Hz) ppm can be assigned to the above-mentioned by-product.

^{13}C NMR (126 MHz, $CDCl_3$):

150.8 (s, 1C$_q$, $CSNCF_3$), 142.6 (s, 1C$_q$, CNO_2), 129.2 (s, CH, C$_{aromatic}$), 125.5 (q, $^{1}J_{CF}$ = 257.2 Hz, 1C$_q$, CF_3), 124.7 (s, CH, C$_{aromatic}$) ppm.

HRMS (ESI, +**)**:

M^+ not found, fragments found: $C_7H_4F_2N_2O_2S^+$ calc.: 217.9956, found: 217.9956 (M–OC_2H_4F–F, = NO_2-Ph-$SNCF_2$), $C_7H_4F_2N_2OS^+$ calc.: 202.0007, found: 202.0005 (M–OC_2H_4F–F–O, = NO-Ph-$SNCF_2$), $C_7H_4F_2NS^{\bullet+}$ calc.: 172.0027, found: 172.0027 (M–OC_2H_4F–F–NO_2), $C_2H_4FO^+$ calc.: 63.0241 found: 63.0235 (OC_2H_4F).

Especially fragments containing the $SNCF_2$-part underline the theory of the existence of the by-product.

6.8.5 SF_5-vinyl-azide as a versatile SF_5-heterocycle building block

General procedure

(E)-(2-Azidovinyl)pentafluoro-λ^6-sulfane **229**

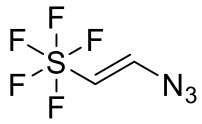

CsF (10.5 mg, 69.8 µmol, 1.00 equiv.) was suspended in 250 µl dry MeCN-d_3 and treated with acetic acid (5.80 mg, 5.52 µL, 96.6 µmol, 1.40 equiv.). The mixture was stirred at 25 °C and SF_5-TIPS-acetylene **228** (21.5 mg, 20 µL, 69.8 µmol, 1.00 equiv.) straight followed by TMS-N_3 (13.7 mg, 15.8 µL, 119 µmol, 1.7 equiv.) were added while stirred vigorously. The reaction mixture was stirred for 1.5 h. The yield was determined out of the crude reaction mixture through ^{1}H NMR and ^{19}F-NMR spectroscopy and the yield was determined using benzotrifluoride (8.57 µl, 10.2 mg, 69.8 µmol, 1.00 equiv.) in 100 µL MeCN-d_3 as an internal standard.

^{1}H NMR (400 MHz, MeCN-d_3):

δ = 6.98 – 6.91 (m, 2H, C*H*N_3), 5.93 (pd, 2H, *J* = 8.8, 7.5 Hz, 2H, SF_5C*H*) ppm.

^{19}F NMR (377 MHz, $CDCl_3$):

δ = 83.8 (p, $^2J_{FF}$ = 149.9 Hz 1F, SF_4*F*), 67.7 (ddd, *J* = 150.0, 9.0, 2.5 Hz, 4F, S*F*$_4$F) ppm.

Ethyl (E)-5-methyl-1-(2-(pentafluoro-λ^6-sulfaneyl)vinyl)-1H-1,2,3-triazole-4-carboxylate (**230**)

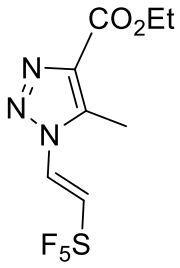

To a mixture of the *in situ* generated vinyl azide, ethylacetoacetate (13.5 mg, 13.1 µL, 104 µmol, 1.50 equiv.) and $Mn(OAc)_3 \times 2H_2O$ (1.9 mg, 7.1 µmol, 0.1 equiv.) were added and stirred at 80 °C for 16 h. Afterward, the solvent was removed under reduced pressure and the crude product was isolated *via* flash column chromatography on silica gel using *n*-hexane/EtOAc (10:1 → 0:1). The title product was afforded as a colorless solid (10.5 mg, 34.2 mmol, 49%).

^{1}H NMR (400 MHz, MeCN-d_3):

δ = 7.24 (dp, *J* = 8.3, 2.7 Hz, 1H, NC*H*), 7.06 (dp, *J* = 8.6, 8.6 Hz, 1H, C*H*SF_5), 4.37 (q, $^3J_{HH}$ = 7.1 Hz, 3H, C*H*$_2$$CH_3$), 2.52 (s, 3H, CH_3), 1.36 (t, $^3J_{HH}$ =7.1 Hz, 2H, CH_2*C*H_3) ppm.

^{19}F NMR (377 MHz, MeCN-d_3):

δ = 78.6 (p, $^2J_{FF}$ = 152.9, SF_4*F*), 66.8 (ddd, *J* = 151.3, 8.6, 2.6 Hz, 4F, S*F*$_4$F) ppm.

^{13}C NMR (101 MHz, MeCN-d_3):

δ = 162.0 (s, *C*OOEt), 153.0 (s, *C*CO_2Et), 139.9 (m, NCH*C*HSF_5, *via* HSQC), 137.0 (s, *C*CH_3, *via* HMBC), 125.7 (m, N*C*HCHSF_5), 61.8 (s, O*C*$H_2$$CH_3$), 14.5 (s, CH_2*C*H_3), 9.6 (s, *C*H_3) ppm.

^{1}H ^{13}C-HMBC:

cross-peak: 2.52 ppm (s, CH_3) and 139.9 ppm (p, NCH*C*HSF_5), indicating that the *trans*-triazole is more likely present.

HRMS (ESI, +):

($C_8H_{11}F_5N_3O_2S$) calc.: 308.0492, found: 308.0485.

(E)-1-(5-Methyl-1-(2-(pentafluoro-λ^6-sulfanyl)vinyl)-1H-1,2,3-triazol-4-yl)ethan-1-one (**232**)

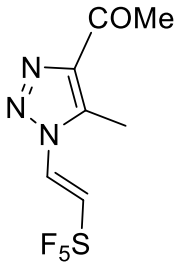

To a mixture of the *in situ* generated vinyl azide, pentane-2,4-dione (10.4 mg, 10.6 µL, 104 µmol, 1.50 equiv.) and $Mn(OAc)_3 \times 2H_2O$ (1.9 mg, 7.1 µmol, 0.1 equiv.) were/was added and stirred at 80 °C for 16 h. Afterward, the solvent was removed under reduced pressure and the crude product was isolated *via* flash column chromatography on silica gel using *n*-hexane/EtOAc (10:1 → 0:1). The title product **232** was afforded as a colorless solid.

^{1}H NMR (400 MHz, MeCN-d_3): δ = 7.24 (dp, *J* = 8.3, 2.8 Hz, 1H, NC*H*), 7.06 (dp, *J* = 8.5, 8.5 Hz, 1H, C*H*SF_5), 2.62 (s, 3H, COCH_3), 2.51 (s, 3H, CH_3) ppm.

^{19}F NMR (377 MHz, MeCN-d_3): δ = 78.7 (p, $^2J_{FF}$ = 150.0, SF_4*F*), 66.8 (ddd, *J* = 150.1, 8.3, 2.8 Hz, 4F, S*F*$_4$F) ppm.

^{13}C NMR too less substance to resolve all peaks.

HRMS (ESI, +) ($C_7H_8F_5N_3Na_1O_1S_1$) calc.: 300.0200, found: 300.0203, as the Na^+ adduct of the molecular mass.

6.9 Crystallographic data

μ-Oxo-bridged dimeric [tetraphenyl-porphyrin]-manganese(III) complex **38**

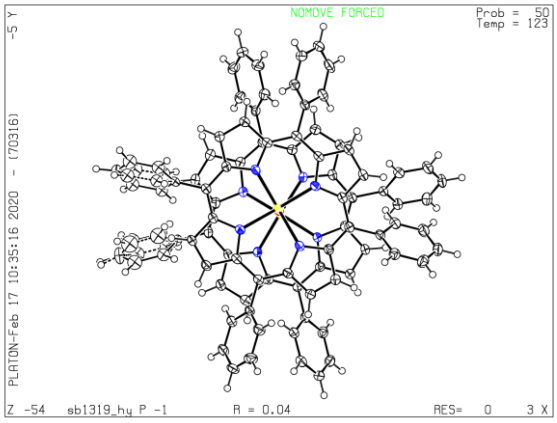

Crystal data

$C_{88}H_{56}Mn_2N_8O$	**Z = 2**
M_r = 1351.28	**F(000) = 1396**
Triclinic, *P*-1 (no.2)	**D_x = 1.359 Mg m^{-3}**
a = 14.4394 (6) Å	**Cu $K\alpha$ radiation, λ = 1.54178 Å**
b = 14.5438 (6) Å	**Cell parameters from 9944 reflections**
c = 17.8672 (8) Å	**θ = 2.6–72.1°**
α = 70.868 (2)°	**μ = 3.56 mm^{-1}**
β = 75.640 (2)°	**T = 123 K**
γ = 70.603 (2)°	**Plates, red-purple**
V = 3302.7 (3) Å^3	**0.10 × 0.06 × 0.02 mm**

Data collection

Bruker D8 VENTURE diffractometer with Photon II CPAD detector	**11370 reflections with $I > 2\sigma(I)$**
Radiation source: INCOATEC microfocus sealed tube	**R_{int} = 0.036**
rotation in ϕ and ω, 0.5°, shutterless scans	**θ_{max} = 72.2°, θ_{min} = 2.7°**
Absorption correction: multi-scan *SADABS* (Sheldrick, 2014)	**h = -17→17**
T_{min} = 0.738, T_{max} = 0.902	**k = -17→17**
38266 measured reflections	**l = -22→21**
12747 independent reflections	

Refinement

Refinement on F^2	**Primary atom site location: dual**
Least-squares matrix: full	**Secondary atom site location: difference Fourier map**
$R[F^2 > 2\sigma(F^2)]$ = 0.044	**Hydrogen site location: inferred from neighboring sites**
$wR(F^2)$ = 0.112	**H-atom parameters constrained**
S = 1.03	**$w = 1/[\sigma^2(F_o^2) + (0.0546P)^2 + 2.7187P]$ where $P = (F_o^2 + 2F_c^2)/3$**
12747 reflections	**$(\Delta/\sigma)_{max}$ = 0.001**
886 parameters	**$\Delta\rangle_{max}$ = 0.72 e Å^{-3}**
120 restraints	**$\Delta\rangle_{min}$ = -0.53 e Å^{-3}**

Crystal data

$C_{88}H_{56}Mn_2N_8O$	$Z = 2$
$M_r = 1351.28$	$F(000) = 1396$
Triclinic, P-1 (no.2)	$D_x = 1.359$ Mg m^{-3}
$a = 14.4394$ (6) Å	Cu $K\alpha$ radiation, $\lambda = 1.54178$ Å
$b = 14.5438$ (6) Å	Cell parameters from 9944 reflections
$c = 17.8672$ (8) Å	$\theta = 2.6–72.1°$
$\alpha = 70.868$ (2)°	$\mu = 3.56$ mm^{-1}
$\beta = 75.640$ (2)°	$T = 123$ K
$\gamma = 70.603$ (2)°	Plates, red-purple
$V = 3302.7$ (3) Å^3	0.10 × 0.06 × 0.02 mm

Data collection

Bruker D8 VENTURE diffractometer with Photon II CPAD detector	11370 reflections with $I > 2\sigma(I)$
Radiation source: INCOATEC microfocus sealed tube	$R_{int} = 0.036$
rotation in ϕ and ω, 0.5°, shutterless scans	$\theta_{max} = 72.2°$, $\theta_{min} = 2.7°$
Absorption correction: multi-scan *SADABS* (Sheldrick, 2014)	$h = -17\rightarrow17$
$T_{min} = 0.738$, $T_{max} = 0.902$	$k = -17\rightarrow17$
38266 measured reflections	$l = -22\rightarrow21$
12747 independent reflections	

Refinement

Refinement on F^2	Primary atom site location: dual
Least-squares matrix: full	Secondary atom site location: difference Fourier map
$R[F^2 > 2\sigma(F^2)] = 0.044$	Hydrogen site location: inferred from neighboring sites
$wR(F^2) = 0.112$	H-atom parameters constrained
$S = 1.03$	$w = 1/[\sigma^2(F_o^2) + (0.0546P)^2 + 2.7187P]$ where $P = (F_o^2 + 2F_c^2)/3$
12747 reflections	$(\Delta/\sigma)_{max} = 0.001$
886 parameters	$\Delta\rangle_{max} = 0.72$ e Å^{-3}
120 restraints	$\Delta\rangle_{min} = -0.53$ e Å^{-3}

minor disordered parts omitted for clarity

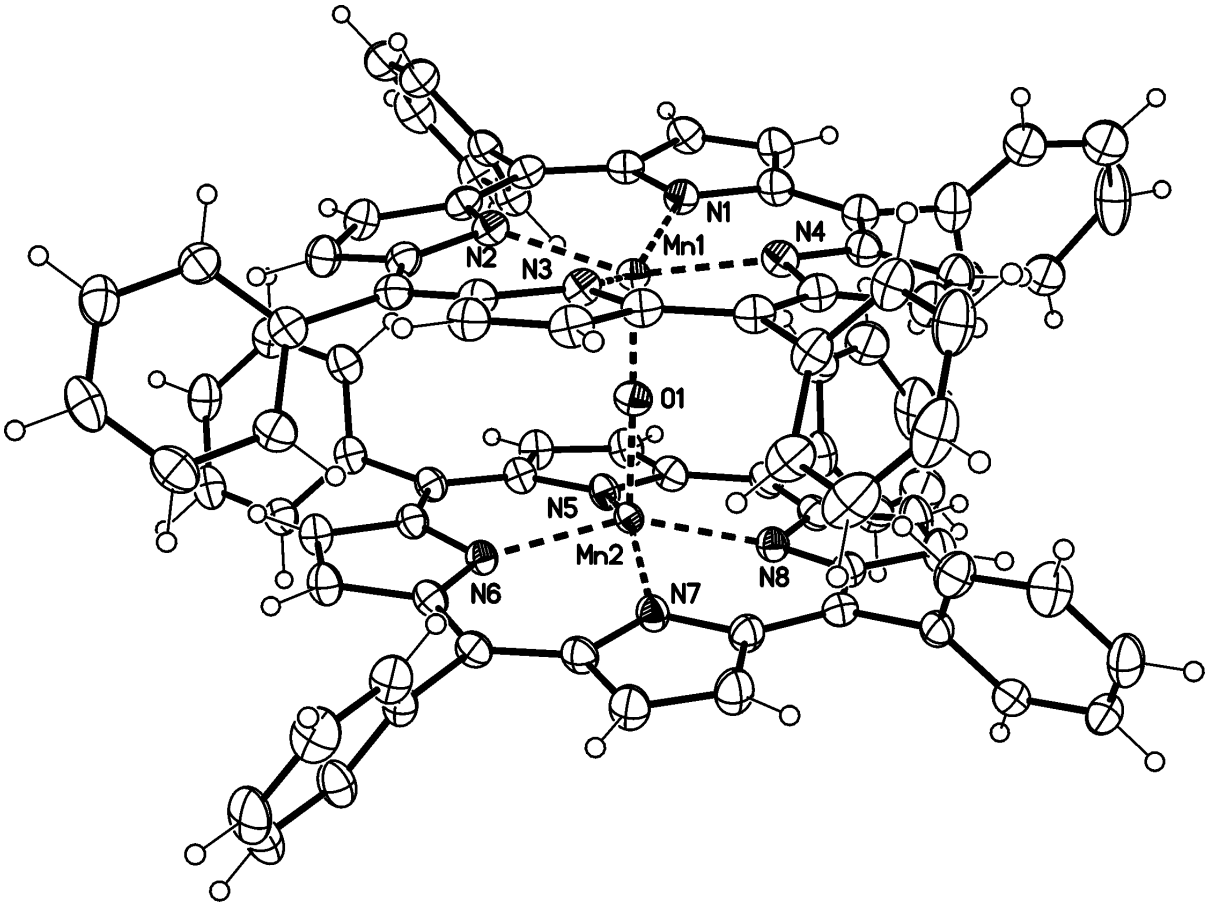

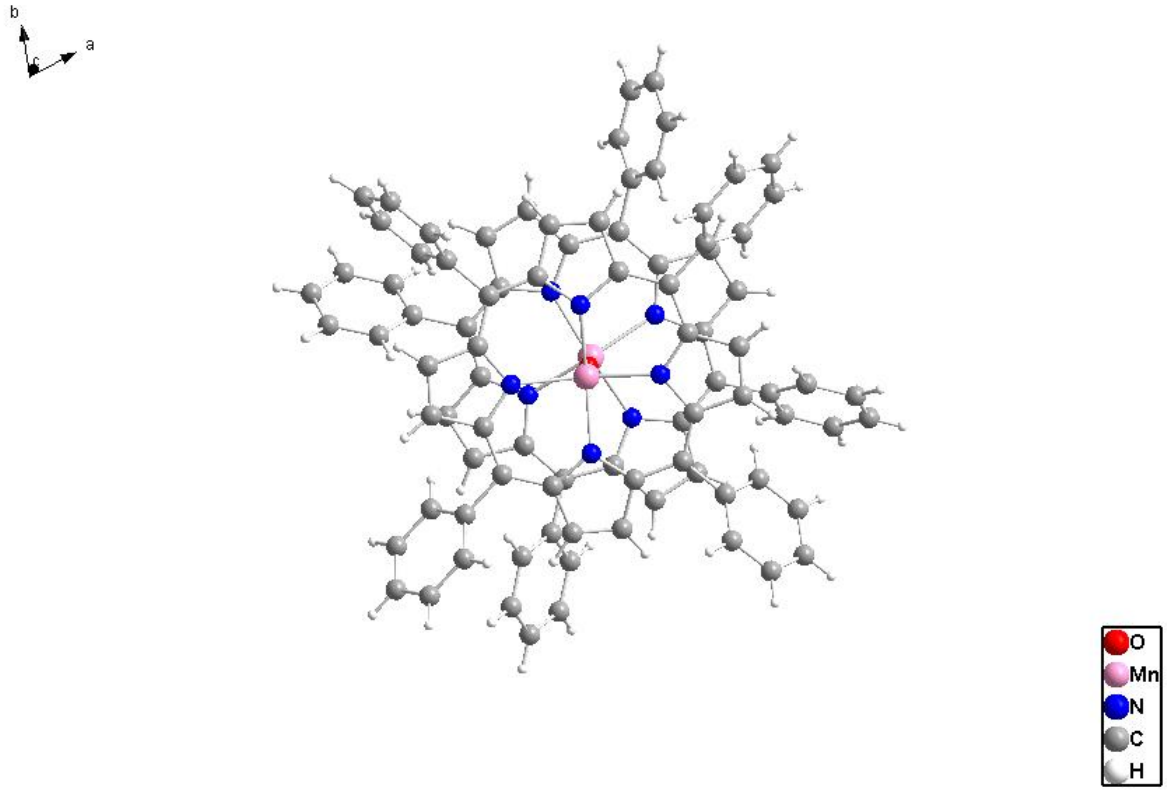
b
a
c
O
Mn
N
C
H

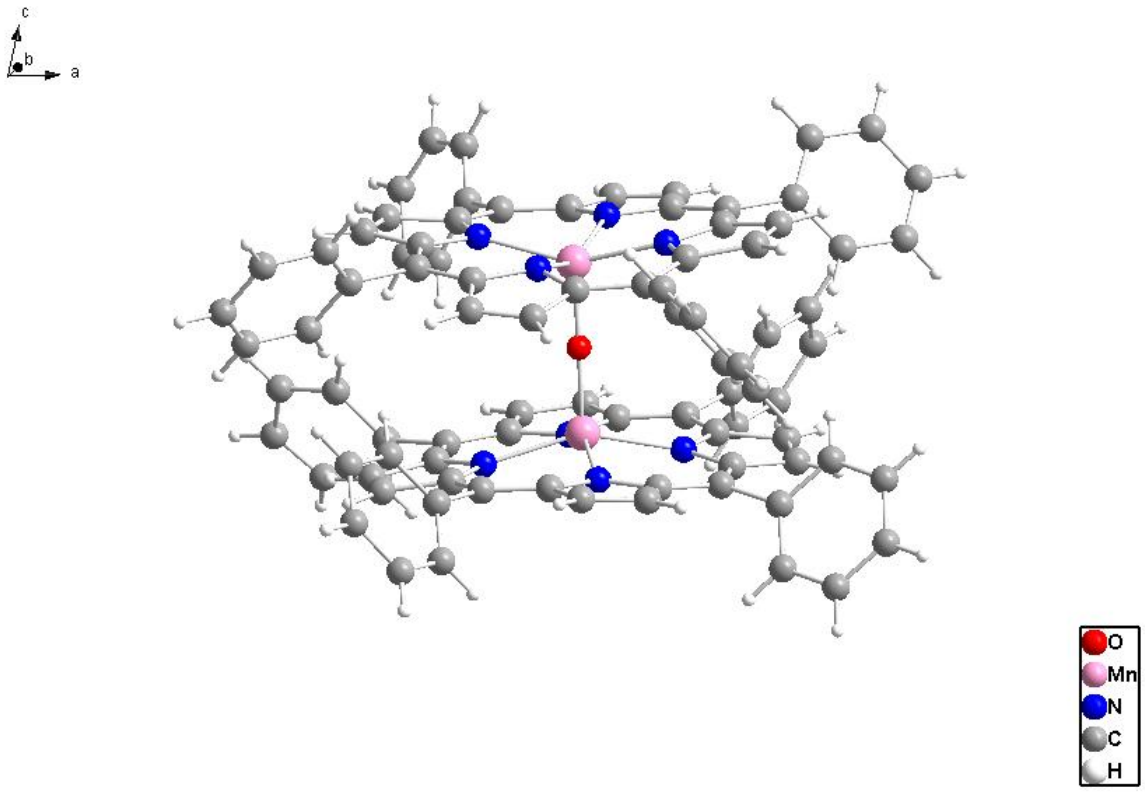
c
b
a
O
Mn
N
C
H

5-(2-Formylphenyl)-10,20-diethoxycarbonylphenylporphyrin (**126**)

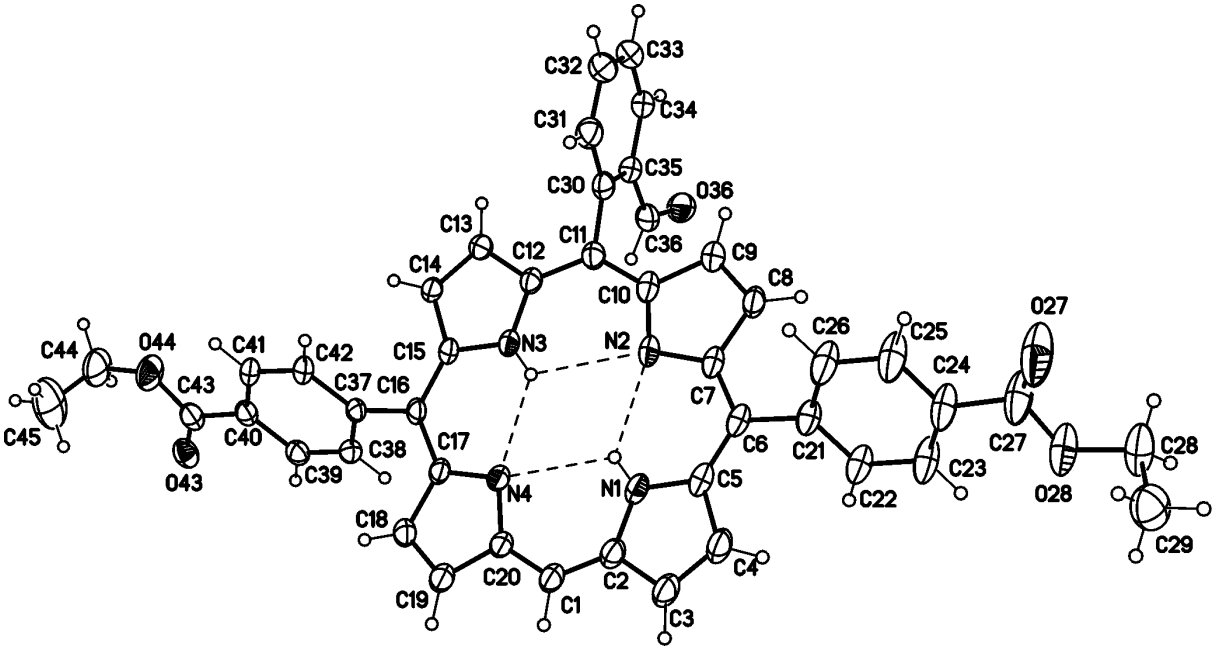

Molecular structure of **126** (displacement parameters are drawn at 30% probability level)

Crystal data

$C_{45}H_{34}N_4O_5$	Z = 8
M_r = 710.76	F(000) = 2976
Orthorhombic, *Pbca (no.61)*	D_x = 1.209 Mg m^{-3}
a = 18.8247 (9) Å	Cu $K\alpha$ radiation, λ = 1.54178 Å
b = 13.4631 (5) Å	μ = 0.64 mm^{-1}
c = 30.8262 (14) Å	T = 123 K
V = 7812.6 (6) Å^3	0.14 × 0.06 × 0.02 mm

Data collection

63387 measured reflections	θ_{max} = 73.1°, θ_{min} = 2.9°
7737 independent reflections	h = -23→23
5052 reflections with $I > 2\sigma(I)$	k = -16→15
R_{int} = 0.130	l = -33→38

[1,2-Phenylene-(5-(10,20-*para*-diethoxycarbonylphenylporphyrin),5-(10,15,20-triphenylporphyrin))]-dinickel(II) (**141**)

Crystal data

$C_{82}H_{54}N_8Ni_2O_4 \cdot C_5H_{12}$	$F(000) = 2928$
$M_r = 1404.89$	$D_x = 1.379$ Mg m^{-3}
Monoclinic, $P2_1$ (no.4)	Cu $K\alpha$ radiation, $\lambda = 1.54178$ Å
$a = 14.6620$ (6) Å	Cell parameters from 9610 reflections
$b = 27.1129$ (12) Å	$\theta = 3.2–72.1°$
$c = 18.2260$ (8) Å	$\mu = 1.18$ mm^{-1}
$\beta = 110.942$ (2)°	$T = 123$ K
$V = 6766.8$ (5) Å^3	Plates, red purple
$Z = 4$	0.12 × 0.06 × 0.03 mm

Data collection

Bruker D8 VENTURE diffractometer with PhotonII CPAD detector	22452 reflections with $I > 2\sigma(I)$
Radiation source: INCOATEC microfocus sealed tube	$R_{int} = 0.048$
rotation in ϕ and ω, 0.5°, shutterless scans	$\theta_{max} = 72.2°$, $\theta_{min} = 2.6°$
Absorption correction: multi-scan *SADABS* (Sheldrick, 2014)	$h = -18 \rightarrow 17$
$T_{min} = 0.819$, $T_{max} = 0.971$	$k = -33 \rightarrow 28$
75718 measured reflections	$l = -22 \rightarrow 22$
24649 independent reflections	

Refinement

Refinement on F^2	Secondary atom site location: difference Fourier map
Least-squares matrix: full	Hydrogen site location: inferred from neighboring sites
$R[F^2 > 2\sigma(F^2)] = 0.053$	H-atom parameters constrained
$wR(F^2) = 0.138$	$w = 1/[\sigma^2(F_o^2) + (0.085P)^2 + 3.120P]$ where $P = (F_o^2 + 2F_c^2)/3$

S = 1.03	$(\Delta/\sigma)_{max}$ = 0.032
24649 reflections	$\Delta\rangle_{max}$ = 0.99 e Å^{-3}
1730 parameters	$\Delta\rangle_{min}$ = -0.39 e Å^{-3}
1819 restraints	Absolute structure: Refined as an inversion twin.
Primary atom site location: dual	Absolute structure parameter: 0.38 (2)

Hydrogen atoms were refined using a riding model. Semi-empirical absorption corrections were applied. **141** is refined as an inversion (racemic) twin with BASF = 0.38(2) (Hooft's y-parameter) y = 0.39(1)[219]. Therefore, the ratio between the two enantiomers is for the measured crystal approx. 62:38. In **141** are two crystallographic independent molecules with identical chirality in the asymmetric unit (see L.S.-fit). Refinement with the listed atoms shows residual electron density due to a heavily disordered solvent molecules that could not be refined with split atoms (*n*-pentane for **141**, see cif-file for details). Therefore, the option "SQUEEZE" of the program package *Platon*[394, 395] was used to create a hkl file considering the residual electron density in the void areas.

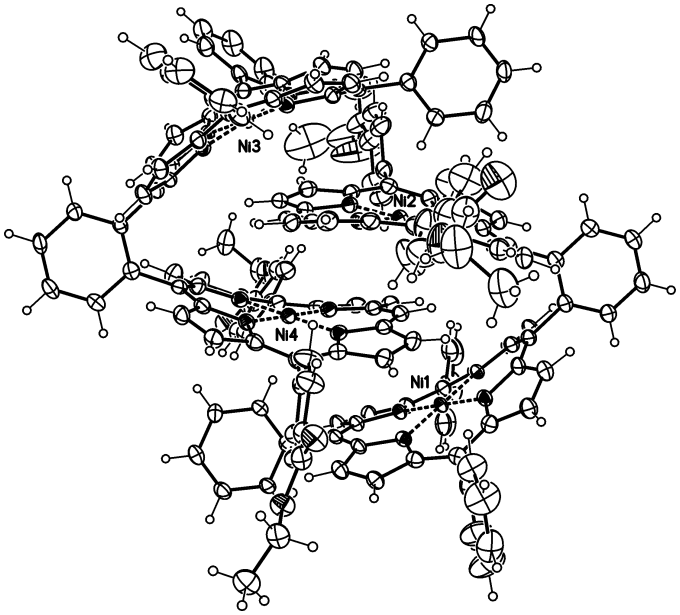

Molecular structure of the two crystallographic independent molecules of **141** in the asymmetric unit (displacement parameters are drawn at 50% probability level)

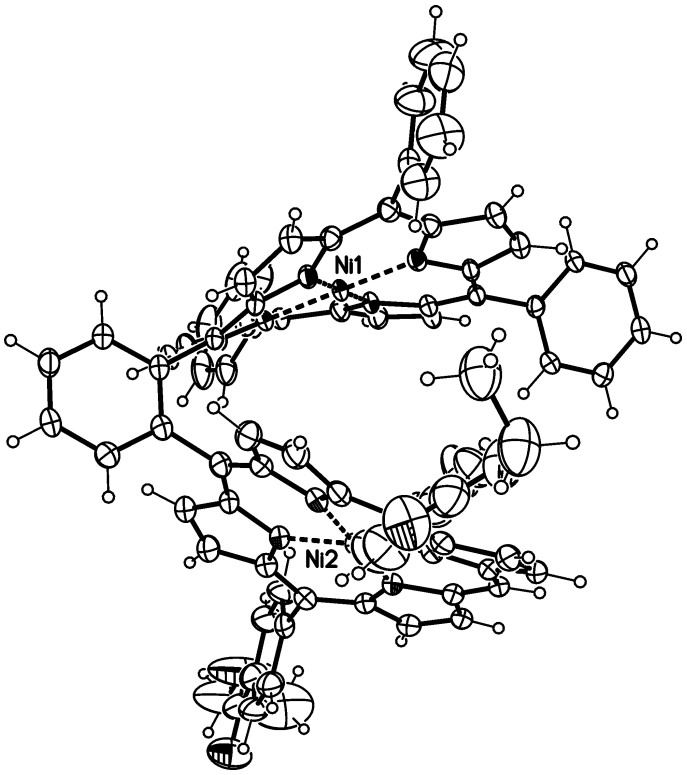

Molecular structure of the 1st crystallographic independent molecule of **141** in the asymmetric unit (displacement parameters are drawn at 50% probability level).

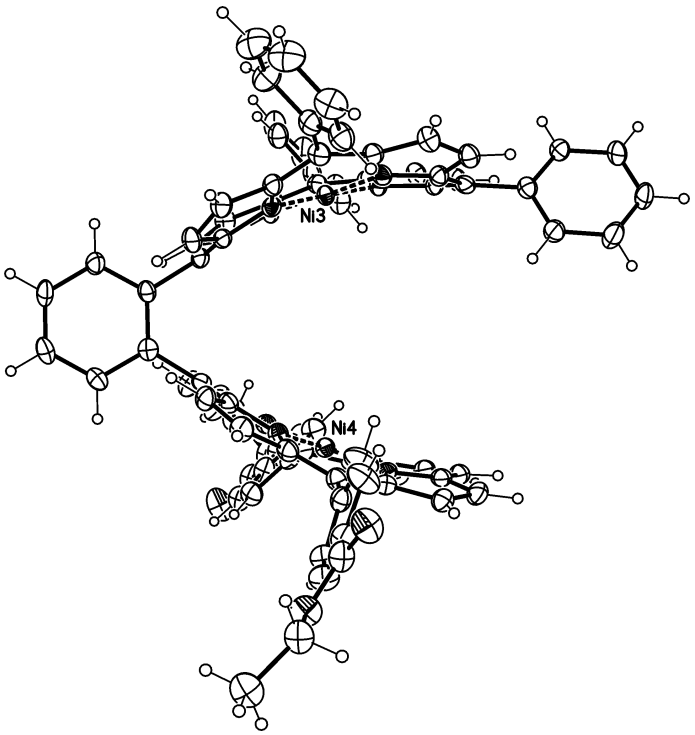

Molecular structure of the 12th crystallographic independent molecule of **141** in the asymmetric unit (displacement parameters are drawn at 50% probability level).

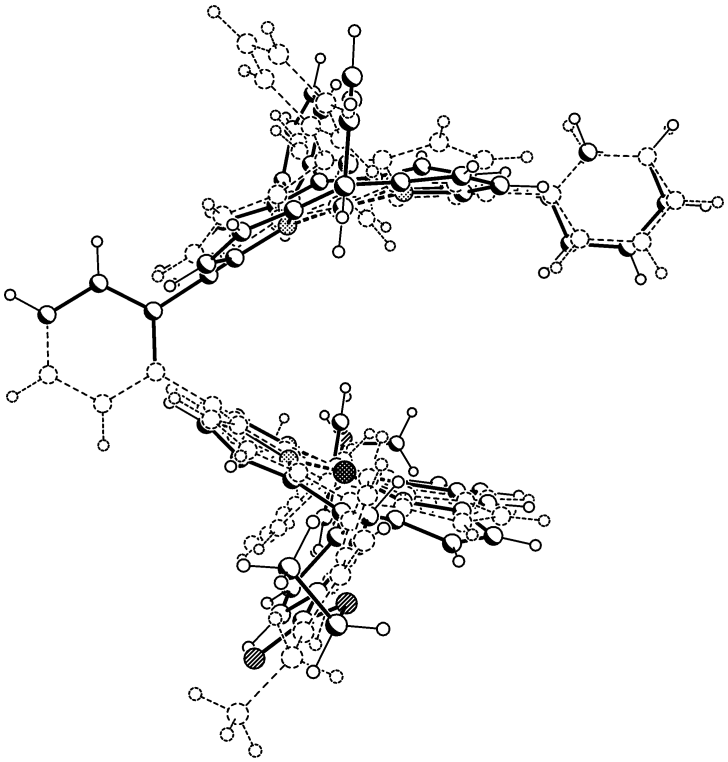

L.S. fit of the two crystallographic independent molecules of **141** (fitted atoms: phenyl spacer and the 1,2-carbon atoms, for the fitted molecules, the configuration in the asymmetric unit is used).

[5-(2-Formylphenyl)-10,15,20-triphenylporphyrin]platinum(II) (**156**)

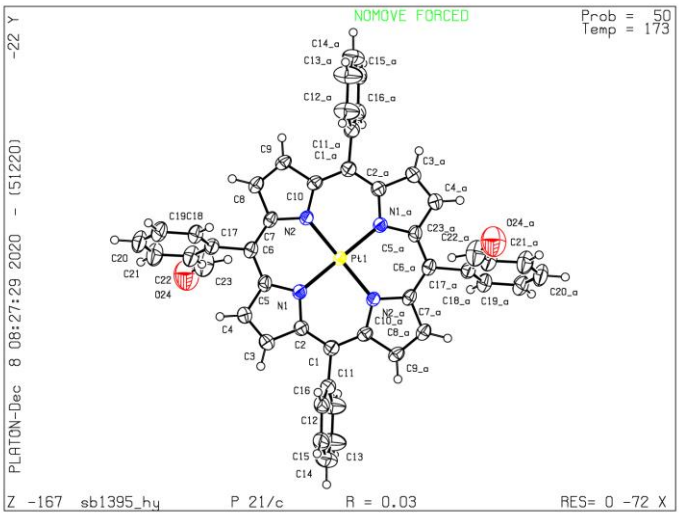

Crystal data

$C_{45}H_{28}N_4OPt$	$F(000)$ = 824
M_r = 835.80	D_x = 1.664 Mg m^{-3}
Monoclinic, $P2_1/c$ *(no.14)*	Cu $K\alpha$ radiation, λ = 1.54178 Å
a = 13.1859 (4) Å	Cell parameters from 9961 reflections
b = 11.4230 (3) Å	θ = 3.4–72.2°
c = 11.5042 (3) Å	μ = 8.21 mm^{-1}
β = 105.751 (1)°	T = 173 K
V = 1667.73 (8) Å^3	Plates, orange
Z = 2	0.12 × 0.06 × 0.02 mm

Data collection

Bruker D8 VENTURE diffractometer with PhotonII CPAD detector	2620 reflections with $I > 2\sigma(I)$
Radiation source: INCOATEC microfocus sealed tube	R_{int} = 0.035
rotation in ϕ and ω, 1°, shutterless scans	θ_{max} = 72.3°, θ_{min} = 3.5°
Absorption correction: multi-scan *SADABS* (Sheldrick, 2014)	h = -16→16
T_{min} = 0.585, T_{max} = 0.841	k = -13→14
21653 measured reflections	l = -13→14
3281 independent reflections	

Refinement

Refinement on F^2	Primary atom site location: dual
Least-squares matrix: full	Secondary atom site location: difference Fourier map
$R[F^2 > 2\sigma(F^2)]$ = 0.026	Hydrogen site location: inferred from neighboring sites
$wR(F^2)$ = 0.070	H-atom parameters constrained
S = 1.10	$w = 1/[\sigma^2(F_o^2) + (0.0376P)^2 + 1.7961P]$ where $P = (F_o^2 + 2F_c^2)/3$
3281 reflections	$(\Delta/\sigma)_{max} < 0.001$
241 parameters	$\Delta\rangle_{max}$ = 1.27 e Å^{-3} (near Pt1)
225 restraints	$\Delta\rangle_{min}$ = -0.52 e Å^{-3}

Crystal data

$C_{45}H_{28}N_4OPt$	$F(000) = 824$
$M_r = 835.80$	$D_x = 1.664$ Mg m^{-3}
Monoclinic, $P2_1/c$ *(no.14)*	Cu $K\alpha$ radiation, $\lambda = 1.54178$ Å
$a = 13.1859$ (4) Å	Cell parameters from 9961 reflections
$b = 11.4230$ (3) Å	$\theta = 3.4$–$72.2°$
$c = 11.5042$ (3) Å	$\mu = 8.21$ mm^{-1}
$\beta = 105.751$ (1)°	$T = 173$ K
$V = 1667.73$ (8) Å^3	Plates, orange
$Z = 2$	0.12 × 0.06 × 0.02 mm

Data collection

Bruker D8 VENTURE diffractometer with PhotonII CPAD detector	2620 reflections with $I > 2\sigma(I)$
Radiation source: INCOATEC microfocus sealed tube	$R_{int} = 0.035$
rotation in ϕ and ω, 1°, shutterless scans	$\theta_{max} = 72.3°$, $\theta_{min} = 3.5°$
Absorption correction: multi-scan *SADABS* (Sheldrick, 2014)	$h = -16 \rightarrow 16$
$T_{min} = 0.585$, $T_{max} = 0.841$	$k = -13 \rightarrow 14$
21653 measured reflections	$l = -13 \rightarrow 14$
3281 independent reflections	

Refinement

Refinement on F^2	Primary atom site location: dual
Least-squares matrix: full	Secondary atom site location: difference Fourier map
$R[F^2 > 2\sigma(F^2)] = 0.026$	Hydrogen site location: inferred from neighboring sites
$wR(F^2) = 0.070$	H-atom parameters constrained
$S = 1.10$	$w = 1/[\sigma^2(F_o^2) + (0.0376P)^2 + 1.7961P]$ where $P = (F_o^2 + 2F_c^2)/3$
3281 reflections	$(\Delta/\sigma)_{max} < 0.001$
241 parameters	$\Delta\rangle_{max} = 1.27$ e Å^{-3} (near Pt1)
225 restraints	$\Delta\rangle_{min} = -0.52$ e Å^{-3}

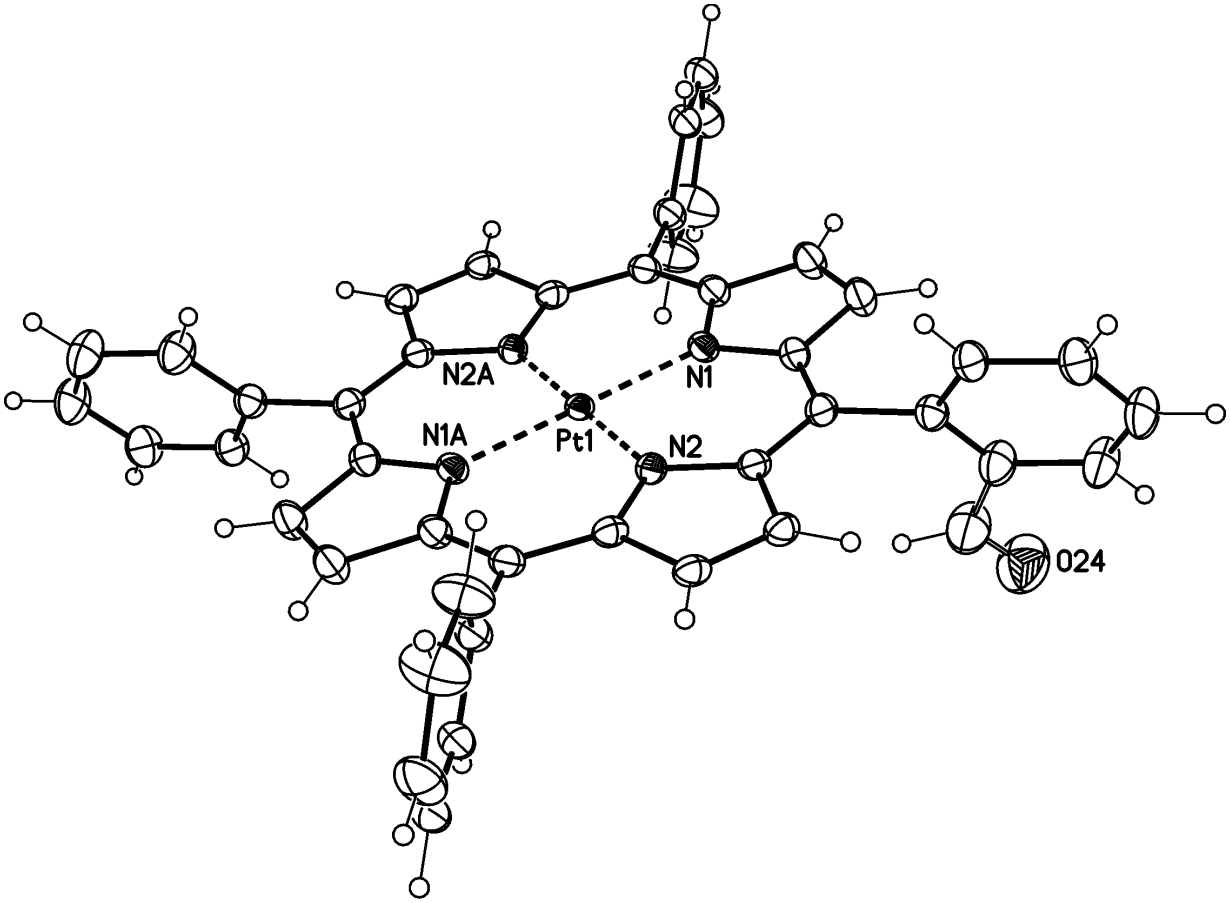
N2A
N1
N1A
Pt1
N2
O24

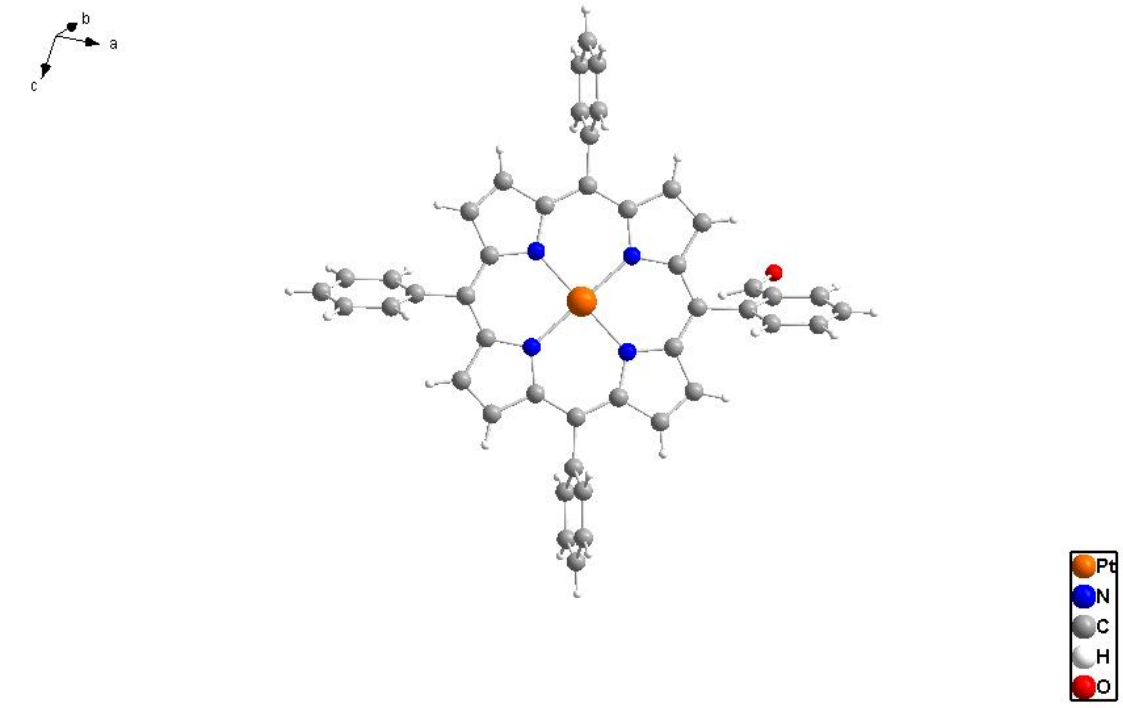
b
a
c
Pt
N
C
H
O

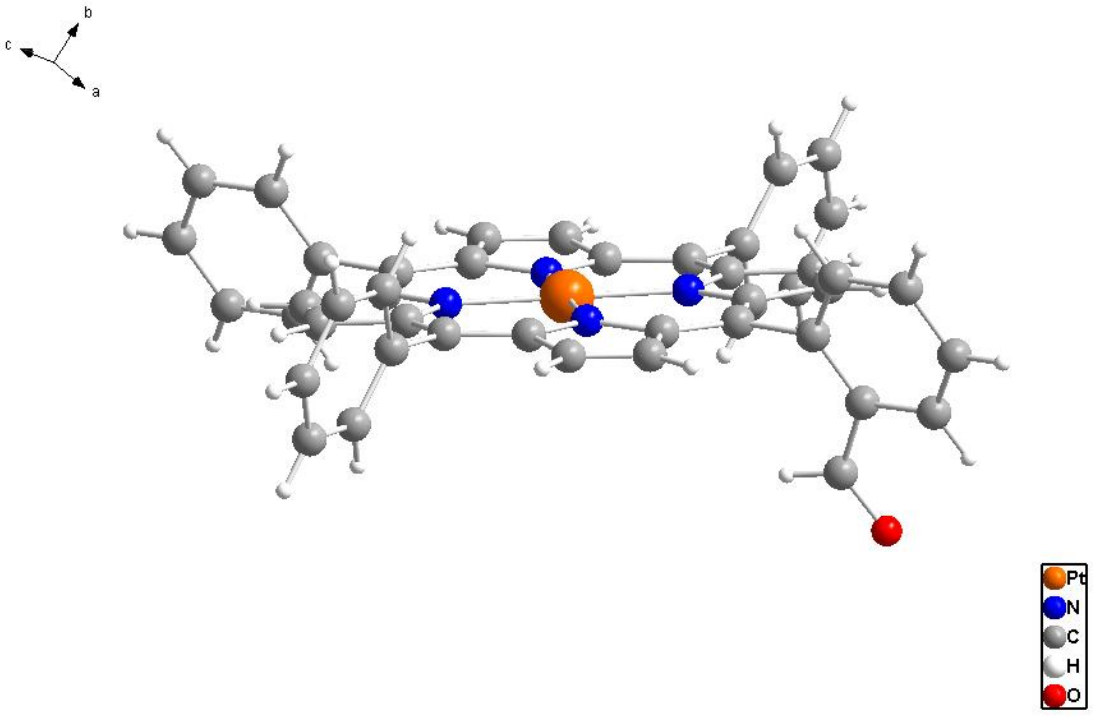
b
c
a
Pt
N
C
H
O

2-Methyl-2-((tetrafluoro(4-nitrophenyl)-λ^6-sulfaneyl)peroxy)propanenitrile (**222**)

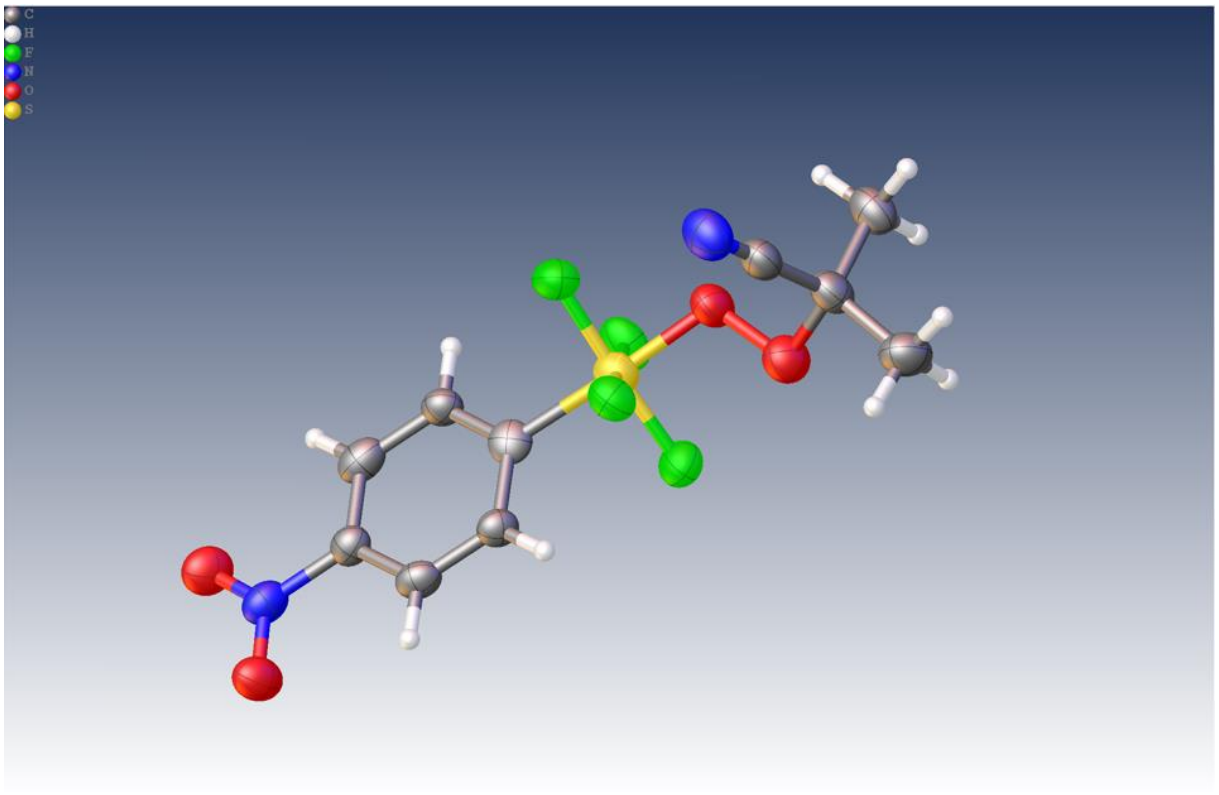

Identification code	ca070721_1_1
Empirical formula	$C_{10}H_{10}F_4N_2O_4S$
Formula weight	330.26
Temperature/K	100.0(1)
Crystal system	monoclinic
Space group	$P2_1/c$
a/Å	11.8522(15)
b/Å	6.0909(6)
c/Å	18.711(2)
α/°	90
β/°	101.350(12)
γ/°	90
Volume/Å^3	1324.3(3)
Z	4
ρ_{calc}g/cm^3	1.656
μ/mm^{-1}	2.848
F(000)	672.0
Crystal size/mm^3	0.076 × 0.022 × 0.012
Radiation	Cu Kα (λ = 1.54184)
2Θ range for data collection/°	7.608 to 106.046
Index ranges	$-12 \leq h \leq 12$, $-6 \leq k \leq 6$, $-16 \leq l \leq 19$
Reflections collected	1525
Independent reflections	1525 [R_{int} = 0.0760, R_{sigma} = 0.0719]
Data/restraints/parameters	1525/0/193

Goodness-of-fit on F^2	1.046
Final R indexes [I>=2σ (I)]	R_1 = 0.0648, wR_2 = 0.1685
Final R indexes [all data]	R_1 = 0.0911, wR_2 = 0.1862
Largest diff. peak/hole / e $Å^{-3}$	0.70/-0.33

Crystal structure determination of 222

Crystal Data for $C_{10}H_{10}F_4N_2O_4S$ (M =330.26 g/mol): monoclinic, space group $P2_1/c$ (no. 14), a = 11.8522(15) Å, b = 6.0909(6) Å, c = 18.711(2) Å, β = 101.350(12)°, V = 1324.3(3) $Å^3$, Z = 4, T = 100.0(1) K, μ(Cu Kα) = 2.848 mm^{-1}, $Dcalc$ = 1.656 g/cm^3, 1525 reflections measured (7.608° ≤ 2Θ ≤ 106.046°), 1525 unique (R_{int} = ?, R_{sigma} = 0.0719) which were used in all calculations. The final R_1 was 0.0648 (I > 2σ(I)) and wR_2 was 0.1862 (all data).

Refinement model description

Number of restraints - 0, number of constraints - unknown.
Details:
1. Twinned data refinement
Scales: 0.754(5)
0.246(5)
2. Fixed Uiso
At 1.2 times of:
All C(H) groups
At 1.5 times of:
All C(H,H,H) groups
3.a Aromatic/amide H refined with riding coordinates:
C6(H6), C7(H7), C9(H9), C10(H10)
3.b Idealized Me refined as a rotating group:
C3(H3A,H3B,H3C), C4(H4A,H4B,H4C)

7 List of abbreviations

3-NBA	3-Nitrobenzyl Alcohol
Å	*Angström*
abs.	absolut
acac	acetylacetonate
aq.	aqueous
Ar	Aryl-
ATR	Attenuated Total Reflection (IR)
BMOBBP	*β-meso-o*-Phenylene bisporphyrin
Bn	Benzyl-
Bu	Butyl-
bs	broad singlet
°C	Grad *Celsius*
c	concentration
calc.	calculated
$CDCl_3$	Chloroform-d_1
CH_2Cl_2	Dichloromethane
$CHCl_3$	Chloroform
C_{hex}	Cyclohexane
cm	centimeter
CODH	Carbon Monoxide Dehydrogenase
COSY	Correlation Spectroscopy (NMR)
cp	cyclopentadienyl
d	day, doublet (NMR), path length
DCM-d_2	Dichloromethane-d_2
DSSC	Dye Sensitized Solar Cells
DDQ	2,3-Dichloro-5,6-Dicyano-1,4-benzoquinone
DEPT	Distortionless Enhancement by Polarization Transfer (NMR)
DFT	Density Functional Theory
DMAC	Dimethylacetamide
DMF	Dimethylformamide
DMSO	Dimethylsulfoxide
E	potential
E^0	standard potential

e.g.	lat. *Exempli gratia*
EI	Electron Impact ionization (MS)
EOAc	Ethylacetate
EOBBP	Ethoxycarbonyl *o*-phenylene bisporphyrin
equiv.	equivalents
ESI	Electrospray Ionization (MS)
Et	ethyl-
et al.	*et alia* (and others)
EtOH	Ethanol
eV	electron volt
FAB	Fast Atom Bombardment (MS)
F	Fluorescence
FRET	*Förster* Resonance Energy Transfer
FTO	Fluorine-doped Tin Oxide
g	gramm
GC	Gas Chromatography
GC-MS	Gas Chromatography Mass Spectrometry
h	hour(s)
HMBC	Heteronuclear Multiple Bond Correlation (NMR)
HPLC	High-Pressure Liquid Chromatography
HRMS	High-Resolution Mass Spectrometry (MS)
HSQC	Heteronuclear Single Quantum Coherence (NMR)
HOMO	Highest Occupied Molecular Orbital
Hz	Hertz
i	lat. *iso*
i.e.	lat. *id est*
IC	Internal Conversion
IMS	Ion Mobility Spectrometry
IR	Infrared (-Spectroscopy)
^{i}Pr	*iso*-Propyl
ISC	Intersystem Crossing
IUPAC	International Union of Pure and Applied Chemistry
J	coupling constant
K	Kelvin

kJ	kilojoule
Ln	Lanthanide
LUMO	Lowest Unoccupied Molecular Orbital
M	molar
m	multiplett (NMR), medium (IR), *milli*
m	*meta*
m/z	mass/charge-ratio
Me	Methyl-
MeOH	Methanol
min	minutes
mL	milliliter
mmol	millimole
µmol	micromole
M	Metal
mol%	mole percent
MO	Molecular Orbital
MeOH	Methanol
MHz	*mega* Hertz
MS	Mass Spectrometry, Molecular Sieve
n	*nano*
NBS	N-Bromosuccinimide
NIR	Near-Infrared
NLO	Non-Linear Optics
nm	nanometer
NMR	Nuclear Magnetic Resonance
NOESY	Nuclear *Overhauser* Effect Spectroscopy (NMR)
o	*ortho*
OAc	acetate
OBBP	*o*-Phenylene bisporphyrin
OBBPS	Sulfonated *o*-phenylene bisporphyrin
P	phosphorescence
p	pentet
p	*para*
p.a	*pro analysis*

PDT	Photodynamic Therapy
Ph	phenyl-
ppm	parts per million
q	quartet (NMR)
quant.	quantitative
r.t.	room temperature
RCB	Repulsive Coulomb Barrier
R_f	Retardation factor
s	singlet (NMR), strong (IR)
sat	sitting-atop, saturated
SCE	Saturated Calomel Electrode
S_EAr	Electrophilic aromatic substitution
T	Temperature
t	triplet (NMR), tertiary
TBAF	Tetra Butyl Ammonium Fluoride
^{t}Bu	*tert*-butyl
TFA	Trifluoro Acetic acid
THF	Tetrahydrofuran
THF-d_8	Tetrahydrofuran-d_8
TLC	Thin Layer Chromatography
TMS	trimethylsilyl-
Tol	Toluene
TPP	Tetraphenylporphyrin
UCNP	Upconverting Nanoparticle
V	Volt
Vis	visible
via	through
vs	very strong (IR)
vs	*versus* (against)
UV	Ultraviolet
w	week, weak (IR)
w/w	weight percent
Y	Yield
δ	chemical shift

ε	extinction coefficient
λ	wavelength
$h\nu$	light
Φ	quantum yield
$\tilde{\nu}$	wavenumber

8 Bibliography

[1] E. Dickens, *Das Da-Vinci-Universum: die Notizbücher des Leonardo*, Ullstein, **2006**.

[2] P. Kang, Z. Chen, M. Brookhart, T. J. Meyer, *Top. Catal.* **2015**, *58*, 30-45.

[3] K. Tanaka, D. Ooyama, *Coord. Chem. Rev.* **2002**, *226*, 211-218.

[4] J.-H. Jeoung, H. Dobbek, *Science* **2007**, *318*, 1461-1464.

[5] H. Dobbek, V. Svetlitchnyi, L. Gremer, R. Huber, O. Meyer, *Science* **2001**, *293*, 1281-1285.

[6] C. L. Drennan, J. Heo, M. D. Sintchak, E. Schreiter, P. W. Ludden, *Proc. Natl. Acad. Sci.* **2001**, *98*, 11973-11978.

[7] E. A. Mohamed, Z. N. Zahran, Y. Naruta, *Chem. Mater.* **2017**, *29*, 7140-7150.

[8] G. Niedner-Schatteburg, *Funding Proposal 2019 - 2022* **2018**.

[9] M. O. Senge, *Chem. Commun.* **2011**, *47*, 1943-1960.

[10] G. Moss, *Pure Appl. Chem.* **1987**, *59*, 779-832.

[11] J. Sessler, A. Gebauer, E. Vogel, K. Kadish, K. Smith, R. Guilard, *Kadish, KM* **2000**, 257-278.

[12] J. Alvarez-Builla, J. J. Vaquero, J. Barluenga, *Modern heterocyclic chemistry, 4 volume set, Vol. 2*, John Wiley & Sons, **2011**.

[13] T. Eicher, S. Hauptmann, A. Speicher, *The chemistry of heterocycles: structures, reactions, synthesis, and applications*, John Wiley & Sons, **2013**.

[14] A. Osuka, S. Saito, *Chem. Commun.* **2011**, *47*, 4330-4339.

[15] H. Furuta, T. Asano, T. Ogawa, *J. Am. Chem. Soc.* **1994**, *116*, 767-768.

[16] J. D. Harvey, C. J. Ziegler, *Coordination chemistry reviews* **2003**, *247*, 1-19.

[17] M. Toganoh, S. Ikeda, H. Furuta, *Inorg. Chem.* **2007**, *46*, 10003-10015.

[18] H. Furuta, T. Ishizuka, A. Osuka, T. Ogawa, *J. Am. Chem. Soc.* **2000**, *122*, 5748-5757.

[19] S. Ikeda, M. Toganoh, S. Easwaramoorthi, J. M. Lim, D. Kim, H. Furuta, *J. Org. Chem.* **2010**, *75*, 8637-8649.

[20] E. Hückel, *Z. physik* **1931**, *70*, 204-286.

[21] J. Jusélius, D. Sundholm, *PCCP* **2000**, *2*, 2145-2151.

[22] H. Fliegl, D. Sundholm, *J. Org. Chem.* **2012**, *77*, 3408-3414.

[23] J. I. Wu, I. Fernández, P. v. R. Schleyer, *J. Am. Chem. Soc.* **2013**, *135*, 315-321.

[24] V. Albers, H. Knorr, *J. Chem. Phys.* **1936**, *4*, 422-425.

[25] M. Gouterman, *J. Mol. Spec.* **1961**, *6*, 138-163.

[26] M. Meot-Ner, A. D. Adler, *J. Am. Chem. Soc.* **1975**, *97*, 5107-5111.

[27] R. Haldar, K. Batra, S. M. Marschner, A. B. Kuc, S. Zahn, R. A. Fischer, S. Bräse, T. Heine, C. Wöll, *Chem. Eur. J.* **2019**, *25*, 7847-7851.

[28] H. L. Anderson, *Chem. Commun.* **1999**, 2323-2330.

[29] W. T. Simpson, *J. Chem. Phys.* **1949**, *17*, 1218-1221.

[30] H. Longuet-Higgins, C. Rector, J. Platt, *J. Mol. Spectrosc.* **1950**, *18*, 1174-1181.

[31] A. Hollaender, *Radiation biology, Vol. III. Visible and near-visible light.* **1956**.

[32] T. Hashimoto, Y.-K. Choe, H. Nakano, K. Hirao, *J. Phys. Chem. A* **1999**, *103*, 1894-1904.

[33] J. Falk, *Porphyrins and metalloporphyrins, Vol. 2*, Elsevier Science & Technology, **1975**.

[34] L. E. Webb, E. B. Fleischer, *J. Am. Chem. Soc.* **1965**, *87*, 667-669.

[35] K. Tatsumi, R. Hoffmann, *J. Am. Chem. Soc.* **1981**, *103*, 3328-3341.

[36] E. Riedel, *Anorganische Chemie*, 9. Auflage ed., De Gruyter, Berlin ; Bosten, **2015**.

[37] S.-C. So, W.-M. Cheung, W.-H. Chiu, M. de Vere-Tucker, H. H.-Y. Sung, I. D. Williams, W.-H. Leung, *Dalton Trans.* **2019**, *48*, 8340-8349.

[38] R.-J. Cheng, P.-Y. Chen, T. Lovell, T. Liu, L. Noodleman, D. A. Case, *J. Am. Chem. Soc.* **2003**, *125*, 6774-6783.

[39] P. Spellane, M. Gouterman, A. Antipas, S. Kim, Y. Liu, *Inorg. Chem.* **1980**, *19*, 386-391.

[40] A. Treibs, *Liebigs Ann.* **1969**, *728*, 115-143.

[41] E. B. Fleischer, *Acc. Chem. Res.* **1970**, *3*, 105-112.

[42] P. P. Kumar, B. G. Maiya, *New J. Chem.* **2003**, *27*, 619-625.

[43] J. M. Kamm, C. P. Iverson, W.-Y. Lau, M. D. Hopkins, *Langmuir* **2016**, *32*, 487-495.

[44] E. B. Fleischer, R. Thorp, D. Venerable, *J. Chem. Soc. D* **1969**, 475a-475a.

[45] J. W. Buchler, *J. Porphyrins Phthalocyanines* **2000**, *4*, 337-339.

[46] J. W. Buchler, J. Hüttermann, J. Löffler, *Bull. Chem. Soc. Jpn.* **1988**, *61*, 71-77.

[47] K. Kim, W. S. Lee, H. J. Kim, S. H. Cho, G. S. Girolami, P. A. Gorlin, K. S. Suslick, *Inorg. Chem.* **1991**, *30*, 2652-2656.

[48] J. W. Buchler, A. De Cian, S. Elschner, J. Fischer, P. Hammerschmitt, R. Weiss, *Chem. Ber.* **1992**, *125*, 107-115.

[49] J. W. Buchler, G. Heinz, *Chem. Ber.* **1996**, *129*, 1073-1081.

[50] M. Ikeda, M. Takeuchi, S. Shinkai, F. Tani, Y. Naruta, *Bull. Chem. Soc. Jpn.* **2001**, *74*, 739-746.

[51] G. S. Girolami, S. N. Milam, K. S. Suslick, *J. Am. Chem. Soc.* **1988**, *110*, 2011-2012.

[52] G. S. Girolami, S. N. Milam, K. S. Suslick, *Inorg. Chem.* **1987**, *26*, 343-344.

[53] G. Ricciardi, A. Rosa, E. J. Baerends, S. A. van Gisbergen, *J. Am. Chem. Soc.* **2002**, *124*, 12319-12334.

[54] G. Ricciardi, A. Rosa, S. Van Gisbergen, E. Baerends, *J. Phys Chem. A* **2000**, *104*, 635-643.

[55] A. Hoffman, D. Collins, V. Day, E. Fleischer, T. Srivastava, J. Hoard, *J. Am. Chem. Soc.* **1972**, *94*, 3620-3626.

[56] J. Collman, C. Barnes, P. Brothers, T. Collins, T. Ozawa, J. Gallucci, J. A. Ibers, *J. Am. Chem. Soc.* **1984**, *106*, 5151-5163.

[57] K. Koizumi, M. Shoji, Y. Nishiyama, Y. Maruno, Y. Kitagawa, K. Soda, S. Yamanaka, M. Okumura, K. Yamaguchi, *Int. J. Quantum Chem* **2004**, *100*, 943-956.

[58] M. A. Torrens, D. K. Straub, L. Epstein, *J. Am. Chem. Soc.* **1972**, *94*, 4160-4162.

[59] H. Maeda, H. Furuta, *Pure Appl. Chem.* **2006**, *78*, 29-44.

[60] H. Furuta, T. Ishizuka, A. Osuka, H. Dejima, H. Nakagawa, Y. Ishikawa, *J. Am. Chem. Soc.* **2001**, *123*, 6207-6208.

[61] J. P. Belair, C. J. Ziegler, C. S. Rajesh, D. A. Modarelli, *J. Phys Chem. A* **2002**, *106*, 6445-6451.

[62] H. Furuta, T. Ogawa, Y. Uwatoko, K. Araki, *Inorganic chemistry* **1999**, *38*, 2676-2682.

[63] P. J. Chmielewski, L. Latos-Grażyński, K. Rachlewicz, T. Glowiak, *Angew. Chem.* **1994**, *33*, 779-781.

[64] H. Maeda, A. Osuka, Y. Ishikawa, I. Aritome, Y. Hisaeda, H. Furuta, *Org. Lett.* **2003**, *5*, 1293-1296.

[65] W.-C. Chen, C.-H. Hung, *Inorg. Chem.* **2001**, *40*, 5070-5071.

[66] R. Myśliborski, K. Rachlewicz, L. Latos-Grażyński, *J. Porphyrins Phthalocyanines* **2007**, *11*, 172-180.

[67] H. Furuta, T. Ishizuka, A. Osuka, *J. Am. Chem. Soc.* **2002**, *124*, 5622-5623.

[68] A. Srinivasan, M. Toganoh, T. Niino, A. Osuka, H. Furuta, *Inorg. Chem.* **2008**, *47*, 11305-11313.

[69] H. Furuta, N. Kubo, H. Maeda, T. Ishizuka, A. Osuka, H. Nanami, T. Ogawa, *Inorg. Chem.* **2000**, *39*, 5424-5425.

[70] M. Toganoh, H. Furuta, *Chem. Lett.* **2019**, *48*, 615-622.

[71] A. Młodzianowska, L. Latos-Grażyński, L. Szterenberg, *Inorg. Chem.* **2008**, *47*, 6364-6374.

[72] S. Ikeda, M. Toganoh, H. Furuta, *Inorg. Chem.* **2011**, *50*, 6029-6043.

[73] T. Yamamoto, J. A. Abraham, S. Mori, M. Toganoh, S. Shimizu, M. Ishida, H. Furuta, *Chem. Asian J.* **2020**, *15*, 748-752.

[74] M. Toganoh, T. Ishizuka, H. Furuta, *Chem. Commun.* **2004**, 2464-2465.

[75] T. Ishizuka, S. Ikeda, M. Toganoh, I. Yoshida, Y. Ishikawa, A. Osuka, H. Furuta, *Tetrahedron* **2008**, *64*, 4037-4050.

[76] C. Bizzarri, *Coord. Chem. Rev.* **2017**.

[77] W. Z. Z. Küster, *Physiology. Chem* **1912**, *82*.

[78] H. Fischer, Zeile, K., *Ann. Chem. Ber. Dtsch. Chem* **1929**, *468*, 98.

[79] P. Rothemund, *J. Am. Chem. Soc.* **1935**, *57*, 2010-2011.

[80] P. Rothemund, *J. Am. Chem. Soc.* **1936**, *58*, 625-627.

[81] P. Rothemund, A. R. Menotti, *J. Am. Chem. Soc.* **1941**, *63*, 267-270.

[82] A. D. Adler, F. R. Longo, J. D. Finarelli, J. Goldmacher, J. Assour, L. Korsakoff, *J. Org. Chem.* **1967**, *32*, 476-476.

[83] J. S. Lindsey, I. C. Schreiman, H. C. Hsu, P. C. Kearney, A. M. Marguerettaz, *J. Org. Chem.* **1987**, *52*, 827-836.

[84] R. K. Sharma, G. Ahuja, I. T. Sidhwani, *Green Chem. Lett. Rev.* **2009**, *2*, 101-105.

[85] P. D. Rao, S. Dhanalekshmi, B. J. Littler, J. S. Lindsey, *J. Org. Chem.* **2000**, *65*, 7323-7344.

[86] E. J. Breitmaier, G., *Georg Thieme Verlag* **2001**, *4. Aufl.*

[87] M. O. Senge, *Acc. Chem. Res.* **2005**, *38*, 733-743.

[88] M. Fazekas, M. Pintea, M. O. Senge, M. Zawadzka, *Tetrahedron Letters* **2008**, *49*, 2236-2239.

[89] B. J. Littler, Y. Ciringh, J. S. Lindsey, *J. Org. Chem.* **1999**, *64*, 2864-2872.

[90] D. M. Wallace, S. H. Leung, M. O. Senge, K. M. Smith, *J. Org. Chem.* **1993**, *58*, 7245-7257.

[91] S. Fox, R. Hudson, R. W. Boyle, *Tetrahedron Lett.* **2003**, *44*, 1183-1185.

[92] G. R. Geier III, B. J. Littler, J. S. Lindsey, *J. Chem. Soc., Perkin Trans. 2* **2001**, 701-711.

[93] W. S. Kaim, B., *Teuner-Verlag* **2004**, *3. Aufl.*

[94] K. N. Ferreira, T. M. Iverson, K. Maghlaoui, J. Barber, S. Iwata, *Science* **2004**, *303*, 1831.

[95] I. Bertini, G. Cavallaro, A. Rosato, *Chem. Rev.* **2006**, *106*, 90-115.

[96] F. P. Guengerich, *J. Biol. Chem.* **1991**, *266*, 10019-10022.

[97] I. S. Isaac, J. H. Dawson, *Essays Biochem* **1999**, *34*, 51-69.

[98] A. R. Battersby, K. Frobel, *Chem. unserer Zeit* **1982**, *16*, 124-134.

[99] M. Ghosh, *Annals of botany* **2006**, *98*, 1145-1153.

[100] C. Glorieux, P. B. Calderon, *Biol. Chem.* **2017**, *398*, 1095-1108.

[101] N. C. Veitch, *Phytochem. Rev.* **2004**, *3*, 3-18.

[102] S. Lesage, H. Xu, L. Durham, *Hydrol. Sci. J.* **1993**, *38*, 343-354.

[103] M. Krüger, A. Meyerdierks, F. O. Glöckner, R. Amann, F. Widdel, M. Kube, R. Reinhardt, J. Kahnt, R. Böcher, R. K. Thauer, S. Shima, *Nature* **2003**, *426*, 878.

[104] K. Karapiperi, C. Gousis, P. Papaioannidou, *Front. pharmacol.* **2010**.

[105] J. Brown, L. Powers, B. Kincaid, J. Larrabee, T. G. Spiro, *J. Am. Chem. Soc.* **1980**, *102*, 4210-4216.

[106] I. M. Klotz, T. A. Klotz, H. A. Fiess, *Arch. Biochem. Biophys.* **1957**, *68*, 284-299.

[107] A. Desideri, M. Falconi, F. Polticelli, M. Bolognesi, K. Djinovic, G. Rotilio, *J. Mol. Biol.* **1992**, *223*, 337-342.

[108] J. P. Collman, N. K. Devaraj, R. A. Decréau, Y. Yang, Y.-L. Yan, W. Ebina, T. A. Eberspacher, C. E. Chidsey, *Science* **2007**, *315*, 1565-1568.

[109] R. A. Capaldi, F. Malatesta, V. Darley-Usmar, *Biochim Biophys Acta Bioenerg* **1983**, *726*, 135-148.

[110] M. I. Verkhovsky, A. Jasaitis, M. L. Verkhovskaya, J. E. Morgan, M. Wikström, *Nature* **1999**, *400*, 480-483.

[111] B. Kadenbach, *Angew. Chem.* **1983**, *95*, 273-281.

[112] G. M. Dubowchik, A. D. Hamilton, *J. Chem. Soc., Chem. Commun.* **1987**, 293-295.

[113] G. M. Dubowchik, A. D. Hamilton, *J. Chem. Soc., Chem. Commun.* **1986**, 1391-1394.

[114] U. Ermler, G. Fritzsch, S. K. Buchanan, H. Michel, *Structure* **1994**, *2*, 925-936.

[115] Yikrazuul, *wikimedia.org* **2009**.

[116] J. M. Berg, J. L. Tymoczko, L. Stryer, New York: WH Freeman, **2002**.

[117] I. Abdalmuhdi, C. Chang, *J. Org. Chem.* **1985**, *50*, 411-413.

[118] T. Nagata, A. Osuka, K. Maruyama, *J. Am. Chem. Soc.* **1990**, *112*, 3054-3059.

[119] M. R. Wasielewski, *Chem. Rev.* **1992**, *92*, 435-461.

[120] O. Liviu, R.-M. Ion, S. Teodorescu, R.-M. Ştirbescu, I. Dulama, I. Bucurică, *Bull. Transilv. Univ. Bras. II* **2017**, *10 (59)*, 47-54.

[121] C. Teng, X. Yang, C. Yuan, C. Li, R. Chen, H. Tian, S. Li, A. Hagfeldt, L. Sun, *Org. Lett.* **2009**, *11*, 5542-5545.

[122] Z. Ning, Q. Zhang, W. Wu, H. Tian, *J. Organomet. Chem.* **2009**, *694*, 2705-2711.

[123] C. Rimington, *Biochem. J.* **1960**, *75*, 620-623.

[124] M. O. Senge, M. Fazekas, E. G. Notaras, W. J. Blau, M. Zawadzka, O. B. Locos, E. M. Ni Mhuircheartaigh, *Adv. Mater.* **2007**, *19*, 2737-2774.

[125] G. Oskam, B. V. Bergeron, G. J. Meyer, P. C. Searson, *J. Phys. Chem. B* **2001**, *105*, 6867-6873.

[126] F. Pichot, B. A. Gregg, *J. Phys. Chem. B* **2000**, *104*, 6-10.

[127] B. A. Gregg, F. Pichot, S. Ferrere, C. L. Fields, *J. Phys. Chem. B* **2001**, *105*, 1422-1429.

[128] S. Hattori, Y. Wada, S. Yanagida, S. Fukuzumi, *J. Am. Chem. Soc.* **2005**, *127*, 9648-9654.

[129] H. Nusbaumer, J.-E. Moser, S. M. Zakeeruddin, M. K. Nazeeruddin, M. Grätzel, *J Phys. Chem. B* **2001**, *105*, 10461-10464.

[130] T. C. Li, A. M. Spokoyny, C. She, O. K. Farha, C. A. Mirkin, T. J. Marks, J. T. Hupp, *J. Am. Chem. Soc.* **2010**, *132*, 4580-4582.

[131] G. Boschloo, A. Hagfeldt, *Acc. Chem. Res.* **2009**, *42*, 1819-1826.

[132] M. O. Senge, M. Fazekas, M. Pintea, M. Zawadzka, W. J. Blau, *Eur. J. Org. Chem.* **2011**, *2011*, 5797-5816.

[133] S. D. Bella, *Chem. Soc. Rev.* **2001**, *30*, 355-366.

[134] H. S. Nalwa, *Adv. Mater.* **1993**, *5*, 341-358.

[135] A. Sen, P. C. Ray, P. K. Das, V. Krishnan, *J. Phys. Chem.* **1996**, *100*, 19611-19613.

[136] V. Rumyantseva, A. Shchelkunova, A. Gorshkova, Y. V. Alekseev, I. Shilov, A. Ivano, E. Davydov, A. Mironov, *Fine Chemical Technologies* **2017**, *12*, 72-80.

[137] V. Rumyantseva, A. Gorshkova, A. Mironov, *Fine Chemical Technologies* **2014**, *9*.

[138] E. Paszko, C. Ehrhardt, M. O. Senge, D. P. Kelleher, J. V. Reynolds, *Photodiagnosis and photodynamic therapy* **2011**, *8*, 14-29.

[139] A. Owen, *Fundamentals of UV-visible spectroscopy* **1996**.

[140] O. Laporte, W. F. Meggers, *J. Opt. Soc. Am.* **1925**, *11*, 459-463.

[141] E. F. F. Silva, C. Serpa, J. M. Dąbrowski, C. J. P. Monteiro, S. J. Formosinho, G. Stochel, K. Urbanska, S. Simões, M. M. Pereira, L. G. Arnaut, *Chem. Eur. J.* **2010**, *16*, 9273-9286.

[142] P. Agostinis, K. Berg, K. A. Cengel, T. H. Foster, A. W. Girotti, S. O. Gollnick, S. M. Hahn, M. R. Hamblin, A. Juzeniene, D. Kessel, *Cancer J. Clin.* **2011**, *61*, 250-281.

[143] T. Nunoshiba, F. Obata, A. C. Boss, S. Oikawa, T. Mori, S. Kawanishi, K. Yamamoto, *J. Biol. Chem.* **1999**, *274*, 34832-34837.

[144] M. Hesse, H. Meier, B. Zeeh, *Spektroskopische Methoden in der organischen Chemie*, Georg Thieme Verlag, **2005**.

[145] A. P. Castano, T. N. Demidova, M. R. Hamblin, *Photodiagnosis and photodynamic therapy* **2004**, *1*, 279-293.

[146] D. Wang, B. Xue, X. Kong, L. Tu, X. Liu, Y. Zhang, Y. Chang, Y. Luo, H. Zhao, H. Zhang, *Nanoscale* **2015**, *7*, 190-197.

[147] X. Wang, R. R. Valiev, T. Y. Ohulchanskyy, H. Ågren, C. Yang, G. Chen, *Chem. Soc. Rev.* **2017**, *46*, 4150-4167.

[148] W. C. Eisenberg, K. Taylor, R. R. Guerrero, *J. Photochem. Photobiol. B: Biol.* **1992**, *16*, 381-384.

[149] D. Carlsson, T. Suprunchuk, D. Wiles, *J. Am. Oil Chem. Soc.* **1976**, *53*, 656-660.

[150] D. Min, J. Boff, *Compr. Rev. Food Sci. Food Saf.* **2002**, *1*, 58-72.

[151] M. Wang, Z. Chen, W. Zheng, H. Zhu, S. Lu, E. Ma, D. Tu, S. Zhou, M. Huang, X. Chen, *Nanoscale* **2014**, *6*, 8274-8282.

[152] Y. I. Park, J. H. Kim, K. T. Lee, K. S. Jeon, H. B. Na, J. H. Yu, H. M. Kim, N. Lee, S. H. Choi, S. I. Baik, *Adv. Mater.* **2009**, *21*, 4467-4471.

[153] J. Barona-Castaño, C. Carmona-Vargas, T. Brocksom, K. de Oliveira, *Molecules* **2016**, *21*, 310.

[154] S. Nakagaki, G. K. B. Ferreira, G. M. Ucoski, K. A. Dias de Freitas Castro, *Molecules* **2013**, *18*, 7279-7308.

[155] B. Akagah, A. T. Lormier, A. Fournet, B. Figadère, *Org. Biomol. Chem.* **2008**, *6*, 4494-4497.

[156] J. Legros, J. R. Dehli, C. Bolm, *Adv. Synth. Catal.* **2005**, *347*, 19-31.

[157] S. Campestrini, U. Tonellato, *J. Mol. Catal. A: Chem.* **2001**, *171*, 37-42.

[158] E. Lamy, L. Nadjo, J. M. Saveant, *J. Electroanal. Chem. Interf. Electrochem.* **1977**, *78*, 403-407.

[159] C. W. Machan, S. A. Chabolla, J. Yin, M. K. Gilson, F. A. Tezcan, C. P. Kubiak, *J. Am. Chem. Soc.* **2014**, *136*, 14598-14607.

[160] R. Kuriki, H. Matsunaga, T. Nakashima, K. Wada, A. Yamakata, O. Ishitani, K. Maeda, *J. Am. Chem. Soc.* **2016**, *138*, 5159-5170.

[161] P. Kang, C. Cheng, Z. Chen, C. K. Schauer, T. J. Meyer, M. Brookhart, *J. Am. Chem. Soc.* **2012**, *134*, 5500-5503.

[162] Y. Chen, C. W. Li, M. W. Kanan, *J. Am. Chem. Soc.* **2012**, *134*, 19969-19972.

[163] C. Costentin, S. Drouet, M. Robert, J.-M. Savéant, *Science* **2012**, *338*, 90-94.

[164] J. Schneider, H. Jia, K. Kobiro, D. E. Cabelli, J. T. Muckerman, E. Fujita, *Energy Environ. Sci.* **2012**, *5*, 9502-9510.

[165] S. Lin, C. S. Diercks, Y.-B. Zhang, N. Kornienko, E. M. Nichols, Y. Zhao, A. R. Paris, D. Kim, P. Yang, O. M. Yaghi, *Science* **2015**, *349*, 1208-1213.

[166] M. Bourrez, F. Molton, S. Chardon-Noblat, A. Deronzier, *Angew. Chem. Int. Ed.* **2011**, *50*, 9903-9906.

[167] M. Hammouche, D. Lexa, M. Momenteau, J. M. Saveant, *J. Am. Chem. Soc.* **1991**, *113*, 8455-8466.

[168] U. Kaiser, E. Heitz, *Ber. Bunsenges. Physik. Chem* **1973**, *77*, 818-823.

[169] J. Gressin, D. Michelet, L. Nadjo, J. Saveant, *Chem. Inform.* **1979**, *10*, no-no.

[170] A. Coehn, S. Jahn, *Ber. Dtsch. Chem. Ges.* **1904**, *37*, 2836-2842.

[171] Y. Hori, K. Kikuchi, S. Suzuki, *Chem. Lett.* **1985**, *14*, 1695-1698.

[172] R. A. Marcus, *J. Chem. Phys.* **1956**, *24*, 966-978.

[173] M. Hammouche, D. Lexa, J. Savéant, M. Momenteau, *J. Electroanal. Chem. Interf. Electrochem.* **1988**, *249*, 347-351.

[174] C. Gueutin, D. Lexa, J. M. Saveant, D. L. Wang, *Organometallics* **1989**, *8*, 1607-1613.

[175] A. Osuka, S. Nakajima, T. Nagata, K. Maruyama, K. Toriumi, *Angew. Chem.* **1991**, *30*, 582-584.

[176] M. Calik, F. Auras, L. M. Salonen, K. Bader, I. Grill, M. Handloser, D. D. Medina, M. Dogru, F. Löbermann, D. Trauner, *J. Am. Chem. Soc.* **2014**, *136*, 17802-17807.

[177] B. Vonhoeren, S. Dalgleish, L. Hu, M. M. Matsushita, K. Awaga, B. J. Ravoo, *ACS Appl. Mater.* **2015**, *7*, 7049-7053.

[178] M. Pizzotti, E. Annoni, R. Ugo, S. Bruni, S. Quici, P. Fantucci, M. Bruschi, G. Zerbi, M. D. Zoppo, *J. Porphyrins Phthalocyanines* **2004**, *8*, 1311-1324.

[179] K. Murakami, Y. Yamamoto, H. Yorimitsu, A. Osuka, *Chem. Eur. J.* **2013**, *19*, 9123-9126.

[180] C. Schissler, Master Thesis (Karlsruhe Institute of Technology), **2018**.

[181] K.-i. Yamashita, K. Kataoka, M. S. Asano, K.-i. Sugiura, *Org. Lett.* **2011**, *14*, 190-193.

[182] Q. Sun, L. Cai, H. Ma, C. Yuan, W. Xu, *ACS nano* **2016**, *10*, 7023-7030.

[183] P. R. Frail, K. Susumu, M. Huynh, J. Fong, J. M. Kikkawa, M. J. Therien, *Chem. Mater.* **2007**, *19*, 6062-6064.

[184] T. E. Screen, I. M. Blake, L. H. Rees, W. Clegg, S. J. Borwick, H. L. Anderson, *J. Chem. Soc., Perkin Trans. 1* **2002**, 320-329.

[185] K. Sindhu, G. Anilkumar, *RSC Adv.* **2014**, *4*, 27867-27887.

[186] C. Maeda, M. Takata, A. Honsho, T. Ema, *Org. Lett.* **2016**, *18*, 6070-6073.

[187] A. Matharu, P. Karadakov, S. Cowling, G. Hegde, L. Komitov, *Liq. Cryst.* **2011**, *38*, 207-232.

[188] H. N. Wong, F. Sondheimer, *Tetrahedron* **1981**, *37*, 99-109.

[189] K. Niedermann, N. Früh, R. Senn, B. Czarniecki, R. Verel, A. Togni, *Angew. Chem.* **2012**, *51*, 6511-6515.

[190] B. C. Berris, G. H. Hovakeemian, Y. H. Lai, H. Mestdagh, K. P. C. Vollhardt, *J. Am. Chem. Soc.* **1985**, *107*, 5670-5687.

[191] J. T. Fletcher, M. J. Therien, *J. Am. Chem. Soc.* **2000**, *122*, 12393-12394.

[192] S. K. Bhasin, *Pharmaceutical Organic Chemistry*, Elsevier, **2012**.

[193] D. Shimizu, K. Fujimoto, A. Osuka, *Angew. Chem. Int. Ed.* **2018**, *57*, 9434-9438.

[194] U. Eisner, R. Linstead, *J. Chem Soc.* **1955**, 3742-3749.

[195] M. Tian, S. Chen, W. Sheng, H. Huang, C. Guo, *Chem. Lett.* **2015**, *44*, 1383-1385.

[196] L. J. Esdaile, M. O. Senge, D. P. Arnold, *Chem. Commun.* **2006**, 4192-4194.

[197] D. J. cram, J. M. Cram, *Acc. Chem. Res.* **1971**, *4*, 204-213.

[198] Z. Hassan, E. Spuling, D. M. Knoll, J. Lahann, S. Bräse, *Chem. Soc. Rev.* **2018**, *47*, 6947-6963.

[199] I. Majerz, T. Dziembowska, *J. Phs. Chem. A* **2016**, *120*, 8138-8147.

[200] D. M. Knoll, H. Šimek, Z. Hassan, S. Bräse, *Eur. J. Org. Chem.* **2019**, *2019*, 6198-6202.

[201] D. S. Seferos, S. A. Trammell, G. C. Bazan, J. G. Kushmerick, *Proc. Natl. Acad. Sci.* **2005**, *102*, 8821-8825.

[202] M. Wielopolski, A. Molina-Ontoria, C. Schubert, J. T. Margraf, E. Krokos, J. Kirschner, A. Gouloumis, T. Clark, D. M. Guldi, N. Martín, *J. Am. Chem. Soc.* **2013**, *135*, 10372-10381.

[203] D. Knoll, *Heterobimetallic [2.2] Paracyclophane Complexes and Their Application in Photoredox Catalysis*, Logos Verlag Berlin GmbH, **2020**.

[204] J. Cámara, M. C. Blanco, A. Laguna, P. Naumov, M. C. Gimeno, *Chem. Commun.* **2017**, *53*, 9202-9205.

[205] C. Braun, M. Nieger, W. R. Thiel, S. Bräse, *Chem. Eur. J.* **2017**, *23*, 15474-15483.

[206] H. Meier, Y. Kobuke, S.-i. Kugimiya, *J. Chem. Soc., Chem. Commun.* **1989**, 923-924.

[207] C. Chang, *J. Heterocycl. Chem.* **1977**, *14*, 1285-1288.

[208] J. P. Collman, P. Denisevich, Y. Konai, M. Marrocco, C. Koval, F. C. Anson, *J. Am. Chem. Soc.* **1980**, *102*, 6027-6036.

[209] J. P. Collman, C. S. Bencosme, C. E. Barnes, B. D. Miller, *J. Am. Chem. Soc.* **1983**, *105*, 2704-2710.

[210] J. T. Landrum, D. Grimmett, K. J. Haller, W. R. Scheidt, C. A. Reed, *J. Am. Chem. Soc.* **1981**, *103*, 2640-2650.

[211] C. Chang, I. Abdalmuhdi, *J. Org. Chem.* **1983**, *48*, 5388-5390.

[212] C. K. Chang, I. Abdalmuhdi, *Angew. Chem.* **1984**, *23*, 164-165.

[213] Y. Deng, C. J. Chang, D. G. Nocera, *J. Am. Chem. Soc.* **2000**, *122*, 410-411.

[214] C. J. Chang, Y. Deng, A. F. Heyduk, C. Chang, D. G. Nocera, *Inorg. Chem.* **2000**, *39*, 959-966.

[215] J. T. Fletcher, M. J. Therien, *J. Am. Chem. Soc.* **2002**, *124*, 4298-4311.

[216] Y. Shimazaki, H. Takesue, T. Chishiro, F. Tani, Y. Naruta, *Chem. Lett.* **2001**, *30*, 538-539.

[217] S. M. Marschner, R. Haldar, O. Fuhr, C. Wöll, S. Bräse, *Chem. Eur. J.* **2021**, *27*, 1390.

[218] H. S. Cho, D. H. Jeong, M.-C. Yoon, Y. H. Kim, Y.-R. Kim, D. Kim, S. C. Jeoung, S. K. Kim, N. Aratani, H. Shinmori, *J. Phs. Chem. A* **2001**, *105*, 4200-4210.

[219] R. W. Hooft, L. H. Straver, A. L. Spek, *J. Appl. Crystallogr.* **2008**, *41*, 96-103.

[220] N. A. Pereira, M. Laranjo, J. Casalta-Lopes, A. C. Serra, M. Piñeiro, J. Pina, J. S. Seixas de Melo, M. O. Senge, M. F. Botelho, L. Martelo, *ACS Med. Chem. Lett.* **2017**, *8*, 310-315.

[221] K. T. Weber, K. Karikis, M. D. Weber, P. B. Coto, A. Charisiadis, D. Charitaki, G. Charalambidis, P. Angaridis, A. G. Coutsolelos, R. D. Costa, *Dalton Trans.* **2016**, *45*, 13284-13288.

[222] U. Eberhardt, W. Schwarz, H. Musso, *Liebigs Ann. Chem.* **1987**, *1987*, 809-810.

[223] C. O. Obondi, G. N. Lim, F. D'Souza, *J. Phys. Chem. C* **2015**, *119*, 176-185.

[224] K.-i. Yamashita, N. Katsumata, S. Tomita, M. Fuwa, K. Fujimaki, T. Yoda, D. Hirano, K.-i. Sugiura, *Chem. Lett.* **2015**, *44*, 492-494.

[225] Z. Valicsek, O. Horváth, *Microchem. J.* **2013**, *107*, 47-62.

[226] E. A. Mason, E. W. McDaniel, *NASA STI/Recon Technical Report A* **1988**, *89*.

[227] F. Fernandez-Lima, D. Kaplan, M. Park, *Rev. Sci. Instrum.* **2011**, *82*, 126106.

[228] J. A. Silveira, K. Michelmann, M. E. Ridgeway, M. A. Park, *J. Am. Soc. Mass. Spectrom.* **2016**, *27*, 585-595.

[229] K. Michelmann, J. A. Silveira, M. E. Ridgeway, M. A. Park, *J. Am. Soc. Mass. Spectrom.* **2014**, *26*, 14-24.

[230] M. E. Ridgeway, J. A. Silveira, J. E. Meier, M. A. Park, *Analyst* **2015**, *140*, 6964-6972.

[231] Y. Pu, M. E. Ridgeway, R. S. Glaskin, M. A. Park, C. E. Costello, C. Lin, *Anal. Chem.* **2016**, *88*, 3440-3443.

[232] P. Weis, F. Hennrich, R. Fischer, E. K. Schneider, M. Neumaier, M. M. Kappes, *PCCP* **2019**, *21*, 18877-18892.

[233] D. Helm, J. P. Vissers, C. J. Hughes, H. Hahne, B. Ruprecht, F. Pachl, A. Grzyb, K. Richardson, J. Wildgoose, S. K. Maier, *Mol. Cell. Proteom.* **2014**, *13*, 3709-3715.

[234] F. Furche, R. Ahlrichs, C. Hättig, W. Klopper, M. Sierka, F. T. Weigend, *Mol. Sci* **2014**, *4*, 91-100.

[235] J. P. Perdew, *Phys. Ref. B* **1986**, *33*, 8822.

[236] A. D. Becke, *Phys. Ref. A* **1988**, *38*, 3098.

[237] F. Weigend, R. Ahlrichs, *PCCP* **2005**, *7*, 3297-3305.

[238] S. Grimme, J. Antony, S. Ehrlich, H. Krieg, *J. Chem. Phys.* **2010**, *132*, 154104.

[239] S. Grimme, S. Ehrlich, L. Goerigk, *J. Comput. Chem.* **2011**, *32*, 1456-1465.

[240] C. Larriba, C. J. Hogan, *J. Comput. Phys.* **2013**, *251*, 344-363.

[241] C. Larriba, C. J. Hogan, *J. Phys. Chem. A* **2013**, *117*, 3887-3901.

[242] C. Schissler, E. K. Schneider, B. Felker, P. Weis, M. Nieger, M. M. Kappes, S. Bräse, *Chem. Eur. J.* **2021**, *27*, 3047-3054.

[243] K. Brendle, U. Schwarz, P. Jäger, P. Weis, M. Kappes, *J. Phs. Chem A* **2016**, *120*, 8716-8724.

[244] P. Jäger, K. Brendle, E. Schneider, S. Kohaut, M. K. Armbruster, K. Fink, P. Weis, M. M. Kappes, *J. Phs. Chem A* **2018**, *122*, 2974-2982.

[245] A. Takai, C. P. Gros, J. M. Barbe, R. Guilard, S. Fukuzumi, *Chem. Eur. J.* **2009**, *15*, 3110-3122.

[246] F. Bolze, C. P. Gros, P. D. Harvey, R. Guilard, *J. Porphyrins Phthalocyanines* **2001**, *5*, 569-574.

[247] N. N. Greenwood, *Mössbauer spectroscopy*, Springer Science & Business Media, **2012**.

[248] E. Riedel, *Anorganische chemie*, Walter de Gruyter, **2011**.

[249] V. Schunemann, H. Paulsen, *Mossbauer Spectroscopy*, John Wiley & Sons, Ltd.: Hoboken, NJ, **2007**.

[250] C. L. Herzenberg, American Association for the Advancement of Science, **1972**.

[251] J. R. Sams, T. Tsin, *The porphyrins* **2012**, *4*, 425-478.

[252] J. R. Polam, J. L. Wright, K. A. Christensen, F. A. Walker, H. Flint, H. Winkler, M. Grodzicki, A. X. Trautwein, *J. Am. Chem. Soc.* **1996**, *118*, 5272-5276.

[253] G. Schapira, J. Elion, *Biochemie* **1980**, *62*.

[254] A. Berlicka, L. Latos-Grażyński, T. Lis, *Inorg. Chem.* **2005**, *44*, 4522-4533.

[255] W.-L. Kwong, R. W.-Y. Sun, C.-N. Lok, F.-M. Siu, S.-Y. Wong, K.-H. Low, C.-M. Che, *Chem. Sci.* **2013**, *4*, 747-754.

[256] A. F. Mironov, *Usp. Khim.* **2013**, *82*, 333-351.

[257] M. R. Wasielewski, M. P. Niemczyk, W. A. Svec, *Tetrahedron Lett.* **1982**, *23*, 3215-3218.

[258] P. Seta, E. Bienvenue, P. Maillard, M. Momenteau, *Photochem. Photobiol.* **1989**, *49*, 537-543.

[259] A. Osuka, F. Kobayashi, K. Maruyama, *Bull. Chem. Soc. Jpn.* **1991**, *64*, 1213-1225.

[260] J.-M. Camus, P. D. Harveya, R. Guilarda, *Macroheterocycles* **2013**, *6*, 13-22.

[261] A. Osuka, S. Nakajima, K. Maruyama, *J. Org. Chem.* **1992**, *57*, 7355-7359.

[262] J. Tao, J. P. Perdew, V. N. Staroverov, G. E. Scuseria, *Phys. Rev. Lett.* **2003**, *91*, 146401.

[263] J. P. Perdew, A. Ruzsinszky, G. I. Csonka, L. A. Constantin, J. Sun, *Phys. Rev. Lett.* **2009**, *103*, 026403.

[264] J. P. Perdew, A. Ruzsinszky, G. I. Csonka, L. A. Constantin, J. Sun, *Phys. Rev. Lett.* **2011**, *106*, 179902.

[265] F. Furche, R. Ahlrichs, C. Hättig, W. Klopper, M. Sierka, F. Weigend, *Rev.: Comput. Mol. Sci* **2014**, *4*, 91-100.

[266] L. Zanetti-Polzi, A. Amadei, R. Djemili, S. p. Durot, L. Schoepff, V. r. Heitz, B. Ventura, I. Daidone, *J. Phys. Chem. C* **2019**, *123*, 13094-13103.

[267] J. B. Callis, M. Gouterman, Y. Jones, B. Henderson, *J. Mol. Spectrosc.* **1971**, *39*, 410-420.

[268] A. Antipas, M. Gouterman, *J. Am. Chem. Soc.* **1983**, *105*, 4896-4901.

[269] A. Khan, M. Kasha, *Proc. Natl. Acad. Sci.* **1979**, *76*, 6047-6049.

[270] R. Baskaran, J. Lee, S.-G. Yang, *Biomater. Res.* **2018**, *22*, 1-8.

[271] A. E. O'Connor, W. M. Gallagher, A. T. Byrne, *Photochem. Photobiol.* **2009**, *85*, 1053-1074.

[272] J. Deng, H. Li, M. Yang, F. Wu, *Photochem. Photobiol. Sci.* **2020**, *19*, 905-912.

[273] W. D. Stohrer, *Photochemie: Konzepte, Methoden, Experimente* **1998**, 5-81.

[274] J. Fabian, H. Nakazumi, M. Matsuoka, *Chem. Rev.* **1992**, *92*, 1197-1226.

[275] J. P. Belair, C. J. Ziegler, C. S. Rajesh, D. A. Modarelli, *J Phys. Chem. A* **2002**, *106*, 6445-6451.

[276] P. J. Chmielewski, L. Latos-Grażyński, K. Rachlewicz, T. Glowiak, *Angew. Chemie* **1994**, *33*, 779-781.

[277] G. R. Geier, D. M. Haynes, J. S. Lindsey, *Org. Lett.* **1999**, *1*, 1455-1458.

[278] H. Furuta, T. Ishizuka, A. Osuka, H. Dejima, H. Nakagawa, Y. Ishikawa, *J Am. Chem. Soc.* **2001**, *123*, 6207-6208.

[279] H. Furuta, H. Maeda, A. Osuka, *J. Org. Chem.* **2001**, *66*, 8563-8572.

[280] T. Ishizuka, H. Yamasaki, A. Osuka, H. Furuta, *Tetrahedron Lett.* **2007**, *63*, 5137-5147.

[281] P. Li, C. Zhao, M. D. Smith, K. D. Shimizu, *J. Org. Chem.* **2013**, *78*, 5303-5313.

[282] K. Billingsley, S. L. Buchwald, *J. Am. Chem. Soc.* **2007**, *129*, 3358-3366.

[283] M. Miura, *Angew. Chem. Int. Ed.* **2004**, *43*, 2201-2203.

[284] Q. Zhao, C. Li, C. H. Senanayake, W. Tang, *Chem. Eur. J.* **2013**, *19*, 2261-2265.

[285] S. Ikeda, M. Toganoh, H. Furuta, *Inorg. Chem.* **2011**, *50*, 6029-6043.

[286] M. Toganoh, T. Ishizuka, H. Furuta, *Chemical communications* **2004**, 2464-2465.

[287] E. Lindner, H. Dreher, *J. Organomet. Chem.* **1973**, *55*, 347-356.

[288] K. M. Kadish, K. M. Smith, R. Guilard, *The Porphyrin Handbook, Vol. 3*, Academic Press, **2000**.

[289] W. A. Herrmann, C. W. Kohlpaintner, *Angew. Chem.* **1993**, *105*, 1588-1609.

[290] P. Jäger, K. Brendle, U. Schwarz, M. Himmelsbach, M. K. Armbruster, K. Fink, P. Weis, M. M. Kappes, *J. Phys. Chem. Lett.* **2016**, *7*, 1167-1172.

[291] U. Schwarz, M. Vonderach, M. K. Armbruster, K. Fink, M. M. Kappes, P. Weis, *J. Phs. Chem A* **2014**, *118*, 369-379.

[292] Z. Dong, P. J. Scammells, *J. Org. Chem.* **2007**, *72*, 9881-9885.

[293] G. Fülling, D. Schröder, B. Franck, *Angew. Chem.* **1989**, *101*, 1550-1552.

[294] J. d. P. Peter W. Atkins, *Physikalische Chemie*, Wiley-VCH, **2013**.

[295] M. Link, Master Thesis (Karlsruhe Institute of Technology), **2020**.

[296] A. Einstein, *Ann. Phys.* **1905**, *322*, 132-148.

[297] X.-B. Wang, L.-S. Wang, *Annu. Rev. Phys. Chem.* **2009**, *60*, 105-126.

[298] J. Simons, P. Skurski, R. Barrios, *J. Am. Chem. Soc.* **2000**, *122*, 11893-11899.

[299] C. Zippel, R. Israil, L. Schüssler, Z. Hasan, E. Schneider, P. Weis, M. Nieger, C. Bizzarri, M. M. Kappes, C. Riehn, *Chem. Eur. J.* **2021**.

[300] L. Wang, J. Cheng, L. Deng, *Inorg. Chim. Acta* **2017**, *460*, 49-54.

[301] C. Schissler, E. K. Schneider, S. Lebedkin, P. Weis, G. Niedner-Schatteburg, M. M. Kappes, S. Bräse, *Chem. Eur. J.* **2021**.

[302] J. P. Collman, J. M. Garner, K. Kim, J. A. Ibers, *Inorg. Chem.* **1988**, *27*, 4513-4516.

[303] J. W. Buchler, L. Puppe, K. Rohbock, H. H. Schneehage, *Chem. Ber.* **1973**, *106*, 2710-2732.

[304] G. M. Godziela, H. M. Goff, *J. Am. Chem. Soc.* **1986**, *108*, 2237-2243.

[305] R. Ragni, A. Punzi, F. Babudri, G. M. Farinola, *Eur. J. Org. Chem.* **2018**, *2018*, 3500-3519.

[306] E. P. Gillis, K. J. Eastman, M. D. Hill, D. J. Donnelly, N. A. Meanwell, *J. Med. Chem.* **2015**, *58*, 8315-8359.

[307] P. Shah, A. D. Westwell, *J. Enzyme Inhib. Med. Chem* **2007**, *22*, 527-540.

[308] S. Swallow, *Progress in medicinal chemistry* **2015**, *54*, 65-133.

[309] P. Jeschke, *ChemBioChem* **2004**, *5*, 570-589.

[310] T. Fujiwara, D. O'Hagan, *J. Fluorine Chem.* **2014**, *167*, 16-29.

[311] R. J. Plunkett, Google Patents, **1941**.

[312] K. Ohlrogge, K. Ebert, *Membranen: Grundlagen, Verfahren und industrielle Anwendungen*, John Wiley & Sons, **2012**.

[313] J. Wang, M. Sánchez-Roselló, J. L. Aceña, C. Del Pozo, A. E. Sorochinsky, S. Fustero, V. A. Soloshonok, H. Liu, *Chem. Rev.* **2014**, *114*, 2432-2506.

[314] M. C. Walker, M. C. Chang, *Chem. Soc. Rev.* **2014**, *43*, 6527-6536.

[315] P. Richardson, *Expert opinion on drug discovery* **2016**, *11*, 983-999.

[316] K. Müller, C. Faeh, F. Diederich, *Science* **2007**, *317*, 1881-1886.

[317] Y. Zhou, J. Wang, Z. Gu, S. Wang, W. Zhu, J. L. Aceña, V. A. Soloshonok, K. Izawa, H. Liu, *Chem. Rev.* **2016**, *116*, 422-518.

[318] P. R. Savoie, J. T. Welch, *Chem. Rev.* **2015**, *115*, 1130-1190.

[319] M. F. Sowaileh, R. A. Hazlitt, D. A. Colby, *ChemMedChem* **2017**, *12*, 1481-1490.

[320] G. A. Silvey, G. H. Cady, *J. Am. Chem. Soc.* **1950**, *72*, 3624-3626.

[321] W. A. Sheppard, *J. Am. Chem. Soc.* **1960**, *82*, 4751-4752.

[322] S. Altomonte, M. Zanda, *J. Fluorine Chem.* **2012**, *143*, 57-93.

[323] R. D. Bowden, P. J. Comina, M. P. Greenhall, B. M. Kariuki, A. Loveday, D. Philp, *Tetrahedron* **2000**, *56*, 3399-3408.

[324] T. Umemoto, L. M. Garrick, N. Saito, *Beilstein J. Org. Chem.* **2012**, *8*, 461-471.

[325] W. R. Dolbier Jr, *Guide to fluorine NMR for organic chemists*, John Wiley & Sons, **2016**.

[326] O. Lösking, H. Willner, *Angew. Chem.* **1989**, *101*, 1283-1284.

[327] M. VOROBEV, A. Filatov, M. Englin, *Zh. Obshch. Khim.* **1973**, *43*, 1653-1653.

[328] D. Leusser, J. Henn, N. Kocher, B. Engels, D. Stalke, *J. Am. Chem. Soc.* **2004**, *126*, 1781-1793.

[329] C. P. Rosenau, B. J. Jelier, A. D. Gossert, A. Togni, *Angew. Chem. Int. Ed.* **2018**, *57*, 9528-9533.

[330] P. Zhou, C. Chen, S. Li, *J. Chem. Res.* **2020**, *44*, 376-380.

[331] X. Ou, G. M. Bernard, A. F. Janzen, *Can. J. Chem.* **1997**, *75*, 1878-1884.

[332] K. Lummer, M. V. Ponomarenko, G.-V. Röschenthaler, M. Bremer, P. Beier, *J. Fluorine Chem.* **2014**, *157*, 79-83.

[333] O. S. Kanishchev, W. R. Dolbier Jr, *Angew. Chem. Int. Ed.* **2015**, *54*, 280-284.

[334] M. Kosobokov, B. Cui, A. Balia, K. Matsuzaki, E. Tokunaga, N. Saito, N. Shibata, *Angew. Chem. Int. Ed.* **2016**, *55*, 10781-10785.

[335] B. Cui, S. Jia, E. Tokunaga, N. Saito, N. Shibata, *Chem. Commun.* **2017**, *53*, 12738-12741.

[336] O. I. Guzyr, V. N. Kozel, E. B. Rusanov, A. B. Rozhenko, V. N. Fetyukhin, Y. G. Shermolovich, *J. Fluorine Chem.* **2020**, *239*, 109635.

[337] K. Tanagawa, Z. Zhao, N. Saito, N. Shibata, *Bull. Chem. Soc. Jpn.* **2021**.

[338] O. V. Boltalina, *J. Fluorine Chem.* **2000**, *101*, 273-278.

[339] J. Mizukado, Y. Matsukawa, H.-d. Quan, M. Tamura, A. Sekiya, *J. Fluorine Chem.* **2006**, *127*, 79-84.

[340] V. Aleshina, A. Y. Borshchevskii, E. Skokan, I. Arkhangel'skii, A. Astakhov, N. Shustova, *Solid State Phys.* **2002**, *44*, 629-630.

[341] J. Burdon, L. Garnier, *J. Fluorine Chem.* **1991**, *54*, 50.

[342] C. R. Pitts, D. Bornemann, P. Liebing, N. Santschi, A. Togni, *Angew. Chem. Int. Ed.* **2019**, *58*, 1950-1954.

[343] P. Erdmann, J. Leitner, J. Schwarz, L. Greb, *ChemPhysChem* **2020**, *21*, 987.

[344] K. D. Gupta, J. n. M. Shreeve, *Inorg. Chem.* **1985**, *24*, 1457-1460.

[345] L. Zhong, P. R. Savoie, A. S. Filatov, J. T. Welch, *Angew. Chem. Int. Ed.* **2014**, *53*, 526-529.

[346] K. Niina, K. Tanagawa, Y. Sumii, N. Saito, N. Shibata, *Org. Chem. Front* **2020**, *7*, 1276-1282.

[347] E. G. Janzen, P. H. Krygsman, D. A. Lindsay, D. L. Haire, *J. Am. Chem. Soc.* **1990**, *112*, 8279-8284.

[348] L. Liu, Z. Wang, X. Fu, C.-H. Yan, *Org. Lett.* **2012**, *14*, 5692-5695.

[349] P. Das, K. Niina, T. Hiromura, E. Tokunaga, N. Saito, N. Shibata, *Chem. Sci.* **2018**, *9*, 4931-4936.

[350] J. Dong, L. Krasnova, M. Finn, K. B. Sharpless, *Angew. Chem.* **2014**, *53*, 9430-9448.

[351] W. Steinkopf, *J. Prakt. Chem.* **1927**, *117*, 1-82.

[352] J. J. Krutak, R. D. Burpitt, W. H. Moore, J. A. Hyatt, *J. Org. Chem.* **1979**, *44*, 3847-3858.

[353] A. Barrow, C. Smedley, Q. Zheng, S. Li, J. Dong, J. Moses, *Chem. Soc. Rev.* **2019**, *48*, 4731-4758.

[354] A. L. Tribby, I. Rodríguez, S. Shariffudin, N. D. Ball, *J. Org. Chem.* **2017**, *82*, 2294-2299.

[355] R. J. Meyer, *Gmelin Handbook of Inorganic Chemistry*, **1969**.

[356] M. l. Cloutier, M. Roudias, J.-F. Paquin, *Org. Lett.* **2019**, *21*, 3866-3870.

[357] W. R. Dolbier Jr, Z. Zheng, *J. Fluorine Chem.* **2011**, *132*, 389-393.

[358] K. Takizawa, H. Nulwala, R. J. Thibault, P. Lowenhielm, K. Yoshinaga, K. L. Wooley, C. J. Hawker, *J. Polym. Sci., Part A: Polym. Chem.* **2008**, *46*, 2897-2912.

[359] Y.-F. Wang, K. K. Toh, S. Chiba, K. Narasaka, *Org. Lett.* **2008**, *10*, 5019-5022.

[360] D. Rombach, Dissertation (Karlsruhe Institute of Technology), **2018**.

[361] L. A. McIver, M. S. Siddique, *StatPearls* **2020**.

[362] K. Schwetlick, *Wiley-VCH, Weinheim* **2015**, *24. Auflage*.

[363] H. E. Gottlieb, V. Kotlyar, A. Nudelman, *J. Org. Chem.* **1997**, *62*, 7512-7515.

[364] S. Budavari, M. J. O'Neil, A. Smith, P. E. Heckelman, *Inc., Rahway, NJ* **1989**, *104*.

[365] W. C. Still, M. Kahn, A. Mitra, *J. Org. Chem.* **1978**, *43*, 2923-2925.

[366] G. M. Sheldrick, *Acta Cryst. A* **2015**, *71*, 3-8.

[367] A. Bruker:, Bruker AXS Inc. Madison, WI, USA, **2016**.

[368] G. Sheldrick, *University of Göttingen, Göttingen, Germany* **2014**.

[369] S. P. Westrip, *J. Appl. Crystallogr.* **2010**, *43*, 920-925.

[370] O. V. Dolomanov, L. J. Bourhis, R. J. Gildea, J. A. Howard, H. Puschmann, *J. Appl. Crystallogr.* **2009**, *42*, 339-341.

[371] G. M. Sheldrick, *Acta Cryst. C* **2015**, *71*, 3-8.

[372] R. Haldar, K. Batra, S. M. Marschner, A. B. Kuc, S. Zahn, R. A. Fischer, S. Bräse, T. Heine, C. Wöll, *Chem. Eur. J.* **2019**, *25*, 7847-7851.

[373] D. C. Götz, T. Bruhn, M. O. Senge, G. Bringmann, *J. Org. Chem.* **2009**, *74*, 8005-8020.

[374] G.-Y. Gao, J. V. Ruppel, D. B. Allen, Y. Chen, X. P. Zhang, *J. Org. Chem.* **2007**, *72*, 9060-9066.

[375] P. R. Frail, K. Susumu, M. Huynh, J. Fong, J. Kikkawa, M. J. Therien, *Chem. Mater.* **2007**, *19*, 6062-6064.

[376] A. Ryan, A. Gehrold, R. Perusitti, M. Pintea, M. Fazekas, O. B. Locos, F. Blaikie, M. O. Senge, *Eur. J. Org. Chem.* **2011**, *2011*, 5817-5844.

[377] C. Glaser, *Ber. Dtsch. Chem. Ges.* **1869**, *2*, 422-424.

[378] D. Shimizu, K. Fujimoto, A. Osuka, *Angew. Chem.* **2018**, *130*, 9578-9582.

[379] D. R. Martir, M. Averardi, D. Escudero, D. Jacquemin, E. Zysman-Colman, *Dalton Trans.* **2017**, *46*, 2255-2262.

[380] Y. Fang, L. Wang, W. Xu, Z. Ou, M. Chen, L. Cong, W. Shan, X. Ke, K. M. Kadish, *Inorg. Chem.* **2019**, *58*, 2576-2587.

[381] V. A. Ol'shevskaya, V. M. Alpatova, A. S. Radchenko, A. A. Ramonova, A. S. Petrova, V. V. Tatarskiy, A. V. Zaitsev, E. G. Kononova, N. S. Ikonnikov, A. A. Kostyukov, *Dyes Pigm.* **2019**, *171*, 107760.

[382] K. U. Rao, R. M. Appa, J. Lakshmidevi, R. Vijitha, K. K. Rao, M. Narasimhulu, K. Venkateswarlu, *Asian J. Org. Chem.* **2017**, *6*, 751-757.

[383] M. John Plater, S. Aiken, G. Bourhill, *Tetrahedron* **2002**, *58*, 2415-2422.

[384] M. L. Gomes, G. DeFreitas-Silva, P. G. dos Reis, M. N. Melo, F. Frezard, C. Demicheli, Y. M. Idemori, *J Biol Inorg Chem* **2015**, *20*, 771-779.

[385] Y. Okabe, S. K. Lee, M. Kondo, S. Masaoka, *J. Biol. Inorg. Chem.* **2017**, *22*, 713-725.

[386] R. Nishibayashi, T. Kurahashi, S. Matsubara, *Synlett* **2014**, *25*, 1287-1290.

[387] S. K. Albert, M. Golla, H. V. P. Thelu, N. Krishnan, P. Deepak, R. Varghese, *Org. Biomol. Chem.* **2016**, *14*, 6960-6969.

[388] S. A. Vail, D. I. Schuster, D. M. Guldi, M. Isosomppi, N. Tkachenko, H. Lemmetyinen, A. Palkar, L. Echegoyen, X. Chen, J. Z. Zhang, *J. Phys. Chem. B* **2006**, *110*, 14155-14166.

[389] S. Ikeda, M. Toganoh, H. Furuta, *Inorg Chem* **2011**, *50*, 6029-6043.

[390] M. Toganoh, S. Ikeda, H. Furuta, *Inorg Chem* **2007**, *46*, 10003-10015.

[391] M. Toganoh, T. Ishizuka, H. Furuta, *Chem Commun (Camb)* **2004**, 2464-2465.

[392] B. B. Beyene, A. W. Yibeltal, C. Hung, *Inorg. Chim. Acta* **2020**, *513*, 119929.

[393] V. Pashinnik, E. Martyniuk, M. Tabachuk, Y. G. Shermolovich, L. Yagupolskii, *Synth. Commun.* **2003**, *33*, 2505-2509.

[394] A. L. Spek, *Acta Crystallogr. Sect. D. Biol. Crystallogr.* **2009**, *65*, 148-155.

[395] A. L. Spek, *Acta Crystallogr. Sect. C. Struct. Chem.* **2015**, *71*, 9-18.

9 Appendix

9.1 Acknowledgement

First, I would like to cordially thank my doctoral supervisor, Prof. Dr. Stefan Bräse for the support, trust and freedom granted in the context of the preparation of this work. This allowed many chemical adventures to be dared and was essential for scientific growth and development. Thank you very much for supervising my doctoral thesis and for all the nice years of working together.

My thanks also go to Prof. Dr. Erick Carreira and Dr. David Rombach, who generously hosted me in the laboratories at ETH Zurich. The view beyond the horizon of preparative chemistry to industry-related chemical method development shaped my chemical education extensively. Prof. Dr. Bill Morandi I thank for making his infrastructure available to carry out air-sensitive experiments without reclaiming something back.

A special thank is dedicated to Prof. Dr. Manfred Kappes, Dr. Patrick Weis and especially to Erik Schneider. Without their help the work would not be as it is – thank you Erik for measuring samples at your spectrometers, when I needed the results most. One of the most exciting periods of my life was when we started getting access to the first cofacial structures. I thank all of you for the fruitful discussions and the many correction cycles leading to two mutual publications already.

Benjamin Felker, Sina Jaschik and Felix Bösch I thank for working with me in the laboratory as trainees for one year. Each of you had specific talents, which inspired me. I am sure that all of you will find your path.

I thank Patrick Kern, Silke Notter and Céline Schoch, who chose to write their theses supervised by me. David Rettinger, Ivana Ladan and Arina Belov I thank for absolving their internal practical courses in my laboratory. Sarah Pallocks and Réne Wurst I thank for working with me as assistants.

Dr. Sergei Lebedkin I thank for measuring revealing absorption and luminescence spectra accurately and on time.

Dr. Martin Nieger, Michael Solar and Dr. Nils Trapp I thank for their single-crystal X-ray analysis and insight full information regarding the practical work.
Dr. Vanessa Koch and Dr. David Rombach I thank for directing me on the right research path. In my eyes nothing is more important in one's development than having the right mentors at the right time. You coined me sustainably in my work ethics.

The AK Bräse I thank for creating an efficient but friendly work environment without being an elbows society. Especially, thanks go to Christiane Lampert and Janine Bolz for holding the group together and helping me overcome any kind of problems with the bureaucracy (there were a lot…). Dr. Christin Bednarek for being around and helping with the trainees. Dr. Nicole Jung for being available literately any time I had issues with the ELN and during the publishing processes.

The Fonds der Chemischen Industrie and the graduate program of the federal state of Baden-Württemberg (LGF) I thank for financial support without restricting my ideas of research. The Collaborative Research Center TRR88 "3MET" and the DFG I thank for making it possible to create a platform under the lead of Prof. Gereon Niedner-Schatteburg and Prof. Manfred Kappes. The interdisciplinarity and the exchange of this gathering could not be better and I mourn that the founding period is over soon. Additionally, I thank 3DMM2O and the implemented graduate school that made it possible for me to graduate within the MBA fundamental program.

Dr. Stefan Marschner I thank for helping me jump on the porphyrin research train. For guaranteeing 100% trustable preliminary results and experiences. Dr. Daniel Knoll I thank for our joined work on paracyclophane-porphyrin conjugates and for sharing long-term experiences.

Dr. Andreas Omlor I thank for insightful Mössbauer spectra. Unfortunately our research paths within 3MET crossed too late but inspiring talks and revealing results were still possible.

Manuel Link I thank for interesting photodissociation and photoelectron spectroscopy and explaining the theoretical insights behind them to me.

Dr. Andreas Rapp and Dr. Norbert Foitzik I thank for having an open ear for all different types of questions regarding, e.g., NMR spectroscopy, the computers or the OC seminar.

A big thank goes to the IOC analytic team: Angelika Mösle, Lara Hirsch, Despina Savvidou, Pia Lang, Tanja Ohmer-Scherrer and Rieke Schulte squeezing in important measurements and being cooperative on many subjects even when I granted to little amount of substance.

Céline Leonhardt, Dr. Christoph Zippel, Sarah Al Muthafer and Dr. David Rombach I thank for correcting this work. You have put so much time and effort in this – without you the thesis wouldn´t look the same. My unconventional time schedule did not make your life easier…. I appreciate that very much and owe you one!

MWS62 I thank for making my ETH time the best half a year I have had so far. Even though you were all super different, everyone took a piece of my heart.

Sarah Al Muthafer and Kevin Keller I thank for being my closest friends during our studies. Even though you are contrary to me, we complement each other perfectly.

Of course, I thank Lovisa Schlenker for showing me how selfless a person can be. You live straight from your heart and I am more than happy to have you by my side.

Mama, Papa, Franzi and Corni… you are the most important people in my life. Always supporting and inspiring me. Thank you for being the best family anyone could ever imagine.